THE UNIVERSITY *of* EDINBURGH

This thesis has been submitted in fulfilment of the requirements for a postgraduate degree (e.g. PhD, MPhil, DClinPsychol) at the University of Edinburgh. Please note the following terms and conditions of use:

This work is protected by copyright and other intellectual property rights, which are retained by the thesis author, unless otherwise stated.
A copy can be downloaded for personal non-commercial research or study, without prior permission or charge.
This thesis cannot be reproduced or quoted extensively from without first obtaining permission in writing from the author.
The content must not be changed in any way or sold commercially in any format or medium without the formal permission of the author.
When referring to this work, full bibliographic details including the author, title, awarding institution and date of the thesis must be given.

Investigating the neuroprotective role of carboxyl-terminus of Hsc70-interacting protein (CHIP) in healthy aging

Janet Poplawski

Doctor of Philosophy

Institute of Genetics and Cancer
College of Medicine and Veterinary Medicine
University of Edinburgh

2025

Dedicated to Marek & Helena

Declaration

I declare that I am the sole author of this thesis, and all work contained within it is my own, unless otherwise indicated or acknowledged.

Edinburgh, 2025

Janet Poplawski

2025

Acknowledgements

The last five years have been a period of immense growth & learning, far beyond just in the academic context, and would not have been possible without the help and support of many people. First and foremost, I would like to thank my supervisors, Kathryn Ball and Maria Doitsidou. Kathryn, thank you so much for your guidance over the years, and for being patient and supportive when I was struggling. You helped me when I needed it while also fostering an environment in which I had the space to learn and grow. Your passion for science is infectious and it's difficult not to get excited about pushing the bounds of knowledge when I hear you talk. You are both kind and ingenious and I am incredibly lucky to have had you as a supervisor. Maria, I've really appreciated your patience and willingness to answer my questions, as well as your generosity in sharing your lab space and equipment. Working in a genetics lab after a background in -omics was definitely a challenge to me, and I would not have been able to work through this project without your guidance and support. I am also thankful to my committee, Douglas Houston and Elizabeth Patton, for all your helpful comments and feedback throughout my program. I would also like to thank Ted Hupp for making sure I was not the only one commuting to and from George Square several times daily, and for always being happy to share fun worm (and Poland) facts at the IGC. I'm counting the days until I can pay it forward and regale other people with Sydney Brenner's experiments and perhaps even Gdańsk's political climate. Running Western blots just wouldn't have been the same without you.

I am also thankful to my lab and PhD cohort – it was a pleasure coming to work knowing you'd all be there. Thanks to Ailish, Yolanda, Jack, and Ashita for making lab work so much fun and answering my endless questions. Thanks to my PhD cohort as well, including Fraser, Ross, Cav, Chloe, Heather, Nathan, and everyone else – it was great to explore Edinburgh with you.

I would also like to thank Jakub Faktor, Sachin Kote, Javier Alfaro, and everyone else at the ICCVS for making my stay so enjoyable, showing me the beauty of Gdańsk, and letting me practice my (admittedly imperfect) Polish. Sachin, thank you so much for inviting me to visit your lab and being such a great collaborator throughout the years.

Jakub, thank you for being both my supervisor and “tour guide” – it was great trying every kind of pierogi with you.

I am grateful to my parents, Marek and Helena, and my sister, Aczi, for always supporting my hopes and dreams and making sure I had all the love and support in the world to achieve them. Thank you to all my friends, both near and far. Jaira, thank you for texting me every day (both because we’re in love, and also to make sure I’m still alive), and for talking me up when I forget what I’m capable of. Thank you to Amy for being there (and drawing beautiful birds on my legs) and to Russ for always making me laugh. To Louise, Morgan, and Jordan: thank you for all the girls’ nights and adventures. Thank you to Tal and Ro for being two of my best friends and arguably one of my favourite couples ever. It was great to explore the world with you (by “world” I mean the UK, but we will add France to the list one day). I loved our weekly games nights and/or afternoons, and your support of my sometimes-questionable fashion choices (even though I think dressing up as a sausage roll should have gotten me British citizenship). I hope we can make our next hiking trip in Canada.

Finally, I’d like to thank my best friend and sister, Ruby. I cannot believe how quickly the past few years have flown by, and I don’t think I would’ve been able to get through it all without you. You were my family away from home, and by far the best friend I’ve ever had. You know me well enough to pick words out of my brain before they even have a chance to leave my mouth. I can’t believe how much we’ve been through together – from the pipes exploding in every house we’ve lived in, to owning a cat together for exactly two weeks, to watching a single mouse run across the carpet of our gargantuan living room (after the cat “left”, of course). Thank you for eating all my experimental dishes, including the world’s worst tacos and the dental anaesthetic stew; on a completely unrelated note, thank you for coincidentally doing all the cooking except for that one time with the tacos and that other time with the stew. I tear up every time I think about leaving you especially, but luckily we call each other three times daily anyways, so maybe we’ll live.

This work was supported by the Natural Sciences and Engineering Research Council of Canada (NSERC PGS D) and the University of Edinburgh (Principal’s Career Development Scholarship & Edinburgh Global Research Scholarship).

Abstract

Throughout the past several decades, the elderly population has increased substantially. Yet, in spite of this enormous shift in age-related demographic characteristics, the cellular and physiological mechanisms underlying aging itself remain ill-defined. Their intrinsic complexity is further exacerbated by the difficulty inherent in segregating processes associated with pathological aging from those related to the normal, healthy aging process. Given that protein homeostasis is a major contributor to both normal and malignant aging, the ubiquitin-proteasome system is a promising candidate for teasing apart the pathways driving both healthy and pathological processes.

E3 ubiquitin ligases catalyse the final step of an enzymatic cascade priming proteins for degradation through the ubiquitin-proteasome system and thus are crucial to protein quality control. Carboxyl terminus of Hsp70-interacting protein (CHIP), one such ligase, was initially found to facilitate the polyubiquitination and eventual degradation of aberrantly folded and/or aggregated client proteins in a complex with Hsp70, an essential component of the chaperone system. More recent studies, however, have identified additional, chaperone-independent functions of CHIP in mediating the activity, localization, and steady-state levels of a targeted protein cohort essential for cellular and organismal well-being, including several involved in interferon and insulin signaling as well as membrane integrity. In animal models, deletion of CHIP imparts an early aging phenotype, along with impaired cognitive function and neurodegeneration. CHIP deletion also predisposed animals to increased cell death, mitochondrial dysfunction, and oxidative stress. The functions of CHIP are also context-dependent, with CHIP being rerouted from mediating insulin receptor degradation in normal cellular conditions to protein quality control pathways under conditions of proteotoxic stress, thus stabilizing the insulin receptor and decreasing lifespan.

While its multifaceted role in neuroprotection makes CHIP a promising subject for the study of healthy aging, little is known about the interplay between its functions and their mechanistic underpinnings. Here, I aim to delineate the cellular pathways mediating the neuroprotective effects of CHIP through the proteomic investigation of a

whole-animal model system, *C. elegans*. **The objectives of this study are (1) to characterize a methodological approach for the experimental conditions relevant to processing *C. elegans* samples for proteomic analyses, (2) to explore the effects of *chn-1* ablation on the proteomic landscape of nematodes, the simplest whole-animal model systems for the study of aging, and (3) to identify and validate proteomic biomarkers found to be implicated in CHIP-mediated processes including cellular transport, protein quality control, and longevity.**

SWATH-MS was performed on *chn-1(by155)* and *chn-1(tm2692)* deletion mutants, in addition to wild-type controls, processed by either SDS or CHAPS/urea-based lysis protocols. Between-buffer analyses revealed 1 092 substantially altered proteins, with methodologically contingent trends in protein expression patterns substantially overshadowing differences between independently-derived strains. Core proteins altered in response to *chn-1* ablation included the transcription factor SMA-9, a key modulator of the TGF-β signaling cascade, as well as mitochondrial pyruvate carrier 1 (MPC1) and FIS-2, suggesting CHIP-associated mitochondrial dysfunction in *chn-1*-null animals. Membrane proteins as well as proteins associated with the regulation of trafficking activity, and more specifically retrograde transport, during which proteins and lipids are shuttled between endosomes and the *trans*-Golgi network, were also preferentially altered in response to *chn-1* ablation. In contrast to the broad spectrum of proteins affected by different lysis methods, *chn-1* ablation itself impacted a more focused subset of proteins, with only 33 and 46 proteins altered across both *chn-1*-null strains in CHAPS/urea- and SDS-processed samples, respectively. These findings suggest a tight substrate specificity, and lend further support to the noncanonical function of CHIP as a chaperone-independent/docking-dependent ubiquitin ligase.

Subsequent validation experiments involving lifespan assays on *chn-1(tm2692); sma-9* double-knock-out nematodes revealed a less-than-additive epistatic double-mutant phenotype, suggesting that *chn-1* and *sma-9* interact in a manner that is overlapping but not entirely redundant. Immunofluorescence and Western blotting experiments were also performed in a SH-SY5Y neuroblastoma cell line to further verify the proteomics results. Specifically, Golgi fragmentation was assessed in both *chn-1* wild-type and knock-out nematodes expressing a Golgi marker, as well as wild-type and

CHIP knock-out cells stained with GM130. Western blotting was performed on several proteins involved in retrograde transport pathways, including COG complex as well as Rab proteins. In CHIP-null cells and animals, aberrant protein expression was correlated with increased Golgi fragmentation, suggesting CHIP loss-of-function may be linked to this early marker of neurodegeneration. Finally, rescue experiments in *C. elegans* using the human and nematode orthologs of CHIP were created using Gateway cloning, and subsequent proteomics experiments performed to identify a focused cohort of CHIP-associated proteins corresponding specifically to lifespan extension.

In addition to elucidating novel methodological considerations for *C. elegans*-based proteomics experiments, these findings provide evidence for CHIP-mediated molecular processes underpinning Golgi integrity, protein transport, mitochondrial dysfunction, and longevity, and provide a foundation for future mechanistic studies to further shed light on these CHIP-associated pathways, processes, and signaling cascades.

Lay Summary

Aging is one of the most ubiquitous and yet poorly understood phenomena. Contributing to this lack of understanding is the difficulty inherent in separating pathological from healthy aging. The protein quality control (or PQC) network is a series of safeguards and processes focused on maintaining the proper configuration (i.e., folding) and functioning of proteins in the organism, and the appropriate functioning of this system is central to healthy aging.

CHIP, a ubiquitin ligase, is a protein that plays a key role in the PQC network. It is responsible for transferring ubiquitin to target proteins, and thus regulating their stability or degradation. In doing so, CHIP plays a key role in maintaining cellular membrane function, immunity, and insulin signaling. Perhaps predictably, animals lacking CHIP experience accelerated aging and cognitive impairment, in tandem with a number of other undesirable effects, such as mitochondrial dysfunction and a vulnerability to oxidative stress. The role of CHIP has also been found to change depending on the cellular environment. For instance, in healthy cells, CHIP mediates the degradation of the insulin receptor. However, under conditions of cellular stress, CHIP is rerouted toward maintaining protein quality control. This results in the stabilization of the insulin receptor, and an associated decrease in longevity.

Here, I further investigated the neuroprotective functions of CHIP through a series of experiments assessing how the protein landscape of the nematode (*C. elegans*), one of the simplest whole-animal model organisms, was changed in response to *chn-1* (the worm orthologue of CHIP) deletion. I first compared two lysis buffers, each with chemical properties predicted to extract a different set of proteins, to both contribute to the methodological literature and ensure I was thorough in capturing how *chn-1* deletion could affect the proteome. I then compared *chn-1* controls with knock-out mutants to investigate the proteomic effects of *chn-1* deletion. Finally, I performed a series of follow-up experiments to further explore these results.

My analyses revealed that the effects of lysis buffer had an enormous impact on protein extraction, with over 1 000 proteins differentially expressed depending on whether a CHAPS/urea- or SDS-based lysis protocol was followed. In contrast to these

results, *chn-1* deletion itself impacted a more refined subset of proteins, including SMA-9, a modulator of TGF-β signaling (playing a large role in development, homeostasis, and tissue repair), as well as several proteins related to mitochondrial function. Membrane proteins and those involved in protein transport were also heavily impacted, especially those implicated in retrograde transport, or the transfer of proteins between endosomes and the *trans*-Golgi network. These findings further support the relatively novel idea that CHIP can function as a chaperone-independent E3 ligase, as opposed to a chaperone-dependent ligase only.

My follow-up experiments included a lifespan assay on *chn-1* and *sma-9* double-knock-out worms, which showed that double mutants displayed lifespans that were shorter than single mutants, but perhaps not as short as would be expected. This implies that *chn-1* and *sma-9* function in a manner that overlaps at least partially, but not entirely. Further validation experiments were also performed in both wild-types and CHIP knock-outs, in both worm and human cell models. Golgi fragmentation, an early marker of neurodegeneration, was assessed in both model systems, and the expression of several proteins involved in protein transport was investigated as well. Aberrant protein expression was found in CHIP-null conditions, along with increased Golgi fragmentation, suggesting the absence of normal CHIP function may be linked to this early marker of pathological aging. Finally, both human and *C. elegans* CHIP rescue worms were created using Gateway cloning, and another proteomics experiment performed to identify the subset of proteins responsible for the lifespan rescue corresponding to the genetic re-addition of CHIP in these animals.

These findings provide evidence that CHIP is involved in regulating processes integral to healthy aging such as Golgi integrity, protein transport, the healthy functioning of the mitochondria, and lifespan itself. They also provide a foundation for future studies aiming to further investigate the mechanisms through which these relationships occur.

Abbreviations

17-AAG	17-allylamino-17-demethoxy geldanamycin
CHAPS	3-[(3-cholamidopropyl)dimethylammonio]-1-propanesulfonate)
AcN	Acetonitrile
ATP	Adenosine triphosphate
AMPK	Adenosine-5'-monophosphate-dependent protein kinase
ARF4	ADP-ribosylation factor 4
APP	Amyloid-β precursor protein
BCA	Bicinchoninic acid
BP	Biological process
BMAL1	Brain and muscle ARNT-like 1
C. elegans	*Caenorhabditis elegans*
CHIP	Carboxyl terminus of Hsp70-interacting protein
CC	Cellular component
COPI	Coat Protein Complex I
COPII	Coat Protein Complex II
CDG-II	Congenital glycosylation disorder type II
COG	Conserved oligomeric Golgi
COG6	Conserved oligomeric Golgi complex subunit 6
CREB3	Cyclic AMP-responsive element-binding protein 3
CDK5	Cyclin-dependent kinase 5
CFTR	Cystic fibrosis transmembrane conductance regulator
DAMPs	Damage-associated molecular proteins
ESCs	Embryonic stem cells
ER	Endoplasmic reticulum
EARP	Endosome-associated recycling protein
eNOS	Endothelial nitric oxide synthase
ECL	Enhanced chemiluminescence
ERES	ER exit sites
ERGIC53	ER-Golgi intermediate compartment 53
E. coli	*Escherichia coli*
EDTA	Ethylenediaminetetraacetic acid
FIRKO	Fat-specific insulin receptor knock-out
FASP	Filter-aided sample preparation
FOXO	Forkhead box protein O
FA	Formic acid
GAPDH	Glyceraldehyde-3-phosphate dehydrogenase
GASE	Golgi apparatus stress response element
GM130	Golgi matrix protein 130
GRASP65	Golgi reassembly stacking protein 65

GARP	Golgi-associated retrograde protein
Hsp70	Heat shock protein 70
HSF	Heat-shock family
HSP47	Heat-shock protein 47
HGF	Hepatocyte growth factor
H3K4	Histone H3 lysine 4
HER2	Human epidermal growth factor receptor 2
pTau	Hyperphosphorylation of tau
IRE1	Inositol-requiring enzyme 1
IIS	Insulin-like growth factor signaling
IGF-1	Insulin-like growth factor-1
IRF-1	Interferon regulatory factor 1
LRRK2	Leucine-rich repeat kinase 2
LC	Liquid chromatography
mTOR	Mechanistic TOR
miRNAs	microRNAs
MT	Microtubule
mtDNA	mitochondrial DNA
MPC1	Mitochondrial pyruvate carrier 1
MF	Molecular function
mTORC2	mTOR complex 2
NGM	Nematode growth medium
NFTs	Neurofibrillary tangles
NAD	Nicotinamide adenine dinucleotide
Pen/Strep	Penicillin/Streptomycin
PTEN	Phosphatase and tensin homolog
PEPCK-C	Phosphoenolpyruvate carboxykinase
pGRASP65	Phosphorylation of GRASP65
PML	Promyelocytic leukaemia
PIM	Protease inhibitor mix
PKB	Protein kinase B
PQC	Protein quality control
PTK6	Protein tyrosine kinase 6
PINK1	PTEN-induced kinase 1
PINK1	PTEN-induced putative kinase 1
ROC/COR	Ras of complex/C-terminal of Roc
Rab	Ras-associated binding
ROS	Reactive oxygen species
SWATH-MS	Sequential window acquisition of all theoretical fragment ion spectra-mass spectrometry
STAT	Signal transducer and activator of transcription

SIRT1	Sirtuin 1
SUMO	Small ubiquitin-like modifier
SDS	Sodium dodecyl sulfate
SNARE	Soluble N-ethylmaleimide-sensitive factor activating protein receptor
SLC	SoLute Carrier
SNX6	Sorting nexin 6
STUB1	STIP1 Homology and U-Box Containing Protein 1
S-trap	Suspension trap
TOR	Target of rapamycin
TPR	Tetratricopeptide repeat
TFE3	Transcription factor binding to IGHM enhancer 3
TFEB	Transcription factor EB
TGF-β	Transforming growth factor-β
tER	transitional ER
TEs	Transposable elements
UPS	Ubiquitin-proteasome system
VPS52	Vacuolar protein sorting-associated protein 52 homolog
VTC	Vesicular-tubular cluster
YAP1	Yes-associated protein 1
α-Syn	α-Synuclein
ULK1	Unc-1 like autophagy activating kinase 1
mTORC1	Mammalian target of rapamycin complex 1
VPS34	Vacuolar protein sorting 34
LC3	1A/1B-light chain 3
CGC	*Caenorhabditis* Genetics Centre
APS	Ammonium persulfate
PCR	Polymerase chain reaction

Contents

Declaration ..... **iv**
Acknowledgements ..... **v**
Abstract ..... **vii**
Lay Summary ..... **x**
Abbreviations ..... **xii**
List of Figures ..... **xix**
List of Tables ..... **xxii**

Chapter 1 ..... **1**
1.1 Overview of C-Terminus of Hsp70-Interacting Protein (CHIP) and Its Effects 1
1.2 The Hallmarks of Aging 3
1.2.1 Introduction to Aging 3
1.2.2 Genomic Instability 5
1.2.3 Telomere Attrition 5
1.2.4 Epigenetic Alterations 6
1.2.5 Loss of Proteostasis 7
1.2.6 Deregulated Nutrient Sensing 11
1.2.7 Mitochondrial Dysfunction 14
1.2.8 Cellular Senescence 15
1.2.9 Stem Cell Exhaustion 16
1.2.10 Impaired Cellular Communication 17
1.3 Introduction to Ubiquitination and the Ubiquitin-Proteasome System 17
1.4 Introduction to Autophagy 19
1.5 The Structure and Functions of CHIP 21
1.5.1 Introduction to CHIP 21
1.5.2 The Structure of CHIP 23
1.5.3 CHIP and Transcriptional Regulation 26
1.5.4 CHIP at the Crossroads of Proteostasis and Insulin Signaling 27
1.5.5 CHIP and Mitochondrial Dysfunction 28
1.5.6 CHIP and Protein Trafficking 28
1.6 Introduction to Models of Aging 29

1.7 Summary, Aims & Hypotheses 31
1.8 Thesis Layout 33

Chapter 2: *C. elegans* Protein Landscape is Altered Depending on Detergent Properties During Lysis 34
2.1 Introduction 34
2.1.1 Introduction to *C. elegans* 36
2.2 Materials and Methods 38
2.2.1 Experiment Overview and Rationale 38
2.2.2 Nematode Strains 40
2.2.2.1 Triple-Backcrossing C. elegans Strains 40
2.2.2.2 Agarose Gel Electrophoresis of DNA 41
2.2.2.3 Polymerase Chain Reaction (PCR) 41
2.2.2.4 DNA Sequencing 42
2.2.4 Preparation of Samples for Proteomic Analyses 42
2.2.5 Mass Spectrometry-Based Proteomics 44
2.2.5.1 Data Processing and Statistical Analyses 45
2.3 Results: Protein Extractability Varies in a Detergent-Dependent Manner 45
2.3.1 Validation of *C. elegans* Strains 45
2.3.2 Overview of the Changes in the Proteome 51
2.3.3 Lysis Procedure Alters Protein Landscape in a Detergent-Dependent Manner 57
2.4 Discussion 75

Chapter 3: *chn-1* Ablation Alters the *C. elegans* Protein Landscape 83
3.1 Introduction 83
3.2 Materials and Methods 84
3.2.1 Experiment Overview and Rationale 84
3.2.2 Lifespan Assay 87
3.2.3 Statistical Analyses 87
3.3 Results: *chn-1* Deletion Alters the *C. elegans* Proteomic Landscape 88
3.3.1 Validation of *C. elegans* Strains 88
3.3.2 Knock-Out Mutants of *chn-1* are Short-Lived 88
3.3.3 Overview of the Changes in the Proteome 89

3.3.4 Shared Proteins Altered Across *chn-1* Deletion Mutants Reveal Focused Changes 92
3.3.5 Pairwise Comparisons Reveal Altered Proteomic Landscape in Response to *chn-1* Deletion 99
3.4 Discussion 116

Chapter 4: *chn-1* Deletion Affects Golgi Morphology, TGF-β Signalling, and Retrograde Transport 123
4.1 Introduction 123
4.1.1 The Role of the Golgi Apparatus in Neuroprotection and Degeneration 123
4.1.1.1 Overview of the Golgi Complex 123
4.1.1.2 Protein Quality Control in the Golgi Apparatus 125
4.1.1.3 Retrograde Transport and the COG Complex 127
4.1.1.4 The Golgi Apparatus and Neurological Diseases 128
4.1.1.5 Membrane Trafficking and Rab Proteins in Pathological Aging 132
4.1.1.6 The Effects of CHIP Ablation on Golgi Morphology, TGF-β Signalling, and Retrograde Transport 133
4.2 Materials and Methods 135
4.2.1 Experiment Overview 135
4.2.2 *C. elegans* and SH-SY5Y Strains Employed 138
4.2.3 Fluorescence Microscopy and Phenotype Analyses 139
4.2.3.1 Quantification of C. elegans Golgi Phenotype 139
4.2.3.2 Cell Culture 139
4.2.3.3 SH-SY5Y Subculture 140
4.2.3.4 Cryopreservation 140
4.2.3.5 Cell Recovery 141
4.2.3.6 Cell Counting 141
4.2.3.7 Coverslip Preparation 141
4.2.3.8 SH-SY5Y Immunofluorescence 141
4.2.3.9 Cell Harvesting 142
4.2.4 Biochemical Techniques 143
4.2.4.1 Cell Pellet Lysis 143
4.2.4.2 SDS-PAGE In-House Polyacrylamide Gels 143
4.2.4.3 Immunoblotting (Western Blotting) 145
4.2.5 Lifespan Assay 146

4.2.6 Statistical Analyses 146
4.2.7 *chn-1* Rescue Proteomics 146
4.3 Results: *chn-1* Ablation Alters Golgi Morphology, TGF-β Signaling, and Retrograde Transport 147
4.3.1 Both Single and Double-Knock-Out Mutants of *chn-1* and *sma-9* are Short-Lived 147
4.3.2 Transport-Related Proteins and Structures Show a CHN-1-Dependent Phenotype 150
4.3.3 Immunoblotting Experiments Revealed CHIP- and Extraction-Dependent Transport Protein Expression 154
4.3.4 Validation of CHIP/*chn-1* Rescue *C. elegans* Strains 156
4.3.5 Rescue of CHIP/*chn-1* Results in a Corresponding Rescue of Lifespan Phenotype 157
4.3.6 Lifespan Rescue is Associated with a Distinct Proteomic Signature 161
4.4 Discussion 175

Chapter 5 182
5.1 Detergent Properties Substantially Alter Protein Profiles 182
5.1.1 Summary of Findings 182
5.1.2 Study Limitations and Considerations for Future Work 183
5.2 *chn-1* Ablation Alters the Nematode Proteomic Landscape 183
5.2.1 Summary of Findings 183
5.2.2 Study Limitations and Considerations for Future Work 185
5.3 CHIP Impacts Golgi Morphology, TGF-β Signaling, and Retrograde Transport 186
5.3.1 Summary of Findings 186
5.3.2 Study Limitations and Considerations for Future Work 187
5.4 Final Conclusion 187

Appendix A 190
Supplemental Results for Chapter 2 190
Appendix B 220
Supplemental Results for Chapter 3 220
Appendix C 245
Supplemental Data for Chapter 4 245
Bibliography 342

List of Figures

Figure 1.1 CHIP promotes either longevity or proteostasis, depending on the cellular environment 2

Figure 1.2 The hallmarks of aging 4

Figure 1.3 The proteostasis network, protein folding intermediates, and the native state 10

Figure 1.4 Protein degradation, ubiquitin, and the ubiquitin-proteasome system 19

Figure 1.5 The structure of CHIP 25

Figure 2.1 Life cycle of *C. elegans* 38

Figure 2.2 Failed experiment examining strain-dependent differences in *chn-1(by155)* and *chn-1(tm2692)* mutants vs. wild-type controls 39

Figure 2.3 Agarose gel electrophoresis of *chn-1(by155)* and *chn-1(tm2692)* PCR amplicons prior to proteomic analyses of *chn-1* deletion mutants 48

Figure 2.4 Genomic maps of *chn-1(by155)* and *chn-1(tm2692)*, including primer binding sites 49

Figure 2.5 Sequence of the *chn-1(by155)* allele 50

Figure 2.6 Sequence of the *chn-1(tm2692)* allele 51

Figure 2.7 Venn diagram showing the overlap of total proteins identified (independent of *p*-value or fold change) in N2 wildtype animals via DDA-MS subjected to lysis by either CHAPS- or SDS-based lysis buffer 52

Figure 2.8 PCA scores plots showing separation between both strains and detergent conditions 54

Figure 2.9 Heatmap showing expression patterns of proteins identified by SWATH-MS across detergents 56

Figure 2.10 Comparative SWATH-MS proteomic analyses of N2 wild-type *C. elegans* samples processed by lysis with CHAPS/Urea- vs. SDS-based lysis buffer 59

Figure 2.11 GO enrichment analysis of the *C. elegans* N2 wild-type proteome of underexpressed proteins identified by SWATH-MS across lysis buffers 62

Figure 2.12 GO enrichment analysis of the *C. elegans* N2 wild-type proteome of overexpressed proteins identified by SWATH-MS across lysis buffers 66

Figure 2.13 Venn diagrams showing overlap of GO terms substantially altered by SWATH-MS across *C. elegans chn-1* mutants 69

Figure 2.14 KEGG pathway analysis derived from the N2 wild-type proteomics of our *C. elegans* model 71
Figure 2.15 Venn diagrams showing overlap of KEGG pathways substantially altered by SWATH-MS across *C. elegans chn-1* mutants 74
Figure 2.16 Subcellular localization and physicochemical characteristics of proteins identified by simultaneous proteo-metabolomic liquid-liquid extraction interphase pellets 81

Figure 3.1 Flowchart of sample preparation and proteomic analyses 85
Figure 3.2 The location and gene structure of *chn-1* 87
Figure 3.3 Lifespan is decreased by *chn-1* deletion 90
Figure 3.4 Venn diagrams showing the overlap of proteins identified by SWATH-MS across *C. elegans* CHIP mutants 91
Figure 3.5 Comparative SWATH-MS proteomic analyses of *chn-1(by155)* vs. N2 wild-type *C. elegans* samples processed by lysis with CHAPS/Urea-based lysis buffer 100
Figure 3.6 Comparative SWATH-MS proteomic analyses of *chn-1(tm2692)* vs. N2 wild-type *C. elegans* samples processed by lysis with CHAPS/Urea-based lysis buffer 103
Figure 3.7 Comparative SWATH-MS proteomic analyses of *chn-1(by155)* vs. N2 wild-type *C. elegans* samples processed by lysis with SDS-based lysis buffer 106
Figure 3.8 Comparative SWATH-MS proteomic analyses of *chn-1(tm2692)* vs. N2 wild-type *C. elegans* samples processed by lysis with SDS-based lysis buffer 109
Figure 3.9 KEGG pathway analysis derived from the proteomics of our *C. elegans* model 114

Figure 4.1 An overview of Golgi proteins involved in mediating vesicular transport and golgins across compartments 126
Figure 4.2 The structure and function of the Golgi apparatus under normal and neurodegenerative conditions 130
Figure 4.3 The deletion of both *chn-1* and *sma-9* leads to reduced lifespan 149
Figure 4.4 The Golgi in *chn-1(tm2692)* exhibit increased fragmentation 151
Figure 4.5 Antibody titration experiment for COG6 and Rab6 152
Figure 4.6 CHIP ablation altered expression of proteins integral to cellular transport . 153
Figure 4.7 CHIP deletion in SH-SY5Y cells alters Rab6 and COG6 expression in a detergent-dependent manner 155
Figure 4.8 Genomic maps of Pchn-1_hCHIP_SL2-mKate-UTR and Pchn-1-CeCHIP-SL2mKateUTR expression clones 156

Figure 4.9 A comparison of human CHIP and *C. elegans* CHN-1 sequences and structures 157

Figure 4.10 Rescuing *chn-1* mutants led to an associated increase in lifespan 160

Supplemental Figure A1 Venn diagrams showing the overlap of proteins identified by SWATH-MS across detergents 191

Supplemental Figure A2 Comparative SWATH-MS proteomic analyses of *chn-1(by155) C. elegans* samples processed by lysis with CHAPS/Urea- vs. SDS-based lysis buffer 193

Supplemental Figure A3 Comparative SWATH-MS proteomic analyses of *chn-1(tm2692) C. elegans* samples processed by lysis with CHAPS/Urea- vs. SDS-based lysis buffer 194

Supplemental Figure A4 GO enrichment analysis of the *C. elegans chn-1(by155)* proteome of underexpressed proteins identified by SWATH-MS across lysis buffers. 201

Supplemental Figure A5 GO enrichment analysis of the *C. elegans chn-1(by155)* proteome of overexpressed proteins identified by SWATH-MS across lysis buffers ... 204

Supplemental Figure A6 GO enrichment analysis of the *C. elegans chn-1(tm2692)* proteome of underexpressed proteins identified by SWATH-MS across lysis buffers. 208

Supplemental Figure A7 GO enrichment analysis of the *C. elegans chn-1(tm2692)* proteome of overexpressed proteins identified by SWATH-MS across lysis buffers ... 212

Supplemental Figure A8 KEGG pathway analysis derived from the *chn-1(by155)* proteomics of our *C. elegans* model 216

Supplemental Figure A9 KEGG pathway analysis derived from the *chn-1(tm2692)* proteomics of our *C. elegans* model 218

Supplemental Figure B1 GO enrichment analysis of the proteome of overlapping proteins identified by SWATH-MS across *C. elegans* mutants 231

Supplemental Figure B2 CHAPS/urea-based GO enrichment analysis derived from the proteomics of our *C. elegans* model 236

Supplemental Figure B3 *chn-1(by155)* GO enrichment analysis derived from the proteomics of our *C. elegans* model 239

Supplemental Figure B4 *chn-1 (tm2692)* GO enrichment analysis derived from the proteomics of our *C. elegans* model 242

Supplemental Figure C1 Additional representative confocal images of wild-type and *chn-1(tm2692)* coelomocytes expressing MANS::GFP Golgi markers 245

List of Tables

Table 1.1 Advantages and disadvantages of some of the most common model systems in aging research 31

Table 2.1 Primers for PCR amplification of *chn-1* wild or mutant type genes..... 41

Table 2.2 Top proteins (based on fold change) identified by SWATH-MS that are over-represented in N2 wild-type *C. elegans* samples processed by lysis with CHAPS/urea- vs. SDS-based lysis buffer..... 60

Table 2.3 Top proteins (based on fold change) identified by SWATH-MS that are under-represented in N2 wild-type *C. elegans* samples processed by lysis with CHAPS/Urea- vs. SDS-based lysis buffer..... 61

Table 2.4 N2 wild-type GO terms related to underexpressed proteins identified by SWATH-MS across lysis buffers..... 63

Table 2.5 N2 wild-type GO terms related to overexpressed proteins identified by SWATH-MS across lysis buffers..... 67

Table 2.6 KEGG pathways related to substantially altered proteins identified by SWATH-MS across lysis buffers in N2 wild-type animals..... 72

Table 3.1 KEGG pathways related to CHIP loss-of-function in both *chn-1(by155)* and *chn-1(tm2692)* mutants..... 92

Table 3.2 Shared proteins (based on fold change) identified by SWATH-MS that are over-represented in both *chn-1(by155)* and *chn-1(tm2692) C. elegans* samples processed by lysis with CHAPS/urea-based lysis buffer 94

Table 3.3 Shared proteins (based on fold change) identified by SWATH-MS that are under-represented in both *chn-1(by155)* and *chn-1(tm2692) C. elegans* samples processed by lysis with CHAPS/urea-based lysis buffer 95

Table 3.4 Shared proteins (based on fold change) identified by SWATH-MS that are over-represented in both *chn-1(by155)* and *chn-1(tm2692) C. elegans* samples processed by lysis with SDS-based lysis buffer 96

Table 3.5 Shared proteins (based on fold change) identified by SWATH-MS that are under-represented in both *chn-1(by155)* and *chn-1(tm2692) C. elegans* samples processed by lysis with SDS-based lysis buffer 98

Table 3.6 Top proteins (based on fold change) identified by SWATH-MS proteomic analyses that are over-represented in *chn-1(by155)* vs. N2 wild-type *C. elegans* samples processed by lysis with CHAPS/urea-based lysis buffer..... 101

Table 3.7 Top proteins (based on fold change) identified by SWATH-MS proteomic analyses that are under-represented in *chn-1(by155)* vs. N2 wild-type *C. elegans* samples processed by lysis with CHAPS/urea-based lysis buffer 102

Table 3.8 Top proteins (based on fold change) identified by SWATH-MS proteomic analyses that are over-represented in *chn-1(tm2692)* vs. N2 wild-type *C. elegans* samples processed by lysis with CHAPS/urea-based lysis buffer 104

Table 3.9 Top proteins (based on fold change) identified by SWATH-MS proteomic analyses that are under-represented in *chn-1(tm2692)* vs. N2 wild-type *C. elegans* samples processed by lysis with CHAPS/urea-based lysis buffer 105

Table 3.10 Top proteins (based on fold change) identified by SWATH-MS proteomic analyses that are over-represented in *chn-1(by155)* vs. N2 wild-type *C. elegans* samples processed by lysis with SDS-based lysis buffer 107

Table 3.11 Top proteins (based on fold change) identified by SWATH-MS proteomic analyses that are under-represented in *chn-1(by155)* vs. N2 wild-type *C. elegans* samples processed by lysis with SDS-based lysis buffer 108

Table 3.12 Top proteins (based on fold change) identified by SWATH-MS proteomic analyses that are over-represented in *chn-1(tm2692)* vs. N2 wild-type *C. elegans* samples processed by lysis with SDS-based lysis buffer 110

Table 3.13 Top proteins (based on fold change) identified by SWATH-MS proteomic analyses that are under-represented in *chn-1(tm2692)* vs. N2 wild-type *C. elegans* samples processed by lysis with SDS-based lysis buffer 111

Table 3.14 KEGG pathways related to CHIP loss-of-function in either *chn-1(by155)* or *chn-1(tm2692)* mutants 115

Table 4.1 Buffer and solution constituents for western blotting 144

Table 4.2 Rescued proteins (based on fold change) identified by SWATH-MS that are either over- or under-represented in both *h*CHIP and *chn-1* rescue strains processed by lysis with CHAPS/urea-based lysis buffer 163

Table 4.3 Rescued proteins (based on fold change) identified by SWATH-MS that are either over- or under-represented in both *h*CHIP and *chn-1* rescue strains processed by lysis with SDS-based lysis buffer 166

Table 4.4 GO terms related to substantially altered proteins identified in both *h*CHIP and *chn-1* rescue strains processed by lysis with CHAPS/urea-based lysis buffer 171

Table 4.5 KEGG pathways related to substantially altered proteins identified in both *h*CHIP and *chn-1* rescue strains processed by lysis with CHAPS/urea-based lysis buffer 172

Table 4.6 GO terms related to substantially altered proteins identified in both *h*CHIP and *chn-1* rescue strains processed by lysis with SDS-based lysis buffer 173

Table 4.7 KEGG pathways related to substantially altered proteins identified in both *h*CHIP and *chn-1* rescue strains processed by lysis with SDS-based lysis buffer 174

Supplemental Table A1 Top proteins (based on fold change) identified by SWATH-MS that are over-represented in *chn-1(by155) C. elegans* samples processed by lysis with CHAPS/Urea- vs. SDS-based lysis buffer 195

Supplemental Table A2 Top proteins (based on fold change) identified by SWATH-MS that are under-represented in *chn-1(by155) C. elegans* samples processed by lysis with CHAPS/Urea- vs. SDS-based lysis buffer 196

Supplemental Table A3 Top proteins (based on fold change) identified by SWATH-MS that are over-represented in *chn-1(tm2692) C. elegans* samples processed by lysis with CHAPS/Urea- vs. SDS-based lysis buffer 197

Supplemental Table A4 Top proteins (based on fold change) identified by SWATH-MS that are under-represented in *chn-1(tm2692) C. elegans* samples processed by lysis with CHAPS/Urea- vs. SDS-based lysis buffer..... 198

Supplemental Table A5 *chn-1(by155)* GO terms related to underexpressed proteins identified by SWATH-MS across lysis buffers 202

Supplemental Table A6 *chn-1(by155)* GO terms related to overexpressed proteins identified by SWATH-MS across lysis buffers 205

Supplemental Table A7 *chn-1(tm2692)* GO terms related to underexpressed proteins identified by SWATH-MS across lysis buffers 209

Supplemental Table A8 *chn-1(tm2692)* GO terms related to overexpressed proteins identified by SWATH-MS across lysis buffers 213

Supplemental Table A9 KEGG pathways related to substantially altered proteins identified by SWATH-MS across lysis buffers in *chn-1(by155) C. elegans* mutants ... 217

Supplemental Table A10 KEGG pathways related to substantially altered proteins identified by SWATH-MS across lysis buffers in *chn-1(tm2692) C. elegans* mutants . 219

Supplemental Table B1 Bonferroni-adjusted *p*-values associated with longevity differences in N2 wild-type, *chn-1(by155)*, and *chn-1(tm2692)* mutants 220

Supplemental Table B2 Restricted mean survival times and final mortalities associated with longevity differences in N2 wild-type, *chn-1(by155)*, and *chn-1(tm2692)* mutant animals..... 221

Supplemental Table B3 Censored animals when comparing N2, *chn-1(by155)*, and *chn-1(tm2692) chn-1* deletion mutants 222

Supplemental Table B4 Genes corresponding to shared proteins (based on fold change) identified by SWATH-MS that are over-represented in both *chn-1(by155)* and *chn-1(tm2692) C. elegans* samples processed by lysis with CHAPS/urea-based lysis buffer..... 226

Supplemental Table B5 Genes corresponding to shared proteins (based on fold change) identified by SWATH-MS that are under-represented in both *chn-1(by155)* and

chn-1(tm2692) C. elegans samples processed by lysis with CHAPS/urea-based lysis buffer 227

Supplemental Table B6 Genes corresponding to shared proteins (based on fold change) identified by SWATH-MS that are over-represented in both *chn-1(by155)* and *chn-1(tm2692) C. elegans* samples processed by lysis with SDS-based lysis buffer . 228

Supplemental Table B7 Genes corresponding to shared proteins (based on fold change) identified by SWATH-MS that are under-represented in both *chn-1(by155)* and *chn-1(tm2692) C. elegans* samples processed by lysis with SDS-based lysis buffer . 229

Supplemental Table B8 GO terms related to CHIP loss-of-function in both *chn-1(by155)* and *chn-1(tm2692)* mutants 232

Supplemental Table B9 GO terms related to CHIP loss-of-function in either *chn-1(by155)* or *chn-1(tm2692)* mutants lysed by CHAPS/urea 237

Supplemental Table B10 GO terms related to CHIP loss-of-function in *chn-1(by155)* mutants lysed by SDS 240

Supplemental Table B11 GO terms related to CHIP loss-of-function in *chn-1(tm2692)* mutants lysed by SDS 243

Supplemental Table C1 Bonferroni-adjusted *p*-values associated with longevity differences in *chn-1* and *sma-9* single- and double-gene mutations 246

Supplemental Table C2 Restricted mean survival times and final mortalities associated with longevity differences in *chn-1* and *sma-9* single- and double-gene mutations 247

Supplemental Table C3 Censored animals when comparing N2 wild-type, *sma-9* mutants, *chn-1* mutants, and *chn-1; sma-9* double-mutants 248

Supplemental Table C4 Bonferroni-adjusted *p*-values associated with longevity differences in *chn-1(by155)*-null mutants, *chn-1(by155)*-derived *h*CHIP/*Ce*CHIP rescue animals, and *m*Kate controls 253

Supplemental Table C5 Restricted mean survival times and final mortalities associated with longevity differences in *chn-1(by155)*-null mutants, *chn-1(by155)*-derived *h*CHIP/*Ce*CHIP rescue animals, and *m*Kate controls 254

Supplemental Table C6 Censored animals when comparing N2 wild-type, *chn-1(by155)* mutants, *chn-1(by155)*-derived *h*CHIP and *Ce*CHIP rescue strains, and *mKate* controls 255

Supplemental Table C7 Bonferroni-adjusted *p*-values associated with longevity differences in *chn-1(tm2692)*-null mutants, *chn-1(tm2692)*-derived *h*CHIP/*Ce*CHIP rescue animals, and *m*Kate controls 263

Supplemental Table C8 Restricted mean survival times and final mortalities associated with longevity differences in *chn-1(tm2692)*-null mutants, *chn-1(tm2692)*-derived *h*CHIP/*Ce*CHIP rescue animals, and *m*Kate controls 264

Supplemental Table C9 Censored animals when comparing N2 wild-type, *chn-1(tm2692)* mutants, *chn-1(tm2692)*-derived *h*CHIP and *Ce*CHIP rescue strains, and *mKate* controls 265

Supplemental Table C10 Rescued proteins (based on fold change) identified by SWATH-MS that are either over- or under-represented in *h*CHIP rescue strain 1 processed by lysis with CHAPS/urea-based lysis buffer 273

Supplemental Table C11 Rescued proteins (based on fold change) identified by SWATH-MS that are either over- or under-represented in *h*CHIP rescue strain 2 processed by lysis with CHAPS/urea-based lysis buffer 278

Supplemental Table C12 Rescued proteins (based on fold change) identified by SWATH-MS that are either over- or under-represented in the *Ce*CHIP rescue strain processed by lysis with CHAPS/urea-based lysis buffer 284

Supplemental Table C13 Rescued proteins (based on fold change) identified by SWATH-MS that are either over- or under-represented in *h*CHIP rescue strain 1 processed by lysis with SDS-based lysis buffer 288

Supplemental Table C14 Rescued proteins (based on fold change) identified by SWATH-MS that are either over- or under-represented in *h*CHIP rescue strain 2 processed by lysis with SDS-based lysis buffer 295

Supplemental Table C15 Rescued proteins (based on fold change) identified by SWATH-MS that are either over- or under-represented in the *Ce*CHIP rescue strain processed by lysis with SDS-based lysis buffer 301

Supplemental Table C16 Genes corresponding to rescued proteins (based on fold change) identified by SWATH-MS that are either over- or under-represented in *h*CHIP rescue strain 1 processed by lysis with CHAPS/urea-based lysis buffer..... 309

Supplemental Table C17 Genes corresponding to rescued proteins (based on fold change) identified by SWATH-MS that are either over- or under-represented in *h*CHIP rescue strain 2 processed by lysis with CHAPS/urea-based lysis buffer..... 314

Supplemental Table C18 Genes corresponding to rescued proteins (based on fold change) identified by SWATH-MS that are either over- or under-represented in the *Ce*CHIP rescue strain processed by lysis with CHAPS/urea-based lysis buffer 319

Supplemental Table C19 Genes corresponding to rescued proteins (based on fold change) identified by SWATH-MS that are either over- or under-represented in *h*CHIP rescue strain 1 processed by lysis with SDS-based lysis buffer..... 323

Supplemental Table C20 Genes corresponding to rescued proteins (based on fold change) identified by SWATH-MS that are either over- or under-represented in *h*CHIP rescue strain 2 processed by lysis with SDS-based lysis buffer..... 330

Supplemental Table C21 Genes corresponding to rescued proteins (based on fold change) identified by SWATH-MS that are either over- or under-represented in the *Ce*CHIP rescue strain processed by lysis with SDS-based lysis buffer..... 335

Chapter 1

1.1 Overview of C-Terminus of Hsp70-Interacting Protein (CHIP) and Its Effects

Carboxyl terminus of Hsp70-interacting protein (CHIP), also known as STIP1 Homology and U-Box Containing Protein 1 (STUB1), is an E3 ligase intricately linked to the regulation of protein quality control through the ubiquitin-proteasome system[1]. CHIP was first shown to enable the polyubiquitination and proteasomal degradation of improperly folded target proteins by forming a complex with Hsp70, an integral component of the chaperone network and critical to triggering cellular processes concerned with the prevention and repair of damage[2,3]. Newer data has shown that CHIP is responsible for several non-canonical E3 activities independent of its chaperone functions mediating the activity, subcellular distribution, and steady-state levels of endogenous proteins essential to health at both the cellular and systems levels. These include native proteins involved in interferon signaling resistance[4,5], insulin signaling[6,7], and neuronal cell membrane integrity[8]. CHIP deletion in animal models has been found to advance aging[9], impede cognitive ability[10], and cause widespread multisystemic neurodegeneration[11], in addition to promoting stress-induced neural cell apoptosis[12], impairing mitophagy[13], and augmenting oxidative stress[14]. The consequences of point or missense mutations have also been found to vary in a location-dependent manner. In observational studies, human subjects with mutations in the tetratricopeptide repeat (TPR) domain of CHIP developed a simpler ataxia phenotype, while those in the U-box domain exhibited neurodegeneration and diminished cognitive function[15,16]. Interestingly, the activities of CHIP have been found to depend on the cellular environment. Under normal conditions, for instance, CHIP regulates insulin signaling and longevity through the mediation of insulin receptor degradation. Conversely, under conditions of proteotoxic stress, or the stress defined by the negative consequences of misfolded proteins in the cell, the functions of CHIP instead coalesce on processes related to protein quality control, thus stabilizing the insulin receptor while simultaneously diminishing longevity[7] (Figure 1.1).

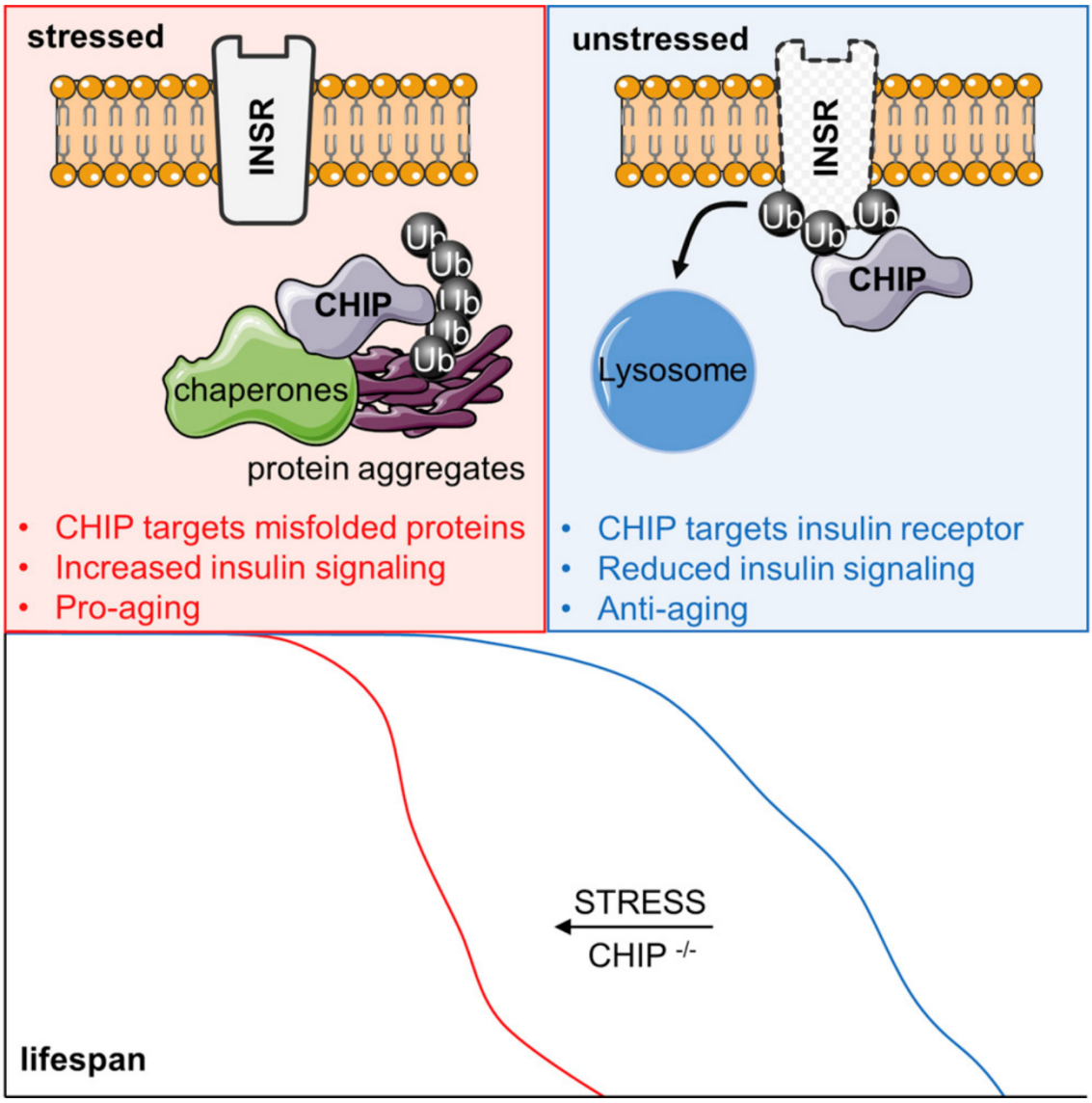

Figure 1.1 **CHIP promotes either longevity or proteostasis, depending on the cellular environment.** Aging is accompanied by a gradual decline in protein homeostasis and an increased vulnerability to neurodegeneration. The ubiquitin ligase CHIP is a key mediator of both homeostasis and insulin receptor turnover, with the insulin receptor itself in turn regulating the IIS pathway, metabolism, and aging. The insulin receptor is a direct substrate of CHIP, which encourages lifespan extension by promoting receptor monoubiquitylation and endosome/lysosome turnover, or the recycling and replacement of the cell's endosomes and lysosomes, under normal conditions. Under proteotoxic conditions, CHIP instead augments its proteostatic role at the expense of its insulin receptor degradation capacity. Thus, there exists a competitive, stress-mediated relationship between CHIP-facilitated protein homeostasis and longevity. Figure reproduced from Tawo et al. 2017, with lifespan data having been collected using *C. elegans*.

1.2 The Hallmarks of Aging

An increase in life expectancy combined with a decrease in fertility rates has led to an unprecedented demographic shift, with 771 million people being 65 years of age or older globally[17]. Despite this societal transition and its associated health impacts, the mechanisms underlying aging remain one of biology's most monumental mysteries. Even more difficult is teasing apart the molecular bases of normal aging from those of pathological significance. Given that protein quality control is central to both[18,19], proteins involved in the maintenance of normal proteostasis – that is, the comprehensive suite of processes driving the maintenance of optimal protein function via the coordinated synthesis, folding, conformational changes, and degradation of the cellular proteome – may be invaluable in defining the processes and mechanisms fundamental to each.

1.2.1 Introduction to Aging

Over the past 50 years, the global population of individuals over 65 has nearly quadrupled[20]. Despite this unprecedented demographic shift, aging remains one of the most poorly understood biological phenomena. Presenting as a gradual deterioration of physiological integrity and increased vulnerability to death, aging is underpinned by several biological processes shared across myriad organisms. Each of these cellular and molecular "hallmarks of aging" satisfies the following three conditions: (1) it is associated with the normal aging process, (2) its exacerbation will further augment the aging phenotype at any given point in time, and conversely, (3) its attenuation will diminish the aging phenotype and increase lifespan[21]. There are nine such hallmarks, further subdivided into three categories: (1) primary hallmarks, or processes eliciting damage that propagates over time (genomic instability, telomere attrition, epigenetic alterations, and loss of proteostasis), (2) antagonistic hallmarks, or processes exerting either beneficial or harmful effects in an intensity-dependent manner (deregulated nutrient sensing, mitochondrial dysfunction, and cellular senescence), and (3) integrative hallmarks, or processes resulting from cumulative damage caused by the primary and antagonistic hallmarks that cannot be compensated for by homeostatic regulation (stem cell exhaustion and altered intercellular communication) (Figure 1.2).

As these facets are intimately interconnected, unravelling the interacting and causal mechanisms will provide groundbreaking insights into our understanding of both healthy and pathological aging (Figure 1.2).

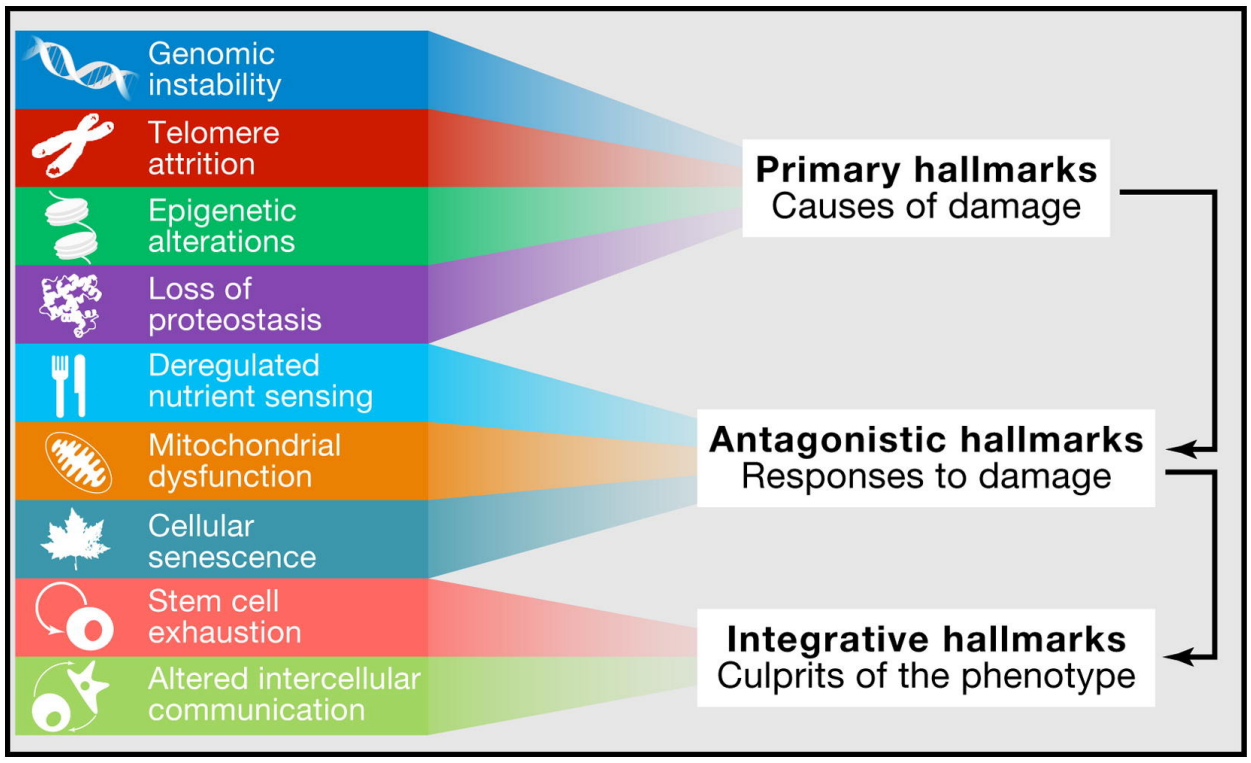

Figure 1.2 **The hallmarks of aging.** Illustration of the nine hallmarks of aging, grouped into three categories. Primary hallmarks are the primary cause of cellular damage, while antagonistic hallmarks exert either beneficial or deleterious effects in an intensity-dependent manner. Integrative hallmarks are a result of the cumulative damage caused by primary and antagonistic hallmarks that cannot be compensated for by homeostatic regulation. Figure reproduced from López-Otín et al. (2013).

1.2.2 Genomic Instability

Living things accumulate damage over time from both extrinsic (e.g., diet) and intrinsic (e.g., DNA replication errors) insults to the homeostatic milieu, leading to an age-associated increase in disease vulnerability coupled with a general decline in organ function. For instance, DNA is constantly exposed to endogenous and exogenous mutagens, such as radiation or free radicals[22]. While cellular DNA repair systems can fix much of this mutagen-induced damage[23], some will evade repair. This can result in genomic alterations ranging from point mutations to chromosomal rearrangements, with consequences ranging from silent mutations to the aberrant expression of oncogenes, tumour suppressor genes, and DNA repair genes. Such DNA mutations and damage, whether caused by extrinsic or intrinsic factors, accumulate over time[24]. As such, older cells have a higher incidence of genetic instability, implicated directly in age-related disorders such as various cancers[25] and neurodegenerative disorders.

1.2.3 Telomere Attrition

Most age-related DNA damage is location-independent, with damage sites randomly located throughout the genome. Some chromosomal regions, however, are more vulnerable to age-associated degradation. Telomeres, the repeat nucleotide sequences at the ends of eukaryotic chromosomes, are one such region[26]. Responsible for protecting the ends of chromosomes and thus preserving genomic integrity, these sequences act as a biological clock on the basis of their length[27]. With the exception of telomerase, most replicative DNA polymerases are unable to fully replicate the terminal ends of linear DNA[28]. The result is a progressive decrease in DNA strand length with increasing rounds of cell division, culminating in the replicative senescence of cells to avoid this deterioration extending to the coding sequences of the DNA (i.e., the Hayflick limit)[29]. However, as telomerase activity is absent in most normal somatic cells – expressed more readily in cancerous tissues, suggesting that telomerase activation is a necessary step in human oncogenesis[30,31] – aging is necessarily associated with the gradual and cumulative deterioration of telomeres[32], further promoting genomic instability by triggering a sustained DNA damage response[33]. Furthermore, telomeres are bound by shelterin, a six-subunit protein complex functioning to protect

chromosome ends from aberrant DNA repair activities[34,35]. As a result of these restrictions in DNA repair, DNA damage at telomeres is especially persistent and likely to induce senescence or apoptosis[36,37].

1.2.4 Epigenetic Alterations

The heritable and reversible modulation of gene expression in the absence of changes to the DNA sequence have also been associated with aging and cellular senescence. Such epigenetic alterations have been linked to deleterious consequences known to either cause or accelerate the aging process and therefore have been studied extensively in the context of cancer and age-related pathologies[38-40]. For instance, genome-wide association studies have revealed an aging-dependent stochastic DNA methylation drift, suggesting impaired maintenance of epigenetic events[41,42]. The consequences of such an epigenetic drift include epigenetic mosaicism in stem cells as well as stem cell exhaustion and proliferative defects. The hypomethylation of some transposable elements (TEs), for example, can lead to an increased risk of cancer and aging-related organ deterioration[40], while many genes whose promoter hypermethylation is associated with increased cancer risk display a direct positive correlation between promoter hypermethylation and age[41].

Mechanisms underlying epigenetic regulation include DNA methylation, chromatin remodelling, post-translational histone modifications, and non-coding RNA-mediated regulation. Genome-wide methylation studies have revealed DNA methylation patterns to be correlated with age in both human and animal studies[43-46]. In this process of epigenetic gene regulation, an increased density of methyl groups physically blocks DNA sites from the transcription machinery. In mammals, this occurs mainly at CpG islands, most often located in the promoter regions of the human genome[47]. Methylation status has been associated with increased mortality independent of other risk factors, including diabetes, hypertension, and smoking. However, some such risk factors have conversely been shown to predict increased methylation. Obesity, for instance, has been causally linked to both increased methylation and accelerated aging of liver tissues[48]. Thus, DNA methylation can accelerate aging both in tandem with and independently of other factors known to affect mortality.

Histone modifications are reversible, post-translational covalent additions to the N- and C-terminals of histone tails or, in some cases, the globular domain[49]. Most commonly, these modifications occur on N-terminal histone tails protruding from the nucleosome core, especially at serine and lysine residues. Histone modifications differentially change the binding affinity between DNA and histones, thus either loosening or tightening the histone-DNA complex and thereby facilitating or preventing access of gene regulatory proteins, respectively. Altered levels of specific histone-modifiers, such as histone deacetylases or methyltransferases, can destabilize chromatin structure and histone-associated epigenetic regulation, leading to a pattern of genetic instability that contributes to an accelerated aging phenotype[50].

Non-coding RNAs, including microRNAs (miRNAs), also play a central role in sculpting patterns of gene expression. miRNAs are short, single-stranded RNA segments of about 22 nucleotides involved in myriad biological functions, including cell proliferation, differentiation, and apoptosis[51] via the regulation of other genes[52]. Aspects of histone modification also appear to be reciprocally influenced by miRNAs, particularly the expression of histone methyltransferases. miRNAs are directly implicated in regulating multiple senescence-related genes and processes[53], and indirectly involved in the regulation of both insulin/insulin-like growth factor (IGF) 1 and target of rapamycin (TOR) signalling pathways[21,54,55]. The crucial role of miRNAs in aging is further supported by the finding that patients with Alzheimer's disease had both significantly altered miRNA population and expression levels in their brain tissues, serum, and cerebrospinal fluid[56].

1.2.5 Loss of Proteostasis

The accumulation and aggregation of toxic misfolded protein species is one of the primary causes of age-related physiological degeneration. The protein homeostasis network functions to ensure the appropriate production and maintenance/turnover of proteins in their native state while simultaneously minimizing harmful or unproductive protein modifications, such as those generating un-/misfolded proteins and protein aggregates[57]. This system of protein quality control functions through chaperone-mediated protein folding, the ubiquitin-proteasomal-mediated degradation of client proteins, and the autophagosomal-lysosomal machinery[21]. Altogether, these processes

are made possible through the carefully orchestrated interplay of nearly 2 000 proteins in human cells, including approximately ~300 molecular chaperones (Figure 1.3A)[58]. Proteins experience several conformational changes prior to reaching their thermodynamically favoured native state, gradually reducing structural frustration in the process[59-61]. Misfolded proteins may accumulate during this time as kinetically constrained species, unable to form functional proteins in the presence of this free-energy barrier[62]. Intermolecular contact between these entities may facilitate the progression of off-pathway aggregation mechanisms, resulting in the formation of aggregate species such as amorphous aggregates, oligomers, and amyloid fibrils[63]. Molecular chaperones also facilitate on-pathway folding of proteins into their native conformations and impede off-pathway reactions leading to the formation of misfolded proteins and protein aggregates (Figure 1.3B)[64].

The failure of the proteostasis network architecture to work as a coordinated whole results in harmful protein aggregation and proteotoxic effects. The consequences of aberrant protein degradation involve, for instance, cellular proteotoxicity, or the culmination of adverse effects resulting from misfolded proteins present in the cell[65]. These misfolded proteins will either be removed immediately by the ubiquitin-proteasome system or aggregate, ultimately forming sequentially soluble oligomers and insoluble aggregates[66]. These are highly toxic to the cell, with effects ranging from 26S proteasome impairment to cell death[67-74]. As a result, proteotoxicity represents a greater threat to tissues with a decreased ability to regenerate their primary cells, such as heart and brain tissues, or to cells required to remain alive and functional for extended periods of time[75]. Although the consequences of proteostasis dysfunction are central pathological features common to numerous neurodegenerative diseases, including Alzheimer's and Parkinson's diseases, the persistent presence of insoluble protein inclusions and aggregates is also a hallmark of some non-neurodegenerative conditions, such as cataracts[76,77]. In general, aging is associated with the progressive decline in proteostasis network capacity and proteome integrity, and protein aggregates/inclusions can in turn be found nearly ubiquitously across aged tissues[18].

Molecular chaperones are a broad class of well-conserved proteins responsible for maintaining the conformational homeostasis of other cellular proteins and RNAs[78].

Central to these processes is the heat-shock family (HSF) of proteins, belonging to a larger network of damage-associated molecular proteins (DAMPs)[79]. This highly conserved group of ubiquitous proteins is known to be transcriptionally upregulated in response to cellular stress[80]. In mammals, heat-shock factor 1 (HSF1) is considered a principal regulator of the heat-shock response[81], a stress-induced protective mechanism characterized by the increased transcription of chaperones to promote the appropriate folding/refolding of misfolded proteins[77]. Deacetylation of HSF1 by sirtuin 1 (SIRT1) prolongs HSF1 binding to heat shock protein 70 (Hsp70), thereby activating Hsp70 transcription[82], with implications for diseases ranging from neurodegeneration to cancer, among others[83,84].

The ubiquitin-proteasomal-mediated degradation of client proteins as well as the autophagy-lysosome system are two of the main protein quality control mechanisms in eukaryotic cells. Proteasome activation has been associated with increased lifespan in an evolutionarily conserved manner[85]. As an example, the assessment of fibroblast cultures taken from healthy centenarian donors revealed a sustained expression of functional proteasome activity, which may promote healthy aging by facilitating the removal of abnormal and oxidatively damaged proteins[86].

The upregulation of autophagy, a highly conserved homeostatic membrane-trafficking pathway mediating the lysosomal degradation of cytosolic constituents[87,88], extends lifespan in nematodes, flies, and mice. Conversely, this lifespan extension is reversed by the experimental obstruction of the autophagy process[88]. Indeed, the mechanistic underpinnings causally linking caloric restriction to extended lifespan involve or are mediated by the autophagy pathway. For instance, caloric restriction stimulates the SIRT1 deacetylase and the adenosine-5'-monophosphate-dependent protein kinase (AMPK) pathways while dampening the rapamycin/S6K pathway, all of which in turn promote autophagy[88-90]. Meanwhile, the TOR inhibitor rapamycin, also having been found to improve neurodegenerative disease outcomes in animal models[91], as well as the acetyltransferase inhibitor spermidine have been shown to extend lifespan across several model organisms[92-95]. Resveratrol, an activator of SIRT1 and several other deacetylases, has been shown to extend lifespan in animals receiving a high-calorie diet[96]. Autophagy activity tends to decline with age, and upregulation of this pathway is

associated with increased lifespan due to the removal of damaged cellular cargo, which might otherwise accumulate and favour neurodegenerative events[97]. Aberrant genetic events within the autophagy cascade have been linked to myriad adverse health outcomes including breast[98] and colorectal[99] cancers as well as aging-associated diseases such as neurodegenerative diseases[100], senile osteoporosis[101], and osteoarthritis[102].

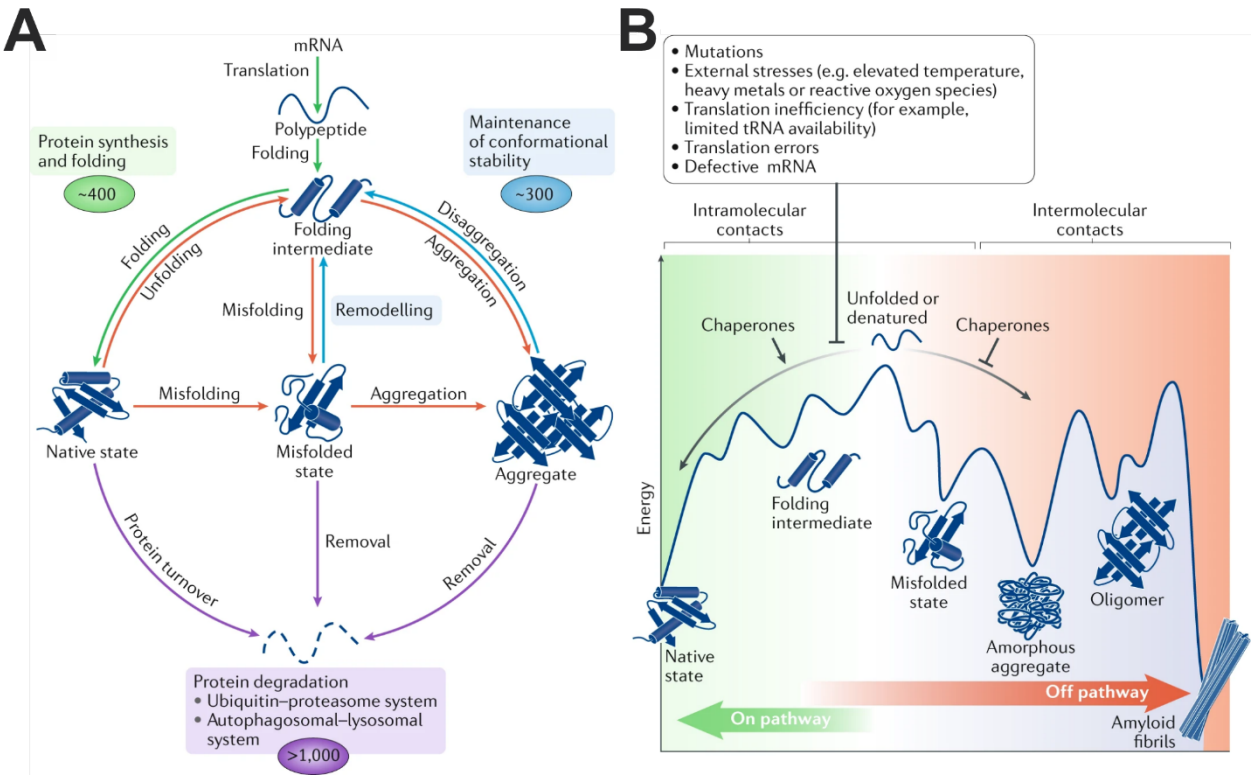

Figure 1.3 **The proteostasis network, protein folding intermediates, and the native state.** (***A***) The proteostasis network. The proteostasis network ensures the appropriate production and maintenance/turnover of proteins in their native state while impeding harmful or unproductive protein modifications, such as those resulting in unfolded proteins or protein aggregates (red). In human cells, the proteostasis network consists of nearly 2 000 proteins, including ~300 molecular chaperones and their regulators, and characteristically includes three major functional components: (1) protein synthesis and folding (green), (2) conformational maintenance (blue), and (3) degradation (purple). (***B***) Protein folding intermediates and the native state. Proteins experience several conformational changes on their way to a thermodynamically favoured state. During this process, misfolded proteins may accumulate as kinetically constrained species unable to form functional proteins as the result of a free-energy barrier. Intermolecular contact between these entities may facilitate the progression of off-pathway aggregation mechanisms, resulting in the formation of aggregate species such as amorphous aggregates, oligomers, and amyloid fibrils. Conversely, molecular chaperones facilitate on-pathway folding of proteins into their native conformations and impede off-pathway

reactions leading to the formation of misfolded proteins and protein aggregates. Several other factors may favour off-pathway reactions leading to protein misfolding and aggregation, such as mutations, external stressors, translation inefficiency/errors, and defects in mRNA. Figure reproduced from Hipp et al. 2019.

1.2.6 Deregulated Nutrient Sensing

Living systems maintain a steady state of glucose homeostasis throughout life. Glucose allows for the production of adenosine triphosphate (ATP) from external nutrients via cellular respiration and as such is ultimately the central energy source of living cells. The mitochondria, as the central hub of energy production, play a crucial role in these processes, with any damage to mitochondrial DNA, biogenesis, dynamics, or general integrity substantially increasing susceptibility to adverse health outcomes in later life[103]. Homeostatic systems respond to both endogenous (e.g., hormones) and exogenous (e.g., nutrients) influences, to maintain glucose levels within a narrow, physiologically acceptable range. However, aging dysregulates the pathways and processes regulating the steady state levels of these molecules, thus in turn disrupting signaling cascades regulating healthy metabolism. These age-associated disruptions in metabolic homeostasis can impact hormone signaling, contributing to reduced insulin sensitivity whereby cells experience decreased glucose tolerance and counterregulation along with an inability to efficiently absorb and utilize nutrients[104]. Altogether, the consequences of these metabolic disruptions converge to have devastating effects on cellular homeostasis more generally. Indeed, the physiological consequences of age-related metabolic dysfunction include an increased susceptibility to “ragged-red” fibres in skeletal muscle, increased visceral fat accumulation, and a decrease in lean muscle mass[105]. These are linked in turn to a number of age-related diseases, including cardiovascular diseases, muscular atrophy, metabolic diseases, various cancers, and neurodegeneration.

Inversely, aberrations in insulin signaling and its downstream effectors may compromise metabolic integrity. Insulin-like growth factor-1 (IGF-1), the principal mediator of pituitary growth hormone, plays a central role in mediating longevity, with both growth hormone and IGF-1 steady state levels declining with age. Indeed, disruptions in the evolutionarily conserved, nutrient-sensing insulin and insulin-like growth factor signaling (IIS) pathway have been associated with drastic increases in

longevity across model systems[54,55,106]. This pathway is a highly conserved signalling network linking nutrient availability to key physiological functions, and mainly regulated by insulin-like peptides mediating the activity of their respective receptors[107]. Interestingly, many IIS pathway genes and targets impacting longevity are also implicated in cancer. These shared underlying mechanisms implicate cancer and aging as two coupled developmental processes spanning the same spectrum, from uncontrolled cell death to excessive cell proliferation[108].

Caloric restriction is the most robust and reproducible anti-aging intervention known to extend lifespan and delay the appearance and progression of age-related pathologies[109-111]. The processes underlying these anti-aging effects include improved mitochondrial function as well as an increased activation of the autophagy pathway. This results in a lower susceptibility to cardiovascular diseases, harmful mutagenesis, oxidative and inflammatory damage, and cancer, as well as increased antibacterial activity[112]. In addition to directing the degradation of long-lived proteins and organelles, the autophagy-lysosomal machinery plays a critical role in balancing energy intake and expenditure under starvation conditions[113]. Autophagy is closely intertwined with apoptosis and necroptosis in directing cell fate, with the latter two predominantly regulating cell death, and the extrinsic apoptotic pathway sharing an upstream signaling cascade with necroptosis[114]. Nevertheless, it remains functionally distinct from its sister pathways as it modulates the balance between cell death and survival[113]. Indeed, in many cases autophagy promotes cell survival, particularly in response to stressors such as starvation and energy depletion[115]. However, under conditions of increased activity, the autophagy pathway transforms into a death-inducing mechanism.

Autophagy and the mitochondrial machinery are intimately connected in the maintenance of energy homeostasis. For instance, mitophagy, the selective degradation of the mitochondria occurring via autophagy, is a first response to mitochondrial damage and crucial to cellular health. Another example is the mitochondrial unfolded-protein response, in which autophagy is triggered[116] by the mitochondrial accumulation of misfolded proteins and subsequent involvement of the protein-folding machinery[116,117].

The metabolic flexibility theory of aging posits that longevity and metabolic health are inextricably linked, and that lifespan extension is achieved by maintaining the ability to switch between substrates for energy metabolism. A heightened energy expenditure across the whole organism has been found to predict increased lifespan[118]. Energy expenditure tends to decrease in an age-associated manner, with older animals also showing decreased activity, endurance, oxygen consumption, and lipid stores in non-adipose tissues. In young animals, the ratio between the volume of oxygen consumption and carbon dioxide production, otherwise known as the respiratory exchange ratio, displays a predictable circadian pattern reflecting a shift from carbohydrate to lipid metabolism. A respiratory exchange ratio of ≥1 indicates that carbohydrates are the main substrate used to provide energy, a ratio of 0.7 indicates that fatty acids are the main fuel source, and a ratio near 0.85 indicates that both carbohydrates and fatty acids are used for energy production. Older animals, however, favour lipid oxidation at the expense of substrate switching, thus exhibiting a lower respiratory exchange ratio as well as an associated increased risk of fat metabolism and storage-associated physiological damage. This metabolic inflexibility is associated with dysregulations in glucose homeostasis as well as an increased risk of age-associated diseases linked to aberrant mitochondrial energy metabolism[119].

As modulators of metabolic activity, nutrient sensing and signaling pathways play a crucial role in longevity. The mechanistic TOR (mTOR) kinase is a central component of one such process, with the chronic inhibition of mTOR pathway constituents acting to promote longevity, although it is unclear whether this pathway inhibition delays aging or simply the onset of age-associated diseases[120-123]. The mTOR pathway induces protein biosynthesis[124] and inhibits autophagy[125] via the phosphorylation of key transcriptional regulators and promotes lipid accumulation by stimulating lipogenesis while suppressing lipid turnover[126,127]. mTOR signaling relies heavily on nucleocytoplasmic compartmentalization, which degrades gradually with increasing age[128]. Indeed, the suppression or deficiency of upstream mTOR pathway regulators at the lysosomal membrane provokes an aging-like phenotype across multiple model systems. The mTOR pathway components at the lysosomal membrane distinctly modulate autophagy through a distinct group of evolutionarily conserved transcription factors, including

forkhead box protein O (FOXO) transcription factors and transcription factor EB (TFEB), both of which are implicated in longevity[128]. The mTOR pathway also regulates cell growth in response to growth factors as well as other upstream regulators[129] and is itself upregulated in cancer[130-132], further highlighting cancer and aging as two distinct manifestations of a shared underlying process.

Energy and nutrient availability are inversely correlated with lifespan extension, with an excess of either leading to increased age-associated disease susceptibility. AMPK serves as a nexus in the regulation of energy homeostasis, nutrient sensing, and stress resistance, these interconnected molecular processes ultimately converging to promote cellular health. AMPK mediates longevity and has been found to enhance cell survival in times of energetic stress through its interaction with mTOR complex 2 (mTORC2)[133]. An inadequate supply of calories or nutrients leads to ATP depletion, increased AMP, and increased AMPK activity, which in turn suppresses mTOR signaling[134]. Under these conditions, AMPK phosphorylates targets stimulating a metabolic shift toward catabolic, ATP-generating pathways, such as autophagy and mitochondrial biogenesis, in lieu of anabolic, ATP-depleting pathways, such as cell growth/proliferation and protein biosynthesis, in an activation-dependent manner[133,135]. High levels of AMP are also associated with an increased accumulation of nicotinamide adenine dinucleotide (NAD), a ubiquitous nucleotide that activates sirtuins[136,137], which in turn regulate insulin signaling and longevity[138].

1.2.7 Mitochondrial Dysfunction

The mitochondrial production of reactive oxygen species (ROS) increases with age, rendering mitochondrial DNA (mtDNA) particularly vulnerable to oxidative damage in later life[139]. If the reducing environment of the cell is not sufficient to prevent oxidative stress, ROS can damage a variety of macromolecules including proteins, lipids, and nucleic acids. However, in some cases, mild mitochondrial damage may have beneficial cellular effects. Mitohormesis, an adaptive cellular response instigated by slight mitochondrial damage, triggers protective mechanisms promoting molecular changes that both compensate for the primary defect and increase lifespan[140,141]. One theory posits that low levels of ROS activate signaling cascades involving AMP and NAD, thus triggering stress response pathways functioning to extend lifespan[142] and increase

overall cellular health[143-146]. The activation of other protective mechanisms in response to mild mitochondrial stressors, such as antioxidant defence[145] and mitochondrial biomass production[147], may also promote longevity.

In animal models, mitochondrial electron transport mutants are particularly valuable in evaluating the effects of mitochondrial oxidative stress on aging. Experiments in nematodes (*Caenorhabditis elegans*) have shown that decreased respiratory activity prolongs lifespan, with distinct mitochondrial mutations instigating an intersecting suite of longevity-promoting processes[148]. Mammalian studies have found a similar relationship between mild mitochondrial damage and extended lifespan[141]. Interestingly, while some of these same mutations in human cohorts have been found to exert catastrophic effects on health outcomes, this apparent paradox was explained by the discovery of a threshold tolerance for respiratory chain damage or dysfunction and the associated increased production of ROS when this damage cannot be attenuated or compensated for by intra- or intermitochondrial complementation[149-151].

Mitochondrial aberrations may also affect the metabolic landscape in a timing-dependent manner. A number of age-associated diseases are linked to mitochondrial dysregulation, including cardiomyopathy[152] and several cancers[153], the latter exploiting defects in mitochondrial function to bypass metabolic checks otherwise preventing uncontrolled cell growth[22].

1.2.8 Cellular Senescence

Cellular senescence, the irreversible arrest of normal cell cycle division, acts as a protective mechanism against uncontrolled cell proliferation[154,155], although more recent evidence has suggested that cellular senescence can paradoxically both stimulate tumorigenesis and promote unhealthy aging via the maintenance of a low-grade inflammatory response[156-158]. Pathways implicated in the induction of cellular senescence include the DNA damage response pathway (triggered by oxidative stress amongst others), DNA damage, telomere shortening, and oncogene activation and/or tumour suppressor gene inactivation[154,158]. For instance, a genome-wide association study found the INK4a/ARF locus to be associated with the greatest number of age-related adverse health outcomes[159], and both $p16^{INK4a}$ tumour suppressor gene expression[160] and protein levels[21,161-163] in both human and mouse tissues correlate

positively with an aged phenotype. Conversely, the removal of $p16^{INK4a}$-expressing senescent cells delays the emergence and development of age-associated diseases in animal models[164]. The signaling cascades stimulating senescence are associated with a characteristic phenotype including a flat and enlarged morphology, increased nonspecific acidic galactosidase activity and chromatin condensation, and changes in the secretome and epigenome[21,158,165-172].

In healthy tissues, the presence of senescent cells is transient and modulated by immunosurveillance and phagocytosis[173-175]. However, senescent cells tend to accumulate in aged tissues, suggesting that either their production is increased, their mechanisms of clearance are compromised, or both. Indeed, the age-associated accumulation of damage to DNA and other cellular components may contribute to the former, while impaired immune clearance due to immunosenescence may contribute to the latter[176]. Senescent cells secrete an assemblage of proinflammatory factors, including cytokines, interleukins, matrixins, and growth factors, altogether known as the senescence-associated secretory phenotype[177,178]. The age-related accumulation of senescent cells and this associated secretory phenotype is one of the underlying mechanisms promoting pathological aging, with an accumulation of senescent cells found in patients with chronic age-associated pathologies[158,179].

1.2.9 Stem Cell Exhaustion

Stem cell exhaustion and altered cellular communication, as integrative hallmarks, are manifestations of the cumulative damage and physiological dysfunction caused by the primary and antagonistic hallmarks of aging. The age-dependent decrease in the regenerative capacity and overall function of cells and tissues is intimately tied to stem cell integrity, with specific age-associated pathologies mirroring the type and manner of stem cell dysfunction. For instance, anemia, osteoporosis, impaired intestinal function, and sarcopenia can be caused by haematopoietic, mesenchymal, intestinal epithelial, and muscle stem cell decline, respectively[21]. However, both deficient and excessive proliferation of stem cells are detrimental to organismal health, with excessive cell proliferation acting to deplete the stem cell niche. This has been shown in both *Drosophila* intestinal stem cells, in which excessive stem cell proliferation led to stem cell niche exhaustion as well as a pro-aging phenotype[180]. Indeed, the compensatory

induction of *INK4a* as well as the decrease in serum levels of IGF-1 during aging represent a physiological stress response acting to maintain stem cell quiescence[21,181].

1.2.10 Impaired Cellular Communication

Impaired intra- and intercellular signaling, including inflammatory, neuronal, endocrine, and neuroendocrine communication, also characterize both healthy and pathological aging. In addition to aberrant insulin secretion, aging is also associated with perturbed insulin growth factor signaling activity, these dysfunctional intercellular signaling cascades contributing to the mechanisms driving the age-associated deterioration of insulin signaling and its downstream pathophysiological effects. Inflammatory processes tend to increase with age, while immunosurveillance against both internal atypical/premalignant factors and external pathogens tends to decrease, thus leaving the cellular environment vulnerable to infection and the growth of cancerous cells. For instance, immunosenescence, the gradual deterioration of immune function, as well as increased cytokine secretion by adipose tissues are both associated with aging and contribute to other age-related disorders – including diabetes, arthritis, and metabolic as well as cardiovascular diseases – through their causative association with a prolonged inflammatory response[182,183].

1.3 Introduction to Ubiquitination and the Ubiquitin-Proteasome System

Protein degradation and homeostasis play a foundational role in both driving cellular health and disease, affecting a broad range of processes ranging from protein recycling, DNA repair, cell cycle regulation, apoptosis, and signal transduction to cellular homeostasis more generally[184]. The ubiquitin-proteasome system (UPS) represents the primary network driving protein degradation and homeostasis in the cell, with aberrations in ubiquitin-related processes having been associated with cancer, neurodegeneration, and metabolic pathologies, highlighting its broad effects on cellular and organismal physiology (Figure 1.4)[184]. Ubiquitin itself, initially discovered by Gideon Goldstein in 1975[185] and further characterized in the decades thereafter[186-188], is a small 8.6 kDa protein found ubiquitously across eukaryotic tissues and coded for in the

human genome by the genes Ubiquitin B, Ubiquitin C, Ubiquitin A-52 residue, and Ribosomal Protein S27A[184]. Ubiquitin E3 ligases are responsible for recognizing target proteins to be degraded, while the 26s proteasome catalyzes protein degradation itself[189]. Interestingly, in addition to degrading damaged, misfolded, and short-lived proteins[190], the UPS also facilitates synaptic remodeling – that is, the activity-dependent strengthening, weakening, or elimination of synapses – via the regulation of scaffolding proteins, receptors, and other signaling molecules integral for both synaptic stability and plasticity[189,191].

The ubiquitin-mediated proteolysis pathway first involves ubiquitin binding to a lysine residue on the target protein[189]. The ATP-dependent activation of ubiquitin's C-terminal carboxyl group catalyzes the formation of an isopeptide bond between a ubiquitin molecule and the target substrate. A second ubiquitin molecule then binds to a lysine residue of the first, and this process is repeated until a polyubiquitin chain of at least four ubiquitin moieties is formed. This polymeric ubiquitin chain functions as a degradation signal necessary for the efficient translocation of the protein substrate to the proteasome[192]. There are three enzymes – the E1 ubiquitin-activating enzymes, E2 ubiquitin-conjugating enzymes, and E3 ubiquitin ligases – involved in this process, with a fourth ubiquitination enzyme, the ubiquitin chain elongation factor E4, sometimes also required to extend a polyubiquitin chain[193]. E1 ubiquitin-activating enzymes bind ubiquitin in an ATP-dependent manner, transferring it to an E2 ubiquitin-conjugating enzyme. E3 ubiquitin ligases then mediate binding to the target protein[194] which is subsequently trafficked to the 26S proteasome. The polyubiquitin chains bind the regulatory caps, and the target proteins then proceed to the catalytic core where they are degraded (Figure 1.4)[195]. Recent evidence suggests that small ubiquitin-like modification (SUMOylation) of proteins may also play a role in the mediation of ubiquitination and protein degradation of at least some target proteins[196,197]. For instance, promyelocytic leukaemia (PML) protein, a tumor suppressor implicated in cell cycle regulation, survival and apoptosis, that is not SUMOylated is not degraded, suggesting that PML SUMOylation is required for ubiquitin ligase-mediated proteasomal degradation[198,199].

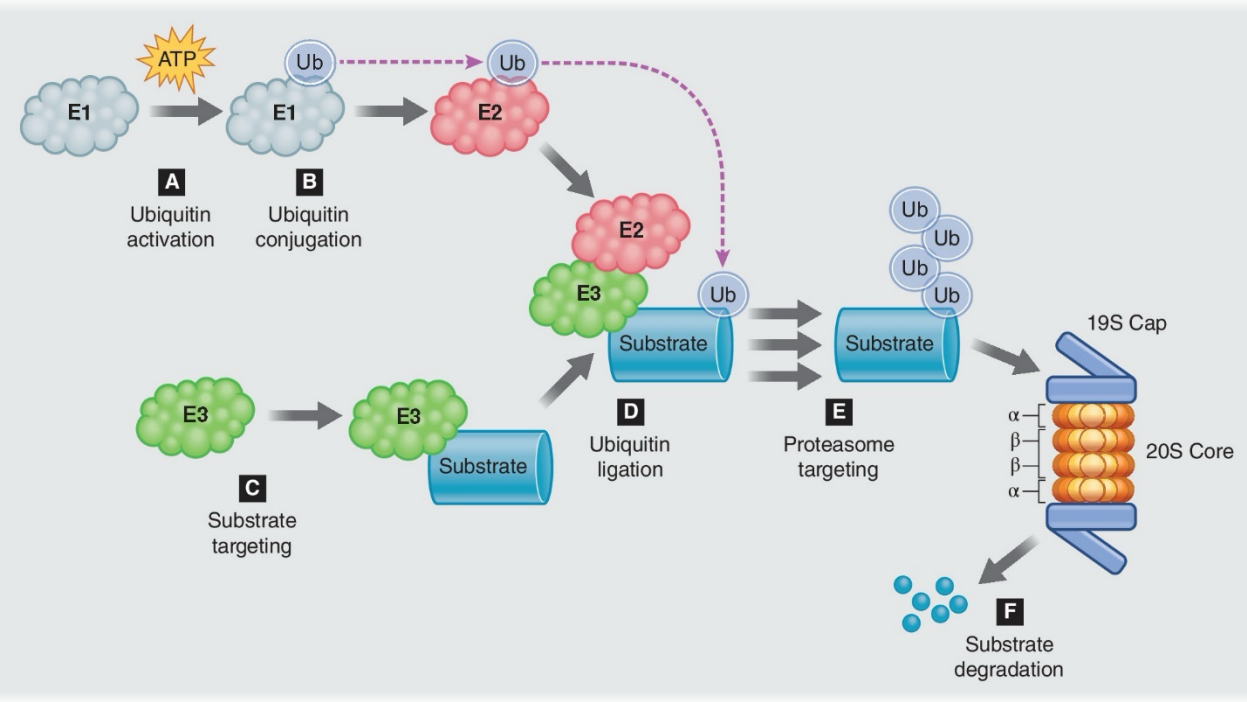

Figure 1.4 **Protein degradation, ubiquitin, and the ubiquitin-proteasome system.** (***A***) Ubiquitin is activated, bound to an E1 ubiquitin-activating enzyme, (***B***) and subsequently conjugated to an E2 ubiquitin-conjugating enzyme. (***C***) The protein substrate to be degraded is then targeted by an E3 ubiquitin ligase and (***D***) ubiquitin is ligated to the substrate. (***E***) Ubiquitin ligation repeats until a polyubiquitin chain is formed, and the substrate is translocated to the proteasome. (***F***) The substrate protein is then recognised by the proteasome 19S cap and shuttled into the 20S core for degradation. Figure reproduced from Schneider et al. 2020.

1.4 Introduction to Autophagy

Autophagy is a highly conserved, self-degradative, homeostatic pathway whereby cellular constituents are enveloped in autophagosomes – double-membrane bound vesicles – and subsequently shuttled to lysosomes for degradation[200]. In mammals, while the proteasome also drives intracellular degradation, autophagy exclusively refers to the lysosome-dependent clearance of cytoplasmic constituents[201]. Autophagy was initially seen as a nonspecific, adaptive, stress-dependent cellular recycling process in response to nutrient deprivation. More recently, however, it has been shown to use selective autophagic receptors and feedback mechanisms to promote homeostasis in non-starved cells[202]. Moreover, autophagy has also been found to mediate the degradation of damaged organelles, including mitochondria (a process known as mitophagy)[203].

Autophagy can be deconstructed into three steps: initiation, elongation, and lysosomal fusion and degradation. To mediate initiation, Unc-1 like autophagy activating kinase 1 (ULK1) is phosphorylated in an opposite manner by the mammalian target of rapamycin complex 1 (mTORC1) and AMPK[125,204,205]. Specifically, in non-starved cells, mTORC1 prevents autophagy initiation via its inhibitory phosphorylation of ULK1's serine 757[125,206,207]. Conversely, in starved cells, autophagy initiation takes place upon phosphorylation of ULK1's serine 317 and serine 377 by AMPK after binding-dependent activation by AMP[208]. Stress-related cellular signaling cascades also trigger the inactivation of mTORC1, and the associated decreased inhibitory phosphorylation by mTORC1 enables ULK1 autophosphorylation. ULK1 is sequestered in complex with autophagy-related proteins ATG101 and ATG13, as well as a FAK family kinase-interacting protein of 200 kDa, and the autophosphorylation of ULK1 in turn allows for the phosphorylation of ATG13 and FAK family kinase-interacting protein of 200 kDa. Finally, nucleation, or creation, of a phagophore (a specialized double-membrane compartment acting as a precursor to an autophagosome) occurs upon the ULK1-mediated activation of the vacuolar protein sorting 34 (VPS34) complex. The VPS34 complex functions as a class III phosphatidylinositol 3-kinase, producing phosphatidylinositol 3-phosphate and thus allowing for the recruitment of phosphatidylinositol 3-phosphate binding proteins and resulting phagophore nucleation[209,210]. Although the primary membrane donor for phagophore formation was previously thought to be the endoplasmic reticulum, it has since been shown that mitochondria, endosomes, and plasma membrane, and the Golgi apparatus may also serve as membrane donors[211,212].

Phagophore elongation is mediated by a number of ubiquitin-like conjugation systems. First, the E1 enzyme ATG7 and E2 enzyme ATG10 allow for the conjugation of ATG12 to ATG5. ATG12-ATG5 then binds ATG16L1, and the resulting complex affixes itself to the phagosome membrane, enabling the subsequent recruitment of the microtubule-associated protein 1A/1B-light chain 3 (LC3)[213]. LC3-II is formed by LC3-I, ATG3, ATG7, and the ATG12-ATG5-ATG16L1 complex once LC3-I is generated by the cleavage of LC3 by ATG4[214]. The fully processed LC3-II then joins the phagosomal

membrane and drives the formation of a mature autophagosome through the extension and closure of the phagophore.

The newly-formed mature autophagosome then fuses with a lysosome, either directly or after first fusing with an endosome. After fusion, the lysosome facilitates the acidification of the autolysosomal compartment through the use of a vacuolar adenosine triphosphatase and activates lysosomal hydrolases capable of autophagic substrate digestion. Any metabolites resulting from the degraded cargo are then available for reuse and redistribution in the cell[215].

Aberrations in autophagy have been suggested to play a pathogenic role in several diseases. For instance, an abnormally high accumulation of autophagosomes has been found in the frontoparietal cortices of Alzheimer's disease patients[216]. Autophagy also plays a crucial role in tau clearance, with aberrant autophagy-lysosomal system functioning promoting the formation of tau oligomers and accumulation of insoluble tau species[217].

1.5 The Structure and Functions of CHIP

1.5.1 Introduction to CHIP

CHIP, a neuroprotective E3 ubiquitin ligase, has been found to support healthy aging in the brain. In human cohorts, CHIP mutations have been causally implicated in cognitive impairment and dementia, while in animal models, knock-outs of the corresponding gene have exhibited accelerated aging and cognitive decline[218-220]. First studied as a member of the protein quality control network, CHIP cooperates with molecular chaperones to ubiquitinate abnormal proteins, thus signalling their degradation and preventing the accumulation of toxic protein intermediates associated with neuronal cell death and dementia[221-224]. More recently, however, CHIP has also been found to have several non-canonical functions which are either independent of chaperone partners, can be negatively regulated by CHIP's association with heat shock proteins, or in which the association between CHIP and Hsp70 in turn regulates processes *other than* the degradation of toxic protein intermediates via the proteasome[225]. Of particular interest is the finding that CHIP acts as an E3 ligase to regulate a small cohort of natively folded proteins in a chaperone-independent manner, thereby contributing to cellular processes

central to organismal health such as insulin signaling[7], membrane homeostasis[226], and interferon signaling[4,227]. Thus, CHIP plays a central role in both abrogating the proliferation of toxic protein intermediates as well as safeguarding cellular processes central to healthy aging.

In order to utilize CHIP as a potential therapeutic target for the treatment and prevention of age-related brain diseases, it is necessary to understand its physiological role in neuroprotective pathways, as well as how its functions are affected by toxic cellular conditions (e.g., the presence of protein aggregates). Animal studies have correlated a CHIP null phenotype with several adverse health outcomes, including neurodegeneration[228], accelerated aging, cognitive impairment, increased cell death, the dysregulation of specific proteins (such as the insulin receptor), and mitochondrial dysfunction[7,219,229]. Conversely, the presence of CHIP confers protection against oxidative stress and the initial development/proliferation of toxic protein aggregates[9,230]. However, when linked to adverse health outcomes in humans, the CHIP gene is not deleted entirely but rather compromised in several ways, such as through the introduction of missense mutations, sequestration into polyglutamate repeat aggregates[7,231], as well as the presence of proteotoxic conditions.

Oxidative stress and other proteotoxic conditions encourage CHIP to form higher order structures & thus limit its activity[232]. There is also evidence (Ball lab, unpublished) that CHIP acts as a direct sensor of oxidative status via the oxidation of Cys residues in its tetratricopeptide repeat (TPR) domain, and that the activity of CHIP, as well as its ability to undergo autoubiquitination, are altered by an increased concentration of alpha-synuclein. CHIP's role in the regulation of other proteins, such as interferon regulatory factor 1 (IRF-1), is also impacted by stress. Specifically, under conditions of proteotoxic stress, CHIP is known to facilitate the ubiquitination and subsequent degradation of the IRF-1 protein. Conversely, in unstressed cells CHIP *enhances* IRF-1 transcriptional activity via the monoubiquitination of IRF-1, which increases its steady-state levels and stabilizes IRF-1:DNA complexes[233]. The central role of oxidative stress and toxic protein intermediates in brain disorders related to aging further highlight CHIP as a promising target for the development of neurodegenerative therapeutics.

The introduction of germline mutations in CHIP has yielded novel insights into its cellular functions, with the phenotype and severity of symptoms dependent on the location of the mutation. For instance, homozygous mutations in the TPR domain of CHIP result in symptoms of ataxia, while those located in the U-box domain of CHIP (thus affecting its E3-ligase activity) lead to symptoms of dementia and cognitive decline. Specific mutations leading to cerebellar degeneration and associated ataxia symptoms have also been identified, such as the autosomal recessive GHS and SCAR16 mutations as well as the autosomal dominant SCA48[234,235]. For individuals with the SCA48 mutation, the early symptoms primarily impact cognitive function, and only later, once neurodegeneration spreads throughout the cerebellum, do patients experience ataxia[234]. Thus, there are mutations that result in individuals exhibiting symptoms of ataxia *only*, and others associated with both ataxia *and* cognitive decline/dementia. These naturally occurring CHIP mutations associated with cerebellar degeneration can be used to generate neuronal cell models, thus letting us better understand the specific role CHIP plays in neuroprotection as well as the prevention and reversal of early signs of dementia.

1.5.2 The Structure of CHIP

CHIP contains three domains, namely an N-terminal TPR domain and a carboxyl-terminal U-box domain separated by a highly charged middle coiled-coil domain (Figure 1.5)[236]. The structure of a U-box is similar to that of a RING-type E3 ligase, but without the zinc chelating residues, and functionally both U-box and zinc-finger domains facilitate the conjugation of Ubiquitin to a substrate[237]. Previously, RING-type E3 ubiquitin enzymes were thought to lack a catalytic site and instead indirectly promote ubiquitination by placing an E2-ubiquitin conjugate into close proximity with a protein substrate[237]. More recent crystallographic diffraction patterns of complexes containing RING finger proteins as well as E2-ubiquitin conjugates suggest that RING finger proteins play a more direct role in moderating the transfer of ubiquitin to client proteins[238,239]. CHIP can facilitate the formation of several lysine-linked ubiquitin chains as a means of regulating its protein substrates, including lysine 27, lysine 48, and lysine 63[240-243]. While Lys48-linked chains are often associated with proteasomal degradation,

the formation of Lys63-linked ubiquitin modifications has been linked to a more diverse range of outcomes[244,245]. Based on murine X-ray crystallography data, the formation of Lys63-linked chains was found to be catalyzed by the C-terminus U-box domain of CHIP bound to the E2 heterodimer Ubc13-Uev1a, in which the hydrophobic ridge of Ubc13 binds to the groove of the U-box domain[240]. The structure of the U-box domain of CHIP in complex with UbcH5a, a human E2 ubiquitin-conjugating enzyme, has also been solved in zebrafish and shows a similar organization to that found in mice[246,247].

In humans, CHIP's N-terminus TPR domain encompasses residues 26–131. It consists of a 34 amino acid motif organized in repeating units of 3–16 motifs, arranged either together of separately, and ultimately forming a pair of anti-parallel helices[248-250]. The TPR domain's hydrophobic surface interacts with Hsp70 and Hsp90[236,251]. In the CHIP–Hsp90 complex, the Hsp90 C-terminal forms a two-carboxylate clamp by binding to the hydrophobic pocket of CHIP's TPR domain, assisted by the electrostatic interactions between an Hsp90 aspartic acid residue and a lysine residue from CHIP's TPR domain[240]. More recent studies have found that residues in both the Hsp70 C-terminal peptide 'PTIEEVD' and the α-helical lid sub domain interact with CHIP, and their affinity can be regulated by post-translational modifications[252].

The coiled-coil region of CHIP connects the U-box domain to the TPR domain and allows for the dimerization of CHIP essential for its catalytic E3 ligase activity[253]. The crystal structure of murine CHIP reveals an asymmetric dimer in which the coiled-coil region adopts a different conformation for each promoter. Specifically, one subunit folds into a hairpin composed of two extended α-helices, while in the second, one of the α-helices is instead fragmented into two. Superimposing the structures for the CHIP-Hsp90 (2C2L) and CHIP-Ubc13-Uev1a (2C2V) complexes reveals that the TPR domain dimer may obscure one of the E2 binding sites in the U-box domain, thus showing that only one U-box binding site is both capable of and sufficient for driving catalysis with E2 enzymes[240].

CHIP exhibits allosteric regulation, with its unbound TPR domain showing remarkable structural flexibility[254], while binding to a Hsp70/90 peptide causes an increased stability. Similarly, certain mutations can affect CHIP TPR domain flexibility, with a missense mutation at Lys30 precipitously decreasing pliability. The allosteric

impacts of TPR domain stabilization also extend to the U-box domain[255], with TPR domain binding to Hsp70/90 or a K30A mutation significantly decreasing E3 ligase activity[256].

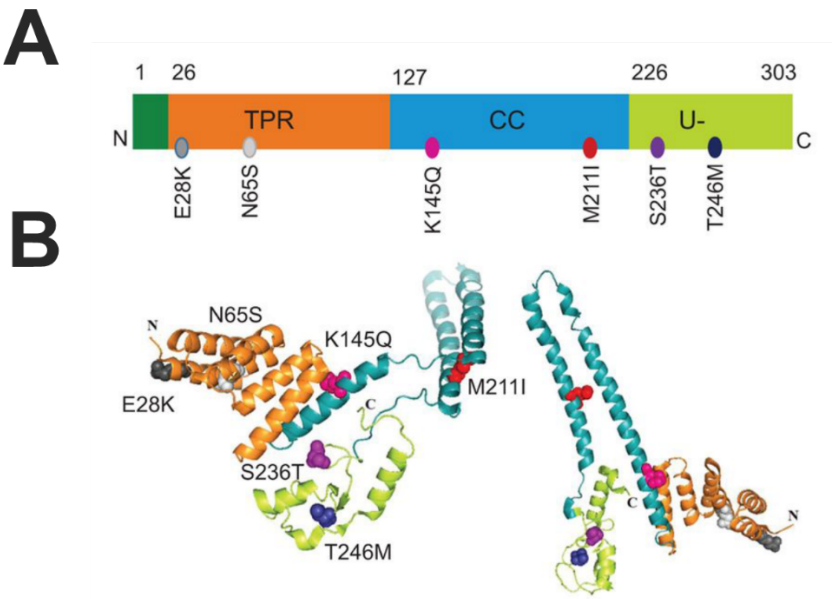

Figure 1.5 **The structure of CHIP**. (***A***) The three domains of CHIP, along with several variants known to impact its function in a 1D protein structure and (***B***) 3D structure of the dimeric protein. PyMOL software (https://www.pymol.org) [Protein Data Bank (PDB) code: 2C2L] was utilized to create the 3D structure, with minor modifications added to better visualize both the different protein domains and the two monomers of the CHIP dimer. Figure reproduced from Pakdaman et al. 2017.

1.5.3 CHIP and Transcriptional Regulation

CHIP is heavily involved in transcriptional regulation across myriad biological processes with wide-ranging cellular and organismal effects. For instance, ectopic STUB1 expression in murine embryonic stem cells (ESCs) was found to significantly reduce the half-lives of SOX2, OCT4, and NANOG, three transcription factors essential in governing the differentiation and pluripotency of ESCs[257]. STUB1 was also found to promote the polyubiquitination and 26S proteasomal degradation of OCT4 through Lys63-linked chains, and SOX2 as well as NANOG through Lys48-linked ubiquitin chains[257]. Thus, the activities of STUB1 were found to elicit ESC differentiation, while its deficiency delayed differentiation and stimulated somatic cell reprogramming, implicating CHIP as a master regulator of pluripotency, albeit through proteasomal degradation-related channels upstream of conventional transcription factors.

Autophagy is a catabolic degradation response whereby long-lived proteins and cytoplasmic organelles are sequestered, digested, and recycled to maintain cellular metabolic homeostasis[258]. Transcription factor EB (TFEB), a transcriptional regulator of autophagy and lysosomal biogenesis, is a target of CHIP-mediated degradation[259]. Specifically, given that phosphorylated TFEB is associated with decreased autophagy activity, and CHIP preferentially targets phosphorylated TFEB for ubiquitin-mediated proteolysis, CHIP augments TFEB activity[259,260]. Additionally, CHIP knockdown has been shown to cause autophagosome formation through simultaneously elevating phosphatase and tensin homolog (PTEN) levels while decreasing protein kinase B (AKT)/mTOR activity[261]. Altogether, this evidence provides strong support for a key role of CHIP in autophagy through its activities impacting autophagy-associated transcriptional regulation.

CHIP is preferentially expressed in adult striated muscle and brain tissue, and was initially found to exhibit cardioprotective effects[236]. CHIP facilitates the ubiquitin-mediated proteasomal degradation of several proteins involved in cardiac homeostasis and function. One such protein, the tumor suppressor p53, acts as an inhibitor of cell growth after acute stress by regulating gene expression[262] in addition to its cancer-related pro-apoptotic functions. However, under certain conditions p53 can have deleterious effects on the cell – for instance, p53 accumulates in the myocardium

subsequent to myocardial infarction, promotes the apoptosis of cardiomyocytes, and ultimately encourages heart failure[263]. Additionally, p53 mutations characterized by a single amino acid change often lead to dominant oncogenic properties[264]. In both cases, CHIP has been found to mediate p53 degradation. Specifically, CHIP facilitates tumor cell apoptosis via the ubiquitination and subsequent proteasomal degradation of oncogenic mutant p53[265]. In heart tissues, myocardial infarction-associated hypoxic stress was found to downregulate CHIP transcription, but pre-emptively increasing CHIP proteins levels prevented the pathological accumulation of p53. Similarly, CHIP overexpression *in vivo* prevented post-myocardial infarction p53 accumulation and subsequent cardiomyocyte apoptosis, as did the enhancement of CHIP function by the Hsp90 inhibitor, 17-allylamino-17-demethoxy geldanamycin (17-AAG), both *in vivo* and *in vitro*[263].

1.5.4 CHIP at the Crossroads of Proteostasis and Insulin Signaling

CHIP is positioned at the nexus of the folding-refolding and degradative pathways, and often involved in facilitating the ubiquitin-mediated proteolysis of improperly folded client proteins. The degradation of aberrant proteins is central to healthy cellular function, and aging itself is characterized by the pathological accumulation of misfolded protein aggregates. Accordingly, CHIP's promotion of the protein quality control system exerts a neuroprotective, anti-aging effect – for instance, STUB1 impedes cellular senescence via the ubiquitination and degradation of inositol-requiring enzyme 1 (IRE1) and brain and muscle ARNT-like 1 (BMAL1)[266,267] – and ablation of CHIP results in an accelerated aging phenotype, implicating CHIP-mediated pathways and processes as a link between proteome imbalance and longevity. Indeed, CHIP deficiency leads to both elevated insulin receptor levels and a decrease in longevity[7]. The membrane-associated insulin receptor links metabolism and aging through its regulation of the IIS pathway. Under normal conditions, CHIP promotes longevity by directly targeting the insulin receptor for ubiquitylation and lysosomal turnover. Conversely, under both aging and conditions of proteotoxic stress, CHIP has instead been found to be rerouted to protein quality control pathways, thus stabilizing the insulin receptor and decreasing lifespan[7]. The discovery of this competitive relationship between proteostasis and longevity

provides novel insights into CHIP-mediated insulin signaling as a mechanistic link connecting proteome imbalances to aging.

1.5.5 CHIP and Mitochondrial Dysfunction

Disruptions in mitophagy and mitochondrial integrity are becoming increasingly implicated in neurodegeneration and pathological aging. In animal studies, loss of CHIP function has been linked to Purkinje neuron degeneration, ataxia[268-270], and mitochondrial dysfunction[268,271-274] in addition to increased PTEN-induced kinase 1 (PINK1) and Parkin protein levels in the central nervous system[268]. Both PINK1, a kinase, and Parkin, another ubiquitin ligase, function in a shared mitophagy pathway. In the absence of mitochondrial stress, PINK1 is targeted for proteasomal degradation. Under conditions of proteotoxic stress, however, PINK1 accumulates on the surface of damaged mitochondria and recruits Parkin to direct the autophagic degradation of mitochondria[275,276]. CHIP has been found to act as a negative regulator of this pathway by stimulating PINK1 degradation, reducing Parkin translocation to the mitochondria, and diminishing mitochondrial autophagy in response to stress[277]. Furthermore, CHIP knockdown has been shown to enhance neuronal mitophagy in *C. elegans*, and several disease-associated STUB1 mutations impair mitochondrial autophagy both *in vivo* and *in vitro*[277], suggesting compromised mitochondrial function could underlie CHIP-associated disease phenotypes.

1.5.6 CHIP and Protein Trafficking

Unexpectedly, CHIP has been shown to cause the chaperone-independent translocation of HSF1, suggesting that it may play a role in protein transport[272]. While studies on CHIP-dependent protein trafficking are scarce, CHIP-mediated ubiquitination has been shown to impede the pro-apoptotic activity of Daxx, a chromatin silencing, death domain-binding protein. However, rather than promoting proteolysis, ubiquitination transiently segregates Daxx into an insoluble fraction from which it is released once the cell restores homeostasis[278,279]. CHIP has also been shown to mediate protein translocation in unstressed cells, suggesting it may play a broader role in protein transport[280]. Specifically, CHIP sequesters soluble endothelial nitric oxide synthase (eNOS), one of three nitric oxide synthases present in human tissues[281], into

an inactive, insoluble cellular fraction[280]. Despite these preliminary findings, the impact of CHIP dysfunction on either the Golgi complex or other transport-associated pathways has not been studied.

1.6 Introduction to Models of Aging

A number of model systems have been used to better understand both healthy and pathophysiological aging, with varying advantages and drawbacks for each (Table 1.1). For instance, rodent models have somewhat short lifespans, reproduce relatively rapidly, and, as mammals, are physiologically similar to humans[282]. The genetic modification of genes encoding proteins driving aging-associated processes in a relatively short-lived mammal may allow, for instance, for the unique assessment of higher order cognitive and behavioural outcomes of particular relevance to humans, such as the ladder rung walking task[283] or RotaRod test[284] to assess motor function and coordination, or the forced swim test to assess learned helplessness or "depression-like behaviour"[285]. However, their inherent complexity can make targeted mechanistic studies particularly difficult. Furthermore, despite the extensive resources available given the popularity of rodents as model systems, much of the husbandry and procedures associated with both their standard care, reproduction, and genetic manipulation are expensive, difficult, and time-consuming. This is especially pertinent in aging research, which by definition operates on a longer timescale than many other subfields of the life sciences.

Cell models, and human cell models in particular, are particularly useful for controlled, mechanistic studies of aging, as well as for drug screening, gene editing, and modeling aging in specific tissues and organs[286]. Genetic manipulation, in particular, can be done efficiently and inexpensively, especially in comparison to mammalian model systems. Indeed, human cell models are generally fast to work with and relatively inexpensive. However, *in vitro* systems lack the full organismal context present in rodent models, including both physiological (i.e., immune and endocrine interactions) and behavioural (cognitive ability, coordination and motor function) processes[287].

C. elegans is a model system often chosen for its anatomical simplicity, genetic tractability, ease and efficiency of use, particularly rapid lifecycle and high reproductive

rate, and inexpensiveness[288]. Its well-defined cellular lineage, transparent body, relatively simple nervous and behavioural systems, and complete neuronal wiring diagram have made it a model system of particular interest to systems neuroscience and the field of aging more generally[289]. Nevertheless, its particularly simplistic biology can also be a limitation. For instance, it lacks several organs and organ systems present in humans (such as a cardiovascular system or bones), and its less complex biology may reduce the translatability of findings to more complex organisms. Furthermore, while behavioural assays of *C. elegans* are both possible and commonly used, its limited complexity is reflected in a limited behavioural repertoire – that is, while behavioural assays examining motility and neuro-muscular function exist[290-293], those examining cognitive function or higher order affect do not.

Many of these higher order behavioural and physiological assays have been done in either mouse or human models in studies focused on the CHIP-associated effects of aging[220,234], and have provided valuable insights. For instance, the introduction of mutations has revealed that impaired function of the U-box (and thus the E3 ligase activity) leads to symptoms of both dementia and cognitive decline, while those affecting only the TPR domain enact a simpler ataxia phenotype[234,235]. Nevertheless, *C. elegans* have also provided particularly valuable CHIP-related insights. For instance, nematode experiments have shown that CHIP mediates a stress-dependent competitive relationship between proteostasis and longevity regulation through its direct action on the insulin receptor[7].

Table 1.1 **Advantages and disadvantages of some of the most common model systems in aging research.**

Model System	Advantages	Disadvantages
Mice/Rodents	1. Assessment of higher order behavioural and physiological outcomes possible 2. Most physiologically similar to humans 3. Full organismal context	1. Expensive 2. Labour-intensive 3. Complexity impedes isolated mechanistic studies of aging
Cells	1. Simplicity allows for mechanistic studies 2. Human cell lines are, by definition, physiologically relevant to humans (can easily use human genes, etc.) 3. Quick, inexpensive, genetically tractable	1. Lack full organismal context, including both physiological and behavioural processes
C. elegans	1. Anatomically simple whole-body organism 2. Behavioural assays possible & common 3. Genetic tractability & well-studied (i.e., availability/accessibility of resources “ready-to-order”)	1. Missing organs/organ systems 2. Complexity can limit breadth of assays, especially behaviourally

1.7 Summary, Aims & Hypotheses

CHIP has been causally associated with the proper functioning of several physiologically integral processes, ranging from proteotoxic stress resistance[9,218] and insulin signaling[7] to multiple subtypes of spinocerebellar ataxia[294]. Indeed, its neuroprotective effects appear to broadly maintain cellular and organismal health via the regulation of the steady state levels of a targeted protein cohort[221,295,296]. Nevertheless, it is clear that the relationship between pathological CHIP function and neurodegeneration is both complex and multifaceted, with many of its mechanistic intricacies remaining unknown. Among its cellular activities, CHIP has been found to interact with and ubiquitinate Daxx, a death domain-associated protein responsible for

regulating transcriptional, apoptotic, and cell cycle activities[297]. However, perhaps unexpectedly, this ubiquitination does not lead to the degradation of Daxx, but rather transiently facilitates its transfer into an insoluble fraction that is released once the cell enters the recovery stage[279,298]. CHIP has also been found to similarly sequester a nitric oxide synthase in *unstressed* cells, thus suggesting it could play a role in protein transport independent of the cell's stress status[280]. Thus, while previous studies have linked aberrant CHIP function to pathological aging, a comprehensive proteomic study of CHIP wild-type and null animals would be invaluable in further elucidating the neuroprotective role of this E3 ligase, linking a loss of CHIP function to neurodegenerative outcomes, and providing clues as to how (and whether) different CHIP-related mechanistic processes, from protein trafficking to ubiquitin/proteasome-related signaling to the regulation of insulin receptor stability, might coalesce upon altered aging-associated phenotypes.

Aims and Hypotheses:

Aims: Here, I address this gap in the literature by (1) first performing a methodological study to investigate differences in lysis buffer composition on protein extraction in *C. elegans*, one of the simplest whole-animal model systems. I then (2) performed proteomic analyses of CHIP wild-type and null animals to further investigate possible CHIP-associated proteins and pathways, and followed up on these results with (3) validation experiments designed to further probe the impact of CHIP deletion on Golgi in cell models, and (4) rescue experiments to determine whether the proteins altered in the initial proteomics experiment were implicated in or independent of CHIP-associated lifespan extension.

Hypotheses: I hypothesize that (1) the lysis buffer composition (and associated biochemical properties) will impact the extraction of myriad proteins, (2) that proteins and pathways related to longevity, protein homeostasis, ubiquitin/proteasome-related processes, protein trafficking, and energy metabolism will be affected by CHIP ablation, (3) that, if CHIP-associated changes in transport-related proteins and organelles are seen, these changes will also be reflected in cell models, and (4) that rescue experiments will reveal many of the proteins and pathways altered in response to CHIP ablation to also be implicated in longevity.

1.8 Thesis Layout

Aging is the progressive, time-dependent accumulation of cellular damage associated with an increased susceptibility to disease and death[299]. The ubiquitin proteasome system orchestrates the turnover of myriad proteins[300], thus playing a neuroprotective role in the homeostatic degradation of both intact and misfolded protein substrates[301]. CHIP, an E3 ubiquitin ligase, was first characterized as a co-chaperone of Hsc/Hsp70[256], with the CHIP:Hsp70 complex positioned at the crossroads of client protein degradation and misfolding[302]. It has since been shown that CHIP has its own substrate specificity[303] as well as several non-canonical functions that are either independent of chaperone partners or unrelated to the proteasome-dependent degradation of misfolded or mutant proteins[303]. Here, I aim to utilize proteomic assays, as well as several validation experiments, in both cell and nematode models to further investigate CHIP's neuroprotective functions. In Chapter 2, I perform a proteomic assay comparing three *C. elegans* strains (two complete loss-of-function *chn-1* mutants, encoding the *C. elegans* orthologue of CHIP) subjected to protein solubilization by either CHAPS/urea or SDS-based lysis buffers to determine the impact of detergent choice on protein extraction profiles and efficiencies. In Chapter 3, I perform proof-of-principle longevity assays to confirm the impact of *chn-1* ablation on lifespan, and subsequently subject *chn-1* wild-type and knock-out strains processed by either CHAPS/urea or SDS-based detergents to a comprehensive between-strain analysis aiming to define the impact of CHIP deletion in a simple, whole-animal model system. Finally, in Chapter 4, I expand upon these initial findings by performing preliminary validation experiments investigating (i) the interaction of CHIP and SMA-9, one of the top proteins differentially expressed in *chn-1*-null animals, on longevity in worms, (ii) the impact of CHIP deletion on Golgi morphology in both worm and human neuroblastoma cell models, (iii) the expression of Rab6 and COG6, two retrograde transport-associated proteins found to be altered in *chn-1*-null samples (Chapter 3) via immunoblotting and immunofluorescence experiments, and (iv) the proteins, pathways, and gene ontology terms associated with a proteomic investigation of *h*CHIP and *Ce*CHIP rescue strains.

Chapter 2: *C. elegans* Protein Landscape is Altered Depending on Detergent Properties During Lysis

2.1 Introduction

Global proteomic analyses provide an invaluable framework for understanding the biochemical underpinnings driving both healthy and pathological aging. This method is not without its obstacles, however. Comparative analyses investigating the relative extraction efficiencies of varying detergents have seldom been performed, despite the diverse physicochemical properties of both subcellular compartments and their associated proteins[304-306]. The isolation of membrane proteins, for instance, is particularly challenging due to their apolar transmembrane domains[307]. Moreover, different classes of membrane proteins and their associated complexes have distinct biochemical characteristics, thereby adding further nuance to specialized protein extractability[308]. For instance, the physicochemical properties of peripheral and lipid-anchored membrane proteins may render them more amenable to extraction by a mild, non-ionic or zwitterionic detergent[309], while integral membrane proteins may require the use of an agent capable of phospholipid bilayer disruption[310].

Proteomic assays using *Escherichia coli* suggest SDS provides the greatest overall protein yield, mainly due to its high efficiency in the extraction of high molecular weight and integral membrane proteins[311], particularly in challenging samples such as muscle tissues and nuts[312,313]. SDS, a widely used anionic surfactant, has an amphiphilic structure characterized by both a hydrophobic dodecyl (12-carbon) tail and a hydrophilic sulfate head group[314,315]. It primarily interacts with proteins via its hydrophobic tail, causing them to unfold and adopt a linear conformation[316,317]. For instance, SDS disrupts lipid bilayer integrity via the insertion of its hydrophobic tail into the membrane, thus extracting and solubilizing membrane proteins, although it can also damage extracellular membrane components[318-320]. Furthermore, in aqueous solutions above its critical micelle concentration, SDS forms micelles, or aggregates capable of

enveloping hydrophobic molecules, thus further facilitating the solubilization of membrane proteins and lipids[317].

Nonetheless, although SDS is highly effective in enhancing and maintaining protein solubility[321], it can interfere with downstream mass spectrometry and electrophoresis unless thoroughly removed (i.e., through filter-aided sample preparation (FASP), which utilizes a molecular weight cut-off membrane to obtain digestion-ready proteins, or a suspension trapping (S-trap), which depletes and digests interfering substances using a three-dimensional porous material as the filter media[322]). That is, it is also among the most deleterious agents in suppressing electrospray ionization, thus complicating MS analyses[323,324] of proteins and peptides. Furthermore, while its powerful detergent action allows for relatively high protein coverage[325], SDS is also a strong, highly denaturing detergent,[325] and thus, while highly effective at solubilizing and denaturing both proteins and protein complexes, is a poor choice for experiments investigating protein structure and interaction partners or extracellular matrix integrity[318,320]. Indeed, its disruption of secondary and tertiary structures, while precluding structural and interactional analyses, facilitates its high extraction yields[312]. Accordingly, a number of cellular fractionation studies assessing lipid profiles as well as mitochondrial and membrane-associated proteins have utilized mild, apolar detergents capable of preserving native protein structure, bioactivity, and interaction partners[311,326-330].

CHAPS, a zwitterionic, non-denaturing detergent, exhibits a high peripheral membrane protein extraction efficiency. It combines features of bile salts (i.e., acting to emulsify fats and modify the permeability of lipid membranes[331]) and sulfobetaine-type (i.e., neutral and efficient at disaggregating proteins but strongly denaturing[332]) detergents, resulting in a polarity that is neutral overall, but contains positive and negative charges[333-335]. CHAPS also forms micelles in aqueous solutions stabilized by both electrostatic interactions among polar groups and hydrophobic interactions among steroid rings[334,335], the clustering of which (in groups of 3–4 molecules) creates small hydrophobic pockets further able to occasionally accommodate hydrophobic residues[334]. However, its small hydrophobic regions prevent it from efficiently penetrating the lipid bilayer[336].

Urea, on the other hand, is a chaotropic agent acting to disrupt hydrogen bonds and weakening both non-covalent and hydrophobic interactions, thus efficiently solubilizing aggregated or otherwise insoluble proteins[337]. Interestingly, urea can alter the micellization behaviour of detergents, both increasing critical micellar concentration as well as altering micelle size and stability. Conveniently, when used with CHAPS, urea increases protein solubilization efficacy[338,339]. While stronger, denaturing detergents such as SDS more efficiently solubilize transmembrane proteins[330], a dual-detergent strategy leveraging both the zwitterionic character of CHAPS as well as the chaotropic properties of urea can effectively target otherwise insoluble superficial membrane proteins.

Despite the interdependent relationship between detergent properties and proteomic output, few studies have directly investigated the relative protein extraction behaviour of multiple detergents in a single experiment. Here, SDS or CHAPS/urea-dependent sample lysis was utilized to explore the interaction of physicochemical protein characteristics, subcellular localization, and detergent choice. We identified clearly distinguishable proteomic signatures linking the biochemical properties of detergents commonly used in proteomic assays and the proteins upon which they act.

2.1.1 Introduction to *C. elegans*

Caenorhabditis elegans is a small, transparent nematode often used as a model of aging. *C. elegans* grows rapidly and reproduces in large numbers, with animals reaching adulthood 38-46 hours after hatching, producing broods of 300 progeny per hermaphrodite, and ultimately living for approximately 21-30 days. Nematodes grow on agar plates while feeding on non-pathogenic *Escherichia coli* (OP50). It was the first animal to have its genome entirely sequenced, and it has since been found that over 65% of all human disease-associated genes have been conserved in *C. elegans*[340,341]. The genetic tractability of *C. elegans* enables the rapid study of cellular mechanisms, signaling pathways, and genetic changes relevant to aging, including those pertaining to proteostasis, mitochondrial function, stress responses, and nutrient-sensing signaling. In addition to being the first to have the entirety of its genome sequenced, *C. elegans* also had the first collection of cloned open reading frames, large-scale protein-protein

interaction map in a metazoan, reverse genetic screens, and the first complete neural wiring diagram[342]. Indeed, nematodes have been at the forefront of aging-related mechanistic discoveries for several decades, with every major *C. elegans* discovery also being later confirmed in both *Drosophila* and mice. For instance, caloric restriction was expected to mediate longevity based on previous experiments in rats. However, the regulatory effects of insulin signaling downregulation on dauer formation (a stress-resistant, dormancy state in *C. elegans* occurring under environmental conditions unfavourable for further growth) were surprising, with this pathway being then shown to have a conserved role in longevity mediation across both flies and mammals[342].

Developmentally, embryogenesis lasts approximately 14 hours at 20^{o}C, resulting in a newly-hatched first larval stage (L1). Animals then progress through four larval stages (L1–L4, increasing in size throughout), although individual sexes are indistinguishable until the L4 stage (Figure 2.1)[343]. L4 hermaphrodites have a tapered tail, and the developing vulva (Figure 2.1, white arrowhead) is visible in the center of the ventral side as a clear half circle[343]. Conversely, L4 males have a wider tail (Figure 2.1, black arrowhead), although are lacking a fan at this stage[343]. The sexes of adult animals can be distinguished by noting the wider girth and tapered tail of hermaphrodites, whereas males appear slimmer with a fan-shaped tail. Oocytes can be fertilized with either sperm from the hermaphrodite or males. Under non-stressed conditions (e.g., when the animals have sufficient food/are not starved), post-embryonic development to reach reproductive adulthood takes approximately 2.5 days[343]. Under adverse conditions (i.e., when animals are starved or subjected to a high population density and/or temperatures), larvae can enter an alternative dauer (a non-feeding, stress-resistant, long-lived state that is reversible when conditions improve) diapause in the transition from L2–L3[343]. Dauer larvae are thinner than all other larval stages. Adult animals undergo a reproductive period, followed by a post-reproductive aging phase during which there is a noticeable decline in locomotion, pharyngeal pumping, and tissue integrity[343].

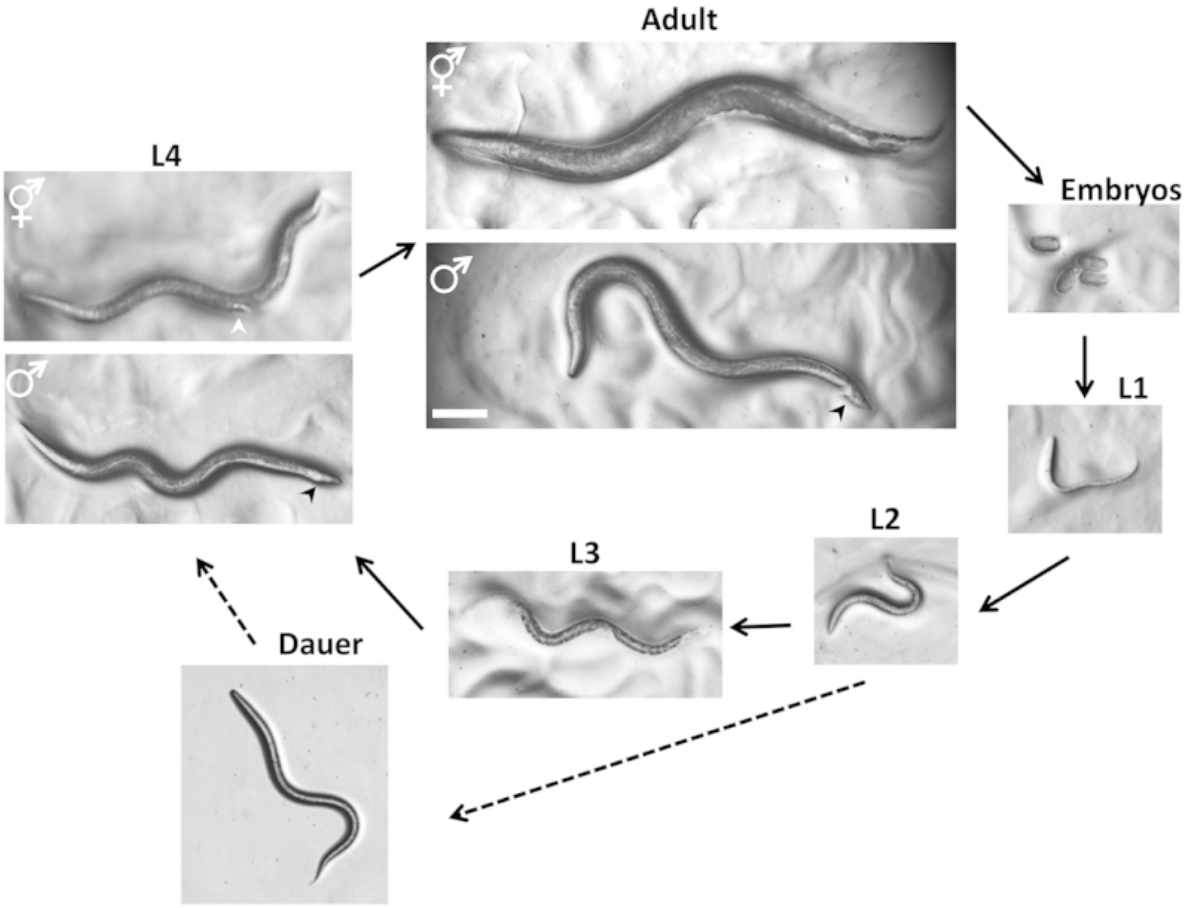

Figure 2.1 **Life cycle of *C. elegans*.** Photographs were taken on Petri dishes (note the bacterial lawns on all but the dauer images). Bar 0.1 mm. Figure reproduced from Corsi et al., 2015.

2.2 Materials and Methods

2.2.1 Experiment Overview and Rationale

A preliminary proteomic experiment was initially performed to investigate strain-dependent differences in *chn-1(by155)* and *chn-1(tm2692)* deletion mutants relative to wild-type controls in exclusively SDS-processed samples. However, upon performing this experiment, an intense peak was found in the total ion chromatogram of all three replicates within each strain (Figure 2.2). This peak was likely due to contamination of the samples; therefore, further analyses could not proceed. Subsequent troubleshooting involved, therefore, rerunning the experiment with additional measures taken to ensure contamination was not an issue moving forward. However, this was also seen as an

opportunity to perform a methodological study examining whether differing lysis detergents would alter (1) the global proteomic landscape of *C. elegans*, and (2) whether specific proteomic pattern changes would occur across detergent conditions in response to *chn-1* ablation, thus potentially giving further insight into novel CHN-1-related functions and protein interactions (Appendix A). To proceed, I first completed an additional preliminary experiment examining the impact of differing detergents on N2 wild-type worms. Finally, I proceeded to generate MS-based proteomic datasets using either CHAPS/Urea- vs. SDS-based lysis buffers and compared wild-type worms to *chn-1(by155)* and *chn-1(tm2692)* deletion mutants (Appendix A).

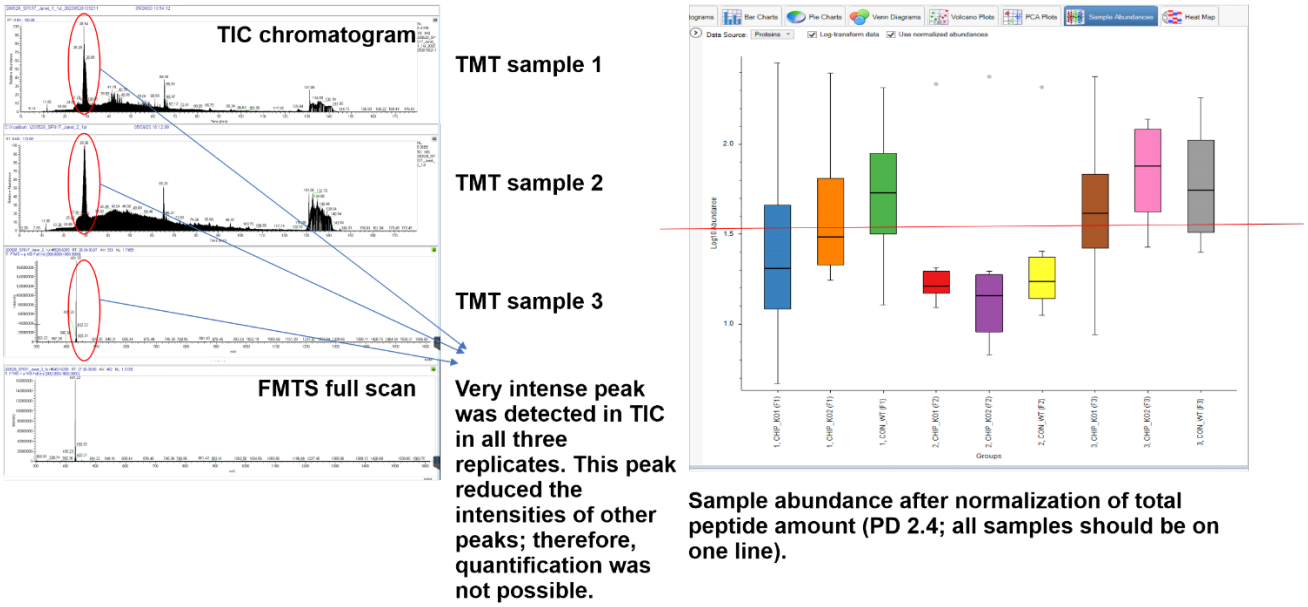

Figure 2.2 **Failed experiment examining strain-dependent differences in *chn-1(by155)* and *chn-1(tm2692)* mutants vs. wild-type controls**. An intense peak was detected in the total ion chromatogram across all replicates, thus reducing the intensities of all other peaks and making further quantification impossible.

2.2.2 Nematode Strains

Animals were cultured using standard methods. Worms were grown at 20ºC on standard nematode growth medium (NGM) plates spread with the *Escherichia coli* (*E. coli*) strain OP50. The following *chn-1* deletion mutants were triple-backcrossed to the laboratory wild-type (Bristol, N2) strain: *chn-1(by155)* and *chn-1(tm2692)*. These (and all other *C. elegans* strains used, apart from *h*/*Ce*CHIP rescue strains constructed in-house as described in Chapter 4) were ordered from the *Caenorhabditis* Genetics Centre (CGC, University of Minnesota, MN, USA).

2.2.2.1 Triple-Backcrossing C. elegans Strains

All strains were triple-backcrossed upon arrival (including *sma-9*-null mutants; Chapter 4), and those created in later chapters (i.e., *sma-9*/*chn-1* double-null mutants as well as final *m*Kate, *h*CHIP, and *Ce*CHIP rescue strains; Chapter 4) were triple-backcrossed prior to experimental/assay use. To do this, each *chn-1* mutant was crossed with N2 males (one hermaphrodite and 3-4 males were placed together on a new plate) and animals from this plate singled onto new plates (i.e., several animals each placed individually onto a new plate and left for 3 days to reproduce). In most populations, male nematodes represent a tiny fraction of all animals (approximately 0.1% – 0.2%). Typically, *C. elegans* is androdioecious – that is, dominated by such self-fertilizing hermaphrodites, with males typically produced from rare, spontaneous X chromosome nondisjunction (the failure of homologous chromosomes or sister chromatids to separate properly during cell division) events during hermaphrodite reproduction. However, in a mating between a male and a hermaphrodite, males constitute 50% of the outcross progeny, as male sperm can outcompete hermaphrodite sperm in fertilization[344,345]. Therefore, crosses were visually inspected under a light microscope, with plates containing a proportion of males nearing 50% deemed the result of a successful cross. Animals from the new plates were genotyped to determine heterozygosity, and animals from a heterozygous plate once again singled onto a new plate and left to grow and reproduce for 3 days. Finally, from this last set of plates, animals were genotyped and those homozygous for the selected *chn-1* mutation were selected for further use. A PCR electrophoresis gel of the final triple-backcrossed

strains is shown in the results, with both the protein ladder as well as heterozygous, homozygous *chn-1*-null, and homozygous wild-type bands labelled (Figure 2.3). This constituted one backcross, and was repeated three times to triple-backcross *chn-1(by155)* and *chn-1(tm2692)* animals.

2.2.2.2 Agarose Gel Electrophoresis of DNA

Agarose gels were prepared by dissolving electrophoresis-grade agarose (Invitrogen) (1% w/v) in 1X TAE buffer (40 mM Tris + 1 mM EDTA, pH 8 with glacial acetic acid). Once cooled, SYBR(R) Safe DNA Gel Stain (1:10 000; Invitrogen) was added to the gel, and the mixture was poured into the chamber. DNA samples were diluted in 6X DNA loading dye (0.25% (w/v) Bromophenol blue + 0.25% (w/v) Xylene cyanol + 15% (v/v) Glycerol) (at a ratio of 5:1, sample:dye) and loaded into the wells of the gel, along with a 1 kb DNA ladder (New England Bioscience). The gel was run in 1X TAE buffer at 80-100 V for 45-60 minutes and subsequently visualized with a UV lamp imaging system and built-in camera.

2.2.2.3 Polymerase Chain Reaction (PCR)

Gene amplification was performed using OneTaq (New England Biolabs, Ipswich, MA) polymerase with reactions prepared as follows: 12.5 µL OneTaq (final concentration: 1x) + 0.5 µL Forward primer (Sigma–Aldrich, St. Louis, MO, USA) + 0.5 µL Reverse primer (Sigma–Aldrich, St. Louis, MO, USA) + 10.5 µL DNAse-free ultrapure water + 1.0 µL genomic DNA lysate as the PCR template. Master mixes were prepared for multiple reactions to minimize inter-sample variation. Final Forward and Reverse primer concentrations: 0.2 µM. Template DNA < 1 000 ng.

Table 2.1 **Primers for PCR amplification of *chn-1* wild or mutant type genes.**

Primer	Sequence	Binding Site	T_m (ºC)
1163.chn-1tm2692ExF	5'-agcgtttgcagcatgtcaag-3'	1355 .. 1374	59
1164.chn-1tm2692ExR	5'-agcatctcaggaacctccct-3'	2328 .. 2347	59
EMD101.chn-1(by155)ExF	5'-gagcccaaacgaagtgaaag-3'	1666 .. 1685	58
EMD102.chn-1(by155)ExR	5'-tgcctccgggttcatattta-3'	3550 .. 3569	54
EMD103.chn-1(by155)IntF	5'-gcacgccatcaaaagtacga-3'	1912 .. 1931	57
EMD104.chn-1(by155)IntR	5'-gtgactggatcgaaatggcc-3'	2448 .. 2467	59

For amplification of *chn-1*, the following PCR cycling program was used: initial denaturation (94°C for 30 seconds), 35 cycles of: 94°C (30 seconds/cycle), T_m as above (Table 2.1, 30 seconds/cycle), 68°C (1 minute/1 000 base pairs), 1 cycle of: 68°C (2:10 minutes), 10°C (forever).

2.2.2.4 DNA Sequencing

DNA Sanger sequencing was performed by Source Bioscience (Cambridge, UK) using the appropriate forward or reverse primers used for PCR (Table 2.1).

2.2.3 Growth and Synchronization of Worms

Worms were chunked from plates of three different types of strains (N2 controls, *chn-1(by155)* and *chn-1(tm2692)*) and transferred to fresh NGM plates spread with the *E. coli* strain OP50 (1X NGM; lifespan analysis, bombardment) or HB101 (3X NGM; proteomics). Animals were allowed to replicate for at least 3 generations, with synchronous growth accomplished by subjecting gravid adults (60 hours post-plating) of the previous generation to bleaching using 0.6 mL H_20 + 1.9 mL 5% bleach + 2.5 mL 1M NaOH.

2.2.4 Preparation of Samples for Proteomic Analyses

All proteomics experiments were conducted with technical and biological triplicate samples for each strain (N2 wildtype, *chn-1(by155)*, and *chn-1(tm2692)*) with 24 000 animals plated per sample (8 000/plate). Sample collection took place 48 hours post-plating, when animals were non-gravid young adults – this was because the presence of eggs in the body, occurring throughout much of adulthood in *C. elegans*, would overwhelm any *chn-1*-deletion-related results of a proteomic screen with proteins related to reproductive processes, including the development and presence of oocytes. Thus, collecting samples in pre-gravid young adulthood would allow for the analysis of *chn-1*-associated changes in adults without also biasing the results toward reproductive changes at the expense of other physiologically relevant age-related processes. Samples were lysed directly in 300 µL of either SDS- (4% SDS, 150 mM NaCl, 10 mM phosphate buffer pH 7.0, 50 mM N-ethylmaleimide, 25 mM TCEP) or CHAPS/Urea- (35 mM Tris, 8M urea, 4% CHAPS, 65 mM DTT, pH 8.0) based lysis buffer. Upon rinsing

from plates, samples were mixed with glass beads, agitated for four cycles in a bead-beater (4 000 shakes per second; 30 seconds per cycle), centrifuged between cycles at 21 913 g for 3 minutes at room temperature, and heated at 65ºC for 15 minutes. The supernatant was transferred from each sample to new 1.5-mL centrifuge tubes and subsequently centrifuged at 15 000 RMP for 5 minutes at room temperature. The supernatant from this step contained the clear lysate for proteomic analyses and was transferred to a separate tube. A 50 µL aliquot was taken from each sample for protein quantification via either BCA (SDS-based lysis buffer) or Bradford (CHAPS/Urea-based lysis buffer) protein assays. Samples were stored at –80ºC until subjected to FASP, and subsequently sequential window acquisition of all theoretical fragment ion spectra-mass spectrometry (SWATH-MS)-based proteomic analyses.

Peptides were generated by FASP, as described previously[346,347]. Briefly, The RC-DC method (Bio-Rad, Watford, UK) was utilized to confirm sample protein concentrations, and protein-normalized samples added to urea buffer-treated (8M urea in 0.1 M Tris pH 8.5) 30 kDa spin filter columns (MRCPRT010; Microcon®, Sigma–Aldrich, St. Louis, MO, USA). Columns were subsequently centrifuged at 14 000 *g* for 15 minutes at 20ºC, mixed with urea-based buffer + 100 mM Tris (2-carboxyethyl) phosphate hydrochloride (Sigma–Aldrich, St. Louis, MO, USA), incubated for 30 minutes in a shaking thermo-block at 37ºC, and centrifuged at 16 099 *g* for 15 minutes at 20ºC. The columns were further treated with urea buffer + 300 mM of iodoacetamide (Sigma–Aldrich, St. Louis, MO, USA), shaken in a thermos-mixer for 1 minute, left at 20ºC in a light-free, stationary environment for 20 minutes, and centrifuged at 16 099 *g* for 15 minutes at 20ºC. The resulting supernatant was discarded, 100 mM ammonium bicarbonate added to each column, and samples again centrifuged at 16 099 *g* for 20 minutes at 20ºC. Upon repetition of this step, the columns were placed in low-binding-affinity tubes. Trypsin diluted in trypsin buffer (Promega, Southampton, UK) + 50 mM ammonium bicarbonate was added at a 1:100 ratio. The columns incubated at 37ºC for 16 hours and subsequently centrifuged at 20ºC and 16 099 *g* for 15 minutes. Peptide concentrations were determined using the Quantitative Colorimetric Peptide Assay (Thermo Scientific, USA).

Peptides desalting was done using C-18 (Harvard Apparatus, Holliston, USA) columns conditioned three times with 100% acetonitrile (AcN) and 0.1% formic acid (FA) prior to centrifugation at 252 *g* for 2 minutes at room temperature. Columns were then hydrated in 0.1% FA for 15 minutes and subsequently centrifuged at 447 *g* at room temperature for 3 minutes. Samples were loaded into columns, centrifuged at 699 *g* for 3 minutes, and washed three times with 0.1% FA. Finally, peptides were eluted via three consecutive centrifugations at 699 *g* for 3 minutes using 50%–80% and 100% AcN with 0.1% FA prior to peptide eluates being evaporated and dissolved in 5% AcN with 0.05% FA.

2.2.5 Mass Spectrometry-Based Proteomics

Dried peptide samples were dissolved in 100 µL of loading buffer (0.08% trifluoroacetic acid in 2.5% acetonitrile in H_2O) and injected into the liquid chromatography (LC) column (1 µL/sample). Sample peptides were separated using the Thermo Scientific UltiMate 3000 (Thermo Scientific, USA) system connected to the Thermo Scientific Exploris 480 mass spectrometer (Thermo Scientific, USA), with µ-precolumn C18 trap cartridges (inner diameter 300 µm, length 5mm) packed with C18 PepMap100 sorbent with PepMap 5 µm sorbent (Thermo Scientific, USA) used to concentrate and desalt immunopeptides via a 5 µL/minute loading buffer flow. Peptides were separated on a fused-silica packed column (inner diameter 75 µm, length 250 mm) packed with PepMap 2 µm sorbent (Thermo Scientific, USA) via a non-linear increase of a mobile phase B (0.1% formic acid in acetonitrile) in a mobile phase A (0.1% formic acid in H_2O). Peptides were separated using a linear gradient beginning at 2.5% B and increasing to 40.0% B in 90 minutes (flow rate 300 nL/minute), subsequently ionized in a nano-electrospray ion source, and introduced to Exploris 480.

Data comparing CHAPS/Urea with SDS-based lysis methods were acquired in data-independent peptide mode. The resolution was set at 120 000 for full scan in profile format, with a full scan range of m/z 350 Th to m/z 1 200 Th and an automatic gain control target of 300% with automatic maximum injection time. After each full scan, the most intense precursor ions picked from the spectrum were fragmented. After the first precursor ion fragmentation, the dynamic mass exclusion was set to 20 seconds,

mass tolerance set to 10 ppm, and precursor isolation window set to 1.6 Th. Minimum precursor ion intensity was set to 5.0E3 and both precursor isotopologues as well as any precursor charge states other than +1, +2, +3, +5, and +6 were excluded. Scans were acquired with normalised collision energy type and fixed collision energy mode, with the collision energy set to 30%. Orbitrap resolution was set to 15 000, the normalised automatic gain control target was set to standard (injection time 40 milliseconds), and the data type was centroid. The total protein count includes single peptide IDs.

2.2.5.1 Data Processing and Statistical Analyses

Raw data files (.raw) were converted into mzXML format and searched with Comet against all *C. elegans* proteins annotated in the UniProt/SwissProt database, including a set of decoy protein sequences comprised of the reverse protein sequence for each database protein. Trypsin was set as the protease, two missed cleavages were allowed, fixed modification was set to the carbamidomethylation of cysteines, and methionine oxidation was set as a variable modification. The tolerated mass errors were 8 ppm on MS1 level and 8 ppm on MS2 level. Search results were processed with PeptideProphet[348] and ProteinProphet[349] as part of the TPP 5.2.0 [350]. Samples were compared pairwise using paired *t*-tests.

2.3 Results: Protein Extractability Varies in a Detergent-Dependent Manner

2.3.1 Validation of *C. elegans* Strains

Agarose PCR gels (Figure 2.3), genomic maps of *chn-1(by155)* and *chn-1(tm2692)* (Figure 2.4) and sequences of both alleles of the *chn-1* knock-outs (Figure 2.5 and Figure 2.6) are shown below. PCR genotyping of *chn-1(by155)* and *chn-1(tm2692)* deletion mutants is shown in Figure 2.3A and Figure 2.3B respectively, with primers either external or internal to the corresponding allele, as described in Figure 2.3 and Table 2.1.

For the *chn-1(by155)* allele, the *chn-1*-null samples contain a truncated CHN-1 protein lacking the U-box domain resulting from the deletion of 989 base pairs removing exons 5 and 6, as depicted in both the genomic map shown in Figure 2.4 (the primer binding sites, which determined the DNA fragment sizes of the PCR products, were also included in Figure 2.4) as well as the sequence of the *chn-1(by155)* allele shown in Figure 2.5. The numbers on the right of Figure 2.3A and Figure 2.3B refer to the DNA fragment sizes (bp). For instance, when using primers external to the *by155* deletion allele as described below in Figure 2.3A, lanes 2, 4, and 12 contain *chn-1(by155)*-null samples with DNA fragment sizes of 918 bps (these DNA fragments are shorter due to the deletion of the *by155 allele*, thus enabling their migration further down the agarose gel than the larger DNA fragments), while lanes 6 and 14 contain WT samples with DNA fragment sizes of 1 904 bps and lanes 8 and 16 contain heterozygous samples. The heterozygosity of lanes 8 and 16 was further confirmed using primers internal to the *by155* deletion allele, with the presence of bands in lanes 9 and 17 (also heterozygous) indicating that the *by(155)* deletion allele was not entirely absent (if it was, no bands would be observed as the primers would not have had sites with which to bind). Internal primers to the *by155* deletion allele also confirmed that lanes 7 and 15 contain WT samples. In contrast, the use of primers internal to the *by155* deletion allele confirmed a *chn-1(by155)*-null genotype in lanes 3, 5, and 13 via the absence of a band (Figure 2.3A).

For the *chn-1(tm2692)* allele, the *chn-1*-null samples consist of a shortened CHN-1 protein lacking the TPR domain due to a 263 base pair deletion (with a 3 base pair insertion) ultimately removing exons 2, 3, and 4, encoding amino acids 26 through 92 (Figure 2.4). The sequence of the *chn-1(tm2692)* allele is shown in Figure 2.6. When using primers containing a primer-binding site internal to the *tm2692* deletion allele (Figure 2.4) as described below in Figure 2.3B, lanes 2, 4, and 12 contain *chn-1(tm2692)*-null samples confirmed by the absence of a band. Lanes 3, 5, and 13, processed using primers external to the *tm2692* deletion allele (Figure 2.3B), also contain *chn-1(tm2692)*-null samples with a DNA fragment size of 681 bps (these DNA fragments are shorter due to the deletion of the *tm2692* allele, thus enabling their migration further down the agarose gel than the larger DNA fragments. Lanes 6 and 14

(processed using primers containing a primer-binding site internal to the *tm2692* deletion allele, as shown in Figure 2.4) contain WT samples with a DNA fragment size of 1 904 bps, confirmed by the presence of a band (the absence of a band would reflect the primer being unable to bind to the primer-binding site internal to the *tm2692* deletion allele and thus indicate the lanes contained *chn-1(tm2692)*-null samples). Lanes 7 and 15 (processed using primers external to the *tm2692* deletion allele, as shown in Figure 2.4) also contain WT samples confirmed by both their DNA fragment sizes (993 bps) and these DNA fragment sizes being larger (and thus migrating a shorter distance down the agarose gel) than the corresponding *chn-1(tm2692)*-null samples (Figure 2.3B and Figure 2.4). Lanes 8 and 16 as well as 9 and 17 contain heterozygous samples processed by primers containing either a primer-binding site internal to or both primer-binding sites external to the *tm2692* deletion allele, respectively (Figure 2.3B and Figure 2.4). The presence of a band in lanes 8 and 16 confirms that these lanes do not contain *chn-1(tm2692)*-null samples, while the presence of two bands in lanes 9 and 17 (with DNA fragment sizes of 993 and 681 bps) confirms the heterozygosity of these samples. For each genotype, the same plate was processed with both external and internal primers to the appropriate deletion allele.

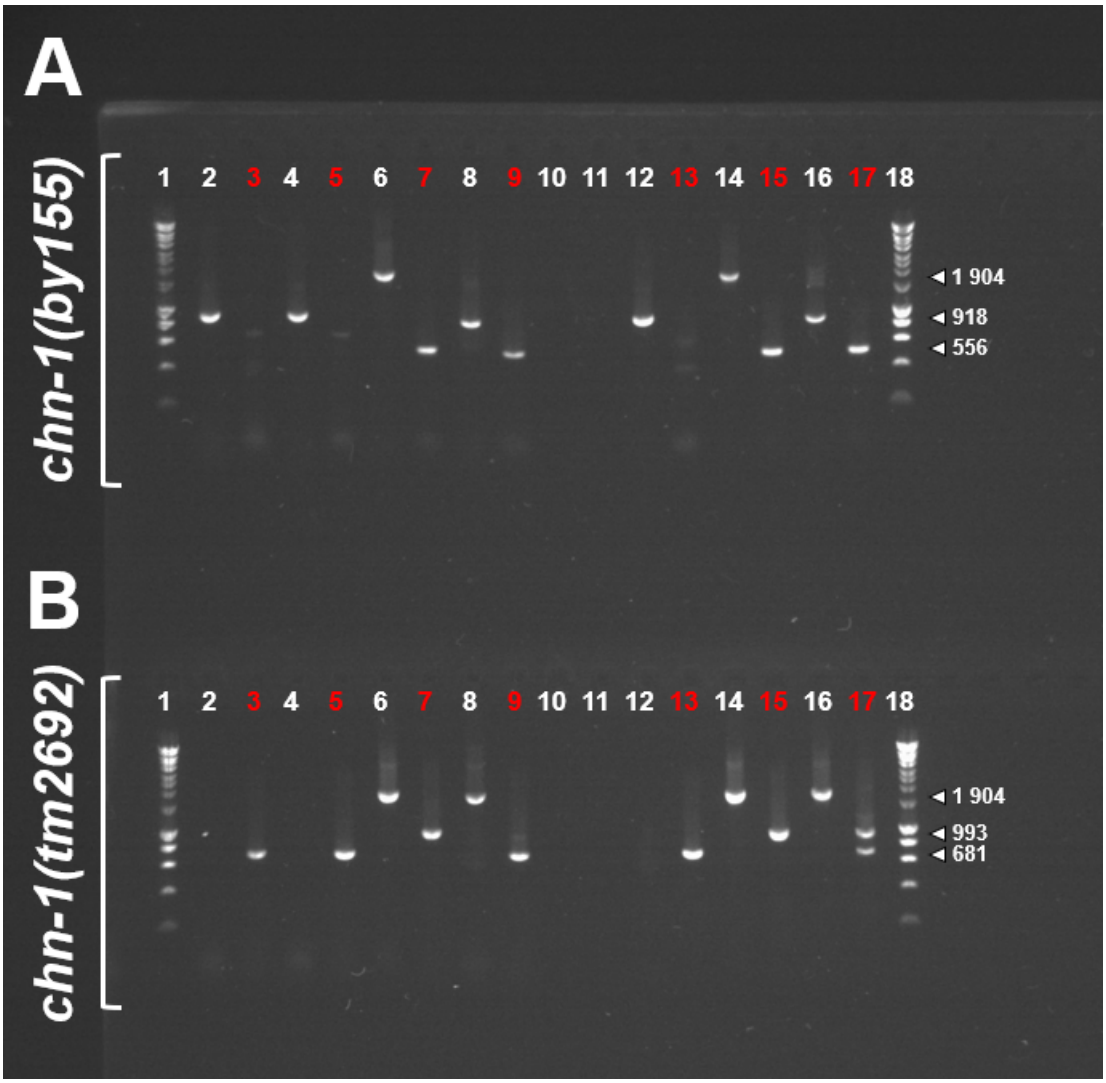

Figure 2.3 **Agarose gel electrophoresis of *chn-1(by155)* and *chn-1(tm2692)* PCR amplicons prior to proteomic analyses of *chn-1* deletion mutants.** Agarose gel electrophoresis of *chn-1* deletion mutant PCR products after triple-backcrossing of (***A***) *chn-1(by155)* and (***B***) *chn-1(tm2692)* mutant animals using either (***A***, ***B***) EMD101.chn-1(by155)ExF and EMD102.chn-1(by155)ExR (white font), (***A***) EMD103.chn-1(by155)IntF and EMD104.chn-1(by155)IntR (red font), or (***B***) 1163.chn-1tm2692ExF and 1164.chn-1tm2692ExR (red font) (Table 2.1). Samples were analyzed by electrophoresis through 1% (wt/vol) agarose gels. (***A***) Lanes: 1, 1 kb DNA ladder marker (New England Bioscience); 2–5, *chn-1(by155)*; 6–7, WT; 8–9, heterozygous samples; 10–11, spaces; 12–13, *chn-1(by155)* controls; 14–15, WT controls; 16–17, heterozygous controls; 18, 1 kb DNA ladder marker. (***B***) Lanes: 1, 1 kb DNA ladder marker; 2–5, *chn-1(tm2692)*; 6–7, WT; 8–9, heterozygous samples; 10–11, spaces; 12–13, *chn-1(tm2692)* controls; 14–15, WT controls; 16–17, heterozygous controls; 18, 1 kb DNA ladder marker. The numbers to the right refer to the DNA fragment sizes (bp).

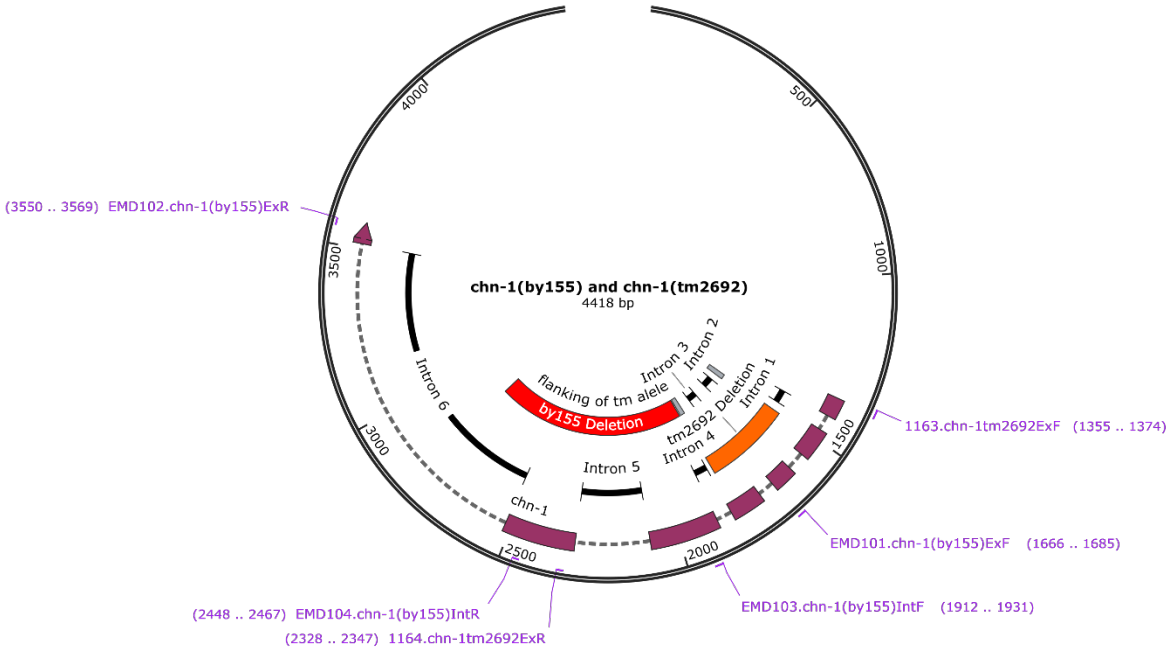

Figure 2.4 **Genomic maps of *chn-1(by155)* and *chn-1(tm2692)*, including primer binding sites.**

Figure 2.5 **Sequence of the *chn-1(by155)* allele.**

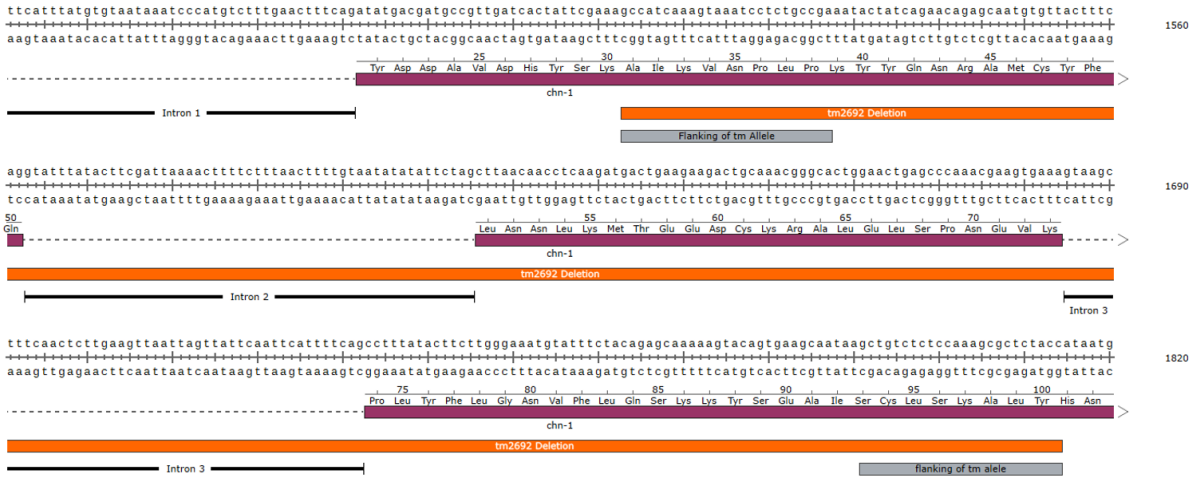

Figure 2.6 **Sequence of the *chn-1(tm2692)* allele.**

2.3.2 Overview of the Changes in the Proteome

Preliminary experiments comparing N2 wild-type animals processed by CHAPS/urea to those lysed by SDS revealed a striking detergent-dependent proteomic landscape, with 1 822 proteins of 11 237 total proteins (16.2%) uniquely seen in CHAPS/urea-processed samples and 3 592 proteins (32.0%) uniquely seen in SDS-processed samples (Figure 2.7). Thus, I proceeded with a larger experiment to further define the CHN-1-dependent proteomic landscape in response to *chn-1* deletion (Appendix A).

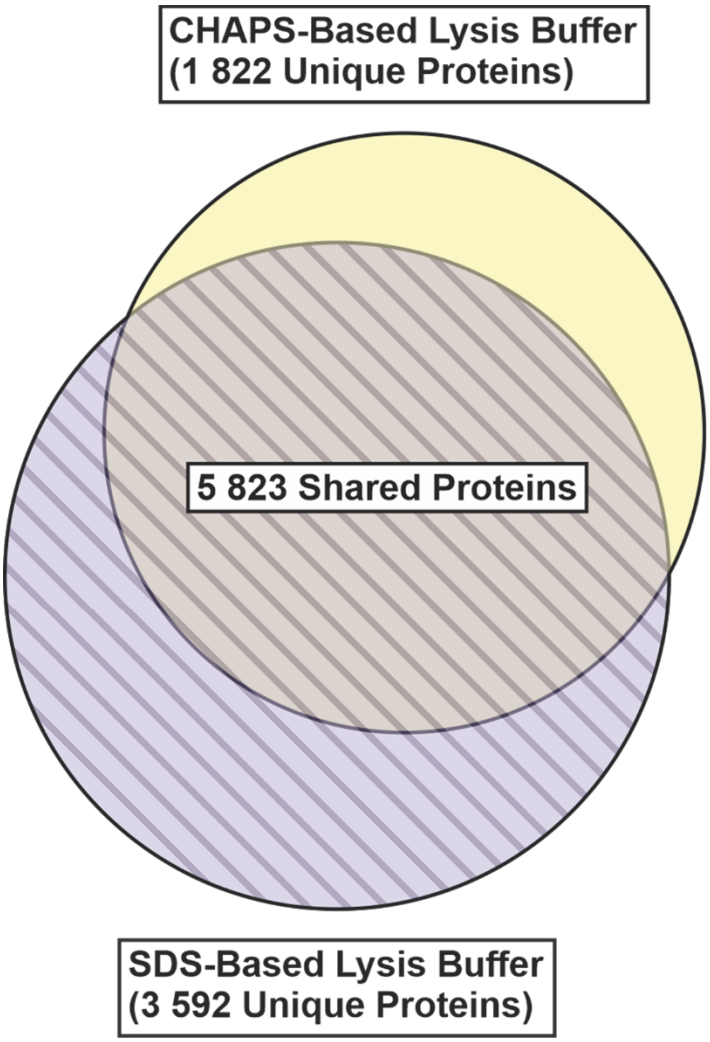

Figure 2.7 **Venn diagram showing the overlap of total proteins identified (independent of *p*-value or fold change) in N2 wildtype animals via DDA-MS subjected to lysis by either CHAPS- or SDS-based lysis buffer.** The total protein count includes single peptide IDs.

Proteins and their relative abundance were quantified between sample pairs – that is, each *chn-1*-null mutant was compared to N2 wild-type controls. Initial quality control analyses showed greater group separation between detergent conditions than between strains, as expected (Figure 2.8), and quantile normalized PCA scores for all strains under both detergent conditions showed principal components 1 and 2 being equal to 34.61% and 6.01% of the total variance, respectively (Figure 2.8A). Conversely, analyses performed on only SDS- (Figure 2.8B) or CHAPS/urea-processed (Figure 2.8C) samples showed principal components accounting for 9.95% to 16.94% of the total variance.

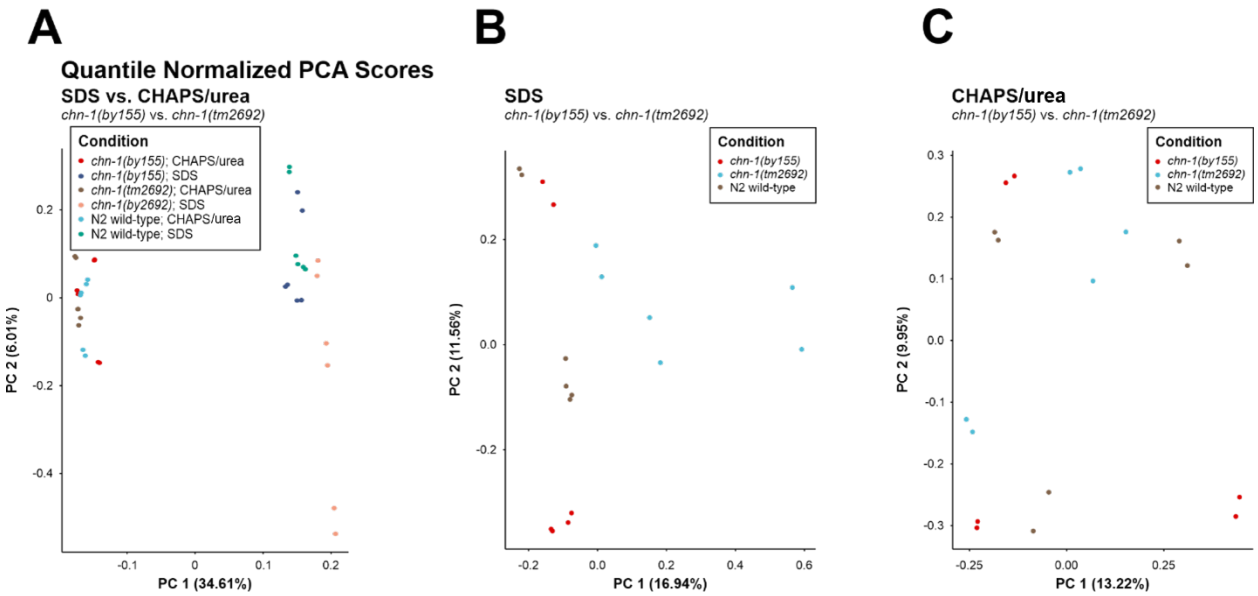

Figure 2.8 **PCA scores plots showing separation between both strains and detergent conditions.** Plots showing separation between (***A***) all samples belonging to both chn-1-null strains, wild-type controls, and CHAPS/urea as well as SDS detergent conditions, (***B***) samples processed only by SDS, and (***C***) samples processed only by CHAPS/urea. The x- and y-axes show principal components 1 and 2, respectively, with the percentages shown in brackets along each axis indicating the amount of data variance explained by that component.

The heatmap presented in Figure 2.9 depicts the relative fold changes of proteins altered in response to lysis procedure, providing a graphical representation of whether protein hits were under- or overexpressed across lysis conditions. The dendrogram to the left of the heat map illustrates the results of unsupervised hierarchical clustering analysis, which was able to group lysis conditions across strains, indicating that broadly, similarities in protein expression patterns due to lysis condition overshadowed differences across *chn-1(by155)* and *chn-1(tm2692) chn-1* deletion mutants.

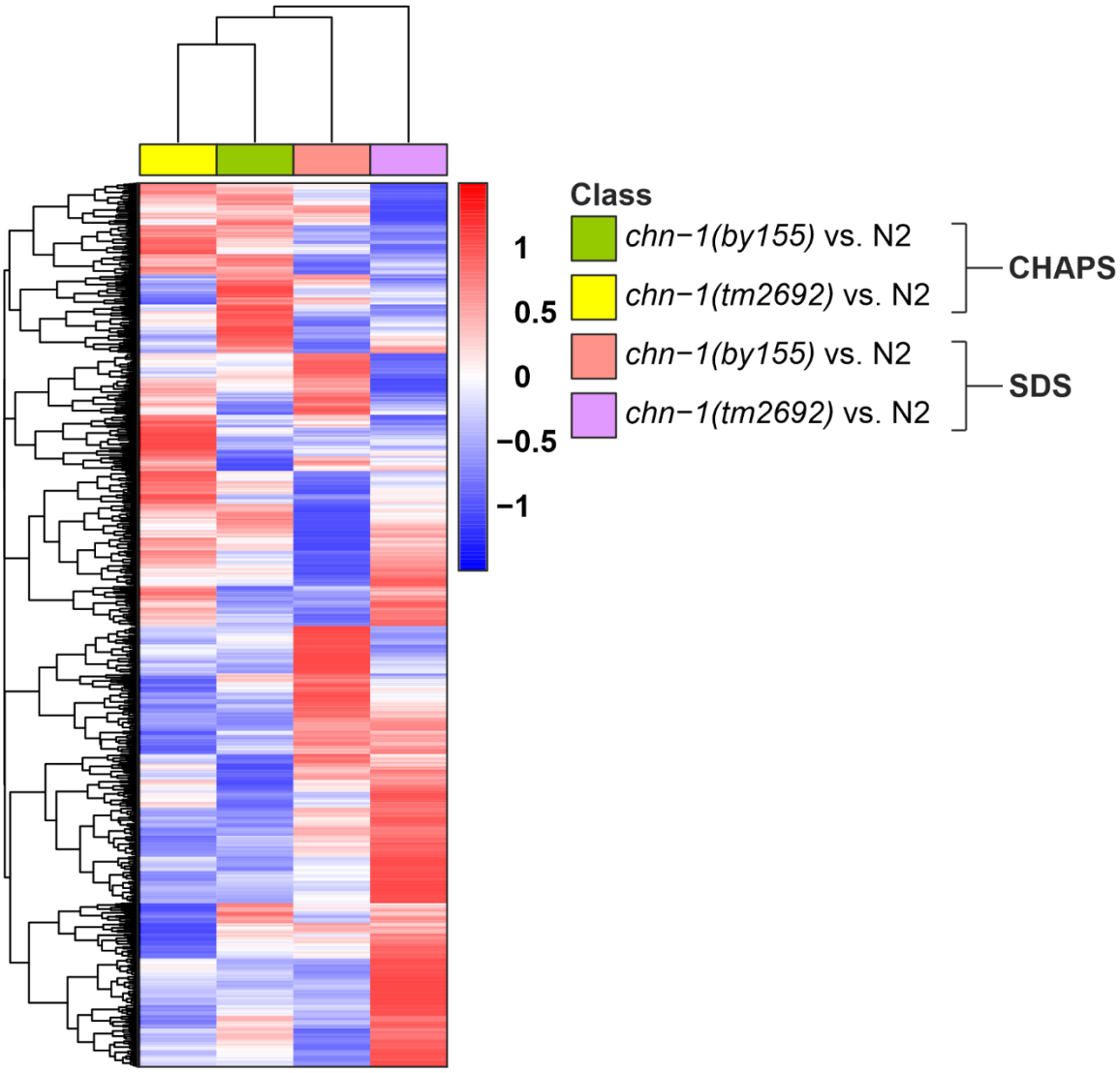

Figure 2.9 **Heatmap showing expression patterns of proteins identified by SWATH-MS across detergents.** Total proteins identified for *chn-1(by155)* (green and pink columns) or *chn-1(tm2692)* (yellow and purple columns) *C. elegans chn-1* mutants compared to wild-type N2 controls are shown. Each *chn-1* mutant was processed with either CHAPS/Urea- (green and yellow columns) or SDS-based (pink and purple columns) lysis buffer. Each row is a protein, with red indicating high expression and blue indicating low expression.

Volcano plots indicate which protein hits contributed most to the detergent-dependent variation observed in the heat map in N2 wild-type animals (Figure 2.10 and Tables 2.2-2.3), with Table 2.2 listing proteins that were most substantially overrepresented in CHAPS/Urea- compared to SDS-processed samples and Table 2.3 listing proteins that were most substantially underrepresented. Proteins most substantially overexpressed in N2 wild-type samples included suppressor of aph-1 and actin-1, with fold changes of 39.39 and 19.97, respectively (Figure 2.10 and Table 2.2). Proteins most substantially underexpressed in N2 wild-type samples included probable acyl-coenzyme A oxidase acox-1.5, peroxisomal membrane protein related, and acyl-coenzyme A oxidase acox-1.2, with fold changes of 0.06, 0.07, and 0.09, respectively (Figure 2.10 and Table 2.3). Recurring overexpressed proteins involved signaling proteins, including those related to Notch and Wnt signaling, as well as longevity and actin cytoskeleton regulation. Proteins related to peroxisomal function and biogenesis, including membrane proteins, were consistently underexpressed in CHAPS/Urea-compared to SDS-processed samples.

2.3.3 Lysis Procedure Alters Protein Landscape in a Detergent-Dependent Manner

A genome-wide network model of *C. elegans* protein expression was used to investigate protein sets altered as a result of lysis protocol (Figures 2.10-2.14 and Supplemental Figures A2-A7 as well as Tables 2.4-2.6 and Supplemental Tables A5-A10). In N2 wild-type animals, the CHAPS/Urea- compared to SDS-based lysis procedure significantly downregulated biological processes related to nucleosome assembly (FDR-adjusted $p < 0.001$) and rRNA processing (FDR-adjusted $p < 0.001$), as well as several processes pertaining to protein transport and membrane trafficking, including IRE1-mediated unfolded protein response (FDR-adjusted $p < 0.001$), intracellular protein transport (FDR-adjusted $p < 0.001$), protein transport (FDR-adjusted $p < 0.01$), vesicle-mediated transport (FDR-adjusted $p < 0.05$), ER to Golgi vesicle-mediated transport (FDR-adjusted $p < 0.05$), and endoplasmic reticulum unfolded protein response (FDR-adjusted $p < 0.05$) (Figure 2.11 and Table 2.4). Underexpressed GO terms related to cellular components included peroxisome (FDR-adjusted $p < 0.001$)

as well as a cluster of terms associated with cellular trafficking and transmembrane transport, including endoplasmic reticulum (FDR-adjusted $p < 0.001$), endoplasmic reticulum membrane (FDR-adjusted $p < 0.001$), endoplasmic reticulum lumen (FDR-adjusted $p < 0.01$), and endoplasmic reticulum-Golgi intermediate compartment (FDR-adjusted $p < 0.05$), mitochondrial inner membrane (FDR-adjusted $p < 0.001$), endomembrane system (FDR-adjusted $p < 0.01$), Golgi apparatus (FDR-adjusted $p < 0.01$), cytoplasmic vesicle (FDR-adjusted $p < 0.01$), mitochondrial outer membrane (FDR-adjusted $p < 0.05$), and membrane coat (FDR-adjusted $p < 0.05$) (Figure 2.11 and Table 2.4). Underexpressed molecular function GO terms included hydrolase activity (FDR-adjusted $p < 0.001$) and oxidoreductase activity (FDR-adjusted $p < 0.001$) (Figure 2.11 and Table 2.4).

The CHAPS/Urea- compared to SDS-based lysis procedure significantly upregulated N2 wild-type biological processes including cell cycle (FDR-adjusted $p < 0.001$), protein modification by small protein conjugation (FDR-adjusted $p < 0.05$), and gene silencing by RNA (FDR-adjusted $p < 0.05$) (Figure 2.12 and Table 2.5). Several overexpressed GO terms in N2 wild-type samples related to cellular components involved intermembrane spaces such as cytoplasm (FDR-adjusted $p < 0.001$), extracellular region (FDR-adjusted $p < 0.001$), and cytosol (FDR-adjusted $p < 0.001$) (Figure 2.12 and Table 2.5). While significantly enriched cellular component GO terms pertaining to intermembrane spaces were also found in the underexpressed wild-type dataset, these made up a substantially smaller subset of enriched terms, with 3 of 26 enriched underexpressed terms related to intermembrane spaces compared to 3 of 14 enriched overexpressed terms (Figure 2.10 and Supplemental Figure A2 as well as Tables 2.4-2.5). Overexpressed molecular function GO terms included nutrient reservoir activity (FDR-adjusted $p < 0.001$) and lipid transporter activity (FDR-adjusted $p < 0.001$) (Figure 2.12 and Table 2.5).

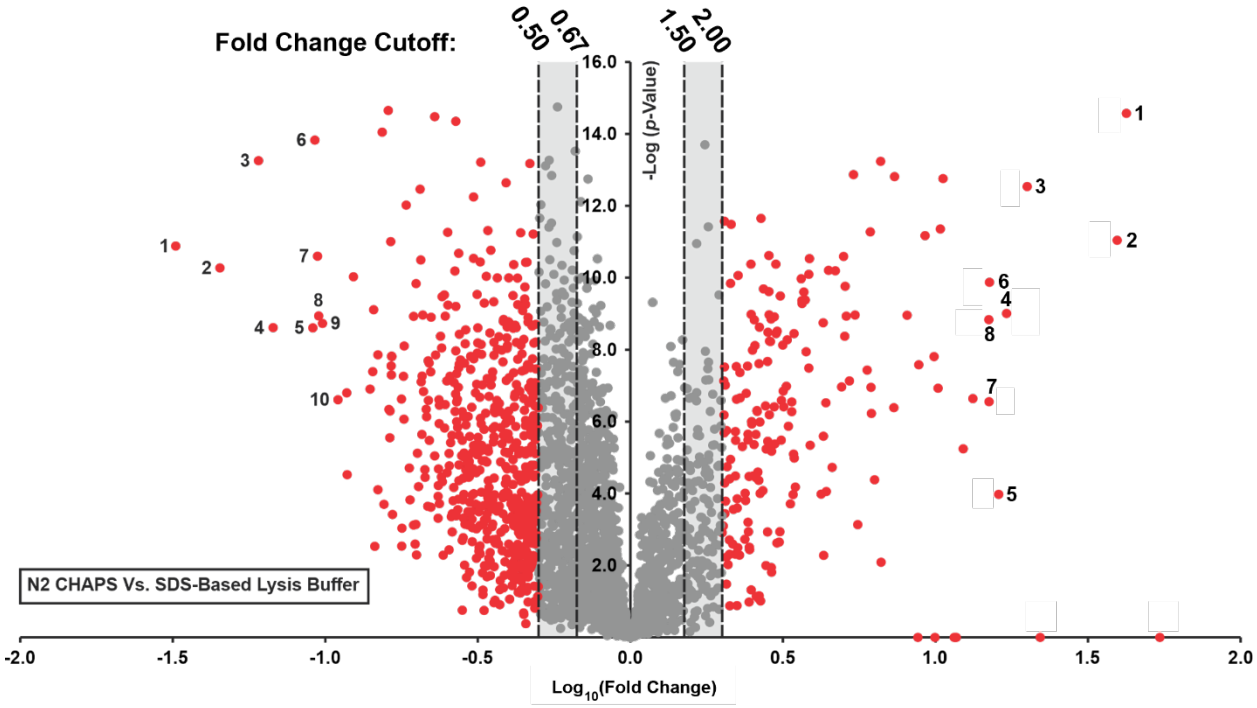

Figure 2.10 **Comparative SWATH-MS proteomic analyses of N2 wild-type *C. elegans* samples processed by lysis with CHAPS/Urea- vs. SDS-based lysis buffer.** Cut-off criteria (fold changes of ≤0.5 and ≥2 or ≤0.67 and ≥1.5) are represented by the dotted lines and shaded areas. Proteins (dots) that do not meet these fold change criteria are colour-coded in grey, while those that do are red. Over-represented proteins in the CHAPS/Urea-processed samples compared to SDS-processed samples have a positive log (fold change), while under-represented proteins have negative values. The top most over- and under-represented proteins that were significantly changed ($p < 0.05$, excluding $p=0$) are numbered and labeled in Tables 2.2 (upregulated proteins) and 2.3 (downregulated proteins).

Table 2.2 **Top proteins (based on fold change) identified by SWATH-MS that are over-represented in N2 wild-type *C. elegans* samples processed by lysis with CHAPS/urea- vs. SDS-based lysis buffer.**

Protein	Gene	*p*-Value	Fold Change	-Log (*p*-Value)	Log (Fold Change)	Regulation	Label
Ubiquitin-like protein 1-40S ribosomal protein S27a [Cleaved into: Ubiquitin-like protein 1; 40S ribosomal protein S27a]	*ubl-1*	2.66E-15	42.232	14.574	1.626	Up	1
Suppressor of aph-1	*sao-1*	9.11E-12	39.394	11.040	1.595	Up	2
Actin-1	*act-1*	2.91E-13	19.967	12.536	1.300	Up	3
SHNi-TPR domain-containing protein	*nasp-2*	9.85E-10	17.088	9.007	1.233	Up	4
FMRF-Like Peptide	*flp-28*	1.06E-04	16.106	3.975	1.207	Up	5
Cuticle collagen 49	*col-49*	1.33E-10	15.037	9.876	1.177	Up	6
Sperm-Specific family, class Q	*ssq-2*	2.81E-07	14.974	6.551	1.175	Up	7
Uncharacterized protein	*Y75B8A.13*	1.46E-09	14.945	8.834	1.175	Up	8

Table 2.3 **Top proteins (based on fold change) identified by SWATH-MS that are under-represented in N2 wild-type *C. elegans* samples processed by lysis with CHAPS/Urea- vs. SDS-based lysis buffer.**

Protein	Gene	*p*-Value	Fold Change	-Log (*p*-Value)	Log (Fold Change)	Label
Putative pterin-4-alpha-carbinolamine dehydratase (PHS) (EC 4.2.1.96) (4-alpha-hydroxy-tetrahydropterin dehydratase) (Pterin carbinolamine dehydratase) (PCD)	*pcbd-1*	1.32E-11	0.032	10.879	-1.490	1
Col_cuticle_N domain-containing protein	*col-97*	5.30E-11	0.045	10.276	-1.345	2
Probable acyl-coenzyme A oxidase acox-1.5 (AOX 1.5) (Acyl-CoA oxidase 1.5) (EC 1.3.3.-)	*acox-1.5*	5.53E-14	0.060	13.257	-1.219	3
Peroxisomal Membrane Protein related	*pmp-2*	2.44E-09	0.067	8.613	-1.171	4
Putative folylpolyglutamate synthase (EC 6.3.2.17) (Folylpoly-gamma-glutamate synthetase) (FPGS) (Tetrahydrofolylpolyglutamate synthase) (Tetrahydrofolate synthase)	*F25B5.6*	2.47E-09	0.091	8.607	-1.041	5
Col_cuticle_N domain-containing protein	*col-104*	1.49E-14	0.092	13.827	-1.035	6
Acyl-coenzyme A oxidase acox-1.2 (EC 1.3.3.-)	*acox-1.2*	2.50E-11	0.094	10.602	-1.026	7
Cuticle collagen dpy-13 (Protein dumpy-13)	*dpy-13*	1.15E-09	0.095	8.941	-1.022	8
Col_cuticle_N domain-containing protein	*bli-6*	1.87E-09	0.098	8.729	-1.009	9
Col_cuticle_N domain-containing protein	*col-175*	2.47E-07	0.110	6.608	-0.959	10

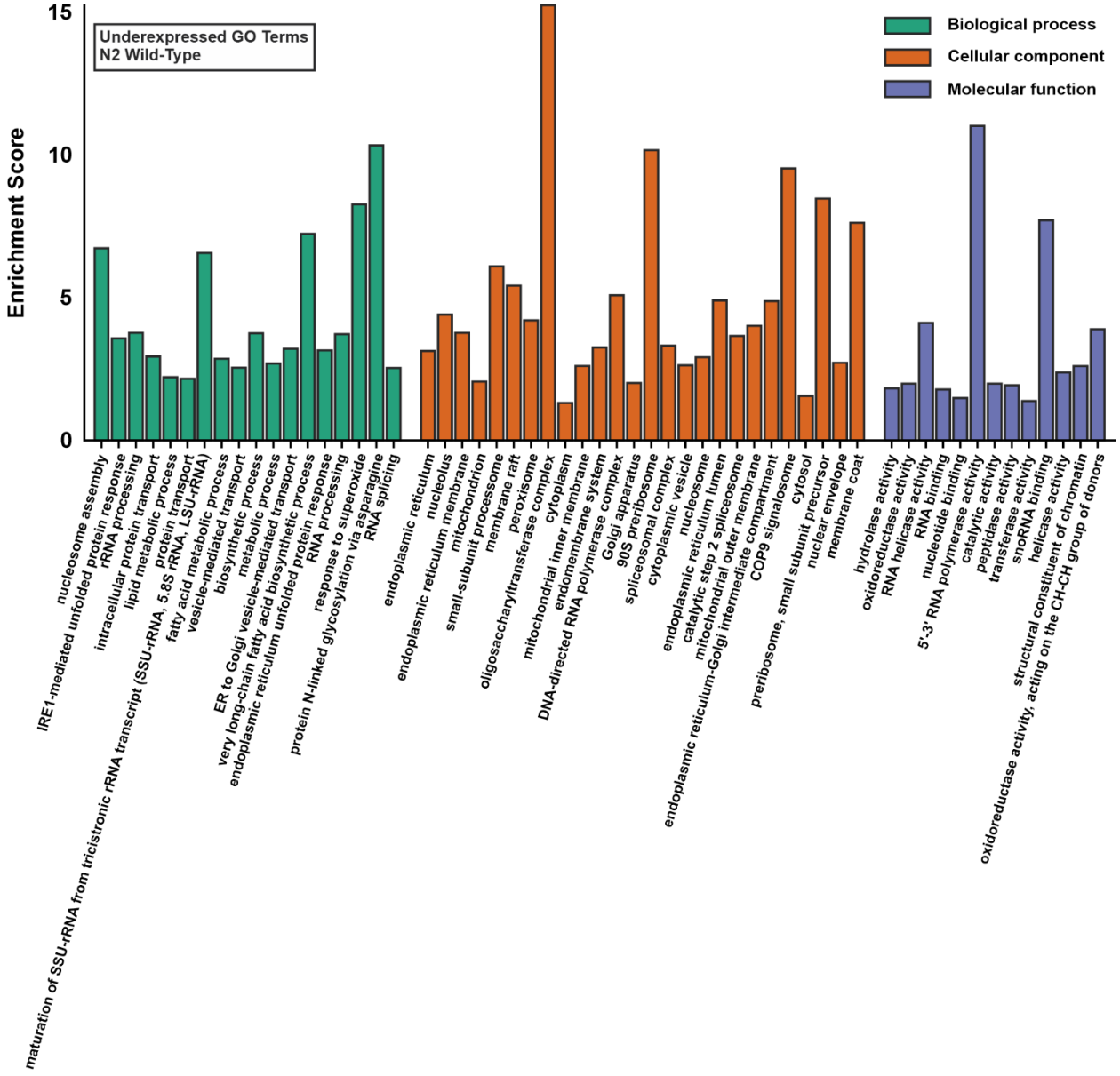

Figure 2.11 **GO enrichment analysis of the *C. elegans* N2 wild-type proteome of underexpressed proteins identified by SWATH-MS across lysis buffers.** The proteomic changes between N2 wild-type animals processed by either CHAPS/Urea- or SDS-based lysis buffer were analyzed by DAVID[346,351]. Significant GO terms (FDR-adjusted $p < 0.05$) were plotted by SRPlot. GO terms shown are related to biological processes, cellular components, and molecular functions, and each term is plotted based on fold enrichment. Only proteins that met the cut-off criteria (fold changes of ≤0.67) were used for the analysis. GO terms related to extraction buffer-dependent underexpressed proteins are listed in Table 2.4. Cross-strain comparisons indicating GO terms overrepresented in more than one strain are noted in Table 2.4 and illustrated in Figure 2.13.

Table 2.4 **N2 wild-type GO terms related to underexpressed proteins identified by SWATH-MS across lysis buffers.** Related to Figure 2.11. Biological process (BP), molecular function (MF) and cellular component (CC) GO terms identified (using DAVID) in N2 wild-type *C. elegans* animals when processed by CHAPS/urea-based lysis buffer compared to SDS-based lysis buffer. The number of associated genes ("count") and an association index (probability (raw and FDR-adjusted *p*-values) as well as enrichment score) for each GO term is included. Cross-strain comparisons were further performed using GO terms with FDR-adjusted $p < 0.05$ (Figure 2.13). † Indicates GO terms shared by two strains. ‡ Indicates GO terms shared by N2 wild-type, *chn-1(by155)*, and *chn-1(tm2692)* deletion mutants.

	GO Term	Count	Enrichment	*p*-Value	FDR-Adjusted *p*-Value
BP	nucleosome assembly†	19	6.729	2.08E-11	2.62E-08
BP	IRE1-mediated unfolded protein response‡	34	3.572	1.07E-10	6.76E-08
BP	rRNA processing‡	24	3.766	3.20E-08	1.34E-05
BP	intracellular protein transport‡	27	2.936	8.77E-07	2.76E-04
BP	lipid metabolic process‡	43	2.212	1.30E-06	3.29E-04
BP	protein transport‡	40	2.156	6.17E-06	1.30E-03
BP	maturation of SSU-rRNA from tricistronic rRNA transcript (SSU-rRNA, 5.8S rRNA, LSU-rRNA)‡	9	6.563	2.16E-05	3.89E-03
BP	fatty acid metabolic process‡	21	2.861	2.83E-05	4.45E-03
BP	vesicle-mediated transport	23	2.546	7.14E-05	1.00E-02
BP	biosynthetic process‡	13	3.748	1.02E-04	1.25E-02
BP	metabolic process‡	20	2.695	1.09E-04	1.25E-02
BP	ER to Golgi vesicle-mediated transport	15	3.206	1.54E-04	1.58E-02
BP	very long-chain fatty acid biosynthetic process	7	7.231	1.62E-04	1.58E-02
BP	endoplasmic reticulum unfolded protein response†	15	3.152	1.88E-04	1.69E-02
BP	RNA processing‡	12	3.719	2.28E-04	1.92E-02
BP	response to superoxide‡	6	8.264	3.21E-04	2.53E-02
BP	protein N-linked glycosylation via asparagine†	5	10.330	5.50E-04	3.96E-02

BP	RNA splicing†	18	2.536	5.65E-04	3.96E-02
CC	endoplasmic reticulum‡	84	3.131	3.46E-21	1.23E-18
CC	nucleolus‡	52	4.403	6.63E-20	8.61E-18
CC	endoplasmic reticulum membrane‡	62	3.765	7.25E-20	8.61E-18
CC	mitochondrion‡	89	2.059	6.88E-11	6.13E-09
CC	small-subunit processome‡	18	6.097	1.24E-09	8.84E-08
CC	membrane raft‡	16	5.420	8.37E-08	4.96E-06
CC	peroxisome‡	16	4.205	3.23E-06	1.64E-04
CC	oligosaccharyltransferase complex‡	6	15.243	6.78E-06	3.02E-04
CC	cytoplasm‡	209	1.308	1.09E-05	4.13E-04
CC	mitochondrial inner membrane‡	27	2.605	1.16E-05	4.13E-04
CC	endomembrane system‡	16	3.252	8.70E-05	2.59E-03
CC	DNA-directed RNA polymerase complex‡	10	5.081	8.72E-05	2.59E-03
CC	Golgi apparatus†	36	2.010	1.02E-04	2.79E-03
CC	90S preribosome‡	6	10.162	1.20E-04	3.00E-03
CC	spliceosomal complex†	15	3.314	1.26E-04	3.00E-03
CC	cytoplasmic vesicle†	20	2.628	1.81E-04	4.02E-03
CC	nucleosome†	17	2.912	1.92E-04	4.02E-03
CC	endoplasmic reticulum lumen‡	9	4.899	3.14E-04	5.90E-03
CC	catalytic step 2 spliceosome‡	12	3.658	3.15E-04	5.90E-03
CC	mitochondrial outer membrane†	10	4.011	6.18E-04	1.10E-02
CC	endoplasmic reticulum-Golgi intermediate compartment‡	8	4.878	8.56E-04	1.45E-02
CC	COP9 signalosome‡	5	9.527	1.04E-03	1.68E-02
CC	cytosol‡	54	1.553	1.30E-03	2.01E-02
CC	preribosome, small subunit precursor‡	5	8.468	1.77E-03	2.62E-02

CC	nuclear envelope†	13	2.714	2.62E-03	3.73E-02
CC	membrane coat	5	7.621	2.79E-03	3.82E-02
MF	hydrolase activity‡	128	1.823	6.97E-12	4.62E-09
MF	oxidoreductase activity‡	70	1.985	3.26E-08	1.08E-05
MF	RNA helicase activity‡	16	4.111	3.40E-06	7.23E-04
MF	RNA binding‡	66	1.781	4.36E-06	7.23E-04
MF	nucleotide binding‡	117	1.481	8.21E-06	1.09E-03
MF	5'-3' RNA polymerase activity‡	6	11.013	5.15E-05	5.70E-03
MF	catalytic activity‡	38	1.985	7.17E-05	6.79E-03
MF	peptidase activity‡	38	1.930	1.30E-04	1.08E-02
MF	transferase activity‡	111	1.377	3.23E-04	2.38E-02
MF	snoRNA binding†	6	7.709	5.07E-04	3.36E-02
MF	helicase activity‡	20	2.379	5.96E-04	3.54E-02
MF	structural constituent of chromatin	17	2.600	6.46E-04	3.54E-02
MF	oxidoreductase activity, acting on the CH-CH group of donors	10	3.893	6.94E-04	3.54E-02

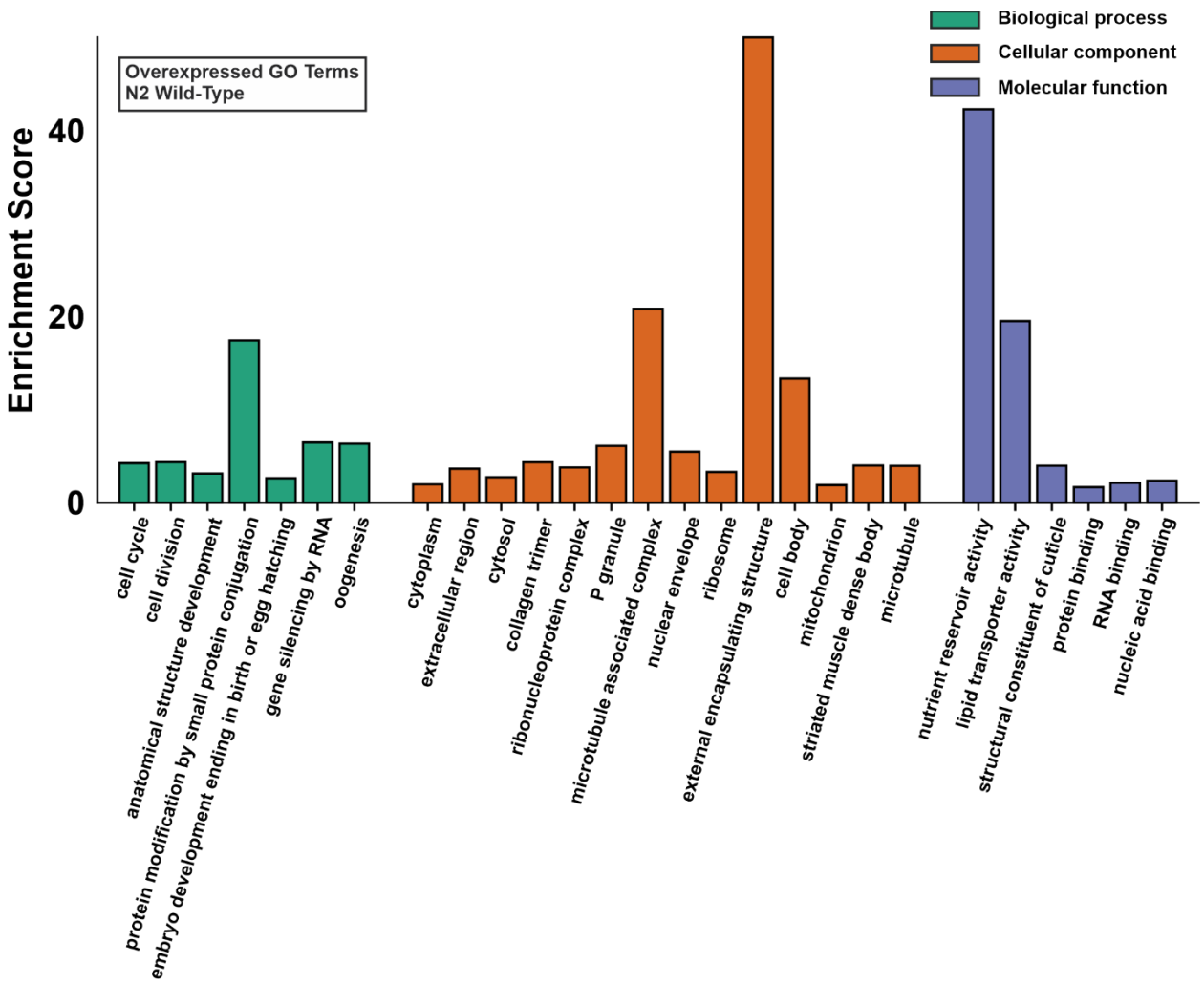

Figure 2.12 **GO enrichment analysis of the *C. elegans* N2 wild-type proteome of overexpressed proteins identified by SWATH-MS across lysis buffers.** The proteomic changes between N2 wild-type animals processed by either CHAPS/Urea- or SDS-based lysis buffer were analyzed by DAVID. Significant GO terms (FDR-adjusted $p < 0.05$) were plotted by SRPlot. GO terms shown are related to biological processes, cellular components, and molecular functions, and each term is plotted based on fold enrichment. Only proteins that met the cut-off criteria (fold changes of ≥1.5) were used for the analysis. GO terms related to extraction buffer-dependent overexpressed proteins are listed in Table 2.5. Cross-strain comparisons indicating GO terms overrepresented in more than one strain are noted in Table 2.5 and illustrated in Figure 2.13.

Table 2.5 **N2 wild-type GO terms related to overexpressed proteins identified by SWATH-MS across lysis buffers.** Related to Figure 2.12. Biological process (BP), molecular function (MF) and cellular component (CC) terms identified in N2 wild-type *C. elegans* animals when processed by CHAPS/urea-based lysis buffer compared to SDS-based lysis buffer. The number of associated genes ("count") and an association index (probability (raw & FDR-adjusted *p*-values) as well as enrichment score) for each term is included. Cross-strain comparisons were further performed using terms with FDR-adjusted $p < 0.05$ (Figure 2.13). † Indicates terms shared by two strains. ‡ Indicates terms shared by N2 wild-type, *chn-1(by155)*, and *chn-1(tm2692)* deletion mutants.

	GO Term	Count	Enrichment	*p*-Value	FDR-Adjusted *p*-Value
BP	cell cycle†	18	4.252	1.02E-06	4.76E-04
BP	cell division†	15	4.361	8.05E-06	1.88E-03
BP	anatomical structure development‡	18	3.128	6.00E-05	9.36E-03
BP	protein modification by small protein conjugation†	5	17.446	1.38E-04	1.62E-02
BP	embryo development ending in birth or egg hatching†	18	2.642	4.54E-04	4.25E-02
BP	gene silencing by RNA	7	6.480	6.63E-04	4.95E-02
BP	Oogenesis	7	6.350	7.40E-04	4.95E-02
CC	cytoplasm‡	96	1.973	3.87E-12	6.62E-10
CC	extracellular region‡	32	3.656	7.66E-10	6.55E-08
CC	cytosol‡	29	2.738	2.36E-06	1.34E-04
CC	collagen trimer‡	16	4.351	4.01E-06	1.71E-04
CC	ribonucleoprotein complex‡	17	3.798	1.04E-05	3.29E-04
CC	P granule‡	11	6.116	1.15E-05	3.29E-04
CC	microtubule associated complex	5	20.850	6.69E-05	1.63E-03
CC	nuclear envelope	8	5.484	6.06E-04	1.30E-02
CC	ribosome‡	12	3.299	1.04E-03	1.98E-02
CC	external encapsulating structure†	3	50.040	1.17E-03	2.00E-02
CC	cell body‡	4	13.344	2.97E-03	4.40E-02
CC	mitochondrion†	25	1.898	3.09E-03	4.40E-02
CC	striated muscle dense body	8	4.003	3.79E-03	4.89E-02
CC	Microtubule	8	3.964	4.00E-03	4.89E-02
MF	nutrient reservoir activity‡	6	42.310	4.07E-08	9.73E-06
MF	lipid transporter activity‡	6	19.528	7.63E-06	8.67E-04
MF	structural constituent of cuticle‡	16	3.982	1.09E-05	8.67E-04
MF	protein binding†	46	1.673	4.75E-04	2.84E-02
MF	RNA binding†	24	2.133	8.21E-04	3.92E-02
MF	nucleic acid binding†	19	2.378	1.03E-03	4.11E-02

The Venn diagrams below illustrate the between-strain overlap of GO terms significantly enriched as a function of lysis condition (Figure 2.13). Comparing CHAPS/Urea- to SDS-processed samples, underexpressed terms outnumbered overexpressed terms across all strains *C. elegans* strains, with 57 enriched underexpressed terms compared to 27 enriched overexpressed terms in N2 wild-type samples, 55 enriched underexpressed terms compared to 17 enriched overexpressed terms in *chn-1(by155)* mutants, and 57 enriched underexpressed terms compared to 35 enriched overexpressed terms in *chn-1(tm2692)* mutants. That is, 67.9% of all significantly enriched terms in N2 wild-type samples, 76.4% of all significantly enriched terms in *chn-1(by155)* animals, and 62.0% of all significantly enriched terms in *chn-1(tm2692)* animals were underexpressed (Figure 2.13).

Within comparisons pertaining to biological processes, cellular components, and molecular functions, the vast majority of significantly enriched terms were shared by more than one strain, with most shared by all three strains (Figure 2.13 as well as Tables 2.4-2.5 and Supplemental Tables A5-A8). In N2 wild-type animals, of 57 enriched underexpressed terms, 40 (70.2%) were found also significantly underexpressed in both deletion mutants, and 11 (19.3%) were shared with either *chn-1(by155)* or *chn-1(tm2692)* mutants, leaving only 6 (10.5%) underexpressed terms unique to wild-type animals (Figure 2.13 and Table 2.4). Of 27 enriched overexpressed terms, 12 (44.4%) are shared with both deletion mutants and 9 (33.3%) are shared with one (Figure 2.13 and Table 2.5). This same trend is seen in *chn-1(by155)* mutants, which share 52 of 72 (72.2%) enriched terms with both N2 wild-type and *chn-1(tm2692)* animals and 9 (12.5%) with one other strain, as well as in *chn-1(tm2692)* mutants, which share 52 of 92 (56.5%) enriched terms with both N2 wild-type and *chn-1(by155)* animals and 19 (20.7%) with one other strain (Figure 2.13 and Tables 2.4-2.5 and Supplemental Tables A5-A8).

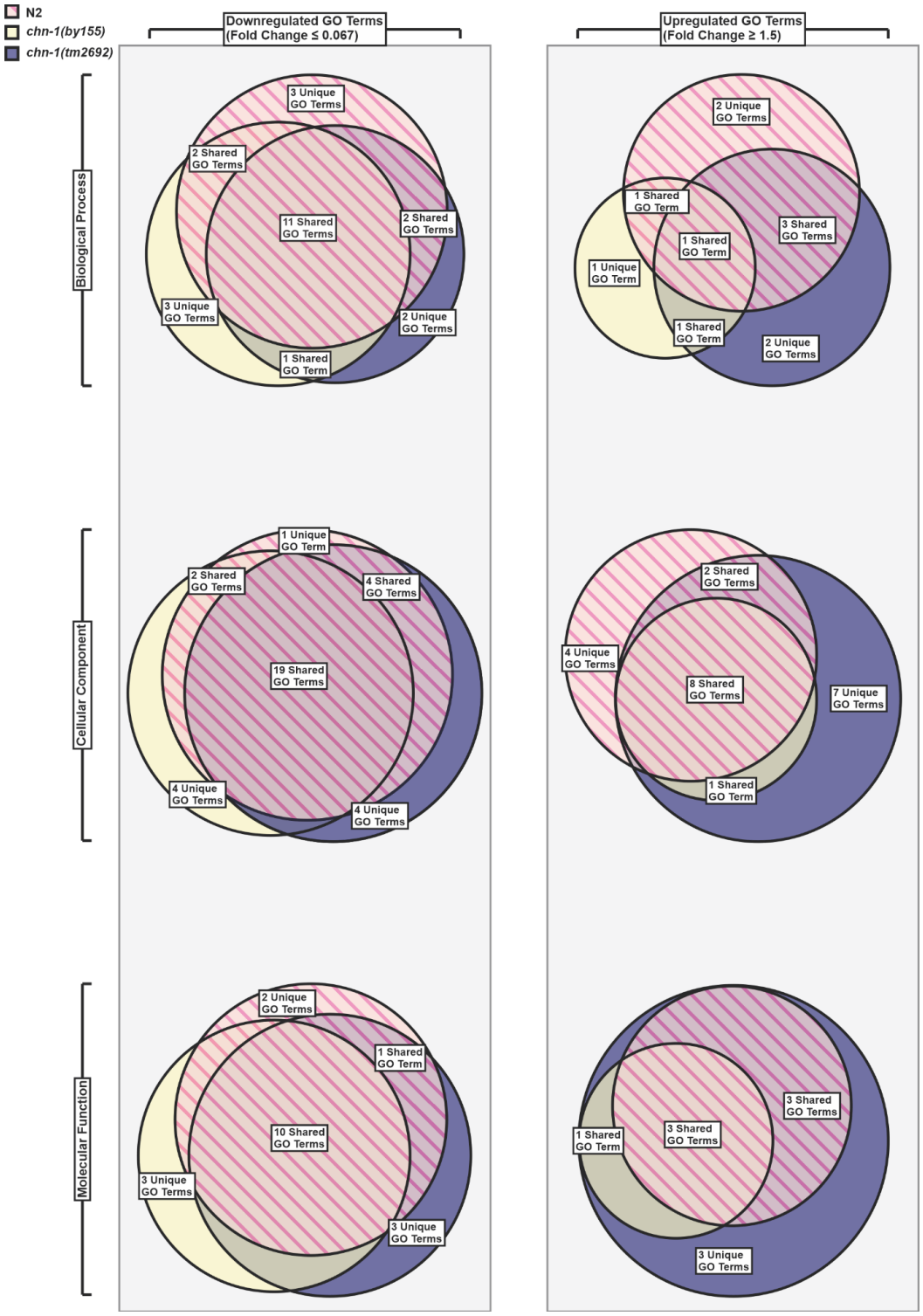

Figure 2.13 **Venn diagrams showing overlap of GO terms substantially altered by SWATH-MS across *C. elegans chn-1* mutants.** Related to Figures 2.11-2.12 and Supplemental Figures A4-A7 as well as Tables 2.4-2.5 and Supplemental Tables A5-A8. Cross-strain comparisons were made using GO terms (FDR-adjusted $p < 0.05$) that were underexpressed (left) or overexpressed (right) in a detergent-dependent manner.

KEGG pathway topology analyses in wild-type worms revealed significant effects on metabolic pathways ($p < 0.001$) and peroxisome ($p < 0.001$) (Figure 2.14 and Table 2.6). Several pathways related to membrane-associated and vesicular trafficking were also underexpressed in wild-type animals, including protein processing in endoplasmic reticulum ($p < 0.001$), protein export ($p < 0.01$), ABC transporters ($p < 0.05$) and endocytosis ($p < 0.05$) (Figure 2.14 and Table 2.6). Longevity regulating pathway was also underexpressed, although this only approached significance ($p = 0.072$) (Figure 2.14 and Table 2.6). Enriched overexpressed pathways included oxidative phosphorylation ($p < 0.001$), DNA replication ($p < 0.01$), ribosome ($p < 0.01$), ubiquitin mediated proteolysis ($p < 0.01$), and phagosome ($p < 0.05$) (Figure 2.14 and Table 2.6).

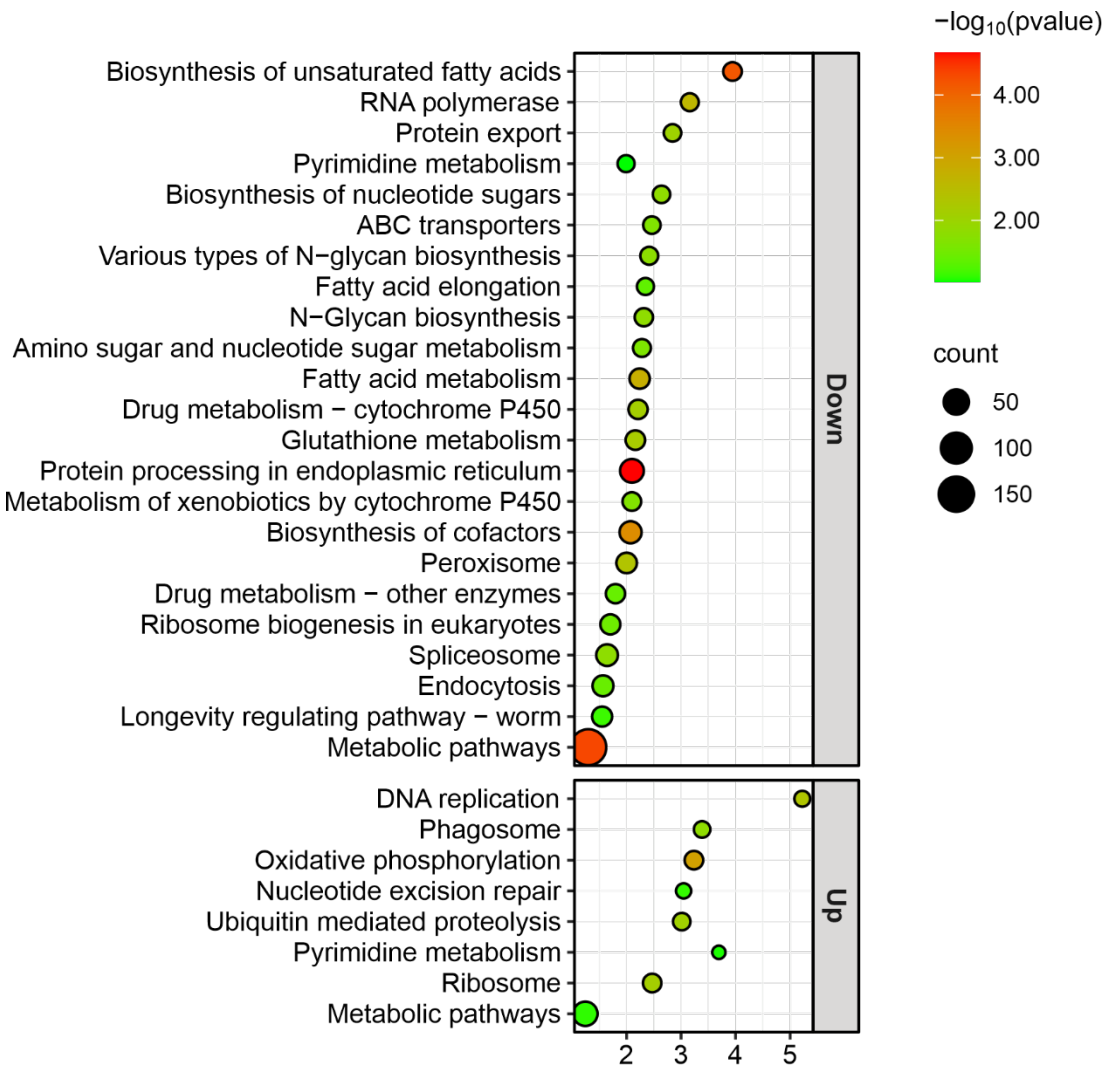

Figure 2.14 **KEGG pathway analysis derived from the N2 wild-type proteomics of our *C. elegans* model.** SWATH-MS data comparing samples processed with either CHAPS/Urea- or SDS-based lysis buffer was analysed using DAVID and plotted by SRPlot. Only proteins that met the cut-off criteria (fold changes of ≤0.67 and ≥1.5) were used for the analysis. Each pathway is colour-coded based on statistical significance (–log10(*p*-value)). Pathways related to *chn-1* loss-of-function are listed in Table 2.6. Cross-strain comparisons indicating pathways overrepresented in more than one strain are noted in Table 2.6 and illustrated in Figure 2.15.

Table 2.6 **KEGG pathways related to substantially altered proteins identified by SWATH-MS across lysis buffers in N2 wild-type animals.** Related to Supplemental Figure A6 and Figure 2.14. Pathways identified in N2 wild-type *C. elegans* animals when processed by CHAPS/urea-based lysis buffer compared to SDS-based lysis buffer. The number of associated genes ("count") and an association index (probability (raw *p*-values) as well as enrichment score) for each pathway is included. Cross-strain comparisons were further performed. † Indicates pathways shared by two strains. ‡ Indicates pathways shared by N2 wild-type, *chn-1(by155)*, and *chn-1(tm2692)* deletion mutants.

Pathway	Count	Enrichment	*p*-Value	Regulation
Protein processing in endoplasmic reticulum‡	35	2.099	2.11E-05	Down
Metabolic pathways‡	151	1.299	4.57E-05	Down
Biosynthesis of unsaturated fatty acids‡	12	3.943	6.69E-05	Down
Biosynthesis of cofactors‡	26	2.074	3.92E-04	Down
Fatty acid metabolism‡	18	2.240	1.67E-03	Down
RNA polymerase‡	10	3.159	2.45E-03	Down
Peroxisome‡	19	2.001	4.57E-03	Down
Glutathione metabolism‡	15	2.162	6.66E-03	Down
Drug metabolism - cytochrome P450‡	14	2.212	7.53E-03	Down
Protein export†	9	2.844	9.44E-03	Down
Biosynthesis of nucleotide sugars‡	9	2.640	1.51E-02	Down
N-Glycan biosynthesis‡	11	2.317	1.52E-02	Down
Spliceosome‡	24	1.643	1.57E-02	Down
Various types of N-glycan biosynthesis‡	10	2.416	1.70E-02	Down
Metabolism of xenobiotics by cytochrome P450‡	12	2.097	2.20E-02	Down
ABC transporters‡	9	2.464	2.29E-02	Down
Amino sugar and nucleotide sugar metabolism†	10	2.282	2.45E-02	Down
Ribosome biogenesis in eukaryotes‡	17	1.703	3.46E-02	Down
Endocytosis†	21	1.568	3.92E-02	Down
Drug metabolism - other enzymes‡	14	1.797	4.04E-02	Down
Fatty acid elongation	8	2.347	4.52E-02	Down
Longevity regulating pathway - worm†	17	1.552	7.23E-02	Down
Pyrimidine metabolism†	8	1.991	9.65E-02	Down
Oxidative phosphorylation‡	12	3.235	9.09E-04	Up
DNA replication	6	5.223	4.91E-03	Up
Ribosome‡	12	2.470	7.72E-03	Up
Ubiquitin mediated proteolysis†	9	3.013	8.63E-03	Up
Phagosome‡	7	3.385	1.54E-02	Up
Nucleotide excision repair	5	3.047	7.75E-02	Up
Metabolic pathways‡	39	1.244	8.05E-02	Up
Pyrimidine metabolism	4	3.693	9.01E-02	Up

Enriched pathways overlapping between N2 wild-type, *chn-1(by155)* and *chn-1(tm2692)* deletion mutants as a function of lysis procedure are illustrated in the Venn diagrams below (Figure 2.15). Comparing CHAPS/Urea- to SDS- processed samples, underexpressed pathways outnumbered overexpressed pathways across all strains, with 23 enriched pathways compared to 8 enriched pathways in N2 wild-type samples (74.2% of enriched pathways being underexpressed), 25 enriched pathways compared to 6 enriched pathways in *chn-1(by155)* mutants (80.6% of enriched pathways being underexpressed), and 22 enriched pathways compared to 9 enriched pathways in *chn-1(tm2692)* mutants (71.0% of enriched pathways being underexpressed) (Figure 2.15). Most enriched pathways were shared by at least two strains (Figure 2.15 as well as Table 2.6 and Supplemental Tables A9-A10). Of all underexpressed pathways enriched in wild-type animals, 17 (73.9%) were also underexpressed in *chn-1(by155)* and *chn-1(tm2692)* mutants, and a further 5 (21.7%) were shared with either *chn-1(by155)* or *chn-1(tm2692)* mutants, leaving only one (4.3%) underexpressed pathway unique to wild-type animals (Figure 2.15 and Table 2.6). Of 8 enriched overexpressed pathways, 4 (50.0%) were overexpressed in all strains and one (12.5%) was common to *chn-1(by155)* mutants, leaving only 3 (37.5%) uniquely overexpressed in wild-type animals (Figure 2.15 and Table 2.6). This also occurs in *chn-1(by155)* mutants, which share 21 of 31 (67.7%) of enriched pathways with both wild-type and *chn-1(tm2692)* mutants and 6 (19.4%) with one other strain, as well as in *chn-1(tm2692)* mutants, which share 21 of 31 (67.7%) of enriched pathways with both wild-type and *chn-1(by155)* animals and 4 (12.9%) with one other strain (Figure 2.15, Table 2.6, and Supplemental Tables A9 and A10).

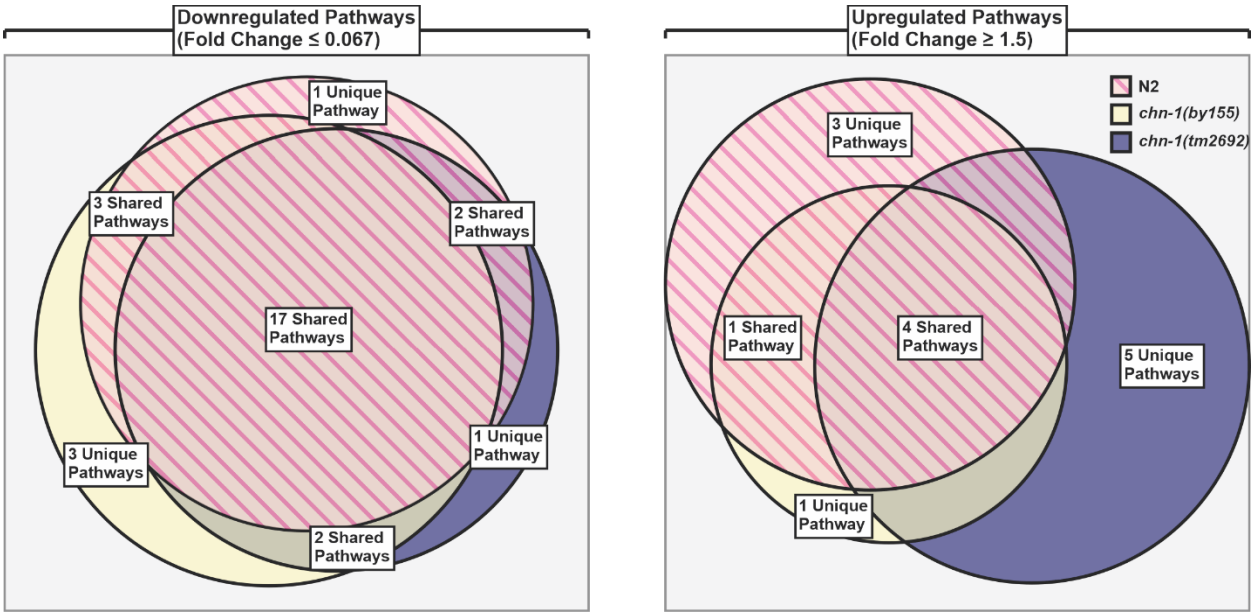

Figure 2.15 **Venn diagrams showing overlap of KEGG pathways substantially altered by SWATH-MS across *C. elegans chn-1* mutants.** Related to Figure 2.14 and Supplemental Figures A8-A9 as well as Table 2.6 and Supplemental Tables A9-A10. Cross-strain comparisons were made using pathways ($p < 0.05$) that were underexpressed (left) or overexpressed (right) in a detergent-dependent manner.

2.4 Discussion

Proteomics is a powerful research approach for untangling the mechanistic underpinnings underlying both healthy and pathological aging. Accordingly, myriad extraction protocols have been developed to facilitate protein isolation for further study. As a genetically tractable model for aging, proteomics experiments in *C. elegans* have been especially valuable in teasing apart molecular pathways associated with aging. Few studies, however, have compared extraction procedures within a single experiment. Here, methodological triangulation in the form of two protein extraction approaches were used to compare the effects of CHAPS/Urea- versus SDS-based sample lysis in *chn-1* wild-type animals (Chapter 2) as well as two *chn-1* deletion mutants, *chn-1(by155)* and *chn-1(tm2692)* (Appendix A).

Initial proteomic experiments showed a large unidentified peak in the TIC chromatogram (Figure 2.2) likely due to contamination (e.g., solvent (i.e., DMSO)/reagent contaminants, plasticizers such as phthalates leached from plastic labware, inadequately removed detergents (i.e., SDS) or surfactants/buffer components, sample carry over due to inadequate cleaning between runs, or matrix effects from proteins or other biological components remaining from prior injections). SDS, in particular, can interfere with trypsin digestion and subsequent MS analyses; for this reason, experiments were repeated with both SDS and CHAPS-based processing of samples, both to (1) rule out the presence of SDS as a source of contamination, and (2) to act as a methodological study assessing the protein extraction capabilities of SDS vs. CHAPS in *C. elegans*. Given that repeating the experiment with new MS-grade reagents eliminated the large unidentified peak in SDS-processed samples, however, its presence was likely due to reagent contaminants (i.e., traces of other lab reagents present during sample lysis and preparation).

Preliminary analyses found that, despite unsupervised hierarchical clustering analysis correctly grouping experimental lysis conditions across strains, there was no trend in the proportion of all substantially altered proteins that were either uniquely under- or overexpressed in CHAPS/Urea- and SDS-processed samples between the two *chn-1*-deletion mutants. That is, SDS-processed samples did not consistently have a greater or lesser proportion of proteins substantially altered compared to CHAPS-

processed samples between the two *chn-1*-null mutants (*chn-1(by155)*, underexpressed:12.9% CHAPS/Urea, 17.1% SDS; *chn-1(by155)*, overexpressed: 12.2% CHAPS/Urea, 27.6% SDS; *chn-1(tm2692)*, underexpressed: 20.1% CHAPS/Urea, 10.9% SDS; *chn-1(tm2692)*, overexpressed: 22.8% CHAPS/Urea, 21.0% SDS) (Appendix A). Despite correctly grouping experimental lysis conditions across strains, unsupervised hierarchical clustering analysis found larger differences in protein expression between the two mutant strains lysed by SDS than those processed by CHAPS (Figure 2.9). This is possibly due to SDS extracting a broader diversity of proteins more generally, and this potentially resulting in more variability between *chn-1*-null strains, whereas CHAPS preferentially solubilized proteins in a subcellular localization-dependent manner, possibly resulting in less variability between the two mutants (Figure 2.9).

Individual differentially-expressed proteins in both CHAPS/urea and SDS-processed samples encompassed both membrane-associated and cytosolic subcellular localization. CHAPS, a zwitterionic, non-denaturing detergent, features a high membrane and membrane-bound protein extraction efficiency. However, and perhaps counterintuitively, it exhibits poor extractability of hydrophobic and high molecular weight proteins[352] due to the relatively small size of its own hydrophobic regions[334]. Indeed, extraction experiments exploring CHAPS-membrane interactions in erythrocytes suggest that CHAPS fails to penetrate the lipid bilayer and instead binds in a flat orientation on the cell surface[353]. The CHAPS-associated preferential extraction of superficial membrane proteins suggests that ideal extraction conditions may be achieved by the addition of a chaotropic agent to the lysis buffer to further disrupt hydrophobic interactions within a polypeptide chain or between protein complex subunits[354]. To this end, the addition of urea, a hydrophilic denaturant acting to disrupt hydrophobic and intraprotein interactions[336,355], may allow for deeper membrane penetration and the extraction of a wider range of membrane proteins and molecular protein weights than CHAPS alone.

Conversely, SDS, a potent, highly-denaturing anionic detergent, is particularly effective in solubilizing membrane proteins due to its dissociation of lipid membranes and subsequent denaturation and solubilization of membrane proteins, as well as other

misfolded, precipitated, or hydrophobic proteins[356-358]. Broadly, it is the most effective additive for the promotion and maintenance of global protein solubility[321], offers unprecedented proteome coverage[359], and even functions to prevent protein adsorption onto container surfaces[360]. Indeed, as an amphipathic synthetic surfactant, high SDS concentrations (i.e., between 1 and 4%) enhance protein extraction and solubilization from cell lysates[359,361-365]. The limited evidence surrounding protein extractability in *C. elegans* lysates, however, is less clear. While SDS remains the standard for protein solubilization of whole animal lysates, the solubilization of the global nematode proteome by urea in combination with NP-40, a relatively non-denaturing, mild non-ionic[366] detergent, caused a more thorough lysis than the SDS-based method[367]. The SDS-based reagent led to the rapid disintegration of the cuticle, thus releasing any still-unaffected tissue fragments into the surrounding medium, while the Urea/NP-40-solubilized animals would gradually lose all opacity, indicating a prolonged dissolution process. Perhaps counterintuitively, the cuticles were sufficiently permeable to allow for urea/NP-40-facilitated internal solubilization, thus enabling a more comprehensive extraction procedure than was found in SDS-processed animals[367]. Nevertheless, SDS has been distinguished as the 'universal' technique for proteome characterization, as demonstrated by Wisniewski et al.'s FASP procedure[359].

Despite these advantages, SDS-based solubilization produces several difficulties when used in MS-based proteomic approaches. Firstly, given its protein-denaturing activities, SDS is an inappropriate choice of detergent for the extraction of native soluble proteins and protein complexes. Furthermore, when purifying membrane proteins, the use of membrane spanning domain-stabilizing detergents, such as CHAPS, is essential. Indeed, SDS processing often destroys the extracellular domain structure of membrane proteins[368]. Finally, with few exceptions – namely, at very low concentrations in electrospray ionization-MS[369] or higher concentrations in matrix-assisted laser desorption/ionization-MS[369,370] – SDS suppresses peptide and protein signals. Further to this, SDS is notoriously difficult to deplete[371,372], leading many to avoid its use entirely.

Compared to SDS, samples processed by CHAPS/urea showed altered specificity for protein solubilization in a subcellular localization-dependent manner.

Specifically, top cellular compartments underexpressed in CHAPS/urea versus SDS-processed animals across all strains analyzed included the nucleolus as well as several membrane-dominant organelles, such as the endoplasmic reticulum, endoplasmic reticulum membrane, mitochondria, and mitochondrial inner membrane. Conversely, overexpressed cellular compartments in CHAPS/urea-processed samples included signaling-related terms such as extracellular response, cytoplasmic terms such as cytoplasm and cytosol, and protein complexes such as P granule. Pathways differentially expressed across wild-type animals and *chn-1*-null mutants also included ribosomal and membrane/vesicle-associated processes, including protein processing in endoplasmic reticulum, endocytosis, RNA polymerase, and ribosome biogenesis in eukaryotes.

Although CHAPS and urea efficiently solubilize membrane-associated proteins – with a particular affinity for superficial membrane proteins, in the case of the former – SDS tends to be broadly more effective at global protein extraction, including that of membrane proteins[356,358]. As such, it is possible that animals having undergone CHAPS/urea-based lysis were characterized by solubilized proteins belonging to a targeted class of superficial membrane proteins, while those having undergone SDS-based lysis were characterized by a broader range of transmembrane proteins. Thus, the far-reaching solubilization behaviour of SDS may have resulted in greater membrane-associated protein coverage than the preferential extraction of superficial membrane proteins in CHAPS-processed samples combined with the broader, chaotropic-induced protein solubilization effect of the urea additive.

SDS has previously been found to preferentially enrich basic proteins, such as ribosomal and ribonuclear proteins[373]. For instance, liquid-liquid extraction experiments have shown that proteins exclusively identified following an SDS solubilization procedure exhibited a shift toward higher, more basic isoelectric points, possibly due to the anionic properties of its sulfate group (Figure 2.16)[373]. Conversely, CHAPS and urea are zwitterionic and non-ionic, respectively, and thus may have preferentially solubilized proteins with domains exhibiting non-ionic/zwitterionic-like properties.

These experiments have far-reaching implications for the field of proteomics, and indeed for any techniques utilizing protein extraction more generally. Through its critical

role in maintaining protein homeostasis, CHIP has been found to exert its neuroprotective influence on processes centred around genome stability – for instance, by its interaction with the tumour suppressor protein p53[374-377] – as well as mitochondrial integrity[268,378], the oxidative stress response[379,380], endoplasmic reticulum-associated degradation pathway regulation[267,381,382], protein trafficking[280,383], neuronal cell membrane integrity[8], and the top-down regulation of epigenetic mechanisms such as histone deacetylation[384,385]. Many of the individual proteins, altered gene ontology terms, and enriched pathways found across *chn-1*-null and wild-type strains were directly related to these activities. Differentially expressed proteins in response to detergent exposure included several involved in actin cytoskeleton organization, peroxisomal function and biogenesis, as well as those related to protein quality control. Enriched gene ontology terms shared across strains included biological processes associated with the ER stress response, RNA processing, metabolism, and protein transport, as well as molecular functions including RNA binding and helicase activity, oxidoreductase activity, peptidase activity, and transferase activity. Finally, pathways altered across strains included those related to ER-associated protein processing, metabolism, endocytosis, ribosome biogenesis, and RNA polymerase, among others. Therefore, detergent exposure substantially effects protein solubilization with profound experimental implications.

Typically, in protein abundance volcano plots, greyed out “non-significant values” sometimes include hits with *p*-values > 0.05 or fold changes greater than 0.5 and less than 2.0. Similarly, some authors determine which hits are “significant” through the calculation of 95% confidence intervals and/or +/- 2.0 standard deviation intervals, using these as the threshold cutoffs. Clearly, there is some subjectivity involved in the process, one example of which is including hits for which the fold change exceeds a cutoff threshold but for which the *p*-values are either non-significant or even *p*=0, as noteworthy in discussions or even validation experiments.

It is possible that large fold changes without adequate statistical support are false positives – instead of indicating a “real” biological change, they may instead be outliers or reflect random variation, technical noise, artifacts, or the presence of low-abundance proteins with high measurement error. Including these hits in downstream analyses may

result in an inflated discovery rate and, ultimately, a misrepresentation/misinterpretation of the data[386-388]. On the other hand, substantial fold changes may be indicative of true biological differences regardless of statistical significance, particularly in an experimental context defined by limited replicates and/or high variability. Likewise, methodological limitations including sample size and quantification method may lead to the exclusion of true positives if only *p*-values are considered, and the inclusion of such hits facilitates scientific transparency in that it provides a more comprehensive view of the proteomic landscape in response to the independent variable[387-389]. While the subjective nature of proteomic threshold cutoffs in the determination of significance is a matter of debate, a context-dependent strategy characterized by the transparent classification of protein hits as either substantially altered or not, combined with an acknowledgment of the study's analytical limitations, may appropriately balance the advantages and disadvantages of either approach.

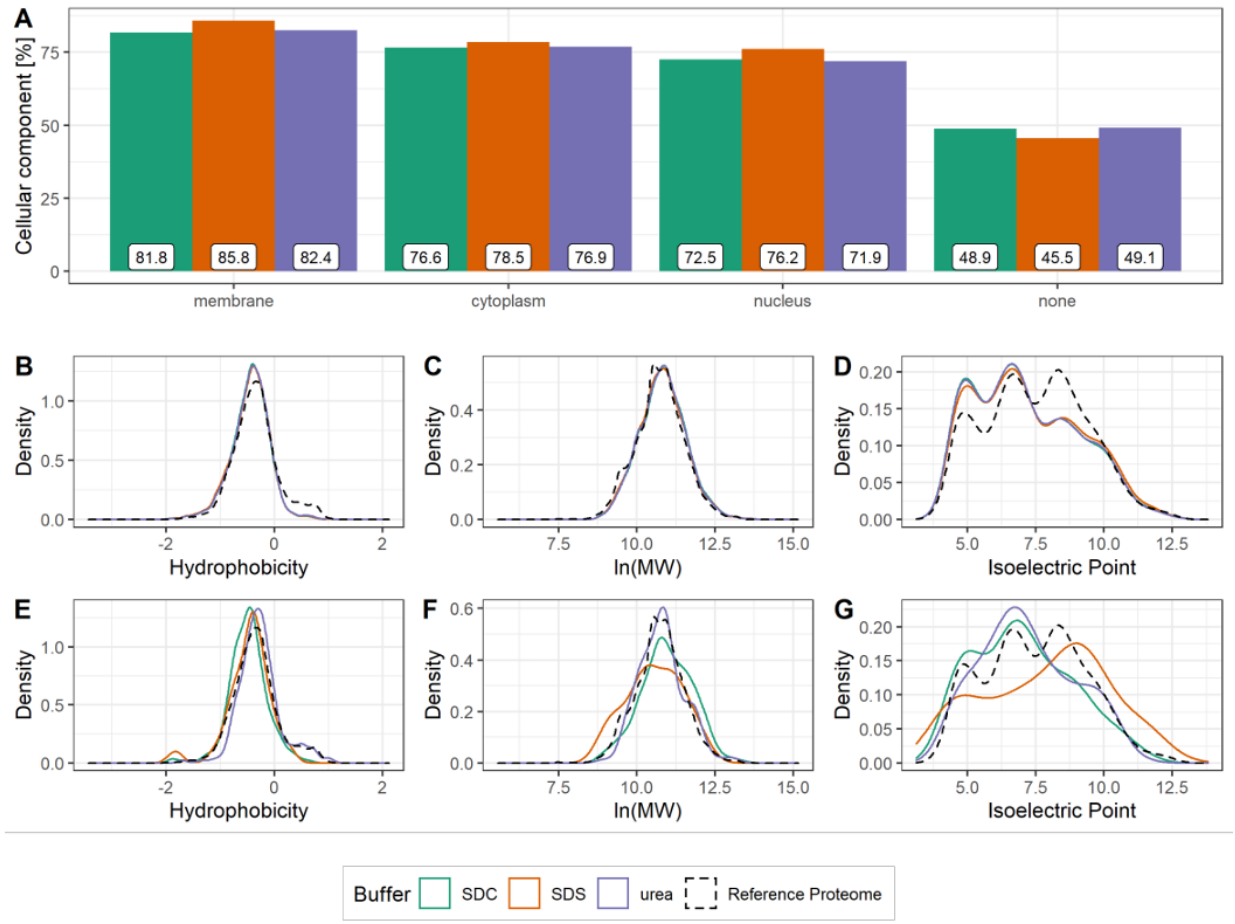

Figure 2.16 **Subcellular localization and physicochemical characteristics of proteins identified by simultaneous proteo-metabolomic liquid-liquid extraction interphase pellets.** (***A***) Protein distribution across cellular compartment categories. (***B***, ***C***, ***D***) Physicochemical properties of all proteins extracted by each of three detergents (SDC, SDS, or urea). (***E***, ***F***, ***G***) Physicochemical properties of only proteins identified exclusively by extraction with SDC, SDS, or urea. Dashed line, human reference proteome (SwissProt, uniport.org). Figure reproduced from Pijkeren et al., 2023.

The present findings provide novel insights into the effects of detergent exposure variability on the solubilized proteome of *C. elegans* by correlating detergent-associated physicochemical properties to the proteins they extract. These data also suggest a role for detergent variability as a potential confound in proteomic experiments, with profound effects on the subcellular localizations, processes, and pathways of solubilized proteins. Future studies should expand upon these data by incorporating additional detergents alongside those already examined and incorporating comparative analyses with alternate model systems, such as human cell lines or mammalian organs. Detergent concentrations could also be adjusted and protein solubility examined accordingly. CHAPS, for example, has two critical micelle concentrations, with concentrations above the second causing molecules to form a two-layer spherical micellar structure characterized by aliphatic molecules of the inner layer interacting with steroid groups of the outer layer[390]. Interestingly, a subgroup of proteins is only soluble and stable at concentrations above the second critical micellar concentration, implying further effects on detergent-dependent solubilization specificity. Finally, protein refolding experiments[391,392] prior to further validation experiments may provide novel insights into protein-protein interaction sites, partners, and functional mechanisms.

Chapter 3: *chn-1* Ablation Alters the *C. elegans* Protein Landscape

3.1 Introduction

Over the past 50 years, the global population of individuals over 65 has nearly quadrupled. Despite these rapid demographic changes, aging remains one of the final frontiers in biology. Indeed, its inherent complexity is further amplified by the difficulty in separating the effects of normal aging from the consequences of age-associated diseases. As proteostasis plays a key role in driving both healthy and pathological aging[17,18], the protein quality control network is a promising target for delineating specific pathways and mechanisms promoting healthy aging as well as defining how these processes are altered in age-associated pathologies.

Carboxyl terminus of Hsp70-interacting protein (CHIP), an E3 ubiquitin ligase, functions as a key regulator of protein quality control[1]. CHIP was initially shown to facilitate the polyubiquitination and subsequent degradation of misfolded client proteins by binding to Hsp/c70, a core component of the molecular chaperone machinery[2,3]. More recent evidence has revealed that CHIP also has a non-canonical role as a chaperone-independent E3 ligase in regulating the activity, localization, and steady-state levels of several native proteins essential for cellular and organismal health, including interferon signaling[4,5], insulin pathways[6,7], and membrane homeostasis[8]. Animal knock-outs of CHIP experience accelerated aging[9], cognitive impairment[10], and neurodegeneration[11], as well as increased cell death[12], mitochondrial dysfunction[13], and oxidative stress[14]. In human observational studies, the consequences of missense mutations vary depending on their location, with those affecting only the tetratricopeptide repeat (TPR) domain of the protein associated with a less complex ataxia phenotype, while mutations in the U-box domain result in neurodegeneration and cognitive decline[15,16]. Interestingly, the functions of CHIP are also context-dependent. For instance, in healthy cells CHIP mediates the degradation of the insulin receptor, thus regulating insulin signaling and longevity. However, proteotoxic stress causes

CHIP to be rerouted into protein quality control pathways, thus stabilizing the insulin receptor and reducing lifespan[7].

While its multifaceted role in neuroprotection makes CHIP a promising subject for the study of healthy aging, little is known about the CHIP-dependent proteomic landscape at the organismal level. Here, I am to delineate the cellular pathways mediating the neuroprotective effects of CHIP through the general mass spectrometry-based proteomic screen of two independently-derived *chn-1*-null *C. elegans* mutants, a genetically tractable and simple whole-animal model for the study of aging. These experiments identified clearly a broad, clearly distinguishable proteomic signature and possible mechanistic pathways linking CHIP to decreased longevity.

3.2 Materials and Methods

3.2.1 Experiment Overview and Rationale

Previously, I performed preliminary experiments to troubleshoot MS-based proteomics experiments on *C. elegans* while exploring methodological considerations (i.e., using multiple detergent conditions) to determine both (1) how lysis by CHAPS/urea vs. SDS changed the global protein landscape of the nematode and (2) how these changes were affected by *chn-1* ablation in a between-buffer analysis of *chn-1*-null mutants (Chapter 2). Here, I aim to expand upon these data by exploring in further detail how different extraction procedures affect the *chn-1*-dependent proteomic landscape, with a focus on a between-strain proteomic analysis. As described in Chapter 2, *chn-1* deletion mutants were validated by PCR genotyping (Figure 2.3). I begin by performing a proof-of-principle lifespan experiment to confirm the three strains employed have the longevity phenotype expected of *chn-1*-null animals, and subsequently proceed to process, run, and analyse *chn-1(by155)*, *chn-1(tm2692)*, and N2 wild-type strains as described in Figure 3.1 below.

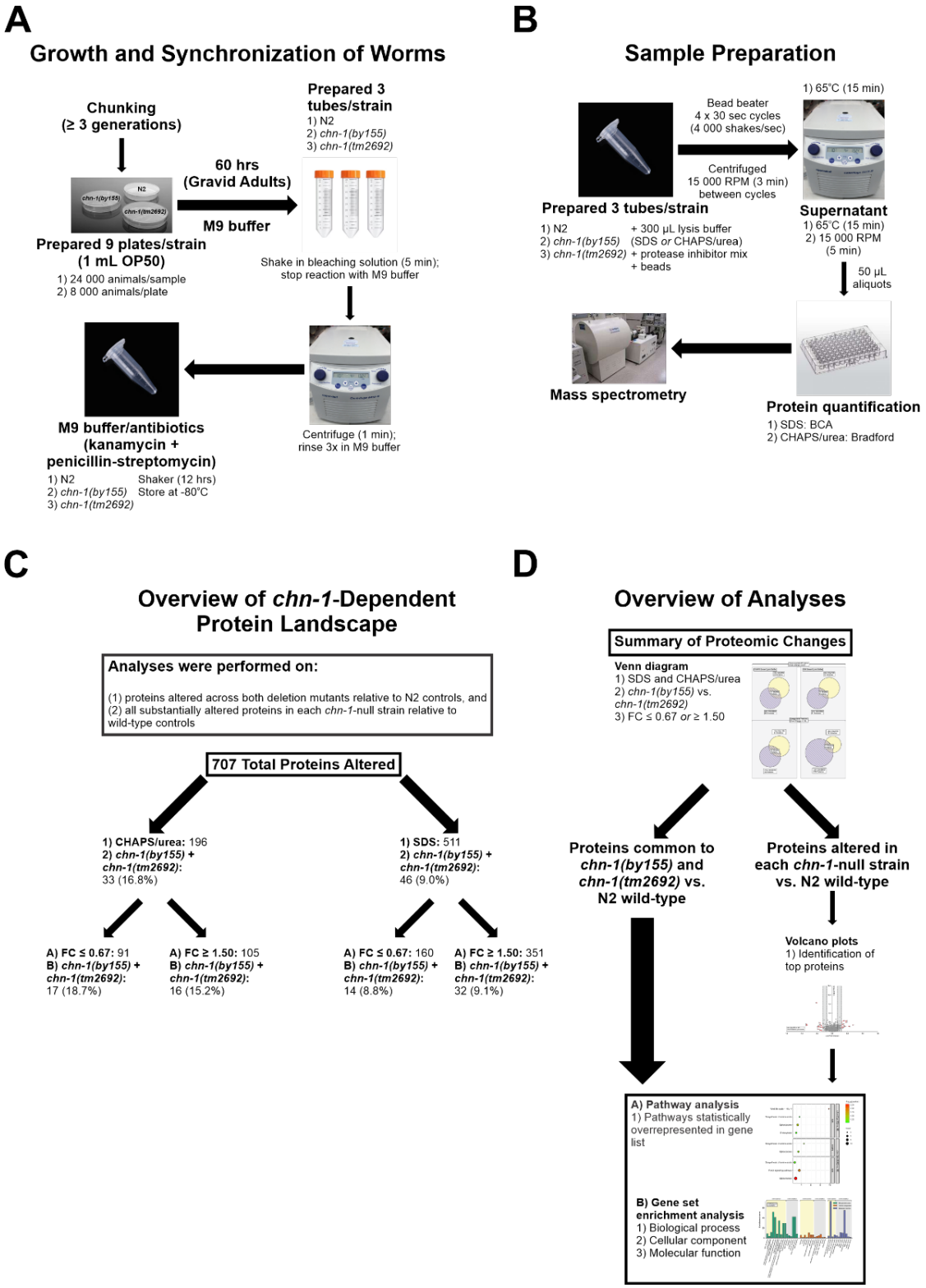

Figure 3.1 **Flowchart of sample preparation and proteomic analyses.** Schematic of (***A***) the growth and synchronization of worms, (***B***) sample lysis and preparation for MS-based proteomics, (***C***) overview of layered analytical approach in this chapter, and (***D***) pipeline for proteomic analyses, including GO and KEGG pathway analyses.

A proof-of-principle lifespan assay using wild-type, *chn-1(by155)*, and *chn-1(tm2692)* deletion mutants was performed to confirm the effects of *chn-1* deletion on lifespan. A schematic detailing the locations of these mutations is shown below (Figure 3.2). As described previously, the full-length CHN-1 protein has three TPR motifs and a U-box domain, and the *by155* and *tm2692* mutations result in truncated CHN-1 proteins lacking the U-box domain and the TPR-domain, respectively. Figure 3.2 shows the *by155* deletion allele, along with the position and extent of the deletion (equal to 989 base pairs), as well as the *tm2692* deletion allele, with a 263 base pair deletion and a 3 base pair insertion removing exons 2, 3, and 4, resulting in a gene product lacking amino acids 26 through 92, encoding most of the TPR repeat. Between-strain comparisons were then performed on MS-based proteomic datasets generated using either wild-type, *chn-1(by155)*, or *chn-1(tm2692)* samples processed with either CHAPS/Urea- or SDS-based lysis buffers. The nematode strains, growth and synchronization of worms, preparation of samples for proteomic analyses, and mass spectrometry-based proteomics methods were as described in Chapter 2, with pre-gravid animals collected early in adulthood (i.e., at the end of the L4-larval stage/beginning of adulthood approximately 48 hours post-plating) to minimize the impact of developmental processes unrelated to *chn-1*-deletion on the proteome. Proteomics analyses were performed on (1) proteins substantially altered across both deletion mutants relative to N2 controls, and (2) independently on all substantially-altered proteins in each *chn-1*-null strain relative to wild-type controls.

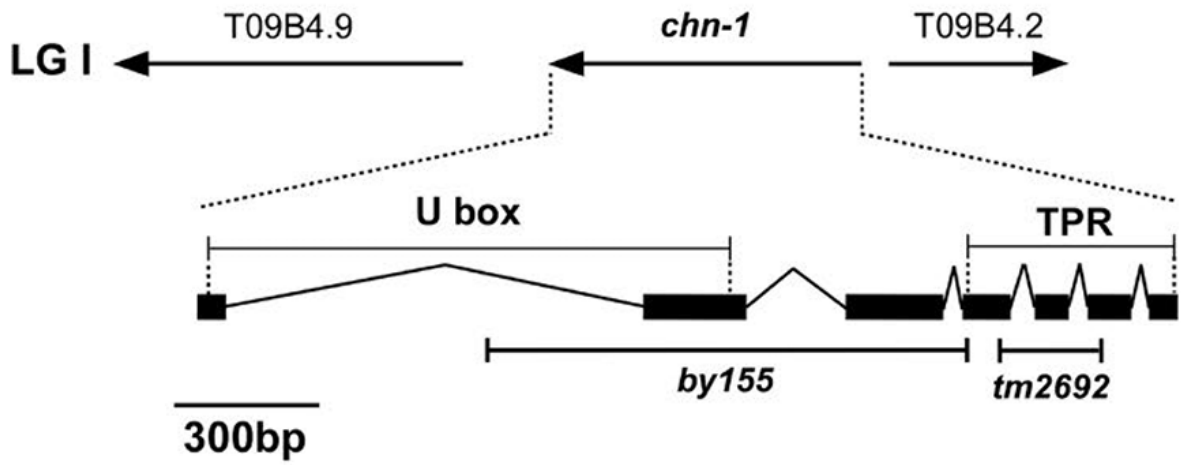

Figure 3.2 **The location and gene structure of *chn-1*.** Black boxes indicate coding segments. The domain structure of CHN-1, as well as the deletion sites in the *by155* and *tm2692* alleles are shown. Figure reproduced from Liu et al. 2018.

3.2.2 Lifespan Assay

Lifespan assays were performed on fresh NGM plates spread with the *E. coli* strain OP50 (1X NGM). The experiment was performed at room temperature, and plates otherwise stored at 20^{o}C. Age-synchronized L1 nematodes were seeded on plates for 48 hours. On day 1 of adult life, 16 worms were transferred to each of 8 feeding plates seeded with 300 µL OP50 24 hours prior (128 animals/strain). Starting 2 days later, worms were scored on alternating days as alive, dead, or censored. Animals were recorded as dead if they filed to exhibit spontaneous movement and subsequently did not respond when gently probed several times by a wire pick. To focus on lifespan, worms that were lost, became desiccated on the side of the plate after crawling off, or died due to extruded internal organs or hatching progeny inside the uterus were censored. Animals were transferred to fresh plates on alternating days until all worms were either dead or censored. Three independent experiments were performed. Each strain utilized *n* = 128 animals, with the exception of *chn-1(by155)* (Replicate 1 only; *n* = 129) and *chn-1(tm2692)* (Replicate 2 only; *n* = 126).

3.2.3 Statistical Analyses

Restricted mean survival times were plotted ± standard error of the mean. For lifespan assays, statistical analyses were performed in OASIS 2 [393] using the Kaplan Meier estimator. Statistical significance was determined using a log-rank test between pooled

populations of animals, and the Bonferroni method was used to adjust for multiple comparisons. Figures were generated using GraphPad Prism (version 10.4.0) (GraphPad, CA, USA).

3.3 Results: *chn-1* Deletion Alters the *C. elegans* Proteomic Landscape

3.3.1 Validation of *C. elegans* Strains

Both *chn-1* mutant alleles were validated by PCR electrophoresis (Figure 2.3), with both a genomic map (Figure 2.4) and sequence deletions for *chn-1(by155)* (Figure 2.5) and *chn-1(tm2692)* (Figure 2.6) shown in Chapter 2.

3.3.2 Knock-Out Mutants of *chn-1* are Short-Lived

Proteostasis and longevity are mediated competitively through CHIP-assisted proteolysis. Under normal conditions, CHIP facilitates the degradation of the insulin receptor, receptor monoubiquitylation, and endocytic-lysosomal turnover, thus regulating the IIS pathway and promoting longevity. Conversely, under conditions of proteotoxic stress, CHIP is instead channeled toward protein quality control pathways at the expense of insulin receptor degradation, thus stabilizing the insulin receptor and accelerating the aging process. The effects of proteotoxic stress are mirrored by CHIP depletion, and *chn-1* deletion mutants consistently exhibiting decreased longevity. Prior to processing samples for proteomics, a proof-of-concept lifespan assay was performed on N2 wild-type *C. elegans* as well as *chn-1(by155)* and *chn-1(tm2692) chn-1* deletion mutants. In this experiment, the control animals showed a restricted mean survival time of 20.94 days whereas the *chn-1(by155)* and *chn-1(tm2692)* had restricted mean survival times of 17.27 and 16.50 days, or 17.53% and 21.20% reduction in restricted mean survival time, respectively ($p < 0.001$, log-rank). The two deletion mutants did not differ in restricted mean survival times ($p = 0.29$, log-rank). The last mortality occurred on days 28, 22, and 19 in controls, *chn-1(by155)*, and *chn-1(tm2692) chn-1* mutants, respectively (Figure 3.3). Bonferroni-adjusted *p*-values (Supplemental Table B1), restricted mean survival times, and final mortalities (Supplemental Table B2) associated

with longevity differences in N2 wild-type, *chn-1(by155)*, and *chn-1(tm2692)* across all 3 replicates are shown in Appendix B, while the number of animals censored at each time-point is shown in Supplemental Table B3.

3.3.3 Overview of the Changes in the Proteome

Proteins and their relative abundance were quantified between sample pairs. Analyses were performed using both *chn-1(by155)* and *chn-1(tm2692)* loss-of-function deletion mutants, each compared to N2 wild-type controls. The inclusion of two *chn-1*-null strains was done with the aim of accounting for between-strain differences in *chn-1* deletion strains. Therefore, these findings are analyzed in two steps. First, only the proteins that were substantially altered in both *chn-1* deletion mutants compared to wild-type animals were pooled and analyzed collectively (an integrated 'high confidence' subset of protein hits). Finally, proteins substantially altered were analyzed in each *chn-1*-null strain independently. To account for the effects of lysis buffer on protein extraction and identification, the experiment was repeated twice: once with samples lysed with SDS, and once with CHAPS/Urea-processed samples.

Between-strain analyses comparing *chn-1(by155)* and *chn-1(tm2692) chn-1* mutants vs. N2 wild-type controls revealed a total of 707 substantially-altered proteins, with 196 and 511 substantially-altered proteins in CHAPS/Urea-processed and SDS-processed samples, respectively. In CHAPS/Urea-processed samples, 33 of the 196 total proteins substantially altered were shared by both *chn-1* deletion strains (16.8% of all proteins altered in CHAPS/Urea-processed samples), whereas in SDS-processed samples, 46 of the 511 total proteins altered were shared by both mutants relative to wild-type controls (9.0% of all changed proteins in SDS-processed samples) (Figure 3.4).

In CHAPS/Urea-processed samples, analyses of underexpressed proteins (i.e., fold change ≤ 0.67) revealed 91 substantially altered proteins, with 17 of these shared by both *chn-1* deletion strains (18.7% of all proteins underexpressed in CHAPS/Urea-processed samples). In SDS-processed samples, 160 proteins were substantially underexpressed, and 14 of these (8.8% of all proteins underexpressed in SDS-processed samples) were shared by both *chn-1(by155)* and *chn-1(tm2692)* mutants. Analyses of overexpressed proteins (i.e., fold change ≥ 1.5) in CHAPS/Urea-processed

samples revealed 105 substantially altered proteins, with 16 of these (15.2% of all proteins overexpressed in CHAPS/Urea-processed samples) shared by both *chn-1* mutants. Of 351 proteins overexpressed in samples lysed with SDS, 32 (9.1% of all proteins overexpressed in SDS-processed samples) were shared by both *chn-1* mutants (Figure 3.4).

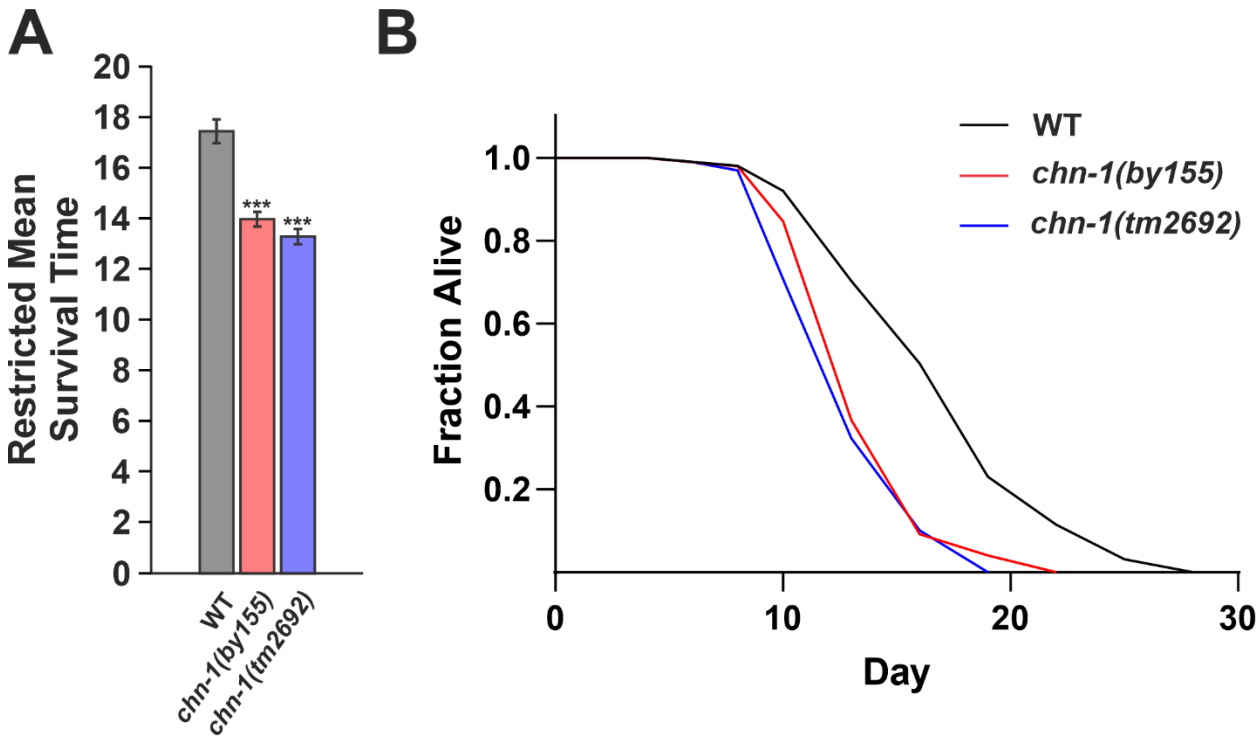

Figure 3.3 **Lifespan is decreased by *chn-1* deletion.** (***A***) Restricted mean survival time and (***B***) cumulative survival graph comparing wild-type N2 controls with *chn-1(by155)* and *chn-1(tm2692) C. elegans chn-1* mutants. Deletion mutants showed decreased restricted mean survival times and significantly decreased lifespans than wild-type N2 controls. Asterisks indicate significances: ****p*<0.001. Error bars represent ± SEM. Bonferroni-adjusted *p*-values as well as restricted mean survival times and final mortalities associated with longevity differences in N2 wild-type, *chn-1(by155)*, and *chn-1(tm2692)* across all 3 replicates are shown in Supplemental Table B1 and Supplemental Table B2, respectively. The number of animals censored at each time-point of the assay is shown in Supplemental Table B3.

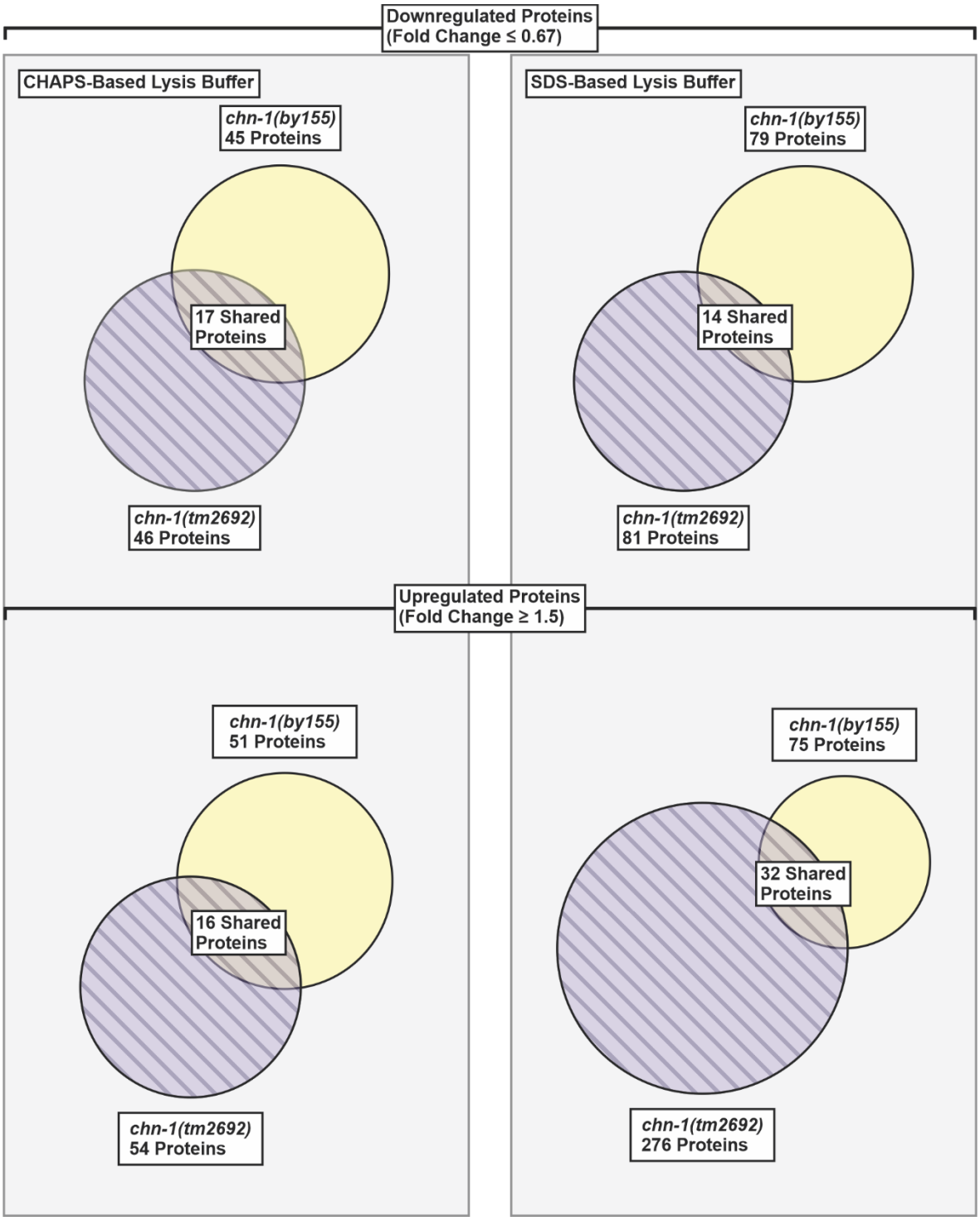

Figure 3.4 **Venn diagrams showing the overlap of proteins identified by SWATH-MS across *C. elegans* CHIP mutants.** Comparisons between *chn-1(by155)* and *chn-1(tm2692) C. elegans chn-1* mutants processed with either CHAPS/Urea- (left) or SDS-based (right) lysis buffer. Proteins with fold changes of ≤ 0.67 (top) and ≥ 1.5 (bottom) compared to wild-type N2 controls are identified. The total protein count includes single peptide IDs.

3.3.4 Shared Proteins Altered Across *chn-1* Deletion Mutants Reveal Focused Changes

KEGG pathway topology analyses performed on protein hits shared by both *chn-1* mutants relative to wild-type controls revealed a focused cohort of enriched pathways in SDS-processed samples. Specifically, significant effects on metabolic pathways ($p < 0.05$), and an effect approaching significance on spliceosome ($p = 0.098$) were found (Table 3.1). These analyses revealed no pathways to be significantly overrepresented in CHAPS/Urea-processed samples, however. For both pathway topology and gene set enrichment analyses (Appendix B) of the 'high confidence' protein subset, underexpressed and overexpressed proteins were pooled.

Table 3.1 **KEGG pathways related to CHIP loss-of-function in both *chn-1(by155)* and *chn-1(tm2692)* mutants.** Shared pathways identified in *chn-1(by155)* and *chn-1(tm2692) C. elegans* mutants when compared to N2 wild-type animals (using DAVID). The lysis buffer, number of associated genes ("count") and an association index (probability (*p*-value) as well as enrichment score) for each pathway is included.

Pathway	Lysis Buffer	Count	Enrichment	*p*-Value
Metabolic pathways	SDS	9	1.970	3.41E-02
Spliceosome	SDS	3	5.225	9.80E-02

Tables 3.2-3.5 indicate which proteins were shared by both *chn-1(by155)* and *chn-1(tm2692) chn-1* mutants relative to wild-type controls, with Tables 3.2 and 3.4 listing proteins that were more abundant in CHAPS/Urea- and SDS-processed samples, respectively, whereas Tables 3.3 and 3.5 indicate proteins that were less abundant in CHAPS/Urea- and SDS-processed samples, respectively. Overrepresented proteins across *chn-1* mutants in CHAPS/Urea-processed samples included aquaporin, bromo domain-containing protein, PLD phosphodiesterase domain-containing protein, HEAT repeat protein, vacuolar protein sorting-associated protein VTA1 homolog, conserved oligomeric Golgi complex subunit 6, BPTI/Kunitz inhibitor domain-containing protein, and probable mitochondrial pyruvate carrier 1 (Table 3.2). Underrepresented proteins across *chn-1*-null worms included transcription factor sma-9, protein-lysine N-methyltransferase M142.8, protein ABHD1, FIS1-related protein fis-2, MTOR-associated protein MEAK7, UBX domain-containing protein 2, and gamma-soluble NSF attachment protein (Table 3.3). The transcription factor sma-9 had a fold change of 0.31 ($p < 0.001$) in *chn-1(by155)* mutants relative to wild-type controls, and 0.25 ($p < 0.001$) in *chn-1(tm2692)* mutants relative to wild-type controls (Table 3.3).

Proteins most substantially overexpressed across *chn-1* mutants in SDS-processed samples included Tudor domain-containing protein, methyltransferase small domain-containing protein, putative 1-acyl-sn-glycerol-3-phosphate acyltransferase, SLC (SoLute Carrier) homolog, mitochondrial ribosomal protein, small, Lissencephaly-1 homolog, EHS-1, MARVEL domain-containing protein, SSD domain-containing protein, and protein-lysine N-methyltransferase M142.8 (Table 3.4). Proteins substantially underexpressed across SDS-processed deletion mutants include polypeptide N-acetylgalactosaminyltransferase 5, probable small nuclear ribonucleoprotein Sm D1, glyceraldehyde-3-phosphate dehydrogenase 3, peptidyl-prolyl cis-trans isomerase E, secreted protein, mitochondrial import inner membrane translocase subunit Tim21, and biogenesis of lysosome-related organelles complex 1 subunit 2 (Table 3.5). Recurring substantially-altered proteins include those with functions related to protein folding and trafficking, aging, mitochondrial function, methylation, as well as the structure and function of the Golgi complex.

Table 3.2 **Shared proteins (based on fold change) identified by SWATH-MS that are over-represented in both *chn-1(by155)* and *chn-1(tm2692) C. elegans* samples processed by lysis with CHAPS/urea-based lysis buffer.** Associated genes for each protein are listed in Supplemental Table B4.

Protein	***chn-1(by155)* vs. N2**				***chn-1(tm2692)* vs. N2**			
	***p*-Value**	**Fold Change**	**-Log (*p*-Value)**	**Log (Fold Change)**	***p*-Value**	**Fold Change**	**-Log (*p*-Value)**	**Log (Fold Change)**
Aquaporin	1.72E-02	4.823	1.763	0.683	2.68E-01	1.738	0.572	0.240
Peptidase M1 leukotriene A4 hydrolase/aminopeptidase C-terminal domain-containing protein	1.18E-03	2.893	2.930	0.461	2.01E-02	1.752	1.698	0.243
Bromo domain-containing protein	2.64E-03	2.838	2.579	0.453	1.06E-02	2.271	1.975	0.356
Zygote defective protein 12	1.60E-02	2.167	1.795	0.336	3.59E-02	1.935	1.445	0.287
PLD phosphodiesterase domain-containing protein	1.18E-01	1.906	0.929	0.280	1.72E-01	1.796	0.765	0.254
HEAT repeat protein	2.31E-02	1.904	1.636	0.280	3.70E-02	1.793	1.431	0.254
Glucuronosyltransferase	1.68E-02	1.805	1.773	0.256	2.31E-02	1.745	1.636	0.242
Vacuolar protein sorting-associated protein VTA1 homolog	7.96E-02	1.785	1.099	0.252	7.86E-02	1.745	1.105	0.242
DUF19 domain-containing protein	2.86E-01	1.732	0.543	0.239	1.39E-01	2.034	0.856	0.308
Conserved oligomeric Golgi complex subunit 6	6.32E-01	1.647	0.199	0.217	4.48E-01	1.697	0.349	0.230
DNA-directed RNA polymerases I, II, and III subunit RPABC5	3.58E-02	1.640	1.446	0.215	2.27E-02	1.763	1.644	0.246
Protein Phosphatase Four Regulatory subunit	2.51E-01	1.603	0.601	0.205	1.74E-01	1.752	0.759	0.244
Translocon Sec61/SecY plug domain-containing protein	2.18E-01	1.575	0.662	0.197	1.90E-02	2.397	1.722	0.380
Aminotran_5 domain-containing protein	5.31E-02	1.539	1.275	0.187	6.97E-02	1.652	1.157	0.218
BPTI/Kunitz inhibitor domain-containing protein	3.47E-01	1.532	0.460	0.185	1.66E-01	2.088	0.779	0.320
Probable mitochondrial pyruvate carrier 1	4.50E-01	1.522	0.347	0.182	4.38E-01	1.539	0.358	0.187

Table 3.3 **Shared proteins (based on fold change) identified by SWATH-MS that are under-represented in both *chn-1(by155)* and *chn-1(tm2692) C. elegans* samples processed by lysis with CHAPS/urea-based lysis buffer.** Associated genes for each protein are listed in Supplemental Table B5.

Protein	*chn-1(by155)* vs. N2				*chn-1(tm2692)* vs. N2			
	p-Value	Fold Change	-Log (*p*-Value)	Log (Fold Change)	*p*-Value	Fold Change	-Log (*p*-Value)	Log (Fold Change)
Transcription factor sma-9	1.36E-08	0.314	7.866	-0.503	3.03E-11	0.246	10.519	-0.610
Uncharacterized protein F44E2.9	4.98E-02	0.347	1.303	-0.460	5.22E-02	0.351	1.282	-0.455
Protein-lysine N-methyltransferase M142.8	4.62E-02	0.374	1.336	-0.428	2.38E-01	0.565	0.624	-0.248
SEA domain-containing protein	6.41E-02	0.435	1.193	-0.361	3.00E-02	0.442	1.522	-0.354
Uncharacterized protein C26F1.3	7.18E-02	0.482	1.144	-0.317	9.50E-02	0.510	1.022	-0.292
Protein ABHD11	6.56E-03	0.500	2.183	-0.301	5.20E-02	0.620	1.284	-0.208
C-type lectin domain-containing protein	1.66E-01	0.513	0.781	-0.290	1.95E-01	0.536	0.711	-0.270
FIS1-related protein fis-2	7.19E-04	0.543	3.143	-0.265	4.53E-03	0.622	2.344	-0.206
MTOR-associated protein MEAK7	5.25E-02	0.553	1.280	-0.257	9.60E-02	0.621	1.018	-0.207
Fatty Acid/Retinol binding protein	1.96E-01	0.573	0.708	-0.242	1.64E-01	0.547	0.786	-0.262
Putative RNA polymerase II transcriptional coactivator	1.51E-01	0.593	0.821	-0.227	7.47E-03	0.371	2.127	-0.430
UBX domain-containing protein 2	2.37E-01	0.627	0.625	-0.203	2.61E-01	0.642	0.583	-0.192
Gamma-soluble NSF attachment protein	1.45E-01	0.629	0.839	-0.201	1.45E-01	0.629	0.838	-0.201
Peptidyl-prolyl cis-trans isomerase E	8.35E-02	0.629	1.078	-0.201	5.48E-02	0.595	1.261	-0.226
Pre-rRNA-processing protein TSR2 homolog	5.64E-02	0.650	1.249	-0.187	1.30E-03	0.439	2.886	-0.358
Brix domain-containing protein F44G4.1	1.52E-01	0.654	0.818	-0.184	1.15E-01	0.612	0.940	-0.214
RNA helicase	4.33E-02	0.669	1.364	-0.175	3.10E-02	0.637	1.509	-0.196

Table 3.4 **Shared proteins (based on fold change) identified by SWATH-MS that are over-represented in both *chn-1(by155)* and *chn-1(tm2692) C. elegans* samples processed by lysis with SDS-based lysis buffer.** Associated genes for each protein are listed in Supplemental Table B6.

Protein	*chn-1(by155)* vs. N2				*chn-1(tm2692)* vs. N2			
	***p*-Value**	**Fold Change**	**-Log (*p*-Value)**	**Log (Fold Change)**	***p*-Value**	**Fold Change**	**-Log (*p*-Value)**	**Log (Fold Change)**
FMRF-Like Peptide	1.49E-03	12.712	2.825	1.104	8.20E-03	7.130	2.086	0.853
Methyltransferase domain-containing protein	2.61E-02	4.100	1.584	0.613	6.66E-03	3.806	2.177	0.580
NADP-dependent oxidoreductase domain-containing protein	5.81E-09	3.051	8.236	0.484	3.60E-03	1.793	2.443	0.254
UDP-glucuronosyltransferase	3.81E-02	2.456	1.419	0.390	7.71E-02	1.648	1.113	0.217
Tudor domain-containing protein	4.16E-01	2.444	0.381	0.388	2.80E-01	4.473	0.554	0.651
Methyltransferase small domain-containing protein	1.02E-07	2.217	6.992	0.346	2.96E-08	2.658	7.528	0.425
HoloCentric chromosome binding Protein	3.40E-02	2.216	1.468	0.345	1.27E-01	1.941	0.896	0.288
Putative 1-acyl-sn-glycerol-3-phosphate acyltransferase	1.05E-01	2.158	0.977	0.334	1.53E-01	1.954	0.815	0.291
Chitin-binding domain protein cbd-1	1.01E-08	2.146	7.997	0.332	6.23E-04	1.544	3.205	0.189
MLt-TeN (Mlt-10) related	1.19E-01	2.123	0.926	0.327	2.79E-01	1.625	0.555	0.211
SLC (SoLute Carrier) homolog	7.00E-02	1.947	1.155	0.289	2.54E-01	1.534	0.595	0.186
Mitochondrial Ribosomal Protein, Small	3.78E-02	1.859	1.423	0.269	7.62E-02	1.682	1.118	0.226
Lissencephaly-1 homolog	1.81E-02	1.852	1.742	0.268	3.56E-02	1.713	1.448	0.234
Acyl carrier protein	1.97E-02	1.819	1.706	0.260	6.36E-02	1.587	1.197	0.201
DUF19 domain-containing protein	2.56E-01	1.803	0.592	0.256	1.45E-02	3.503	1.838	0.544
EHS-1	2.18E-02	1.799	1.662	0.255	3.03E-02	1.732	1.519	0.239
Albumin	3.89E-03	1.720	2.410	0.236	5.10E-03	1.868	2.292	0.271
Pseudouridine synthase I TruA alpha/beta domain-containing protein	7.39E-02	1.718	1.132	0.235	3.87E-03	2.505	2.413	0.399
5'-AMP-activated protein kinase subunit beta-1	3.18E-01	1.700	0.498	0.231	3.48E-01	1.560	0.459	0.193
Remorin_C domain-containing protein	6.13E-02	1.684	1.213	0.226	4.69E-02	1.745	1.329	0.242
PIPK domain-containing protein	1.02E-02	1.665	1.992	0.221	4.66E-04	2.067	3.332	0.315

Dual specificity mitogen-activated protein kinase kinase	3.76E-02	1.645	1.424	0.216	7.48E-02	1.521	1.126	0.182
BING4 C-terminal domain-containing protein	6.24E-02	1.625	1.205	0.211	2.15E-03	2.235	2.667	0.349
Tudor domain-containing protein	6.48E-02	1.609	1.188	0.207	1.08E-01	1.654	0.968	0.218
MARVEL domain-containing protein	4.96E-04	1.604	3.304	0.205	1.89E-04	1.994	3.725	0.300
CRAL-TRIO domain-containing protein	2.22E-01	1.602	0.653	0.205	3.43E-02	2.256	1.465	0.353
Endoribonuclease	6.02E-02	1.588	1.220	0.201	2.35E-03	2.262	2.629	0.355
Acyl-coenzyme A thioesterase 8	8.88E-02	1.583	1.051	0.199	9.64E-02	1.565	1.016	0.194
SSD domain-containing protein	5.54E-02	1.568	1.256	0.195	7.50E-02	1.514	1.125	0.180
DUF19 domain-containing protein	1.02E-01	1.544	0.993	0.189	2.70E-03	1.792	2.568	0.253
Microtubule-associated protein futsch	2.48E-02	1.527	1.605	0.184	1.76E-02	1.571	1.755	0.196
Protein-lysine N-methyltransferase M142.8	4.05E-01	1.520	0.392	0.182	1.91E-01	1.884	0.720	0.275

Table 3.5 **Shared proteins (based on fold change) identified by SWATH-MS that are under-represented in both *chn-1(by155)* and *chn-1(tm2692) C. elegans* samples processed by lysis with SDS-based lysis buffer.** Associated genes for each protein are listed in Supplemental Table B7.

Protein	***chn-1(by155)* vs. N2**				***chn-1(tm2692)* vs. N2**			
	***p*-Value**	**Fold Change**	**-Log (*p*-Value)**	**Log (Fold Change)**	***p*-Value**	**Fold Change**	**-Log (*p*-Value)**	**Log (Fold Change)**
Nematode cuticle collagen N-terminal domain-containing protein	3.95E-04	0.271	3.403	-0.567	5.07E-02	0.490	1.295	-0.310
Uncharacterized protein	9.81E-02	0.279	1.009	-0.555	2.70E-01	0.479	0.569	-0.320
Ribosomal protein S10 domain-containing protein	2.47E-03	0.306	2.608	-0.514	1.44E-02	0.402	1.840	-0.396
RNA helicase	1.15E-02	0.450	1.941	-0.346	1.39E-01	0.626	0.856	-0.203
Polypeptide N-acetylgalactosaminyltransferase 5	8.81E-03	0.451	2.055	-0.346	1.68E-02	0.489	1.776	-0.311
Probable small nuclear ribonucleoprotein Sm D1	1.28E-01	0.469	0.894	-0.329	2.51E-01	0.589	0.600	-0.230
Tyrosine-protein phosphatase domain-containing protein	1.74E-02	0.529	1.759	-0.276	4.64E-02	0.519	1.334	-0.285
Glyceraldehyde-3-phosphate dehydrogenase 3	2.06E-01	0.533	0.687	-0.273	2.49E-01	0.605	0.604	-0.218
cystathionine gamma-lyase	1.19E-02	0.576	1.926	-0.240	5.65E-02	0.607	1.248	-0.217
Peptidyl-prolyl cis-trans isomerase E	8.03E-02	0.626	1.095	-0.204	1.30E-01	0.669	0.888	-0.175
Probable glucosamine-6-phosphate isomerase	6.78E-03	0.634	2.169	-0.198	1.37E-02	0.665	1.865	-0.177
Secreted protein	3.15E-01	0.644	0.501	-0.191	2.27E-01	0.577	0.645	-0.239
Mitochondrial import inner membrane translocase subunit Tim21	1.86E-02	0.645	1.730	-0.190	1.66E-02	0.639	1.780	-0.194
Biogenesis of lysosome-related organelles complex 1 subunit 2	1.26E-01	0.646	0.898	-0.190	1.74E-02	0.385	1.759	-0.414

3.3.5 Pairwise Comparisons Reveal Altered Proteomic Landscape in Response to *chn-1* Deletion

Volcano plots indicate which proteins contributed most proteomic variation in response to *chn-1* deletion in *chn-1(by155)* versus N2 wild-type and *chn-1(tm2692)* versus wild-type controls in CHAPS/Urea (Supplemental Figure B1 and Figure 3.5 as well as Tables 3.6-3.9) and SDS-lysed samples (Figures 3.6-3.7 and Tables 3.10-3.13), with Tables 3.6, 3.8, 3.10, and 3.12 listing proteins that were most substantially overrepresented and Tables 3.7, 3.9, 3.11, and 3.13 listing proteins that were most substantially underrepresented. Proteins most substantially overexpressed in CHAPS/Urea-processed *chn-1(by155)* versus N2 wild-type samples included aquaporin, leuk-A4-hydro_C domain-containing protein, midasin, and protein patched homolog 3, with fold changes of 4.82, 2.89, 2.25, and 2.20, respectively (Figure 3.5 and Table 3.6). Proteins most substantially underexpressed in CHAPS/Urea-lysed *chn-1(by155)* versus N2 wild-type samples included MFS domain-containing protein, ASC-1, transcription factor sma-9, protein-lysine N-methyltransferase M142.8, and SHSP domain-containing protein, with fold changes of 0.146, 0.149, 0.314, 0.374, and 0.421, respectively (Figure 3.5 and Table 3.7). Proteins most substantially overexpressed in CHAPS/Urea-processed *chn-1(tm2692)* versus N2 wild-type animals included lysozyme-like protein 7, smu-1 suppressor of mec-8 and unc-52 protein, and protein up-regulated in *daf-2*(Gf), with fold changes of 2.67, 2.57, and 2.14, respectively (Figure 3.6 and Table 3.8). Proteins substantially underexpressed in CHAPS/Urea-lysed *chn-1(tm2692)* versus N2 controls included transcription factor sma-9, F-spondin, AMPHiphysin homolog, putative RNA polymerase II transcriptional coactivator, and pre-rRNA processing protein TSR2 homolog, with fold changes of 0.25, 0.33, 0.33, 0.37, and 0.44 (Figure 3.6 and Table 3.9).

Proteins most substantially overexpressed in SDS-processed *chn-1(by155)* versus N2 controls included polyglutamine-repeat protein *pqn-41*, glyceraldehyde-3-phosphate dehydrogenase 4, NADH-ubiquinone oxidoreductase chain 3, C-mannosyltransferase *dpy-19*, U1 small nuclear ribonucleoprotein C, and putative aquaporin-10, with fold changes of 12.71, 3.33, 3.05, 3.05, 2.42, and 2.22 (Figure 3.7 and Supplemental Table A7). Proteins most substantially underexpressed in SDS-lysed

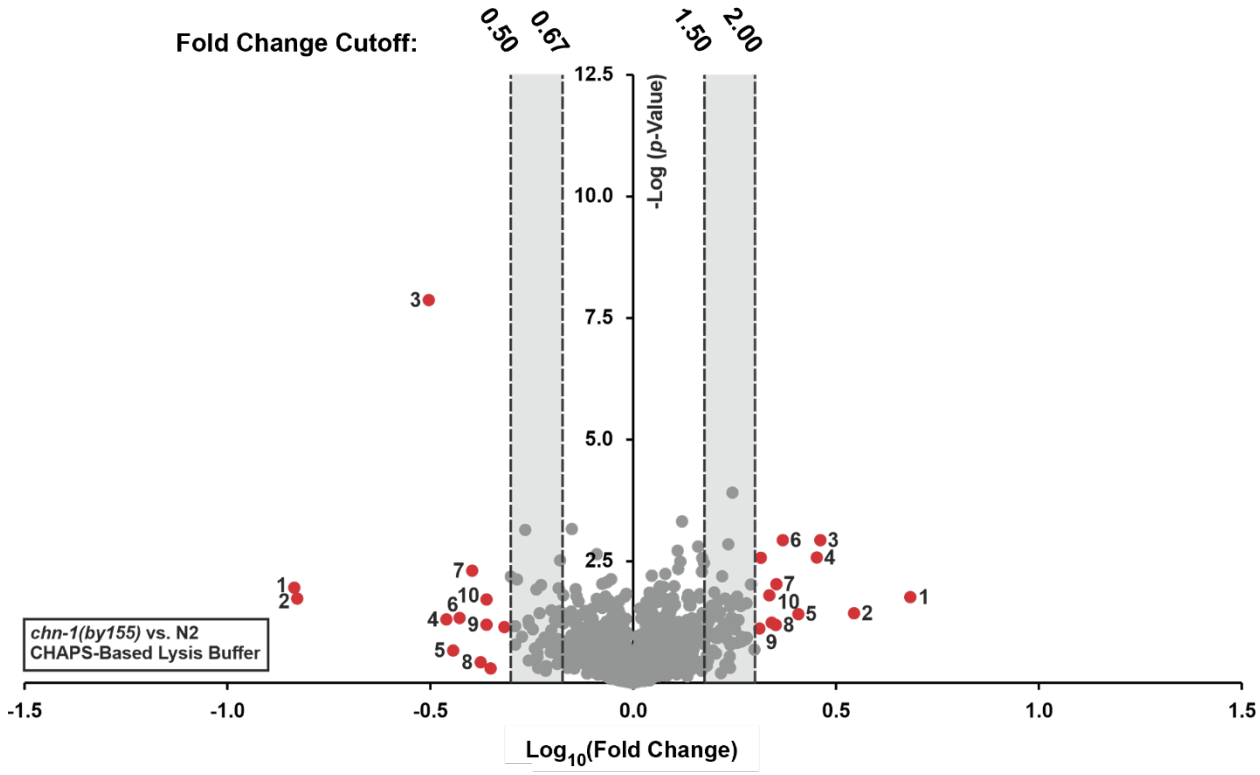

Figure 3.5 **Comparative SWATH-MS proteomic analyses of *chn-1(by155)* vs. N2 wild-type *C. elegans* samples processed by lysis with CHAPS/Urea-based lysis buffer.** Cut-off criteria (fold changes of ≤0.5 and ≥2 or ≤0.67 and ≥1.5) are represented by the dotted lines and shaded areas. Proteins (dots) that do not meet these fold change criteria are colour-coded in grey, while those that do are red. Over-represented proteins in the *chn-1(by155)* samples compared to N2 wild-type samples have a positive log (fold change), while under-represented proteins have negative values. The top 10 most over- and under-represented proteins are numbered and labeled in Tables 3.6 (upregulated proteins) and 3.7 (downregulated proteins).

Table 3.6 **Top proteins (based on fold change) identified by SWATH-MS proteomic analyses that are over-represented in *chn-1(by155)* vs. N2 wild-type *C. elegans* samples processed by lysis with CHAPS/urea-based lysis buffer.**

Protein	Gene	*p*-Value	Fold Change	-Log (*p*-Value)	Log (Fold Change)	Regulation	Label
Aquaporin	*aqp-11*	1.72E-02	4.823	1.763	0.683	Up	1
Col_cuticle_N domain-containing protein	*ram-2*	3.72E-02	3.509	1.430	0.545	Up	2
Leuk-A4-hydro_C domain-containing protein	*ltah-1.2*	1.18E-03	2.893	2.930	0.461	Up	3
Bromo domain-containing protein	*F13C5.2*	2.64E-03	2.838	2.579	0.453	Up	4
Allophagy receptor allo-1	*allo-1*	3.89E-02	2.556	1.410	0.408	Up	5
Putative folylpolyglutamate synthase	*F25B5.6*	1.17E-03	2.339	2.931	0.369	Up	6
Col_cuticle_N domain-containing protein	*col-97*	9.34E-03	2.258	2.030	0.354	Up	7
Midasin	*F55F10.1*	6.51E-02	2.249	1.187	0.352	Up	8
Protein patched homolog 3	*ptc-3*	5.78E-02	2.196	1.238	0.342	Up	9
Zygote defective protein 12	*zyg-12*	1.60E-02	2.167	1.795	0.336	Up	10

Table 3.7 **Top proteins (based on fold change) identified by SWATH-MS proteomic analyses that are under-represented in *chn-1(by155)* vs. N2 wild-type *C. elegans* samples processed by lysis with CHAPS/urea-based lysis buffer.**

Protein	Gene	*p*-Value	Fold Change	-Log (*p*-Value)	Log (Fold Change)	Regulation	Label
MFS domain-containing protein	*Y51A2D.18*	1.11E-02	0.146	1.956	-0.835	Down	1
ASC-1	*trip-4*	1.87E-02	0.149	1.729	-0.828	Down	2
Transcription factor sma-9	*sma-9*	1.36E-08	0.314	7.866	-0.503	Down	3
Uncharacterized protein F44E2.9	*F44E2.9*	4.98E-02	0.347	1.303	-0.460	Down	4
Uncharacterized protein	*B0513.4*	2.17E-01	0.360	0.664	-0.443	Down	5
Protein-lysine N-methyltransferase M142.8	*M142.8*	4.62E-02	0.374	1.336	-0.428	Down	6
PUD1_2 domain-containing protein	*pud-4*	4.94E-03	0.402	2.306	-0.396	Down	7
SHSP domain-containing protein	*ZK1128.7*	3.79E-01	0.421	0.421	-0.375	Down	8
SEA domain-containing protein	*Y48G1BR.1*	6.41E-02	0.435	1.193	-0.361	Down	9
Sulfotransfer_1 domain-containing protein	*hst-3.1*	1.95E-02	0.435	1.710	-0.361	Down	10

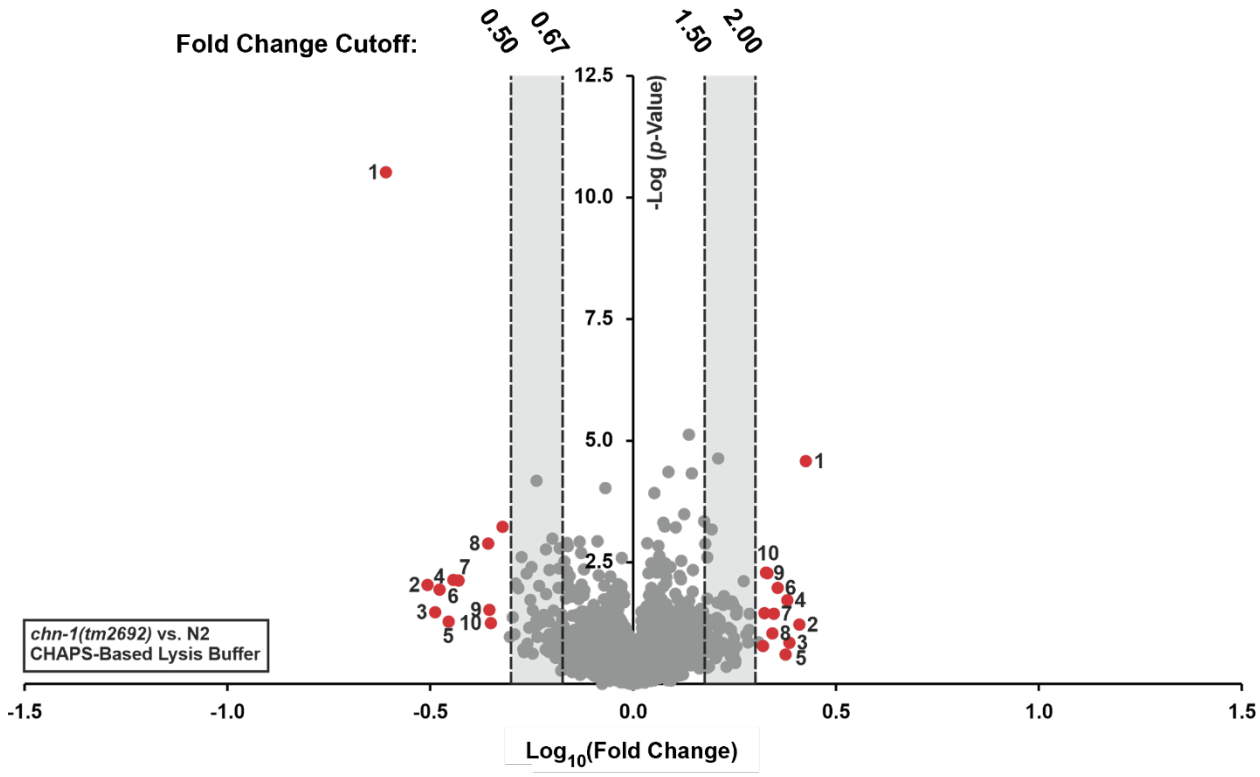

Figure 3.6 **Comparative SWATH-MS proteomic analyses of *chn-1(tm2692)* vs. N2 wild-type *C. elegans* samples processed by lysis with CHAPS/Urea-based lysis buffer.** Cut-off criteria (fold changes of ≤0.5 and ≥2 or ≤0.67 and ≥1.5) are represented by the dotted lines and shaded areas. Proteins (dots) that do not meet these fold change criteria are colour-coded in grey, while those that do are red. Over-represented proteins in the *chn-1(tm2692)* samples compared to N2 wild-type samples have a positive log (fold change), while under-represented proteins have negative values. The top 10 most over- and under-represented proteins are numbered and labeled in Tables 3.8 (upregulated proteins) and 3.9 (downregulated proteins).

Table 3.8 **Top proteins (based on fold change) identified by SWATH-MS proteomic analyses that are over-represented in *chn-1(tm2692)* vs. N2 wild-type *C. elegans* samples processed by lysis with CHAPS/urea-based lysis buffer.**

Protein	Gene	*p*-Value	Fold Change	-Log (*p*-Value)	Log (Fold Change)	Regulation	Label
Lysozyme-like protein 7	*lys-7*	2.63E-05	2.665	4.580	0.426	Up	1
Smu-1 suppressor of mec-8 and unc-52 protein	*smu-1*	6.05E-02	2.567	1.218	0.409	Up	2
Uncharacterized protein ZK1320.3	*ZK1320.3*	1.42E-01	2.427	0.847	0.385	Up	3
Plug_translocon domain-containing protein	*sec-61.a*	1.90E-02	2.397	1.722	0.380	Up	4
NAD(P)-bd_dom domain-containing protein	*bus-5*	2.47E-01	2.376	0.607	0.376	Up	5
Bromo domain-containing protein	*F13C5.2*	1.06E-02	2.271	1.975	0.356	Up	6
5C820	*pud-3*	3.61E-02	2.221	1.443	0.346	Up	7
Uncharacterized protein	*smgl-1*	9.16E-02	2.203	1.038	0.343	Up	8
Protein Up-regulated in Daf-2(Gf)	*pud-2.1*	5.28E-03	2.144	2.277	0.331	Up	9
PUD1_2 domain-containing protein	*pud-1.2*	5.18E-03	2.123	2.286	0.327	Up	10

Table 3.9 **Top proteins (based on fold change) identified by SWATH-MS proteomic analyses that are under-represented in *chn-1(tm2692)* vs. N2 wild-type *C. elegans* samples processed by lysis with CHAPS/urea-based lysis buffer.**

Protein	Gene	*p*-Value	Fold Change	-Log (*p*-Value)	Log (Fold Change)	Regulation	Label
Transcription factor sma-9	*sma-9*	3.03E-11	0.246	10.519	-0.610	Down	1
Uncharacterized protein	*F38B2.6*	9.22E-03	0.311	2.035	-0.507	Down	2
F-spondin	*spon-1*	3.38E-02	0.325	1.471	-0.488	Down	3
AMPHiphysin homolog	*amph-1*	1.16E-02	0.333	1.937	-0.477	Down	4
Uncharacterized protein F44E2.9	*F44E2.9*	5.22E-02	0.351	1.282	-0.455	Down	5
RNA/RNP complex-1-interacting phosphatase homolog	*pir-1*	7.28E-03	0.361	2.138	-0.443	Down	6
Putative RNA polymerase II transcriptional coactivator	*T13F2.2*	7.47E-03	0.371	2.127	-0.430	Down	7
Pre-rRNA-processing protein TSR2 homolog	*Y51H4A.15*	1.30E-03	0.439	2.886	-0.358	Down	8
SEA domain-containing protein	*Y48G1BR.1*	3.00E-02	0.442	1.522	-0.354	Down	9
MLt-TeN (Mlt-10) related	*mltn-8*	5.65E-02	0.446	1.248	-0.351	Down	10

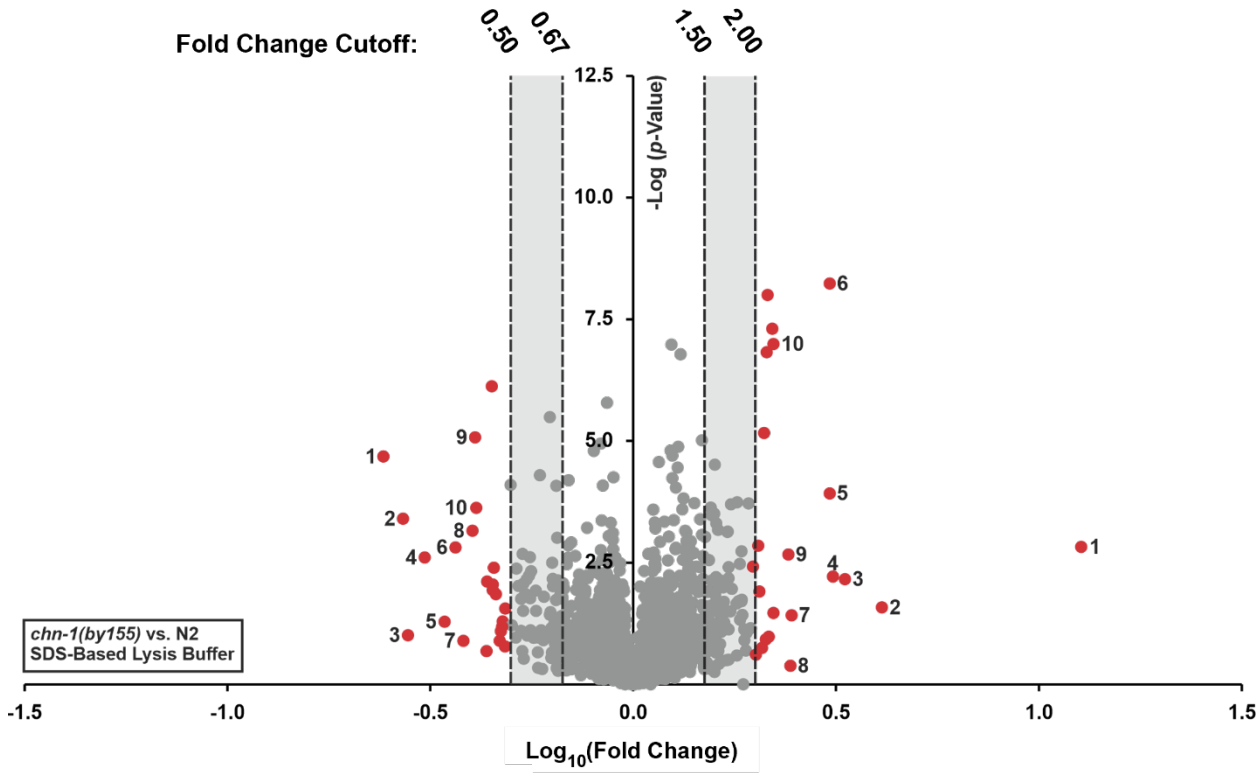

Figure 3.7 **Comparative SWATH-MS proteomic analyses of *chn-1(by155)* vs. N2 wild-type *C. elegans* samples processed by lysis with SDS-based lysis buffer.** Cut-off criteria (fold changes of ≤0.5 and ≥2 or ≤0.67 and ≥1.5) are represented by the dotted lines and shaded areas. Proteins (dots) that do not meet these fold change criteria are colour-coded in grey, while those that do are red. Over-represented proteins in the *chn-1(by155)* samples compared to N2 wild-type samples have a positive log (fold change), while under-represented proteins have negative values. The top 10 most over- and under-represented proteins are numbered and labeled in Tables 3.10 (upregulated proteins) and 3.11 (downregulated proteins).

Table 3.10 **Top proteins (based on fold change) identified by SWATH-MS proteomic analyses that are over-represented in *chn-1(by155)* vs. N2 wild-type *C. elegans* samples processed by lysis with SDS-based lysis buffer.**

Protein	Gene	*p*-Value	Fold Change	-Log (*p*-Value)	Log (Fold Change)	Regulation	Label
Polyglutamine-repeat protein pqn-41	*flp-28*	1.49E-03	12.712	2.825	1.104	Up	1
Protein phosphatase 2B regulatory subunit cnb-1	*prmt-6*	2.61E-02	4.100	1.584	0.613	Up	2
Glyceraldehyde-3-phosphate dehydrogenase 4	*nspd-5*	6.85E-03	3.327	2.164	0.522	Up	3
Cuticle collagen 6	*nspd-6*	6.08E-03	3.106	2.216	0.492	Up	4
NADH-ubiquinone oxidoreductase chain 3	*Y57E12AL.6*	1.20E-04	3.052	3.921	0.485	Up	5
C-mannosyltransferase dpy-19	*C35D10.6*	5.81E-09	3.051	8.236	0.484	Up	6
Major sperm protein 33	*ugt-5*	3.81E-02	2.456	1.419	0.390	Up	7
Probable peptidyl-glycine alpha-amidating monooxygenase pamn-1	*Y50D4C.3*	4.16E-01	2.444	0.381	0.388	Up	8
U1 small nuclear ribonucleoprotein C	*nasp-2*	2.16E-03	2.415	2.665	0.383	Up	9
Putative aquaporin-10	*mtq-2*	1.02E-07	2.217	6.992	0.346	Up	10

Table 3.11 **Top proteins (based on fold change) identified by SWATH-MS proteomic analyses that are under-represented in *chn-1(by155)* vs. N2 wild-type *C. elegans* samples processed by lysis with SDS-based lysis buffer.**

Protein	Gene	*p*-Value	Fold Change	-Log (*p*-Value)	Log (Fold Change)	Regulation	Label
Col_cuticle_N domain-containing protein	*rol-1*	2.08E-05	0.242	4.683	-0.616	Down	1
Col_cuticle_N domain-containing protein	*col-143*	3.95E-04	0.271	3.403	-0.567	Down	2
Uncharacterized protein	*F17E9.5*	9.81E-02	0.279	1.009	-0.555	Down	3
Ribosomal_S10 domain-containing protein	*mrpl-48*	2.47E-03	0.306	2.608	-0.514	Down	4
Guanine nucleotide-binding protein subunit beta-2	*gpb-2*	5.16E-02	0.343	1.288	-0.465	Down	5
Sperm-Specific family, class Q	*ssq-1*	1.54E-03	0.365	2.812	-0.438	Down	6
PIP-1	*spn-4*	1.27E-01	0.382	0.896	-0.418	Down	7
Col_cuticle_N domain-containing protein	*col-88*	6.99E-04	0.402	3.156	-0.396	Down	8
Cuticle collagen dpy-13	*dpy-13*	8.39E-06	0.408	5.076	-0.389	Down	9
Cuticle collagen dpy-5	*dpy-5*	2.35E-04	0.410	3.629	-0.387	Down	10

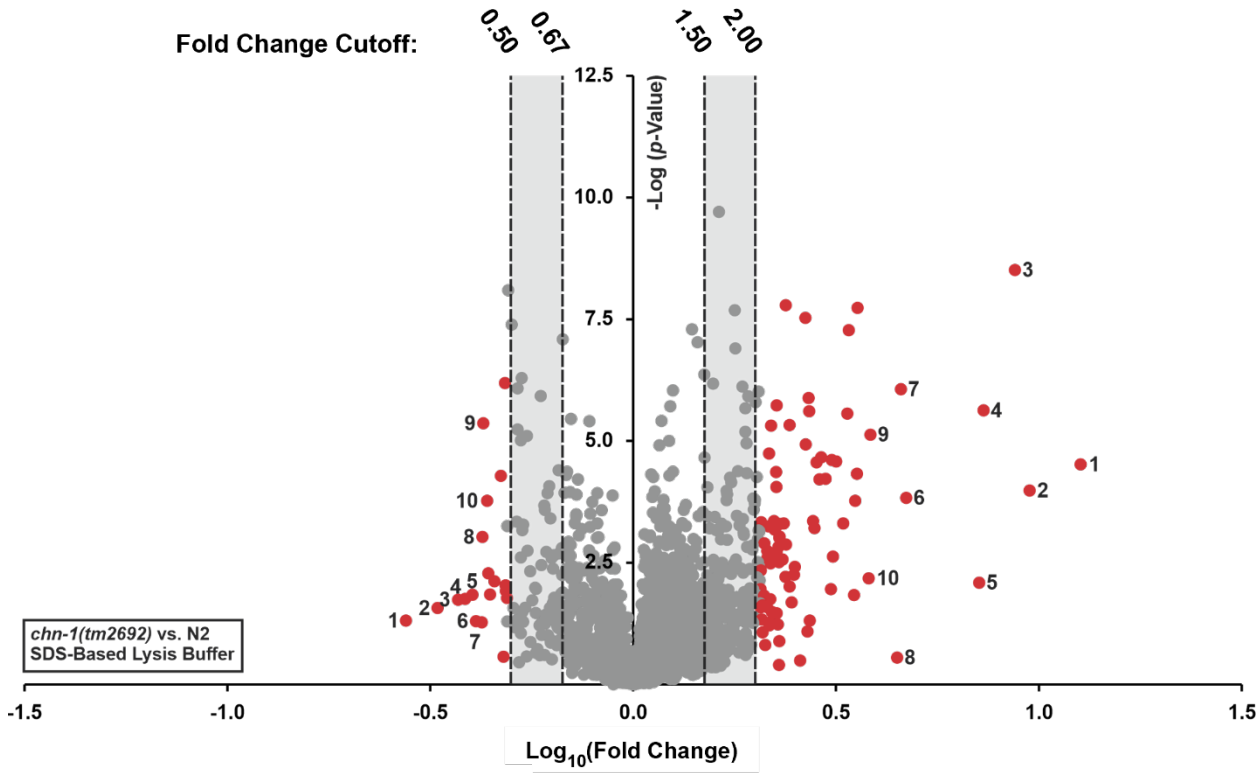

Figure 3.8 **Comparative SWATH-MS proteomic analyses of *chn-1(tm2692)* vs. N2 wild-type *C. elegans* samples processed by lysis with SDS-based lysis buffer.** Cut-off criteria (fold changes of ≤0.5 and ≥2 or ≤0.67 and ≥1.5) are represented by the dotted lines and shaded areas. Proteins (dots) that do not meet these fold change criteria are colour-coded in grey, while those that do are red. Over-represented proteins in the *chn-1(tm2692)* samples compared to N2 wild-type samples have a positive log (fold change), while under-represented proteins have negative values. The top 10 most over- and under-represented proteins are numbered and labeled in Tables 3.12 (upregulated proteins) and 3.13 (downregulated proteins).

Table 3.12 **Top proteins (based on fold change) identified by SWATH-MS proteomic analyses that are over-represented in *chn-1(tm2692)* vs. N2 wild-type *C. elegans* samples processed by lysis with SDS-based lysis buffer.**

Protein	Gene	*p*-Value	Fold Change	-Log (*p*-Value)	Log (Fold Change)	Regulation	Label
Ground-like domain-containing protein	*grl-15*	3.02E-05	12.663	4.520	1.103	Up	1
BPTI/Kunitz inhibitor domain-containing protein	*R12A1.3*	1.03E-04	9.483	3.985	0.977	Up	2
IF rod domain-containing protein	*ifc-2*	3.06E-09	8.736	8.514	0.941	Up	3
Col_cuticle_N domain-containing protein	*col-38*	2.34E-06	7.304	5.631	0.864	Up	4
FMRF-Like Peptide	*flp-28*	8.20E-03	7.130	2.086	0.853	Up	5
NAD(P)-bd_dom domain-containing protein	*bus-5*	1.48E-04	4.709	3.830	0.673	Up	6
Col_cuticle_N domain-containing protein	*col-49*	8.68E-07	4.574	6.062	0.660	Up	7
Tudor domain-containing protein	*Y50D4C.3*	2.80E-01	4.473	0.554	0.651	Up	8
Uncharacterized protein	*F30H5.3*	7.41E-06	3.844	5.130	0.585	Up	9
Methyltransf_25 domain-containing protein	*prmt-6*	6.66E-03	3.806	2.177	0.580	Up	10

Table 3.13 **Top proteins (based on fold change) identified by SWATH-MS proteomic analyses that are under-represented in *chn-1(tm2692)* vs. N2 wild-type *C. elegans* samples processed by lysis with SDS-based lysis buffer.**

Protein	Gene	*p*-Value	Fold Change	-Log (*p*-Value)	Log (Fold Change)	Regulation	Label
Glutamine synthetase	*gln-6*	4.90E-02	0.275	1.309	-0.560	Down	1
Structural maintenance of chromosomes protein 3	*smc-3*	2.69E-02	0.330	1.570	-0.482	Down	2
Probable pre-mRNA-splicing factor ATP-dependent RNA helicase mog-5	*mog-5*	1.82E-02	0.370	1.739	-0.432	Down	3
Biogenesis of lysosome-related organelles complex 1 subunit 2	*blos-2*	1.74E-02	0.385	1.759	-0.414	Down	4
Ribosomal_S10 domain-containing protein	*mrpl-48*	1.44E-02	0.402	1.840	-0.396	Down	5
Peptidyl-prolyl cis-trans isomerase	*pinn-4*	5.04E-02	0.410	1.298	-0.388	Down	6
Matrin-type domain-containing protein	*T13H5.4*	5.35E-02	0.424	1.272	-0.373	Down	7
Uncharacterized protein	*D1086.6*	9.31E-04	0.425	3.031	-0.371	Down	8
Vitellogenin-5	*vit-5*	4.31E-06	0.428	5.366	-0.369	Down	9
Col_cuticle_N domain-containing protein	*col-119*	1.69E-04	0.437	3.772	-0.360	Down	10

chn-1(by155) versus wild-type controls included ribosomal_S10 domain-containing protein and Guanine nucleotide-binding protein subunit beta-2, with fold changes of 0.31 and 0.34, respectively (Figure 3.7 and Supplemental Table A8). Proteins most substantially overexpressed in SDS-processed *chn-1(tm2692)* versus N2 controls included BPTI/Kunitz inhibitor domain-containing protein and Tudor domain-containing protein, with fold changes of 9.48 and 4.47, respectively (Figure 3.8 and Table 2.6). Top proteins underexpressed in SDS-lysed *chn-1(tm2692)* versus wild-type animals included probable pre-mRNA-splicing factor ATP-dependent RNA helicase *mog-5*, biogenesis of lysosome-related organelles complex 1 subunit 2, peptidyl-prolyl cis-trans isomerase, Matrin-type domain-containing protein, and vitellogenin-5, with fold changes of 0.37, 0.39, 0.41, 0.42, and 0.43 (Figure 3.8 and Table 3.13). Proteins substantially altered in response to *chn-1* ablation were frequently involved in cellular transport/secretion, including processes such as protein and amino acid trafficking, endo- and exocytosis, lipid transport, the intracellular transport of organelles, and modulating channel activity more generally. Recurrent processes associated with proteins altered in response to *chn-1* deletion also encompassed several pertaining to the protein quality control network, including protein folding/refolding, modulating the functions of proteases and protein aggregation, and ameliorating the effects of aging and neurodegeneration more generally, as well as proteins associated with oxidative stress resilience. The *chn-1*-null mutants also exhibited protein changes suggesting a susceptibility to altered epigenetic regulation, including that pertaining to methylation and transcriptional regulation, as well as proteins implicated in DNA damage repair. Finally, recurrent experimental hits also included several mitochondrial, spliceosomal, and ribosomal proteins.

KEGG pathway topology analyses in SDS-processed *chn-1(by155) chn-1* mutants versus wild-type controls revealed significant effects on viral life cycle – HIV-1 ($p < 0.01$) and spliceosome ($p < 0.05$), and enrichment approaching significance in endocytosis ($p = 0.086$) and biosynthesis of amino acids ($p = 0.094$) (Figure 3.9 and Table 3.14). In SDS-lysed *chn-1(tm2692) chn-1* mutants versus wild-type controls, spliceosome ($p < 0.01$) and FoxO signaling pathway ($p < 0.05$) were significantly enriched, and biosynthesis of amino acids approached significance ($p = 0.079$) (Figure

3.9 and Table 3.14). In CHAPS/Urea-processed *chn-1(tm2692)* mutants versus N2 controls, both biosynthesis of amino acids (p = 0.053) and spliceosome (p = 0.055) approached significance, but neither CHAPS/Urea-processed *chn-1(by155)* mutants versus N2 controls nor *chn-1(tm2692)* mutants versus wild-type controls had any significantly enriched pathways (Figure 3.9 and Table 3.14).

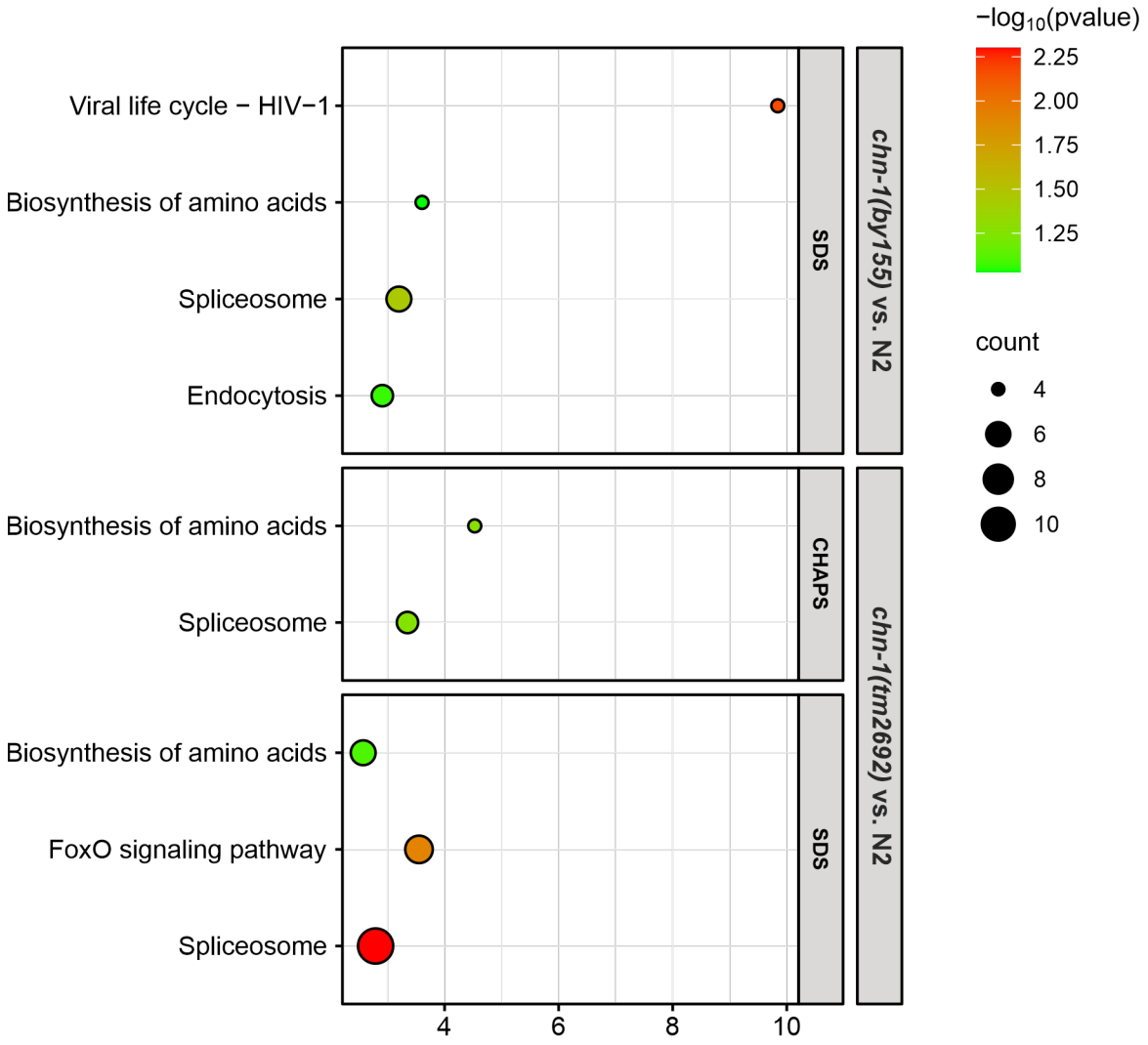

Figure 3.9 **KEGG pathway analysis derived from the proteomics of our *C. elegans* model.** SWATH-MS data comparing either *chn-1(by155)* or *chn-1(tm2692) C. elegans* mutants with N2 wild-type controls was analysed using DAVID and plotted by SRPlot. Samples were processed with either CHAPS/Urea- or SDS-based lysis buffer. Only proteins that met the cut-off criteria (fold changes of ≤0.67 and ≥1.5) were used for the analysis. Each pathway is colour-coded based on statistical significance (–log10(*p*-value)). Pathways related to CHIP loss-of-function are listed in Table 3.14.

Table 3.14 **KEGG pathways related to CHIP loss-of-function in either *chn-1(by155)* or *chn-1(tm2692)* mutants.** Shared pathways identified in either *chn-1(by155)* or *chn-1(tm2692) C. elegans* mutants when compared to N2 wild-type animals (using DAVID). The lysis buffer, strain, number of associated genes ("count") and an association index (probability (*p*-value) as well as enrichment score) for each pathway is included.

Pathway	Strain	Lysis Buffer	Count	Enrichment	*p*-Value
Biosynthesis of amino acids	*chn-1(tm2692)*	CHAPS/Urea	4	4.529	5.34E-02
Spliceosome	*chn-1(tm2692)*	CHAPS/Urea	5	3.349	5.53E-02
Viral life cycle - HIV-1	*chn-1(by155)*	SDS	4	9.843	6.84E-03
Spliceosome	*chn-1(by155)*	SDS	6	3.199	3.48E-02
Endocytosis	*chn-1(by155)*	SDS	5	2.908	8.58E-02
Biosynthesis of amino acids	*chn-1(by155)*	SDS	4	3.604	9.35E-02
Spliceosome	*chn-1(tm2692)*	SDS	11	2.790	5.01E-03
FoxO signaling pathway	*chn-1(tm2692)*	SDS	7	3.551	1.23E-02
Biosynthesis of amino acids	*chn-1(tm2692)*	SDS	6	2.572	7.93E-02

3.4 Discussion

Through both its chaperone-dependent and non-canonical activities, CHIP is central to the global protein landscape. Here, I found that *chn-1* ablation was linked to lifelong global proteomic changes based on *chn-1*-null nematodes having (i) altered expression of a focused array of proteins, (ii) differentially enriched gene ontology terms related to protein transport, rRNA processing, macromolecule methylation, primary metabolic processes, and endosomal transport (Appendix B), (iii) variably expressed pathways related to the biosynthesis of amino acids, spliceosome, endocytosis, and the FoxO signaling pathway linked to (iv) a substantially shortened lifespan. Particularly overrepresented among global *chn-1*-dependent proteomic markers were proteins involved in the structure and function of the Golgi and associated membrane networks, proteins regulating mitochondrial biogenesis and dynamics, as well as proteins involved in the epigenetic regulation of gene transcription. Moreover, many of the proteins found to be substantially altered by *chn-1* ablation are involved in both the pathogenesis of neurodegenerative diseases and cancer, highlighting the possible inverse comorbidity and biological connection between the two conditions[394].

Although proteomic analyses were performed on pre-gravid animals collected early in adulthood to minimize the impact of developmental and reproductive processes unrelated to *chn-1* deletion on the proteome, some natural variation in developmental rate between individuals was inevitable. Therefore, it is possible that some proteins, pathways, and gene ontology terms found in the results may reflect developmental or reproductive processes rather than the presence or absence of CHN-1. While this would be true in any study, further validation experiments to both confirm and replicate these results would be valuable and add strength to the findings. It is also of note that, while the deletion of some genes can impact developmental rate in mutant vs. N2 wild-type animals (e.g., *npr-1* and *glb-5*)[395], there are no studies that directly compare the developmental rate of *chn-1*-null mutants to N2 wild-type *C. elegans*. To account for inter-strain variation in developmental rate, animals were visually examined under a microscope on an hourly basis on the day of sample collection, with no notable between-strain differences observed. Similarly, while reproductive output in relation to genotype has been observed in response to the deletion of a number of other genes

(e.g.,lincRNAs, *clk-1*, *daf-2*, *dhc-1*, *mel-28*, and yolk protein regulators), no studies investigate the effects of *chn-1* deletion on fertility or brood size in *C. elegans*, and visual examination under a microscope revealed no discernable differences between N2 wild-type, *chn-1(by155)*, and *chn-1(tm2692)* mutants[396-399]. Future studies should further delineate the role of *chn-1* in development and reproduction throughout the lifespan, especially as the impact of *chn-1* deletion on longevity may also depend at least partially on the developmental timing of its effects. For instance, the deletion of several aging-related genes (e.g., *unc-36*)[400] impairs development and shortens lifespan, while RNAi knockdown of these same genes may instead avoid the disruption of developmental processes and even *extend* lifespan through the reduction of age-related damage, as posited by the antagonistic pleiotropy theory of aging[401].

A large number of protein hits did not overlap between *chn-1(by155)* and *chn-1(tm2692)* mutants. In proteomics studies, many reported hits fail to replicate or correspond to physiologically meaningful changes. More generally, noise in proteomics experiments may be introduced by technical variability (e.g., minor variability in sample handling, storage, peptide recovery, and instrument performance, including variations in ionization variability, for instance), batch effects, minor differences in sample preparation, or incomplete or inconsistent peptide identification and quantification (e.g., due to low signal-to-noise, co-eluting peptides) ultimately creating apparent differences in protein abundance unrelated to biological phenomena. Additionally, aging is intrinsically variable between animals, tissues, and cells, with small cohort sizes further amplifying this variability and leading to the detection of spurious apparent patterns between strains. Finally, the complexity and dynamic range intrinsic to the proteome may impact protein hits shown in analyses that do not reflect true, long-term aging-related physiological changes. Altogether, protein hits shared between both *chn-1* deletion mutants are more likely to be reproducible and physiologically meaningful as a starting point for additional validation experiments.

In both *chn-1(by155)* and *chn-1(tm2692)* mutants, *chn-1* ablation substantially changed 33 proteins in CHAPS/urea-processed samples and 46 proteins in SDS-processed samples. KEGG pathways related to the biosynthesis of amino acids as well as the spliceosome were among the most substantially altered across both mutants and

detergent conditions. Thus, while individual protein changes were not identical across detergents, aggregate *chn-1*-dependent proteomic changes ultimately led to a shared proteomic phenotype. Accordingly, previous work has shown CHIP-associated impacts on protein trafficking[280,402], mRNA production and splicing during heat stress[403], transcriptional regulation[404], and mitochondrial integrity[277,404].

The covalent attachment of ubiquitin to its substrates facilitates several distinct functions[405-408]. Substrates can be either mono- or poly-ubiquitinated, or both[409], with the point of attachment between adjacent ubiquitin moieties determining both the nature of the chain and the fate of the substrate[405,410]. CHIP interacts with chaperones through its TPR domain, resulting in the formation of a complex that promotes conformational changes in CHIP itself, thus allowing it to ubiquitinate other chaperone-bound client proteins or chaperones themselves[224]. CHIP mediates lysine 27, lysine 48, and lysine 63 polyubiquitin chains[223,240,247,411,412]. CHIP facilitates the formation of several structurally and functionally distinct polyubiquitin chains, and CHIP-mediated substrate ubiquitination can be either proteolytic or non-proteolytic[412]. Lysine 48-linked polyubiquitin chains, for example, are primarily associated with proteasomal degradation[413-415]. Conversely, lysine 63-linked chains largely mediate non-proteolytic processes, such as DNA repair, endocytosis, and autophagy[416,417], while lysine 27-linked chains moderate processes related to both mitochondrial integrity and proteasomal degradation, among others[197,405,412,418].

Evidence exists of crosstalk between different histone modifications. Previous studies have linked myriad episignature-associated genes to the ubiquitination pathway, thus suggesting a link between ubiquitylation and methylation[419]. For instance, monoubiquitination of the histone protein H2B at lysine 120 by the RAD6/BRE1 ubiquitin ligase complex is both sufficient and necessary for the methylation of histone H3 lysine 4 (H3K4) in human cells[420]. One of the most substantially overexpressed proteins in response to *chn-1* ablation across both deletion mutants was the bromodomain-containing protein. Bromodomains specifically bind to acetylated lysine residues on histone tails, and directly mediate chromatin remodeling and transcriptional regulation[421,422]. Other proteins differentially expressed in *chn-1*-null animals included protein-lysine N-methyltransferase M142.8, a catalyst of histone lysine methylation, and

methyltransferase small domain-containing protein, predicted to be a catalytic subunit of the eRF1 methyltransferase complex. In *S. cerevisiae*, Mtq2 forms a heterodimer with Trm112, a methyltransferase protein activator, to methylate the translation release factor eRF1 and thus terminate translation[423,424]. Additionally, macromolecule methylation was among the most significantly enriched biological processes. Thus, the present findings suggest CHIP-mediated processes may be implicated in post-translational modifications beyond ubiquitination, such as histone-associated chromatin remodeling, among others.

The transcription factor SMA-9 was one of the most substantially underexpressed proteins across both *chn-1(by155)* and *chn-1(tm2692)* mutants. SMA-9, a member of the neuroprotective transforming growth factor-β (TGF-β) pathway[425-427], is a zinc finger protein involved in several key functions. For instance, RNAi-mediated *sma-9* silencing in amyloid-β-expressing transgenic *C. elegans* strains resulted in both increased amyloid plaque formation as well as elevated levels of reactive oxygen species[428], corroborating previous evidence for the role of TGF-β in amyloid-β clearance as well as plaque reduction[429]. The absence of TGF-β has previously been associated with an increase in reactive oxygen species[427,430], suggesting that an amyloid-β-dependent increase in the steady-state levels of oxidative species may contribute to the clearance of these misfolded aggregates[428]. Aberrant *sma-9* expression has also been linked to reduced motor activity and altered excitatory neurotransmission[428,431], suggesting a role for the TGF-β signaling cascade in connecting the altered neurotransmitter profile and neuronal death to the disordered movement characteristic of Alzheimer's disease[432,433]. Finally, both *chn-1* and *sma-9*-null animals have significantly reduced longevity, mediated by the phosphorylation of DAF-16 through insulin/IGF-1 signaling[7,428], altogether indicating that both CHN-1 and SMA-9 may both play crucial roles in the mitigation of pathological aging-associated changes. Indeed, SMAD proteins, central players in the regulation of TGF-β signaling, are degraded in a ubiquitin/proteasome system-dependent manner[434], and CHIP has been shown to indirectly regulate TGF-β signaling by directing the basal Smad3 level[435,436].

Altered metabolic and mitochondrial dynamics were heavily overrepresented in the chn-1-*null* proteomic landscape. Previously, CHIP rescued several mitochondrial

defects in mutants of the mitochondrial kinase PINK1 (PTEN-induced putative kinase 1), including excessive fusion, reduced ATP content, and crista disorganization in *D. melanogaster*[378]. Here, *chn-1* ablation led to significant underexpression of FIS1-related protein fis-2, previously found to play a key role in mitochondrial fission[437], implicating CHIP in both mitochondrial fission and fusion processes. *chn-1*-null animals also showed changes in the FoxO signaling pathway. Interestingly, FoxO transcription factors mediate both mitochondrial fusion (via mitofusin 1 and 2) and fission (via dynamin-related protein 1, mitochondrial fission protein 1, and mitochondrial elongation factor 1) during transcriptional, posttranscriptional, and posttranslational pathways[438]. Similar mitochondrial dysfunction was ameliorated in mutants of the E3 ubiquitin ligase Parkin, which has in turn been found to control the stability of the downstream CHIP-IRF1 axis through its proteolytic functions[439]. Altogether, these results suggest that CHIP, Pink1, and Parkin act in a shared pathway to maintain mitochondrial integrity while attenuating mitochondrial defects associated with Parkinson's disease[437].

chn-1 mutants also exhibited changes in the biosynthesis of amino acids and rRNA processing, with individual proteins such as mitochondrial ribosomal protein, small, being differentially expressed in *chn-1*-null animals. Under conditions of proteotoxic stress, including those causing proteasomal inhibition, Hsp70 is separated from the ribosomal machinery by the accumulation of misfolded proteins, thus promoting the aberrant folding of newly synthesized polypeptides and resulting in the general inhibition of global protein synthesis[440]. It is possible that the inhibition of CHIP's protein quality control-associated functions in the *chn-1*-null animals led to a similar cellular phenotype, with an increased concentration of misfolded, newly synthesized proteins impacting both ribosome-associated processes as well as protein and amino acid biosynthesis.

The spliceosome was among the top KEGG pathways enriched in *chn-1* mutants. Although research related to the interplay between CHIP and splicing activity is scarce, preliminary data have found that CHIP-mediated splicing, chaperone-independent ubiquitination of RNA binding proteins, and mRNA production may take place under certain cellular conditions[403]. Specifically, RNAseq and splicing analyses revealed that over two-thirds of transcripts induced during heat stress were dependent

upon CHIP, with a subset of these being entirely dependent on CHIP[403]. Pathway analyses of transcripts with alterations in stress induced CHIP-dependent splicing found significant enrichment in processes related to aging and mortality, preweaning lethality, and abnormal survival[403]. In conjunction with this, other studies have found that, among CHIP knock-out mice, approximately 20% die prior to weaning and those that survive exhibit both decreased longevity as well as an accelerated aging phenotype[9]. Altogether, these results suggest that an impaired RNA processing and splicing-related stress response contributes to longevity-associated phenotypes in CHIP-null animals.

Consistent with differentially expressed fold changes of individual proteins including Conserved oligomeric Golgi complex subunit 6 (COG6) and Rab6, a Golgi-associated GTPase[441], both *chn-1(by155)* and *chn-1(tm2692)* gene set enrichment analyses (Appendix B) and KEGG pathway topology analyses revealed changes in such processes as protein transport, endosomal transport, and endocytosis. This draws attention to possible proteomic dysregulation of protein trafficking in *chn-1*-null animals. For instance, protein quality control in the endoplasmic reticulum has been found to depend largely on the cooperative interaction between CHIP and the Hsp70 protein, with a CHIP mutation eliminating E3 ligase activity inhibiting Hsp70-dependent ubiquitination and degradation of a model client, Cystic Fibrosis Transmembrane Conductance Regulator (CFTR)[442]. Interestingly, both COG6 and Rab6 are implicated in retrograde transport, with the two proteins sharing a Golgi retrograde trafficking pathway defined initially by the endogenous intracellular transport of subtilase cytotoxin[443]. Rab6 is also a known binding partner of COG6, which itself interacts with a subset of Golgi SNARE proteins to maintain Golgi complex integrity[444]. Indeed, the disruption of Golgi morphology and protein trafficking is a pathological feature of several neurodegenerative disorders, with ineffectual intracellular trafficking machinery contributing to the accumulation and aggregation of misfolded proteins[445].

The following genes/proteins were altered in *chn-1* deletion mutants under the Viral life cycle – HIV1 KEGG pathway: Charged multivesicular body protein 4b (CHMP4B, UniProt ID: Q21959), *vps-20*/Charged multivesicular body protein 6 (CHMP6, UniProt ID: Q9BL60), *spt-5*/Transcription elongation factor SPT5 (UniProt ID: Q21338), and *hgrs-1*/Hepatocyte growth factor-regulated tyrosine kinase substrate

(UniProt ID: Q17796). CHMP4B mediates membrane scission during multivesicular body formation and is critical for virion release, with aberrant CHMP4B function possibly impairing antiviral endosomal sorting and autophagic responses[446,447]. CHMP6 mediates viral egress efficiency as well as endosomal cargo sorting, with CHMP6 dysregulation altering antigen-presentation pathways relevant to innate immunity[448-450]. Similarly, SPT5 and HRS modulate viral transcription/immunity-related gene expression[451-455] and innate immune receptor turnover[456,457], respectively. Thus, the enrichment of this pathway in *chn-1*-null mutants likely reflects immunity-related changes with a shared relevance to HIV1 in humans.

The present findings provide novel insights into the potential mechanisms underlying the pro-aging effects of aberrant CHIP function by correlating *chn-1* deletion in *C. elegans* to a proteomic landscape characterized by changes in protein trafficking, rRNA processing, epigenetic modifications, as well as splicing and mitochondrial integrity. These data also support previous work suggesting a CHIP-dependent spliceosomal and RNA-related stress response[403], and suggest a novel role for CHIP in both the TGF-β signaling cascade[428] and maintaining Golgi complex integrity. Future studies should validate these findings, in addition to further characterizing the relationship between the neuroprotective functions of CHIP, SMA-9, and protein trafficking.

Chapter 4: *chn-1* Deletion Affects Golgi Morphology, TGF-β Signalling, and Retrograde Transport

4.1 Introduction

The Golgi complex, an organelle central to regulating secretory functions in the cell, plays a crucial role in the sorting and processing of cargo. Cellular stress, however, has been found to disrupt the unique structure and organization of the Golgi, with neurons being particularly sensitive to Golgi stress[1]. Indeed, the early dissassembly and fragmentation of the Golgi apparatus correlates with a number of neurodegenerative conditions[1]. Here, I include background information on the general structure and function of the Golgi complex as well as its role in both healthy and pathological aging. I conclude with an introduction to E3 ligases and the Golgi, culminating in an introduction to and overview of the validation experiments performed in this chapter (i.e., focusing on the effects of CHIP deletion on Golgi organization and proteins involved in retrograde transport as well as TGF-beta signalling and lifespan regulation).

4.1.1 The Role of the Golgi Apparatus in Neuroprotection and Degeneration

4.1.1.1 Overview of the Golgi Complex

The Golgi apparatus comprises several dispersed but interconnected structures including an assemblage of layered lamellar sacks, known as cisternae, as well as their associated vesicles[479,480]. These layered cisternae are organized parallel to one another in units known as Golgi stacks, which are themselves laterally connected by tubules to form a continuous ribbon-like network[480,481].

In the biosynthetic secretory pathway, Coat Protein Complex II (COPII) facilitates the formation of transport vesicles to carry cargo molecules from the endoplasmic reticulum (ER) to the Golgi apparatus or the ER-Golgi intermediate compartment in a process known as anterograde transport[482]. These COPII-coated vesicles detach from

ER exit sites (ERES) or transitional ER (tER), specialized ribosome-free ER regions subclustered proximally to the Golgi and allowing for the transport of biological cargo from the ER to the Golgi apparatus. The COPII-coated vesicles discard their coats upon budding from the ER, thus leaving them vulnerable to membrane fusion with other vesicles. This can occur in both vesicles sharing a compartment (homotypic fusion) or in those occupying different compartments (heterotypic fusion)[483]. Both processes depend on a particular suite of compatible soluble N-ethylmaleimide-sensitive factor activating protein receptor (SNARE) proteins interacting between membranes[484].

Secretory proteins of high abundance can bypass the need for sorting receptors to leave the ER, however the mechanisms underlying this phenomenon remain poorly understood. One noteworthy exception is the ER-Golgi intermediate compartment 53 (ERGIC53) protein, a receptor acting as a mannose-binding lectin to encase a discrete set of secretory proteins into COPII-coated transport vesicles by binding to mannose residues on target proteins[485]. Its role was elucidated when patients carrying a loss-of-function mutation in ERGIC53 exhibited decreased levels of two blood-clotting factors, Factor V and Factor VIII, leading to coagulation deficiencies and excessive bleeding[485,486].

On its way to the Golgi apparatus, secretory cargo traverses a tubulo-vesicular system known as the ERGIC or vesicular-tubular cluster (VTC). The ERGIC is closely associated with ERES[487] and acts as a sorting station for cargo leaving the ER[486]. The Golgi complex itself can be subdivided into the *cis*-Golgi, medial, and *trans*-Golgi compartments, with ER-derived cargo traversing the peripheral Golgi structures to then enter the Golgi cisternae stacks through the *cis*- end and progressing through the medial compartment towards the *trans*- end[488], from which transport carriers and secretory cargo are further sorted for transport to their final destinations[489,490]. The addition of oligosaccharide side chains to lipids and proteins traversing the Golgi stacks also function to aid their lysosome-bound vesicular transport, with specific side chains associated with the direction of molecules to specific transport vesicles[491,492].

The Golgi apparatus functions to sort and subsequently prepare lipids as well as soluble and transmembrane proteins synthesized by the endoplasmic reticulum for transport to the cell surface, large dense-core vesicles, or the endosomal-lysosomal

system[493,494], with secretion-associated Golgi proteins including golgins, the conserved oligomeric Golgi (COG) complex, and the Golgi-associated retrograde protein (GARP) complex, among others (Figure 4.1). In addition to its essential role in the regulation of secretory processes and signaling molecules[495], the Golgi complex also facilitates carbohydrate synthesis as well as the synthesis of glycosaminoglycans for animals[496], and is involved in myriad activities including glycosylation, mitosis, DNA repair, stress responses, autophagy, apoptosis, and inflammation[497,498].

4.1.1.2 Protein Quality Control in the Golgi Apparatus

Secretory proteins must pass stringent quality control checkpoints prior to leaving the ER, as improperly formed dysfunctional proteins may interfere with proteins and processes further downstream in the biosynthetic secretory pathway, necessitating extensive remedial action[499]. Misfolded proteins are kept from leaving the ER, and in some instances, such as in the case of multimeric complexes, proteins must undergo full assembly before exiting the ERES. Indeed, more than 90% of proteins fail to reach their final destination on the cell surface, thus requiring cells to maintain an abundant supply of newly synthesized proteins to ensure the functional subset that has been correctly folded and assembled is sufficient to meet the needs of the cell[500,501]. The departure of misfolded and/or improperly assembled proteins from the ER is impeded, for example by the chaperone-dependent disruption of molecular processes and signaling cascades[499], and these proteins are then ushered back into the cytosol and subsequently degraded by the proteasomal machinery.

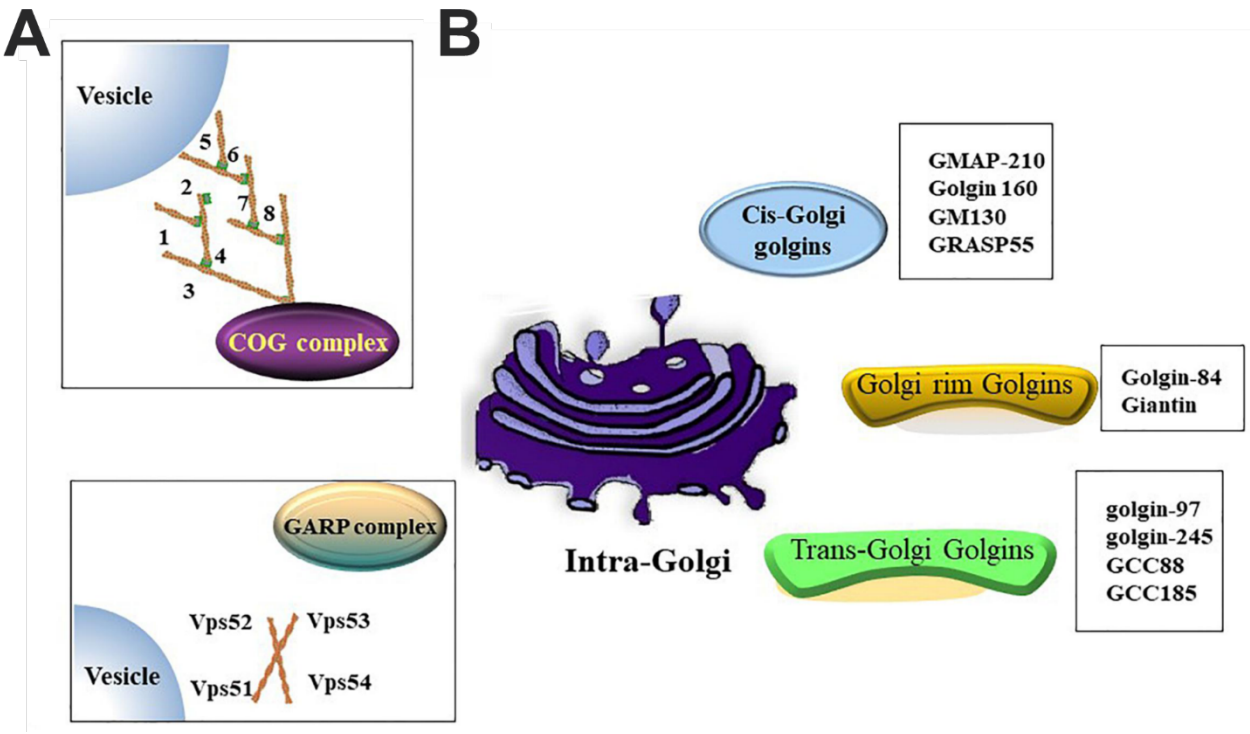

Figure 4.1 **An overview of Golgi proteins involved in mediating vesicular transport and golgins across compartments**. (***A***) An overview of Golgi proteins involved in mediating vesicular transport. Both the COG complex, made up of eight COG subunits (COG1-8), and the GARP complex (comprised of VPS51, VPS52, VPS53, and VPS54) are membrane tethering complexes acting to facilitate cargo trafficking. (***B***) A summary of golgins across compartments. Golgins act to selectively tether transport cargo-containing transport vesicles at the Golgi complex. Figure reproduced from Deng et al. 2020.

4.1.1.3 Retrograde Transport and the COG Complex

Improperly folded or assembled proteins, as well as displaced ER-resident and budding proteins, cannot proceed through the Golgi-dependent secretory trafficking pathway for further transport and modification and are instead recovered from or near to the ER via a process known as retrograde (or retrieval) transport. Newly forming VTCs will give rise to budding Coat Protein Complex I (COPI) vesicles of their own, in addition to the COPII-coated vesicles facilitating anterograde transport. These COPI-coated vesicle retrieval mechanism regulates coatomer assembly reactions, in particular the consecutive assembly of COPI-coated vesicles immediately following COPII shedding upon vesicular budding from the ER. Retrograde transport occurs as the VTCs travel from the ER to the Golgi complex, with the ratio of the COPI/COPII-coated clusters gradually changing as proteins and VTCs themselves are retrieved for transport back to the ER[502-504].

Two primary, non-mutually exclusive models have emerged to describe the movement of secretory cargo proteins through the Golgi cisternae along with the fixed positions of cisternal enzymes. The vesicular transport model posits that cisternae are stable compartments allowing the passage of coated vesicles containing secretory cargo from the ER to the *trans*-Golgi in an enzyme-dependent manner, with glycosylation enzymes localized at each cisterna modifying secretory cargo to facilitate passage. The cisternal maturation model, on the other hand, posits that cisternae are transient structures, forming and maturing as needed from *cis*-to-*trans* prior to disassembling[505].

The COG complex, consisting of eight COG subunits (COG1-8), facilitates the retrograde transport of protein cargo both within the Golgi itself and from the Golgi to the ER by acting as a cytoplasmic tether connecting COPI-coated vesicles to *cis*-Golgi membranes[506]. The functions of this complex are congruent with the cisternal maturation model as COG subunit mutations greatly impact both Golgi enzyme distribution and protein glycosylation patterns[507], indicating that the function and location of Golgi enzymes is dynamic at least some of the time. COG subunit mutations may spur Golgi glycosyltransferase dysfunction, leading to aberrant glycosylation patterns

and associated pathological consequences. Mutations in COG subunits have been causatively linked to congenital glycosylation disorder type II (CDG-II), for example[508].

4.1.1.4 The Golgi Apparatus and Neurological Diseases

The Golgi complex adapts to the physiological needs of the cell. Golgi fragmentation, a morphological phenomenon characterized by the dispersal or thorough disintegration of cisternal stacks, is one such adaptation (Figure 4.2). The causes of Golgi fragmentation are diverse and include growth factor signaling dysregulating ER-Golgi trafficking, the compromised retrieval of membrane proteins from endosomes to the Golgi apparatus, and aberrant protein glycosylation due to ER-lysosome-Golgi network dysregulation[509,510]. Protein glycosylation is an essential co- and post-translational modification of membrane and secretory proteins. Glycosylation increases the hydrophilicity of protein intermediates and impedes the formation of aggregates, thus playing a central role in protein quality control and the prevention of neurodegeneration.

Stressors typically trigger an initial compensatory response from the Golgi apparatus, such as compensatory expansion, manifesting as an adaptive reorganization of the cellular machinery. In non-neuronal cells, Golgi fragmentation may initially ameliorate disruptions to cellular homeostasis by facilitating the rapid transport of proteins to their final destinations. In neurons, the sustained presence of excitotoxins and oxidative stressors negate the initial benefits of Golgi fragmentation, instead promoting atrophy and other negative cellular effects including cell death and neurodegeneration. Indeed, Golgi fragmentation has been found to precede apoptosis in *in vitro* models of mechanical cell damage. Oxidative insults are both a cause and consequence of Golgi fragmentation, resulting in a negative feedback cycle ultimately culminating in augmented stress signaling as well as neuronal dysfunction and deterioration. Conversely, the experimental attenuation of Golgi fragmentation decreases and decelerates apoptosis.

Oxidative insults or toxicant exposure can trigger physiological changes in the Golgi-ER network affecting the secretory pathway, including luminal pH alterations, ionic imbalances, cargo overload, and disruptions in glycosylation and glycosylation-related processes. Aberrant glycosylation is associated with impaired membrane trafficking, thus further amplifying Golgi stress. In response to this stress-mediated feedback loop,

cells will initiate compensatory processes and signaling pathways aiming to repair the Golgi machinery while limiting any associated adverse effects. Stress-repair signaling cascades include the procaspase-2/golgins-160 pathway, wherein procaspase-2 associates with upstream apoptotic regulators to shepherd Golgi matrix proteins containing nuclear localization signals, such as golgin-160 and giantin, to the nucleus[511,512]. The heat-shock protein 47 (HSP47) pathway protects cells from apoptosis induced by Golgi stress, with the downregulation of HSP47 leading to Golgi fragmentation and subsequently stress-induced apoptosis[513,514]. The transcription factor binding to IGHM enhancer 3 (TFE3) pathway ensures the dephosphorylation of TFE3 and mediates its nuclear translocation. Dephosphorylated TFE3 then binds a Golgi apparatus stress response element (GASE), thus activating the transcription of stress-response genes as well as increasing glycosylation enzyme and membrane trafficking protein expression[514,515]. The cyclic AMP-responsive element-binding protein 3 (CREB3)/ADP-ribosylation factor 4 (ARF4) pathway mediates ARF4, which regulates the trafficking of cargo proteins between the Golgi and ER[516-518]. Under conditions of Golgi stress, decreased ARF4 protein levels trigger the activation and nuclear translocation of CREB3, which in turn initiates transcription of ARF4[519]. The failure of these stress-repair pathways, however, ensures the degradation of the Golgi machinery and the death of the cell.

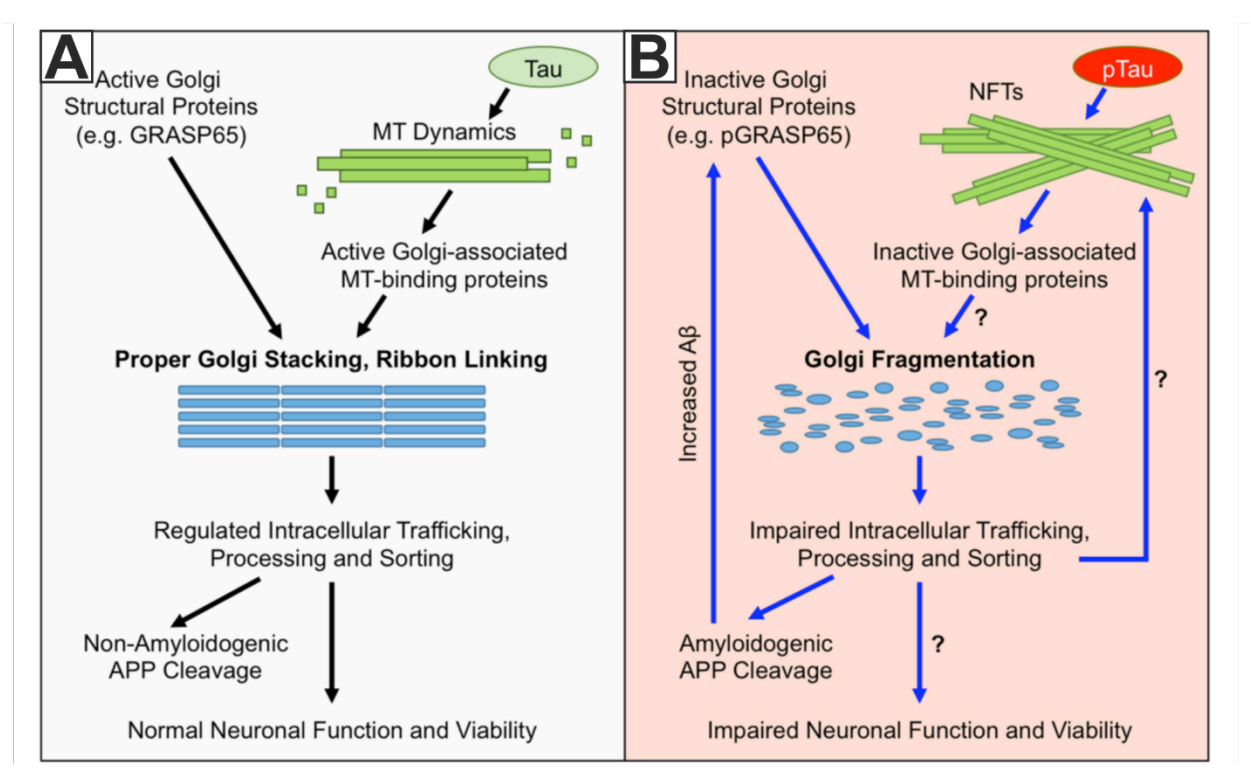

Figure 4.2 **The structure and function of the Golgi apparatus under normal and neurodegenerative conditions**. (***A***) The Golgi apparatus under normal conditions. The structural integrity of the Golgi complex is essential for healthy biosynthetic secretory processes, as well as the processing of amyloid-β precursor protein (APP) and APP-associated enzymes. Most APP processing occurs in a non-amyloidogenic manner. Golgi-associated structural proteins such as (unphosphorylated) Golgi reassembly stacking protein 65 (GRASP65) as well as a functional microtubule (MT) system maintain the structural integrity of the Golgi. In normal healthy cells, secretory cargo essential for neuronal function, including lipids, polysaccharides, and cell-surface proteins is appropriately modified, sorted, and transported to its final destination. Altogether, these processes culminate in a neuroprotective phenotype, sustaining neuronal health and integrity. (***B***) An overview of structural and functional Golgi defects in Alzheimer's disease. The function of Golgi-associated structural proteins may be compromised in a number of ways. For example, the degradation or phosphorylation of GRASP65 (pGRASP65), the hyperphosphorylation of tau (pTau), and the formation of neurofibrillary tangles (NFTs) disrupt MT function and impede protein trafficking. This leads to Golgi fragmentation and is characteristic of Alzheimer's disease. In turn, Golgi fragmentation leads to the dysregulated sorting, trafficking, and processing of APP and APP-associated enzymes, thus spurring amyloidogenic APP processing and further impairing GRASP65 function. More broadly, Golgi fragmentation impedes the sorting, processing, and trafficking of lipids, proteins, and polysaccharides essential for neuronal health, thus promoting neurodegeneration and cell death. Figure reproduced from Joshi et al. 2015.

Many neurodegenerative diseases are characterised by a complex and multifaceted pathogenesis involving both environmental and genetic influences affecting mitochondrial dysfunction, protein aggregation, oxidative stress exposure, autophagy impairment, neuroinflammation, and dopamine deficiencies, among others[520]. Structural and functional aberrations of the Golgi complex are also linked to myriad neurodegenerative conditions, including Alzheimer's disease, Parkinson's disease, amyotrophic lateral sclerosis, Huntington's disease, multiple-system atrophy, and Creutzfeldt-Jacob disease[521,522]. For instance, Golgi fragmentation is an early event across multiple neurodegenerative disorders, confirmed by *in vitro* and *in vivo* studies as well as postmortem analyses of tissue samples[514,522]. α-Synuclein (α-syn), implicated in the pathophysiology of synucleopathies including Parkinson's disease with and without dementia, dementia with Lewy bodies, and multiple-system atrophy, forms intercellular aggregates during the onset of Golgi fragmentation. This results in the formation of inclusions prone to amassing toxins, thus increasing a cell's vulnerability to oxidative stress and apoptosis[523].

Leucine-rich repeat kinase 2 (LRRK2), Ras-associated binding (Rab) proteins, vacuolar protein sorting-associated protein 52 homolog (VPS52), and cyclin-dependent kinase 5 (CDK5) all play a role in maintaining Golgi complex integrity and secretory transport[524]. For example, aberrant CDK5 activation results in CDK5 phosphorylating Golgi structural proteins and fragmenting Golgi, thus accelerating APP trafficking, increasing amyloid-β production and compromising secretory pathway function as well as neuronal integrity[525]. VPS52, a subunit of the GARP and endosome-associated recycling protein (EARP) complexes, interacts with LRRK2 to mediate retrograde protein sorting and membrane fusion at the *trans*-Golgi network[526]. LRRK2 itself plays a key role in the Golgi apparatus, with LRRK2 mutants disrupting its structural and functional integrity as well as Golgi-associated vesicular transport[527-530]. Moreover, complete inactivation of LRRK2 has been found to fragment Golgi and impair vesicular transport, endocytosis, and autophagy in human kidney proximal tubular epithelial cells[514].

4.1.1.5 Membrane Trafficking and Rab Proteins in Pathological Aging

Rabs are an evolutionarily conserved, membrane-localized family of small GTPases that play an essential role in regulating vesicle formation, transport, fusion, and intracellular membrane trafficking more generally. Acting as molecular switches, Rab proteins recruit effectors via their binding domain into distinct subcellular regions in their GTP-bound state and are inactive in their GDP-bound state[531-533].

When overexpressed, 14 Rab proteins can be directly phosphorylated by endogenous LRRK2. Rab8a, Rab8b and Rab10 act downstream of LRRK2, and when phosphorylated tend to localize and accumulate at the centrosome, thus impeding centrosome cohesion[534-536]. A subset of Rab GTPases are key LRRK2 substrates, with Rab10 and Rab12 phosphorylation increasing in the presence of malignant LRRK2 mutants[514]. A Rab32 missense mutation has been linked with Parkinson's disease, for example. The G2019S and I2020T LRRK2 mutations, along with the R1441C LRRK2 mutation in the Ras of complex/C-terminal of Roc (ROC/COR) GTPase domain, are also associated with Parkinson's disease[537]. Several mutations causally associated with Parkinson's disease alter LRRK2 kinase activity, for example by encouraging LRRK2 autophosphorylation. 14-3-3 proteins, regulatory adapter proteins that often bind to phosphorylated residues in signaling cascades, are integral to myriad biological processes underpinning neurodegeneration and pathological aging[538,539]. LRRK2 mutations that impede its interaction with 14-3-3 proteins may lead to a pathological accumulation of LRRK2 in tissues, potentially leading to the formation of large vacuoles and protein aggregates[540-542] as well as perturbations in autophagy[541,543].

Rab29 and LRRK2 engage in a reciprocal regulatory relationship, with Rab29 both acting upstream of and being phosphorylated by LRRK2. Rab29, along with Rab 32 and Rab38, interact directly with LRRK2 to influence its subcellular location. Rab 29 regulates LRRK2 activation in response to lysosomal stress and shuttles mutant LRRK2 into transport vesicles derived from the *trans*-Golgi network. Rab32 and Rab38 also interact directly with sorting nexin 6 (SNX6), a predominantly cytoplasmic protein involved in the intracellular trafficking of membrane receptors. SNX6 belongs to the sorting nexin family of proteins and is a component of the retromer. Rab32, together with Rab38, SNX6, and the retromer complex regulates signaling cascades mediating

LRRK2 activation. The Rab32-SNX6/retromer interaction mediates mannose-6-phosphate receptor localization on the *trans*-Golgi network, which contributes to Golgi trafficking[544,545].

Rab6, the most abundant Golgi-associated Rab protein, is crucial to both anterograde and retrograde transport as well as the maintenance of Golgi organization[546-551]. There are four Rab6 isoforms in mammalian cells, Rab6A, Rab6A', Rab6B, and Rab6C[552]. Rab6 deficiency in HeLa cells increases the number, length, and continuity of Golgi cisternae and results in a marked accumulation of both COPI- and clathrin-coated vesicular structures as well as coated membrane fission/fusion components[548]. In epistasis experiments, co-depletion of Rab6 impeded Golgi ribbon disruption caused by COG knockdown[553]. Interestingly, overexpression of either wild-type or GTP-restricted (Q72L) mutant Rab6A shepherded β-1,4-galactosyltransferase from the *trans*-Golgi network to the ER, thus facilitating retrograde transport, while overexpression of the GDP-restricted (T27N) mutant Rab6A inhibited retrograde transport[441,547,554], indicating that functional Rab6 activity is essential to retrograde Golgi trafficking. Indeed, one retrograde transport pathway is COPI-independent and regulated by Rab6[555,556].

4.1.1.6 The Effects of CHIP Ablation on Golgi Morphology, TGF-β Signalling, and Retrograde Transport

E3 ubiquitin ligases play a pivotal role in both healthy and pathological aging[458,459]. CHIP, an E3 ligase with intrinsic chaperone activity, was initially identified as a molecular triage causing proteins to undergo either refolding or degradation[1,460]. In addition to its E3 ubiquitin ligase-dependent targeting of partially or entirely unfolded proteins for destruction by the proteasome, CHIP also functions independently to mediate the structure and function of a distinct cohort of client proteins essential for myriad cellular processes[256]. In addition to its role in ubiquitin-dependent proteolysis, CHIP has been implicated in protein trafficking[278-280], TGF-β signaling[278,436,461-464], insulin pathways[7], and longevity[7,9]. CHIP plays a crucial cytoprotective role against pathological aging, and aberrant CHIP function has been implicated in a wide range of adverse health outcomes. In cancer, CHIP functions to inhibit tumor progression by facilitating the ubiquitination and degradation of various substrates, including human

epidermal growth factor receptor 2 (HER2)[465,466], yes-associated protein 1 (YAP1)[467], and protein tyrosine kinase 6 (PTK6)[468], among others. Many CHIP-related pathologies also converge on neurodegeneration, with CHIP-mediated proteins involved in the pathogenesis of Alzheimer's disease[223,469], amyotrophic lateral sclerosis[470,471], Parkinson's diseases[472-474], as well as several polyglutamine diseases, including Huntington's disease[475,476] and spinocerebellar ataxias[234].

CHIP has a broad influence on the cellular environment, impacting processes including transcriptional regulation[477], mitophagy[277], the ER stress response[12,478], and protein trafficking[278-280]. Indeed, previous research has suggested CHIP-dependent effects on epigenetic regulation[257], metabolic[374] and mitochondrial activities[268,378], as well as Golgi complex association and function[280] (Chapter 3). Notably, the insulin receptor is a direct target of CHIP, and experiments in *C. elegans* show a competitive relationship between proteostasis and longevity regulation through CHIP-assisted proteolysis, thus integrating metabolic and aging-associated processes. However, despite its involvement in protein trafficking and the ER stress response, little is known about the impact of CHIP on Golgi complex function and organization. Furthermore, while its role in the insulin receptor-dependent regulation of lifespan is well established[7], research concerning alternative mechanistic possibilities for the CHIP-dependent regulation of lifespan is scarce.

My previous proteomics experiments in *C. elegans* show sma-9 was one of the most substantially underexpressed proteins in response to *chn-1* deletion (Chapter 3). Both CHIP[435,436] and SMA-9[425-427] play crucial roles in modulating amyloid-β aggregation and cytotoxicity via the TGF-β signaling cascade. TGF-β deficiency has been associated with both increased levels of reactive oxygen species[427,430] and amyloid plaques[429], further supporting previous findings suggesting a TGF-β-mediated clearance of misfolded protein aggregates and amyloid-β-dependent oxidative stress[428]. Elevated levels of both amyloid plaques and reactive oxygen intermediates were also found in transgenic amyloid-β-expressing *C. elegans* strains subjected to RNAi-mediated knockdown of *sma-9*[428]. Aberrant *sma-9* expression has also been associated with motor deficits and altered excitatory neurotransmission[428,431], suggesting a possible association between TGF-β signaling, *sma-9* activity, and the altered neurotransmitter

profile, neuronal death, and disordered movement phenotype characteristic of Alzheimer's disease[432,433]. Finally, similar to *chn-1*-null animals, *sma-9*-null mutants exhibit decreased longevity due to the insulin/IGF-1 signaling-mediated phosphorylation of DAF-16[7,428], altogether suggesting that both CHN-1 and SMA-9 play a central role in mitigating pathological aging. Indeed, SMAD proteins are themselves degraded by the ubiquitin-proteasome system[434], and CHIP itself has been shown to indirectly affect TGF-β signaling by regulating the basal Smad3 level[435,436]. Thus, experiments aiming to both validate the proteomics results seen in Chapter 3 and further define the role of SMA-9 and CHIP in mediating longevity would be valuable.

Here, I (i) explore the interaction of CHIP with SMA-9 through longevity assays on *chn-1(tm2692); sma-9* double-knock-out mutants, (ii) explore the CHIP-dependent morphology of the Golgi complex in *C. elegans* by crossing *chn-1*-null mutants with a mannosidase Golgi marker, and in a human neuroblastoma cell line by analysing GM130 staining, (iii) validate the findings from previous proteomics experiments (Chapter 3) using immunofluorescence and immunoblotting for Rab6 and COG6, two proteins integral to retrograde transport, and (iv) distinguish the subset of proteins most likely to contribute to CHIP-mediated lifespan extension through the use of *CHIP*/*chn-1* rescue experiments. These experiments identified CHIP-related changes to Golgi morphology, the expression of proteins involved in retrograde trafficking, and a targeted subset of processes and pathways potentially implicated in CHIP-mediated lifespan regulation.

4.2 Materials and Methods

4.2.1 Experiment Overview

Previous proteomics data revealed SMA-9 to be among the most substantially underexpressed proteins in response to *chn-1* ablation (Chapter 3). To investigate whether the transcription factor SMA-9 and CHN-1 function in an integrative or independent manner, as well as to validate the proteomics data showing that SMA-9 was one of the most substantially underexpressed proteins in response to *chn-1* ablation across both CHAPS/Urea- and SDS-based sample processing, lifespan assays

were performed on *chn-1(tm2692)* and *sma-9* deletion mutants, as well as *chn-1(tm2692); sma-9* double-knock-out mutants.

The proteomics data suggested altered Golgi function in response to *chn-1* ablation. Thus, the CHN-1/CHIP-dependent Golgi phenotype was further assessed in *chn-1(tm2692)* mutants relative to wild-type controls using a mannosidase II::GFP marker. Additional validation experiments of individual protein hits included immunofluorescent staining of Rab6, COG6, and GM130, a cis-Golgi matrix protein, in wild-type and CHIP knock-out human SH-SY5Y neuroblastoma cells. These data were further supplemented by Western blotting experiments investigating Rab6, COG6, and GM130 expression in wild-type and CHIP knock-out SH-SY5Y cells lysed with either Tween 20, Triton X-100, RIPA, or CHAPS/Urea-based lysis buffers to quantify total CHIP-dependent protein-of-interest levels while accounting for buffer-dependent protein extraction variability.

Preliminary lifespan validation experiments involved the generation of both human and *C. elegans* orthologue CHIP rescue strains via bombardment and subsequent hygromycin B selection, followed by the visual selection of fluorescent transgenic animals. The following primers were used to clone the *chn-1* promoter region: Pchn-1_AttB4-F (5'-GGGGACAACTTTGTATAGAAAAGTTGTAACCGCGTGTAGTTTTACCAACC-3'); Pchn-1_AttB1-R (5'-GGGGACTGCTTTTTTGTACAAACTTGTGCTGCAAACGCTGAAAATAAGCGGA-3'); 1163.chn-1tm2692Ex-F (5'-AGCGTTTGCAGCATGTCAAG-3'); and 1164.chn-1tm2692Ex-R (5'-AGCATCTCAGGAACCTCCCT-3'). Gateway Cloning was performed as previously described with slight modifications[557] using the following entry vectors: pDONR P4-P1R (Position 1, *chn-1* promoter); pDONR 221 (Position 2, *h*CHIP/*Ce*CHIP); and pDONR P2r-P3 (Position 3, *m*Kate entry vector: SL2-mKate::let-858 3'UTR) (Invitrogen). Where appropriate, successful incorporation into each vector was verified by transforming into DH5α cells and sequencing the purified DNA (Source Bioscience, Cambridge, UK).

Two independently-derived *h*CHIP, one *Ce*CHIP strain, and an *m*Kate control were generated from each *chn-1*-null mutant (*chn-1(by155)* and *chn-1(tm2692)*), and

lifespan assays performed to confirm the rescue of nematode lifespan in rescue strains. N2 wild-type controls, *chn-1(tm2692)* mutants, and I then subjected the *h*CHIP/*Ce*CHIP rescue strains derived from *chn-1(tm2692)* mutants to extensive proteomic analyses for by either CHAPS/urea- or SDS-based lysis approaches, and proteins rescued in the *h*CHIP/*Ce*CHIP strains were thus inferred to drive CHIP/CHN-1-associated lifespan extension.

Both CHAPS/urea- and SDS-based lysis approaches were employed, as my previous data showed substantial detergent-based differences in protein solubility (Chapter 2 and Chapter 3). That is, lysis by SDS, a highly-denaturing anionic detergent, resulted in a significantly altered protein solubilization profile when compared to lysis by CHAPS/urea, a mild, non-denaturing zwitterionic detergent conbined with a chaotropic agent, respectively (Chapter 2). Specifically, CHAPS and urea effectively solubilized membrane-associated proteins, and in particular, peripheral membrane proteins, while SDS was more effective at global protein extraction as well as the solubilization of transmembrane proteins. SDS-based sample processing has also been found to enrich basic proteins due to the anionic properties of its sulfate group, while CHAPS and urea may be predisposed to the preferential extraction of proteins with zwitterionic and non-ionic properties, respectively (Chapter 2). Therefore, to gain the best possible understanding of the interplay between CHIP ablation and the *C. elegans* global proteomic landscape, the proteomics experiments both here and in previous chapters were performed with both CHAPS/urea- and SDS-based processing. Furthermore, this rationale was expanded to the immunoblotting validation experiments below (Figure 4.7) – that is, multiple detergents were used to incorporate the effects of detergent-dependent protein solubility in relation to the presence of absence of CHIP.

I performed all validation experiments at the University of Edinburgh (Institute of Genetics and Cancer/Hugh Robson Building) apart from the comparative proteomic data collection of *h*CHIP/*Ce*CHIP rescue strains, which I performed as a visiting researcher at the University of Gdańsk (International Centre for Cancer Vaccine Science).

4.2.2 *C. elegans* and SH-SY5Y Strains Employed

The *C. elegans* strains used in the *sma-9* lifespan experiments are as follows: N2, wild-type Bristol; *chn-1*(*tm2692*(*chn-1* deletion)); VC1183, *sma-9*(*ok1628*(allele deletion)); and *chn-1(tm2692); sma-9(ok1628)*(double-null mutants).

The strains used in epifluorescent Golgi imaging were: NP822, *chn-1(tm2692)* I/xxx;cdIs54[pcc1::MANS::GFP + myo-2p::GFP + unc-119(+)], along with the corresponding wild-type control.

The *C. elegans* strains used in the lifespan validation and proteomics experiments are as follows: N2, wild-type Bristol; *chn-1*(*by155*(allele deletion)); *chn-1*(*tm2692*(allele deletion)); MDH1081, referred to hereafter as "*h*CHIP rescue 1", derived from the *chn-1(by155)* mutant (*chn-1(by155)* I/xxx;norIs34[Pchn-1::hCHIP::SL2::mKate2-let-858UTR](389-4)); MDH1082, referred to hereafter as "*h*CHIP rescue 2", derived from the *chn-1(by155)* mutant (*chn-1(by155)* I/xxx;norIs35[Pchn-1::hCHIP::SL2::mKate2-let-858UTR](389-7)); MDH1083, referred to hereafter as "*Ce*CHIP rescue", derived from the *chn-1(by155)* mutant (*chn-1(by155)* I/xxx;norIs36[Pchn-1::CHN-1::SL2::mKate2-let-858UTR](390-1)); MDH1084, referred to hereafter as "*m*Kate Control", dervied from the *chn-1(by155)* mutant (*chn-1(by155)* I/xxx;norIs37[Pchn-1::mKate::let-858UTR](391-8)); MDH1085, referred to hereafter as "*h*CHIP rescue 1", derived from the *chn-1(tm2692)* mutant (*chn-1(tm2692)* I/xxx;norIs34[Pchn-1::hCHIP::SL2::mKate2-let-858UTR](389-4)); MDH1086, referred to hereafter as "*h*CHIP rescue 2", derived from the *chn-1(tm2692)* mutant (*chn-1(tm2692)* I/xxx;norIs35[Pchn-1::hCHIP::SL2::mKate2-let-858UTR](389-7)); MDH1087, referred to hereafter as "*Ce*CHIP rescue", derived from the *chn-1(tm2692)* mutant (*chn-1(tm2692)* I/xxx;norIs36[Pchn-1::CHN-1::SL2::mKate2-let-858UTR](390-1)); and MDH1088, referred to hereafter as "*m*Kate Control", derived from the *chn-1(tm2692)* mutant (*chn-1(tm2692)* I/xxx;norIs37[Pchn-1::mKate::let-858UTR](391-8)).

All *C. elegans strains* were either made in-house or sourced from the *Caenorhabditis* Genetics Center (University of Minnesota). The CHIP SH-SY5Y model was engineered by Erisa Nita[558].

4.2.3 Fluorescence Microscopy and Phenotype Analyses

4.2.3.1 Quantification of C. elegans Golgi Phenotype

Synchronization was performed using standard alkaline hypochlorite methods, as described in Chapter 2. Age synchronous populations of L4 larval animals were obtained after growth of synchronized L1 larvae on OP50-seeded plates. For immobilization, worms were mounted on agarose pads and treated with 5 µL of 60 mM levamisole as an anesthetic. Fluorescent confocal imaging was performed using a Zeiss Imager M2 (Zeiss, Oberkochen, Germany) equipped with an Orca R2 (Hamamatsu) camera. High magnification (63X objective) z-stack images of the head region were obtained, and analyses on endocytic/secretory compartments performed for the two coelomocytes closest to the head in each animal. Images were quantified manually with Fiji (National Institutes of Health open source). For each cell, z-stacks with signal of GFP fluorescence were projected using the "sum slices" algorithm in Fiji. The polygon selection tool was used to select both the area encompassing all endosomal compartments per coelomocyte ("Golgi Area (μm^2)") (Figure 4.4C). The mean and maximum fluorescence intensities of each coelomocyte were determined using the measure tool, thus estimating both the average fluorescence intensity over the entire Golgi stack as well as the maximum fluorescence intensity within the stack. An area near each Golgi stack was also measured, and this background value subtracted from each mean and maximum expression data point. The multi-point tool was used to quantify the number of Golgi fragments per cell, and this measure was divided by the cell's Golgi area to find the Golgi's fragment density ("Density (Fragments/μm^2)") (Figure 4.4H). The polygon selection tool was again used to measure the area of 10 randomly selected endosomal compartments, and the mean of these values calculated as the average fragment area per cell. Each reported value is the average of both coelomocyte measurements per animal. At least 10 animals were quantified per condition, and the experiment performed in triplicate. The images presented are representative of each treatment group.

4.2.3.2 Cell Culture

Tissue culture plasticwares were sourced from Greiner Bio-One (Kremsmünster, Austria) or TPP Techno Plastic Products AG (Trasadingen, Switzerland). Wild-type and

CHIP knock-out SH-SY5Y human neuroblastoma cell lines were acquired under informed consent as per the appropriate ethical guidelines. Cells were maintained in a humid atmosphere at 37°C and 5% CO_2. SH-SY5Y cells were grown in DMEM (GIBCO, Grand Island, USA) after supplementing with 10% FBS and 0.5 U/mL Penicillin and 500 ng/mL Streptomycin (1% Pen/Strep, Invitrogen). Cell growth was monitored daily using a phase-contrast microscope. Cell cultures were kept in a mycoplasma-free incubator and tested intermittently for *mycoplasma* contamination using the luciferase-based MycoAlert® *Mycoplasma* Detection Kit (Lonza Group Ltd, Basel, Switzerland) following the manufacturer's instructions.

4.2.3.3 SH-SY5Y Subculture

For routine subculture, cells were cultured to 80% confluency in a 10 cm plate. Cell culture media were aspirated and cells were gently washed with 5 mL sterile Ca^{2+}/Mg^{2+}-free PBS (pH 7.4) prior to being incubated with 2 mL 0.05% trypsin-0.02% EDTA (ethylenediaminetetraacetic acid) for 5 minutes at 37°C and 5% CO_2. The plates were then checked for the physical detachment of the cell monolayer from the plate. Once this was observed, 8 mL of media was added to each plate and cells were suspended by gentle pipetting. One mL of the cell suspension was aliquoted into a new 10 cm plate, along with 9 mL of fresh media (i.e., a 1:10 dilution). This stock plate was used to maintain the cell line. The remaining cell suspension was utilized in experiments as needed.

4.2.3.4 Cryopreservation

For optimal cryoprotection, cells from confluent plates were harvested using trypsin-EDTA as described above and centrifuged for 5 minutes at 168 *g*. Upon aspiration of the supernatant, the pellet was resuspended in 3 mL of a cryopreservation solution composed of 50% FBS + 10% DMSO + 40% DMEM (without FBS or Pen/Strep). Cell aggregates suspended in the freezing solution were transferred to cryogenic vials (Nunc CryoTubes, Thermo Fisher Scientific Inc, Cambridge, UK) in 1 mL aliquots. The cryogenic vials were then placed in a NALGENE™ cryo freezing container (Nalgene, VWR Inc, Belgium) at room temperature and transferred to -80°C for 24 hours for controlled-rate freezing. Frozen cells were then transferred to liquid nitrogen, and stored long-term in the gas phase above the liquid nitrogen.

4.2.3.5 Cell Recovery

Fully supplemeted DMEM (containing 10% FBS and 1% Pen/Strep) was pre-warmed at 37^{o}C in a water bath. Individual cryovials were rapidly thawed by pipetting 1 mL of the pre-warmed media back and forth several times. Residual DMSO was removed by centrifuging this suspension at 377 *g* for 3 minutes and aspirating the supernatant. The remaining pellet was gently resuspended in 2 mL of pre-warmed fully supplemented DMEM and transferred to a 10 cm plate along with an additional 8 mL of supplemented media. Cells were cultured at 37^{o}C and 5% CO_2.

4.2.3.6 Cell Counting

To approximately standardize the number and confluency of cells across conditions in *in-vivo* experiments, cells were seeded in pre-determined densities. SH-SY5Y cell monolayers were detached using trypsin-EDTA, as described above. Cells were then resuspended in 8 mL of fully supplemented DMEM and centrifuged for 3 minutes at 377 *g*. Upon aspiration of the supernatant, the cell pellet was resuspended in 2 mL of supplemented DMEM. From this cell suspension, a 10 µL aliquot was gently mixed with 0.4% trypan blue solution (Cat # T13000, Labtech International Ltd, East Sussex, UK) in a 1:1 v/v ratio. Automated cell counting was performed using LUNA Cell Counting Slides (Cat # L12001, Logos Biosystems, Anyang, Korea) in a cell counter (Logos Biosystems, Anyang, Korea). Cell count measurements for each sample were repeated in triplicate.

4.2.3.7 Coverslip Preparation

In immunofluorescence experiments, cells were grown on 13-mm diameter round glass coverslips (Cat # 631-0149, VWR Inc, Belgium). Coverslips were washed with 70% ethanol, autoclaved for 30 minutes at 180^{o}C, and individually placed in the wells of a 12-well tissue culture plate. SH-SY5Y cell suspensions were added to each well and topped up with fully supplemented DMEM to a final volume of 1 mL.

4.2.3.8 SH-SY5Y Immunofluorescence

Cells were grown on sterile coverslips in 12-well cell culture plates in a humidified 5% CO_2 at 37^{o}C. Once cells reached approximately 80% confluence, the growth media was removed and coverslips were gently washed three times for 5 minutes each with 700 µL room temperature PBS per well. Cells in each well were then fixed with 600 µL 4% PFA

at room temperature for 15 minutes and washed another three times with room temperature PBS, after which they were permeabilized in 800 µL 0.01% Triton X-100 (PBS-Triton) for a further 5 minutes. Blocking was performed using 5% donkey serum in 0.01% PBS-Triton for one hour and subsequently incubated in primary antibody for 16 hours at 4°C. An antibody titration experiment was performed, and the resulting staining used to determine optimal antibody concentrations (Figure 4.5). Wild-type and CHIP knock-out SH-SY5Y cells were co-stained with either Rab6 (dilution 1:200, rabbit polyclonal, Abcam Inc, Cambridge, UK) and GM130 (1:200, mouse monoclonal, Thermo Fisher Scientific Inc, Cambridge, UK) or COG6 (dilution 1:200, rabbit polyclonal, Atlas Antibodies, Stockholm, Sweden) and GM130 in blocking buffer. A separate set of wild-type and CHIP knock-out wells was also stained with CHIP (1:200, mouse monoclonal, provided by collaborators). Cells were washed twice with PBS-Triton and incubated with either anti-mouse or anti-rabbit Alexa Fluorochrome (488 or 594, Thermo Fisher Scientific Inc, Cambridge, UK) for 1 hour at room temperature. Cells were then washed twice with PBS-Triton and nuclei stained with DAPI (0.5 µg/mL in PBS) for 5 minutes at room temperature. Finally, coverslips were gently washed twice in PBS, mounted with 10 µL of Vectashield mounting medium, and stored in a light-protected container overnight. If longer storage was required prior to imaging, microscope slides were stored in the dark at 4°C. Imaging was performed using a Zeiss Imager M2.

Specificity of the Rab6, COG6, and GM130 antibodies has been confirmed in human cells. Non-specific labelling was controlled for by incubating coverslips with blocking buffer instead of primary antibody. All negative controls resulted in the absence of immunoreactivity.

4.2.3.9 Cell Harvesting

Growth media was aspirated and cells were washed three times with 5 mL of sterile PBS at room temperature. Sterile room temperature PBS (700 µL) was added to each 10 cm plate, and a disposable rubber plate scraper was used to gently scrape cells from the dish surface. The PBS-cell suspension was transferred to a 1.5-mL microcentrifuge tube on ice. The scraping process was repeated for a second time, after which each sample was spun for 5 minutes at 447 *g* in a bench-top centrifuge. The supernatant was

discarded, and the samples either used immediately or snap-frozen in liquid nitrogen and stored at -80ºC.

4.2.4 Biochemical Techniques

4.2.4.1 Cell Pellet Lysis

After harvesting, cell lysis was performed using a 3:1 ratio of the appropriate lysis buffer to the cell pellet mass. SH-SY5Y cells were lysed using buffers containing either Tween 20 (50 mM HEPES pH 7.5, 0.1% (v/v) Tween 20, 150 mM NaCl, 0.1 mM EDTA, 2 mM DTT, and 1X protease inhibitor mix (PIM)), Triton X-100 (50mM HEPES pH 7.5, 0.2% (v/v) Triton X-100, 150 mM NaCl, 10 mM NaF, 2 mM DTT, 0.1 mM EDTA and 1X PIM), RIPA (50 mM Tris HCl pH 7.4, 150 mM NaCl, 1% Triton X-100, 0.5% sodium deoxylcholate, 0.1% SDS, 1 mM EDTA, 10 mM NaF, 1 mM PMSF, and 1X PIM), or CHAPS-Urea (35 mM Tris, 8M urea, 4% CHAPS, 65 mM DTT, pH 8.0). Cells pellets mixed with the appropriate lysis buffer were left on ice for 30 minutes and subsequently spun at 18,894 *g* for 20 minutes at 4ºC. The supernatants were then transferred to new 1.5-mL microcentrifuge tubes, and total protein concentrations were determined using either a Bradford (Tween 20 & Triton X-100; Bio-Rad, Watford, UK) or BCA (RIPA & CHAPS/Urea; Thermo Fisher Scientific Inc, Cambridge, UK)-based protein assay system, as per the manufacturer's instructions.

4.2.4.2 SDS-PAGE In-House Polyacrylamide Gels

Polyacrylamide gels were made in-house using Mini-Protean 3 cell apparatus-associated casting molds (Bio-Rad, Watford, UK) with 10-well combs and 1.0- or 1.5-mm thick glass spacers, depending on the protein loading volume. Stacking and resolving gels, along with other immunoblotting-related solutions, were prepared as described in Table 4.1, with higher percentage resolving gels reserved for proteins with smaller molecular weights. A layer of isopropyl alcohol was placed on top of each resolving gel during the gel casting procedure to facilitate straight gel solidication and prevent the formation of bubbles. Once the resolving gel solidified, the stacking gel was prepared and poured appropriately prior to the comb being placed. Twenty µg of protein from each cell lysate was then mixed with 2x sample buffer in a 1:1 (v/v) ratio, incubated for 4 minutes at 85ºC, and loaded into the appropriate wells of the gel. All samples to be

compared were loaded concurrently alongside a pre-stained protein ladder (PageRuler™ Prestained Protein Ladder, Thermo Fisher Scientific Inc, Cambridge, UK), to generate a molecular weight scale. Gels were run at 120V in Tris-Glycine SDS Running Buffer 1x until the lowest molecular marker reached the bottom of the gel.

Table 4.1 **Buffer and solution constituents for western blotting**

2x Sample Buffer	**Running Buffer**
5% (w/v) SDS, 125 mM	192 mM Glycine
25% (v/v) Glycerol	25 mM Tris-HCl (pH 6.8)
0.3 M Tris, pH 6.8	0.1% w/v SDS in dH_2O
200 mM DTT	**Transfer Buffer**
Bromophenol blue (to desired colour)	192 mM Glycine
Running Gel	25 mM Tris-HCl (pH 6.8)
30% Acrylamide (Protogel)	20% v/v Methanol in dH_2O
0.39 M Tris-HCl (pH 8.8)	**PBS**
0.1% (w/v) SDS	1.37 M NaCl
0.1% (w/v) Ammonium Persulphate (APS)	0.1 M Na_2HPO_4
0.04% (v/v) TEMED in dH_2O	27 mM KCl
Stacking Gel	18 mM KH_2PO_4
5% Acrylamide Mix	**PBS-Tween**
0.13 M Tris-HCl (pH 6.8)	1x PBS + 0.1% (v/v) Tween 20
0.1% (w/v) APS	**5% Milk in PBS-Tween**
0.1% (w/v) SDS	5% w/v Non-Fat Dry Milk (Marvel) + PBS-Tween
0.04% (v/v) TEMED in dH_2O	**ECL Solution 1**
Separation Gel	100 mM Tris-HCl (pH 8.5)
8-15% Acrylamide Mix	2.5 mM Luminol Stock
0.39 M Tris-HCl (pH 8.8)	0.4 mM *p*-Coumaric Acid in dH_2O
0.1% (w/v) APS	**ECL Solution 2**
0.1% (w/v) SDS	100 mM Tris-HCl (pH 8.5)
0.04% (v/v) TEMED in dH_2O	0.02% (v/v) H_2O_2 in dH_2O

4.2.4.3 Immunoblotting (Western Blotting)

SDS-polyacrylamide slab gels containing resolved proteins and prestained marker proteins were transferred to 0.2-µm pore nitrocellulose blotting membranes (Advantec MFS Inc, Dublin, CA, USA) using the Mini Trans-Blot wet transfer system (Bio-Rad, Watford, UK) and 1x Transfer Buffer (Table 4.1) in the transfer apparatus. Transfer took place in a Trans-Blot cell either with ice packs to prevent overheating for 1 hour at 110V or at 4°C overnight at 30 mA. Membranes were rinsed with PBS at room temperature for 5 minutes with agitation, stained with India ink (Pelikan) to confirm the presence of protein bands, rinsed briefly with PBS-Tween (Table 4.1), and subjected to blocking for either 1 hour at room temperature or 16 hours at 4°C with PBS-Tween + 5% bovine serum albumin (BSA; A9647, Sigma–Aldrich, St. Louis, MO, USA). Blotting membranes were washed with PBS three times for 5 minutes per wash with agitation at room temperature and subseqently incubated with the following pimary antibodies diluted in 5% Milk in PBS-Tween for either 1 hour at room temperature or overnight at 4°C: CHIP (dilution 1:1,000, mouse monoclonal), Rab6 (1:500, rabbit polyclonal), or COG6 (1:250, rabbit polyclonal) followed by the appropriate secondary antibodies (1:1,000) for 1 hour at room temperature. Three PBS washes (room temperature, 5 minutes each) were performed between and after antibody incubations. β-Actin was used as a control.

For antibody detection, Enhanced Chemiluminescence (ECL) Solutions 1 and 2 (Table 4.1) were mixed in an equal ratio (1:1 v/v) and poured to cover the membrane surfaces for 1 minute. Upon the removal of excess solution, blots were developed using an ImageQuant LAS 4000 biomolecular imager (GE Healthcare Life Sciences, Buc, France) for the appropriate exposure duration. Experimental repeats for SH-SY5Y wild-type and CHIP knock-outs lysed with either Tween, Triton, RIPA, or CHAPS/Urea-based lysis buffers were as follows: CHIP Tween 20, $n = 4$; COG6 Tween 20, $n = 5$; all others, $n = 1$.

4.2.5 Lifespan Assay

Lifespan assays were performed as described in Chapter 3. Three independent experiments were performed for both the *sma-9* and *h*CHIP/*Ce*CHIP rescue experiments. For assays investigating the longevity of *sma-9* and *chn-1* single- and double-deletion mutants relative to both one another and N2 wild-type controls, each strain per replicate used *n* = 128 animals. For assays quantifying the longevity of N2 wild-type and *mKate* controls, *chn-1(by155)* mutants, and *chn-1(by155)*-derived *h*CHIP and *Ce*CHIP rescue strains, each strain per replicate used *n* = 128 animals. For assays quantifying the longevity of N2 wild-type and *mKate* controls, *chn-1(tm2692)* mutants, and *chn-1(tm2692)*-derived *h*CHIP and *Ce*CHIP rescue strains, each strain per replicate used *n* = 128 animals, with the exception of *h*CHIP Rescue 1 (Replicate 3 only; *n* = 129), *chn-1* Rescue (Replicate 3 only; *n* = 123), *mKate* Control (Replicate 3 only; *n* = 133), and N2 (Replicate 3 only; *n* = 127).

4.2.6 Statistical Analyses

Data for all results are given as mean ± standard error of the mean. When comparing treatment groups, significance levels were determined using Students *t*-tests via SPSS (version 26.0, SPSS Inc., IL, USA). For lifespan analyses, *Kaplan-Meier* estimates and restricted mean survival times were obtained using OASIS[559]. Proteomics analyses were performed as described in Chapter 2.

4.2.7 *chn-1* Rescue Proteomics

Between-strain comparisons were performed on MS-based proteomic datasets generated using either wild-type, *chn-1(tm2692)*, or *chn-1(tm2692)*-derived *h*/*Ce*CHIP rescue strains processed with either CHAPS/Urea- or SDS-based lysis buffers. The nematode strains, growth and synchronization of worms, preparation of samples, and mass spectrometry-based proteomics methods and analyses were as described in Chapter 2. PCR and DNA sequencing were done as described in Chapter 2, with primer sequences found in Table 2.1. The final list-of-interests for proteins most relevant to the lifespan reversal phenotype was filtered as follows: (1) data was sorted such that separate lists were made for proteins with a fold change of at least 1.5x or at most 0.67x, (2) a reference list of proteins substantially altered in *chn-1(tm2692)* mutants

relative to controls was created, (3) initial comparisons were made highlighting proteins that were either over- or underexpressed in each rescue strain relative to the *chn-1*-null mutants in a direction opposite to that found in the reference list, (4) from this list, proteins that were shared between all three rescue strains were listed, and all others were excluded. Gene ontology and KEGG pathway analyses were performed on this final list of protein hits found by either CHAPS/Urea- (Table 4.2) or SDS-based lysis methods (Table 4.3). The full list of proteins rescued by CHAPS/Urea- and SDS-based processing can be found in Supplemental Tables C10-12 and C13-15, respectively (proteins rescued in *h*CHIP rescue 1: Supplemental Tables C10 and C13; *h*CHIP rescue 2: Supplemental Tables C11 and C14; Supplemental Tables C12 and C15: *Ce*CHIP rescue).

4.3 Results: *chn-1* Ablation Alters Golgi Morphology, TGF-β Signaling, and Retrograde Transport

Validating Proteomics Data

4.3.1 Both Single and Double-Knock-Out Mutants of *chn-1* and *sma-9* are Short-Lived

The transcription factor SMA-9 was one of the most substantially underexpressed protein hits in response to *chn-1* ablation. Moreover, SMA-9 expression was reduced under both CHAPS/Urea- and SDS-based lysis conditions. To validate these proteomic findings, as well as to tease apart whether SMA-9 and CHN-1 function in an integrative or independent manner, both *chn-1(tm2692)* and *sma-9* deletion mutants, as well as *chn-1(tm2692); sma-9* double-knock-out mutants were subjected to lifespan analyses. In the first experimental replicate, the control animals had a restricted mean survival time of 16.35 days, whereas the *chn-1(tm2692)* and *sma-9* single-gene knock-out mutants had restricted mean survival times of 13.28 (or an 18.78% reduction from the baseline survival score) and 12.93 days (a 20.92% lifespan reduction), respectively (log-rank test compared with wild-type, *chn-1(tm2692)*, $p < 0.001$; *sma-9*, $p < 0.001$) (Figure 4.3). The *chn-1(tm2692); sma-9* double mutants had a restricted mean survival time of

11.95 days (a 26.91% reduction in lifespan relative to wild-type animals, or a 10.02% and a 7.58% lifespan reduction relative to *chn-1(tm2692)* and *sma-9* mutants, respectively) (log-rank test compared with *chn-1(tm2692); sma-9* double-knock-outs, wild-type controls, $p < 0.001$; *chn-1(tm2692)*, $p = 0.047$; *sma-9*, $p = 0.11$) (Figure 4.3). The double mutants differed significantly from *chn-1* mutants and N2 controls, but only approached significance when compared to *sma-9* mutants. The last mortality occurred on days 28, 25, 22, and 22 in control animals, *chn-1(tm2692)*, *sma-9*, and *chn-1(tm2692); sma-9* mutants, respectively (Figure 4.3).

Interestingly, in the second replicate of this experiment (Supplemental Table C1), the double mutants instead differed significantly from *sma-9*-null animals ($p = 0.045$, log-rank) but not *chn-1*-null mutants ($p = 0.077$, log-rank), despite approaching statistical significance. Once more, *chn-1(tm2692); sma-9* animals exhibited the shortest lifespan, followed by *chn-1*, *sma-9*, and finally wild-type worms (with restricted mean survival times of 12.62, 13.86, 13.91, and 17.01 days, respectively) (Supplemental Table C2). Again, the two single-gene knock-outs did not differ significantly from one another, but both the single- and double-gene mutants exhibited significantly reduced longevity relative to wild-type animals (*chn-1(tm2692)*, $p < 0.001$; *sma-9*, $p < 0.001$; *chn-1(tm2692); sma-9*, $p < 0.001$; log-rank) (Supplemental Table C1). Trending similarly to the first experimental replicate, the last mortality occurred on days 28, 25, 25, and 22 in N2 controls, *chn-1(tm2692)*, *sma-9*, and *chn-1(tm2692); sma-9* mutants, respectively (Supplemental Table C2).

Results from the third experimental replicate trended similarly to those of the first two, with both the single- (*chn-1(tm2692)*, $p < 0.001$; *sma-9*, $p < 0.001$, log-rank) and double-gene ($p < 0.001$, log-rank) mutations associated with a significant decrease in lifespan relative to wild-type controls, while the two single-gene knock-outs did not differ significantly from one another. Here, however, neither single mutant differed significantly from the double mutant (log-rank test compared with *chn-1(tm2692); sma-9* double-knock-outs, *chn-1(tm2692)*, $p = 0.083$; *sma-9*, $p = 0.070$), although both approached statistical significance (Supplemental Table C1). Double-gene mutants had the shortest lifespan, followed by *chn-1*, *sma-9*, and finally wild-type animals, with restricted mean survival times of 12.71, 14.22, 14.51, and 16.96 days, respectively. The

last mortality occurred on days 28, 22, 22, and 25 in wild-type controls, *chn-1(tm2692)*, *sma-9*, and *chn-1(tm2692); sma-9* mutants, respectively (Supplemental Table C2). Information pertaining to animals censored across all replicates can be found in Supplemental Table C3.

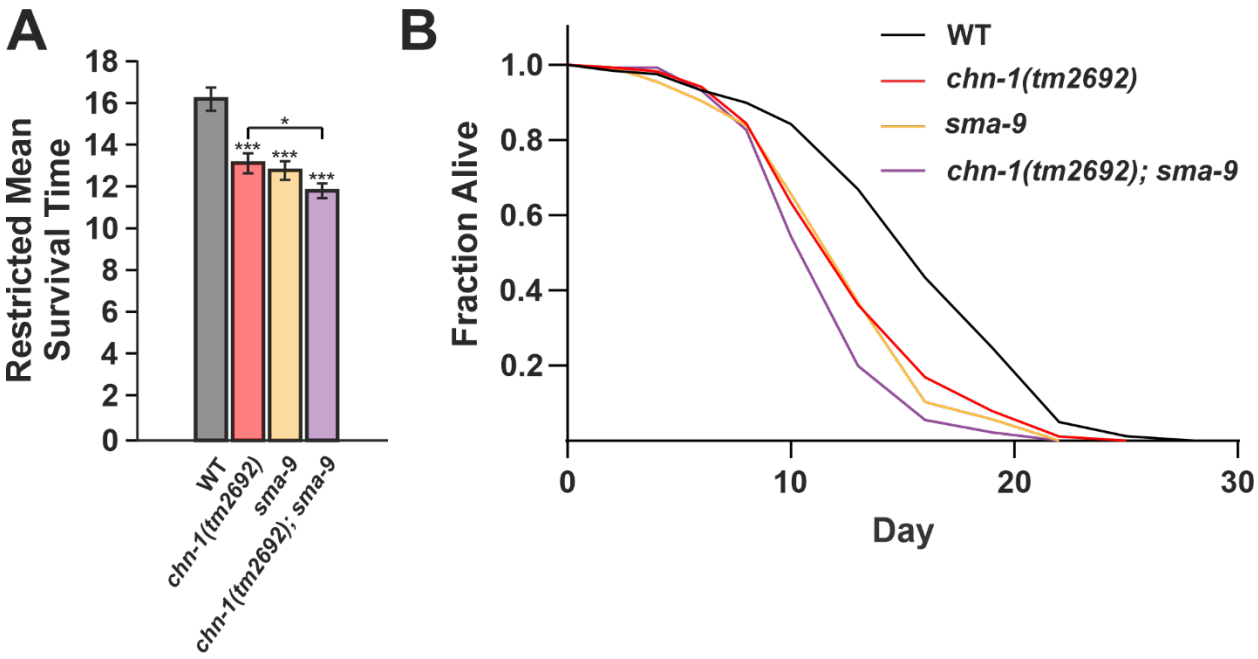

Figure 4.3 **The deletion of both *chn-1* and *sma-9* leads to reduced lifespan**. (***A***) Restricted mean survival time and (***B***) cumulative survival graph comparing wild-type N2 controls with *chn-1(tm2692)*, *sma-9*, and *chn-1(tm2692); sma-9 C. elegans chn-1* mutants. Deletion mutants showed decreased restricted mean survival times and significantly decreased lifespans relative to wild-type N2 controls, with double mutants exhibiting the shortest restricted mean survival time. Asterisks indicate significances: **p*<0.05, ****p*<0.001. Error bars represent ± SEM (identical experiments repeated *n* = 3 times). Bonferroni-adjusted *p*-values as well as restricted mean survival times and final mortalities associated with longevity differences in N2 wild-types, *sma-9* single- and double-mutants, and *chn-1* single- and double-mutants across all 3 replicates are shown in Supplemental Table C1 and Supplemental Table C2, respectively. The number of animals censored at each time-point of the assay is shown in Supplemental Table C3.

4.3.2 Transport-Related Proteins and Structures Show a CHN-1-Dependent Phenotype

Global proteomics analyses comparing *chn-1*-null animals to wild-type controls suggested an altered Golgi-related phenotype resulting from *chn-1* ablation. Therefore, initial validation experiments focused on proteins and organelles of immediate relevance to protein trafficking. Specifically, the CHN-1-dependent Golgi phenotype was further assessed in *chn-1(tm2692)* mutants relative to wild-type controls using a mannosidase II::GFP marker (Figure 4.4A and Figure 4.4B). Area measurements encompassing the Golgi-resident protein showed that *chn-1* ablation did not lead to an increase in the area of the Golgi in terms of spatial signal distribution ($t(21) = -0.955$, $p = 0.35$) (Figure 4.4C). The *chn-1*-null animals showed a significant increase in mean fluorescence intensity ($t(21) = -2.332$, $p < 0.05$) and an increase in maximum fluorescence intensity ($t(21) = -2.004$, $p = 0.058$), though this measure only approached statistical significance (Figure 4.4D and 4.4E). Mutant *chn-1* animals had a 15.83% increase in the mean number of fragments per coelemocyte, although this relationship was not significant ($t(21) = -1.835$, $p = 0.081$) (Figure 4.4F). The average area of each individual fragment was significantly decreased in the *chn-1* knock-outs, with endosomal compartments in *chn-1*-null animals exhibiting a 31.66% decrease in area ($t(21) = 7.729$, $p < 0.001$) (Figure 4.4G). The fragment density per area did not change between treatment groups ($t(16.67) = -1.179$, $p = 0.26$). Overall, *chn-1* ablation led to a phenotype in which Golgi fragments were brighter, smaller, and more numerous than those of wild-type controls (Figure 4.4 and Supplemental Figure C1).

An antibody titration experiment confirmed optimal primary antibody concentrations for COG6 (dilution 1:200) and Rab6 (dilution 1:200), two proteins integral to retrograde transport and protein trafficking (Figure 4.5). CHIP deletion was found to also alter the expression patterns of GM130, a Golgi marker, as well as Rab6 and COG6 in SH-SY5Y human neuroblastoma cells (Figure 4.6). Rab6 and COG6 staining were brighter in CHIP wild-type cells, and both partially co-localised with GM130 (Figure 4.6A and 4.6B). Similar to the *C. elegans* experiments, CHIP-null SH-SY5Y cells exhibited significantly higher expression of GM130 (Figure 4.6A and 4.6B).

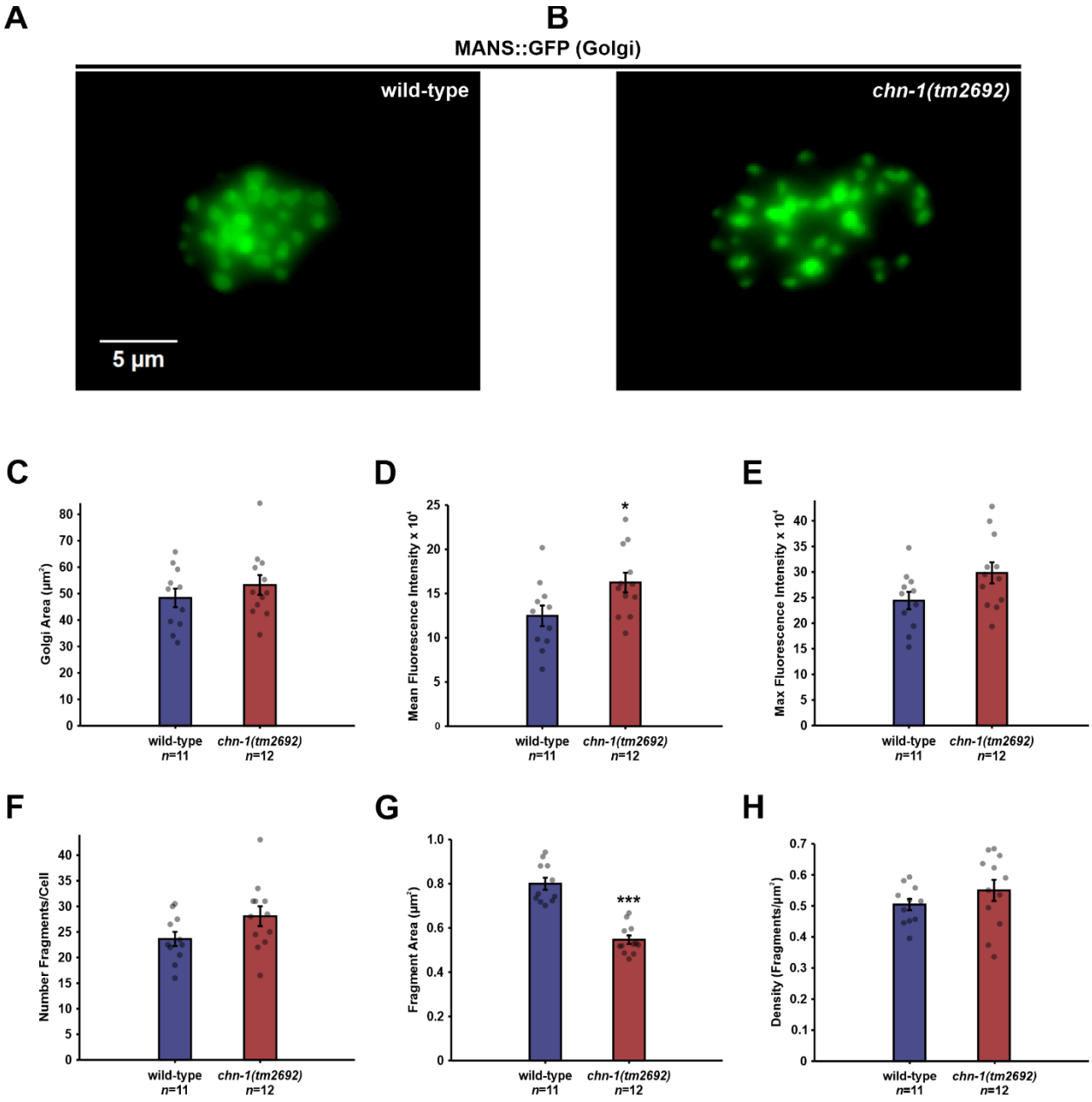

Figure 4.4 **The Golgi in *chn-1(tm2692)* exhibit increased fragmentation.** Representative confocal images of (***A***) wild-type and (***B***) *chn-1(tm2692)* coelomocytes expressing MANS::GFP Golgi markers. Quantification of the diameter of GFP-positive structures demonstrates a decrease in size and increase in endosomal density outlined by MANS::GFP in *chn-1*-null animals, while measurements of fluorescence intensity indicated that *chn-1* ablation was associated with increased brightness. Asterisks indicate significances: ***p*<0.01, ****p*<0.001. Error bars represent ± SEM. Scale bar 5 µm (identical experiments repeated *n* = 3 times).

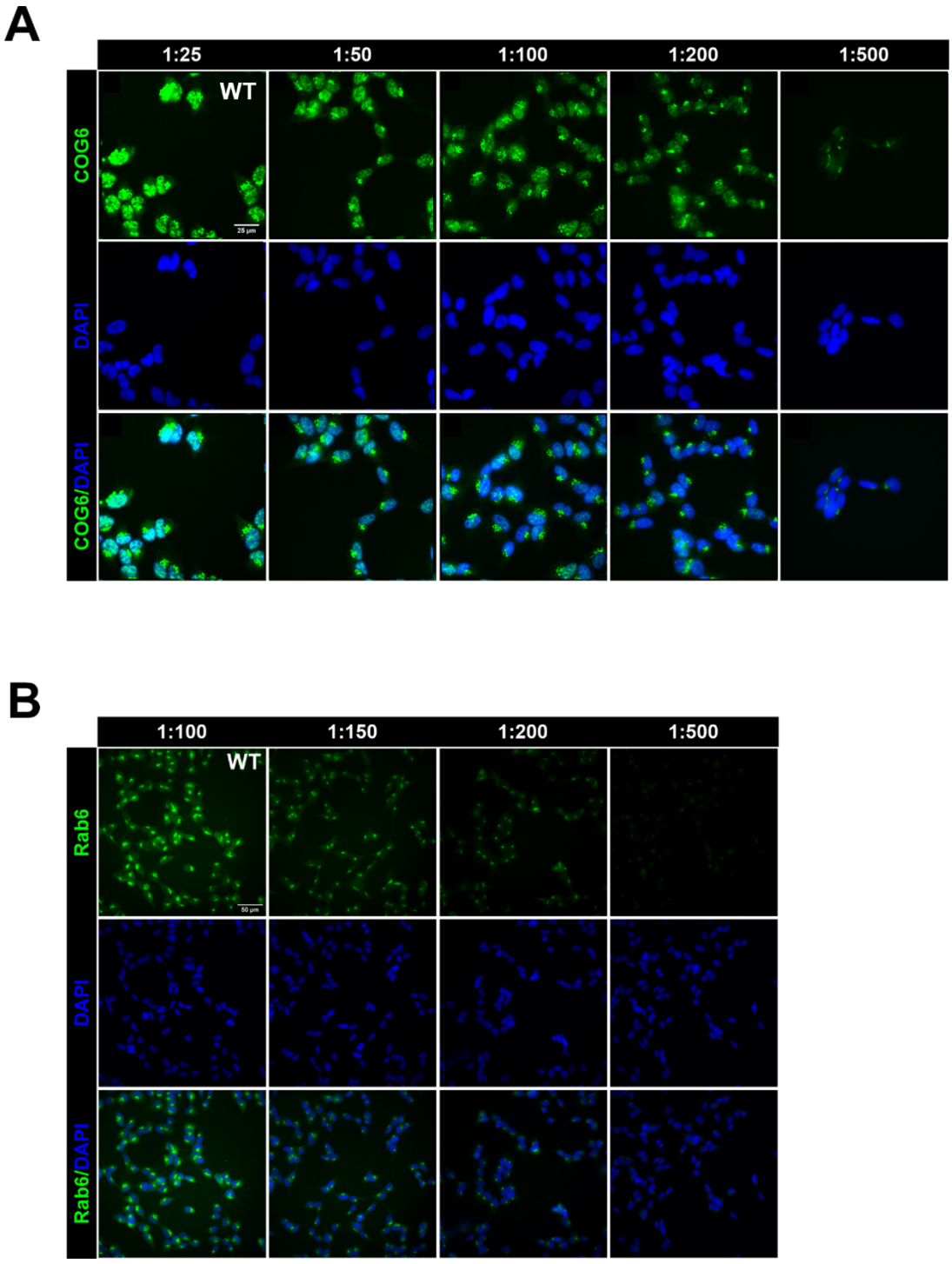

Figure 4.5 **Antibody titration experiment for COG6 and Rab6.** Immunofluorescence of wild-type patient-derived SH-SY5Y neuroblastoma cells stained for (***A***) COG6 and (***B***) COG6. Primary antibody concentrations are listed above the images. Rab6 and COG6 were detected using Alexa 488 (green) secondary antibody. Nuclei were stained with DAPI (blue). Scale bar either (***A***) 25 µm or (***B***) 50 µm (representative of experiments repeated at least *n* = 3 times).

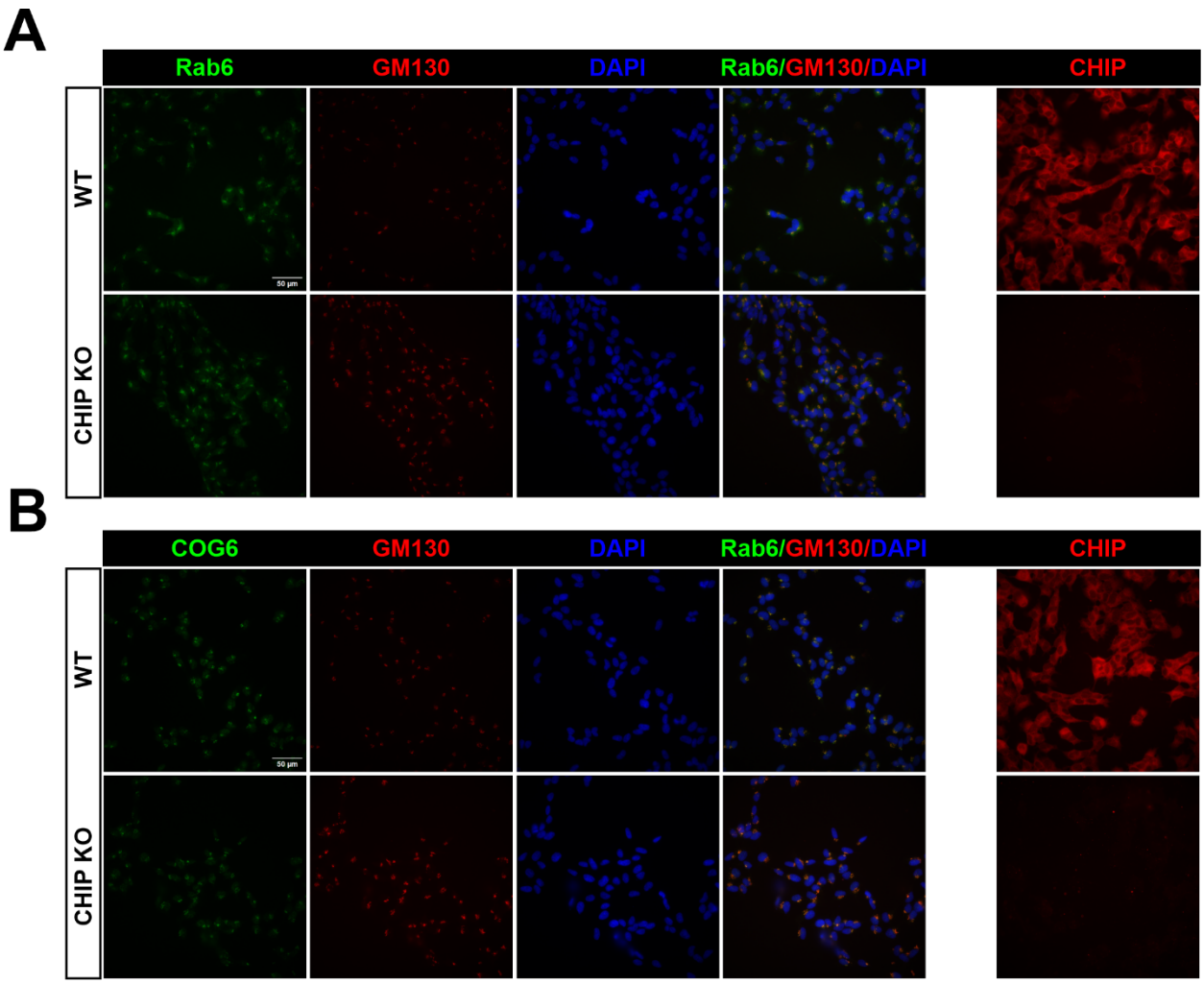

Figure 4.6 **CHIP ablation altered expression of proteins integral to cellular transport.** Immunofluorescence of wild-type and CHIP KO patient-derived SH-SY5Y neuroblastoma cells stained for Rab6 (***A***), COG6 (***B***), and GM130 (***A***, ***B***). Rab6 and COG6 were detected using Alexa 488 (green) secondary antibody, while GM130 and CHIP were detected using Alexa 594 (red) secondary antibody. Nuclei were stained with DAPI (blue). Scale bar 50 μm (representative of experiments repeated at least *n* = 3 times).

4.3.3 Immunoblotting Experiments Revealed CHIP- and Extraction-Dependent Transport Protein Expression

Proteomics, *C. elegans* mannosidase marker, and immunofluorescence experiments indicated an altered transport phenotype in response to CHIP ablation. Furthermore, the proteomics data in showed substantial extraction-dependent variability in proteins altered by *chn-1* deletion (Chapter 2 and Chapter 3). Thus, immunoblotting with several extraction detergents was performed to further investigate (1) the expression patterns of Rab6 and COG6 in a wild-type and CHIP knock-out human neuroblastoma (SH-SY5Y) cells, and (2) whether varying extraction procedures would affect target protein expression. Mean relative Rab6 protein expression in CHIP knock-out versus wild-type cell extracts was increased by 83.04% in Tween-processed samples, although the variability was large (SEM = 0.67) and the relationship not statistically significant ($t(3) = -1.237$, $p = 0.30$) (Figure 4.7A). Relative levels of Rab6 expression were increased in Triton, RIPA, and CHAPS/Urea-processed samples by 29.32%, 28.26%, and 9.97%, respectively (Figure 4.7B). Meanwhile, mean relative COG6 protein expression in CHIP knock-out versus wild-type extracts was increased by 70.44% in Tween-processed samples ($t(4) = -3.791$, $p < 0.05$) (Figure 4.7A) and by 30.60% in RIPA-processed samples. COG6 expression was decreased in Triton and CHAPS/Urea-processed samples, however, by 44.08% and 67.65%, respectively (Figure 4.7C).

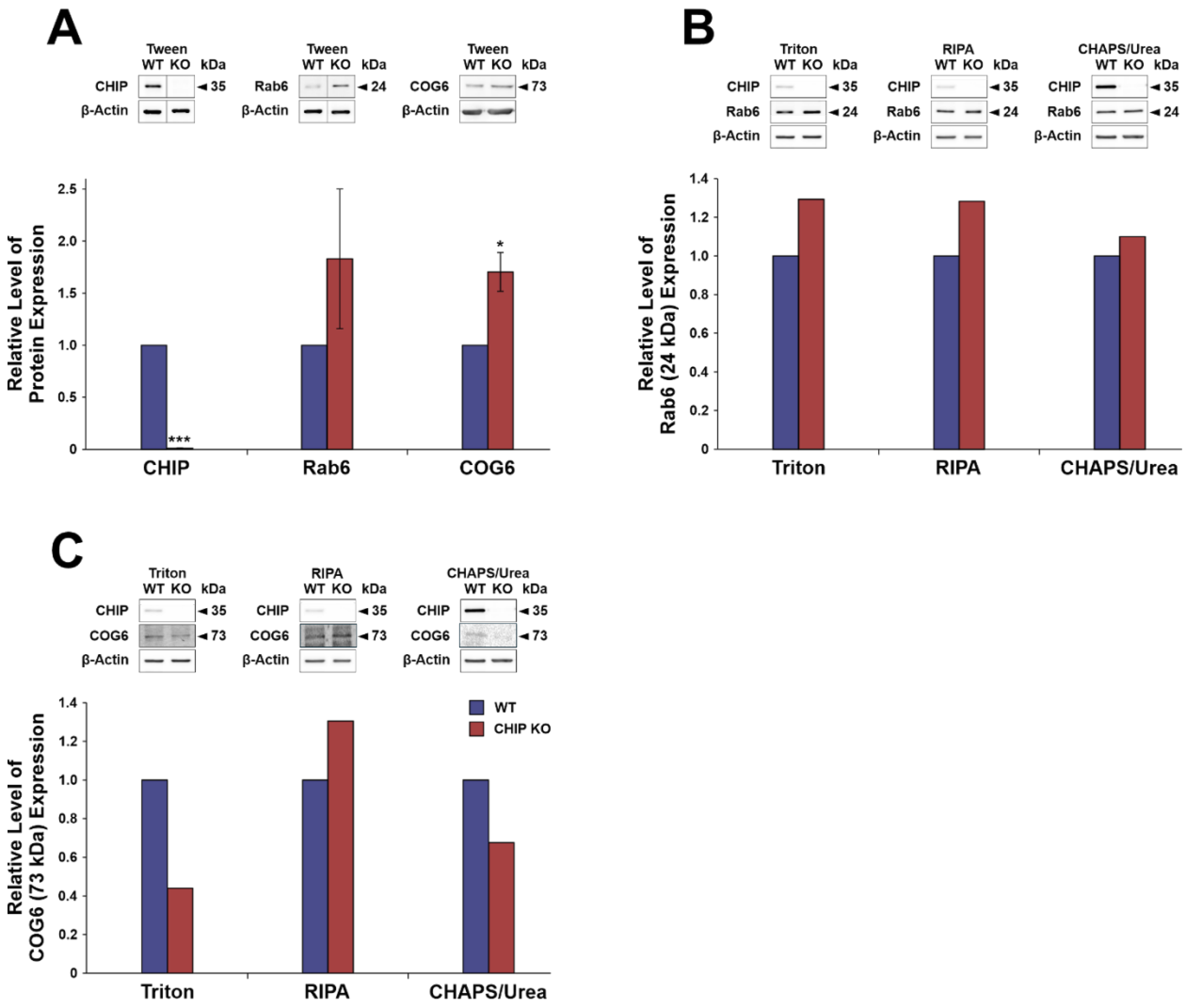

Figure 4.7 **CHIP deletion in SH-SY5Y cells alters Rab6 and COG6 expression in a detergent-dependent manner.** Western blot analyses and quantification of CHIP (***A***), Rab6 (***A***, ***B***) or COG6 (***A***, ***C***) protein expression in wild-type and CHIP knock-out SH-SY5Y cell extracts lysed with either (***A***) Tween 20, (***B***, ***C***) Triton X-100, RIPA, or CHAPS/urea-based lysis buffers. Asterisks indicate significances: **p*<0.05, ****p*<0.001. Error bars represent ± SEM (Rab6 and CHIP Tween 20, *n* = 4; COG6 Tween 20, *n* = 5; all others, *n* = 1).

Complementation of Human/*C. elegans* CHIP

4.3.4 Validation of CHIP/*chn-1* Rescue *C. elegans* Strains

Validation of *h*CHIP and *Ce*CHIP rescue strains was done by PCR electrophoresis (as described in Chapter 2), with genomic maps of both expression clones shown below (Figure 4.8).

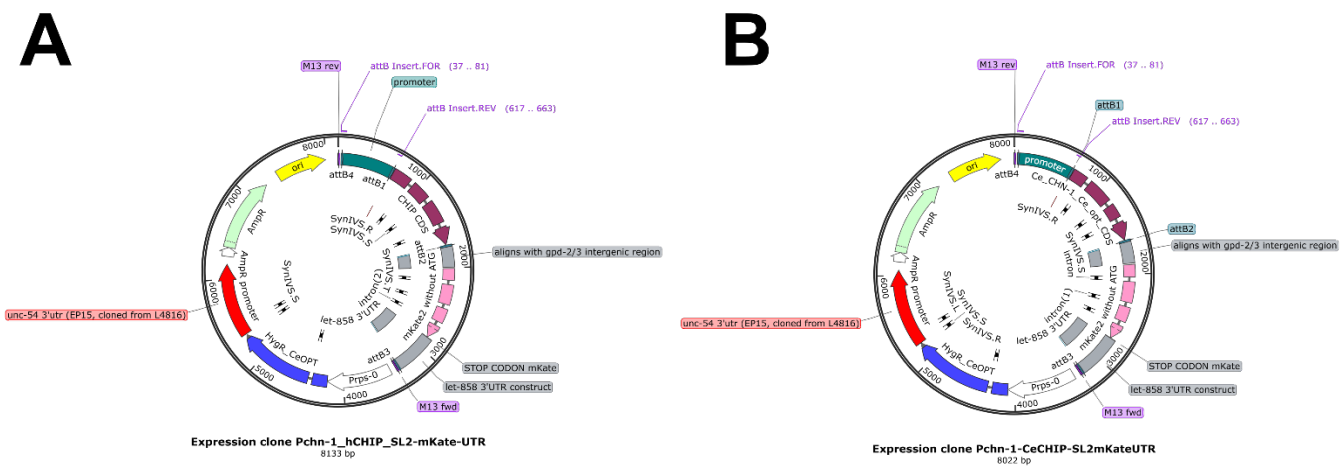

Figure 4.8 **Genomic maps of (*A*) Pchn-1_hCHIP_SL2-mKate-UTR and (*B*) Pchn-1-CeCHIP-SL2mKateUTR expression clones.**

A comparison of human CHIP and *C. elegans* CHN-1 sequence and structure is shown below (Figure 4.9).

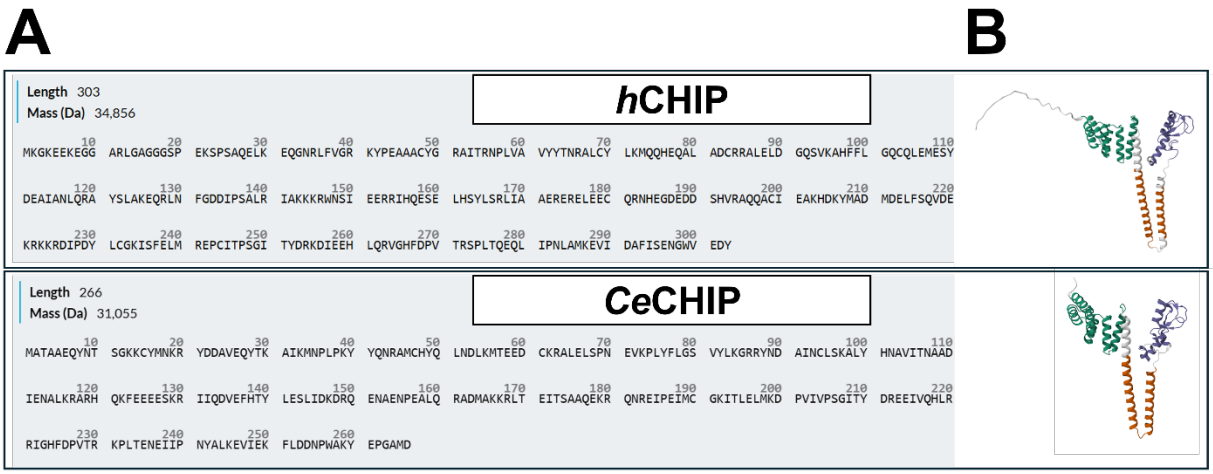

C

BLAST Metrics: *h*CHIP vs. *Ce*CHIP

Maximum Score	Total Score	Query Cover	E Value	Percentage Identity
201	201	91%	4E-68	39.35%

Figure 4.9 **A comparison of human CHIP and *C. elegans* CHN-1 sequences and structures.** (***A***) A comparison of human *h*CHIP and *Ce*CHIP sequences, (***B***) protein structures, and (***C***) BLAST metrics.

4.3.5 Rescue of CHIP/*chn-1* Results in a Corresponding Rescue of Lifespan Phenotype

Both *C. elegans* CHN-1 and human CHIP rescue strains were constructed by bombardment and hygromycin B selection followed by visual selection of transgenic animals under fluorescence. Two independently-derived *h*CHIP, one *Ce*CHIP strain, and an mKate control were created from each *chn-1*-null mutant (*chn-1(by155)* and *chn-1(tm2692)*), and lifespan assays performed to confirm lifespan extension alongside genotype rescue. The *h*CHIP and *Ce*CHIP rescue strains were constructed to (1) provide a comprehensive overview of proteins that were rescued by complementation of both human and *C. elegans* CHIP, and ultimately (2) to identify which proteins contribute to CHIP-associated lifespan extension in the human orthologue of the gene. The use of three rescue strains acted as a means to further distinguish which rescued proteins are most likely to contribute to CHIP-associated lifespan extension (i.e., those rescued across all three strains). Finally, an mKate control was also constructed.

As expected, rescuing both *chn-1(by155)* and *chn-1(tm2692)* mutants led to an associated increase in lifespan (Figure 4.10). In the first experimental replicate of strains derived from *chn-1(by155)* mutants, the wild-type control animals, *chn-1(by155)*

mutants, and *m*Kate controls had restricted mean survival times of 19.93 days, 15.97 days, and 15.02 days (or a 19.87% and 24.64% reduction from the baseline survival score), respectively (log-rank test compared with wild-type, *chn-1(by155)*, $p < 0.001$; *m*Kate control, $p < 0.001$) (Figure 4.10A and 4.10B). Conversely, the *h*CHIP rescue strains 1 and 2, as well as the *Ce*CHIP rescue strain, had restricted mean survival times of 18.93 days, 18.60 days, and 18.79 days (or an increase of 15.64%, 14.14%, 15.01% relative to *chn-1(by155)* mutants), respectively (log-rank test compared with *chn-1(by155)*, *h*CHIP rescue 1, $p < 0.001$; *h*CHIP rescue 2, $p < 0.001$; *Ce*CHIP rescue, $p < 0.001$) (Figure 4.10A and 4.10B). None of the rescue strains differed significantly from the N2 controls (log-rank test compared with wild-type, *h*CHIP rescue 1, $p = 1.00$; *h*CHIP rescue 2, $p = 0.62$; *Ce*CHIP rescue, $p = 0.19$). The last mortality occurred on day 26 in both the *chn-1(by155)* mutants and *m*Kate controls, and on days 28, 30, 30, and 28 in the wild-type controls, *h*CHIP rescues 1 and 2, and *Ce*CHIP rescues, respectively (Figure 4.10A and 4.10B). The second and third experimental replicates for *chn-1(by155)*-derived strains trend similarly, with rescue animals exhibiting increased longevity and a delayed last mortality relative to *chn-1(by155)* (Supplemental Tables C4 and C5). Of note, the wild-type strain of the second replicate had an unusually short lifespan, possibly due to agar plate contamination throughout the course of the assay (Supplemental Tables C4 and C5).

In the first experimental replicate of strains derived from *chn-1(tm2692)* mutants, the wild-type animals, *chn-1(tm2692)* mutants, and *m*Kate controls had restricted mean survival times of 20.02 days, 16.80 days, and 17.25 days (or a 16.08% and 13.84% reduction from the baseline survival score), respectively (log-rank test compared with wild-type, *chn-1(tm2692)*, $p < 0.001$; *m*Kate control, $p < 0.001$) (Figure 4.10C and 4.10D). Conversely, the *h*CHIP rescue strains 1 and 2, as well as the *Ce*CHIP rescue strain, had restricted mean survival times of 20.35 days, 20.01 days, and 19.74 days (or an increase of 17.44%, 16.04%, and 14.89% relative to *chn-1(tm2692)* mutants), respectively (log-rank test compared with *chn-1(tm2692)*, *h*CHIP rescue 1, $p < 0.001$; *h*CHIP rescue 2, $p < 0.001$; *Ce*CHIP rescue, $p < 0.001$) (Figure 4.10C and 4.10D). As in the *chn-1(by155)*-derived strains, none of the rescues differed significantly from the N2 controls (log-rank test compared with wild-type, *h*CHIP rescue 1, $p = 0.22$; *h*CHIP

rescue 2, p = 1.00; *Ce*CHIP rescue, p = 1.00). The last mortality occurred on day 24 in both the *chn-1(tm2692)* mutants and *m*Kate controls, and on days 30, 32, 32, and 30 in the wild-type controls, *h*CHIP rescues 1 and 2, and *Ce*CHIP rescues, respectively (Figure 4.10C and 4.10D). The second and third experimental replicates for *chn-1(tm2692)*-derived strains trend similarly, with rescue animals having an increased lifespan along with a delayed last mortality relative to *chn-1(tm2692)* (Supplemental Tables C7 and C8). Information pertaining to animals censored across all replicates for *chn-1(by155)*- and *chn-1(tm2692)*-derived strains can be found in Supplemental Table C6 and Supplemental Table C9, respectively.

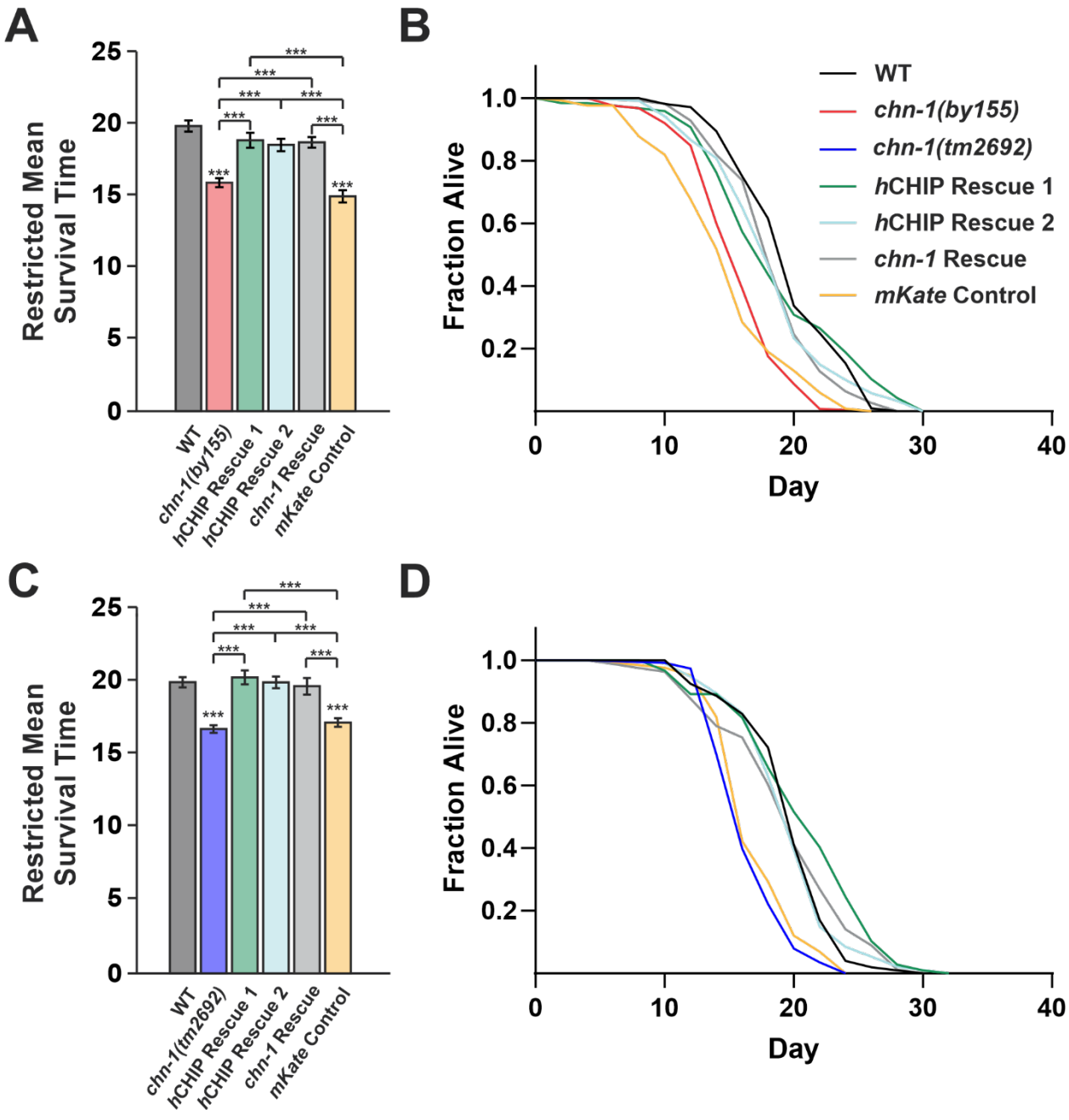

Figure 4.10 **Rescuing *chn-1* mutants led to an associated increase in lifespan.** (***A***, ***C***) Restricted mean survival time and (***B***, ***D***) cumulative survival graphs comparing wild-type N2 controls with *chn-1(by155)* (***A***, ***B***) and *chn-1(tm2692)* (***C***, ***D***) *C. elegans chn-1* mutants, as well as *chn-1* and *h*CHIP rescues derived from each deletion mutant. Deletion mutants showed decreased restricted mean survival times and significantly decreased lifespans than wild-type N2 controls, while rescue strains did not differ significantly from controls. Asterisks indicate significances: ***$p<0.001$. Error bars represent ± SEM (identical experiments repeated $n = 3$ times). Bonferroni-adjusted *p*-values as well as restricted mean survival times and final mortalities associated with longevity differences in N2 wild-types, *chn-1(by155)* and *chn-1(tm2692) chn-1* deletion

mutants, and *chn-1(by155)*- as well as *chn-1(tm2692)*-derived *h*CHIP rescue strains, *Ce*CHIP rescue strains, and *mKate* controls across all 3 replicates are shown in Supplemental Table C4, Supplemental Table C5 (*chn-1(by155)*-derived strains), Supplemental Table C7 and Supplemental Table C8 (*chn-1(tm2692)*-derived strains) (Bonferroni-adjusted *p*-values: Supplemental Table C4 and Supplemental Table C7; restricted mean survival times and final mortalities: Supplemental Table C5 and Supplemental Table C8). The number of animals censored at each time-point of the assay are shown in Supplemental Table C6 and Supplemental Table C9 for *chn-1(by155)*- and *chn-1(tm2692)*-derived strains, respectively.

4.3.6 Lifespan Rescue is Associated with a Distinct Proteomic Signature

Protein relative abundance was quantified between treatment pairs. That is, in this experiment, protein relative abundance was quantified comparing wild-type animals to either *chn-1(by155)* or *chn-1(tm2692)* mutants, and subsequently comparing each *chn-1*-null mutant to each rescue strain. Analyses were performed using *chn-1(tm2692)* deletion mutants, along with three *chn-1(tm2692)*-derived rescue strains ("*h*CHIP rescue 1", "*h*CHIP rescue 2", and "*Ce*CHIP rescue") and N2 controls. Proteins meeting a fold change cutoff of either ≤ 0.67 or ≥ 1.5 in pairwise comparisons were considered substantially altered, with proteins differentially expressed in opposite directions from wild-type to knock-out animals and knock-out to rescue strains being defined as "rescued". To account for protein extraction variability, analyses were performed on both samples processed by CHAPS-Urea and SDS-based lysis methods. Proteins rescued across all three rescue strains independently are listed in Tables 4.2 (CHAPS/Urea-processed samples) and 4.3 (SDS-processed samples), while all rescued proteins are listed in Supplemental Tables C10-C15.

Sequential comparisons revealed 151 rescued proteins common to the 3 rescue strains across both CHAPS/Urea- and SDS-processed samples (CHAPS/Urea: 61 proteins, or 40.13% of all commonly-shared rescued proteins; SDS: 91 proteins, or 59.87% of all commonly-shared rescued proteins) (Tables 4.2 and 4.3). In CHAPS/Urea-processed samples, 29 of these were overexpressed and 32 were underexpressed, while SDS-processed samples had 65 overexpressed and 26 underexpressed proteins, respectively (Tables 4.2 and 4.3). Overexpressed rescued proteins in CHAPS-lysed samples included Small RNA 2'-O-methyltransferase, Myosin

IA, COP9 signalosome complex subunit 2, Dymeclin, Uncharacterized Golgi apparatus membrane protein-like protein C34D4.4, Ubiquinone biosynthesis monooxygenase COQ6, mitochondrial, while underexpressed proteins included BPTI/Kunitz inhibitor domain-containing protein, Long chain fatty acid elongase 6, and Cytochrome b, among others (Table 4.2). In SDS-processed samples, overexpressed proteins included sn-1-specific diacylglycerol lipase ABHD11, PHAF1 protein T01G9.2, Saposin B-type domain-containing protein, Stomatin-1, Histone H2A, Probable mitochondrial import inner membrane translocase subunit tim-17B.1, and Probable Golgi transport protein 1. Conversely, overexpressed proteins included Fibulin-1, Endoplasmic reticulum lectin 1, and Transport and Golgi organization protein 1 homolog (Table 4.3). There were no overexpressed proteins shared across CHAPS/urea- and SDS-processed samples, while in underexpressed proteins, only Proton-coupled zinc antiporter SLC30A5, a secretory pathway-related protein involved in mediating zinc entry into the lumen of organelles[560-564], was shared between CHAPS/urea- and SDS-processed samples (Table 4.2 and 4.3).

Table 4.2 **Rescued proteins (based on fold change) identified by SWATH-MS that are either over- or under-represented in both *h*CHIP and *chn-1* rescue strains processed by lysis with CHAPS/urea-based lysis buffer.** Each protein listed below met the fold change cutoff criteria of either ≤ 0.67 or ≥ 1.5 compared to *chn-1(tm2692) C. elegans chn-1* mutants across the three rescue strains, as well as at each stage of comparison. Initially, a reference list was created comparing N2 wild-type worms and *chn-1* mutants. Proteins differentially expressed in opposite directions from wild-type to knock-out animals and knock-out to rescue strains were defined as "rescued".

Expression	Protein	*h*CHIP rescue 1 vs. *chn-1(tm2692)*		*h*CHIP rescue 2 vs. *chn-1(tm2692)*		*chn-1* Rescue vs. *chn-1(tm2692)*	
		p-Value	Fold Change	*p*-Value	Fold Change	*p*-Value	Fold Change
Over	Prolyl carboxy peptidase like protein 5	1.05E-03	3.302	1.02E-02	2.489	1.96E-01	1.559
Over	Uncharacterized protein C56G2.3	5.74E-03	2.909	2.72E-01	1.536	2.80E-02	2.303
Over	Small RNA 2'-O-methyltransferase	1.16E-01	2.757	2.04E-01	2.001	3.00E-02	3.219
Over	PUM-HD domain-containing protein	2.53E-01	2.677	1.91E-01	2.731	1.06E-01	4.641
Over	Nucleolar protein 9	3.71E-02	2.551	1.60E-01	1.883	1.28E-01	1.947
Over	RNA helicase	3.37E-03	2.454	1.74E-04	3.731	6.59E-04	3.035
Over	3'-5' exonuclease domain-containing protein	4.55E-04	2.299	1.23E-04	2.543	5.21E-04	2.275
Over	DNA-directed RNA polymerase subunit beta	1.64E-01	2.123	5.38E-02	2.866	8.52E-02	2.550
Over	Uncharacterized protein	9.59E-02	2.078	1.55E-01	2.260	2.49E-01	2.352
Over	L-serine ammonia-lyase	4.07E-03	2.029	3.96E-03	2.034	5.76E-02	1.614
Over	GRounDhog	7.20E-02	2.024	2.70E-01	1.522	8.03E-02	1.982
Over	m7GpppX diphosphatase	9.61E-03	2.011	6.13E-02	1.642	1.72E-02	1.894
Over	Probable urocanate hydratase	3.15E-02	1.906	3.13E-02	1.907	8.85E-03	2.213
Over	Myosin IA	3.70E-02	1.873	2.17E-02	2.002	1.99E-03	2.605
Over	COP9 signalosome complex subunit 2	4.15E-03	1.853	9.37E-03	1.818	1.13E-02	1.652
Over	Probable glutamine synthetase	4.28E-01	1.827	2.68E-01	2.349	8.15E-02	4.045
Over	Aldehyde dehydrogenase domain-containing protein	6.70E-02	1.782	8.85E-03	2.435	1.50E-04	4.417
Over	Peptidase S28	3.35E-01	1.773	4.29E-01	1.556	4.40E-01	1.580
Over	High mobility group protein hmg-12	6.55E-02	1.749	1.66E-01	1.518	9.00E-02	1.671
Over	Ribosomal protein S6 kinase beta	1.46E-01	1.738	1.37E-01	1.761	2.55E-01	1.537
Over	Dymeclin	6.26E-02	1.723	1.12E-01	1.624	4.31E-02	1.969

Over	Uncharacterized Golgi apparatus membrane protein-like protein C34D4.4	2.84E-01	1.721	1.03E-01	2.304	5.47E-02	2.694
Over	Putative choline-phosphate cytidylyltransferase	1.18E-01	1.662	2.80E-02	2.072	1.13E-02	2.343
Over	Tubby protein homolog 1	2.38E-01	1.564	4.87E-03	3.017	3.68E-02	2.233
Over	Ubiquinone biosynthesis monooxygenase COQ6, mitochondrial	5.86E-02	1.563	3.42E-02	1.656	1.57E-02	1.789
Over	Glycoside hydrolase family 1 protein	2.22E-01	1.558	2.69E-02	2.270	1.96E-01	1.634
Over	Patched-related protein 18	3.83E-02	1.555	3.69E-02	1.561	7.59E-03	1.786
Over	Probable peptidyl-tRNA hydrolase 2	1.13E-01	1.536	1.57E-02	1.949	3.24E-02	1.798
Over	Serine/threonine-protein phosphatase 4 catalytic subunit 1	1.09E-01	1.505	2.52E-03	2.233	1.07E-01	1.508
Under	BPTI/Kunitz inhibitor domain-containing protein	1.48E-02	0.232	1.06E-01	0.463	7.93E-02	0.432
Under	Long chain fatty acid elongase 6	8.78E-03	0.250	6.69E-02	0.390	1.72E-01	0.500
Under	Putative metallophosphoesterase F40B5.2	4.84E-02	0.251	2.51E-01	0.405	5.56E-01	0.667
Under	Heat shock 70 kDa protein 13	1.92E-03	0.263	6.28E-02	0.477	2.33E-01	0.626
Under	Nematode cuticle collagen N-terminal domain-containing protein	7.09E-03	0.299	5.77E-02	0.442	1.23E-01	0.519
Under	Proton-coupled zinc antiporter SLC30A5	2.54E-02	0.311	1.08E-02	0.223	1.25E-01	0.455
Under	RRM domain-containing protein	1.01E-01	0.322	4.69E-01	0.661	2.40E-01	0.475
Under	Uncharacterized protein D2096.6	4.59E-02	0.350	2.01E-03	0.181	2.53E-02	0.305
Under	Uncharacterized protein	2.71E-02	0.438	1.39E-01	0.554	2.10E-02	0.398
Under	TOG domain-containing protein	3.25E-02	0.453	6.69E-03	0.308	1.81E-03	0.320
Under	Carnitine O-palmitoyltransferase	3.42E-02	0.469	3.68E-02	0.474	7.01E-02	0.527
Under	DUF19 domain-containing protein	2.19E-03	0.474	4.29E-02	0.625	1.16E-02	0.550
Under	Fatty acid-binding protein homolog 4	2.80E-01	0.489	1.78E-01	0.407	5.28E-01	0.660
Under	Uncharacterized protein	1.00E-01	0.491	5.74E-02	0.436	4.37E-02	0.413
Under	Fungal lipase-like domain-containing protein	2.43E-01	0.520	1.99E-01	0.525	8.20E-02	0.424
Under	EGF-like domain-containing protein	2.30E-03	0.522	7.47E-06	0.361	2.14E-05	0.367
Under	Bestrophin homolog 14	2.23E-01	0.524	1.70E-01	0.468	1.76E-01	0.473
Under	CaDmium Responsive	8.26E-02	0.524	1.80E-01	0.610	6.76E-02	0.505

Under	Putative 1-acyl-sn-glycerol-3-phosphate acyltransferase acl-1	4.38E-02	0.527	3.09E-03	0.376	1.86E-01	0.663
Under	Glycoside hydrolase 35 catalytic domain-containing protein	4.84E-02	0.535	3.68E-02	0.545	7.05E-02	0.498
Under	DeHydrogenases, Short chain	1.25E-01	0.536	8.76E-02	0.512	2.12E-01	0.620
Under	Long chain fatty acid elongase 5	2.61E-03	0.545	9.13E-04	0.463	7.46E-04	0.557
Under	Cytochrome b	8.87E-02	0.552	1.68E-01	0.619	1.85E-01	0.631
Under	Epoxide hydrolase	3.04E-01	0.574	3.13E-01	0.627	2.96E-01	0.617
Under	Putative aquaporin-10	1.07E-01	0.577	1.71E-03	0.313	1.49E-01	0.613
Under	Probable manganese-transporting ATPase catp-8	3.53E-02	0.604	5.78E-03	0.510	8.67E-02	0.665
Under	Large ribosomal subunit protein uL5A	5.02E-01	0.608	9.30E-02	0.355	1.31E-01	0.419
Under	SOSS complex subunit A homolog	2.98E-02	0.613	1.91E-03	0.522	1.40E-02	0.591
Under	CRAL-TRIO domain-containing protein	5.92E-01	0.624	3.03E-01	0.505	5.78E-01	0.613
Under	DeHydrogenases, Short chain	8.28E-02	0.625	3.11E-02	0.553	2.52E-03	0.422
Under	Retinol dehydrogenase 13	1.03E-01	0.640	1.61E-02	0.508	1.31E-01	0.662
Under	Nematode cuticle collagen N-terminal domain-containing protein	3.98E-01	0.654	1.15E-01	0.447	9.38E-02	0.424

Table 4.3 **Rescued proteins (based on fold change) identified by SWATH-MS that are either over- or under-represented in both *h*CHIP and *chn-1* rescue strains processed by lysis with SDS-based lysis buffer.** Each protein listed below met the fold change cutoff criteria of either ≤ 0.67 or ≥ 1.5 compared to *chn-1(tm2692) C. elegans chn-1* mutants across the three rescue strains, as well as at each stage of comparison. Initially, a reference list was created comparing N2 wild-type worms and *chn-1* mutants. Proteins differentially expressed in opposite directions from wild-type to knock-out animals and knock-out to rescue strains were defined as "rescued".

Expression	Protein	*h*CHIP rescue 1 vs. *chn-1(tm2692)*		*h*CHIP rescue 2 vs. *chn-1(tm2692)*		*chn-1* Rescue vs. *chn-1(tm2692)*	
		p-Value	Fold Change	*p*-Value	Fold Change	*p*-Value	Fold Change
Over	sn-1-specific diacylglycerol lipase ABHD11	4.01E-02	6.513	4.15E-01	1.804	1.38E-01	2.868
Over	PHAF1 protein T01G9.2	3.84E-03	5.186	3.48E-02	2.933	2.64E-03	6.012
Over	Saposin B-type domain-containing protein	2.38E-04	4.538	1.81E-02	2.475	1.45E-03	3.567
Over	Stomatin-1	2.74E-02	4.450	2.74E-01	2.172	3.21E-01	2.189
Over	Carboxypeptidase E	2.00E-03	4.114	1.90E-02	2.839	1.50E-05	10.088
Over	Intrinsically Disordered Protein, class C	1.07E-01	3.800	2.61E-01	3.662	9.50E-04	22.859
Over	Histone H2A	2.44E-02	3.555	2.92E-01	1.776	9.12E-02	2.544
Over	Probable mitochondrial import inner membrane translocase subunit tim-17B.1	1.15E-01	3.464	5.36E-01	1.794	1.17E-01	6.351
Over	Prolyl Carboxy Peptidase like	9.79E-04	3.244	1.26E-01	1.715	9.16E-03	2.570
Over	Extracellular protein	1.37E-01	3.087	1.16E-01	2.982	6.08E-02	3.586
Over	Glutathione S-transferase 4	1.22E-05	2.985	1.73E-05	3.227	1.64E-01	1.517
Over	Large ribosomal subunit protein bL9m	4.38E-03	2.918	2.04E-01	1.569	3.19E-02	2.186
Over	SURF1-like protein	5.37E-02	2.799	5.49E-02	2.987	6.87E-02	2.633
Over	Acyl-coenzyme A thioesterase 8	8.89E-02	2.763	1.11E-01	2.585	2.66E-03	6.086
Over	Mitochondrial import receptor subunit TOM7 homolog	8.22E-02	2.670	5.19E-02	3.225	2.23E-02	4.082
Over	Not3 domain-containing protein	2.17E-03	2.593	3.40E-03	2.838	5.23E-03	2.684
Over	RNA polymerase II transcription factor SIII p18 subunit	4.42E-03	2.584	1.85E-01	1.533	1.71E-03	2.875
Over	UBX domain-containing protein 4	1.01E-01	2.583	4.41E-01	1.547	8.23E-02	2.741
Over	Peptidyl-prolyl cis-trans isomerase 10	1.50E-02	2.547	2.14E-01	1.647	4.22E-03	3.578
Over	Coatomer subunit epsilon	2.15E-04	2.510	3.93E-03	1.981	1.79E-02	1.729
Over	Protein mac-1	1.65E-02	2.495	1.60E-01	1.691	3.82E-02	2.190
Over	HEAT repeat protein	1.04E-02	2.455	3.11E-02	2.103	2.98E-02	3.272

Over	Peroxidasin homolog pxn-2	5.40E-03	2.434	3.83E-02	1.951	6.55E-05	3.933
Over	ATP synthase subunit C lysine N-methyltransferase	8.92E-02	2.386	1.19E-01	2.321	4.78E-03	4.602
Over	Cytoplasmic tRNA 2-thiolation protein 1	1.28E-01	2.208	2.13E-01	1.904	5.43E-02	2.758
Over	Proliferating cell nuclear antigen	6.74E-03	2.199	3.83E-02	1.798	5.73E-03	2.238
Over	5'-3' exoribonuclease 2 homolog	5.95E-06	2.170	1.05E-04	1.904	6.24E-05	1.951
Over	Probable Golgi transport protein 1	1.40E-01	2.168	3.53E-01	1.619	2.15E-01	1.907
Over	MICOS complex subunit MIC60-2	1.22E-01	2.101	2.26E-01	1.777	1.72E-01	1.919
Over	SUI1 domain-containing protein	3.04E-03	2.088	8.57E-04	2.330	1.19E-03	2.266
Over	Glucuronosyltransferase	5.27E-02	2.085	6.70E-02	2.000	3.27E-02	2.256
Over	Chromatin target of PRMT1 protein C-terminal domain-containing protein	8.65E-02	2.079	5.16E-02	2.306	2.11E-03	3.922
Over	Skp1-related protein	8.57E-03	2.053	4.62E-02	1.702	1.17E-02	1.986
Over	Probable mitochondrial pyruvate carrier 1	2.08E-01	2.027	1.14E-01	2.359	4.62E-03	5.207
Over	ERCC4 domain-containing protein	8.59E-02	1.999	7.40E-02	2.061	8.32E-03	3.024
Over	AP-2 complex subunit alpha	4.86E-03	1.993	6.09E-04	2.356	5.39E-07	3.849
Over	Putative cystathionine gamma-lyase 2	3.17E-02	1.965	6.07E-02	1.794	4.25E-03	2.529
Over	BPI1 domain-containing protein	1.81E-02	1.875	3.08E-02	1.511	5.13E-03	1.769
Over	U5 small nuclear ribonucleoprotein 200 kDa helicase	2.98E-02	1.851	2.54E-02	1.887	5.03E-02	1.734
Over	Ribonucleoside-diphosphate reductase large subunit	6.74E-02	1.840	7.38E-02	1.814	2.00E-01	1.524
Over	E3 ubiquitin-protein ligase hecd-1	2.50E-02	1.839	1.08E-02	2.010	2.82E-02	1.814
Over	Proteasome subunit alpha type-7	4.21E-03	1.836	8.10E-03	1.744	1.53E-02	1.656
Over	UBX domain-containing protein 3	1.84E-01	1.835	2.46E-01	1.696	4.88E-02	2.501
Over	Cysteine protease atg-4.1	1.24E-01	1.826	1.04E-01	1.893	2.49E-02	2.528
Over	Probable 26S proteasome complex subunit dss-1	3.84E-02	1.815	1.28E-02	2.073	1.38E-02	2.054
Over	Uncharacterized oxidoreductase F53C11.3	8.23E-02	1.796	4.88E-02	1.953	3.81E-02	2.028
Over	Golgi-specific brefeldin A-resistance guanine nucleotide exchange factor 1 homolog	1.73E-02	1.761	8.43E-04	2.264	1.47E-04	2.575
Over	Uncharacterized protein C18H9.6	1.07E-01	1.738	1.07E-01	1.737	2.26E-02	2.294

Over	Pinin/SDK/MemA protein domain-containing protein	2.06E-02	1.705	1.01E-02	1.819	8.33E-05	2.652
Over	Dihydropyrimidinase 2	7.82E-02	1.680	6.50E-03	2.299	2.48E-02	1.959
Over	Fatty acyl-CoA reductase	8.70E-02	1.662	6.87E-02	1.720	5.79E-02	1.761
Over	Nuclear hormone receptor family member nhr-49	2.29E-01	1.643	3.61E-02	2.288	9.13E-02	1.877
Over	Signal peptidase complex subunit 2	4.90E-02	1.640	5.52E-02	1.618	1.30E-02	1.891
Over	KH domain-containing protein akap-1	2.91E-02	1.640	1.95E-02	1.703	2.70E-02	1.651
Over	Small ribosomal subunit protein mS31	1.97E-02	1.634	1.92E-02	1.637	4.24E-03	1.841
Over	Neuronal calcium sensor 2	1.39E-02	1.632	1.39E-02	1.632	1.51E-02	1.622
Over	Intestinal acid phosphatase	1.08E-01	1.626	1.28E-01	1.582	7.24E-02	1.726
Over	Gut esterase 1	2.25E-01	1.616	1.12E-02	2.854	1.09E-02	2.865
Over	CYtochrome P450 family	5.20E-01	1.595	3.80E-01	1.617	3.35E-01	1.789
Over	Integrin-linked protein kinase homolog pat-4	9.81E-02	1.591	2.46E-02	1.904	1.18E-02	2.074
Over	Probable glutathione S-transferase gst-36	1.34E-02	1.583	3.89E-03	1.729	1.07E-02	1.609
Over	DDRGK domain-containing protein 1	2.41E-01	1.557	2.24E-01	1.584	1.17E-01	1.818
Over	alpha-1,2-Mannosidase	1.20E-01	1.540	1.40E-01	1.577	3.09E-03	2.467
Over	Innexin-5	1.32E-01	1.537	4.65E-03	2.336	5.21E-02	1.753
Over	Multifunctional procollagen lysine hydroxylase and glycosyltransferase	2.19E-01	1.523	2.01E-02	2.277	5.59E-02	1.947
Under	Fibulin-1	5.03E-03	0.053	3.90E-02	0.112	1.32E-02	0.100
Under	Protein kinase domain-containing protein		0.089		0.255		0.416
Under	Sm domain-containing protein	2.03E-02	0.118	9.86E-02	0.193	7.98E-02	0.213
Under	JNK-interacting protein	5.67E-03	0.127	8.33E-03	0.132	1.08E-02	0.160
Under	39S ribosomal protein L55, mitochondrial	1.57E-03	0.162	3.49E-02	0.315	6.59E-02	0.356
Under	PI31_Prot_N domain-containing protein	1.56E-02	0.167	2.25E-01	0.498	2.81E-01	0.539
Under	Cytochrome P450	6.15E-02	0.204	3.42E-02	0.159	6.03E-02	0.202
Under	Flavin-containing monooxygenase	2.35E-03	0.205	3.90E-02	0.352	1.20E-02	0.295
Under	Nematode cuticle collagen N-terminal domain-containing protein	7.14E-02	0.212	1.89E-03	0.071	4.39E-02	0.191
Under	Fanconi anemia group I protein	3.50E-02	0.216	2.44E-02	0.184	6.28E-02	0.265
Under	GTP-binding protein	6.18E-03	0.224	6.58E-02	0.379	1.99E-02	0.287
Under	V-type proton ATPase subunit e	2.84E-03	0.245	6.67E-02	0.464	1.96E-01	0.579

Under	Membrane insertase YidC/Oxa/ALB C-terminal domain-containing protein	3.25E-04	0.273	3.73E-03	0.360	7.03E-04	0.297
Under	G-patch domain-containing protein	5.39E-02	0.297	3.80E-01	0.572	1.40E-01	0.371
Under	Endoplasmic reticulum lectin 1	3.94E-04	0.309	3.27E-02	0.484	8.03E-02	0.556
Under	Transport and Golgi organization protein 1 homolog	4.52E-02	0.346	2.55E-01	0.555	5.39E-02	0.361
Under	Fcf2 pre-rRNA processing C-terminal domain-containing protein	8.56E-02	0.350	1.12E-01	0.379	3.94E-01	0.598
Under	Extracellular superoxide dismutase	1.30E-01	0.358	4.24E-01	0.572	1.10E-01	0.337
Under	Proton-coupled zinc antiporter SLC30A5	4.52E-02	0.399	6.68E-02	0.473	8.57E-02	0.497
Under	Serpentine Receptor, class T	2.62E-02	0.412	8.55E-03	0.444	1.90E-01	0.667
Under	CMP/dCMP-type deaminase domain-containing protein	1.11E-01	0.473	5.10E-02	0.364	1.17E-01	0.467
Under	Aspartate dehydrogenase domain-containing protein	1.39E-01	0.516	6.20E-02	0.430	1.44E-01	0.520
Under	NADH-ubiquinone oxidoreductase chain 4	1.35E-01	0.525	1.44E-01	0.533	2.62E-01	0.618
Under	Histidine-rich glycoprotein-like	3.29E-01	0.594	3.31E-01	0.595	1.98E-01	0.501
Under	Uterine Lumin Expressed/localized	2.77E-01	0.596	6.04E-02	0.425	2.09E-01	0.531
Under	Probable dynactin subunit 2	2.46E-01	0.638	2.09E-01	0.614	8.52E-02	0.508

Pathways and processes related to DNA methylation and chromatin accessibility, the ubiquitin-proteasome system, the regulation of membrane integrity, Golgi-mediated protein trafficking, mitochondrial dysfunction, and lipid biogenesis and metabolism featured prominently among rescued proteins. Indeed, gene ontology enrichment analyses of CHAPS-processed samples revealed several GO terms related to fatty acid biosynthesis and elongation, particularly methyl-branched fatty acid biosynthetic process and fatty acid elongation of polyunsaturated, saturated, and monounsaturated fatty acids (all $p < 0.05$) (Table 4.4). The cellular compartment most impacted by rescue of *chn-1* was the endoplasmic reticulum ($p < 0.05$) (Table 4.4). Oxidoreductase activity and metabolic pathways were also significantly altered in a rescue-dependent manner ($p < 0.05$) (Table 4.4 and Table 4.5). The only GO term shared by both CHAPS/urea- and SDS-processed samples across both *h*CHIP and *Ce*CHIP rescue strains was endoplasmic reticulum (cellular compartment; $p < 0.05$) (Table 4.4 and 4.6).

Epigenetic processes and pathways related to DNA repair were significantly affected by *chn-1* rescue in SDS-processed samples, including heterochromatin formation, DNA repair, and regulation of DNA-templated transcription (all $p < 0.001$) (Table 4.6). Mitochondrion organization was also altered ($p < 0.01$), followed by vesicle-mediated as well as protein transport (both $p < 0.05$) (Table 4.6). Perhaps unsurprisingly, the cellular compartments most affected by *chn-1* rescue included the nucleosome ($p < 0.001$), endoplasmic reticulum ($p < 0.001$), and mitochondria ($p < 0.01$), as well as compartments related to these organelles, while significant molecular functions included several related to epigenetic regulation, namely nucleosomal DNA binding and structural constituent of chromatin (both $p < 0.05$) (Table 4.6). Accordingly, the most substantially-altered pathway was ATP-dependent chromatin remodeling ($p < 0.001$). DNA binding ($p < 0.001$) and protein binding ($p < 0.01$) were also significant, along with protein heterodimerization activity ($p < 0.001$) (Table 4.7).

Table 4.4 **GO terms related to substantially altered proteins identified in both *h*CHIP and *chn-1* rescue strains processed by lysis with CHAPS/urea-based lysis buffer.** Biological process (BP), molecular function (MF) and cellular component (CC) GO terms identified (using DAVID) in *h*CHIP/*Ce*CHIP rescue strains after being altered in the opposite direction from N2 wild-type to *chn-1(tm2692)* deletion mutants. The number of associated genes ("count") and an association index (probability (raw *p*-values) as well as enrichment score) for each GO term is included. † Indicates GO terms shared by both CHAPS/urea- and SDS-processed samples.

	GO Term	Count	Enrichment	*p*-Value
BP	methyl-branched fatty acid biosynthetic process	2	141.688	1.38E-02
BP	fatty acid elongation, polyunsaturated fatty acid	2	47.229	4.07E-02
BP	fatty acid elongation, saturated fatty acid	2	47.229	4.07E-02
BP	fatty acid elongation, monounsaturated fatty acid	2	47.229	4.07E-02
BP	mRNA catabolic process	2	38.642	4.95E-02
CC	endoplasmic reticulum†	6	4.297	1.12E-02
MF	oxidoreductase activity	6	3.721	2.01E-02
MF	hydrolase activity	7	2.750	3.68E-02
MF	fatty acid elongase activity	2	45.483	4.23E-02
MF	serine-type exopeptidase activity	2	40.935	4.69E-02

Table 4.5 **KEGG pathways related to substantially altered proteins identified in both *h*CHIP and *chn-1* rescue strains processed by lysis with CHAPS/urea-based lysis buffer.** Pathways identified (using DAVID) in *h*CHIP/*Ce*CHIP rescue strains after being altered in the opposite direction from N2 wild-type to *chn-1(tm2692)* deletion mutants. The number of associated genes ("count") and an association index (probability (raw *p*-values) as well as enrichment score) for each pathway is included. ‡ Indicates pathways shared by both CHAPS/urea- and SDS-processed samples.

Pathway	Count	Enrichment	*p*-Value
Metabolic pathways	11	1.824	3.33E-02

Table 4.6 **GO terms related to substantially altered proteins identified in both *h*CHIP and *chn-1* rescue strains processed by lysis with SDS-based lysis buffer.** Biological process (BP), molecular function (MF) and cellular component (CC) GO terms identified (using DAVID) in *h*CHIP/*Ce*CHIP rescue strains after being altered in the opposite direction from N2 wild-type to *chn-1(tm2692)* deletion mutants. The number of associated genes ("count") and an association index (probability (raw *p*-values) as well as enrichment score) for each GO term is included. † Indicates GO terms shared by both CHAPS/urea- and SDS-processed samples.

	GO Term	Count	Enrichment	*p*-Value
BP	heterochromatin formation	16	37.757	3.35E-20
BP	DNA repair	17	13.200	8.94E-14
BP	regulation of DNA-templated transcription	18	3.882	2.13E-06
BP	mitochondrion organization	4	13.011	3.39E-03
BP	vesicle-mediated transport	5	4.457	2.48E-02
BP	protein transport	6	3.034	4.57E-02
CC	Nucleosome	16	24.183	7.45E-17
CC	endoplasmic reticulum†	12	3.890	2.27E-04
CC	Mitochondrion	14	2.741	1.50E-03
CC	Nucleus	34	1.669	1.55E-03
CC	endoplasmic reticulum lumen	3	14.412	1.79E-02
CC	mitochondrial inner membrane	5	3.980	3.60E-02
MF	nucleosomal DNA binding	16	70.939	1.97E-25
MF	structural constituent of chromatin	16	21.957	2.49E-16
MF	protein heterodimerization activity	16	17.078	1.30E-14
MF	DNA binding	19	2.381	6.74E-04
MF	protein binding	19	1.877	9.14E-03

Table 4.7 **KEGG pathways related to substantially altered proteins identified in both *h*CHIP and *chn-1* rescue strains processed by lysis with SDS-based lysis buffer.** Pathways identified (using DAVID) in *h*CHIP/*Ce*CHIP rescue strains after being altered in the opposite direction from N2 wild-type to *chn-1(tm2692)* deletion mutants. The number of associated genes ("count") and an association index (probability (raw *p*-values) as well as enrichment score) for each pathway is included. ‡ Indicates pathways shared by both CHAPS/urea- and SDS-processed samples.

Pathway	Count	Enrichment	*p*-Value
ATP-dependent chromatin remodeling	16	12.588	2.88E-13
Drug metabolism - other enzymes	5	4.364	2.50E-02

4.4 Discussion

Congruent with its neuroprotective effects[385], functional deficits in CHIP contribute to a plethora of malignant health outcomes, with many CHIP-related pathologies converging on neurodegenerative disorders[256]. Here, I show that the ablation of both CHIP and SMA-9 had a mildly additive effect on nematode longevity, suggesting the two genes function in a distinct but perhaps somewhat overlapping manner within the TGF-β signaling cascade. I also show that abrogation of CHIP function alters Golgi morphology and expression of Rab6 and COG6, two proteins sharing a Golgi-associated retrograde trafficking pathway, and that CHIP rescue is causally associated with restored longevity linked to altered protein expression converging upon chromatin formation and remodeling, protein transport, metabolic pathways, and mitochondrial organization. Interestingly, the majority of proteins substantially altered from N2 wild-type to each *chn-1* deletion mutant were altered in the opposite direction from the *chn-1*-null mutants to the rescues, suggesting that longevity interacts with and is affected by a broad suite of proteins that may also intersect with other processes. These findings suggest a correlation between normal CHIP function, Golgi complex integrity, and healthy aging, further underpinning the neuroprotective role of CHIP.

SMA-9 was significantly underexpressed in both *chn-1(by155)* and *chn-1(tm2692)* animals, and *chn-1; sma-9* double-mutants were shorter-lived than both *chn-1* and *sma-9* single-gene knock-out mutants, although only the former was significant. The proteomic correlation between CHIP deletion and SMA-9 underexpression suggests an interdependent relationship between CHIP and SMA-9, while the relatively modest difference between the *chn-1; sma-9* double-mutants and each single-gene knock-out mutant suggests overlapping but not entirely redundant activities within the TGF-β signaling pathway. This is reinforced by the absence of consistent statistically significant differences between single- and double-gene-deficient animals across experimental replicates, even while double-gene mutants showed a persistent decrease in longevity. As mentioned previously, SMA-9 has been implicated in several neuroprotective functions including amyloid-β clearance, plaque reduction[427-430], deficits in motor coordination, altered excitatory neurotransmission[428,431], and insulin/IGF-1 signaling-mediated longevity[7,428]. Interestingly, Proton-coupled zinc antiporter SLC30A5,

the only rescued protein shared by *h*CHIP and *Ce*CHIP rescue strains across both CHAPS/urea- and SDS-processed samples, plays a crucial role in insulin storage and secretion via the transport of zinc into the secretory granules of pancreatic β-cells, suggesting a CHIP-associated interplay between insulin signaling and secretory processes in the mediation of aging[561]. While the mechanisms underlying the interdependence between CHIP and SMA-9 remain unknown, CHIP-mediated TGF-β signaling has been found to occur via the regulation of basal Smad3 levels[435,436], and SMAD proteins more generally are degraded in a ubiquitin-dependent proteolytic cascade[434]. Future studies should also investigate whether overexpression of *sma-9* would rescue the *chn-1* deletion phenotype. While this was not empirically tested here, the overlapping but not entirely redundant activities of *sma-9* and *chn-1* (as implied in the lifespan assay results) within the same TGF-β pathway suggest *sma-9* overexpression may at least partially rescue longevity in *chn-1*-null mutants, although this may also be contextually dependent (e.g., at what stage of the lifespan *sma-9* is overexpressed).

CHIP-null animal and cell experiments showed altered Golgi morphology, fluorescence, and expression of associated retrograde trafficking proteins. Specifically, both *chn-1*-null MANS-positive nematode Golgi stacks and GM130-stained human neuroblastoma cells showed increased immunofluorescence expression, and individual Golgi compartments in animals significantly decreased in area while increasing in number. Morphological analyses of Golgi structures have revealed neurodegeneration-associated changes across a spectrum of conditions, including Amyotrophic lateral sclerosis[565], Alzheimer's disease[566], Parkinson's disease[567], Huntington's disease[568], Creutzfeldt-Jacob disease[569], and multiple system atrophy[570]. Golgi fragmentation, for instance, may detrimentally alter neuronal physiology as well as axonal, dendritic, and synaptic transport[571]. Rather than being a downstream consequence of the apoptotic process, Golgi fragmentation precedes other malignant changes in the neurodegenerative pathological cascade[572]. The neurodegenerative fragmentation of Golgi morphology maladaptively alters protein biogenesis and transport, including that of the amyloid precursor protein in Alzheimer's disease[573] and sodium-dependent vitamin C transporter 2 in Huntington's disease[574]. More generally, pathophysiological

changes in the Golgi complex may trigger a stress response ultimately resulting in neuronal death[575]. While the distribution of stacked cisternae into diffused smaller elements is characteristic of fragmentation, the increased fluorescence across both worm and cell models may instead suggest a distinct, knock-out-dependent downstream signaling cascade characteristic of the Golgi stress response[576].

Immunoblotting and immunofluorescence revealed differential expression of COG6 and Rab6, two retrograde trafficking-associated proteins, in response to CHIP ablation. Specifically, Western blotting revealed relatively high but variable expression of Rab6 in response to CHIP ablation across extraction buffers, whereas COG6 expression was significantly increased in Tween-solubilized CHIP-null samples but variable across other detergents. One possible interpretation for the variability in Rab6 and COG6 expression suggests that, under normal conditions, CHIP may be involved in sequestering these proteins in specific subcellular compartments, or otherwise impact their localization in an alternative manner, whether directly or indirectly. Conversely, as discussed in Chapter 2, the steady-state localisations of the proteins themselves may simply be more amenable to solubilization by certain detergents based on their biochemical properties in a CHIP-dependent manner, although both possibilities are purely speculative and require further validation. Indeed, CHIP has previously been implicated in protein trafficking. For instance, it has been shown to induce the chaperone-independent translocation of HSF1[272] as well as mediating the translocation of eNOS, one of three nitric oxide synthases present in human tissues[281], in unstressed cells[280]. Interestingly, CHIP-directed ubiquitination has also been shown to disrupt the apoptotic activity of Daxx, a chromatin-silencing, death domain-binding protein, by temporarily sequestering it into an insoluble fraction until the cell returns to homeostasis[278,279]. Thus, the detergent-dependent differences in protein solubilization seen here may reflect a broader role of CHIP in protein trafficking, although further work is needed to elucidate the mechanisms underlying the intersection between CHIP activity, the physicochemical characteristics of different extraction buffers, and Rab6/COG6 expression.

Immunofluorescent staining also showed that COG6 and Rab6 were partially co-localised with GM130, likely due to their shared overarching role in maintaining Golgi

dynamics, associated functions, and structural integrity[444,577]. For instance, the golgins – a family of Golgi-associated coiled-coil proteins required to provide structural support for Golgi cisternae and enable tethering events during membrane fusion, including GM130[578] – function in Rab6-regulated membrane-tethering events[577]. COG6, in turn, is known to interact with several Golgi Rabs[579], but its partial co-localisation with GM130 has been found to persist even in cells lacking Rab6, suggesting that COG6-SNARE interactions play a larger role in COG6 localization and Golgi integrity[444].

Golgi complex fragmentation has been causally linked to α-Synuclein (α-Syn) prefibrillar aggregate formation[580] as well as an ER-Golgi trafficking imbalance[567,581], and the α-Syn accumulation-induced dysregulation of ER-to-Golgi transport has in turn been associated with the Rab1, 3A, and 8-dependent inhibition of SNARE complex assembly[567]. Notably, cooperative interactions between Hsp/c70 and CHIP have been found to regulate ER protein quality control more generally, with reciprocal allosteric interactions between its TPR and U-box domains and the substrate-binding and C-terminal domains of Hsp/c70 facilitating the ubiquitination of misfolded cystic fibrosis transmembrane conductance regulator (CFTR), a model substrate for ER-associated quality control[442]. Indeed, the overexpression of these Rabs is both necessary and sufficient to rescue ER-to-Golgi trafficking in yeast and mammalian cells[567]. It is possible that Rab6 and COG6 are implicated in an analogous retrograde signaling cascade, and their overexpression in CHIP-null cell extracts reflected an early, compensatory stress response to the pro-aging cellular processes brought about by CHIP deletion. The decreased immunofluorescence expression in CHIP knock-outs may reflect a more diffused distribution pattern throughout the cells – indeed, the variable expression of COG6 and Rab6 in response to extraction with different detergents suggests a variable localization of these two proteins – while the relative immunoblotting expression variability of Rab6 may be influenced by cellular stress response pathways induced by pockets of increased confluency[582,583].

A proteomic assay of proteins associated with CHN-1-dependent lifespan rescue revealed differential enrichment converging upon chromatin formation and remodeling. Aging itself is characterized by a stochastic deregulation of gene expression. Here, DNA repair was one of the most significantly enriched biological processes in rescued

nematodes. Indeed, murine embryonic fibroblasts treated with DNA-damaging H_2O_2 mirrored this aging-associated increase in transcriptional noise, suggesting DNA damage plays a critical role[584]. Work in senescent human cells has linked aging to altered transcriptional programming characterized by the upregulation of alternative histone transcripts[585] as well as the induction of several cellular defense and inflammatory response genes. Many of the corresponding proteins are relevant to the senescence-associated secretory phenotype[586], the chronic induction of which can decrease longevity[587], thus potentially linking transport-related processes to a shortened lifespan.

In senescent human fibroblasts, CHIP is upregulated in tandem with a downregulation of p53, and CHIP silencing results in considerable p53 accumulation[588]. Indeed, CHIP-dependent p53 regulation occurs specifically during senescence[588]. More broadly, CHIP has also been found to affect cellular senescence through the modulation of oxidative load[589]. Ubiquitylated and sumoylated proteins, including telomerase, p53, histone H2A, and proliferating cell nuclear antigen, are also upregulated in senescent cells, resulting in proteasomal degradation[590]. Interestingly, the sumoylation of p53/pRb and associated proteins impacts both senescence-specific transcriptional programming[591] and longevity more generally[592]; however, more work is needed to untangle the chromatin mechanisms linking CHIP-mediated proteasomal degradation and lifespan[593].

CHIP has also been implicated in the modulation of Met receptor degradation, thus indirectly modulating a downstream, chromatin remodeling-associated signaling cascade[594]. Specifically, Met receptor interaction with CHIP led to proteasomal degradation in vitro, while CHIP knockdown increased Met receptor expression[594]. Conversely, CHIP overexpression destabilized endogenous Met receptor in lung cancer cells while simultaneously impeding Met-directed cancerous cell growth and proliferation[594]. Notably, hepatocyte growth factor (HGF)-dependent Met receptor activation results in receptor dimerization as well as the activation of its intrinsic intracellular tyrosine kinase[595]. This results in the transient appearance of phosphorylation sites in the Met receptor tail, which in turn recruit signaling proteins and trigger their associated signaling cascades, including signal transducer and activator of

transcription (STAT), among others[595]. Previously, growth factor receptors were thought to function through membrane-associated proximal signaling events, resulting in the downstream activation of nuclear transcription factors or STAT proteins[595]. Upon HGF-associated activation, however, Janus kinases have been implicated in the Met receptor-triggered signal transduction events[596]. Interestingly, these kinases can translocate to the nucleus, where they in turn mediate the phosphorylation of histones and otherwise contribute to myriad processes associated with chromatin remodeling and gene expression[595].

Metabolic and mitochondrial pathways and gene ontology terms were noticeably enriched amongst rescued proteins. Myriad gerontological studies over the last several decades posit mitochondria as a key regulator of longevity[597-605]. The 'uncoupling to survive' hypothesis suggests that energy metabolism correlates with longevity[597] – specifically, that inefficient mitochondrial ATP synthesis may be necessary to limit pathological oxygen radical-mediated damage in the cell[597]. The insulin receptor, a direct target of CHIP, regulates the insulin and IGF-1 signaling pathway, thus mediating metabolism and aging[7]. However, the relationship between deregulated insulin and insulin-like growth factor 1 signaling and mitochondrial activity is less clear. Emerging evidence suggests inflammation, insulin resistance, and mitochondrial dysfunction to be common features underlying the epidemiological connection between Alzheimer's disease and type 2 diabetes, for instance[606]. In *C. elegans*, long-lived *daf-2* mutants deficient in the insulin/IGF receptor showed both decreased metabolic rate and oxygen consumption compared to control strains[607]; however, long-lived *D. melanogaster* insulin/IGF receptor substrate mutants did not differ in either of these parameters[608]. In mice, a fat-specific insulin receptor knock-out (FIRKO) extended lifespan by 18% along with increasing oxygen consumption per gram of body weight, associated mitochondrial mtDNA content, size, and gene expression for proteins involved in mitochondrial biogenesis[609], altogether implicating increased white adipose tissue oxidative metabolism and metabolic rate in the increased longevity and metabolic disease resistance of FIRKO mice[610]. In contrast, however, differential expression of PEPCK-C (phosphoenolpyruvate carboxykinase), a protein involved in gluconeogenesis and glyceroneogenesis, in white adipose tissue caused obesity or lipodystrophy,

respectively, but did not extend lifespan[611], suggesting a variable effect of adipose-associated metabolic changes on lifespan. Conversely, PEPCK-C overexpression in skeletal muscles led to increased oxygen consumption, mitochondrial biogenesis, and lifespan[611], suggesting variability in the relationship between model organisms, tissue types, and the effects of oxidative metabolism on longevity. In rats, aging is correlated with an increased formation of intra-mitochondrial reactive oxygen species, oxidative damage, proton leak-rates resulting in the reduction of membrane potential, as well as decreased ATPase and complex IV activities[612]. Interestingly, treatment with IGF-1 reversed these detrimental effects, suggesting that the antioxidative properties of this hormone are associated with mitochondrial protection[612]. Future studies should focus on further elucidating how the interaction dynamics between the CHIP-dependent regulation of insulin receptor turnover[7] and mitochondrial dynamics influence longevity.

The present findings provide novel insights into possible CHIP-dependent perturbations linking TGF-β signaling, Golgi morphology, retrograde trafficking pathways, epigenetic processes, and mitochondrial aberrations to decreased longevity. These results suggest that CHIP ablation is associated with differential expression of Golgi markers across model systems that may be indicative of an early stress response[575,576] and provide the foundations for further exploring the mechanistic interplay between Golgi complex dysfunction and neurodegenerative disease. Proteomic analyses of *h*CHIP and *Ce*CHIP rescue strains suggest CHIP may enact broad effects on processes related to transcriptional regulation as well as metabolic and mitochondrial pathways to mediate longevity, possibly through its regulation of the insulin receptor. Future studies should aim to define the mechanistic underpinnings of linking the neuroprotective functions of CHIP to altered Golgi activity, TGF-β signaling, and longevity.

Chapter 5
General Discussion

5.1 Detergent Properties Substantially Alter Protein Profiles

5.1.1 Summary of Findings

The present findings provide novel insights into methodological considerations that should be taken into account when extracting proteins for -omic analyses. Specifically, global protein solubilization was performed on three *C. elegans* strains to determine how lysis with SDS, a highly-denaturing anionic detergent, and CHAPS/urea, a mild, non-denaturing zwitterionic detergent combined with a chaotropic agent, respectively, affected protein extraction. Preliminary unsupervised hierarchical clustering analyses correctly grouped experimental lysis conditions across strains, suggesting that the effects of detergent choice superseded between-strain differences. Although CHAPS and urea efficiently solubilized membrane-associated proteins – and in particular, peripheral membrane proteins – SDS was broadly more effective at global protein extraction, and particularly at the solubilization of transmembrane proteins. One possible explanation for these data is that a focused cohort of superficial membrane proteins were overrepresented amongst all proteins solubilized by CHAPS/urea, while a broader class of transmembrane proteins were solubilized in SDS-processed samples. In other words, the broader protein solubilization activity of SDS may have led to more extensive coverage of membrane proteins than the biased extraction of peripheral membrane proteins by CHAPS combined with the chaotropic activity of urea. Pathways differentially expressed across all strains also included ribosomal-associated processes. Interestingly, SDS has previously been found to enrich basic proteins – such as ribosomal and ribonuclear proteins – due to the anionic character of its sulfate group. On the other hand, as CHAPS and urea are zwitterionic and non-ionic, respectively, they may be predisposed to extracting proteins with domains containing zwitterionic and non-ionic properties.

5.1.2 Study Limitations and Considerations for Future Work

These findings highlight the impact of detergent variability on global protein solubilization in *C. elegans* and suggest a role for the physicochemical properties of detergents as a possible confound when comparing proteomic experiments. This data can be improved upon by including additional buffers, particularly those previously used in cellular fractionation studies of *C. elegans*, such as NP-40, Tween 20[613], and Triton X-100[614]. Additional cross-strain comparisons of detergent-dependent patterns in protein solubilization, gene ontology term enrichment, and pathway changes would also strengthen the conclusions. Additionally, if single-gene knock-out of known CHN-1 interaction partners are used, for instance, these cross-comparisons would simultaneously provide additional insights into CHN-1-associated functions and downstream effects. Repeating these experiments in other model systems – such as the SH-SY5Y human neuroblastoma cell line or mammalian organs – to investigate detergent-dependent protein solubilization would also be valuable.

Finally, detergent concentrations could be adjusted and protein extraction patterns examined as a result. CHAPS, for example, has two critical micelle concentrations, with molecules above the second critical micelle concentration forming double-layered micelles with an aliphatic inner shell interacting with steroid groups in the outer shell[390]. This property also affects protein solubilization, with a number of proteins only extracted by CHAPS in this state. Finally, protein refolding experiments[391,392] in conjunction with further validation experiments may further our understanding of protein-protein interaction sites, partners, and downstream effects.

5.2 *chn-1* Ablation Alters the Nematode Proteomic Landscape

5.2.1 Summary of Findings

CHIP functions both as a co-chaperone and E3 ubiquitin ligase, thus underpinning both pathways related to chaperone networks and proteasomal degradation[402]. Notably, CHIP can also act independently of its chaperone partners to regulate the structure and function of several client proteins involved in a diverse range of cellular processes,

altogether culminating in broad pathophysiological consequences should its activities be hindered. Here, a proteomic assay was performed to explore the functions of CHIP in *C. elegans*, a whole-animal, genetically tractable model organism. Specifically, two independently-derived *chn-1*-null mutants, *chn-1(by155)* and *chn-1(tm2692)*, were compared to N2 wild-type animals upon protein solubilization with either CHAPS and urea or SDS. The results linked decreased longevity associated with *chn-1* deletion to differentially expressed proteins, gene ontology terms, and pathways related to protein trafficking, endosomal transport, and endocytosis, rRNA processing, macromolecular methylation, metabolic processes, the biosynthesis of amino acid, splicing, and FoxO signaling. Proteomic markers associated with mitochondrial and Golgi complex integrity, as well as transcriptional regulators, were especially enriched in *chn-1*-null animals, suggesting that inefficiencies the oxidative stress response as well as Golgi-associated protein trafficking may contribute to the mechanistic underpinnings of CHIP-related disorders, including both neurodegenerative and cancerous conditions.

These data provide novel protein hits for further study in known CHIP-dependent pathways while suggesting that its activities extend beyond the main findings seen in previous studies. For instance, altered metabolic and mitochondrial dynamics were heavily enriched in null to wild-type comparisons, further implicating metabolic abnormalities as well as the oxidative stress response in the pathophysiology of CHIP-mediated disorders. For instance, CHIP was previously found to rescue several mitochondrial defects in *Pink1* mutants, including excessive fusion, reduced ATP content, and crista disorganization[378]. Here, *chn-1*-null mutants showed a significant underexpression of FIS1-related protein fis-2, known to play a central role in mitochondrial fission[437], along with enriched FoxO signaling, implicating CHIP in imbalanced mitochondrial fission–fusion. Mitochondrial fission–fusion is essential to mitochondrial homeostasis, morphology, and network connectivity, as well as the repair of defective mitochondria, mitochondrial segregation during cell division, oxidative phosphorylation, and intramitochondrial calcium signal transduction[615]. Indeed, aberrations in fission–fusion are associated with several adverse effects[616,617], including neuronal injury[618-620] and cellular senescence[621], among others[622,623].

Splicing, Golgi-associated protein transport, and TBF-β signaling were also altered in response to *chn-1* deletion. Previous RNAseq and splicing analyses found the majority of transcripts induced during heat stress were at least partially dependent on CHIP, and subsequent pathway analyses of these CHIP-dependent transcripts found enrichment in processes related to a pro-aging phenotype[403]. This mirrors the decreased longevity and accelerated aging found in other studies focused on abrogated CHIP function[9], and suggests an impaired stress response culminating in both dysregulated RNA processing and splicing may contribute to the accelerated aging observed in CHIP-null animals. Several proteins altered in *chn-1*-null samples, such as Rab6 and COG6, were also implicated in both retrograde transport and Golgi complex integrity. These proteins converged with enriched KEGG pathways as well as gene ontology terms including protein transport, endosomal transport, and endocytosis, suggesting altered CHIP-mediated trafficking activities may contribute to protein transport deficiencies culminating in the disruption of Golgi morphology and the deleterious accumulation of improperly trafficked, misfolded proteins[445]. Finally, the transcription factor SMA-9 was one of the most substantially underexpressed proteins across both *chn-1(by155)* and *chn-1(tm2692)* deletion mutants, suggesting that CHN-1 may participate or interact with the TGF-β signaling pathway[428].

5.2.2 Study Limitations and Considerations for Future Work

These data provide a foundation for further validation experiments exploring the neuroprotective role of CHIP. As these preliminary results suggest CHIP ablation affects cellular processes in a location-dependent manner, further research may benefit from cellular fractionation experiments comparing the protein landscapes of the organelles most sensitive to CHIP deletion, such as the mitochondria and Golgi complex. Since metabolic pathways were significantly altered in *chn-1*-null worms, future experiments may also benefit from a quantitative ^{1}H NMR-based metabolomic assay of the downstream metabolites associated with CHIP deletion. Furthermore, given that the TPR and U-box domains of CHIP reflect distinct functions of the protein, repeating these proteomic, metabolomic, and cellular fractionation experiments subsequent to the targeted introduction of site-specific point mutations affecting either its chaperone or E3 ligase activity may provide a more nuanced overview of CHIP's complex biology.

Finally, specific interaction partners of CHIP may be isolated and further characterized using pull-down or proximity ligation assays, for example.

5.3 CHIP Impacts Golgi Morphology, TGF-β Signaling, and Retrograde Transport

5.3.1 Summary of Findings

The neuroprotective functions of CHIP have a broad range of health implications, ranging from tumor suppression to the prevention of several neurodegenerative disorders. The cellular processes impacted by its activities are equally varied, and include lifespan regulation, mitophagy, transcriptional regulation, TGF-β signaling, and protein trafficking, among others. Nevertheless, little is known about the impacts of CHIP on Golgi complex morphology or retrograde trafficking, and the nuances of its role in lifespan determination has seldom been explored outside the context of insulin signaling. Here, I explored CHIP-dependent Golgi morphology using Golgi markers in both cell and worm models, and performed preliminary validation experiments on three differentially-expressed proteins (SMA-9, COG6, and Rab6) previously found in *chn-1*-null mutants (Chapter 3). Finally, I performed a proteomics assay on *h*CHIP and *Ce*CHIP rescue strains processed by either CHAPS/urea or SDS-based lysis to determine which proteins, gene ontology terms, and pathways were rescued along with lifespan. Firstly, deletion of *CHIP* and *sma-9* had a mildly additive effect on nematode longevity, suggesting the two proteins function in a primarily distinct but somewhat overlapping manner within the TBF-β signaling pathway. Secondly, abrogation of CHIP function was found to alter Golgi morphology in both cell and worm models, in addition to resulting in altered expression of two retrograde trafficking-associated proteins, Rab6 and COG6, suggesting the neuroprotective functions of CHIP may extend into the Golgi as well. Finally, proteomic assays of rescue strains showed a distinct subset of proteins, pathways, and gene ontology terms associated with the rescue of CHIP-related lifespan extension, many of which converged upon processes related to the epigenetic regulation of gene expression as well as mitochondrial and metabolic pathways.

5.3.2 Study Limitations and Considerations for Future Work

Taken together, these findings provide a strong foundation for further research into the mechanisms connecting CHIP function to Golgi integrity, TGF-β signaling, transcriptional regulation, and mitochondrial as well as metabolic pathways. Future experiments could aim to define the interaction, whether direct or indirect, between CHIP and SMA-9, for instance through the use of pull-down or proximity ligation assays. Future work could also aim to define both the mechanisms underlying the CHIP-dependent morphological changes seen here. While I suggested the increased Golgi complex fluorescence may have been due to an early stress response preceding the Golgi fragmentation often observed in neurodegenerative disorders, this was just one interpretation of the data. This hypothesis could be tested, for instance, by monitoring early changes in Golgi organization after the induction of a cellular stressor, such as exposure to hydrogen peroxide, in both wild-type and CHIP knock-out samples. Finally, validation experiments could be performed to further investigate the mechanistic underpinnings linking lifespan extension in both *h*CHIP and *Ce*CHIP rescue strains to mitochondrial, metabolic, and epigenetic processes. For example, experiments investigating protein-protein interactions can be performed in mitochondria specifically to explore the activities of CHIP in these organelles.

5.4 Final Conclusion

CHIP plays a crucial neuroprotective role healthy aging, with aberrations in its structure and function leading to considerable shifts in myriad cellular processes, including protein homeostasis, insulin signaling, and mitochondrial integrity. However, there is a great deal yet unknown about the intricacies of these CHIP-dependent processes and signaling cascades, as well as how they intersect to ultimately impact longevity. Here, the foundation for a suite of proteomic analyses was established through a methodological study examining the impact of detergent choice on protein solubility and extraction efficiency within *C. elegans* strains. Building upon this knowledge, the proteomic landscapes of two complete loss-of-function *chn-1* deletion mutants were compared to N2 wild-type controls using both CHAPS/urea- and SDS-processed samples to elucidate the impact of *chn-1* ablation on the global proteome. Finally,

validation experiments were performed on protein hits of interest in both *C. elegans* as well as CHIP knock-out and wild-type strains in the SH-SY5Y human neuroblastoma cell line. A final 'rescue' proteomics experiment in nematodes was carried out using the human and *C. elegans* orthologues of CHIP, in conjunction with a 'rescue' lifespan assay, to determine which proteins and pathways were altered along with CHIP-dependent changes in longevity.

Altogether, these findings highlight that (1) detergent and cellular properties interact to influence global protein solubilization, while (2) expanding upon proteins, pathways, and signaling cascades previously known to be impacted by CHIP, such as those related to mitochondrial integrity, insulin signaling, and the oxidative stress response, and (3) implicating Golgi integrity and trafficking-related processes in both healthy and pathophysiological aging in a CHIP-dependent manner. These findings were also supplemented by (4) 'rescue' proteomics analyses and longevity assays suggesting that CHIP-related lifespan mediation occurs in conjunction with a broad range of other cellular processes, as opposed to a few targeted proteins and/or pathways. The association of *chn-1* ablation with both Golgi-related proteins and pathways, as well as altered Golgi morphology, was particularly unexpected and calls for further study. While preliminary data implicate CHIP in protein trafficking under both stressed (i.e., by interacting with, ubiquitinating, and ultimately transiently sequestering Daxx into an insoluble cellular fraction, thereby countering its pro-apoptotic activity[279,298]) and non-stressed (i.e., by partitioning eNOS into an inactive and insoluble cellular component[280]) conditions, thus suggesting CHIP may play both a stress-dependent and more general role in protein trafficking. Perhaps the most striking finding was the CHIP-dependent alteration of Golgi morphology in both cell and nematode models, given that it did not necessarily mimic Golgi fragmentation, but perhaps another yet-unidentified process requiring further study.

Unraveling the intricacies of CHIP, as well as its impact on healthy and pathological aging, presents a promising opportunity for the development of therapeutic clinical interventions. These could involve, for instance, modulating CHIP activity or targeting specific components of CHIP-mediated pathways identified in this study.

Additional research is needed to further identify and tease apart CHIP-dependent processes, as well as how these processes go awry in neurodegenerative conditions.

Appendix A

Supplemental Results for Chapter 2

Analyses were performed using both *chn-1(by155)* and *chn-1(tm2692)* loss-of-function deletion mutants, each compared to N2 wild-type control animals, with the aim of accounting for between-strain variability when assessing lysis buffer-dependent proteomic changes. Analyses comparing lysis conditions of *chn-1(by155)* and *chn-1(tm2692)* loss-of-function mutants vs. N2 wild-type revealed 505 and 587 substantially-altered proteins, respectively. In *chn-1(by155)* mutants, analyses of underexpressed proteins revealed 153 substantially underexpressed proteins (i.e., fold change ≤ 0.67) uniquely altered in samples lysed with CHAPS/Urea (12.9% of all *chn-1(by155)* underexpressed proteins), while 202 substantially underexpressed proteins were uniquely altered in SDS-processed samples (17.1% of all *chn-1(by155)* underexpressed proteins). Analyses of overexpressed proteins (i.e., fold change ≥ 1.5) revealed 46 proteins uniquely altered in CHAPS/Urea-processed samples (12.2% of all *chn-1(by155)* overexpressed proteins) and 104 proteins uniquely altered in samples lysed with SDS (27.6% of all *chn-1(by155)* overexpressed proteins). In *chn-1(tm2692)* mutants, 259 underexpressed proteins were uniquely altered in samples lysed with CHAPS/Urea (20.1% of all *chn-1(tm2692)* underexpressed proteins), while 140 proteins were uniquely altered in SDS-processed samples (10.9% of all *chn-1(tm2692)* underexpressed proteins). Analyses of overexpressed proteins revealed 98 and 90 proteins uniquely altered in CHAPS/Urea- and SDS-processed samples, respectively (22.8% and 21.0% of all *chn-1(tm2692)* overexpressed proteins, respectively) (Supplemental Figure A1).

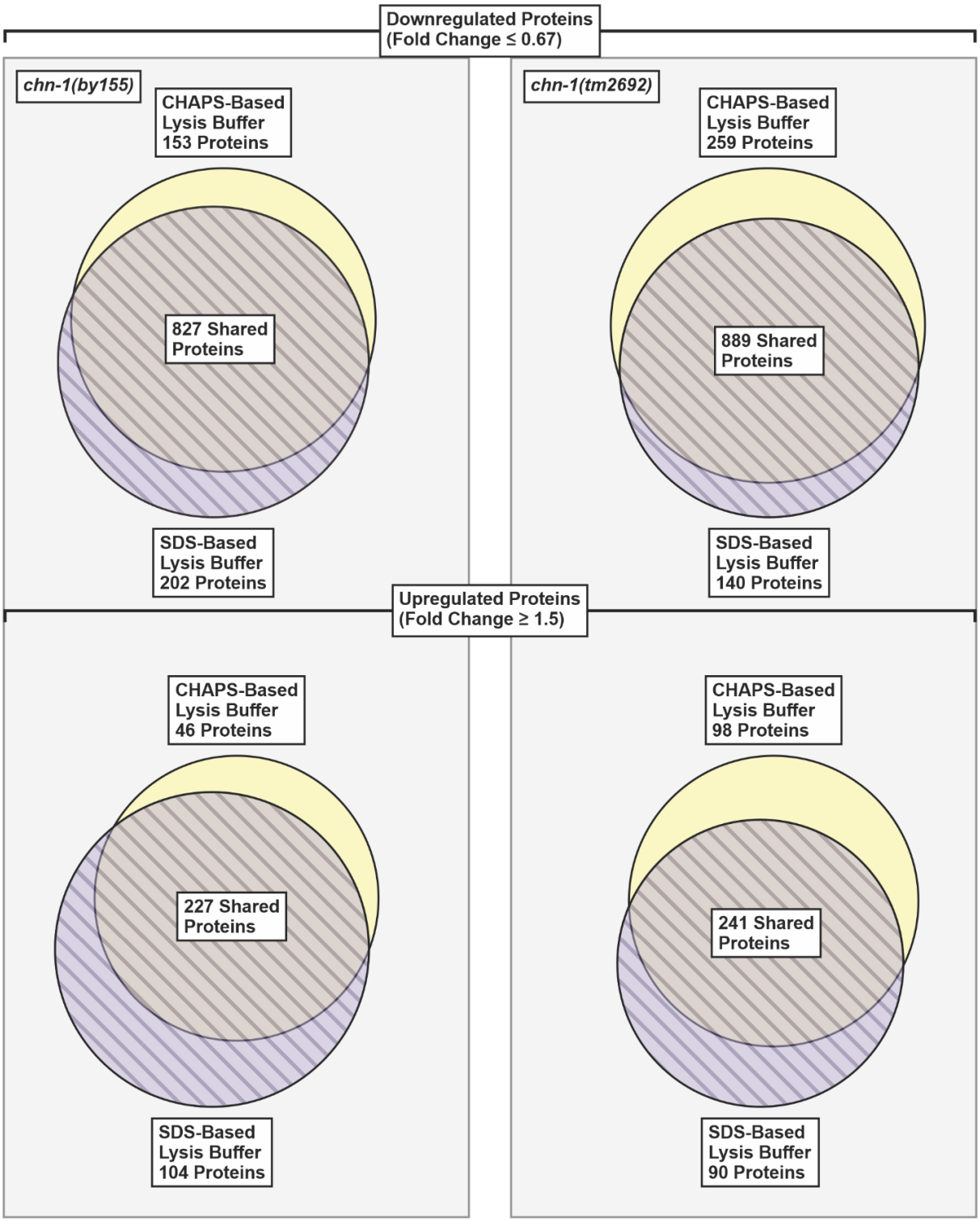

Supplemental Figure A1 **Venn diagrams showing the overlap of proteins identified by SWATH-MS across detergents**. Comparisons between CHAPS/Urea- and SDS-based lysis buffers for *chn-1(by155)* (left) and *chn-1(tm2692)* (right) *C. elegans chn-1* mutants. Proteins with fold changes of ≤ 0.67 (top) and ≥ 1.5 (bottom) compared to wild-type N2 controls are identified. The total protein count includes single peptide IDs.

Volcano plots indicate which protein hits contributed most to the detergent-dependent variation observed in the heat map in *chn-1(by155)* (Supplemental Figure A2 and Supplemental Tables A1-A2) and *chn-1(tm2692)* (Supplemental Figure A3 and Supplemental Tables A3-A4) *chn-1* deletion mutants, with Supplemental Tables A1 and A3 listing proteins that were most substantially overrepresented in CHAPS/Urea-compared to SDS-processed samples and Supplemental Tables A2 and A4 listing proteins that were most substantially underrepresented. Proteins most substantially overexpressed in *chn-1(by155) chn-1* deletion mutants included suppressor of aph-1, actin-1, and diSHevelled related, with fold changes of 23.83, 14.58, and 13.40, respectively (Supplemental Figure A2 and Supplemental Table A1). Proteins most substantially underexpressed in *chn-1(by155) chn-1* deletion mutants included peroxisome membrane protein related, putative peroxisome assembly protein 12, asparagine synthetase, and TUG-UBL1 domain-containing protein, with fold changes of 0.10, 0.13, 0.15, and 0.16, respectively (Supplemental Figure A2 and Supplemental Table A2). Proteins most substantially overexpressed in *chn-1(tm2692) chn-1* deletion mutants included suppressor of aph-1, CCHC-type domain containing protein, diSHevelled related, and actin-1, with fold changes of 39.43, 27.41, 14.89, and 11.03, respectively (Supplemental Figure A3 and Supplemental Table A3). Proteins most substantially underexpressed in *chn-1(tm2692) chn-1* deletion mutants included peroxisomal membrane protein related, probable acyl-coenzyme A oxidase acox-1.5, and inactive angiotensin-converting enzyme-related protein, with fold changes of 0.04, 0.05, and 0.05, respectively (Supplemental Figure A3 and Supplemental Table A4).

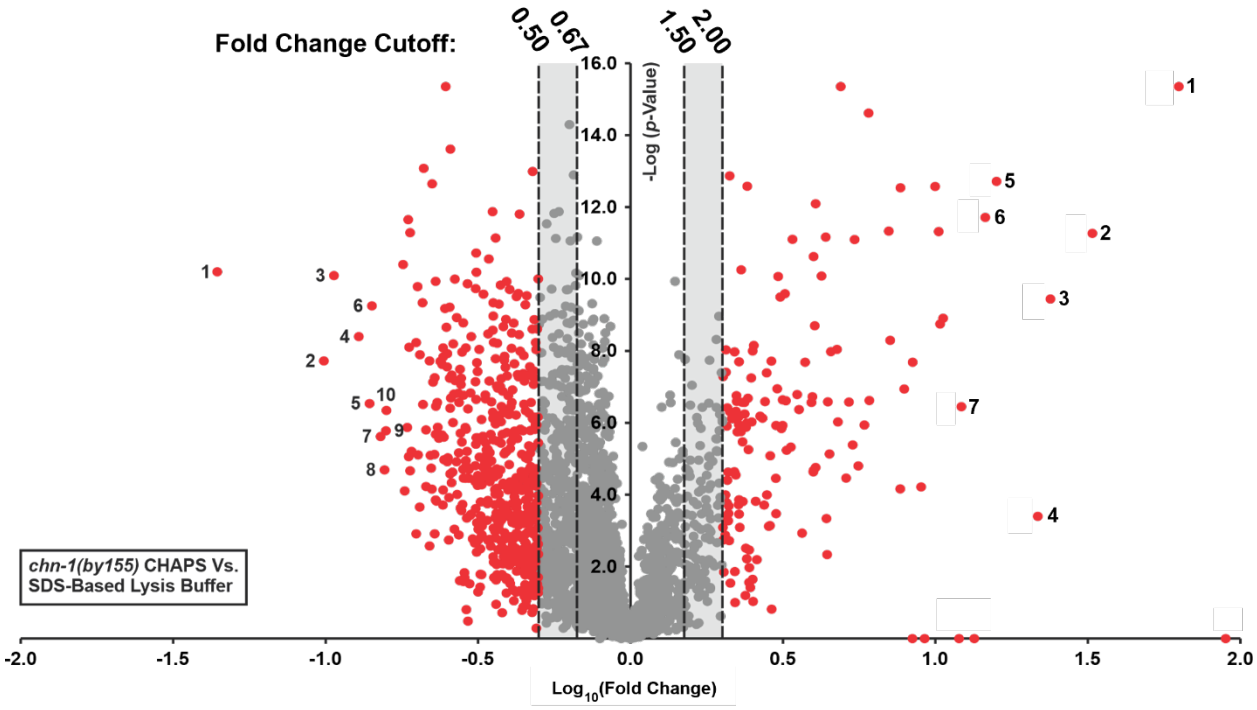

Supplemental Figure A2 **Comparative SWATH-MS proteomic analyses of *chn-1(by155) C. elegans* samples processed by lysis with CHAPS/Urea- vs. SDS-based lysis buffer.** Cut-off criteria (fold changes of ≤0.5 and ≥2 or ≤0.67 and ≥1.5) are represented by the dotted lines and shaded areas. Proteins (dots) that do not meet these fold change criteria are colour-coded in grey, while those that do are red. Over-represented proteins in the CHAPS/Urea-processed samples compared to SDS-processed samples have a positive log (fold change), while under-represented proteins have negative values. The top most over- and under-represented proteins that were significantly changed ($p < 0.05$, excluding $p=0$) are numbered and labeled in Supplemental Table A1 (upregulated proteins) and 2.4 (downregulated proteins).

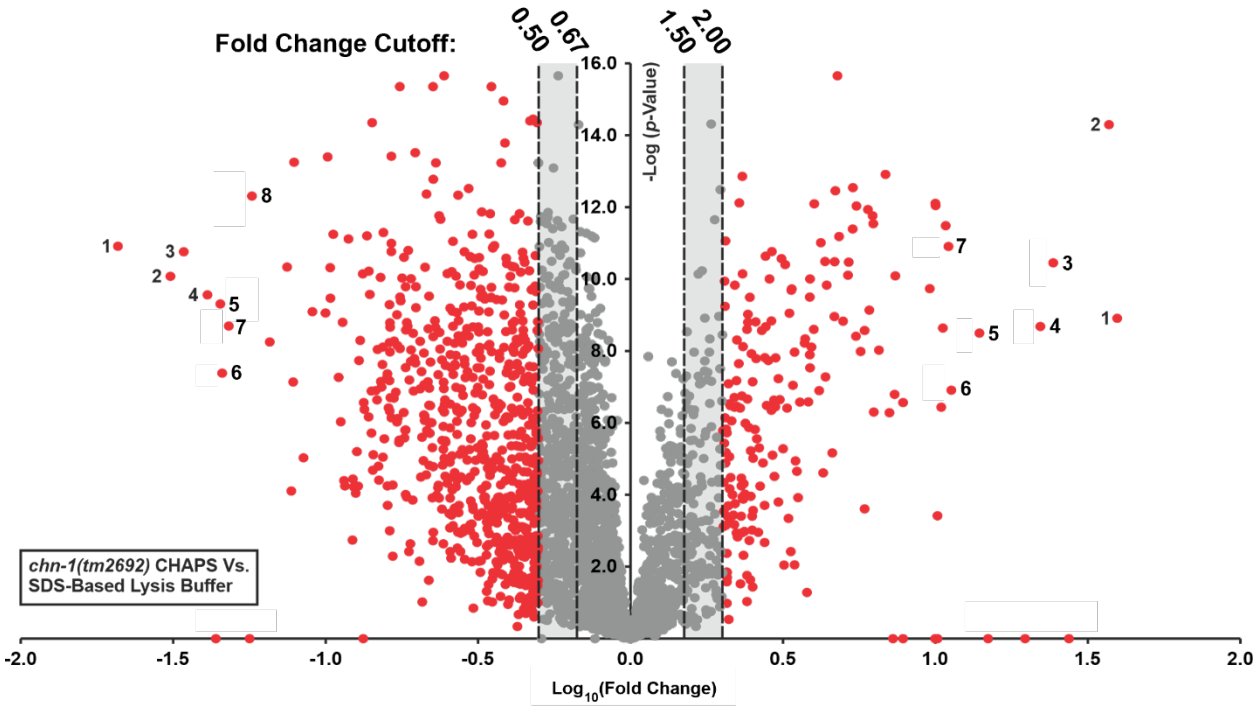

Supplemental Figure A3 **Comparative SWATH-MS proteomic analyses of *chn-1(tm2692) C. elegans* samples processed by lysis with CHAPS/Urea- vs. SDS-based lysis buffer.** Cut-off criteria (fold changes of ≤0.5 and ≥2 or ≤0.67 and ≥1.5) are represented by the dotted lines and shaded areas. Proteins (dots) that do not meet these fold change criteria are colour-coded in grey, while those that do are red. Over-represented proteins in the CHAPS/Urea-processed samples compared to SDS-processed samples have a positive log (fold change), while under-represented proteins have negative values. The top most over- and under-represented proteins that were significantly changed ($p < 0.05$, excluding $p=0$) are numbered and labeled in Supplemental Table A3 (upregulated proteins) and Supplemental Table A4 (downregulated proteins).

Supplemental Table A1 **Top proteins (based on fold change) identified by SWATH-MS that are over-represented in *chn-1(by155) C. elegans* samples processed by lysis with CHAPS/Urea- vs. SDS-based lysis buffer.**

Protein	Gene	*p*-Value	Fold Change	-Log (*p*-Value)	Log (Fold Change)	Label
Ubiquitin-like protein 1-40S ribosomal protein S27a [Cleaved into: Ubiquitin-like protein 1; 40S ribosomal protein S27a]	*ubl-1*	4.44E-16	62.793	15.353	1.798	1
Col_cuticle_N domain-containing protein	*col-143*	5.35E-12	32.727	11.271	1.515	2
Suppressor of aph-1	*sao-1*	3.62E-10	23.834	9.441	1.377	3
Uncharacterized protein	*D1069.3*	4.01E-04	21.661	3.397	1.336	4
Uncharacterized protein	*Y75B8A.13*	1.94E-13	15.870	12.712	1.201	5
Actin-1	*act-1*	1.94E-12	14.580	11.713	1.164	6
Aldo_ket_red domain-containing protein	*rps-29*	3.58E-07	12.167	6.446	1.085	7

Supplemental Table A2 **Top proteins (based on fold change) identified by SWATH-MS that are under-represented in *chn-1(by155) C. elegans* samples processed by lysis with CHAPS/Urea- vs. SDS-based lysis buffer.**

Protein	Gene	*p*-Value	Fold Change	-Log (*p*-Value)	Log (Fold Change)	Label
Putative pterin-4-alpha-carbinolamine dehydratase (PHS) (EC 4.2.1.96) (4-alpha-hydroxy-tetrahydropterin dehydratase) (Pterin carbinolamine dehydratase) (PCD)	*pcbd-1*	6.34E-11	0.044	10.198	-1.356	1
Peroxisomal Membrane Protein related	*pmp-2*	1.89E-08	0.099	7.724	-1.006	2
Probable acyl-coenzyme A oxidase acox-1.5 (AOX 1.5) (Acyl-CoA oxidase 1.5) (EC 1.3.3.-)	*acox-1.5*	8.01E-11	0.106	10.096	-0.973	3
Putative peroxisome assembly protein 12 (Peroxin-12)	*prx-12*	3.98E-09	0.128	8.400	-0.891	4
Ground-like domain-containing protein	*grl-5*	2.92E-07	0.139	6.534	-0.856	5
Acyl-coenzyme A oxidase acox-1.2 (EC 1.3.3.-)	*acox-1.2*	5.62E-10	0.142	9.251	-0.848	6
Asparagine synthetase [glutamine-hydrolyzing] (Glutamine-dependent asparagine synthetase)	*asns-2*	2.41E-06	0.151	5.617	-0.820	7
PIPK domain-containing protein	*ppk-1*	2.03E-05	0.156	4.693	-0.807	8
TUG-UBL1 domain-containing protein	*asps-1*	1.66E-06	0.158	5.780	-0.803	9
Col_cuticle_N domain-containing protein	*col-97*	4.54E-07	0.158	6.343	-0.801	10

Supplemental Table A3 **Top proteins (based on fold change) identified by SWATH-MS that are over-represented in *chn-1(tm2692) C. elegans* samples processed by lysis with CHAPS/Urea- vs. SDS-based lysis buffer.**

Protein	Gene	*p*-Value	Fold Change	-Log (*p*-Value)	Log (Fold Change)	Label
Suppressor of aph-1	*sao-1*	1.23E-09	39.425	8.909	1.596	1
Ubiquitin-like protein 1-40S ribosomal protein S27a [Cleaved into: Ubiquitin-like protein 1; 40S ribosomal protein S27a]	*ubl-1*	5.11E-15	37.060	14.292	1.569	2
Uncharacterized protein	*Y37D8A.19*	3.55E-11	24.355	10.450	1.387	3
Col_cuticle_N domain-containing protein	*col-143*	2.08E-09	22.095	8.683	1.344	4
SHNi-TPR domain-containing protein	*nasp-2*	3.21E-09	13.931	8.494	1.144	5
Aldo_ket_red domain-containing protein	*Y39G8B.1*	1.23E-07	11.271	6.912	1.052	6
Actin-1	*act-1*	1.24E-11	11.026	10.907	1.042	7

Supplemental Table A4 **Top proteins (based on fold change) identified by SWATH-MS that are under-represented in *chn-1(tm2692) C. elegans* samples processed by lysis with CHAPS/Urea- vs. SDS-based lysis buffer.**

Protein	Gene	*p*-Value	Fold Change	-Log (*p*-Value)	Log (Fold Change)	Label
Col_cuticle_N domain-containing protein	*col-97*	1.23E-11	0.021	10.912	-1.681	1
Col_cuticle_N domain-containing protein	*bli-6*	8.39E-11	0.031	10.076	-1.509	2
Putative pterin-4-alpha-carbinolamine dehydratase (PHS) (EC 4.2.1.96) (4-alpha-hydroxy-tetrahydropterin dehydratase) (Pterin carbinolamine dehydratase) (PCD)	*pcbd-1*	1.74E-11	0.034	10.759	-1.466	3
Peroxisomal Membrane Protein related	*pmp-2*	2.74E-10	0.041	9.563	-1.388	4
Probable acyl-coenzyme A oxidase acox-1.5 (AOX 1.5) (Acyl-CoA oxidase 1.5) (EC 1.3.3.-)	*acox-1.5*	4.92E-10	0.045	9.308	-1.345	5
Inactive angiotensin-converting enzyme-related protein (ACE-like non-metallopeptidase protein 1)	*acn-1*	4.17E-08	0.046	7.380	-1.340	6
Col_cuticle_N domain-containing protein	*col-175*	2.03E-09	0.048	8.692	-1.318	7
Uncharacterized protein	*H23N18.5*	4.89E-13	0.057	12.311	-1.242	8

In *chn-1(by155)* deletion mutants, CHAPS/Urea- compared to SDS-processing resulted in the underexpression of a wide range of biological processes, including rRNA processing (FDR-adjusted $p < 0.001$), lipid metabolic process (FDR-adjusted $p < 0.001$), and biosynthetic process (FDR-adjusted $p < 0.001$) (Supplemental Figure A4 and Supplemental Table A5). Similar to N2 wild-type samples, biological processes related to protein transport were overrepresented amongst significantly underexpressed GO terms in *chn-1(by155)* mutants, including protein transport (FDR-adjusted $p < 0.01$) and intracellular protein transport (FDR-adjusted $p < 0.01$) (Supplemental Figure A4 and Supplemental Table A5). Significantly underexpressed cellular component GO terms included peroxisome (FDR-adjusted $p < 0.001$) and peroxisomal membrane (FDR-adjusted $p < 0.05$), as well as a number of enriched terms associated with protein trafficking and membrane-related processes including endoplasmic reticulum (FDR-adjusted $p < 0.001$) and endoplasmic reticulum membrane (FDR-adjusted $p < 0.001$), membrane raft (FDR-adjusted $p < 0.001$), mitochondrial inner (FDR-adjusted $p < 0.01$) and outer membrane (FDR-adjusted $p < 0.05$), endomembrane system (FDR-adjusted $p < 0.05$), and endoplasmic reticulum-Golgi intermediate compartment (FDR-adjusted $p < 0.05$) (Supplemental Figure A4 and Supplemental Table A5). Cellular component GO terms related to intermembrane spaces were also enriched but made up a substantially smaller proportion of significantly underexpressed than overexpressed terms in *chn-1(by155)* mutants, with 2 of 25 enriched underexpressed terms pertaining to intermembrane spaces compared to 3 of 9 enriched overexpressed terms (Supplemental Figure A3 and Figure 2.11 as well as Supplemental Tables A5-A6). Top underexpressed molecular function GO terms included hydrolase activity (FDR-adjusted $p < 0.001$), oxidoreductase activity (FDR-adjusted $p < 0.001$), and RNA binding (FDR-adjusted $p < 0.001$) (Supplemental Figure A4 and Supplemental Table A5).

Overexpressed terms enriched in *chn-1(by155)* mutants lysed by CHAPS/Urea compared to SDS included biological processes such as anatomical structure development (FDR-adjusted $p < 0.001$) and translation (FDR-adjusted $p < 0.05$) (Supplemental Figure A5 and Supplemental Table A6). Significantly enriched overexpressed cellular component terms included ribonucleoprotein complex (FDR-adjusted $p < 0.001$) and ribosome (FDR-adjusted $p < 0.001$). Enriched terms related to

intermembrane spaces were also represented, including cytoplasm (FDR-adjusted $p < 0.001$), extracellular region (FDR-adjusted $p < 0.001$), and cytosol (FDR-adjusted $p < 0.001$) (Supplemental Figure A5 and Supplemental Table A6). Enriched overexpressed molecular function GO terms included nutrient reservoir activity (FDR-adjusted $p < 0.001$), lipid transporter activity (FDR-adjusted $p < 0.001$), and structural constituent of ribosome (FDR-adjusted $p < 0.01$) (Supplemental Figure A5 and Supplemental Table A6).

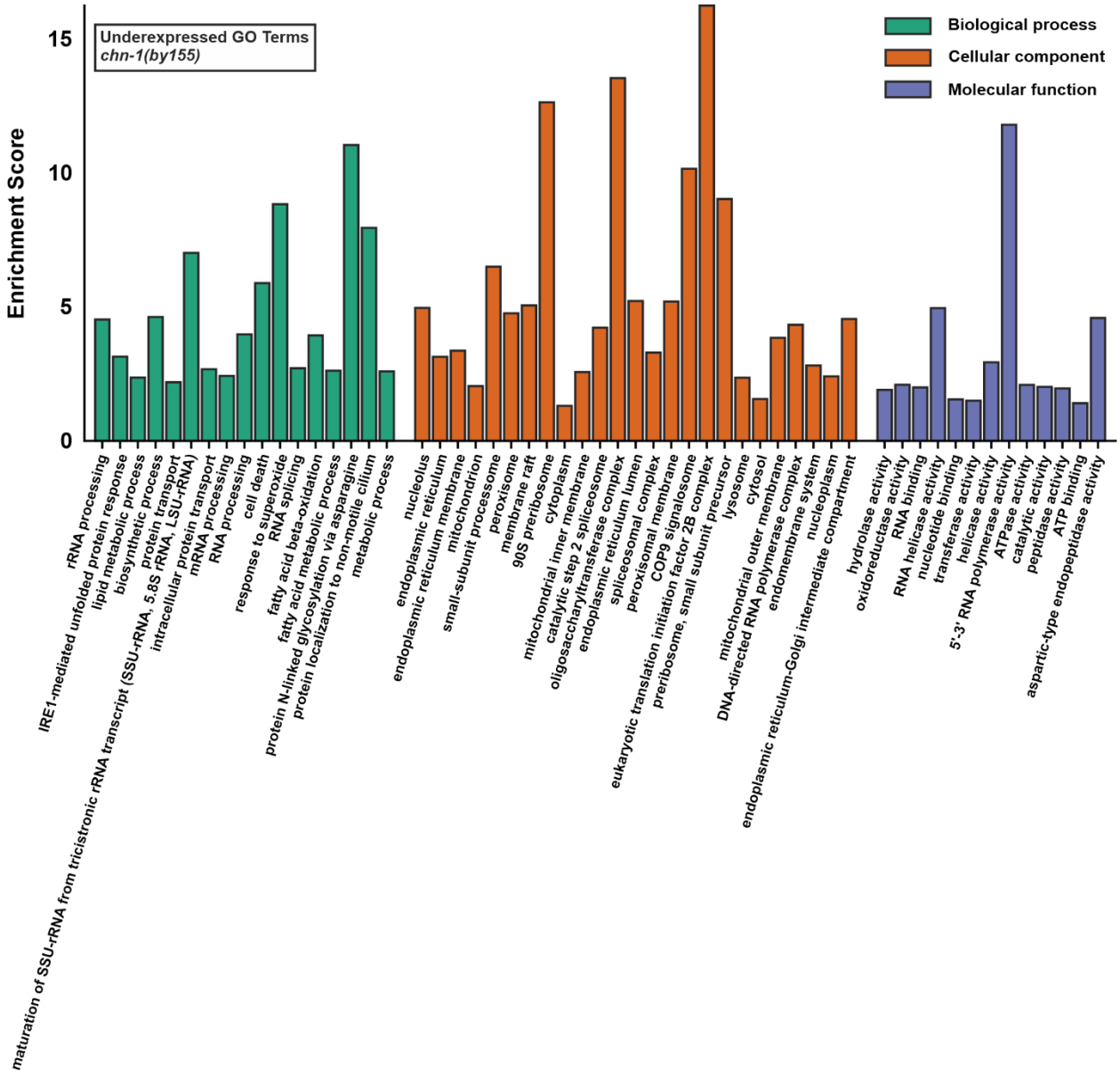

Supplemental Figure A4 **GO enrichment analysis of the *C. elegans chn-1(by155)* proteome of underexpressed proteins identified by SWATH-MS across lysis buffers.** The proteomic changes between *chn-1(by155) C. elegans* mutants processed by either CHAPS/Urea- or SDS-based lysis buffer were analyzed by DAVID. Significant GO terms (FDR-adjusted $p < 0.05$) were plotted by SRPlot. GO terms shown are related to biological processes, cellular components, and molecular functions, and each term is plotted based on fold enrichment. Only proteins that met the cut-off criteria (fold changes of ≤0.67) were used for the analysis. GO terms related to extraction buffer-dependent underexpressed proteins are listed in Supplemental Table A5. Cross-strain comparisons indicating GO terms overrepresented in more than one strain are noted in Supplemental Table A5 and illustrated in Figure 2.13.

Supplemental Table A5 ***chn-1(by155)* GO terms related to underexpressed proteins identified by SWATH-MS across lysis buffers.** Related to Supplemental Figure A4. Biological process (BP), molecular function (MF) and cellular component (CC) GO terms identified (using DAVID) in *chn-1(by155) C. elegans* mutants when processed by CHAPS/urea-based lysis buffer compared to SDS-based lysis buffer. The number of associated genes ("count") and an association index (probability (raw and FDR-adjusted *p*-values) as well as enrichment score) for each GO term is included. Cross-strain comparisons were further performed using GO terms with FDR-adjusted $p < 0.05$ (Figure 2.13). † Indicates GO terms shared by two strains. ‡ Indicates GO terms shared by N2 wild-type, *chn-1(by155)*, and *chn-1(tm2692)* deletion mutants.

	GO Term	Count	Enrichment	*p*-Value	FDR-Adjusted *p*-Value
BP	rRNA processing‡	27	4.529	4.67E-11	5.69E-08
BP	IRE1-mediated unfolded protein response‡	28	3.145	1.32E-07	8.02E-05
BP	lipid metabolic process‡	43	2.365	2.17E-07	8.83E-05
BP	biosynthetic process‡	15	4.623	1.68E-06	5.13E-04
BP	protein transport‡	38	2.190	8.04E-06	1.96E-03
BP	maturation of SSU-rRNA from tricistronic rRNA transcript (SSU-rRNA, 5.8S rRNA, LSU-rRNA)‡	9	7.016	1.32E-05	2.68E-03
BP	intracellular protein transport‡	23	2.674	3.45E-05	6.01E-03
BP	mRNA processing†	24	2.428	1.08E-04	1.64E-02
BP	RNA processing‡	12	3.976	1.26E-04	1.71E-02
BP	cell death	8	5.890	2.04E-04	2.49E-02
BP	response to superoxide‡	6	8.835	2.34E-04	2.59E-02
BP	RNA splicing†	18	2.711	2.59E-04	2.63E-02
BP	fatty acid beta-oxidation	11	3.940	2.98E-04	2.79E-02
BP	fatty acid metabolic process‡	18	2.621	3.92E-04	3.21E-02
BP	protein N-linked glycosylation via asparagine†	5	11.044	4.24E-04	3.21E-02
BP	protein localization to non-motile cilium	6	7.951	4.39E-04	3.21E-02
BP	metabolic process‡	18	2.593	4.48E-04	3.21E-02
CC	nucleolus‡	55	4.965	1.33E-23	4.58E-21
CC	endoplasmic reticulum‡	79	3.138	6.02E-20	1.04E-17
CC	endoplasmic reticulum membrane‡	52	3.366	1.87E-14	2.15E-12
CC	mitochondrion‡	83	2.046	4.63E-10	3.20E-08
CC	small-subunit processome‡	18	6.499	4.64E-10	3.20E-08
CC	peroxisome‡	17	4.762	2.49E-07	1.43E-05
CC	membrane raft‡	14	5.055	1.88E-06	9.26E-05
CC	90S preribosome‡	7	12.638	3.79E-06	1.63E-04

CC	cytoplasm‡	196	1.308	2.14E-05	8.22E-04
CC	mitochondrial inner membrane‡	25	2.571	3.42E-05	1.16E-03
CC	catalytic step 2 spliceosome‡	13	4.225	3.71E-05	1.16E-03
CC	oligosaccharyltransferase complex‡	5	13.540	1.92E-04	5.38E-03
CC	endoplasmic reticulum lumen‡	9	5.223	2.03E-04	5.38E-03
CC	spliceosomal complex†	14	3.297	2.53E-04	6.23E-03
CC	peroxisomal membrane	8	5.199	5.83E-04	1.34E-02
CC	COP9 signalosome‡	5	10.155	8.12E-04	1.75E-02
CC	eukaryotic translation initiation factor 2B complex	4	16.248	8.83E-04	1.79E-02
CC	preribosome, small subunit precursor‡	5	9.027	1.39E-03	2.67E-02
CC	Lysosome	18	2.359	1.50E-03	2.73E-02
CC	cytosol‡	51	1.564	1.60E-03	2.75E-02
CC	mitochondrial outer membrane†	9	3.848	1.85E-03	2.92E-02
CC	DNA-directed RNA polymerase complex‡	8	4.333	1.89E-03	2.92E-02
CC	endomembrane system‡	13	2.816	1.94E-03	2.92E-02
CC	nucleoplasm	16	2.407	2.44E-03	3.51E-02
CC	endoplasmic reticulum-Golgi intermediate compartment‡	7	4.550	3.42E-03	4.71E-02
MF	hydrolase activity‡	125	1.908	4.95E-13	3.35E-10
MF	oxidoreductase activity‡	69	2.097	4.60E-09	1.56E-06
MF	RNA binding‡	69	1.996	3.52E-08	6.07E-06
MF	RNA helicase activity‡	18	4.956	3.58E-08	6.07E-06
MF	nucleotide binding‡	114	1.546	1.37E-06	1.86E-04
MF	transferase activity‡	113	1.502	6.27E-06	7.08E-04
MF	helicase activity‡	23	2.932	7.74E-06	7.50E-04
MF	5'-3' RNA polymerase activity‡	6	11.800	3.68E-05	3.03E-03
MF	ATPase activity	36	2.091	4.03E-05	3.03E-03
MF	catalytic activity‡	36	2.015	8.77E-05	5.95E-03
MF	peptidase activity‡	36	1.959	1.55E-04	9.54E-03
MF	ATP binding	101	1.406	2.90E-04	1.64E-02
MF	aspartic-type endopeptidase activity	9	4.589	4.73E-04	2.47E-02

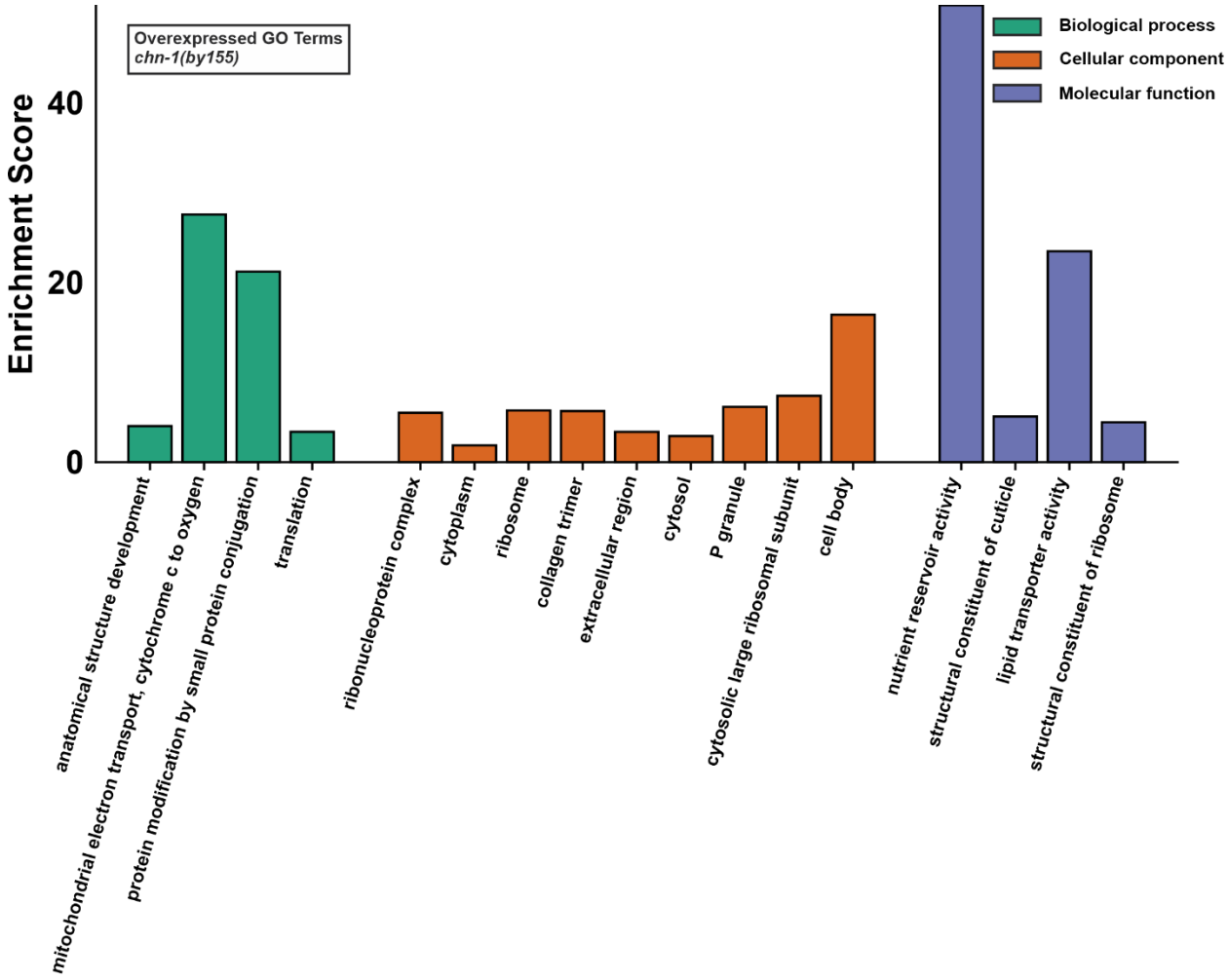

Supplemental Figure A5 **GO enrichment analysis of the *C. elegans chn-1(by155)* proteome of overexpressed proteins identified by SWATH-MS across lysis buffers.** The proteomic changes between *chn-1(by155) C. elegans* mutants processed by either CHAPS/Urea- or SDS-based lysis buffer were analyzed by DAVID. Significant GO terms (FDR-adjusted $p < 0.05$) were plotted by SRPlot. GO terms shown are related to biological processes, cellular components, and molecular functions, and each term is plotted based on fold enrichment. Only proteins that met the cut-off criteria (fold changes of ≥1.5) were used for the analysis. GO terms related to extraction buffer-dependent overexpressed proteins are listed in Supplemental Table A6. Cross-strain comparisons indicating GO terms overrepresented in more than one strain are noted in Supplemental Table A6 and illustrated in Figure 2.13.

Supplemental Table A6 ***chn-1(by155)* GO terms related to overexpressed proteins identified by SWATH-MS across lysis buffers.** Related to Supplemental Figure A5. Biological process (BP), molecular function (MF) and cellular component (CC) GO terms identified (using DAVID) in *chn-1(by155) C. elegans* mutants when processed by CHAPS/urea-based lysis buffer compared to SDS-based lysis buffer. The number of associated genes ("count") and an association index (probability (raw and FDR-adjusted *p*-values) as well as enrichment score) for each GO term is included. Cross-strain comparisons were further performed using GO terms with FDR-adjusted $p < 0.05$ (Figure 2.13). † Indicates GO terms shared by two strains. ‡ Indicates GO terms shared by N2 wild-type, *chn-1(by155)*, and *chn-1(tm2692)* deletion mutants.

	GO Term	Count	Enrichment	*p*-Value	FDR-Adjusted *p*-Value
BP	anatomical structure development‡	19	4.013	1.05E-06	4.09E-04
BP	mitochondrial electron transport, cytochrome c to oxygen	5	27.566	1.98E-05	3.84E-03
BP	protein modification by small protein conjugation†	5	21.205	6.45E-05	8.36E-03
BP	translation†	13	3.381	4.49E-04	4.37E-02
CC	ribonucleoprotein complex‡	20	5.497	3.67E-09	6.05E-07
CC	cytoplasm‡	74	1.871	1.90E-08	1.57E-06
CC	ribosome‡	17	5.751	3.99E-08	1.93E-06
CC	collagen trimer‡	17	5.688	4.67E-08	1.93E-06
CC	extracellular region‡	24	3.374	6.40E-07	2.11E-05
CC	cytosol‡	25	2.904	4.87E-06	1.34E-04
CC	P granule‡	9	6.157	1.01E-04	2.38E-03
CC	cytosolic large ribosomal subunit†	6	7.388	1.23E-03	2.54E-02
CC	cell body‡	4	16.418	1.64E-03	3.01E-02
MF	nutrient reservoir activity‡	6	50.860	1.61E-08	3.28E-06
MF	structural constituent of cuticle‡	17	5.086	1.98E-07	2.02E-05
MF	lipid transporter activity‡	6	23.474	3.08E-06	2.09E-04
MF	structural constituent of ribosome†	13	4.437	3.40E-05	1.74E-03

Analyses comparing CHAPS/Urea- and SDS-lysed *chn-1(tm2692)* mutant samples revealed enriched underexpressed biological processes including rRNA processing (FDR-adjusted $p < 0.001$) and nucleosome assembly (FDR-adjusted $p < 0.001$). Membrane and protein trafficking-associated biological processes were heavily represented and included IRE1-mediated unfolded protein response (FDR-adjusted $p < 0.001$), intracellular protein transport (FDR-adjusted $p < 0.001$), protein transport (FDR-adjusted $p < 0.001$), and endoplasmic reticulum unfolded protein response (FDR-adjusted $p < 0.05$) (Supplemental Figure A6 and Supplemental Table A7). Enriched underexpressed cellular components included peroxisome (FDR-adjusted $p < 0.001$), cytosol (FDR-associated $p < 0.001$), cytoplasm (FDR-associated $p < 0.001$), endoplasmic reticulum lumen (FDR-associated $p < 0.001$), and nucleus (FDR-adjusted $p < 0.05$), with peroxisome and cytoplasm-associated cellular components represented among enriched terms. However, a larger subset of enriched underexpressed cellular components were related to vesicle-associated and cross-membrane protein transport, including endoplasmic reticulum (FDR-adjusted $p < 0.001$) and endoplasmic reticulum membrane (FDR-adjusted $p < 0.001$), mitochondrial inner membrane (FDR-adjusted $p < 0.001$), membrane raft (FDR-adjusted $p < 0.001$), cytoplasmic vesicle (FDR-adjusted $p < 0.01$), endoplasmic reticulum-Golgi intermediate compartment (FDR-adjusted $p < 0.01$), endomembrane system (FDR-adjusted $p < 0.01$), Golgi apparatus (FDR-adjusted $p < 0.01$), nuclear envelope (FDR-adjusted $p < 0.05$), and nuclear pore (FDR-adjusted $p < 0.05$) (Supplemental Figure A6 and Supplemental Table A7). Significantly enriched underexpressed molecular functions included hydrolase activity (FDR-adjusted $p < 0.001$), RNA binding (FDR-adjusted $p < 0.001$), and RNA helicase activity (FDR-adjusted $p < 0.001$) (Supplemental Figure A6 and Supplemental Table A7).
Enriched overexpressed biological processes in *chn-1(tm2692)* deletion mutants included anatomical structure development (FDR-adjusted $p < 0.01$) and cell division (FDR-adjusted $p < 0.01$) (Supplemental Figure A7 and Supplemental Table A8). Enriched overexpressed cellular components included ribonucleoprotein complex (FDR-adjusted $p < 0.001$), cytoplasm (FDR-adjusted $p < 0.001$), ribosome (FDR-adjusted $p < 0.001$), extracellular region (FDR-adjusted $p < 0.001$), and cytosol (FDR-adjusted $p < 0.001$) (Supplemental Figure A7 and Supplemental Table A8). As in N2 wild-type

animals and *chn-1(by155)* mutants, GO terms related to intermembrane spaces made up a larger proportion of significantly enriched overexpressed terms than underexpressed terms, with 3 of 18 enriched overexpressed terms pertaining to intermembrane spaces compared to 3 of 27 enriched underexpressed terms (Figure 2.12 and Supplemental Figure A4 as well as Supplemental Tables A7-A8). Enriched overexpressed molecular function GO terms included structural constituent of ribosome (FDR-adjusted $p < 0.001$), nutrient reservoir activity (FDR-adjusted $p < 0.001$), and lipid transporter activity (FDR-adjusted $p < 0.001$) (Supplemental Figure A7 and Supplemental Table A8).

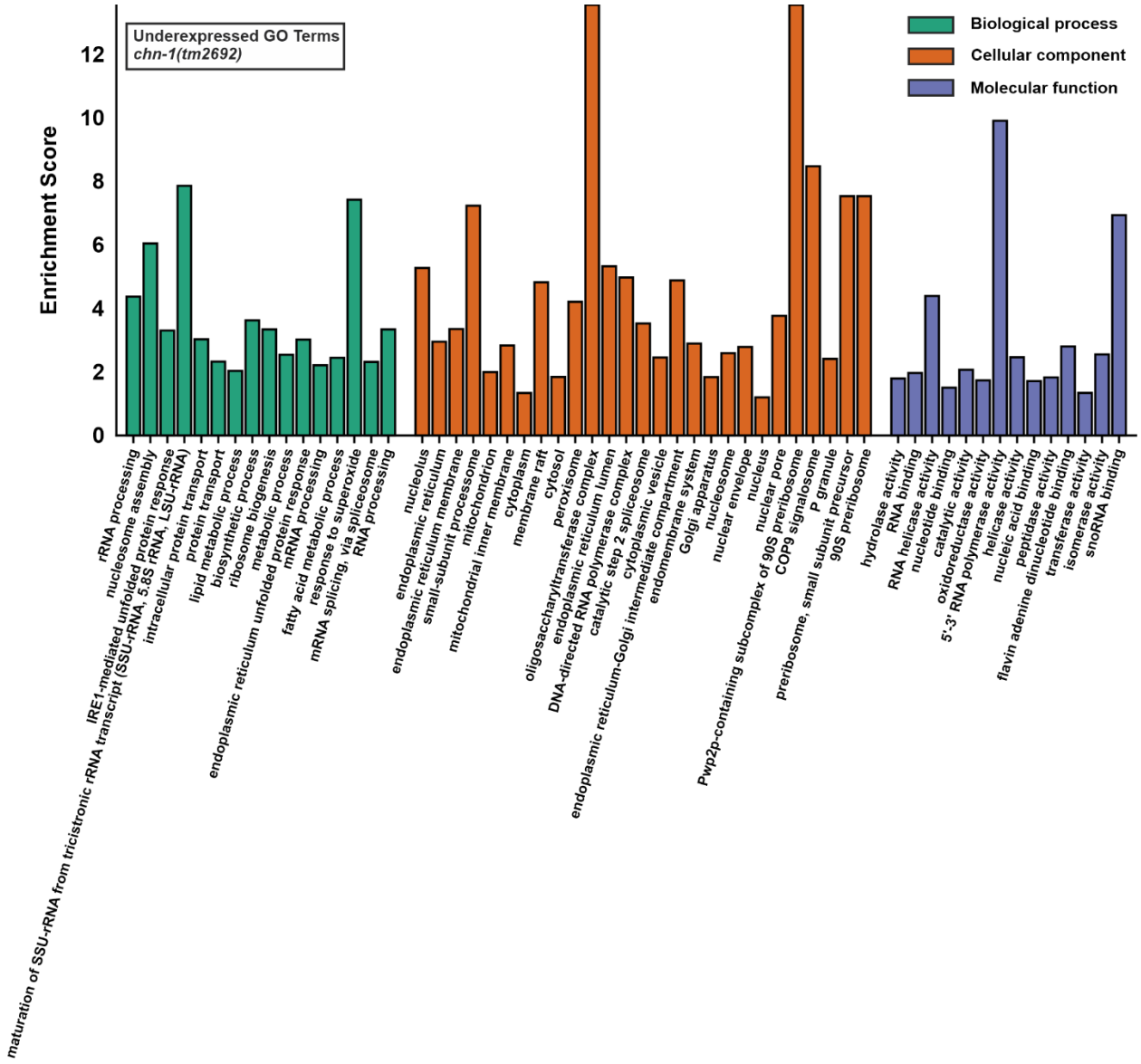

Supplemental Figure A6 **GO enrichment analysis of the *C. elegans* proteome of underexpressed proteins identified by SWATH-MS across lysis buffers.** The proteomic changes between *chn-1(tm2692) C. elegans* mutants processed by either CHAPS/Urea- or SDS-based lysis buffer were analyzed by DAVID. Significant GO terms (FDR-adjusted $p < 0.05$) were plotted by SRPlot. GO terms shown are related to biological processes, cellular components, and molecular functions, and each term is plotted based on fold enrichment. Only proteins that met the cut-off criteria (fold changes of ≤0.67) were used for the analysis. GO terms related to extraction buffer-dependent underexpressed proteins are listed in Supplemental Table A7. Cross-strain comparisons indicating GO terms overrepresented in more than one strain are noted in Supplemental Table A7 and illustrated in Figure 2.13.

Supplemental Table A7 ***chn-1(tm2692)* GO terms related to underexpressed proteins identified by SWATH-MS across lysis buffers.** Related to Supplemental Figure A6. Biological process (BP), molecular function (MF) and cellular component (CC) GO terms identified (using DAVID) in *chn-1(tm2692) C. elegans* mutants when processed by CHAPS/urea-based lysis buffer compared to SDS-based lysis buffer. The number of associated genes ("count") and an association index (probability (raw and FDR-adjusted *p*-values) as well as enrichment score) for each GO term is included. Cross-strain comparisons were further performed using GO terms with FDR-adjusted $p < 0.05$ (Figure 2.13). † Indicates GO terms shared by two strains. ‡ Indicates GO terms shared by N2 wild-type, *chn-1(by155)*, and *chn-1(tm2692)* deletion mutants.

	GO Term	Count	Enrichment	*p*-Value	FDR-Adjusted *p*-Value
BP	rRNA processing‡	31	4.370	1.83E-12	2.41E-09
BP	nucleosome assembly†	19	6.046	1.25E-10	8.22E-08
BP	IRE1-mediated unfolded protein response‡	35	3.303	4.13E-10	1.81E-07
BP	maturation of SSU-rRNA from tricistronic rRNA transcript (SSU-rRNA, 5.8S rRNA, LSU-rRNA)‡	12	7.862	2.13E-08	7.01E-06
BP	intracellular protein transport‡	31	3.029	4.42E-08	1.14E-05
BP	protein transport‡	48	2.324	5.20E-08	1.14E-05
BP	lipid metabolic process‡	44	2.033	8.39E-06	1.58E-03
BP	biosynthetic process‡	14	3.626	6.37E-05	1.05E-02
BP	ribosome biogenesis	15	3.341	8.56E-05	1.25E-02
BP	metabolic process‡	21	2.542	1.50E-04	1.92E-02
BP	endoplasmic reticulum unfolded protein response†	16	3.020	1.60E-04	1.92E-02
BP	mRNA processing†	26	2.210	2.18E-04	2.40E-02
BP	fatty acid metabolic process‡	20	2.448	3.76E-04	3.82E-02
BP	response to superoxide‡	6	7.425	5.32E-04	4.76E-02
BP	mRNA splicing, via spliceosome	21	2.316	5.53E-04	4.76E-02
BP	RNA processing‡	12	3.341	5.77E-04	4.76E-02
CC	nucleolus‡	70	5.275	1.48E-32	5.58E-30

CC	endoplasmic reticulum‡	89	2.952	8.77E-21	1.65E-18
CC	endoplasmic reticulum membrane‡	62	3.350	2.20E-17	2.76E-15
CC	small-subunit processome‡	24	7.234	5.86E-15	5.53E-13
CC	mitochondrion‡	97	1.996	4.51E-11	3.40E-09
CC	mitochondrial inner membrane‡	33	2.833	1.22E-07	7.65E-06
CC	cytoplasm‡	240	1.337	3.70E-07	1.81E-05
CC	membrane raft‡	16	4.823	3.84E-07	1.81E-05
CC	cytosol‡	72	1.843	5.12E-07	1.98E-05
CC	peroxisome‡	18	4.209	5.26E-07	1.98E-05
CC	oligosaccharyltransferase complex‡	6	13.564	1.21E-05	4.14E-04
CC	endoplasmic reticulum lumen‡	11	5.329	1.72E-05	5.41E-04
CC	DNA-directed RNA polymerase complex‡	11	4.973	3.45E-05	9.99E-04
CC	catalytic step 2 spliceosome‡	13	3.527	2.10E-04	5.66E-03
CC	cytoplasmic vesicle†	21	2.456	2.87E-04	6.90E-03
CC	endoplasmic reticulum-Golgi intermediate compartment‡	9	4.883	2.93E-04	6.90E-03
CC	endomembrane system‡	16	2.894	3.15E-04	6.99E-03
CC	Golgi apparatus†	37	1.838	4.55E-04	9.53E-03
CC	nucleosome†	17	2.591	7.06E-04	1.40E-02
CC	nuclear envelope†	15	2.787	7.70E-04	1.45E-02
CC	Nucleus	236	1.200	9.07E-04	1.61E-02
CC	nuclear pore	10	3.768	9.40E-04	1.61E-02
CC	Pwp2p-containing subcomplex of 90S preribosome	4	13.564	1.51E-03	2.47E-02
CC	COP9 signalosome‡	5	8.477	1.61E-03	2.53E-02
CC	P granule	16	2.411	2.25E-03	3.40E-02
CC	preribosome, small subunit precursor‡	5	7.535	2.73E-03	3.81E-02

CC	90S preribosome‡	5	7.535	2.73E-03	3.81E-02
MF	hydrolase activity‡	140	1.795	1.89E-12	1.34E-09
MF	RNA binding‡	81	1.967	3.08E-09	1.09E-06
MF	RNA helicase activity‡	19	4.393	7.61E-08	1.79E-05
MF	nucleotide binding‡	132	1.504	8.37E-07	1.48E-04
MF	catalytic activity‡	44	2.068	5.54E-06	7.83E-04
MF	oxidoreductase activity‡	68	1.736	7.17E-06	8.45E-04
MF	5'-3' RNA polymerase activity‡	6	9.910	8.62E-05	8.70E-03
MF	helicase activity‡	23	2.462	1.13E-04	1.00E-02
MF	nucleic acid binding	50	1.710	2.02E-04	1.59E-02
MF	peptidase activity‡	40	1.828	2.54E-04	1.80E-02
MF	flavin adenine dinucleotide binding	16	2.803	4.00E-04	2.57E-02
MF	transferase activity‡	120	1.339	5.25E-04	3.09E-02
MF	isomerase activity	17	2.553	7.50E-04	4.08E-02
MF	snoRNA binding†	6	6.937	8.29E-04	4.19E-02

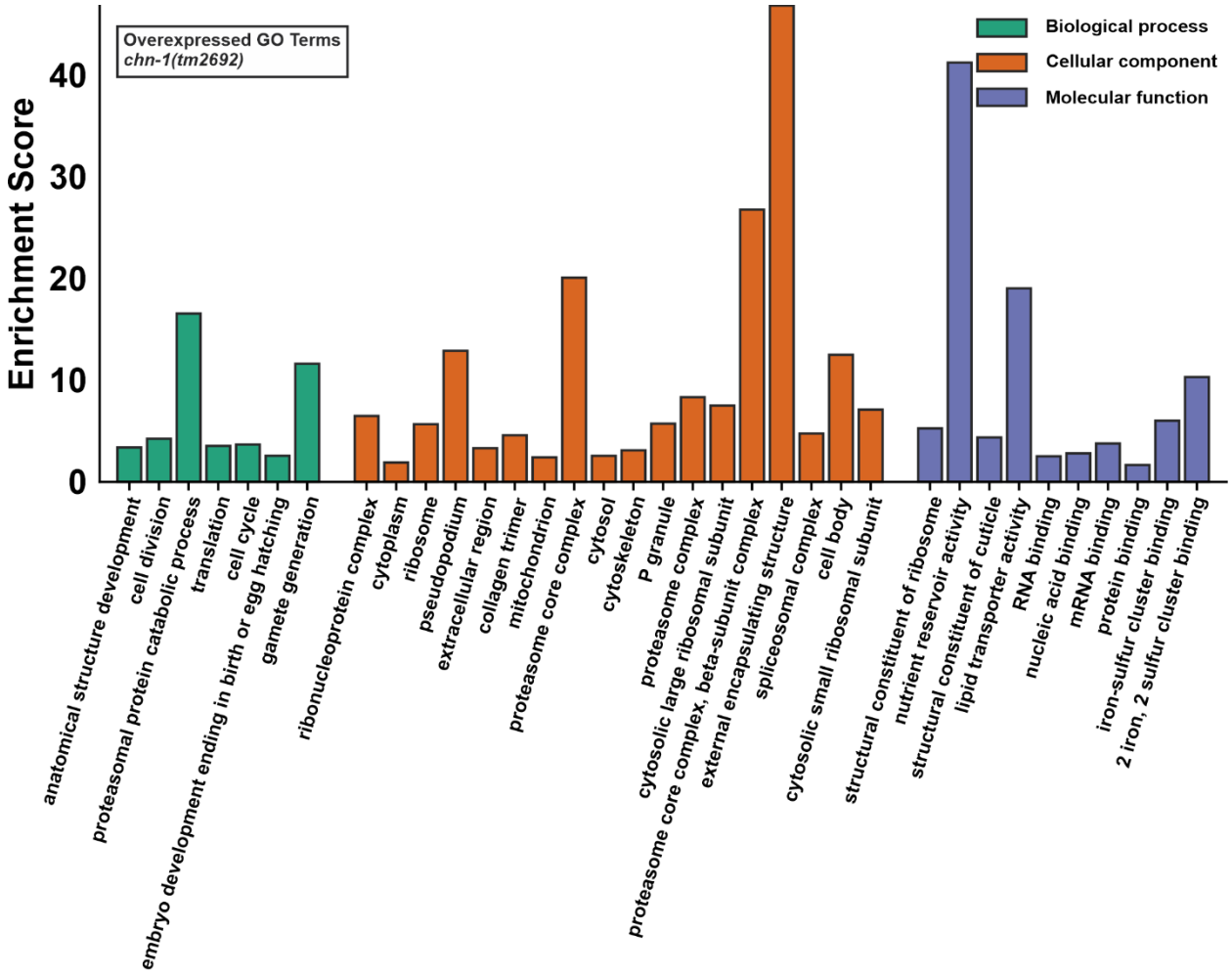

Supplemental Figure A7 **GO enrichment analysis of the *C. elegans* proteome of overexpressed proteins identified by SWATH-MS across lysis buffers.** The proteomic changes between *chn-1(tm2692) C. elegans* mutants processed by either CHAPS/Urea- or SDS-based lysis buffer were analyzed by DAVID. Significant GO terms (FDR-adjusted $p < 0.05$) were plotted by SRPlot. GO terms shown are related to biological processes, cellular components, and molecular functions, and each term is plotted based on fold enrichment. Only proteins that met the cut-off criteria (fold changes of ≥1.5) were used for the analysis. GO terms related to extraction buffer-dependent overexpressed proteins are listed in Supplemental Table A8. Cross-strain comparisons indicating GO terms overrepresented in more than one strain are noted in Supplemental Table A8 and illustrated in Figure 2.13.

Supplemental Table A8 ***chn-1(tm2692)* GO terms related to overexpressed proteins identified by SWATH-MS across lysis buffers.** Related to Supplemental Figure A7. Biological process (BP), molecular function (MF) and cellular component (CC) GO terms identified (using DAVID) in *chn-1(tm2692) C. elegans* mutants when processed by CHAPS/urea-based lysis buffer compared to SDS-based lysis buffer. The number of associated genes ("count") and an association index (probability (raw and FDR-adjusted *p*-values) as well as enrichment score) for each GO term is included. Cross-strain comparisons were further performed using GO terms with FDR-adjusted $p < 0.05$ (Figure 2.13). † Indicates GO terms shared by two strains. ‡ Indicates GO terms shared by N2 wild-type, *chn-1(by155)*, and *chn-1(tm2692)* deletion mutants.

	GO Term	Count	Enrichment	*p*-Value	FDR-Adjusted *p*-Value
BP	anatomical structure development‡	20	3.384	6.63E-06	2.46E-03
BP	cell division†	15	4.246	1.10E-05	2.46E-03
BP	proteasomal protein catabolic process	6	16.558	1.99E-05	2.52E-03
BP	translation†	17	3.541	2.32E-05	2.52E-03
BP	cell cycle†	16	3.680	2.81E-05	2.52E-03
BP	embryo development ending in birth or egg hatching†	18	2.572	6.18E-04	4.63E-02
BP	gamete generation	5	11.620	7.47E-04	4.79E-02
CC	ribonucleoprotein complex‡	31	6.486	5.95E-16	1.05E-13
CC	cytoplasm‡	99	1.905	1.87E-11	1.66E-09
CC	ribosome‡	22	5.665	2.76E-10	1.63E-08
CC	Pseudopodium	11	12.888	7.70E-09	3.41E-07
CC	extracellular region‡	31	3.317	1.50E-08	5.30E-07
CC	collagen trimer‡	18	4.585	3.87E-07	1.14E-05
CC	mitochondrion†	34	2.418	3.92E-06	9.92E-05
CC	proteasome core complex	6	20.085	7.16E-06	1.58E-04
CC	cytosol‡	29	2.564	8.43E-06	1.66E-04
CC	Cytoskeleton	21	3.105	1.44E-05	2.55E-04
CC	P granule‡	11	5.728	2.04E-05	3.28E-04
CC	proteasome complex	8	8.332	4.12E-05	6.08E-04
CC	cytosolic large ribosomal subunit†	8	7.499	8.29E-05	1.13E-03
CC	proteasome core complex, beta-subunit complex	4	26.780	3.12E-04	3.95E-03
CC	external encapsulating structure†	3	46.866	1.33E-03	1.57E-02
CC	spliceosomal complex	7	4.754	3.41E-03	3.72E-02
CC	cell body‡	4	12.498	3.58E-03	3.72E-02
CC	cytosolic small ribosomal subunit	5	7.101	5.03E-03	4.95E-02
MF	structural constituent of ribosome†	19	5.259	1.72E-08	4.03E-06

MF	nutrient reservoir activity‡	6	41.244	4.63E-08	5.42E-06
MF	structural constituent of cuticle‡	18	4.367	6.91E-07	5.39E-05
MF	lipid transporter activity‡	6	19.036	8.64E-06	5.06E-04
MF	RNA binding†	29	2.513	1.09E-05	5.09E-04
MF	nucleic acid binding†	23	2.807	2.20E-05	8.56E-04
MF	mRNA binding	14	3.774	8.18E-05	2.73E-03
MF	protein binding†	47	1.667	4.49E-04	1.31E-02
MF	iron-sulfur cluster binding	7	6.015	9.76E-04	2.54E-02
MF	2 iron, 2 sulfur cluster binding	5	10.311	1.18E-03	2.77E-02

In *chn-1(by155)* deletion mutants, CHAPS/Urea compared to SDS lysis resulted in the underexpression of KEGG pathways related to peroxisome ($p < 0.001$), metabolic pathways ($p < 0.001$), and longevity regulating pathway ($p = 0.050$) (Supplemental Figure A8 and Supplemental Table A9). Once again, pathways related to protein transport were highly enriched, including protein processing in endoplasmic reticulum ($p < 0.001$), ABC transporters ($p < 0.01$), lysosome ($p < 0.01$), and protein export ($p < 0.05$) (Supplemental Figure A8 and Supplemental Table A9). Nuclear cytoplasmic transport was also overexpressed in *chn-1(by155)* mutants, approaching significance at $p = 0.072$ (Supplemental Figure A8 and Supplemental Table A9). Enriched overexpressed pathways included ribosome ($p < 0.001$), oxidative phosphorylation ($p < 0.001$), ubiquitin mediated proteolysis ($p < 0.05$), metabolic pathways (approaching significance at $p = 0.079$), and phagosome (approaching significance at $p = 0.096$) (Supplemental Figure A8 and Supplemental Table A9). KEGG pathways underexpressed in CHAPS/Urea- compared to SDS-processed *chn-1(tm2692)* mutant animals included metabolic pathways ($p < 0.001$) and peroxisome ($p < 0.01$) as well as protein processing in endoplasmic reticulum ($p < 0.001$), endocytosis ($p < 0.001$), nucleocytoplasmic transport ($p < 0.01$), ABC transporters ($p < 0.05$), and lysosome (approaching significance at $p < 0.082$) (Supplemental Figure A9 and Supplemental Table A10). Overexpressed KEGG pathways included ribosome ($p < 0.001$), proteasome ($p < 0.01$), phagosome (approaching significance at $p < 0.059$), and metabolic pathways (approaching significance at $p < 0.092$) (Supplemental Figure A9 and Supplemental Table A10).

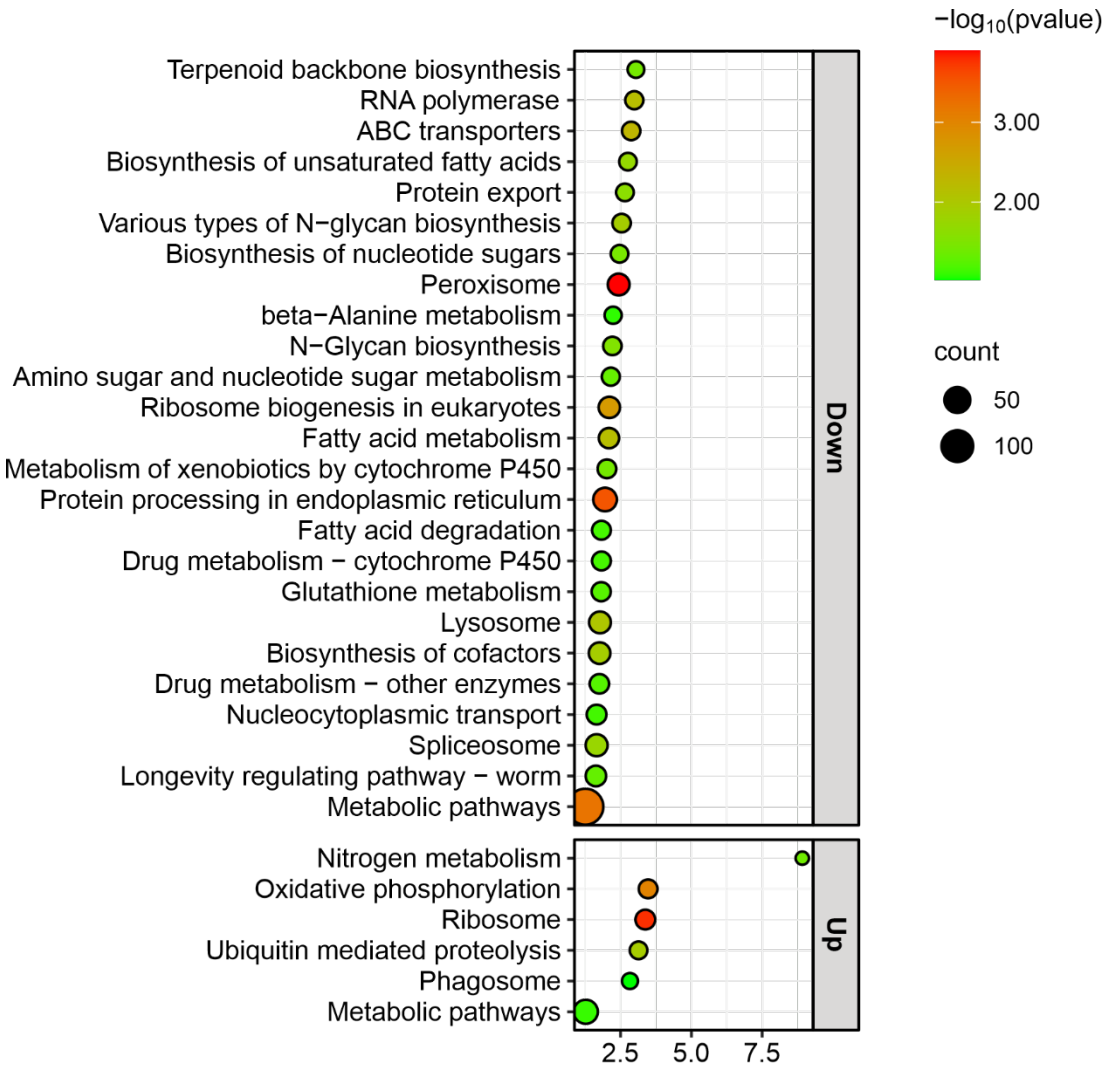

Supplemental Figure A8 **KEGG pathway analysis derived from the *chn-1(by155)* proteomics of our *C. elegans* model.** SWATH-MS data comparing samples processed with either CHAPS/Urea- or SDS-based lysis buffer was analysed using DAVID and plotted by SRPlot. Only proteins that met the cut-off criteria (fold changes of ≤0.67 and ≥1.5) were used for the analysis. Each pathway is colour-coded based on statistical significance (–log10(*p*-value)). Pathways related to *chn-1* loss-of-function are listed in Supplemental Table A9. Cross-strain comparisons indicating pathways overrepresented in more than one strain are noted in Supplemental Table A9 and illustrated in Figure 2.15.

Supplemental Table A9 **KEGG pathways related to substantially altered proteins identified by SWATH-MS across lysis buffers in *chn-1(by155) C. elegans* mutants.** Related to Supplemental Figure A7 & Figure 2.14. Pathways identified in *chn-1(by155)* animals when processed by CHAPS/urea-based lysis buffer compared to SDS-based lysis buffer. The number of associated genes ("count") and an association index (probability (raw *p*-values) as well as enrichment score) for each pathway is included. Cross-strain comparisons were further performed. † Indicates pathways shared by two strains. ‡ Indicates pathways shared by N2 wild-type, *chn-1(by155)*, and *chn-1(tm2692)* deletion mutants.

Pathway	Count	Enrichment	*p*-Value	Regulation
Peroxisome‡	22	2.432	1.26E-04	Down
Protein processing in endoplasmic reticulum‡	31	1.951	3.03E-04	Down
Metabolic pathways‡	139	1.255	6.24E-04	Down
Ribosome biogenesis in eukaryotes‡	20	2.103	1.96E-03	Down
ABC transporters‡	10	2.874	5.22E-03	Down
Fatty acid metabolism‡	16	2.090	6.91E-03	Down
RNA polymerase‡	9	2.984	7.06E-03	Down
Lysosome†	22	1.773	9.37E-03	Down
Biosynthesis of cofactors‡	21	1.758	1.25E-02	Down
Various types of N-glycan biosynthesis‡	10	2.536	1.26E-02	Down
Spliceosome‡	23	1.652	1.74E-02	Down
Biosynthesis of unsaturated fatty acids‡	8	2.759	1.97E-02	Down
Protein export†	8	2.653	2.44E-02	Down
N-Glycan biosynthesis‡	10	2.210	3.03E-02	Down
Biosynthesis of nucleotide sugars‡	8	2.463	3.59E-02	Down
Terpenoid backbone biosynthesis	6	3.043	3.84E-02	Down
Metabolism of xenobiotics by cytochrome P450‡	11	2.018	3.88E-02	Down
Amino sugar and nucleotide sugar metabolism†	9	2.155	4.90E-02	Down
Longevity regulating pathway - worm†	17	1.628	5.03E-02	Down
Glutathione metabolism‡	12	1.815	5.84E-02	Down
Drug metabolism - other enzymes‡	13	1.751	5.96E-02	Down
Fatty acid degradation	11	1.824	7.06E-02	Down
Drug metabolism - cytochrome P450‡	11	1.824	7.06E-02	Down
Nucleocytoplasmic transport†	14	1.653	7.24E-02	Down
beta-Alanine metabolism	7	2.235	8.32E-02	Down
Ribosome‡	14	3.373	1.67E-04	Up
Oxidative phosphorylation‡	11	3.471	9.52E-04	Up
Ubiquitin mediated proteolysis†	8	3.135	1.21E-02	Up
Nitrogen metabolism	3	8.915	4.19E-02	Up
Metabolic pathways‡	34	1.270	7.92E-02	Up

Phagosome‡	5	2.830	9.55E-02	Up

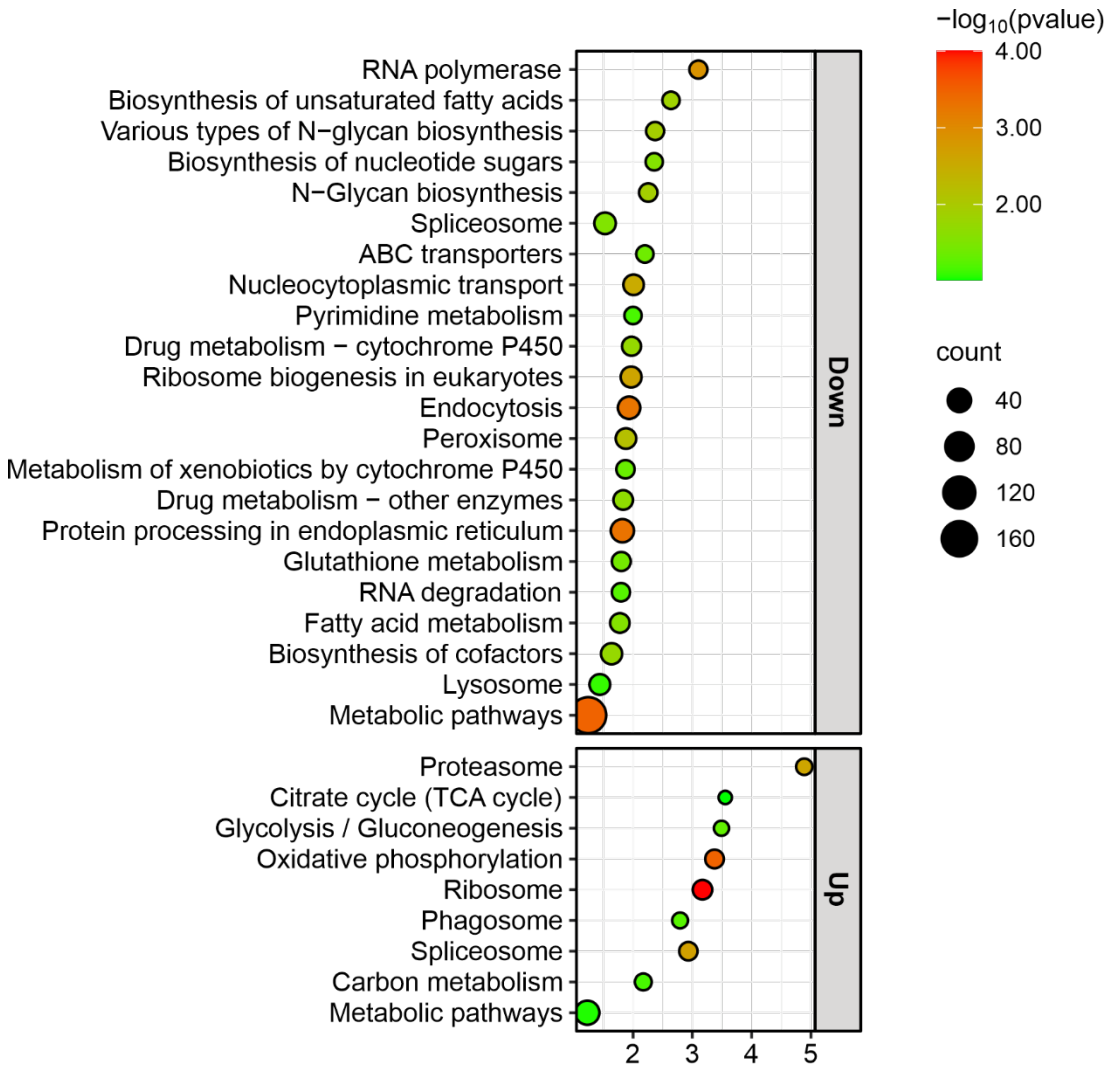

Supplemental Figure A9 **KEGG pathway analysis derived from the *chn-1(tm2692)* proteomics of our *C. elegans* model.** SWATH-MS data comparing samples processed with either CHAPS/Urea- or SDS-based lysis buffer was analysed using DAVID and plotted by SRPlot. Only proteins that met the cut-off criteria (fold changes of ≤0.67 and ≥1.5) were used for the analysis. Each pathway is colour-coded based on statistical significance (–log10(*p*-value)). Pathways related to *chn-1* loss-of-function are listed in Supplemental Table A10. Cross-strain comparisons indicating pathways overrepresented in more than one strain are noted in Supplemental Table A10 and illustrated in Figure 2.15.

Supplemental Table A10 **KEGG pathways related to substantially altered proteins identified by SWATH-MS across lysis buffers in *chn-1(tm2692) C. elegans* mutants.** Related to Figures 2.13 & 2.14. Pathways identified in *chn-1(tm2692)* animals when processed by CHAPS/urea-based lysis buffer compared to SDS-based lysis buffer. The number of associated genes ("count") and an association index (probability (raw *p*-values) as well as enrichment score) for each pathway is included. Cross-strain comparisons were further performed. † Indicates pathways shared by two strains. ‡ Indicates pathways shared by N2 wild-type, *chn-1(by155)*, and *chn-1(tm2692)* deletion mutants.

Pathway	Count	Enrichment	*p*-Value	Regulation
Metabolic pathways‡	162	1.244	3.29E-04	Down
Protein processing in endoplasmic reticulum‡	34	1.820	5.05E-04	Down
Endocytosis†	29	1.933	5.24E-04	Down
RNA polymerase‡	11	3.102	1.36E-03	Down
Ribosome biogenesis in eukaryotes‡	22	1.967	2.38E-03	Down
Nucleocytoplasmic transport†	20	2.009	3.11E-03	Down
Peroxisome‡	20	1.880	6.82E-03	Down
N-Glycan biosynthesis‡	12	2.256	1.22E-02	Down
Various types of N-glycan biosynthesis‡	11	2.372	1.22E-02	Down
Biosynthesis of unsaturated fatty acids‡	9	2.639	1.44E-02	Down
Biosynthesis of cofactors‡	23	1.637	1.84E-02	Down
Drug metabolism - cytochrome P450‡	14	1.974	1.89E-02	Down
Drug metabolism - other enzymes‡	16	1.833	2.18E-02	Down
Fatty acid metabolism‡	16	1.777	2.83E-02	Down
Biosynthesis of nucleotide sugars‡	9	2.357	2.86E-02	Down
Spliceosome‡	25	1.527	3.02E-02	Down
Glutathione metabolism‡	14	1.801	3.87E-02	Down
ABC transporters‡	9	2.200	4.22E-02	Down
Metabolism of xenobiotics by cytochrome P450‡	12	1.872	4.63E-02	Down
RNA degradation	12	1.796	6.05E-02	Down
Pyrimidine metabolism†	9	2.000	6.97E-02	Down
Lysosome†	21	1.439	8.22E-02	Down
Ribosome‡	16	3.170	9.85E-05	Up
Oxidative phosphorylation‡	13	3.374	3.35E-04	Up
Spliceosome	12	2.933	2.06E-03	Up
Proteasome	7	4.888	2.51E-03	Up
Glycolysis / Gluconeogenesis	5	3.491	5.15E-02	Up
Phagosome‡	6	2.793	5.98E-02	Up
Carbon metabolism	8	2.172	7.04E-02	Up
Metabolic pathways‡	40	1.228	9.16E-02	Up
Citrate cycle (TCA cycle)	4	3.555	9.84E-02	Up

Appendix B

Supplemental Results for Chapter 3

Supplemental Table B1 **Bonferroni-adjusted *p*-values associated with longevity differences in N2 wild-type, *chn-1(by155)*, and *chn-1(tm2692)* mutants.** Data correspond to Figure 3.3, Supplemental Table B2, and Supplemental Table B3.

Replicate	Comparison	Adjusted *p*-Value
1	N2 vs. *chn-1(by155)*	0.00E+00
1	N2 vs. *chn-1(tm2692)*	5.20E-08
1	*chn-1(by155)* vs. *chn-1(tm2692)*	3.00E-03
2	N2 vs. *chn-1(by155)*	0.00E+00
2	N2 vs. *chn-1(tm2692)*	0.00E+00
2	*chn-1(by155)* vs. *chn-1(tm2692)*	5.47E-01
3	N2 vs. *chn-1(by155)*	0.00E+00
3	N2 vs. *chn-1(tm2692)*	0.00E+00
3	*chn-1(by155)* vs. *chn-1(tm2692)*	2.92E-01

Supplemental Table B2 **Restricted mean survival times and final mortalities associated with longevity differences in N2 wild-type, *chn-1(by155)*, and *chn-1(tm2692)* mutants.** Data correspond to Figure 3.3, Supplemental Table B1, and Supplemental Table B3.

Replicate	Group	Restricted Mean Survival Time (Day)	SEM (Day)	Final Mortality (Day)
1	N2	19.85	0.54	28
1	*chn-1(by155)*	12.70	0.37	22
1	*chn-1(tm2692)*	14.71	0.61	25
2	N2	20.94	0.54	31
2	*chn-1(by155)*	17.27	0.39	22
2	*chn-1(tm2692)*	16.50	0.40	25
3	N2	17.47	0.47	28
3	*chn-1(by155)*	14.00	0.29	22
3	*chn-1(tm2692)*	13.31	0.30	19

Supplemental Table B3 **Censored animals when comparing N2, *chn-1(by155)*, and *chn-1(tm2692) chn-1* deletion mutants.** Data representing the number of animals censored during each time-point of the assay (of *n* = 126-129 total animals per strain), including animals that were lost (i.e., likely crawled into the agar between measurements), crawled up the plate walls and desiccated, crawled into the agar, bagged (i.e., exhibited internal progeny hatching), or ruptured. Lifespan experiments were carried out at room temperature, and plates otherwise stored at 20ºC. Data correspond to Figure 3.3, Supplemental Table B1, and Supplemental Table B2.

N2 vs. *chn-1by155)* vs. *chn-1(tm2692)*					
Replicate	**Strain**	**Day**	**Dead**	**Censored**	**Reason**
1	N2	0	0	0	--
1	N2	2	0	24	14 lost, 7 dried out on walls of plate, 3 crawled into cracks of agar
1	N2	4	1	6	2 lost, 3 dried out on walls of plate, 1 crawled into cracks of agar
1	N2	6	0	2	1 dried out on walls of plate, 1 "bag of worms" phenotype
1	N2	8	2	5	1 dried out on walls of plate, 1 crawled into cracks of agar, 3 ruptured
1	N2	10	1	0	--
1	N2	13	13	1	1 crawled into cracks of agar
1	N2	16	11	1	1 crawled into cracks of agar
1	N2	19	18	0	--
1	N2	22	20	0	--
1	N2	25	14	0	--
1	N2	28	9	0	--
1	*chn-1(by155)*	0	0	0	--
1	*chn-1(by155)*	2	0	6	6 lost
1	*chn-1(by155)*	4	1	12	4 lost, 6 dried out on walls of plate, 2 crawled into cracks of agar
1	*chn-1(by155)*	6	5	0	--
1	*chn-1(by155)*	8	13	3	1 dried out on walls of plate, 1 crawled into cracks of agar, 1 "bag of worms" phenotype
1	*chn-1(by155)*	10	27	1	1 ruptured
1	*chn-1(by155)*	13	24	1	1 ruptured
1	*chn-1(by155)*	16	26	0	--
1	*chn-1(by155)*	19	7	0	--

1	*chn-1(by155)*	22	3	0	--
1	*chn-1(tm2692)*	0	0	0	--
1	*chn-1(tm2692)*	2	2	40	36 lost (likely crawled into cracked agar since last measurement), 4 dried out on walls of plate
1	*chn-1(tm2692)*	4	0	6	5 lost, 1 crawled into cracks of agar
1	*chn-1(tm2692)*	6	4	5	2 lost, 3 dried out on walls of plate
1	*chn-1(tm2692)*	8	4	2	1 crawled into cracks of agar, 1 ruptured
1	*chn-1(tm2692)*	10	10	0	--
1	*chn-1(tm2692)*	13	23	0	--
1	*chn-1(tm2692)*	16	8	0	--
1	*chn-1(tm2692)*	19	9	0	--
1	*chn-1(tm2692)*	22	8	1	1 ruptured
1	*chn-1(tm2692)*	25	4	0	--
2	N2	0	0	0	--
2	N2	2	3	0	--
2	N2	4	2	25	21 lost (likely crawled into agar since last measurement), 1 crawled into cracks of agar, 3 dried out on walls of plate
2	N2	6	0	14	11 lost (likely crawled into agar since last measurement), 1 dried out on walls of plate, 2 ruptured
2	N2	8	0	0	--
2	N2	10	1	1	1 ruptured
2	N2	13	2	1	1 ruptured
2	N2	16	7	0	--
2	N2	19	23	0	--
2	N2	22	22	0	--
2	N2	25	18	0	--
2	N2	28	7	0	--

2	N2	31	2	0	--
2	*chn-1(by155)*	0	0	0	--
2	*chn-1(by155)*	2	0	0	--
2	*chn-1(by155)*	4	0	13	9 lost, 3 dried out on walls of plate, 1 crawled into cracks of agar
2	*chn-1(by155)*	6	2	4	4 dried out on walls of plate
2	*chn-1(by155)*	8	2	18	7 lost, 9 crawled into cracks of agar, 2 ruptured
2	*chn-1(by155)*	10	5	1	1 dried out on walls of plate
2	*chn-1(by155)*	13	11	2	2 ruptured
2	*chn-1(by155)*	16	18	1	1 ruptured
2	*chn-1(by155)*	19	36	0	--
2	*chn-1(by155)*	22	15	0	--
2	*chn-1(tm2692)*	0	0	0	--
2	*chn-1(tm2692)*	2	1	37	36 lost, 1 dried out on walls of plate
2	*chn-1(tm2692)*	4	0	0	--
2	*chn-1(tm2692)*	6	0	1	1 "bag of worms" phenotype
2	*chn-1(tm2692)*	8	0	1	1 crawled into cracks of agar
2	*chn-1(tm2692)*	10	2	0	--
2	*chn-1(tm2692)*	13	33	0	--
2	*chn-1(tm2692)*	16	16	0	--
2	*chn-1(tm2692)*	19	20	0	--
2	*chn-1(tm2692)*	22	16	0	--
2	*chn-1(tm2692)*	25	1	0	--
3	N2	0	0	0	--
3	N2	2	0	0	--
3	N2	4	0	24	19 lost, 3 crawled into cracks of agar, 2 dried out on walls of plate
3	N2	6	0	0	--

3	N2	8	2	6	4 crawled into cracks of agar, 1 dried out on walls of plate, 1 "bag of words" phenotype
3	N2	10	6	1	1 ruptured
3	N2	13	21	1	1 ruptured
3	N2	16	19	0	--
3	N2	19	26	0	--
3	N2	22	11	0	--
3	N2	25	8	0	--
3	N2	28	3	0	--
3	*chn-1(by155)*	0	0	0	--
3	*chn-1(by155)*	2	0	11	9 lost, 2 dried out on walls of plate
3	*chn-1(by155)*	4	0	19	11 lost, 8 dried out on walls of plate
3	*chn-1(by155)*	6	0	0	--
3	*chn-1(by155)*	8	2	0	--
3	*chn-1(by155)*	10	13	0	--
3	*chn-1(by155)*	13	47	0	--
3	*chn-1(by155)*	16	27	0	--
3	*chn-1(by155)*	19	5	0	--
3	*chn-1(by155)*	22	4	0	--
3	*chn-1(tm2692)*	0	0	0	--
3	*chn-1(tm2692)*	2	0	28	25 lost, 3 dried out on walls of plate
3	*chn-1(tm2692)*	4	0	1	1 crawled into cracks of agar
3	*chn-1(tm2692)*	6	1	0	--
3	*chn-1(tm2692)*	8	2	0	--
3	*chn-1(tm2692)*	10	26	0	--
3	*chn-1(tm2692)*	13	38	0	--
3	*chn-1(tm2692)*	16	22	2	2 ruptured
3	*chn-1(tm2692)*	19	8	0	--

Supplemental Table B4 **Genes corresponding to shared proteins (based on fold change) identified by SWATH-MS that are over-represented in both *chn-1(by155)* and *chn-1(tm2692) C. elegans* samples processed by lysis with CHAPS/urea-based lysis buffer.** Associated fold changes and *p*-values for each pairwise comparison are listed in Table 3.2.

Protein	Gene
Aquaporin	*aqp-11*
Zygote defective protein 12	*zyg-12*
Glucuronosyltransferase	*ugt-1*
Probable mitochondrial pyruvate carrier 1	*mpc-1*
Vacuolar protein sorting-associated protein VTA1 homolog	*T23G11.7*
Translocon Sec61/SecY plug domain-containing protein	*sec-61.a*
HEAT repeat protein 27	*hpo-27*
Protein Phosphatase Four Regulatory subunit	*ppfr-2*
Bromo domain-containing protein	*F13C5.2*
BPTI/Kunitz inhibitor domain-containing protein	*F30H5.3*
Conserved oligomeric Golgi complex subunit 6	*cogc-6*
PLD phosphodiesterase domain-containing protein	*T05C3.6*
DNA-directed RNA polymerases I, II, and III subunit RPABC5	*rpb-10*
Aminotran_5 domain-containing protein	*Y71H2B.5*
Peptidase M1 leukotriene A4 hydrolase/aminopeptidase C-terminal domain-containing protein	*ltah-1.2*
DUF19 domain-containing protein	*ZK105.1*

Supplemental Table B5 **Genes corresponding to shared proteins (based on fold change) identified by SWATH-MS that are under-represented in both *chn-1(by155)* and *chn-1(tm2692) C. elegans* samples processed by lysis with CHAPS/urea-based lysis buffer.** Associated fold changes and *p*-values for each pairwise comparison are listed in Table 3.3.

Protein	Gene
Transcription factor sma-9	*sma-9*
Uncharacterized protein F44E2.9	*F44E2.9*
Protein-lysine N-methyltransferase M142.8	*M142.8*
Uncharacterized protein C26F1.3	*C26F1.3*
MTOR-associated protein MEAK7	*eak-7*
Gamma-soluble NSF attachment protein	*Y59A8B.8*
UBX domain-containing protein 2	*ubxn-2*
Brix domain-containing protein F44G4.1	*F44G4.1*
Protein ABHD11	*abhd-11.2*
Putative RNA polymerase II transcriptional coactivator	*T13F2.2*
C-type lectin domain-containing protein	*clec-218*
FIS1-related protein fis-2	*fis-2*
Fatty Acid/Retinol binding protein	*far-8*
Peptidyl-prolyl cis-trans isomerase E	*cyn-13*
Pre-rRNA-processing protein TSR2 homolog	*tsr-2*
RNA helicase	*Y48G1BR.1*

Supplemental Table B6 **Genes corresponding to shared proteins (based on fold change) identified by SWATH-MS that are over-represented in both *chn-1(by155)* and *chn-1(tm2692) C. elegans* samples processed by lysis with SDS-based lysis buffer.** Associated fold changes and *p*-values for each pairwise comparison are listed in Table 3.4.

Protein	Gene
FMRF-Like Peptide	*flp-28*
Methyltransferase domain-containing protein	*prmt-6*
NADP-dependent oxidoreductase domain-containing protein	*C35D10.6*
UDP-glucuronosyltransferase	*ugt-5*
Tudor domain-containing protein	*smr-1*
Methyltransferase small domain-containing protein	*mtq-2*
HoloCentric chromosome binding Protein	*hcp-2*
Putative 1-acyl-sn-glycerol-3-phosphate acyltransferase	*acl-1*
Chitin-binding domain protein cbd-1	*cbd-1*
MLt-TeN (Mlt-10) related	*mltn-8*
SLC (SoLute Carrier) homolog	*R07B7.10*
Mitochondrial Ribosomal Protein, Small	*mrps-34*
Lissencephaly-1 homolog	*lis-1*
Acyl carrier protein	*ndab-1*
DUF19 domain-containing protein	*C17B7.15*
EHS-1	*ehs-1*
Pseudouridine synthase I TruA alpha/beta domain-containing protein	*pus-1*
5'-AMP-activated protein kinase subunit beta-1	*aakb-1*
Remorin_C domain-containing protein	*hpo-32*
PIPK domain-containing protein	*ppk-1*
Dual specificity mitogen-activated protein kinase kinase	*mek-2*
BING4 C-terminal domain-containing protein	*wdr-46*
Tudor domain-containing protein	*Y50D4C.3*
MARVEL domain-containing protein	*C49A1.10*
CRAL-TRIO domain-containing protein	*F20G2.3*
Endoribonuclease	*endu-2*
Acyl-coenzyme A thioesterase 8	*C37H5.13*
SSD domain-containing protein	*ptr-21*
DUF19 domain-containing protein	*ZK105.1*
Microtubule-associated protein futsch	*maph-1.3*
Protein-lysine N-methyltransferase M142.8	*M142.8*
Albumin	*C37H5.13*

Supplemental Table B7 **Genes corresponding to shared proteins (based on fold change) identified by SWATH-MS that are under-represented in both *chn-1(by155)* and *chn-1(tm2692) C. elegans* samples processed by lysis with SDS-based lysis buffer.** Associated fold changes and *p*-values for each pairwise comparison are listed in Table 3.5.

Protein	Gene
Nematode cuticle collagen N-terminal domain-containing protein	*col-143*
Uncharacterized protein	*F17E9.5*
Ribosomal protein S10 domain-containing protein	*mrpl-48*
RNA helicase	*sacy-1*
Polypeptide N-acetylgalactosaminyltransferase 5	*gly-5*
Probable small nuclear ribonucleoprotein Sm D1	*snr-3*
Tyrosine-protein phosphatase domain-containing protein	*spe-54*
Glyceraldehyde-3-phosphate dehydrogenase 3	*gpd-3*
cystathionine gamma-lyase	*cth-1*
Peptidyl-prolyl cis-trans isomerase E	*cyn-13*
Probable glucosamine-6-phosphate isomerase	*T03F6.3*
Secreted protein	*W09D6.4*
Mitochondrial import inner membrane translocase subunit Tim21	*F56B3.11*
Biogenesis of lysosome-related organelles complex 1 subunit 2	*blos-2*

A genome-wide network model of *C. elegans* protein expression was used to investigate protein sets altered as a result of *chn-1* deletion in both *chn-1(by155)* and *chn-1(tm2692) chn-1* mutants compared to wild-type controls (Supplemental Figure B1 and Supplemental Table B8). In CHAPS/Urea-processed samples, significantly enriched biological processes included those related to protein transport ($p < 0.05$) and rRNA processing ($p < 0.05$), while enriched molecular function GO terms included nucleic acid binding ($p < 0.05$). In samples lysed by SDS, significantly enriched biological processes included macromolecule methylation ($p < 0.05$) and primary metabolic process ($p < 0.05$), while endosomal transport approached significance ($p = 0.068$). Cellular components significantly enriched by *chn-1* ablation across mutants included cytoplasm ($p < 0.05$). Molecular functions enriched across *chn-1*-null mutants included RNA binding ($p < 0.05$), while nucleic acid binding and transferase activity approached significance ($p = 0.093$ and 0.098, respectively).

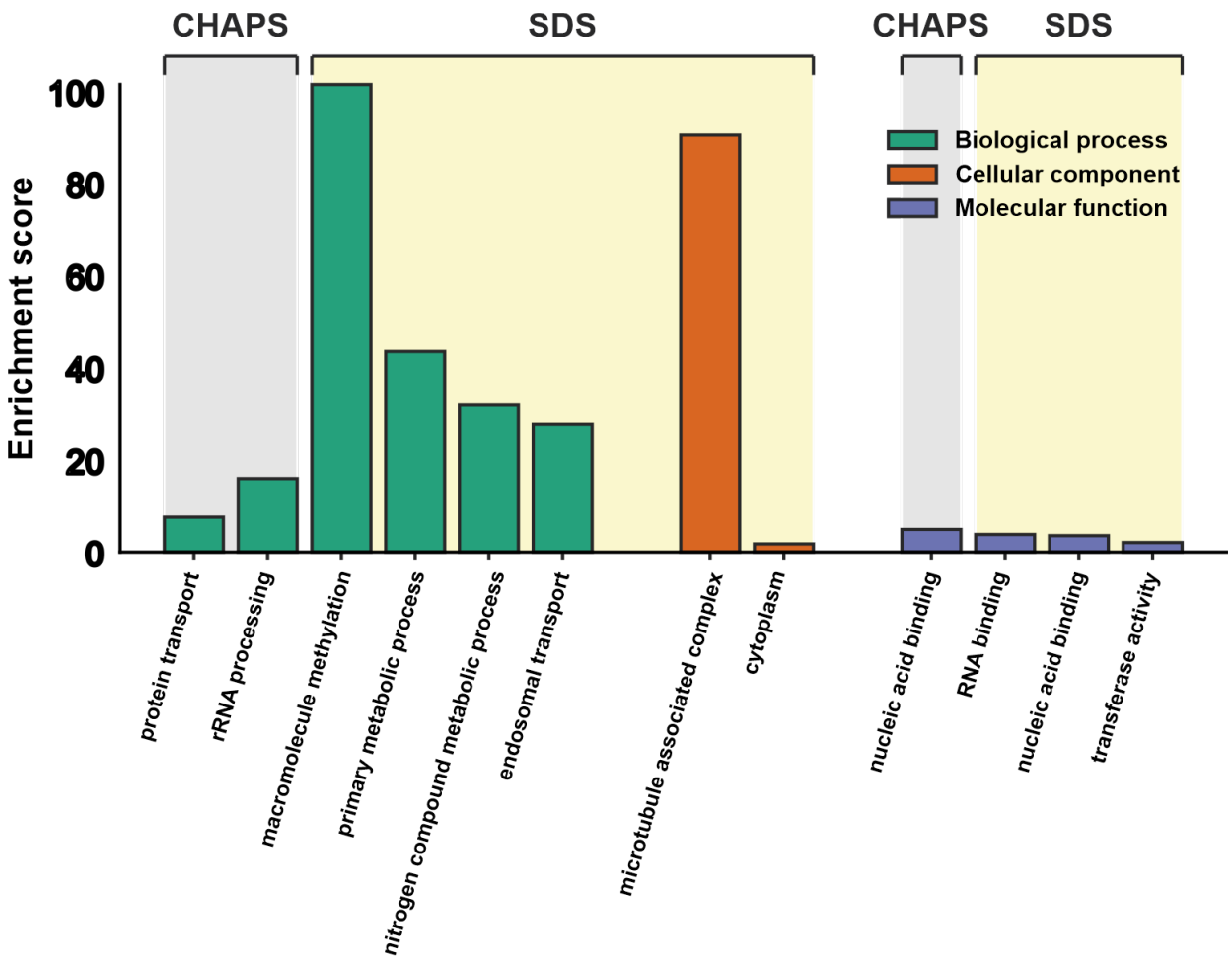

Supplemental Figure B1 **GO enrichment analysis of the proteome of overlapping proteins identified by SWATH-MS across *C. elegans* mutants.** The shared proteomic changes between *chn-1(by155)* and *chn-1(tm2692) C. elegans* mutants when compared to N2 wild-type animals were analyzed by DAVID. Samples were processed with either CHAPS/Urea- or SDS-based lysis buffer. GO terms derived were plotted by SRPlot. GO terms shown are related to biological processes, cellular components, and molecular functions, and each term is plotted based on fold enrichment. Only proteins that met the cut-off criteria (fold changes of ≤0.67 and ≥1.5) were used for the analysis. GO terms related to CHIP loss-of-function are listed in Supplemental Table B8.

Supplemental Table B8 **GO terms related to CHIP loss-of-function in both *chn-1(by155)* and *chn-1(tm2692)* mutants.** Related to Supplemental Figure B1. Shared biological process (BP), molecular function (MF) and cellular component (CC) GO terms identified in *chn-1(by155)* and *chn-1(tm2692) C. elegans* mutants when compared to N2 wild-type animals (using DAVID). The lysis buffer, number of associated genes ("count") and an association index (probability (*p*-value) as well as enrichment score) for each GO term is included.

	GO Term	Lysis Buffer	Count	Enrichment	*p*-Value
BP	Protein transport	CHAPS/Urea	4	7.598	1.32E-02
	rRNA processing	CHAPS/Urea	3	15.985	1.37E-02
	Macromolecule methylation	SDS	2	101.505	1.90E-02
	Primary metabolic process	SDS	2	43.502	4.37E-02
	Nitrogen compound metabolic process	SDS	2	32.054	5.89E-02
	Endosomal transport	SDS	2	27.683	6.78E-02
CC	Microtubule associated complex	SDS	2	90.514	2.13E-02
	Cytoplasm	SDS	12	1.792	4.68E-02
MF	Nucleic acid binding	CHAPS/Urea	4	4.928	4.12E-02
	RNA binding	SDS	6	3.843	1.62E-02
	Nucleic acid binding	SDS	4	3.584	9.26E-02
	Transferase activity	SDS	7	2.097	9.82E-02

Gene set enrichment analyses comparing either *chn-1(by155) chn-1* mutants versus N2 controls or *chn-1(tm2692)* mutants versus wild-type controls, each processed by either CHAPS/Urea- or SDS-based lysis protocols, revealed a number of significantly altered gene ontology sets in response to *chn-1* ablation (Supplemental Figures B2-B4 and Supplemental Tables B9-B11). In CHAPS/Urea-processed *chn-1(by155)* mutants versus N2 controls, *chn-1* deletion significantly enriched biological processes related to rRNA processing ($p < 0.001$), protein transport ($p < 0.01$), and regulation of cell projection organization ($p < 0.05$). Additionally, protein targeting to vacuole involved in ubiquitin-dependent protein catabolic process via the multivesicular body sorting pathway ($p = 0.056$) and mitochondrial fission ($p = 0.065$) approached significance (Supplemental Figure B2 and Supplemental Table B9). In CHAPS/Urea-lysed *chn-1(tm2692)* mutants versus N2 controls, biological processes pertaining to RNA ($p = 0.054$) and rRNA processing ($p < 0.001$) were enriched, as well as those pertaining to methylation ($p < 0.05$) and protein transport ($p < 0.05$) (Supplemental Figure B2 and Supplemental Table B9).

In CHAPS/Urea-processed *chn-1(by155) chn-1* mutants compared to N2 controls, significantly enriched cellular components included nucleus ($p < 0.01$), cytoplasm ($p < 0.05$), and mitochondrial outer membrane ($p < 0.05$), with peroxisome approaching significance ($p = 0.072$) (Supplemental Figure B2 and Supplemental Table B9). Compared to wild-type controls, cellular components enriched in *chn-1(tm2692)* mutants included cytoplasm ($p < 0.01$), intracellular membrane-bounded organelle ($p < 0.05$), catalytic step 2 spliceosome ($p = 0.062$), and mitochondrion ($p = 0.10$) (Supplemental Figure B2 and Supplemental Table B9).

Enriched molecular functions in CHAPS/Urea-lysed *chn-1(by155) chn-1* mutants compared to N2 controls included phosphotyrosine binding ($p < 0.05$), nucleic acid binding ($p < 0.05$), and transcription coactivator activity ($p = 0.079$), while those enriched in *chn-1(tm2692)* mutants relative to wild-type controls included methyltransferase activity ($p < 0.05$), RNA ($p < 0.05$), rRNA ($p < 0.05$), and SNARE binding ($p < 0.05$) (Supplemental Figure B2 and Supplemental Table B9). In SDS-processed *chn-1(by155)* mutants versus wild-type controls, *chn-1* ablation significantly enriched biological processes related to mRNA splicing, via spliceosome ($p < 0.05$),

methylation ($p < 0.05$), and tRNA methylation ($p < 0.05$). Additionally, macromolecule methylation ($p = 0.082$), membrane budding ($p = 0.082$), negative regulation of ubiquitin protein ligase activity ($p = 0.096$), and proteasome assembly ($p = 0.096$) approached significance (Supplemental Figure B3 and Supplemental Table B10).

In SDS-processed *chn-1(by155) chn-1* mutants compared to wild-type controls, significantly enriched cellular components included extracellular region ($p < 0.001$), cytoplasm ($p < 0.01$), spliceosomal complex ($p < 0.05$), cytoplasmic side of plasma membrane ($p < 0.05$), and transcription factor TFIIF complex ($p < 0.05$). Cellular components approaching significance included COP9 signalosome ($p = 0.092$) as well as ESCRT III complex ($p = 0.092$) (Supplemental Figure B3 and Supplemental Table B10).

Significantly enriched molecular functions in SDS-lysed *chn-1(by155) chn-1* mutants compared to N2 controls included RNA binding ($p < 0.001$), methyltransferase activity ($p < 0.05$), NADP binding ($p < 0.05$), cystathionine gamma-lyase activity ($p < 0.05$), and L-cystine L-cysteine-lyase (deaminating) ($p < 0.05$). Molecular functions related to glyceraldehyde-3-phosphate dehydrogenase (GAPDH) (phosphorylating) activity ($p = 0.058$) and serine-type endopeptidase inhibitor activity ($p = 0.092$) approached significance (Supplemental Figure B3 and Supplemental Table B10).

In SDS-processed *chn-1(tm2692) chn-1* deletion mutants versus wild-type control animals, several biological processes related to protein transport ($p < 0.01$) and localization ($p < 0.05$) as well as endocytosis ($p < 0.05$) were significantly enriched. In line with these observations, protein transport into the mitochondrial matrix ($p = 0.0841$) was also enriched, although this finding only approached significance. Other biological processes related to the mitochondria were also augmented, including endoplasmic reticulum unfolded protein response ($p = 0.072$), mitochondrial translation ($p = 0.055$), and mitochondrial organization ($p = 0.063$). Biological processes associated with lipid transport ($p < 0.001$) and metabolism were disproportionately represented. Positive regulation of triglyceride lipase activity ($p = 0.053$), for instance, a process facilitating the degradation and subsequent transmembrane redistribution of triglycerides, was also enriched (Supplemental Figure B4 and Supplemental Table B11).

Cellular components augmented in *chn-1(tm2692) chn-1* mutants relative to N2 controls were related to protein trafficking, uptake, sorting, and delivery, including endocytic vesicle ($p = 0.073$) and intracellular membrane-bounded organelle ($p < 0.05$). Cellular components associated with transcription and DNA repair were also enriched, such as DNA-directed RNA polymerase III complex ($p = 0.060$) and FACT complex ($p = 0.069$). The SCAR complex ($p = 0.091$), a key catalyst for actin cytoskeleton-mediated cell migration, was also overrepresented in response to *chn-1* deletion, along with annuli extracellular matrix ($p < 0.05$), involved in structural support and cell communication, and microtubule associated complex ($p < 0.05$), involved in modulating cytoskeletal integrity. Cellular components associated with the small-subunit processome ($p < 0.05$), a large ribonucleoprotein complex fundamental in organizing eukaryotic small ribosomal subunit assembly, were also enriched, along with ribosome ($p < 0.05$) and ribonucleoprotein complex ($p = 0.096$) more generally. Cellular components pertaining to RNA splicing as well as the mitochondria were also enriched, including the spliceosomal complex ($p < 0.05$), catalytic step 2 spliceosome ($p < 0.05$), and mitochondrion ($p < 0.001$) (Supplemental Figure B4 and Supplemental Table B11).

Insulin signaling and proteotoxic stress resilience are mediated competitively in a CHIP-dependent manner [7]. The insulin and insulin-like growth factor 1 signaling pathway modulates the well-established link between lifespan and nutrient status. Specifically, decreased insulin signaling has been shown to increase longevity while simultaneously increasing resilience to proteotoxicity through the orchestrated response of various transcription factors [55,624-626]. Interestingly, nutrient reservoir activity ($p < 0.001$) was one of the most strongly enriched molecular functions in SDS-processed *chn-1(tm2692) chn-1*-null mutants relative to wild-type controls, along with transcription factor binding ($p = 0.088$), although this did not reach statistical significance. Consistent with results concerning enriched terms related to RNA function, processing, and biogenesis, molecular functions including RNA binding ($p < 0.001$), RNA helicase activity ($p < 0.05$), and RNA polymerase II core binding ($p = 0.080$) were augmented in *chn-1(tm2692)* mutants. ATPase activity ($p < 0.05$), crucial in catalysing the hydrolysis of ATP, was also enriched. Finally, several molecular functions integral to protein transport pathways were overrepresented in SDS-processed *chn-1(tm2692)* animals

relative to wild-type controls, including lipid transporter activity ($p < 0.001$) and protein transmembrane transporter activity ($p < 0.05$) (Supplemental Figure B4 and Supplemental Table B11).

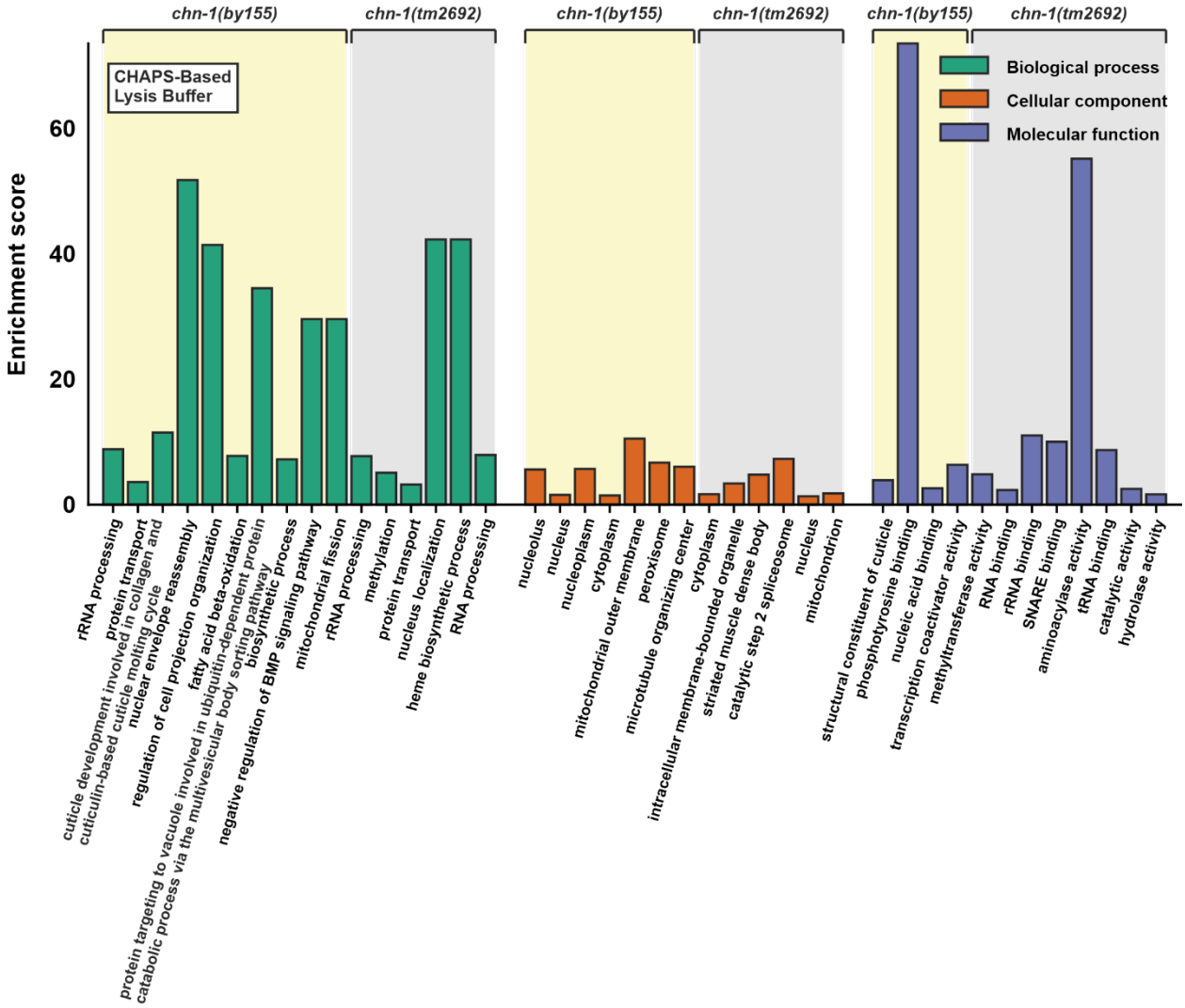

Supplemental Figure B2 **CHAPS/urea-based GO enrichment analysis derived from the proteomics of our *C. elegans* model.** SWATH-MS data comparing either *chn-1(by155)* or *chn-1(tm2692) C. elegans* mutants with N2 wild-type controls was analysed using DAVID and GO terms derived were plotted by SRPlot. Samples were processed with CHAPS/Urea-based lysis buffer. GO terms shown are related to biological processes, cellular components, and molecular functions, and each term is plotted based on fold enrichment. Only proteins that met the cut-off criteria (fold changes of ≤0.67 and ≥1.5) were used for the analysis. GO terms related to CHIP loss-of-function are listed in Supplemental Table B9.

Supplemental Table B9 **GO terms related to CHIP loss-of-function in either *chn-1(by155)* or *chn-1(tm2692)* mutants lysed by CHAPS/urea.** Related to Supplemental Figure B2. Biological process (BP), molecular function (MF) and cellular component (CC) GO terms identified in *chn-1(by155)* or *chn-1(tm2692) C. elegans* mutants when compared to N2 wild-type animals (using DAVID) processed by lysis with CHAPS/urea-based lysis buffer. The strain, number of associated genes ("count") and an association index (probability (*p*-value) as well as enrichment score) for each GO term is included. † Indicates GO terms shared by both *chn-1(by155)* and *chn-1(tm2692)* mutants.

	GO Term	Strain	Count	Enrichment	*p*-Value
BP	rRNA processing†	*chn-1(by155)*	7	8.844	1.27E-04
	protein transport†	*chn-1(by155)*	8	3.603	6.38E-03
	cuticle development involved in collagen and cuticulin-based cuticle molting cycle	*chn-1(by155)*	3	11.511	2.71E-02
	nuclear envelope reassembly	*chn-1(by155)*	2	51.799	3.77E-02
	regulation of cell projection organization	*chn-1(by155)*	2	41.439	4.69E-02
	fatty acid beta-oxidation	*chn-1(by155)*	3	7.770	5.57E-02
	protein targeting to vacuole involved in ubiquitin-dependent protein catabolic process via the multivesicular body sorting pathway	*chn-1(by155)*	2	34.533	5.60E-02
	biosynthetic process	*chn-1(by155)*	3	7.228	6.33E-02
	negative regulation of BMP signaling pathway	*chn-1(by155)*	2	29.599	6.50E-02
	mitochondrial fission	*chn-1(by155)*	2	29.599	6.50E-02
	rRNA processing	*chn-1(tm2692)*	6	7.740	9.95E-04
	Methylation	*chn-1(tm2692)*	5	5.086	1.62E-02
	protein transport	*chn-1(tm2692)*	7	3.219	2.06E-02
	nucleus localization	*chn-1(tm2692)*	2	42.312	4.59E-02
	heme biosynthetic process	*chn-1(tm2692)*	2	42.312	4.59E-02
	RNA processing	*chn-1(tm2692)*	3	7.933	5.37E-02
CC	Nucleolus	*chn-1(by155)*	8	5.624	5.21E-04
	nucleus†	*chn-1(by155)*	34	1.558	5.52E-03
	Nucleoplasm	*chn-1(by155)*	5	5.696	1.12E-02
	cytoplasm†	*chn-1(by155)*	29	1.471	2.54E-02
	mitochondrial outer membrane	*chn-1(by155)*	3	10.545	3.21E-02
	Peroxisome	*chn-1(by155)*	3	6.711	7.24E-02
	microtubule organizing center	*chn-1(by155)*	3	6.051	8.65E-02
	Cytoplasm	*chn-1(tm2692)*	34	1.676	1.72E-03
	intracellular membrane-bounded organelle	*chn-1(tm2692)*	6	3.383	3.14E-02
	striated muscle dense body	*chn-1(tm2692)*	4	4.782	5.02E-02
	catalytic step 2 spliceosome	*chn-1(tm2692)*	3	7.319	6.22E-02
	Nucleus	*chn-1(tm2692)*	30	1.336	6.98E-02
	Mitochondrion	*chn-1(tm2692)*	10	1.798	9.99E-02

MF	structural constituent of cuticle	*chn-1(by155)*	6	3.896	1.81E-02
	phosphotyrosine binding	*chn-1(by155)*	2	73.585	2.66E-02
	nucleic acid binding	*chn-1(by155)*	8	2.628	3.08E-02
	transcription coactivator activity	*chn-1(by155)*	3	6.368	7.89E-02
	methyltransferase activity	*chn-1(tm2692)*	5	4.841	1.90E-02
	RNA binding	*chn-1(tm2692)*	10	2.348	2.45E-02
	rRNA binding	*chn-1(tm2692)*	3	11.038	2.93E-02
	SNARE binding	*chn-1(tm2692)*	3	10.034	3.50E-02
	aminoacylase activity	*chn-1(tm2692)*	2	55.189	3.54E-02
	tRNA binding	*chn-1(tm2692)*	3	8.714	4.53E-02
	catalytic activity	*chn-1(tm2692)*	6	2.518	8.69E-02
	hydrolase activity	*chn-1(tm2692)*	13	1.646	8.81E-02

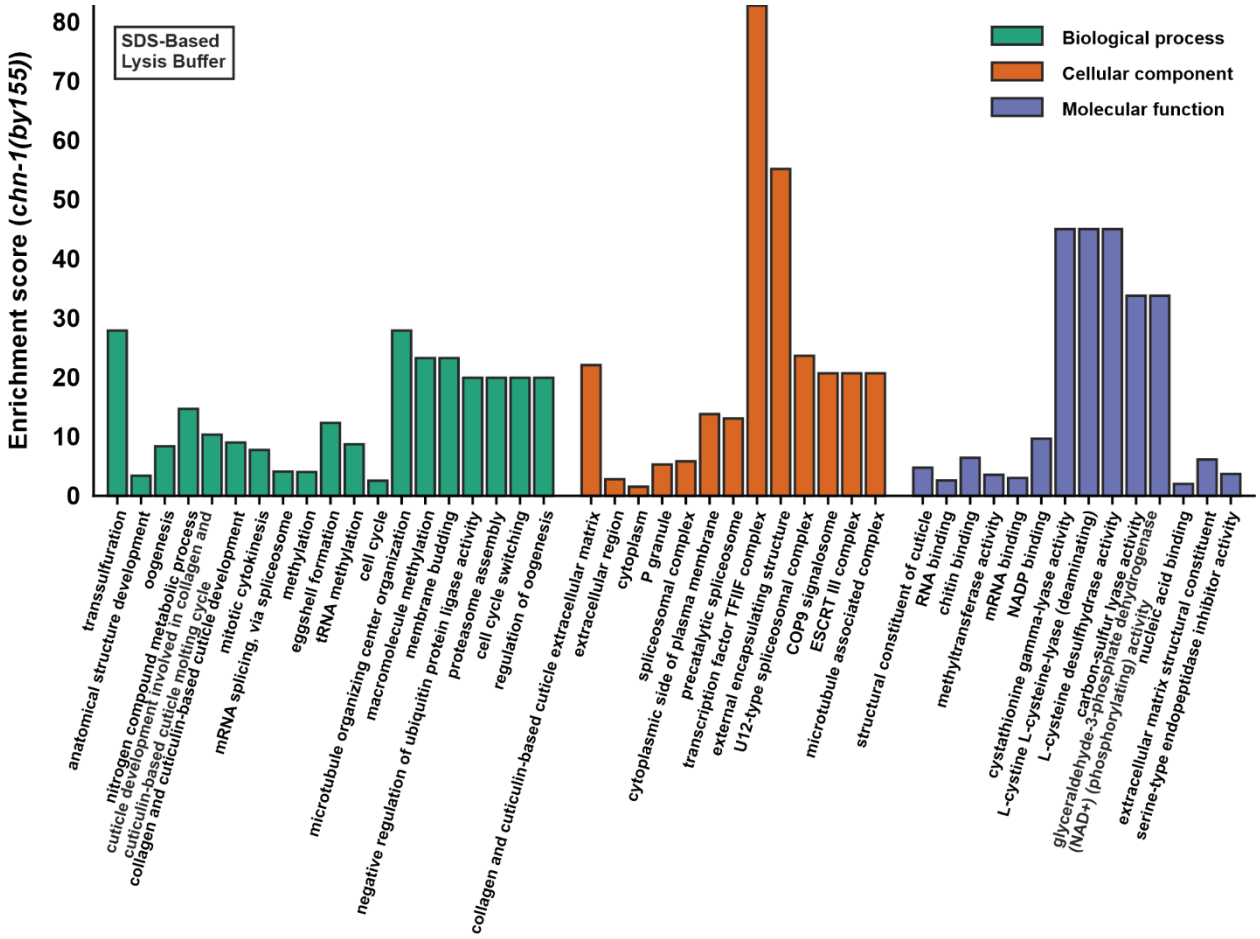

Supplemental Figure B3 **GO enrichment analysis derived from the proteomics of our *C. elegans* model.** SWATH-MS data comparing *chn-1(by155) C. elegans* mutants with N2 wild-type controls was analysed using DAVID and GO terms derived were plotted by SRPlot. Samples were processed with SDS-based lysis buffer. GO terms shown are related to biological processes, cellular components, and molecular functions, and each term is plotted based on fold enrichment. Only proteins that met the cut-off criteria (fold changes of ≤0.67 and ≥1.5) were used for the analysis. GO terms related to CHIP loss-of-function are listed in Supplemental Table B10.

Supplemental Table B10 **GO terms related to CHIP loss-of-function in *chn-1(by155)* mutants lysed by SDS.** Related to Supplemental Figure B3. Biological process (BP), molecular function (MF) and cellular component (CC) GO terms identified in *chn-1(by155) C. elegans* mutants when compared to N2 wild-type animals (using DAVID) processed by lysis with SDS-based lysis buffer. The number of associated genes ("count") and an association index (probability (*p*-value) as well as enrichment score) for each GO term is included. † Indicates GO terms shared by both *chn-1(by155)* and *chn-1(tm2692)* mutants.

	GO Term	Count	Enrichment	*p*-Value
BP	Transsulfuration	4	27.914	3.15E-04
	anatomical structure development†	13	3.411	4.04E-04
	Oogenesis	6	8.374	6.89E-04
	nitrogen compound metabolic process†	4	14.692	2.31E-03
	cuticle development involved in collagen and cuticulin-based cuticle molting cycle†	4	10.338	6.43E-03
	collagen and cuticulin-based cuticle development†	4	9.004	9.48E-03
	mitotic cytokinesis	4	7.754	1.43E-02
	mRNA splicing, via spliceosome†	6	4.105	1.51E-02
	Methylation	6	4.026	1.63E-02
	eggshell formation	3	12.315	2.38E-02
	tRNA methylation	3	8.723	4.52E-02
	cell cycle	7	2.558	5.51E-02
	microtubule organizing center organization	2	27.914	6.92E-02
	macromolecule methylation	2	23.262	8.24E-02
	membrane budding	2	23.262	8.24E-02
	negative regulation of ubiquitin protein ligase activity	2	19.938	9.55E-02
	proteasome assembly	2	19.938	9.55E-02
	cell cycle switching	2	19.938	9.55E-02
	regulation of oogenesis	2	19.938	9.55E-02
CC	collagen and cuticulin-based cuticle extracellular matrix†	4	22.086	6.93E-04
	extracellular region†	15	2.817	8.48E-04
	cytoplasm†	45	1.537	2.14E-03
	P granule†	6	5.287	5.42E-03
	spliceosomal complex†	5	5.833	1.04E-02
	cytoplasmic side of plasma membrane	3	13.804	1.93E-02
	precatalytic spliceosome	3	13.077	2.14E-02
	transcription factor TFIIF complex	2	82.824	2.38E-02
	external encapsulating structure	2	55.216	3.56E-02
	U12-type spliceosomal complex	2	23.664	8.10E-02

	COP9 signalosome	2	20.706	9.21E-02
	ESCRT III complex	2	20.706	9.21E-02
	microtubule associated complex†	2	20.706	9.21E-02
MF	structural constituent of cuticle†	12	4.770	3.97E-05
	RNA binding†	18	2.588	5.22E-04
	chitin binding	4	6.436	2.35E-02
	methyltransferase activity	6	3.557	2.62E-02
	mRNA binding	7	3.013	2.82E-02
	NADP binding	3	9.654	3.75E-02
	cystathionine gamma-lyase activity	2	45.052	4.35E-02
	L-cystine L-cysteine-lyase (deaminating)	2	45.052	4.35E-02
	L-cysteine desulfhydrase activity	2	45.052	4.35E-02
	carbon-sulfur lyase activity	2	33.789	5.75E-02
	glyceraldehyde-3-phosphate dehydrogenase (GAPDH) (phosphorylating) activity	2	33.789	5.75E-02
	nucleic acid binding	10	2.011	5.94E-02
	extracellular matrix structural constituent	3	6.143	8.43E-02
	serine-type endopeptidase inhibitor activity	4	3.703	9.21E-02

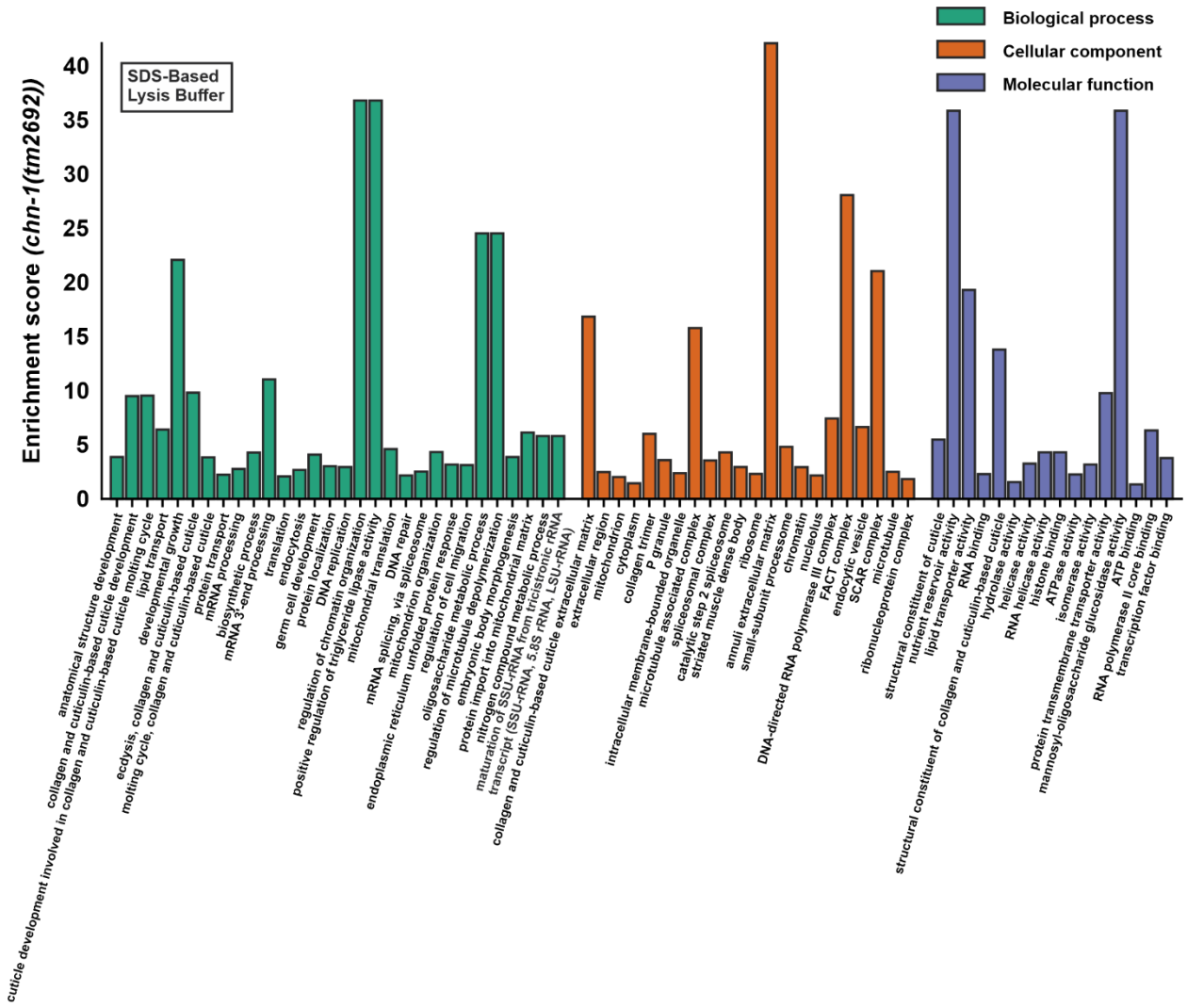

Supplemental Figure B4 **GO enrichment analysis derived from the proteomics of our *C. elegans* model.** SWATH-MS data comparing *chn-1(tm2692) C. elegans* mutants with N2 wild-type controls was analysed using DAVID and GO terms derived were plotted by SRPlot. Samples were processed with SDS-based lysis buffer. GO terms shown are related to biological processes, cellular components, and molecular functions, and each term is plotted based on fold enrichment. Only proteins that met the cut-off criteria (fold changes of ≤0.67 and ≥1.5) were used for the analysis. GO terms related to CHIP loss-of-function are listed in Supplemental Table B11.

Supplemental Table B11 **GO terms related to CHIP loss-of-function in *chn-1(tm2692)* mutants lysed by SDS.** Related to Supplemental Figure B4. Biological process (BP), molecular function (MF) and cellular component (CC) GO terms identified in *chn-1(tm2692) C. elegans* mutants when compared to N2 wild-type animals (using DAVID) processed by lysis with SDS-based lysis buffer. The number of associated genes ("count") and an association index (probability (*p*-value) as well as enrichment score) for each GO term is included. † Indicates GO terms shared by both *chn-1(by155)* and *chn-1(tm2692)* mutants.

	GO Term	Count	Enrichment	*p*-Value
BP	anatomical structure development†	28	3.875	2.88E-09
	collagen and cuticulin-based cuticle development†	8	9.499	1.48E-05
	cuticle development involved in collagen and cuticulin-based cuticle molting cycle†	7	9.543	6.82E-05
	lipid transport	8	6.402	2.14E-04
	developmental growth	3	22.086	6.92E-03
	ecdysis, collagen and cuticulin-based cuticle	4	9.816	7.01E-03
	molting cycle, collagen and cuticulin-based cuticle	7	3.846	9.34E-03
	protein transport	14	2.241	9.73E-03
	mRNA processing	10	2.768	1.00E-02
	biosynthetic process	5	4.280	2.83E-02
	mRNA 3'-end processing	3	11.043	2.85E-02
	Translation	12	2.084	2.92E-02
	Endocytosis	8	2.677	2.96E-02
	germ cell development	5	4.090	3.28E-02
	protein localization	6	3.025	4.74E-02
	DNA replication	6	2.945	5.22E-02
	regulation of chromatin organization	2	36.810	5.34E-02
	positive regulation of triglyceride lipase activity	2	36.810	5.34E-02
	mitochondrial translation	4	4.601	5.46E-02
	DNA repair	9	2.165	5.60E-02
	mRNA splicing, via spliceosome†	7	2.526	5.82E-02
	mitochondrion organization	4	4.331	6.34E-02
	endoplasmic reticulum unfolded protein response	5	3.173	7.15E-02
	regulation of cell migration	5	3.119	7.52E-02
	oligosaccharide metabolic process	2	24.540	7.90E-02
	regulation of microtubule depolymerization	2	24.540	7.90E-02
	embryonic body morphogenesis	4	3.875	8.27E-02
	protein import into mitochondrial matrix	3	6.135	8.41E-02
	nitrogen compound metabolic process†	3	5.812	9.23E-02
	maturation of SSU-rRNA from tricistronic rRNA transcript (SSU-rRNA, 5.8S rRNA, LSU-rRNA)	3	5.812	9.23E-02

CC	collagen and cuticulin-based cuticle extracellular matrix†	6	16.840	1.78E-05
	extracellular region†	26	2.482	4.94E-05
	Mitochondrion	32	2.026	2.41E-04
	cytoplasm†	83	1.441	2.96E-04
	collagen trimer	8	6.014	3.34E-04
	P granule†	8	3.583	6.88E-03
	intracellular membrane-bounded organelle	12	2.383	1.22E-02
	microtubule associated complex†	3	15.787	1.42E-02
	spliceosomal complex†	6	3.558	2.63E-02
	catalytic step 2 spliceosome	5	4.296	2.83E-02
	striated muscle dense body	7	2.947	3.13E-02
	Ribosome	9	2.310	4.14E-02
	annuli extracellular matrix	2	42.100	4.68E-02
	small-subunit processome	4	4.811	4.93E-02
	Chromatin	6	2.937	5.31E-02
	Nucleolus	9	2.165	5.66E-02
	DNA-directed RNA polymerase III complex	3	7.429	6.01E-02
	FACT complex	2	28.066	6.94E-02
	endocytic vesicle	3	6.647	7.33E-02
	SCAR complex	2	21.050	9.14E-02
	Microtubule	6	2.501	9.15E-02
	ribonucleoprotein complex	10	1.830	9.56E-02
MF	structural constituent of cuticle†	26	5.485	6.70E-12
	nutrient reservoir activity	6	35.863	9.37E-08
	lipid transporter activity	7	19.311	6.35E-07
	RNA binding†	30	2.289	4.53E-05
	structural constituent of collagen and cuticulin-based cuticle	5	13.793	3.42E-04
	hydrolase activity	38	1.563	6.02E-03
	helicase activity	9	3.260	6.19E-03
	RNA helicase activity	6	4.304	1.22E-02
	histone binding	6	4.304	1.22E-02
	ATPase activity	13	2.263	1.23E-02
	isomerase activity	7	3.178	2.23E-02
	protein transmembrane transporter activity	3	9.781	3.59E-02
	mannosyl-oligosaccharide glucosidase activity	2	35.863	5.48E-02
	ATP binding	37	1.338	5.69E-02
	RNA polymerase II core binding	3	6.329	7.95E-02
	transcription factor binding	4	3.775	8.79E-02

Appendix C

Supplemental Data for Chapter 4

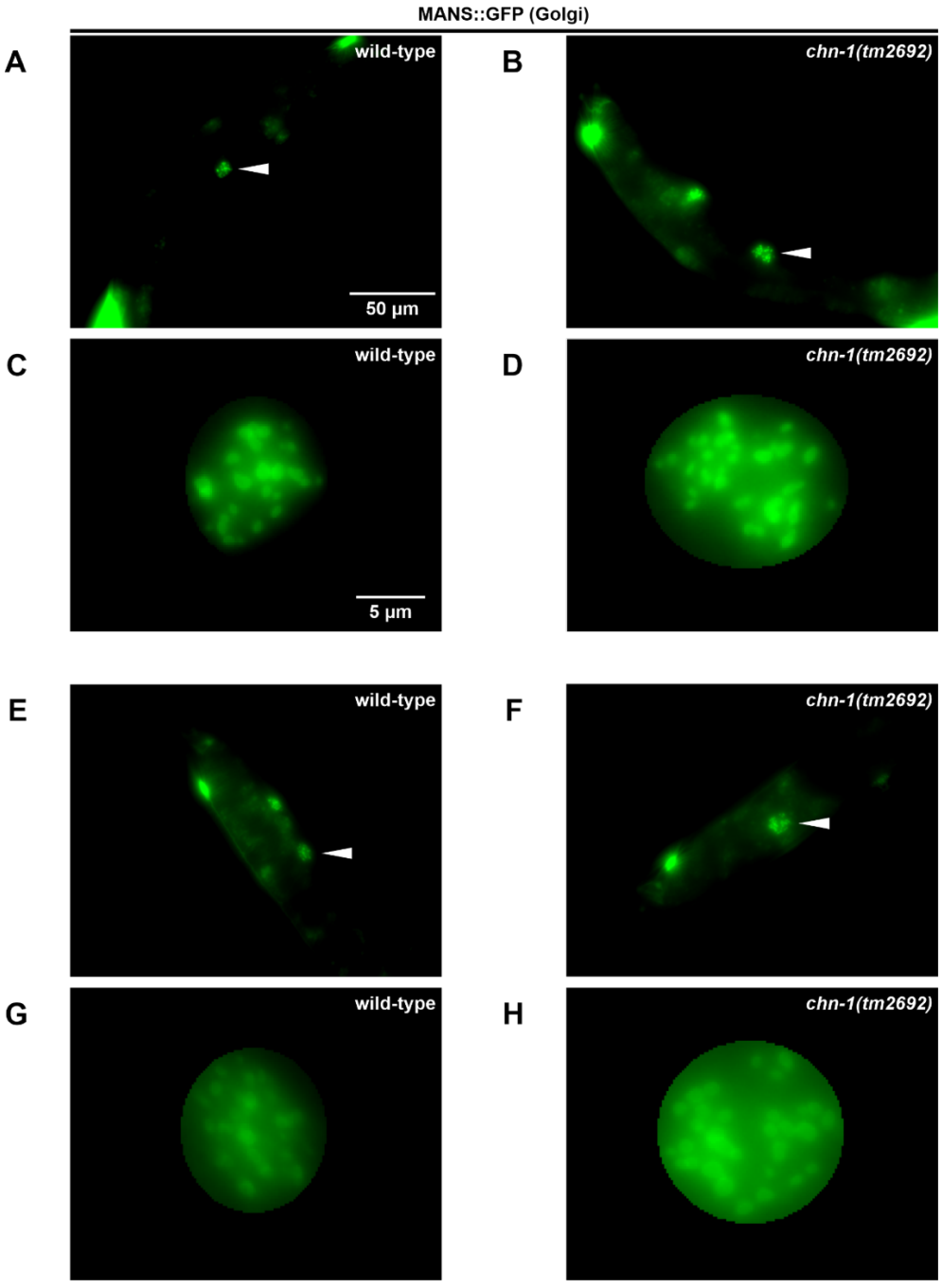

Supplemental Figure C1 **Additional representative confocal images of wild-type and *chn-1(tm2692)* coelomocytes expressing MANS::GFP Golgi markers.** Wild-type: ***A***, ***C***, ***E***, ***G***; *chn-1(tm2692)*: ***B***, ***D***, ***F***, ***H***. Scale bar either 50 µm (***A***) or 5 µm (***C***). Identical experiments repeated *n* = 3 times.

Supplemental Table C1 **Bonferroni-adjusted *p*-values associated with longevity differences in *chn-1* and *sma-9* single- and double-gene mutations.** Data correspond to Figure 4.3, Supplemental Table C2, and Supplemental Table C3.

Replicate	Comparison	Adjusted *p*-Value
1	N2 vs. *chn-1(tm2692)*	1.00E-04
1	N2 vs. *sma-9*	2.30E-06
1	N2 vs. *chn-1(tm2692); sma-9*	0.00E+00
1	*chn-1(tm2692)* vs. *sma-9*	1.00E+00
1	*chn-1(tm2692)* vs. *chn-1(tm2692); sma-9*	4.69E-02
1	*sma-9* vs. *chn-1(tm2692); sma-9*	1.09E-01
2	N2 vs. *chn-1(tm2692)*	6.30E-06
2	N2 vs. *sma-9*	8.30E-06
2	N2 vs. *chn-1(tm2692); sma-9*	0.00E+00
2	*chn-1(tm2692)* vs. *sma-9*	1.00E+00
2	*chn-1(tm2692)* vs. *chn-1(tm2692); sma-9*	7.66E-02
2	*sma-9* vs. *chn-1(tm2692); sma-9*	4.51E-02
3	N2 vs. *chn-1(tm2692)*	5.00E-04
3	N2 vs. *sma-9*	1.10E-05
3	N2 vs. *chn-1(tm2692); sma-9*	0.00E+00
3	*chn-1(tm2692)* vs. *sma-9*	1.00E+00
3	*chn-1(tm2692)* vs. *chn-1(tm2692); sma-9*	8.33E-02
3	*sma-9* vs. *chn-1(tm2692); sma-9*	7.03E-02

Supplemental Table C2 **Restricted mean survival times and final mortalities associated with longevity differences in *chn-1* and *sma-9* single- and double-gene mutations.** Data correspond to Figure 4.3, Supplemental Table C1, and Supplemental Table C3.

Replicate	Group	Restricted Mean Survival Time (Day)	SEM (Day)	Final Mortality (Day)
1	N2	16.35	0.55	28
1	*chn-1(tm2692)*	13.28	0.47	25
1	*sma-9*	12.93	0.44	22
1	*chn-1(tm2692); sma-9*	11.95	0.36	22
2	N2	17.01	0.57	28
2	*chn-1(tm2692)*	13.86	0.46	25
2	*sma-9*	13.91	0.45	25
2	*chn-1(tm2692); sma-9*	12.62	0.35	22
3	N2	16.96	0.37	28
3	*chn-1(tm2692)*	14.22	0.49	22
3	*sma-9*	14.51	0.36	22
3	*chn-1(tm2692); sma-9*	12.71	0.44	25

Supplemental Table C3 **Censored animals when comparing N2 wild-type, *sma-9* mutants, *chn-1* mutants, and *chn-1; sma-9* double-mutants.** Data representing the number of animals censored during each time-point of the assay (of *n* = 128 total animals per strain), including animals that were lost (i.e., likely crawled into the agar between measurements), crawled up the plate walls and desiccated, crawled into the agar, bagged (i.e., exhibited internal progeny hatching), or ruptured. Lifespan experiments were carried out at room temperature, and plates otherwise stored at 20°C. Data correspond to Figure 4.3, Supplemental Table C1, and Supplemental Table C2.

N2, *sma-9* and *chn-1* single & double mutants					
Replicate	**Strain**	**Day**	**Dead**	**Censored**	**Reason**
1	N2	0	0	0	--
1	N2	2	2	21	20 lost, 1 dried out on walls of plate
1	N2	4	1	13	7 lost, 4 dried out on walls of plate, 2 crawled into cracks of agar
1	N2	6	4	3	1 dried out on walls of plate, 2 "bag of worms" phenotype
1	N2	8	3	2	2 crawled into cracks of agar
1	N2	10	5	1	1 ruptured
1	N2	13	15	1	1 ruptured
1	N2	16	20	2	2 ruptured
1	N2	19	15	0	--
1	N2	22	16	0	--
1	N2	25	3	0	--
1	N2	28	1	0	--
1	*chn-1(tm2692)*	0	0	0	--
1	*chn-1(tm2692)*	2	1	23	17 lost, 6 dried out on walls of plate
1	*chn-1(tm2692)*	4	1	9	6 dried out on walls of plate, 3 crawled into cracks of agar
1	*chn-1(tm2692)*	6	4	3	1 dried out on walls of plate, 1 crawled into cracks of agar, 1 "bag of worms" phenotype
1	*chn-1(tm2692)*	8	9	2	2 dried out on walls of plate
1	*chn-1(tm2692)*	10	19	1	1 ruptured
1	*chn-1(tm2692)*	13	24	0	--
1	*chn-1(tm2692)*	16	17	0	--

1	*chn-1(tm2692)*	19	8	0	--
1	*chn-1(tm2692)*	22	6	0	--
1	*chn-1(tm2692)*	25	1	0	--
1	*sma-9*	0	0	0	--
1	*sma-9*	2	1	22	21 lost, 1 dried out on walls of plate
1	*sma-9*	4	4	8	4 lost, 3 dried out on walls of plate, 1 crawled into cracks of agar
1	*sma-9*	6	5	4	1 dried out on walls of plate, 2 crawled into cracks of agar, 1 "bag of worms" phenotype
1	*sma-9*	8	6	0	--
1	*sma-9*	10	17	4	4 ruptured
1	*sma-9*	13	25	0	--
1	*sma-9*	16	23	0	--
1	*sma-9*	19	4	0	--
1	*sma-9*	22	5	0	--
1	*sma-9*chn-1(tm2692)*	0	0	0	--
1	*sma-9*chn-1(tm2692)*	2	1	18	12 lost, 6 dried out on walls of plate
1	*sma-9*chn-1(tm2692)*	4	0	12	5 dried out on walls of plate, 7 crawled into cracks of agar
1	*sma-9*chn-1(tm2692)*	6	6	2	1 dried out on walls of plate, 1 "bag of worms" phenotype
1	*sma-9*chn-1(tm2692)*	8	10	3	3 ruptured
1	*sma-9*chn-1(tm2692)*	10	26	1	1 ruptured
1	*sma-9*chn-1(tm2692)*	13	31	0	--
1	*sma-9*chn-1(tm2692)*	16	13	0	--
1	*sma-9*chn-1(tm2692)*	19	3	0	--
1	*sma-9*chn-1(tm2692)*	22	2	0	--
2	N2	0	0	0	--
2	N2	2	0	24	24 lost
2	N2	4	1	4	4 dried out on walls of plate

2	N2	6	5	3	1 dried out on walls of plate, 1 crawled into cracks of agar, 1 "bag of worms" phenotype
2	N2	8	7	0	--
2	N2	10	3	1	1 crawled into cracks of agar
2	N2	13	16	1	1 ruptured
2	N2	16	12	1	1 ruptured
2	N2	19	21	0	--
2	N2	22	20	0	--
2	N2	25	8	0	--
2	N2	28	1	0	--
2	*chn-1(tm2692)*	0	0	0	--
2	*chn-1(tm2692)*	2	0	39	31 lost, 6 dried out on walls of plate, 2 crawled into cracks of agar
2	*chn-1(tm2692)*	4	1	2	2 dried out on walls of plate
2	*chn-1(tm2692)*	6	1	0	--
2	*chn-1(tm2692)*	8	7	0	--
2	*chn-1(tm2692)*	10	21	0	--
2	*chn-1(tm2692)*	13	17	0	--
2	*chn-1(tm2692)*	16	24	0	--
2	*chn-1(tm2692)*	19	11	0	--
2	*chn-1(tm2692)*	22	3	0	--
2	*chn-1(tm2692)*	25	2	0	--
2	*sma-9*	0	0	0	--
2	*sma-9*	2	1	19	14 lost, 5 dried out on walls of plate
2	*sma-9*	4	1	10	7 dried out on walls of plate, 3 crawled into cracks of agar
2	*sma-9*	6	5	0	--
2	*sma-9*	8	4	2	1 crawled into cracks of agar, 1 ruptured
2	*sma-9*	10	18	0	--
2	*sma-9*	13	26	1	1 crawled into cracks of agar

2	*sma-9*	16	22	1	1 ruptured
2	*sma-9*	19	12	1	1 ruptured
2	*sma-9*	22	3	0	--
2	*sma-9*	25	2	0	--
2	*sma-9*chn-1(tm2692)*	0	0	0	--
2	*sma-9*chn-1(tm2692)*	2	1	2	2 lost
2	*sma-9*chn-1(tm2692)*	4	1	3	3 lost
2	*sma-9*chn-1(tm2692)*	6	6	0	--
2	*sma-9*chn-1(tm2692)*	8	10	6	4 dried out on walls of plate, 1 crawled into cracks of agar, 1 ruptured
2	*sma-9*chn-1(tm2692)*	10	32	0	--
2	*sma-9*chn-1(tm2692)*	13	29	1	1 ruptured
2	*sma-9*chn-1(tm2692)*	16	25	0	--
2	*sma-9*chn-1(tm2692)*	19	10	0	--
2	*sma-9*chn-1(tm2692)*	22	2	0	--
3	N2	0	0	0	--
3	N2	2	0	3	3 lost
3	N2	4	2	0	--
3	N2	6	0	1	1 dried out on walls of plate
3	N2	8	1	0	--
3	N2	10	6	2	2 crawled into cracks of agar
3	N2	13	20	4	4 ruptured
3	N2	16	36	1	1 ruptured
3	N2	19	34	1	1 ruptured
3	N2	22	12	0	--
3	N2	25	4	0	--
3	N2	28	1	0	--
3	*chn-1(tm2692)*	0	0	0	--
3	*chn-1(tm2692)*	2	0	13	12 lost, 1 dried out on walls of plate

3	*chn-1(tm2692)*	4	2	11	3 lost, 7 dried out on walls of plate, 1 crawled into cracks of agar
3	*chn-1(tm2692)*	6	2	9	8 dried out on walls of plate, 1 crawled into cracks of agar
3	*chn-1(tm2692)*	8	10	1	1 ruptured
3	*chn-1(tm2692)*	10	17	0	--
3	*chn-1(tm2692)*	13	19	1	1 ruptured
3	*chn-1(tm2692)*	16	21	1	1 ruptured
3	*chn-1(tm2692)*	19	8	1	1 ruptured
3	*chn-1(tm2692)*	22	12	0	--
3	*sma-9*	0	0	0	--
3	*sma-9*	2	0	5	5 lost
3	*sma-9*	4	0	6	3 lost, 1 dried out on walls of plate, 2 crawled into cracks of agar
3	*sma-9*	6	1	9	5 dried out on walls of plate, 4 crawled into cracks of agar
3	*sma-9*	8	2	3	2 crawled into cracks of agar, 1 ruptured
3	*sma-9*	10	22	3	1 dried out on walls of plate, 2 crawled into cracks of agar
3	*sma-9*	13	28	2	2 ruptured
3	*sma-9*	16	26	0	--
3	*sma-9*	19	15	1	1 ruptured
3	*sma-9*	22	5	0	--
3	*sma-9*chn-1(tm2692)*	0	0	0	--
3	*sma-9*chn-1(tm2692)*	2	2	9	9 lost
3	*sma-9*chn-1(tm2692)*	4	2	1	1 crawled into cracks of agar
3	*sma-9*chn-1(tm2692)*	6	11	1	1 "bag of worms" phenotype
3	*sma-9*chn-1(tm2692)*	8	13	1	1 ruptured
3	*sma-9*chn-1(tm2692)*	10	20	0	--

3	*sma-9*chn-1(tm2692)*	13	28	0	--
3	*sma-9*chn-1(tm2692)*	16	20	0	--
3	*sma-9*chn-1(tm2692)*	19	13	0	--
3	*sma-9*chn-1(tm2692)*	22	6	0	--
3	*sma-9*chn-1(tm2692)*	25	1	0	--

Supplemental Table C4 **Bonferroni-adjusted *p*-values associated with longevity differences in *chn-1(by155)*-null mutants, *chn-1(by155)*-derived *h*CHIP/*Ce*CHIP rescue animals, and *m*Kate controls.** Data correspond to Figure 4.10A and 4.10B, as well as Supplemental Table C5 and Supplemental Table C6.

Replicate	Comparison	Adjusted *p*-Value
1	N2 vs. *chn-1(by155)*	0.00E+00
1	N2 vs. *h*CHIP rescue 1	1.00E+00
1	N2 vs. *h*CHIP rescue 2	6.18E-01
1	N2 vs. *Ce*CHIP rescue	1.94E-01
1	N2 vs. *m*Kate Control	0.00E+00
1	*chn-1(by155)* vs. *h*CHIP rescue 1	2.40E-07
1	*chn-1(by155)* vs. *h*CHIP rescue 2	8.70E-07
1	*chn-1(by155)* vs. *Ce*CHIP rescue	8.60E-08
1	*chn-1(by155)* vs. *m*Kate Control	1.00E+00
1	*h*CHIP rescue 1 vs. *h*CHIP rescue 2	1.00E+00
1	*h*CHIP rescue 1 vs. *Ce*CHIP rescue	1.00E+00
1	*h*CHIP rescue 1 vs. *m*Kate Control	3.20E-08
1	*h*CHIP rescue 2 vs. *Ce*CHIP rescue	1.00E+00
1	*h*CHIP rescue 2 vs. *m*Kate Control	5.10E-07
1	*Ce*CHIP rescue vs. *m*Kate Control	1.70E-07
2	N2 vs. *chn-1(by155)*	3.70E-03
2	N2 vs. *h*CHIP rescue 1	1.00E+00
2	N2 vs. *h*CHIP rescue 2	1.00E+00
2	N2 vs. *Ce*CHIP rescue	1.00E+00
2	N2 vs. *m*Kate Control	8.00E-03
2	*chn-1(by155)* vs. *h*CHIP rescue 1	2.00E-04
2	*chn-1(by155)* vs. *h*CHIP rescue 2	2.30E-05
2	*chn-1(by155)* vs. *Ce*CHIP rescue	1.80E-06
2	*chn-1(by155)* vs. *m*Kate Control	1.00E+00
2	*h*CHIP rescue 1 vs. *h*CHIP rescue 2	1.00E+00
2	*h*CHIP rescue 1 vs. *Ce*CHIP rescue	1.00E+00
2	*h*CHIP rescue 1 vs. *m*Kate Control	5.00E-04
2	*h*CHIP rescue 2 vs. *Ce*CHIP rescue	1.00E+00
2	*h*CHIP rescue 2 vs. *m*Kate Control	1.00E-04
2	*Ce*CHIP rescue vs. *m*Kate Control	2.30E-06
3	N2 vs. *chn-1(by155)*	1.00E+00

3	N2 vs. *h*CHIP rescue 1	6.80E-03
3	N2 vs. *h*CHIP rescue 2	1.10E-05
3	N2 vs. *Ce*CHIP rescue	2.20E-08
3	N2 vs. *m*Kate Control	4.51E-01
3	*chn-1(by155)* vs. *h*CHIP rescue 1	2.37E-02
3	*chn-1(by155)* vs. *h*CHIP rescue 2	3.00E-05
3	*chn-1(by155)* vs. *Ce*CHIP rescue	5.20E-08
3	*chn-1(by155)* vs. *m*Kate Control	1.12E-01
3	*h*CHIP rescue 1 vs. *h*CHIP rescue 2	1.00E+00
3	*h*CHIP rescue 1 vs. *Ce*CHIP rescue	1.62E-01
3	*h*CHIP rescue 1 vs. *m*Kate Control	3.30E-05
3	*h*CHIP rescue 2 vs. *Ce*CHIP rescue	1.00E+00
3	*h*CHIP rescue 2 vs. *m*Kate Control	0.00E+00
3	*Ce*CHIP rescue vs. *m*Kate Control	0.00E+00

Supplemental Table C5 **Restricted mean survival times and final mortalities associated with longevity differences in *chn-1(by155)*-null mutants, *chn-1(by155)*-derived *h*CHIP/*Ce*CHIP rescue animals, and *m*Kate controls.** Data correspond to Figure 4.10A and 4.10B, as well as Supplemental Table C4 and Supplemental Table C6.

Replicate	Group	Restricted Mean Survival Time (Day)	SEM (Day)	Final Mortality (Day)
1	N2	19.93	0.39	28
1	*chn-1(by155)*	15.97	0.32	26
1	*h*CHIP rescue 1	18.93	0.52	30
1	*h*CHIP rescue 2	18.60	0.43	30
1	*Ce*CHIP rescue	18.79	0.37	28
1	*m*Kate Control	15.02	0.43	26
2	N2	18.96	0.48	32
2	*chn-1(by155)*	16.65	0.42	26
2	*h*CHIP rescue 1	19.31	0.47	32
2	*h*CHIP rescue 2	19.56	0.39	30
2	*Ce*CHIP rescue	19.70	0.46	28
2	*m*Kate Control	17.10	0.37	26
3	N2	14.49	0.45	26
3	*chn-1(by155)*	14.91	0.44	26
3	*h*CHIP rescue 1	16.47	0.56	30
3	*h*CHIP rescue 2	17.67	0.56	30
3	*Ce*CHIP rescue	18.60	0.52	30
3	*m*Kate Control	13.41	0.45	24

Supplemental Table C6 **Censored animals when comparing N2 wild-type, *chn-1(by155)* mutants, *chn-1(by155)*-derived *h*CHIP and *Ce*CHIP rescue strains, and *mKate* controls.** Data representing the number of animals censored during each time-point of the assay (of *n* = 128 total animals per strain), including animals that were lost (i.e., likely crawled into the agar between measurements), crawled up the plate walls and desiccated, crawled into the agar, bagged (i.e., exhibited internal progeny hatching), or ruptured. Lifespan experiments were carried out at room temperature, and plates otherwise stored at 20°C. Data correspond to Figure 4.10A and 4.10B, as well as Supplemental Table C4 and Supplemental Table C5.

N2, *chn-1(by155)*, *hCHIP*/Ce*CHIP* Rescues, and *mKate* Controls					
Replicate	**Strain**	**Day**	**Dead**	**Censored**	**Reason**
1	*h*CHIP Rescue 1	0	0	0	--
1	*h*CHIP Rescue 1	2	2	7	7 lost
1	*h*CHIP Rescue 1	4	0	4	1 dried out on walls of plate, 3 crawled into cracks of agar
1	*h*CHIP Rescue 1	6	0	0	--
1	*h*CHIP Rescue 1	8	2	0	--
1	*h*CHIP Rescue 1	10	1	0	--
1	*h*CHIP Rescue 1	12	6	0	--
1	*h*CHIP Rescue 1	14	17	0	--
1	*h*CHIP Rescue 1	16	22	0	--
1	*h*CHIP Rescue 1	18	16	0	--
1	*h*CHIP Rescue 1	20	15	0	--
1	*h*CHIP Rescue 1	22	5	0	--
1	*h*CHIP Rescue 1	24	9	0	--
1	*h*CHIP Rescue 1	26	10	0	--
1	*h*CHIP Rescue 1	28	7	0	--
1	*h*CHIP Rescue 1	30	5	0	--
1	*h*CHIP Rescue 2	0	0	0	--
1	*h*CHIP Rescue 2	2	0	7	5 lost, 2 dried out on walls of plate
1	*h*CHIP Rescue 2	4	0	1	1 crawled into cracks of agar
1	*h*CHIP Rescue 2	6	0	0	--
1	*h*CHIP Rescue 2	8	1	0	--
1	*h*CHIP Rescue 2	10	6	0	--
1	*h*CHIP Rescue 2	12	9	0	--
1	*h*CHIP Rescue 2	14	7	0	--
1	*h*CHIP Rescue 2	16	19	0	--
1	*h*CHIP Rescue 2	18	22	0	--

1	*h*CHIP Rescue 2	20	28	0	--
1	*h*CHIP Rescue 2	22	10	0	--
1	*h*CHIP Rescue 2	24	6	0	--
1	*h*CHIP Rescue 2	26	5	0	--
1	*h*CHIP Rescue 2	28	3	0	--
1	*h*CHIP Rescue 2	30	4	0	--
1	*chn-1* Rescue	0	0	0	--
1	*chn-1* Rescue	2	0	3	3 lost
1	*chn-1* Rescue	4	0	6	6 crawled into cracks of agar
1	*chn-1* Rescue	6	0	0	--
1	*chn-1* Rescue	8	1	7	6 crawled into cracks of agar, 1 "bag of worms" phenotype
1	*chn-1* Rescue	10	1	1	1 ruptured
1	*chn-1* Rescue	12	6	1	1 ruptured
1	*chn-1* Rescue	14	12	0	--
1	*chn-1* Rescue	16	9	0	--
1	*chn-1* Rescue	18	29	0	--
1	*chn-1* Rescue	20	25	0	--
1	*chn-1* Rescue	22	13	0	--
1	*chn-1* Rescue	24	7	0	--
1	*chn-1* Rescue	26	4	0	--
1	*chn-1* Rescue	28	3	0	--
1	*mKate* Control	0	0	0	--
1	*mKate* Control	2	1	3	3 lost
1	*mKate* Control	4	2	2	2 crawled into cracks of agar
1	*mKate* Control	6	0	1	1 "bag of worms" phenotype
1	*mKate* Control	8	12	2	2 ruptured
1	*mKate* Control	10	7	0	--
1	*mKate* Control	12	17	0	--
1	*mKate* Control	14	19	2	2 ruptured
1	*mKate* Control	16	27	0	--
1	*mKate* Control	18	11	0	--
1	*mKate* Control	20	7	0	--
1	*mKate* Control	22	8	0	--
1	*mKate* Control	24	6	0	--
1	*mKate* Control	26	1	0	--
1	*chn-1(by155)*	0	0	0	--

1	*chn-1(by155)*	2	0	2	2 dried out on walls of plate
1	*chn-1(by155)*	4	0	1	1 lost
1	*chn-1(by155)*	6	3	0	--
1	*chn-1(by155)*	8	1	0	--
1	*chn-1(by155)*	10	6	0	--
1	*chn-1(by155)*	12	9	0	--
1	*chn-1(by155)*	14	31	0	--
1	*chn-1(by155)*	16	26	0	--
1	*chn-1(by155)*	18	27	0	--
1	*chn-1(by155)*	20	11	0	--
1	*chn-1(by155)*	22	10	0	--
1	*chn-1(by155)*	24	0	0	--
1	*chn-1(by155)*	26	1	0	--
1	N2	0	0	0	--
1	N2	2	0	11	9 lost, 2 dried out on walls of plate
1	N2	4	0	9	5 dried out on walls of plate, 4 crawled into cracks of agar
1	N2	6	0	0	--
1	N2	8	0	2	2 ruptured
1	N2	10	2	1	1 ruptured
1	N2	12	1	1	1 ruptured
1	N2	14	8	0	--
1	N2	16	15	0	--
1	N2	18	14	0	--
1	N2	20	29	0	--
1	N2	22	9	0	--
1	N2	24	10	0	--
1	N2	26	15	0	--
1	N2	28	1	0	--
2	*h*CHIP Rescue 1	0	0	0	--
2	*h*CHIP Rescue 1	2	0	9	7 lost, 2 dried out on walls of plate
2	*h*CHIP Rescue 1	4	0	1	1 dried out on walls of plate
2	*h*CHIP Rescue 1	6	0	0	--
2	*h*CHIP Rescue 1	8	0	2	2 ruptured
2	*h*CHIP Rescue 1	10	1	0	--
2	*h*CHIP Rescue 1	12	8	0	--

2	*h*CHIP Rescue 1	14	13	0	--
2	*h*CHIP Rescue 1	16	26	0	--
2	*h*CHIP Rescue 1	18	15	0	--
2	*h*CHIP Rescue 1	20	18	0	--
2	*h*CHIP Rescue 1	22	8	0	--
2	*h*CHIP Rescue 1	24	6	0	--
2	*h*CHIP Rescue 1	26	8	0	--
2	*h*CHIP Rescue 1	28	9	0	--
2	*h*CHIP Rescue 1	30	1	0	--
2	*h*CHIP Rescue 1	32	3	0	--
2	*h*CHIP Rescue 2	0	0	0	--
2	*h*CHIP Rescue 2	2	0	13	7 lost, 6 dried out on walls of plate
2	*h*CHIP Rescue 2	4	0	2	2 crawled into cracks of agar
2	*h*CHIP Rescue 2	6	0	0	--
2	*h*CHIP Rescue 2	8	2	1	1 ruptured
2	*h*CHIP Rescue 2	10	0	0	--
2	*h*CHIP Rescue 2	12	5	0	--
2	*h*CHIP Rescue 2	14	7	0	--
2	*h*CHIP Rescue 2	16	6	0	--
2	*h*CHIP Rescue 2	18	30	0	--
2	*h*CHIP Rescue 2	20	34	0	--
2	*h*CHIP Rescue 2	22	11	0	--
2	*h*CHIP Rescue 2	24	2	0	--
2	*h*CHIP Rescue 2	26	6	0	--
2	*h*CHIP Rescue 2	28	8	0	--
2	*h*CHIP Rescue 2	30	1	0	--
2	*chn-1* Rescue	0	0	0	--
2	*chn-1* Rescue	2	2	6	6 dried out on walls of plate
2	*chn-1* Rescue	4	1	2	2 crawled into cracks of agar
2	*chn-1* Rescue	6	0	0	--
2	*chn-1* Rescue	8	0	0	--
2	*chn-1* Rescue	10	0	0	--
2	*chn-1* Rescue	12	7	0	--
2	*chn-1* Rescue	14	15	0	--
2	*chn-1* Rescue	16	3	0	--
2	*chn-1* Rescue	18	20	0	--
2	*chn-1* Rescue	20	20	0	--

2	*chn-1* Rescue	22	21	0	--
2	*chn-1* Rescue	24	16	0	--
2	*chn-1* Rescue	26	7	0	--
2	*chn-1* Rescue	28	8	0	--
2	*mKate* Control	0	0	0	--
2	*mKate* Control	2	0	1	1 dried out on walls of plate
2	*mKate* Control	4	0	6	6 lost
2	*mKate* Control	6	0	2	1 dried out on walls of plate, 1 "bag of worms" phenotype
2	*mKate* Control	8	0	1	1 ruptured
2	*mKate* Control	10	8	1	1 ruptured
2	*mKate* Control	12	8	1	1 ruptured
2	*mKate* Control	14	21	0	--
2	*mKate* Control	16	26	0	--
2	*mKate* Control	18	16	0	--
2	*mKate* Control	20	16	0	--
2	*mKate* Control	22	9	0	--
2	*mKate* Control	24	11	0	--
2	*mKate* Control	26	1	0	--
2	*chn-1(by155)*	0	0	0	--
2	*chn-1(by155)*	2	0	13	9 lost, 4 dried out on walls of plate
2	*chn-1(by155)*	4	0	1	1 dried out on walls of plate
2	*chn-1(by155)*	6	0	0	--
2	*chn-1(by155)*	8	8	3	1 crawled into cracks of agar, 2 ruptured
2	*chn-1(by155)*	10	3	0	--
2	*chn-1(by155)*	12	8	0	--
2	*chn-1(by155)*	14	25	0	--
2	*chn-1(by155)*	16	17	0	--
2	*chn-1(by155)*	18	19	0	--
2	*chn-1(by155)*	20	9	0	--
2	*chn-1(by155)*	22	10	0	--
2	*chn-1(by155)*	24	10	0	--
2	*chn-1(by155)*	26	2	0	--
2	N2	0	0	0	--
2	N2	2	0	11	10 lost, 1 dried out on walls of plate

2	N2	4	0	12	5 dried out on walls of plate, 7 crawled into cracks of agar
2	N2	6	0	0	--
2	N2	8	0	1	1 ruptured
2	N2	10	2	0	--
2	N2	12	6	0	--
2	N2	14	12	0	--
2	N2	16	25	0	--
2	N2	18	14	0	--
2	N2	20	14	0	--
2	N2	22	8	0	--
2	N2	24	12	0	--
2	N2	26	3	0	--
2	N2	28	3	0	--
2	N2	30	3	0	--
2	N2	32	2	0	--
3	*h*CHIP Rescue 1	0	0	0	--
3	*h*CHIP Rescue 1	2	0	0	--
3	*h*CHIP Rescue 1	4	0	2	2 dried out on walls of plate
3	*h*CHIP Rescue 1	6	2	3	1 crawled into cracks of agar, 2 "bag of worms" phenotype
3	*h*CHIP Rescue 1	8	16	1	1 ruptured
3	*h*CHIP Rescue 1	10	7	2	2 ruptured
3	*h*CHIP Rescue 1	12	20	2	2 ruptured
3	*h*CHIP Rescue 1	14	14	2	2 ruptured
3	*h*CHIP Rescue 1	16	1	0	--
3	*h*CHIP Rescue 1	18	9	0	--
3	*h*CHIP Rescue 1	20	19	0	--
3	*h*CHIP Rescue 1	22	14	0	--
3	*h*CHIP Rescue 1	24	4	0	--
3	*h*CHIP Rescue 1	26	4	0	--
3	*h*CHIP Rescue 1	28	3	0	--
3	*h*CHIP Rescue 1	30	3	0	--
3	*h*CHIP Rescue 2	0	0	0	--
3	*h*CHIP Rescue 2	2	0	2	2 dried out on walls of plate
3	*h*CHIP Rescue 2	4	1	0	--

3	*h*CHIP Rescue 2	6	0	3	1 crawled into cracks of agar, 2 "bag of worms" phenotype
3	*h*CHIP Rescue 2	8	13	3	3 ruptured
3	*h*CHIP Rescue 2	10	5	2	2 ruptured
3	*h*CHIP Rescue 2	12	17	0	--
3	*h*CHIP Rescue 2	14	6	0	--
3	*h*CHIP Rescue 2	16	8	0	--
3	*h*CHIP Rescue 2	18	16	0	--
3	*h*CHIP Rescue 2	20	10	0	--
3	*h*CHIP Rescue 2	22	15	0	--
3	*h*CHIP Rescue 2	24	16	0	--
3	*h*CHIP Rescue 2	26	4	0	--
3	*h*CHIP Rescue 2	28	6	0	--
3	*h*CHIP Rescue 2	30	1	0	--
3	*chn-1* Rescue	0	0	0	--
3	*chn-1* Rescue	2	0	0	--
3	*chn-1* Rescue	4	1	1	1 dried out on walls of plate
3	*chn-1* Rescue	6	0	5	2 dried out on walls of plate, 1 crawled into cracks of agar, 2 "bag of worms" phenotype
3	*chn-1* Rescue	8	9	1	1 ruptured
3	*chn-1* Rescue	10	4	1	1 ruptured
3	*chn-1* Rescue	12	7	1	1 ruptured
3	*chn-1* Rescue	14	11	0	--
3	*chn-1* Rescue	16	11	0	--
3	*chn-1* Rescue	18	24	0	--
3	*chn-1* Rescue	20	6	0	--
3	*chn-1* Rescue	22	12	0	--
3	*chn-1* Rescue	24	17	0	--
3	*chn-1* Rescue	26	12	0	--
3	*chn-1* Rescue	28	4	0	--
3	*chn-1* Rescue	30	1	0	--
3	*mKate* Control	0	0	0	--
3	*mKate* Control	2	0	1	1 lost
3	*mKate* Control	4	2	4	4 dried out on walls of plate
3	*mKate* Control	6	5	1	1 "bag of worms" phenotype

3	*mKate* Control	8	24	4	4 ruptured
3	*mKate* Control	10	17	1	1 ruptured
3	*mKate* Control	12	8	0	--
3	*mKate* Control	14	17	0	--
3	*mKate* Control	16	15	0	--
3	*mKate* Control	18	12	0	--
3	*mKate* Control	20	7	0	--
3	*mKate* Control	22	7	0	--
3	*mKate* Control	24	3	0	--
3	*chn-1(by155)*	0	0	0	--
3	*chn-1(by155)*	2	0	0	--
3	*chn-1(by155)*	4	2	2	2 dried out on walls of plate
3	*chn-1(by155)*	6	4	0	--
3	*chn-1(by155)*	8	7	0	--
3	*chn-1(by155)*	10	24	0	--
3	*chn-1(by155)*	12	5	0	--
3	*chn-1(by155)*	14	23	0	--
3	*chn-1(by155)*	16	14	0	--
3	*chn-1(by155)*	18	23	0	--
3	*chn-1(by155)*	20	7	0	--
3	*chn-1(by155)*	22	10	0	--
3	*chn-1(by155)*	24	6	0	--
3	*chn-1(by155)*	26	1	0	--
3	N2	0	0	0	--
3	N2	2	1	1	1 lost
3	N2	4	1	0	--
3	N2	6	3	1	1 dried out on walls of plate
3	N2	8	10	2	1 crawled into cracks of agar, 1 ruptured
3	N2	10	17	3	3 crawled into cracks of agar
3	N2	12	23	3	3 ruptured
3	N2	14	19	1	1 ruptured
3	N2	16	4	0	--
3	N2	18	13	0	--
3	N2	20	16	0	--
3	N2	22	4	0	--
3	N2	24	4	0	--
3	N2	26	2	0	--

Supplemental Table C7 **Bonferroni-adjusted *p*-values associated with longevity differences in *chn-1(tm2692)*-null mutants, *chn-1(tm2692)*-derived *h*CHIP/*Ce*CHIP rescue animals, and *m*Kate controls.** Data correspond to Figure 4.10C and 4.10D, as well as Supplemental Table C8 and Supplemental Table C9.

Replicate	Comparison	Adjusted *p*-Value
1	N2 vs. *chn-1(by155)*	0.00E+00
1	N2 vs. *h*CHIP rescue 1	2.23E-01
1	N2 vs. *h*CHIP rescue 2	1.00E+00
1	N2 vs. *Ce*CHIP rescue	1.00E+00
1	N2 vs. *m*Kate Control	5.20E-08
1	*chn-1(by155)* vs. *h*CHIP rescue 1	0.00E+00
1	*chn-1(by155)* vs. *h*CHIP rescue 2	0.00E+00
1	*chn-1(by155)* vs. *Ce*CHIP rescue	2.50E-08
1	*chn-1(by155)* vs. *m*Kate Control	5.75E-01
1	*h*CHIP rescue 1 vs. *h*CHIP rescue 2	6.58E-01
1	*h*CHIP rescue 1 vs. *Ce*CHIP rescue	1.00E+00
1	*h*CHIP rescue 1 vs. *m*Kate Control	0.00E+00
1	*h*CHIP rescue 2 vs. *Ce*CHIP rescue	1.00E+00
1	*h*CHIP rescue 2 vs. *m*Kate Control	5.20E-07
1	*Ce*CHIP rescue vs. *m*Kate Control	5.40E-06
2	N2 vs. *chn-1(by155)*	0.00E+00
2	N2 vs. *h*CHIP rescue 1	1.00E+00
2	N2 vs. *h*CHIP rescue 2	1.00E+00
2	N2 vs. *Ce*CHIP rescue	1.00E+00
2	N2 vs. *m*Kate Control	0.00E+00
2	*chn-1(by155)* vs. *h*CHIP rescue 1	0.00E+00
2	*chn-1(by155)* vs. *h*CHIP rescue 2	0.00E+00
2	*chn-1(by155)* vs. *Ce*CHIP rescue	0.00E+00
2	*chn-1(by155)* vs. *m*Kate Control	1.00E+00
2	*h*CHIP rescue 1 vs. *h*CHIP rescue 2	1.00E+00
2	*h*CHIP rescue 1 vs. *Ce*CHIP rescue	1.00E+00
2	*h*CHIP rescue 1 vs. *m*Kate Control	0.00E+00
2	*h*CHIP rescue 2 vs. *Ce*CHIP rescue	1.00E+00
2	*h*CHIP rescue 2 vs. *m*Kate Control	0.00E+00
2	*Ce*CHIP rescue vs. *m*Kate Control	0.00E+00
3	N2 vs. *chn-1(by155)*	0.00E+00
3	N2 vs. *h*CHIP rescue 1	1.20E-03
3	N2 vs. *h*CHIP rescue 2	1.00E+00
3	N2 vs. *Ce*CHIP rescue	7.79E-01
3	N2 vs. *m*Kate Control	0.00E+00
3	*chn-1(by155)* vs. *h*CHIP rescue 1	4.20E-03
3	*chn-1(by155)* vs. *h*CHIP rescue 2	0.00E+00
3	*chn-1(by155)* vs. *Ce*CHIP rescue	1.40E-07
3	*chn-1(by155)* vs. *m*Kate Control	8.55E-02
3	*h*CHIP rescue 1 vs. *h*CHIP rescue 2	2.29E-02
3	*h*CHIP rescue 1 vs. *Ce*CHIP rescue	8.95E-02
3	*h*CHIP rescue 1 vs. *m*Kate Control	5.50E-08

3	*h*CHIP rescue 2 vs. *Ce*CHIP rescue	1.00E+00
3	*h*CHIP rescue 2 vs. *m*Kate Control	0.00E+00
3	*Ce*CHIP rescue vs. *m*Kate Control	0.00E+00

Supplemental Table C8 **Restricted mean survival times and final mortalities associated with longevity differences in *chn-1(tm2692)*-null mutants, *chn-1(tm2692)*-derived *h*CHIP/*Ce*CHIP rescue animals, and *m*Kate controls.** Data correspond to Figure 4.10C and 4.10D, as well as Supplemental Table C7 and Supplemental Table C9.

Replicate	Group	Restricted Mean Survival Time (Day)	SEM (Day)	Final Mortality (Day)
1	N2	20.02	0.35	30
1	*chn-1(by155)*	16.80	0.26	24
1	*h*CHIP rescue 1	20.35	0.48	32
1	*h*CHIP rescue 2	20.01	0.40	32
1	*Ce*CHIP rescue	19.74	0.57	30
1	*m*Kate Control	17.25	0.30	24
2	N2	19.75	0.51	30
2	*chn-1(by155)*	16.53	0.25	24
2	*h*CHIP rescue 1	19.90	0.43	28
2	*h*CHIP rescue 2	20.77	0.37	32
2	*Ce*CHIP rescue	20.09	0.41	28
2	*m*Kate Control	15.80	0.35	24
3	N2	16.55	0.41	22
3	*chn-1(by155)*	13.26	0.34	24
3	*h*CHIP rescue 1	14.93	0.36	30
3	*h*CHIP rescue 2	16.19	0.42	28
3	*Ce*CHIP rescue	16.04	0.43	26
3	*m*Kate Control	12.12	0.33	24

Supplemental Table C9 **Censored animals when comparing N2 wild-type, *chn-1(tm2692)* mutants, *chn-1(tm2692)*-derived *h*CHIP and *Ce*CHIP rescue strains, and *mKate* controls.** Data representing the number of animals censored during each time-point of the assay (of *n* = 123-139 total animals per strain), including animals that were lost (i.e., likely crawled into the agar between measurements), crawled up the plate walls and desiccated, crawled into the agar, bagged (i.e., exhibited internal progeny hatching), or ruptured. Lifespan experiments were carried out at room temperature, and plates otherwise stored at 20°C. Data correspond to Figure 4.10C and 4.10D, as well as Supplemental Table C7 and Supplemental Table C8.

N2, *chn-1(tm2692)*, *h*CHIP/*Ce*CHIP Rescues, and *mKate* Controls					
Replicate	**Strain**	**Day**	**Dead**	**Censored**	**Reason**
1	*h*CHIP Rescue 1	0	0	0	--
1	*h*CHIP Rescue 1	2	0	4	3 lost, 1 dried out on walls of plate
1	*h*CHIP Rescue 1	4	0	1	1 dried out on walls of plate
1	*h*CHIP Rescue 1	6	0	1	1 "bag of worms" phenotype
1	*h*CHIP Rescue 1	8	0	2	1 crawled into cracks of agar, 1 ruptured
1	*h*CHIP Rescue 1	10	4	1	1 ruptured
1	*h*CHIP Rescue 1	12	9	1	1 ruptured
1	*h*CHIP Rescue 1	14	10	0	--
1	*h*CHIP Rescue 1	16	8	0	--
1	*h*CHIP Rescue 1	18	17	0	--
1	*h*CHIP Rescue 1	20	15	0	--
1	*h*CHIP Rescue 1	22	12	0	--
1	*h*CHIP Rescue 1	24	17	0	--
1	*h*CHIP Rescue 1	26	15	0	--
1	*h*CHIP Rescue 1	28	8	0	--
1	*h*CHIP Rescue 1	30	2	0	--
1	*h*CHIP Rescue 1	32	1	0	--
1	*h*CHIP Rescue 2	0	0	0	--
1	*h*CHIP Rescue 2	2	0	14	14 lost
1	*h*CHIP Rescue 2	4	0	11	11 lost
1	*h*CHIP Rescue 2	6	0	4	4 dried out on walls of plate
1	*h*CHIP Rescue 2	8	0	3	2 crawled into cracks of agar, 1 ruptured
1	*h*CHIP Rescue 2	10	1	1	1 ruptured

1	*h*CHIP Rescue 2	12	4	1	1 ruptured
1	*h*CHIP Rescue 2	14	5	0	--
1	*h*CHIP Rescue 2	16	6	0	--
1	*h*CHIP Rescue 2	18	19	0	--
1	*h*CHIP Rescue 2	20	22	0	--
1	*h*CHIP Rescue 2	22	23	0	--
1	*h*CHIP Rescue 2	24	6	0	--
1	*h*CHIP Rescue 2	26	3	0	--
1	*h*CHIP Rescue 2	28	3	0	--
1	*h*CHIP Rescue 2	30	1	0	--
1	*h*CHIP Rescue 2	32	1	0	--
1	*chn-1* Rescue	0	0	0	--
1	*chn-1* Rescue	2	0	39	38 lost, 1 dried out on walls of plate
1	*chn-1* Rescue	4	0	8	8 lost
1	*chn-1* Rescue	6	1	0	--
1	*chn-1* Rescue	8	1	0	--
1	*chn-1* Rescue	10	1	0	--
1	*chn-1* Rescue	12	7	0	--
1	*chn-1* Rescue	14	7	0	--
1	*chn-1* Rescue	16	3	1	1 ruptured
1	*chn-1* Rescue	18	12	1	1 ruptured
1	*chn-1* Rescue	20	15	0	--
1	*chn-1* Rescue	22	11	0	--
1	*chn-1* Rescue	24	10	0	--
1	*chn-1* Rescue	26	4	0	--
1	*chn-1* Rescue	28	6	0	--
1	*chn-1* Rescue	30	1	0	--
1	*mKate* Control	0	0	0	--
1	*mKate* Control	2	0	1	1 dried out on walls of plate
1	*mKate* Control	4	0	3	3 crawled into cracks of agar
1	*mKate* Control	6	1	0	--
1	*mKate* Control	8	1	2	2 ruptured
1	*mKate* Control	10	1	1	1 ruptured
1	*mKate* Control	12	3	0	--
1	*mKate* Control	14	16	4	4 ruptured
1	*mKate* Control	16	46	0	--
1	*mKate* Control	18	15	0	--

1	*mKate* Control	20	20	0	--
1	*mKate* Control	22	6	0	--
1	*mKate* Control	24	8	0	--
1	*chn-1(tm2692)*	0	0	0	--
1	*chn-1(tm2692)*	2	0	14	14 lost
1	*chn-1(tm2692)*	4	0	1	1 dried out on walls of plate
1	*chn-1(tm2692)*	6	0	0	--
1	*chn-1(tm2692)*	8	0	0	--
1	*chn-1(tm2692)*	10	1	0	--
1	*chn-1(tm2692)*	12	2	0	--
1	*chn-1(tm2692)*	14	31	0	--
1	*chn-1(tm2692)*	16	34	0	--
1	*chn-1(tm2692)*	18	20	0	--
1	*chn-1(tm2692)*	20	16	0	--
1	*chn-1(tm2692)*	22	5	0	--
1	*chn-1(tm2692)*	24	4	0	--
1	N2	0	0	0	--
1	N2	2	0	0	--
1	N2	4	0	10	2 lost, 8 dried out on walls of plate
1	N2	6	0	9	2 dried out on walls of plate, 4 crawled into cracks of agar, 3 "bag of worms" phenotype
1	N2	8	0	0	--
1	N2	10	0	3	3 ruptured
1	N2	12	8	2	2 ruptured
1	N2	14	4	0	--
1	N2	16	6	1	1 ruptured
1	N2	18	11	2	2 ruptured
1	N2	20	31	0	--
1	N2	22	24	0	--
1	N2	24	13	0	--
1	N2	26	2	0	--
1	N2	28	1	0	--
1	N2	30	1	0	--
2	*h*CHIP Rescue 1	0	0	0	--

2	*h*CHIP Rescue 1	2	0	11	10 lost, 1 dried out on walls of plate
2	*h*CHIP Rescue 1	4	0	1	1 dried out on walls of plate
2	*h*CHIP Rescue 1	6	0	0	--
2	*h*CHIP Rescue 1	8	1	0	--
2	*h*CHIP Rescue 1	10	6	0	--
2	*h*CHIP Rescue 1	12	3	0	--
2	*h*CHIP Rescue 1	14	5	0	--
2	*h*CHIP Rescue 1	16	15	0	--
2	*h*CHIP Rescue 1	18	20	0	--
2	*h*CHIP Rescue 1	20	15	0	--
2	*h*CHIP Rescue 1	22	19	0	--
2	*h*CHIP Rescue 1	24	9	0	--
2	*h*CHIP Rescue 1	26	22	0	--
2	*h*CHIP Rescue 1	28	1	0	--
2	*h*CHIP Rescue 2	0	0	0	--
2	*h*CHIP Rescue 2	2	0	9	7 lost, 2 dried out on walls of plate
2	*h*CHIP Rescue 2	4	0	1	1 lost
2	*h*CHIP Rescue 2	6	0	1	1 crawled into cracks of agar
2	*h*CHIP Rescue 2	8	0	3	1 crawled into cracks of agar, 2 ruptured
2	*h*CHIP Rescue 2	10	2	1	1 ruptured
2	*h*CHIP Rescue 2	12	2	1	1 ruptured
2	*h*CHIP Rescue 2	14	6	0	--
2	*h*CHIP Rescue 2	16	7	0	--
2	*h*CHIP Rescue 2	18	11	0	--
2	*h*CHIP Rescue 2	20	29	0	--
2	*h*CHIP Rescue 2	22	31	0	--
2	*h*CHIP Rescue 2	24	11	0	--
2	*h*CHIP Rescue 2	26	4	0	--
2	*h*CHIP Rescue 2	28	7	0	--
2	*h*CHIP Rescue 2	30	1	0	--
2	*h*CHIP Rescue 2	32	1	0	--
2	*chn-1* Rescue	0	0	0	--
2	*chn-1* Rescue	2	0	3	1 lost, 2 dried out on walls of plate
2	*chn-1* Rescue	4	0	9	9 lost

2	*chn-1* Rescue	6	0	1	1 "bag of worms" phenotype
2	*chn-1* Rescue	8	0	0	--
2	*chn-1* Rescue	10	0	0	--
2	*chn-1* Rescue	12	9	0	--
2	*chn-1* Rescue	14	10	0	--
2	*chn-1* Rescue	16	7	0	--
2	*chn-1* Rescue	18	19	0	--
2	*chn-1* Rescue	20	21	0	--
2	*chn-1* Rescue	22	18	0	--
2	*chn-1* Rescue	24	16	0	--
2	*chn-1* Rescue	26	6	0	--
2	*chn-1* Rescue	28	9	0	--
2	*mKate* Control	0	0	0	--
2	*mKate* Control	2	0	14	11 lost, 3 dried out on walls of plate
2	*mKate* Control	4	0	2	2 dried out on walls of plate
2	*mKate* Control	6	2	1	1 ruptured
2	*mKate* Control	8	2	1	1 ruptured
2	*mKate* Control	10	7	0	--
2	*mKate* Control	12	13	0	--
2	*mKate* Control	14	18	0	--
2	*mKate* Control	16	27	0	--
2	*mKate* Control	18	19	0	--
2	*mKate* Control	20	14	0	--
2	*mKate* Control	22	7	0	--
2	*mKate* Control	24	1	0	--
2	*chn-1(tm2692)*	0	0	0	--
2	*chn-1(tm2692)*	2	0	3	3 lost
2	*chn-1(tm2692)*	4	0	0	--
2	*chn-1(tm2692)*	6	0	1	1 "bag of worms" phenotype
2	*chn-1(tm2692)*	8	0	2	1 crawled into cracks of agar, 1 ruptured
2	*chn-1(tm2692)*	10	0	8	2 dried out on walls of plate, 6 ruptured
2	*chn-1(tm2692)*	12	11	2	2 ruptured
2	*chn-1(tm2692)*	14	21	9	9 ruptured
2	*chn-1(tm2692)*	16	30	0	--

2	*chn-1(tm2692)*	18	23	0	--
2	*chn-1(tm2692)*	20	14	0	--
2	*chn-1(tm2692)*	22	3	0	--
2	*chn-1(tm2692)*	24	1	0	--
2	N2	0	0	0	--
2	N2	2	0	6	6 lost
2	N2	4	0	0	--
2	N2	6	0	1	1 crawled into cracks of agar
2	N2	8	1	1	1 ruptured
2	N2	10	3	0	--
2	N2	12	13	0	--
2	N2	14	9	0	--
2	N2	16	13	0	--
2	N2	18	15	0	--
2	N2	20	22	0	--
2	N2	22	10	0	--
2	N2	24	13	0	--
2	N2	26	7	0	--
2	N2	28	1	0	--
2	N2	30	13	0	--
3	*h*CHIP Rescue 1	0	0	0	--
3	*h*CHIP Rescue 1	2	0	9	9 lost
3	*h*CHIP Rescue 1	4	1	0	--
3	*h*CHIP Rescue 1	6	1	3	2 dried out on walls of plate, 1 ruptured
3	*h*CHIP Rescue 1	8	11	0	--
3	*h*CHIP Rescue 1	10	10	1	1 ruptured
3	*h*CHIP Rescue 1	12	10	0	--
3	*h*CHIP Rescue 1	14	28	0	--
3	*h*CHIP Rescue 1	16	29	2	2 ruptured
3	*h*CHIP Rescue 1	18	17	0	--
3	*h*CHIP Rescue 1	20	11	0	--
3	*h*CHIP Rescue 1	22	5	0	--
3	*h*CHIP Rescue 1	24	0	0	--
3	*h*CHIP Rescue 1	26	0	0	--
3	*h*CHIP Rescue 1	28	0	0	--
3	*h*CHIP Rescue 1	30	1	0	--
3	*h*CHIP Rescue 2	0	0	0	--

3	*h*CHIP Rescue 2	2	0	9	8 lost, 1 dried out on walls of plate
3	*h*CHIP Rescue 2	4	1	4	1 dried out on walls of plate, 3 crawled into cracks of agar
3	*h*CHIP Rescue 2	6	4	2	2 crawled into cracks of agar
3	*h*CHIP Rescue 2	8	7	0	--
3	*h*CHIP Rescue 2	10	5	0	--
3	*h*CHIP Rescue 2	12	6	0	--
3	*h*CHIP Rescue 2	14	14	0	--
3	*h*CHIP Rescue 2	16	16	0	--
3	*h*CHIP Rescue 2	18	31	0	--
3	*h*CHIP Rescue 2	20	18	0	--
3	*h*CHIP Rescue 2	22	9	0	--
3	*h*CHIP Rescue 2	24	0	0	--
3	*h*CHIP Rescue 2	26	1	0	--
3	*h*CHIP Rescue 2	28	1	0	--
3	*chn-1* Rescue	0	0	0	--
3	*chn-1* Rescue	2	2	14	7 lost, 7 dried out on walls of plate
3	*chn-1* Rescue	4	1	10	10 dried out on walls of plate
3	*chn-1* Rescue	6	4	4	3 crawled into cracks of agar, 1 "bag of worms" phenotype
3	*chn-1* Rescue	8	0	1	1 ruptured
3	*chn-1* Rescue	10	6	1	1 ruptured
3	*chn-1* Rescue	12	3	1	1 ruptured
3	*chn-1* Rescue	14	12	0	--
3	*chn-1* Rescue	16	15	0	--
3	*chn-1* Rescue	18	35	0	--
3	*chn-1* Rescue	20	8	0	--
3	*chn-1* Rescue	22	5	0	--
3	*chn-1* Rescue	24	0	0	--
3	*chn-1* Rescue	26	1	0	--
3	*mKate* Control	0	0	0	--
3	*mKate* Control	2	2	8	8 lost
3	*mKate* Control	4	3	2	2 dried out on walls of plate

3	*mKate* Control	6	6	1	1 ruptured
3	*mKate* Control	8	7	0	--
3	*mKate* Control	10	25	0	--
3	*mKate* Control	12	34	0	--
3	*mKate* Control	14	20	0	--
3	*mKate* Control	16	15	0	--
3	*mKate* Control	18	7	0	--
3	*mKate* Control	20	2	0	--
3	*mKate* Control	22	0	0	--
3	*mKate* Control	24	1	0	--
3	*chn-1(tm2692)*	0	0	0	--
3	*chn-1(tm2692)*	2	1	10	1 lost, 9 dried out on walls of plate
3	*chn-1(tm2692)*	4	1	3	1 dried out on walls of plate, 2 "bag of worms" phenotype
3	*chn-1(tm2692)*	6	2	2	2 ruptured
3	*chn-1(tm2692)*	8	6	1	1 ruptured
3	*chn-1(tm2692)*	10	23	0	--
3	*chn-1(tm2692)*	12	27	0	--
3	*chn-1(tm2692)*	14	10	0	--
3	*chn-1(tm2692)*	16	22	0	--
3	*chn-1(tm2692)*	18	17	0	--
3	*chn-1(tm2692)*	20	2	0	--
3	*chn-1(tm2692)*	22	0	0	--
3	*chn-1(tm2692)*	24	1	0	--
3	N2	0	0	0	--
3	N2	2	2	9	9 lost
3	N2	4	2	9	8 dried out on walls of plate, 1 crawled into cracks of agar
3	N2	6	1	0	--
3	N2	8	5	0	--
3	N2	10	3	1	1 ruptured
3	N2	12	4	3	3 ruptured
3	N2	14	11	0	--
3	N2	16	17	0	--
3	N2	18	25	0	--
3	N2	20	28	0	--

3	N2	22	7	0	--

Supplemental Table C10 **Rescued proteins (based on fold change) identified by SWATH-MS that are either over- or under-represented in *h*CHIP rescue strain 1 processed by lysis with CHAPS/urea-based lysis buffer.** Each protein listed below met the fold change cutoff criteria of either ≤ 0.67 or ≥ 1.5 compared to *chn-1(tm2692) C. elegans chn-1* mutants in *h*CHIP rescue strain 1. Initially, a reference list was created comparing N2 wild-type worms and *chn-1* mutants. Proteins differentially expressed in opposite directions from wild-type to knock-out animals and knock-out to rescue strains were defined as "rescued". Associated genes for each protein are listed in Supplemental Table C16.

	***chn-1(tm2692)* vs. N2**		***h*CHIP rescue 1 vs. *chn-1(tm2692)***	
Protein	***p*-Value**	**Fold Change**	***p*-Value**	**Fold Change**
Putative zinc finger matrin-type protein snu-23	1.15E-01	0.155	1.67E-01	5.650
Dual specificity mitogen-activated protein kinase kinase sek-1	1.24E-03	0.150	6.15E-03	4.148
C2 domain-containing protein	4.54E-03	0.255	6.36E-03	3.478
START domain-containing protein	2.18E-01	0.553	2.06E-02	3.312
Prolyl carboxy peptidase like protein 5	7.42E-04	0.251	1.05E-03	3.302
Putative cuticle collagen 80	1.45E-03	0.336	1.65E-02	3.190
Multifunctional methyltransferase subunit TRM112-like protein	4.32E-03	0.321	4.72E-03	3.079
Uncharacterized protein C56G2.3	1.41E-02	0.405	5.74E-03	2.909
Small RNA 2'-O-methyltransferase	1.16E-01	0.415	1.16E-01	2.757
PUM-HD domain-containing protein	1.27E-01	0.293	2.53E-01	2.677
Nucleolar protein 9	1.13E-01	0.361	3.71E-02	2.551
Glutathione peroxidase 3	7.36E-03	0.332	5.03E-02	2.463
RNA helicase	6.46E-05	0.241	3.37E-03	2.454
Helicase SKI2W	3.77E-02	0.383	5.24E-02	2.433
3'-5' exonuclease domain-containing protein	5.89E-06	0.312	4.55E-04	2.299
DNA-directed RNA polymerase subunit beta	6.49E-02	0.366	1.64E-01	2.123
Phosphatidate cytidylyltransferase, mitochondrial	1.86E-03	0.303	5.56E-02	2.092
N-acetyltransferase domain-containing protein	6.68E-03	0.313	4.31E-02	2.085
Uncharacterized protein	3.56E-02	0.334	9.59E-02	2.078
UBX domain-containing protein 6	7.80E-02	0.281	1.39E-01	2.051
Cysteine protease atg-4.1	2.80E-02	0.403	5.58E-02	2.030
L-serine ammonia-lyase	6.68E-02	0.644	4.07E-03	2.029
39S ribosomal protein L55, mitochondrial	3.60E-02	0.522	1.84E-02	2.028
GRounDhog	4.76E-02	0.416	7.20E-02	2.024

N-alpha-acetyltransferase 20	2.36E-02	0.521	1.47E-02	2.024
Domain of unknown function DX domain-containing protein	6.77E-02	0.524	4.78E-02	2.019
Putative pyridoxal kinase	1.62E-01	0.627	3.82E-02	2.015
m7GpppX diphosphatase	7.84E-02	0.628	9.61E-03	2.011
Anaphase-promoting complex subunit 4-like WD40 domain-containing protein	7.30E-02	0.522	6.71E-02	1.944
Probable urocanate hydratase	1.33E-01	0.640	3.15E-02	1.906
Myosin IA	9.07E-03	0.451	3.70E-02	1.873
DeHydrogenases, Short chain	1.69E-02	0.519	2.20E-02	1.869
Apple domain-containing protein	1.35E-01	0.657	2.88E-02	1.868
COP9 signalosome complex subunit 2	6.85E-03	0.464	4.15E-03	1.853
Large ribosomal subunit protein bL17m	7.18E-03	0.440	4.23E-02	1.828
Probable glutamine synthetase	2.62E-01	0.432	4.28E-01	1.827
Sjogren's syndrome/scleroderma autoantigen 1	1.60E-01	0.606	9.44E-02	1.822
Saposin B-type domain-containing protein	1.29E-01	0.568	1.11E-01	1.813
DNA replication licensing factor MCM7	3.60E-04	0.534	7.24E-04	1.803
Aldehyde dehydrogenase domain-containing protein	7.34E-02	0.438	6.70E-02	1.782
Peptidase S28	6.77E-02	0.343	3.35E-01	1.773
Tudor domain-containing protein	2.90E-01	0.639	4.38E-01	1.761
High mobility group protein hmg-12	3.84E-02	0.532	6.55E-02	1.749
Protein male abnormal 7	1.74E-01	0.571	2.26E-01	1.746
Ribosomal protein S6 kinase beta	2.57E-01	0.652	1.46E-01	1.738
Glycolipid transfer protein domain-containing protein	5.46E-02	0.636	2.23E-02	1.724
Dymeclin	8.02E-02	0.560	6.26E-02	1.723
Uncharacterized Golgi apparatus membrane protein-like protein C34D4.4	3.29E-02	0.331	2.84E-01	1.721
Cytochrome c oxidase assembly protein COX20, mitochondrial	3.18E-01	0.669	1.64E-01	1.714
CMP/dCMP-type deaminase domain-containing protein	3.18E-02	0.477	1.17E-01	1.702
EB domain-containing protein	1.28E-01	0.429	4.27E-01	1.679
C-type lectin domain-containing protein	4.61E-01	0.660	4.58E-01	1.671
Nematode cuticle collagen N-terminal domain-containing protein	1.01E-02	0.331	2.16E-01	1.669
Putative choline-phosphate cytidylyltransferase	1.27E-01	0.609	1.18E-01	1.662
Nucleotidyl transferase domain-containing protein	3.65E-02	0.564	3.60E-02	1.659
Retinoid-inducible serine carboxypeptidase	9.50E-03	0.575	1.71E-02	1.657
JmjC domain-containing protein	8.46E-02	0.363	1.87E-01	1.646
DUF3945 domain-containing protein	1.47E-03	0.552	9.06E-03	1.637

Intestinal acid PHOsphatase	1.61E-01	0.571	1.39E-01	1.624
Probable 26S proteasome non-ATPase regulatory subunit 9	2.32E-01	0.602	2.82E-01	1.623
Large ribosomal subunit protein mL51	1.38E-02	0.502	7.92E-02	1.586
Tubby protein homolog 1	7.94E-04	0.262	2.38E-01	1.564
Ubiquinone biosynthesis monooxygenase COQ6, mitochondrial	7.49E-03	0.521	5.86E-02	1.563
Probable pyruvate dehydrogenase acetyl-transferring kinase, mitochondrial	2.08E-01	0.663	1.74E-01	1.559
Glycoside hydrolase family 1 protein	1.17E-02	0.390	2.22E-01	1.558
Patched-related protein 18	3.67E-02	0.640	3.83E-02	1.555
PUA domain-containing protein	2.44E-01	0.639	2.58E-01	1.544
Probable peptidyl-tRNA hydrolase 2	2.51E-02	0.540	1.13E-01	1.536
Small-subunit processome Utp12 domain-containing protein	2.48E-02	0.592	6.57E-02	1.528
DUF148 domain-containing protein	2.84E-01	0.529	4.74E-01	1.528
Sperm-specific class P protein 34	1.74E-01	0.610	2.29E-01	1.517
Splicing factor U2AF 35 kDa subunit	7.81E-02	0.619	1.29E-01	1.506
Elongin-C	7.28E-02	0.658	9.40E-02	1.506
Serine/threonine-protein phosphatase 4 catalytic subunit 1	4.60E-03	0.473	1.09E-01	1.505
Acireductone dioxygenase	1.61E-01	0.663	1.30E-01	1.504
UDP-N-acetylglucosamine/UDP-N-acetylgalactosamine transporter nstp-4	7.97E-03	1.737	4.00E-02	0.669
Kunitz/Bovine pancreatic trypsin inhibitor domain protein	1.28E-01	1.917	3.63E-01	0.667
Ubiquitin-conjugating enzyme E2 1	1.51E-03	2.709	1.72E-01	0.665
Long chain fatty acid elongase 2	9.59E-02	1.799	2.41E-01	0.665
Excitatory amino acid transporter	3.41E-01	1.780	4.08E-01	0.665
Large ribosomal subunit protein uL10m	9.55E-04	2.516	1.22E-01	0.662
Vacuolar protein-sorting-associated protein 25	1.24E-03	3.711	1.66E-01	0.662
Nucleoside-diphosphatase uda-1	2.68E-01	1.557	2.27E-01	0.661
Probable RNA methyltransferase Y17G7B.18		1.593		0.654
Nematode cuticle collagen N-terminal domain-containing protein	1.13E-02	3.810	3.98E-01	0.654
Translocon-associated protein subunit gamma	6.86E-03	1.887	5.75E-02	0.649
Odorant response abnormal protein 4	2.43E-01	1.703	2.41E-01	0.647
J domain-containing protein	4.66E-02	1.760	1.15E-01	0.643
Retinol dehydrogenase 13	2.66E-02	1.858	1.03E-01	0.640
Nicalin	6.05E-02	1.591	6.97E-02	0.639
cystathionine gamma-lyase	1.12E-01	1.645	1.31E-01	0.637
ABC transmembrane type-1 domain-containing protein	1.53E-02	1.776	4.28E-02	0.636

V-type proton ATPase 21 kDa proteolipid subunit c"	2.95E-03	1.947	3.46E-02	0.634
Huntington interacting protein related 1	3.89E-02	1.874	1.29E-01	0.634
Casein kinase I gamma	8.50E-02	1.987	1.92E-01	0.632
Charged multivesicular body protein 1b	4.63E-02	2.353	2.67E-01	0.628
BTB domain-containing protein	3.60E-01	1.895	5.01E-01	0.626
DeHydrogenases, Short chain	2.73E-02	1.837	8.28E-02	0.625
CRAL-TRIO domain-containing protein	2.13E-01	2.203	5.92E-01	0.624
Delta 12 fatty acid desaturase fat-2	2.21E-03	1.884	1.84E-02	0.624
Glucuronosyltransferase	2.41E-01	1.565	9.14E-02	0.620
Large ribosomal subunit protein mL52	1.72E-01	2.357	4.11E-01	0.617
LITAF domain-containing protein	1.29E-02	2.281	1.30E-01	0.616
Ectopic P granules protein 3	1.39E-01	1.777	2.07E-01	0.614
Warthog protein 1	7.60E-02	2.755	3.83E-01	0.614
SOSS complex subunit A homolog	2.18E-02	1.679	2.98E-02	0.613
Acyl-coenzyme A diphosphatase FITM2	9.14E-02	1.590	7.32E-02	0.610
Large ribosomal subunit protein uL5A	1.91E-01	2.109	5.02E-01	0.608
Acyltransferase 3 domain-containing protein	3.21E-02	1.837	7.40E-02	0.605
Probable manganese-transporting ATPase catp-8	1.51E-02	1.799	3.53E-02	0.604
Trimeric intracellular cation channel type 1B.1	2.00E-01	1.648	1.80E-01	0.593
DnaJ homolog dnj-2	1.69E-01	1.663	1.38E-01	0.592
Sidoreflexin	1.28E-01	1.774	8.79E-02	0.591
NADH-ubiquinone oxidoreductase chain 1	6.61E-03	2.661	1.27E-01	0.591
Probable glycerol-3-phosphate acyltransferase, mitochondrial	2.46E-02	1.940	7.91E-02	0.588
Rab5-interacting protein	1.00E-01	1.584	5.38E-02	0.582
Putative aquaporin-10	3.25E-02	2.186	1.07E-01	0.577
NAD-capped RNA hydrolase ndx-9	2.11E-01	1.606	1.47E-01	0.576
Epoxide hydrolase	9.93E-03	3.231	3.04E-01	0.574
Putative endoplasmic reticulum metallopeptidase 1-A	4.26E-03	2.060	2.28E-02	0.571
Metaxin-1 homolog	4.95E-02	2.351	1.88E-01	0.570
Cytochrome c oxidase subunit 2	9.21E-05	2.961	2.35E-02	0.563
Surfeit locus protein 4 homolog	3.73E-04	2.311	7.94E-03	0.552
Cytochrome b	4.29E-02	2.039	8.87E-02	0.552
Histone H4	8.95E-04	2.137	6.55E-03	0.548
Glucuronosyltransferase	1.64E-01	1.700	1.15E-01	0.546
Long chain fatty acid elongase 5	4.62E-02	1.758	2.61E-03	0.545
DeHydrogenases, Short chain	1.74E-01	1.729	1.25E-01	0.536
Glycoside hydrolase 35 catalytic domain-containing protein	9.91E-02	1.676	4.84E-02	0.535

CaDmium Responsive	9.41E-02	1.750	7.36E-02	0.533
Probable mitochondrial pyruvate carrier 1	2.36E-01	1.771	1.86E-01	0.528
Putative 1-acyl-sn-glycerol-3-phosphate acyltransferase acl-1	1.23E-02	2.247	4.38E-02	0.527
ATP synthase subunit a	3.51E-06	2.645	7.03E-04	0.527
CaDmium Responsive	5.10E-02	2.078	8.26E-02	0.524
Bestrophin homolog 14	8.51E-02	2.555	2.23E-01	0.524
EGF-like domain-containing protein	1.17E-02	1.698	2.30E-03	0.522
Fungal lipase-like domain-containing protein	2.36E-01	1.812	2.43E-01	0.520
Ragulator complex protein LAMTOR2 homolog	1.28E-02	2.820	9.93E-02	0.510
Large ribosomal subunit protein uL5B	2.61E-01	2.074	3.68E-01	0.507
Uncharacterized protein	1.14E-01	1.980	1.00E-01	0.491
Fatty acid-binding protein homolog 4	3.61E-01	1.830	2.80E-01	0.489
EOG090X04TT	1.76E-02	3.330	1.30E-01	0.475
DUF19 domain-containing protein	2.26E-04	2.541	2.19E-03	0.474
Putative UDP-glucuronosyltransferase ugt-46	1.38E-01	1.654	2.96E-02	0.470
Carnitine O-palmitoyltransferase	2.34E-02	2.261	3.42E-02	0.469
G-patch domain-containing protein	1.59E-01	2.187	2.26E-01	0.462
Dolichyl-diphosphooligosaccharide--protein glycosyltransferase subunit 2	1.14E-01	1.561	5.69E-02	0.462
TOG domain-containing protein	3.05E-01	1.512	3.25E-02	0.453
Pyr_redox_2 domain-containing protein	2.48E-01	1.898	1.46E-01	0.444
Histidine-rich glycoprotein-like	1.49E-01	2.006	9.26E-02	0.442
Tubulin beta chain	7.08E-02	2.884	1.58E-01	0.442
Uncharacterized protein	1.07E-01	1.850	2.71E-02	0.438
NADH-ubiquinone oxidoreductase chain 3	8.49E-05	4.685	8.71E-03	0.417
Iron-sulfur clusters transporter ABCB7, mitochondrial	3.88E-05	2.969	2.66E-04	0.406
CRAL-TRIO domain-containing protein	1.21E-01	2.166	4.67E-02	0.396
Uncharacterized protein C29G2.6	2.80E-01	1.743	6.29E-02	0.365
Rab8	2.90E-02	2.048	2.26E-03	0.358
Uncharacterized protein D2096.6	5.25E-04	7.109	4.59E-02	0.350
Endoplasmic reticulum lectin 1	2.16E-01	1.953	4.42E-02	0.349
RRM domain-containing protein	1.74E-02	4.434	1.01E-01	0.322
Proton-coupled zinc antiporter SLC30A5	1.85E-02	3.438	2.54E-02	0.311
ER membrane protein complex subunit 3	5.76E-02	2.813	2.57E-03	0.302
Nematode cuticle collagen N-terminal domain-containing protein	9.08E-04	5.093	7.09E-03	0.299
NADH-ubiquinone oxidoreductase chain 5	8.07E-04	5.576	1.11E-02	0.287
Heat shock 70 kDa protein 13	4.51E-02	2.223	1.92E-03	0.263
Putative metallophosphoesterase F40B5.2	3.06E-01	2.752	4.84E-02	0.251

Long chain fatty acid elongase 6	4.64E-02	2.798	8.78E-03	0.250
BPTI/Kunitz inhibitor domain-containing protein	2.14E-01	1.861	1.48E-02	0.232
mRNA stability protein	2.05E-02	2.732	7.71E-03	0.069

Supplemental Table C11 **Rescued proteins (based on fold change) identified by SWATH-MS that are either over- or under-represented in *h*CHIP rescue strain 2 processed by lysis with CHAPS/urea-based lysis buffer.** Each protein listed below met the fold change cutoff criteria of either ≤ 0.67 or ≥ 1.5 compared to *chn-1(tm2692) C. elegans chn-1* mutants in *h*CHIP rescue strain 2. Initially, a reference list was created comparing N2 wild-type worms and *chn-1* mutants. Proteins differentially expressed in opposite directions from wild-type to knock-out animals and knock-out to rescue strains were defined as “rescued”. Associated genes for each protein are listed in Supplemental Table C17.

	***chn-1(tm2692)* vs. N2**		***h*CHIP rescue 2 vs. *chn-1(tm2692)***	
Protein	***p*-Value**	**Fold Change**	***p*-Value**	**Fold Change**
Dehydrogenase/reductase SDR family member 4	2.10E-01	0.451	2.70E-02	4.242
N-acetyltransferase domain-containing protein	6.68E-03	0.313	5.31E-03	4.040
RNA helicase	6.46E-05	0.241	1.74E-04	3.731
Tubby protein homolog 1	7.94E-04	0.262	4.87E-03	3.017
DNA-directed RNA polymerase subunit beta	6.49E-02	0.366	5.38E-02	2.866
PUM-HD domain-containing protein	1.27E-01	0.293	1.91E-01	2.731
Saposin B-type domain-containing protein	1.29E-01	0.568	1.04E-02	2.694
3'-5' exonuclease domain-containing protein	5.89E-06	0.312	1.23E-04	2.543
Prolyl carboxy peptidase like protein 5	7.42E-04	0.251	1.02E-02	2.489
Aldehyde dehydrogenase domain-containing protein	7.34E-02	0.438	8.85E-03	2.435
Probable glutamine synthetase	2.62E-01	0.432	2.68E-01	2.349
Serine/threonine-protein phosphatase PP1-gamma	1.17E-02	0.234	8.04E-02	2.330
Uncharacterized Golgi apparatus membrane protein-like protein C34D4.4	3.29E-02	0.331	1.03E-01	2.304
Glycoside hydrolase family 1 protein	1.17E-02	0.390	2.69E-02	2.270
Uncharacterized protein	3.56E-02	0.334	1.55E-01	2.260
Serine/threonine-protein phosphatase 4 catalytic subunit 1	4.60E-03	0.473	2.52E-03	2.233
Sjogren's syndrome/scleroderma autoantigen 1	1.60E-01	0.606	3.27E-02	2.176
Cysteine protease atg-4.1	2.80E-02	0.403	3.92E-02	2.152
Intestinal acid PHOsphatase	1.61E-01	0.571	3.39E-02	2.122
Protein male abnormal 7	1.74E-01	0.571	7.55E-02	2.097

Cytochrome c oxidase assembly protein COX20, mitochondrial	3.18E-01	0.669	2.08E-01	2.076
Putative choline-phosphate cytidylyltransferase	1.27E-01	0.609	2.80E-02	2.072
EB domain-containing protein	6.09E-02	0.199	4.14E-01	2.071
L-serine ammonia-lyase	6.68E-02	0.644	3.96E-03	2.034
Myosin IA	9.07E-03	0.451	2.17E-02	2.002
Small RNA 2'-O-methyltransferase	1.16E-01	0.415	2.04E-01	2.001
Putative pyrroline-5-carboxylate reductase 4	1.05E-01	0.549	7.93E-02	1.984
Ubiquitin fusion degradation protein 1 homolog	5.18E-03	0.530	2.99E-03	1.974
Probable peptidyl-tRNA hydrolase 2	2.51E-02	0.540	1.57E-02	1.949
Methyltransferase BUD23	1.08E-01	0.669	1.14E-02	1.921
39S ribosomal protein L55, mitochondrial	3.60E-02	0.522	4.82E-02	1.910
Probable urocanate hydratase	1.33E-01	0.640	3.13E-02	1.907
Nucleolar protein 9	1.13E-01	0.361	1.60E-01	1.883
Glyceraldehyde-3-phosphate dehydrogenase 1	4.68E-01	0.612	3.55E-01	1.877
Putative zinc finger matrin-type protein snu-23	1.15E-01	0.155	5.57E-01	1.861
Putative cuticle collagen 80	1.45E-03	0.336	1.03E-01	1.856
Serum response factor-binding protein 1	1.30E-01	0.477	2.55E-01	1.854
Probable pyruvate dehydrogenase acetyl-transferring kinase, mitochondrial	2.08E-01	0.663	6.34E-02	1.850
COP9 signalosome complex subunit 2	6.85E-03	0.464	9.37E-03	1.818
Protein transport protein sec-16A.1	9.72E-02	0.664	1.97E-02	1.807
Phosphoinositide phospholipase C	7.26E-03	0.391	1.16E-01	1.779
VWFA domain-containing protein	1.80E-01	0.494	2.76E-01	1.767
DUF3945 domain-containing protein	1.47E-03	0.552	3.00E-03	1.766
Ribosomal protein S6 kinase beta	2.57E-01	0.652	1.37E-01	1.761
C-type lectin domain-containing protein	2.01E-01	0.502	2.94E-01	1.757
Cobalamin adenosyltransferase-like domain-containing protein	1.46E-02	0.464	6.97E-02	1.746
Putative pyridoxal kinase	1.62E-01	0.627	9.91E-02	1.738
Putative thiosulfate sulfurtransferase mpst-4	1.82E-01	0.654	9.26E-02	1.714
Ubiquinone biosynthesis monooxygenase COQ6, mitochondrial	7.49E-03	0.521	3.42E-02	1.656
m7GpppX diphosphatase	7.84E-02	0.628	6.13E-02	1.642
C-factor	2.92E-02	0.622	2.60E-02	1.625
Dymeclin	8.02E-02	0.560	1.12E-01	1.624
VWFA domain-containing protein	1.79E-01	0.619	1.78E-01	1.618
RING-type E3 ubiquitin transferase	3.38E-01	0.635	3.11E-01	1.617
WD_REPEATS_REGION domain-containing protein	4.15E-01	0.645	3.53E-01	1.607
Periplasmic protein	2.09E-01	0.627	2.07E-01	1.600
Glutathione peroxidase 1	5.26E-05	0.401	2.15E-02	1.595

Glutathione peroxidase 3	7.36E-03	0.332	2.37E-01	1.586
CaLponIn-liKe proteins	3.94E-01	0.655	3.56E-01	1.582
DeHydrogenases, Short chain	1.69E-02	0.519	8.72E-02	1.581
SUPpressor	1.38E-02	0.433	1.66E-01	1.574
Small ribosomal subunit protein mS31	1.51E-02	0.613	2.37E-02	1.573
Patched-related protein 18	3.67E-02	0.640	3.69E-02	1.561
Peptidase S28	6.77E-02	0.343	4.29E-01	1.556
Phosphatidate cytidylyltransferase, mitochondrial	1.86E-03	0.303	2.06E-01	1.550
Suppressor of forked domain-containing protein	7.55E-02	0.196	5.84E-01	1.548
Uncharacterized protein C56G2.3	1.41E-02	0.405	2.72E-01	1.536
MO25-like protein 2	7.10E-02	0.666	5.82E-02	1.533
Uridine and thymidine phosphorylase	3.02E-02	0.630	4.45E-02	1.531
COP9 signalosome complex subunit 1	4.44E-02	0.571	1.23E-01	1.528
Domain of unknown function DX domain-containing protein	6.77E-02	0.524	2.24E-01	1.527
UBX domain-containing protein 6	7.80E-02	0.281	2.98E-01	1.523
Large ribosomal subunit protein bL9m	1.79E-01	0.620	2.36E-01	1.522
GRounDhog	4.76E-02	0.416	2.70E-01	1.522
Elongator complex protein 4	4.94E-02	0.548	1.91E-01	1.520
arginine kinase	3.04E-01	0.621	3.64E-01	1.520
Secretory carrier-associated membrane protein	6.29E-02	0.489	2.19E-01	1.519
High mobility group protein hmg-12	3.84E-02	0.532	1.66E-01	1.518
Serine protease inhibitor swm-1	1.41E-01	0.503	3.51E-01	1.515
CMP/dCMP-type deaminase domain-containing protein	3.18E-02	0.477	1.98E-01	1.514
Nose resistant to fluoxetine protein 5	1.22E-01	0.487	3.67E-01	1.512
Nudix hydrolase domain-containing protein	3.24E-02	1.595	6.12E-02	0.666
ER membrane protein complex subunit 3	5.76E-02	2.813	2.81E-01	0.664
RRM domain-containing protein	1.74E-02	4.434	4.69E-01	0.661
Cytochrome c oxidase subunit 2	9.21E-05	2.961	9.24E-02	0.658
Mitochondrial glutamate carrier 1	3.10E-01	1.527	2.43E-01	0.657
Dolichyl-diphosphooligosaccharide--protein glycosyltransferase subunit 2	1.14E-01	1.561	1.19E-01	0.653
UDP-N-acetylglucosamine/UDP-N-acetylgalactosamine transporter nstp-4	7.97E-03	1.737	2.91E-02	0.652
Acyl-coenzyme A diphosphatase FITM2	9.14E-02	1.590	8.80E-02	0.650
Probable rho GDP-dissociation inhibitor	1.08E-01	1.534	2.27E-01	0.649
Brix domain-containing protein ZK795.3	9.15E-02	1.532	1.93E-01	0.642
V-type proton ATPase 21 kDa proteolipid subunit c''	2.95E-03	1.947	3.68E-02	0.638
Nucleolar protein 6	2.18E-01	1.659	2.69E-01	0.636

Endoplasmic reticulum-Golgi intermediate compartment protein 3	2.40E-01	1.576	1.65E-02	0.628
Odorant response abnormal protein 4	2.43E-01	1.703	1.72E-01	0.628
Nematode cuticle collagen N-terminal domain-containing protein	8.44E-02	2.419	3.10E-01	0.628
Epoxide hydrolase	9.93E-03	3.231	3.13E-01	0.627
Translocon-associated protein subunit gamma	6.86E-03	1.887	4.07E-02	0.626
Rab5-interacting protein	1.00E-01	1.584	9.64E-02	0.625
DUF19 domain-containing protein	2.26E-04	2.541	4.29E-02	0.625
Sidoreflexin	1.28E-01	1.774	1.67E-01	0.623
Cytochrome b	4.29E-02	2.039	1.68E-01	0.619
Strictosidine synthase conserved region domain-containing protein	2.41E-01	1.525	9.14E-02	0.619
Ribosome production factor 2 homolog	8.66E-03	1.731	1.85E-02	0.615
Long chain fatty acid elongase 2	9.59E-02	1.799	1.63E-01	0.614
LITAF domain-containing protein	1.29E-02	2.281	1.25E-01	0.611
CaDmium Responsive	5.10E-02	2.078	1.80E-01	0.610
DOMON domain-containing protein	2.45E-01	1.514	2.02E-01	0.610
Membrane magnesium transporter	3.45E-02	1.851	7.67E-02	0.600
UDP-glucuronosyltransferase	1.89E-01	1.651	1.79E-01	0.598
Putative UDP-glucuronosyltransferase ugt-46	1.38E-01	1.654	1.19E-01	0.588
NADH-ubiquinone oxidoreductase chain 1	6.61E-03	2.661	1.23E-01	0.588
Fatty acid amide hydrolase 1	5.13E-02	1.518	2.02E-01	0.585
Glucuronosyltransferase	2.41E-01	1.565	1.95E-01	0.584
Mannosyl-oligosaccharide 1,2-alpha-mannosidase mans-2	8.47E-02	1.573	4.23E-02	0.584
J domain-containing protein	4.66E-02	1.760	5.36E-02	0.579
Metaxin-1 homolog	4.95E-02	2.351	1.85E-01	0.567
Ectopic P granules protein 3	1.39E-01	1.777	1.43E-01	0.567
Nicalin	6.05E-02	1.591	2.32E-02	0.566
Exosome complex component RRP45	6.58E-02	1.708	7.13E-02	0.560
Putative endoplasmic reticulum metallopeptidase 1-A	4.26E-03	2.060	1.75E-02	0.556
Uncharacterized protein	1.07E-01	1.850	1.39E-01	0.554
DeHydrogenases, Short chain	2.73E-02	1.837	3.11E-02	0.553
Histone H4	8.95E-04	2.137	7.31E-03	0.553
tRNA guanine 26-N2-dimethyltransferase	2.84E-01	1.538	1.03E-01	0.549
Choline/ethanolaminephosphotransferase 1-like	1.81E-01	2.375	3.47E-01	0.549
Glycoside hydrolase 35 catalytic domain-containing protein	9.91E-02	1.676	3.68E-02	0.545
DNA replication licensing factor mcm-6	1.92E-01	2.753	3.82E-01	0.537
C6 domain-containing protein	1.69E-01	1.861	1.66E-01	0.535

Surfeit locus protein 4 homolog	3.73E-04	2.311	5.44E-03	0.535
Diminuto-like protein	3.33E-03	2.030	6.84E-03	0.525
Fungal lipase-like domain-containing protein	2.36E-01	1.812	1.99E-01	0.525
SOSS complex subunit A homolog	2.18E-02	1.679	1.91E-03	0.522
DeHydrogenases, Short chain	1.74E-01	1.729	8.76E-02	0.512
Charged multivesicular body protein 1b	4.63E-02	2.353	1.13E-01	0.511
Probable manganese-transporting ATPase catp-8	1.51E-02	1.799	5.78E-03	0.510
LEM protein 2	1.33E-01	2.300	1.04E-01	0.510
DnaJ homolog dnj-2	1.69E-01	1.663	5.83E-02	0.510
ER membrane protein complex subunit 7 homolog	3.21E-01	1.828	4.07E-01	0.509
Retinol dehydrogenase 13	2.66E-02	1.858	1.61E-02	0.508
U3 small nucleolar ribonucleoprotein protein MPP10	1.09E-01	1.985	1.36E-01	0.506
CRAL-TRIO domain-containing protein	2.13E-01	2.203	3.03E-01	0.505
Cleft lip and palate transmembrane protein 1 homolog	1.28E-01	1.539	2.80E-02	0.496
Lipid scramblase CLPTM1L	1.26E-01	2.336	1.47E-01	0.488
CHCH domain-containing protein	9.69E-02	2.123	9.56E-02	0.487
Endoplasmic reticulum lectin 1	2.16E-01	1.953	1.54E-01	0.485
Tetratricopeptide repeat protein 38	2.01E-02	2.477	5.95E-02	0.483
Heat shock 70 kDa protein 13	4.51E-02	2.223	6.28E-02	0.477
Carnitine O-palmitoyltransferase	2.34E-02	2.261	3.68E-02	0.474
NADH-ubiquinone oxidoreductase chain 3	8.49E-05	4.685	2.42E-03	0.474
Splicing factor 3B subunit 6-like protein	1.73E-01	1.533	7.94E-03	0.468
Bestrophin homolog 14	8.51E-02	2.555	1.70E-01	0.468
Delta 12 fatty acid desaturase fat-2	2.21E-03	1.884	3.55E-04	0.467
NAD-capped RNA hydrolase ndx-9	2.11E-01	1.606	1.07E-01	0.464
NADH-ubiquinone oxidoreductase chain 4	9.18E-04	5.196	4.85E-02	0.464
BPTI/Kunitz inhibitor domain-containing protein	2.14E-01	1.861	1.06E-01	0.463
Long chain fatty acid elongase 5	4.62E-02	1.758	9.13E-04	0.463
Iron-sulfur clusters transporter ABCB7, mitochondrial	3.88E-05	2.969	1.35E-03	0.458
Kunitz/Bovine pancreatic trypsin inhibitor domain protein	1.28E-01	1.917	6.69E-02	0.455
Protein KRI1 homolog	1.00E-01	1.893	7.52E-02	0.455
Dynactin subunit 5	3.41E-02	1.773	1.90E-02	0.449
Nematode cuticle collagen N-terminal domain-containing protein	1.13E-02	3.810	1.15E-01	0.447
C3H1-type domain-containing protein	3.20E-02	3.298	1.40E-01	0.446
Acyltransferase 3 domain-containing protein	3.21E-02	1.837	5.12E-03	0.445

Nematode cuticle collagen N-terminal domain-containing protein	9.08E-04	5.093	5.77E-02	0.442
Uncharacterized protein	1.14E-01	1.980	5.74E-02	0.436
ATP synthase subunit a	3.51E-06	2.645	1.78E-05	0.430
DUF155 domain-containing protein	2.14E-01	1.571	2.55E-03	0.427
DUF3598 domain-containing protein	5.01E-02	2.270	2.43E-02	0.426
Excitatory amino acid transporter	3.41E-01	1.780	8.43E-02	0.422
Fatty acid-binding protein homolog 4	3.61E-01	1.830	1.78E-01	0.407
NADH-ubiquinone oxidoreductase chain 5	8.07E-04	5.576	6.06E-02	0.407
Large ribosomal subunit protein uL5B	2.61E-01	2.074	1.68E-01	0.406
Putative metallophosphoesterase F40B5.2	3.06E-01	2.752	2.51E-01	0.405
hydroxyacylglutathione hydrolase	3.72E-01	1.956	1.72E-01	0.405
Long chain fatty acid elongase 6	4.64E-02	2.798	6.69E-02	0.390
Putative 1-acyl-sn-glycerol-3-phosphate acyltransferase acl-1	1.23E-02	2.247	3.09E-03	0.376
EOG090X04TT	1.76E-02	3.330	4.76E-02	0.372
Probable mitochondrial pyruvate carrier 1	2.36E-01	1.771	3.95E-02	0.364
EGF-like domain-containing protein	1.17E-02	1.698	7.47E-06	0.361
Large ribosomal subunit protein uL5A	1.91E-01	2.109	9.30E-02	0.355
Multidrug resistance protein mrp-7	5.81E-01	1.685	2.75E-01	0.352
Putative aquaporin-10	3.25E-02	2.186	1.71E-03	0.313
TOG domain-containing protein	3.05E-01	1.512	6.69E-03	0.308
RRM domain-containing protein	1.22E-01	2.850	6.10E-02	0.271
Proton-coupled zinc antiporter SLC30A5	1.85E-02	3.438	1.08E-02	0.223
Arf-GAP domain-containing protein	5.95E-02	3.655	2.00E-02	0.211
Uncharacterized protein D2096.6	5.25E-04	7.109	2.01E-03	0.181

Supplemental Table C12 **Rescued proteins (based on fold change) identified by SWATH-MS that are either over- or under-represented in the *Ce*CHIP rescue strain processed by lysis with CHAPS/urea-based lysis buffer.** Each protein listed below met the fold change cutoff criteria of either ≤ 0.67 or ≥ 1.5 compared to *chn-1(tm2692) C. elegans chn-1* mutants in the *Ce*CHIP rescue strain. Initially, a reference list was created comparing N2 wild-type worms and *chn-1* mutants. Proteins differentially expressed in opposite directions from wild-type to knock-out animals and knock-out to rescue strains were defined as "rescued". Associated genes for each protein are listed in Supplemental Table C18.

	***chn-1(tm2692)* vs. N2**		***Ce*CHIP rescue vs. *chn-1(tm2692)***	
Protein	***p*-Value**	**Fold Change**	***p*-Value**	**Fold Change**
PUM-HD domain-containing protein	1.27E-01	0.293	1.06E-01	4.641
Aldehyde dehydrogenase domain-containing protein	7.34E-02	0.438	1.50E-04	4.417
Probable glutamine synthetase	2.62E-01	0.432	8.15E-02	4.045
Serine/threonine-protein phosphatase PP1-gamma	1.17E-02	0.234	1.13E-02	3.623
C-type lectin domain-containing protein	2.01E-01	0.502	3.34E-02	3.243
Small RNA 2'-O-methyltransferase	1.16E-01	0.415	3.00E-02	3.219
RNA helicase	6.46E-05	0.241	6.59E-04	3.035
RING-type E3 ubiquitin transferase	3.38E-01	0.635	3.33E-02	2.948
Protein BCCIP homolog	4.50E-01	0.625	9.30E-02	2.910
Uncharacterized Golgi apparatus membrane protein-like protein C34D4.4	3.29E-02	0.331	5.47E-02	2.694
Myosin IA	9.07E-03	0.451	1.99E-03	2.605
DNA-directed RNA polymerase subunit beta	6.49E-02	0.366	8.52E-02	2.550
Uncharacterized protein	3.56E-02	0.334	2.49E-01	2.352
Putative choline-phosphate cytidylyltransferase	1.27E-01	0.609	1.13E-02	2.343
Uncharacterized protein C56G2.3	1.41E-02	0.405	2.80E-02	2.303
3'-5' exonuclease domain-containing protein	5.89E-06	0.312	5.21E-04	2.275
Tubby protein homolog 1	7.94E-04	0.262	3.68E-02	2.233
Probable urocanate hydratase	1.33E-01	0.640	8.85E-03	2.213
Serum response factor-binding protein 1	1.30E-01	0.477	1.11E-01	2.182
Gamma-soluble NSF attachment protein	3.65E-01	0.504	3.21E-01	2.163
FeS cluster biogenesis domain-containing protein	1.14E-01	0.579	5.67E-02	2.068
CaLponIn-liKe proteins	3.94E-01	0.655	1.63E-01	2.012
Small subunit of serine palmitoyltransferase	3.56E-01	0.494	2.71E-01	1.994
GRounDhog	4.76E-02	0.416	8.03E-02	1.982
Dymeclin	8.02E-02	0.560	4.31E-02	1.969
Nucleolar protein 9	1.13E-01	0.361	1.28E-01	1.947

m7GpppX diphosphatase	7.84E-02	0.628	1.72E-02	1.894
FACT complex subunit ssrp1-B	1.13E-01	0.496	1.62E-01	1.849
Serine protease inhibitor swm-1	1.41E-01	0.503	2.00E-01	1.815
Probable peptidyl-tRNA hydrolase 2	2.51E-02	0.540	3.24E-02	1.798
Ubiquinone biosynthesis monooxygenase COQ6, mitochondrial	7.49E-03	0.521	1.57E-02	1.789
Patched-related protein 18	3.67E-02	0.640	7.59E-03	1.786
DUF148 domain-containing protein	2.84E-01	0.529	3.74E-01	1.695
Cobalamin adenosyltransferase-like domain-containing protein	1.46E-02	0.464	9.14E-02	1.676
High mobility group protein hmg-12	3.84E-02	0.532	9.00E-02	1.671
COP9 signalosome complex subunit 2	6.85E-03	0.464	1.13E-02	1.652
Calcium-transporting ATPase	3.41E-02	0.619	2.87E-02	1.643
Small ribosomal subunit protein mS31	1.51E-02	0.613	1.37E-02	1.643
Anaphase-promoting complex subunit 4-like WD40 domain-containing protein	7.30E-02	0.522	1.70E-01	1.635
Glycoside hydrolase family 1 protein	1.17E-02	0.390	1.96E-01	1.634
Elongin-C	7.28E-02	0.658	3.78E-02	1.629
FErroChelatase-Like	2.26E-01	0.611	2.14E-01	1.624
L-serine ammonia-lyase	6.68E-02	0.644	5.76E-02	1.614
Glycolipid transfer protein domain-containing protein	5.46E-02	0.636	4.44E-02	1.607
mRNA-decapping enzyme 1	7.82E-02	0.496	2.34E-01	1.599
Probable ubiquitin-conjugating enzyme E2 7	5.95E-02	0.539	1.49E-01	1.594
C-factor	2.92E-02	0.622	3.31E-02	1.589
Glutathione peroxidase 1	5.26E-05	0.401	2.39E-02	1.581
Peptidase S28	6.77E-02	0.343	4.40E-01	1.580
Seryl-tRNA synthetase	5.17E-01	0.649	3.80E-01	1.578
Suppressor of forked domain-containing protein	7.55E-02	0.196	5.83E-01	1.564
Complex 1 LYR protein domain-containing protein	1.35E-02	0.521	8.26E-02	1.562
Prolyl carboxy peptidase like protein 5	7.42E-04	0.251	1.96E-01	1.559
Large ribosomal subunit protein bL17m	7.18E-03	0.440	1.39E-01	1.540
Ribosomal protein S6 kinase beta	2.57E-01	0.652	2.55E-01	1.537
N-alpha-acetyltransferase 20	2.36E-02	0.521	1.30E-01	1.537
COP9 signalosome complex subunit 1	4.44E-02	0.571	1.18E-01	1.536
Serine/threonine-protein phosphatase 4 catalytic subunit 1	4.60E-03	0.473	1.07E-01	1.508
Ribosomal protein S10 domain-containing protein	3.40E-04	0.560	7.57E-03	1.507
NADP-dependent oxidoreductase domain-containing protein	3.21E-02	0.543	1.48E-01	1.503
Putative metallophosphoesterase F40B5.2	3.06E-01	2.752	5.56E-01	0.667

Probable manganese-transporting ATPase catp-8	1.51E-02	1.799	8.67E-02	0.665
Putative 1-acyl-sn-glycerol-3-phosphate acyltransferase acl-1	1.23E-02	2.247	1.86E-01	0.663
Retinol dehydrogenase 13	2.66E-02	1.858	1.31E-01	0.662
Fatty acid-binding protein homolog 4	3.61E-01	1.830	5.28E-01	0.660
Ribosome production factor 2 homolog	8.66E-03	1.731	3.77E-02	0.654
tRNA guanine 26-N2-dimethyltransferase	2.84E-01	1.538	2.83E-01	0.650
Tetratricopeptide repeat protein 38	2.01E-02	2.477	2.58E-01	0.649
Probable rho GDP-dissociation inhibitor	1.08E-01	1.534	9.96E-02	0.645
Cytochrome b	4.29E-02	2.039	1.85E-01	0.631
Heat shock 70 kDa protein 13	4.51E-02	2.223	2.33E-01	0.626
DeHydrogenases, Short chain	1.74E-01	1.729	2.12E-01	0.620
Epoxide hydrolase	9.93E-03	3.231	2.96E-01	0.617
CRAL-TRIO domain-containing protein	2.13E-01	2.203	5.78E-01	0.613
Putative aquaporin-10	3.25E-02	2.186	1.49E-01	0.613
Exosome complex component RRP45	6.58E-02	1.708	1.17E-01	0.607
DUF155 domain-containing protein	2.14E-01	1.571	1.61E-01	0.600
SOSS complex subunit A homolog	2.18E-02	1.679	1.40E-02	0.591
Alpha-mannosidase	3.14E-01	1.510	1.31E-01	0.587
Nudix hydrolase domain-containing protein	3.24E-02	1.595	1.46E-02	0.585
Protein LTV1 homolog	1.75E-01	2.020	2.97E-01	0.584
DNA replication licensing factor mcm-6	1.92E-01	2.753	5.22E-01	0.575
CRAL-TRIO domain-containing protein	1.21E-01	2.166	2.33E-01	0.568
Probable DNA-directed RNA polymerases I, II, and III subunit RPABC2	1.80E-01	1.548	8.62E-02	0.568
Cleft lip and palate transmembrane protein 1 homolog	1.28E-01	1.539	4.86E-02	0.568
Medium-chain specific acyl-CoA dehydrogenase, mitochondrial	9.14E-02	2.074	2.02E-01	0.567
CHCH domain-containing protein	9.69E-02	2.123	1.85E-01	0.566
Long chain fatty acid elongase 5	4.62E-02	1.758	7.46E-04	0.557
DUF19 domain-containing protein	2.26E-04	2.541	1.16E-02	0.550
Transthyretin-like family protein	8.25E-02	1.576	2.29E-02	0.545
Protein KRI1 homolog	1.00E-01	1.893	1.53E-01	0.536
Nucleoside-diphosphatase uda-1	2.68E-01	1.557	1.32E-01	0.532
Probable glycerol-3-phosphate acyltransferase, mitochondrial	2.46E-02	1.940	3.62E-02	0.528
ER membrane protein complex subunit 7 homolog	3.21E-01	1.828	4.31E-01	0.527
Carnitine O-palmitoyltransferase	2.34E-02	2.261	7.01E-02	0.527
Mitochondrial glutamate carrier 1	3.10E-01	1.527	1.22E-01	0.520

Nematode cuticle collagen N-terminal domain-containing protein	9.08E-04	5.093	1.23E-01	0.519
CaDmium Responsive	5.10E-02	2.078	6.76E-02	0.505
Long chain fatty acid elongase 6	4.64E-02	2.798	1.72E-01	0.500
Strictosidine synthase conserved region domain-containing protein	2.41E-01	1.525	7.25E-02	0.499
Glycoside hydrolase 35 catalytic domain-containing protein	9.91E-02	1.676	7.05E-02	0.498
Uncharacterized protein C29G2.6	2.80E-01	1.743	2.17E-01	0.477
RRM domain-containing protein	1.74E-02	4.434	2.40E-01	0.475
Bestrophin homolog 14	8.51E-02	2.555	1.76E-01	0.473
Rab8	2.90E-02	2.048	1.87E-02	0.461
Lipid scramblase CLPTM1L	1.26E-01	2.336	1.16E-01	0.458
Proton-coupled zinc antiporter SLC30A5	1.85E-02	3.438	1.25E-01	0.455
Vacuolar protein-sorting-associated protein 25	1.24E-03	3.711	8.71E-03	0.440
DOMON domain-containing protein	2.45E-01	1.514	1.72E-02	0.437
BPTI/Kunitz inhibitor domain-containing protein	2.14E-01	1.861	7.93E-02	0.432
DUF3598 domain-containing protein	5.01E-02	2.270	2.50E-02	0.428
Fungal lipase-like domain-containing protein	2.36E-01	1.812	8.20E-02	0.424
Nematode cuticle collagen N-terminal domain-containing protein	1.13E-02	3.810	9.38E-02	0.424
DeHydrogenases, Short chain	2.73E-02	1.837	2.52E-03	0.422
cystathionine gamma-lyase	1.12E-01	1.645	1.28E-02	0.421
Large ribosomal subunit protein uL5A	1.91E-01	2.109	1.31E-01	0.419
Large ribosomal subunit protein mL52	1.72E-01	2.357	2.00E-01	0.417
Uncharacterized protein	1.14E-01	1.980	4.37E-02	0.413
Uncharacterized protein	1.07E-01	1.850	2.10E-02	0.398
EGF-like domain-containing protein	1.17E-02	1.698	2.14E-05	0.367
E3 ubiquitin-protein ligase UBR5	2.60E-01	1.820	1.02E-01	0.365
Arf-GAP domain-containing protein	5.95E-02	3.655	1.08E-01	0.353
TOG domain-containing protein	3.05E-01	1.512	1.81E-03	0.320
Protein CASC3	1.61E-02	3.309	1.55E-02	0.317
Uncharacterized protein D2096.6	5.25E-04	7.109	2.53E-02	0.305
C3H1-type domain-containing protein	3.20E-02	3.298	2.42E-02	0.267
mRNA stability protein	2.05E-02	2.732	9.72E-03	0.120

Supplemental Table C13 **Rescued proteins (based on fold change) identified by SWATH-MS that are either over- or under-represented in *h*CHIP rescue strain 1 processed by lysis with SDS-based lysis buffer.** Each protein listed below met the fold change cutoff criteria of either ≤ 0.67 or ≥ 1.5 compared to *chn-1(tm2692) C. elegans chn-1* mutants in *h*CHIP rescue strain 1. Initially, a reference list was created comparing N2 wild-type worms and *chn-1* mutants. Proteins differentially expressed in opposite directions from wild-type to knock-out animals and knock-out to rescue strains were defined as "rescued". Associated genes for each protein are listed in Supplemental Table C19.

	***chn-1(tm2692)* vs. N2**		***h*CHIP rescue 1 vs. *chn-1(tm2692)***	
Protein	***p*-Value**	**Fold Change**	***p*-Value**	**Fold Change**
Nematode cuticle collagen N-terminal domain-containing protein	6.03E-05	0.087	5.12E-04	7.809
sn-1-specific diacylglycerol lipase ABHD11	3.22E-01	0.488	4.01E-02	6.513
PHAF1 protein T01G9.2	1.09E-03	0.127	3.84E-03	5.186
Saposin B-type domain-containing protein	1.42E-02	0.389	2.38E-04	4.538
DDRGK domain-containing protein 1	1.84E-01	0.604	2.74E-02	4.450
Carboxypeptidase E	3.54E-02	0.395	2.00E-03	4.114
Intrinsically Disordered Protein, class C	4.06E-01	0.490	1.07E-01	3.800
Histone H2A	3.27E-02	0.302	2.44E-02	3.555
Probable glutathione S-transferase gst-36	2.05E-03	0.554	1.15E-01	3.464
Protein-tyrosine-phosphatase	1.56E-02	0.402	1.56E-03	3.385
Protein LTV1 homolog	1.72E-01	0.439	4.30E-02	3.284
Prolyl Carboxy Peptidase like	8.01E-02	0.538	9.79E-04	3.244
Extracellular protein	2.82E-01	0.447	1.37E-01	3.087
Host cell factor homolog hcf-1	6.09E-02	0.609	1.22E-05	2.985
ShKT domain-containing protein	1.18E-01	0.332	1.38E-01	2.936
Large ribosomal subunit protein bL9m	9.23E-02	0.547	4.38E-03	2.918
TransThyretin-Related family domain	1.63E-01	0.343	3.45E-01	2.884
SURF1-like protein	5.21E-02	0.383	5.37E-02	2.799
Peptidase M14 carboxypeptidase A domain-containing protein	5.23E-03	0.465	5.33E-04	2.771
Ig-like domain-containing protein	1.00E-01	0.656	8.89E-02	2.763
Large ribosomal subunit protein uL10m	6.01E-02	0.584	1.20E-02	2.719
Mitochondrial import receptor subunit TOM7 homolog	3.96E-02	0.287	8.22E-02	2.670
Mitochondrial import inner membrane translocase subunit TIM50	5.34E-02	0.658	1.97E-02	2.625
Not3 domain-containing protein	4.08E-02	0.520	2.17E-03	2.593

RNA polymerase II transcription factor SIII p18 subunit	4.50E-03	0.370	4.42E-03	2.584
UBX domain-containing protein 4	1.30E-01	0.418	1.01E-01	2.583
Peptidyl-prolyl cis-trans isomerase 10	8.89E-04	0.261	1.50E-02	2.547
Uncharacterized protein C05D11.1	1.12E-03	0.576	3.48E-02	2.538
MICOS complex subunit MIC60-2	2.35E-01	0.569	2.15E-04	2.510
RIIa domain-containing protein	3.54E-01	0.522	1.75E-01	2.508
Dynamin	9.24E-02	0.624	1.65E-02	2.495
Probable mitochondrial import inner membrane translocase subunit tim-17B.1	5.77E-01	0.634	1.04E-02	2.455
Peroxidasin homolog pxn-2	5.22E-04	0.323	5.40E-03	2.434
ATP synthase subunit C lysine N-methyltransferase	1.11E-03	0.145	8.92E-02	2.386
Vitellogenin-1	5.29E-03	0.232	8.50E-02	2.375
polyribonucleotide nucleotidyltransferase	9.44E-02	0.461	6.51E-02	2.365
Ribonucleoside-diphosphate reductase large subunit	1.23E-01	0.601	1.33E-02	2.259
SUMO-activating enzyme subunit aos-1	2.73E-01	0.658	4.66E-03	2.254
GTP-binding protein drn-1	2.73E-01	0.452	2.42E-01	2.235
Glutathione S-transferase 4	6.40E-02	0.633	2.90E-02	2.227
Cytoplasmic tRNA 2-thiolation protein 1	2.16E-01	0.528	1.28E-01	2.208
Proliferating cell nuclear antigen	1.16E-02	0.483	6.74E-03	2.199
Vitellogenin-5	8.35E-02	0.314	2.34E-01	2.194
5'-3' exoribonuclease 2 homolog	2.36E-05	0.490	5.95E-06	2.170
Phosphatidate cytidylyltransferase, mitochondrial	1.64E-01	0.605	1.40E-01	2.168
AB hydrolase-1 domain-containing protein	3.46E-01	0.604	4.98E-02	2.154
PH domain-containing protein	1.57E-01	0.626	1.08E-01	2.114
CYtochrome P450 family	4.17E-01	0.666	1.68E-01	2.105
DeHydrogenases, Short chain	1.43E-01	0.626	1.22E-01	2.101
SUI1 domain-containing protein	5.96E-04	0.416	3.04E-03	2.088
Glucuronosyltransferase	2.34E-03	0.305	5.27E-02	2.085
Chromatin target of PRMT1 protein C-terminal domain-containing protein	1.17E-01	0.513	8.65E-02	2.079
Uncharacterized protein C18H9.6	1.95E-01	0.644	2.76E-02	2.057
Skp1-related protein	2.00E-02	0.534	8.57E-03	2.053
DNA-directed RNA polymerase II subunit RPB1	1.18E-02	0.464	1.78E-02	2.051
Major facilitator superfamily	3.74E-01	0.610	2.08E-01	2.027
ERCC4 domain-containing protein	4.74E-03	0.279	8.59E-02	1.999
AP-2 complex subunit alpha	5.49E-05	0.356	4.86E-03	1.993
Large ribosomal subunit protein P2	2.64E-02	0.642	6.56E-03	1.982
Putative cystathionine gamma-lyase 2	2.00E-03	0.362	3.17E-02	1.965

Splicing factor 3B subunit 1 domain-containing protein	2.72E-02	0.476	4.38E-02	1.958
Tyrosine aminotransferase	8.76E-02	0.516	7.50E-02	1.946
Coatomer subunit epsilon	4.02E-02	0.626	1.42E-02	1.944
Zwei Ig domain protein zig-1	2.93E-02	0.599	5.85E-02	1.942
DB domain-containing protein	1.54E-02	0.314	1.52E-01	1.941
Cystatin domain-containing protein	4.13E-03	0.436	2.09E-02	1.919
Proteasome subunit alpha type-7	7.50E-03	0.570	9.04E-02	1.893
Probable UDP-N-acetylglucosamine pyrophosphorylase	1.83E-01	0.616	7.54E-02	1.875
BPI1 domain-containing protein	7.37E-03	0.534	1.81E-02	1.875
U5 small nuclear ribonucleoprotein 200 kDa helicase	2.23E-02	0.522	2.98E-02	1.851
Transthyretin-like family protein	2.75E-03	0.517	5.01E-03	1.844
Nematode cuticle collagen N-terminal domain-containing protein	5.34E-02	0.472	1.44E-01	1.844
Probable Golgi transport protein 1	3.17E-01	0.595	6.74E-02	1.840
BTB domain-containing protein	5.94E-02	0.668	5.21E-02	1.839
E3 ubiquitin-protein ligase hecd-1	3.29E-03	0.443	2.50E-02	1.839
Stomatin-1	4.67E-01	0.620	4.21E-03	1.836
Uncharacterized protein ZK1320.3	8.73E-02	0.551	1.84E-01	1.835
Molting protein mlt-10	2.76E-02	0.367	1.53E-01	1.831
Cysteine protease atg-4.1	7.79E-02	0.500	1.24E-01	1.826
ER membrane protein complex subunit 1	1.85E-01	0.623	3.84E-02	1.815
glutamine synthetase	2.53E-01	0.618	8.23E-02	1.796
SAM50-like protein gop-3	1.68E-04	0.435	6.67E-03	1.784
RING-type E3 ubiquitin transferase	1.46E-02	0.361	1.47E-01	1.783
Prion-like-(Q/N-rich)-domain-bearing protein	4.20E-03	0.263	1.07E-01	1.778
GM2 Activator Protein family member	1.92E-02	0.368	1.69E-01	1.766
hydroxyacylglutathione hydrolase	1.16E-02	0.392	1.06E-01	1.766
Golgi-specific brefeldin A-resistance guanine nucleotide exchange factor 1 homolog	2.10E-05	0.339	1.73E-02	1.761
Domain of unknown function DX domain-containing protein	3.11E-03	0.334	1.11E-01	1.748
Vesicle-trafficking protein SEC22b	1.00E-02	0.389	1.16E-01	1.742
Fungal lipase-like domain-containing protein	8.76E-03	0.299	1.62E-01	1.740
Major sperm protein	3.64E-03	0.595	1.07E-01	1.738
Ran GTPase-activating protein 2	7.11E-02	0.611	1.32E-02	1.731
Argonaute protein wago-4	2.52E-01	0.653	2.69E-03	1.711
Pre-mRNA-splicing factor ATP-dependent RNA helicase ddx-15	2.72E-02	0.495	8.63E-02	1.710
Small ribosomal subunit protein mS31	2.71E-02	0.629	1.98E-03	1.707
Probable mitochondrial pyruvate carrier 1	4.86E-01	0.664	1.79E-02	1.707

Pinin/SDK/MemA protein domain-containing protein	3.23E-03	0.499	2.06E-02	1.705
CRAL-TRIO domain-containing protein	2.03E-02	0.564	2.18E-02	1.702
DUF19 domain-containing protein	7.01E-03	0.549	4.60E-02	1.690
Nuclear hormone receptor family member nhr-49	1.39E-01	0.562	6.18E-02	1.687
V-type proton ATPase 116 kDa subunit a 1	2.47E-02	0.574	3.36E-02	1.687
Uncharacterized protein R05D3.9	2.60E-01	0.651	6.72E-02	1.687
C6 domain-containing protein	1.45E-02	0.547	6.07E-02	1.681
Dihydropyrimidinase 2	7.73E-03	0.444	7.82E-02	1.680
26S rRNA cytosine-C5-methyltransferase nsun-5	1.09E-02	0.507	4.78E-02	1.676
mRNA export factor rae-1	1.50E-01	0.467	3.32E-01	1.664
Vitellogenin-3	5.62E-02	0.486	1.72E-01	1.663
Fatty acyl-CoA reductase	9.97E-03	0.454	8.70E-02	1.662
Splicing factor 3B subunit 6-like protein	1.18E-01	0.577	6.55E-02	1.654
Ubiquinone biosynthesis O-methyltransferase, mitochondrial	9.42E-02	0.667	1.31E-02	1.650
Proline dehydrogenase 1, mitochondrial	8.95E-02	0.560	2.29E-01	1.643
MATH domain-containing protein	4.59E-02	0.379	2.82E-01	1.643
Signal peptidase complex subunit 2	6.36E-03	0.493	4.90E-02	1.640
Ig-like domain-containing protein	4.51E-01	0.597	2.91E-02	1.640
SURF6 homolog gldi-11	1.46E-01	0.655	4.36E-02	1.637
HEAT repeat protein	1.98E-01	0.648	3.76E-01	1.636
Glycoside hydrolase 35 catalytic domain-containing protein	1.31E-02	0.594	3.09E-03	1.635
Peptidase M16 N-terminal domain-containing protein	1.87E-02	0.597	1.97E-02	1.634
Vacuolar protein sorting-associated protein 28 homolog	6.62E-02	0.476	2.01E-01	1.633
Neuronal calcium sensor 2	1.22E-03	0.512	1.39E-02	1.632
Vitelline membrane outer layer protein 1	2.39E-01	0.651	2.34E-02	1.630
Intestinal acid phosphatase	4.97E-03	0.411	1.08E-01	1.626
Gut esterase 1	1.99E-02	0.385	2.25E-01	1.616
Actin	4.93E-02	0.646	2.31E-02	1.603
Probable 26S proteasome regulatory subunit 6B	4.09E-03	0.615	1.07E-01	1.602
Vitellogenin-2	1.98E-02	0.440	1.69E-01	1.600
Malate dehydrogenase	1.57E-02	0.667	5.20E-01	1.595
Integrin-linked protein kinase homolog pat-4	3.43E-02	0.547	9.81E-02	1.591
LIM domain-containing protein unc-95	8.32E-02	0.662	2.00E-01	1.591
Ribulose-phosphate 3-epimerase	1.14E-01	0.649	5.00E-01	1.586
Putative cuticle collagen 80	4.71E-03	0.476	8.67E-02	1.586

Protein mac-1	1.08E-01	0.548	8.10E-02	1.584
HECT domain-containing protein	2.02E-01	0.603	1.34E-02	1.583
Probable 26S proteasome complex subunit dss-1	4.08E-02	0.555	1.75E-01	1.582
Uterine Lumin Expressed/localized	1.77E-02	0.248	4.21E-01	1.582
KH domain-containing protein akap-1	1.90E-02	0.586	6.30E-02	1.579
Nucleoside hydrolase	5.00E-02	0.428	2.82E-01	1.577
Putative transcription elongation factor S-II	1.13E-01	0.519	2.68E-01	1.574
Saposin B-type domain-containing protein	3.32E-02	0.541	1.12E-01	1.561
Serine/threonine-protein phosphatase 2A activator	1.49E-03	0.524	1.37E-02	1.558
Ribosomal Protein, Small subunit	3.62E-03	0.544	2.89E-02	1.557
Tubulin--tyrosine ligase-like protein 12	9.44E-02	0.585	2.41E-01	1.557
2-hydroxyacyl-CoA lyase 2	1.20E-01	0.650	1.84E-01	1.551
F-actin-capping protein subunit alpha	6.41E-02	0.635	4.31E-02	1.548
VWFA domain-containing protein	3.42E-01	0.527	4.87E-01	1.548
alpha-1,2-Mannosidase	7.42E-02	0.624	3.46E-01	1.545
Exportin-2	4.56E-02	0.539	1.54E-01	1.542
Proteasome subunit beta type-1	3.08E-01	0.646	1.20E-01	1.540
NEDD8-conjugating enzyme ubc-12	3.14E-02	0.517	1.38E-01	1.539
Innexin-5	1.11E-02	0.472	1.32E-01	1.537
Acyl-coenzyme A thioesterase 8	4.68E-01	0.652	4.47E-01	1.537
Nucleolar complex protein 2 homolog	1.08E-02	0.541	3.35E-02	1.534
Acidic leucine-rich nuclear phosphoprotein 32-related protein 1	1.00E-01	0.665	4.92E-02	1.531
UBX domain-containing protein 3	2.45E-01	0.589	1.29E-01	1.528
Uncharacterized oxidoreductase F53C11.3	1.32E-01	0.604	2.44E-01	1.524
Multifunctional procollagen lysine hydroxylase and glycosyltransferase	7.75E-02	0.542	2.19E-01	1.523
Uncharacterized protein byn-1	1.56E-02	0.464	1.70E-01	1.523
Nematode Specific Peptide family	1.64E-01	0.651	1.04E-01	1.518
riboflavin kinase	2.02E-02	0.376	1.92E-01	1.514
Secreted protein	3.38E-01	0.594	1.43E-02	1.501
Glyceraldehyde-3-phosphate dehydrogenase 3	8.91E-02	1.874	3.20E-01	0.670
Protein jagunal homolog	2.40E-03	5.416	4.05E-01	0.650
Protein kinase domain-containing protein	7.06E-03	1.604	1.16E-02	0.645
Probable dynactin subunit 2	5.56E-02	2.133	2.46E-01	0.638
START domain-containing protein	6.55E-02	1.950	1.99E-01	0.632
LIM and SH3 domain protein F42H10.3	7.36E-02	1.728	1.23E-01	0.626
Nuclear pore complex protein 14	4.77E-01	1.760	5.17E-01	0.625
Uncharacterized protein D2096.6	1.85E-01	2.145	3.56E-01	0.624

Nuclear pore complex protein npp-16	1.87E-02	3.410	2.97E-01	0.622
Nematode cuticle collagen N-terminal domain-containing protein	7.89E-02	1.983	1.92E-01	0.621
Nematode cuticle collagen N-terminal domain-containing protein	1.67E-02	2.178	1.32E-01	0.621
Heat shock protein Hsp-12.2	3.45E-03	2.537	1.06E-01	0.613
ALG-1 INteracting protein	1.36E-01	1.512	7.28E-02	0.605
LITAF domain-containing protein	3.79E-02	1.969	1.15E-01	0.602
Uterine Lumin Expressed/localized	1.90E-01	1.936	2.77E-01	0.596
Histidine-rich glycoprotein-like	3.90E-01	1.652	3.29E-01	0.594
Alpha-tubulin N-acetyltransferase 1	1.15E-01	1.765	1.07E-01	0.594
Cuticle collagen 1	4.79E-01	1.649	4.51E-01	0.587
Small ribosomal subunit protein mS23	1.12E-01	1.509	5.27E-02	0.586
Ribonucleoside-diphosphate reductase small chain	6.09E-02	1.880	1.10E-01	0.586
Peptidyl-prolyl cis-trans isomerase 4	3.73E-02	1.635	5.03E-02	0.584
Putative cuticle collagen 91	1.19E-01	1.740	1.11E-01	0.584
EF-hand domain-containing protein	1.59E-02	1.699	1.01E-02	0.582
YKT6	2.19E-02	1.852	3.98E-02	0.578
Mitochondrial Ribosomal Protein, Large	2.87E-01	1.743	2.65E-01	0.559
WaRThog	1.30E-01	1.988	1.96E-01	0.558
Soluble NSF attachment protein 29	5.50E-02	1.581	1.53E-02	0.557
Cuticle collagen 10	1.07E-02	1.681	4.43E-03	0.556
Warthog protein 4	2.95E-03	2.046	1.13E-02	0.548
Neprilysin-1	1.71E-01	2.049	2.41E-01	0.543
Onchocerca Related Antigen family	4.57E-02	1.957	8.82E-02	0.541
Large ribosomal subunit protein uL3m	1.08E-02	2.044	2.22E-02	0.530
NADH-ubiquinone oxidoreductase chain 4	2.87E-01	1.578	1.35E-01	0.525
Nematode cuticle collagen N-terminal domain-containing protein	9.52E-02	1.708	4.44E-02	0.521
Aspartate dehydrogenase domain-containing protein	5.96E-02	2.348	1.39E-01	0.516
Putative dihydrofolate reductase	9.19E-02	1.859	5.44E-02	0.514
Nematode cuticle collagen N-terminal domain-containing protein	8.44E-03	2.303	3.02E-02	0.510
Putative cuticle collagen 145	4.26E-04	1.597	1.02E-06	0.501
Probable 2,4-dienoyl-CoA reductase 3	2.83E-02	2.078	1.34E-02	0.499
Nematode cuticle collagen N-terminal domain-containing protein	6.55E-02	1.801	2.39E-02	0.498
Transthyretin-like family protein	6.46E-02	1.941	5.06E-02	0.495
Rhodanese domain-containing protein	3.49E-01	1.574	2.59E-01	0.484
Beta/gamma crystallin 'Greek key' domain-containing protein	6.50E-02	2.392	8.81E-02	0.480

CMP/dCMP-type deaminase domain-containing protein	1.34E-01	2.312	1.11E-01	0.473
Probable maleylacetoacetate isomerase	1.21E-01	1.606	1.40E-02	0.464
Nematode cuticle collagen N-terminal domain-containing protein	2.55E-01	1.847	4.75E-02	0.461
NADAR domain-containing protein	1.43E-01	2.466	2.07E-01	0.461
Domain of unknown function DB domain-containing protein	4.45E-02	1.875	1.46E-02	0.460
Cuticle collagen 14	6.40E-03	2.508	1.62E-02	0.450
Cuticle collagen 38	9.76E-02	2.188	8.04E-02	0.437
BPTI/Kunitz inhibitor domain-containing protein	4.97E-03	2.649	1.43E-02	0.434
Serpentine Receptor, class T	9.20E-02	1.774	2.62E-02	0.412
mannose-6-phosphate isomerase	2.19E-01	1.723	4.68E-02	0.410
Proton-coupled zinc antiporter SLC30A5	5.44E-03	3.217	4.52E-02	0.399
Protein CASC3	3.22E-01	1.981	7.69E-02	0.398
Small ribosomal subunit protein uS14m	1.84E-01	2.394	1.06E-01	0.395
C6 domain-containing protein	2.36E-02	2.829	3.55E-02	0.382
Metal transporter cnnm-1	2.43E-01	2.327	1.85E-01	0.382
Probable inactive acireductone dioxygenase 1	5.92E-03	3.593	1.96E-02	0.360
Extracellular superoxide dismutase [Cu-Zn]	5.55E-01	1.557	1.30E-01	0.358
Fcf2 pre-rRNA processing C-terminal domain-containing protein	3.07E-02	4.312	8.56E-02	0.350
Transport and Golgi organization protein 1 homolog	3.68E-01	1.590	4.52E-02	0.346
C6 domain-containing protein	9.99E-02	2.378	2.47E-02	0.332
Endoplasmic reticulum lectin 1	7.78E-05	3.321	3.94E-04	0.309
EOG090X04TT	1.97E-01	2.026	3.32E-02	0.303
Cytochrome c oxidase subunit 1	3.91E-01	1.550	2.69E-02	0.298
G-patch domain-containing protein	4.74E-01	1.763	5.39E-02	0.297
Membrane insertase YidC/Oxa/ALB C-terminal domain-containing protein	1.36E-02	2.360	3.25E-04	0.273
Activated in Blocked Unfolded protein response	5.36E-02	2.071	6.29E-04	0.261
V-type proton ATPase subunit e	3.80E-02	2.612	2.84E-03	0.245
GTP-binding protein	7.07E-02	2.588	6.18E-03	0.224
Fanconi anemia group I protein	4.83E-01	1.698	3.50E-02	0.216
Putative UDP-glucuronosyltransferase ugt-47	1.22E-01	2.324	8.08E-03	0.213
Nematode cuticle collagen N-terminal domain-containing protein	3.21E-01	2.610	7.14E-02	0.212
Flavin-containing monooxygenase	8.63E-02	2.260	2.35E-03	0.205
Cytochrome P450	4.13E-02	5.808	6.15E-02	0.204
PI31_Prot_N domain-containing protein	1.62E-02	5.933	1.56E-02	0.167
39S ribosomal protein L55, mitochondrial	1.37E-03	6.711	1.57E-03	0.162

E3 ubiquitin-protein ligase listerin	2.98E-01	1.692	2.17E-02	0.159
JNK-interacting protein	3.34E-02	7.594	5.67E-03	0.127
Sm domain-containing protein	3.38E-02	7.028	2.03E-02	0.118
Protein kinase domain-containing protein		4.287		0.089
Fibulin-1	7.44E-03	23.546	5.03E-03	0.053

Supplemental Table C14 **Rescued proteins (based on fold change) identified by SWATH-MS that are either over- or under-represented in *h*CHIP rescue strain 2 processed by lysis with SDS-based lysis buffer.** Each protein listed below met the fold change cutoff criteria of either ≤ 0.67 or ≥ 1.5 compared to *chn-1(tm2692) C. elegans chn-1* mutants in *h*CHIP rescue strain 2. Initially, a reference list was created comparing N2 wild-type worms and *chn-1* mutants. Proteins differentially expressed in opposite directions from wild-type to knock-out animals and knock-out to rescue strains were defined as "rescued". Associated genes for each protein are listed in Supplemental Table C20.

	***chn-1(tm2692)* vs. N2**		***h*CHIP rescue 2 vs. *chn-1(tm2692)***	
Protein	***p*-Value**	**Fold Change**	***p*-Value**	**Fold Change**
Putative metallophosphoesterase F40B5.2	2.91E-01	0.404	9.42E-02	4.462
Exosome complex component RRP45	1.86E-01	0.467	1.90E-02	4.149
Intrinsically Disordered Protein, class C	4.06E-01	0.490	2.61E-01	3.662
Major facilitator superfamily	3.74E-01	0.610	1.73E-05	3.227
Mitochondrial import receptor subunit TOM7 homolog	3.96E-02	0.287	5.19E-02	3.225
Ribosomal RNA-processing protein 7 homolog	8.34E-02	0.278	7.70E-02	3.168
Fungal lipase-like domain-containing protein	8.76E-03	0.299	3.84E-02	3.100
SURF1-like protein	5.21E-02	0.383	5.49E-02	2.987
Extracellular protein	2.82E-01	0.447	1.16E-01	2.982
Myb-binding protein 1A-like protein	4.12E-01	0.357	3.95E-01	2.982
PHAF1 protein T01G9.2	1.09E-03	0.127	3.48E-02	2.933
Gut esterase 1	1.99E-02	0.385	1.12E-02	2.854
Carboxypeptidase E	3.54E-02	0.395	1.90E-02	2.839
Not3 domain-containing protein	4.08E-02	0.520	3.40E-03	2.838
G domain-containing protein	4.77E-04	0.259	1.10E-02	2.737
RIIa domain-containing protein	3.54E-01	0.522	1.63E-01	2.733
RING-type domain-containing protein	2.11E-01	0.383	2.09E-01	2.719
HEAT repeat protein	1.98E-01	0.648	1.11E-01	2.585
ADP-ribosylation factor 6	7.88E-02	0.513	6.09E-02	2.518
Stomatin-1	4.67E-01	0.620	2.07E-02	2.476

Saposin B-type domain-containing protein	1.42E-02	0.389	1.81E-02	2.475
Sensitive to high expression protein 9, mitochondrial	1.19E-01	0.561	2.92E-02	2.434
Thioredoxin-like protein	4.98E-04	0.128	8.80E-02	2.398
DOMON domain-containing protein	7.31E-03	0.373	1.76E-02	2.376
Actin	4.93E-02	0.646	1.74E-01	2.366
Uncharacterized protein C18H9.6	1.95E-01	0.644	1.28E-01	2.361
Ran GTPase-activating protein 2	7.11E-02	0.611	1.14E-01	2.359
AP-2 complex subunit alpha	5.49E-05	0.356	6.09E-04	2.356
60S ribosomal protein L23	2.49E-01	0.554	1.02E-01	2.355
Innexin-5	1.11E-02	0.472	4.65E-03	2.336
SUI1 domain-containing protein	5.96E-04	0.416	8.57E-04	2.330
ATP synthase subunit C lysine N-methyltransferase	1.11E-03	0.145	1.19E-01	2.321
Chromatin target of PRMT1 protein C-terminal domain-containing protein	1.17E-01	0.513	5.16E-02	2.306
Dihydropyrimidinase 2	7.73E-03	0.444	6.50E-03	2.299
Nuclear hormone receptor family member nhr-49	1.39E-01	0.562	3.61E-02	2.288
Multifunctional procollagen lysine hydroxylase and glycosyltransferase	7.75E-02	0.542	2.01E-02	2.277
ANK_REP_REGION domain-containing protein	2.64E-02	0.362	1.31E-01	2.266
Golgi-specific brefeldin A-resistance guanine nucleotide exchange factor 1 homolog	2.10E-05	0.339	8.43E-04	2.264
RRM domain-containing protein	1.17E-01	0.392	2.14E-01	2.239
Uncharacterized protein T19C3.2	1.64E-02	0.516	5.32E-03	2.187
Uncharacterized oxidoreductase F53C11.3	1.32E-01	0.604	2.74E-01	2.172
Proteasome subunit beta type-1	3.08E-01	0.646	1.74E-02	2.132
Protein kinase domain-containing protein	1.38E-01	0.633	3.11E-02	2.103
Nudix hydrolase domain-containing protein	2.70E-03	0.495	1.64E-03	2.098
Probable 26S proteasome complex subunit dss-1	4.08E-02	0.555	1.28E-02	2.073
MTTase N-terminal domain-containing protein	2.98E-01	0.581	5.30E-03	2.062
ERCC4 domain-containing protein	4.74E-03	0.279	7.40E-02	2.061
Probable phosphoribosylformylglycinamidine synthase	1.56E-03	0.529	3.96E-04	2.060
KH domain-containing protein akap-1	1.90E-02	0.586	1.36E-01	2.026
Transmembrane protein 256 homolog	8.82E-02	0.230	3.73E-01	2.024

E3 ubiquitin-protein ligase hecd-1	3.29E-03	0.443	1.08E-02	2.010
Glucuronosyltransferase	2.34E-03	0.305	6.70E-02	2.000
Facilitated glucose transporter protein 1	2.49E-02	0.584	3.93E-03	1.981
Coatomer subunit epsilon	4.02E-02	0.626	7.58E-02	1.972
SAP domain-containing protein	2.44E-01	0.571	1.50E-01	1.961
alpha-1,2-Mannosidase	7.42E-02	0.624	4.88E-02	1.953
Peroxidasin homolog pxn-2	5.22E-04	0.323	3.83E-02	1.951
Neuropeptide-Like Protein		0.551		1.931
Cytoplasmic tRNA 2-thiolation protein 1	2.16E-01	0.528	2.13E-01	1.904
Integrin-linked protein kinase homolog pat-4	3.43E-02	0.547	2.46E-02	1.904
5'-3' exoribonuclease 2 homolog	2.36E-05	0.490	1.05E-04	1.904
Ubiquitin carboxyl-terminal hydrolase	3.56E-01	0.564	2.66E-01	1.897
Cysteine protease atg-4.1	7.79E-02	0.500	1.04E-01	1.893
U5 small nuclear ribonucleoprotein 200 kDa helicase	2.23E-02	0.522	2.54E-02	1.887
Epoxide hydrolase	1.36E-02	0.326	1.56E-01	1.874
Uncharacterized protein ZK1320.3	8.73E-02	0.551	8.28E-02	1.832
Pinin/SDK/MemA protein domain-containing protein	3.23E-03	0.499	1.01E-02	1.819
Ribonucleoside-diphosphate reductase large subunit	1.23E-01	0.601	7.38E-02	1.814
Domain of unknown function DX domain-containing protein	3.11E-03	0.334	9.09E-02	1.813
Uncharacterized protein C29G2.6	1.82E-02	0.433	9.59E-02	1.808
sn-1-specific diacylglycerol lipase ABHD11	3.22E-01	0.488	4.15E-01	1.804
Uncharacterized protein byn-1	1.56E-02	0.464	5.89E-02	1.800
Proliferating cell nuclear antigen	1.16E-02	0.483	3.83E-02	1.798
Splicing factor 3B subunit 6-like protein	1.18E-01	0.577	5.36E-01	1.794
Ubiquinone biosynthesis O-methyltransferase, mitochondrial	9.42E-02	0.667	2.76E-01	1.794
Putative cystathionine gamma-lyase 2	2.00E-03	0.362	6.07E-02	1.794
Dynactin subunit 4	1.19E-01	0.482	2.11E-01	1.787
Protein ctg-1	1.30E-02	0.564	1.21E-02	1.785
MICOS complex subunit MIC60-2	2.35E-01	0.569	2.26E-01	1.777
Histone H2A	3.27E-02	0.302	2.92E-01	1.776
Lipid scramblase CLPTM1L	1.87E-01	0.389	4.59E-01	1.774
Leucine carboxyl methyltransferase 1	5.68E-02	0.463	1.51E-01	1.771
D-2-hydroxyglutarate dehydrogenase, mitochondrial	6.32E-03	0.663	1.35E-03	1.756
UBX domain-containing protein 3	2.45E-01	0.589	1.92E-01	1.755
DNA topoisomerase 2 top-2	2.70E-02	0.565	3.03E-02	1.749

Proteasome subunit alpha type-7	7.50E-03	0.570	8.10E-03	1.744
BIG2 domain-containing protein	2.97E-02	0.603	1.07E-01	1.737
Probable glutathione S-transferase gst-36	2.05E-03	0.554	3.89E-03	1.729
Fatty acyl-CoA reductase	9.97E-03	0.454	6.87E-02	1.720
Dynein heavy chain, cytoplasmic	6.38E-03	0.465	4.72E-02	1.717
Prolyl Carboxy Peptidase like	8.01E-02	0.538	1.26E-01	1.715
Probable Golgi transport protein 1	3.17E-01	0.595	2.33E-02	1.706
HECT domain-containing protein	2.02E-01	0.603	1.95E-02	1.703
Skp1-related protein	2.00E-02	0.534	4.62E-02	1.702
Geranylgeranyl transferase type-2 subunit alpha	7.50E-02	0.602	1.30E-01	1.701
Glutathione S-transferase	3.03E-02	0.572	2.46E-01	1.696
Protein Scribble homolog let-413	1.83E-01	0.490	2.78E-01	1.691
Protein mac-1	1.08E-01	0.548	1.60E-01	1.691
NADH-ubiquinone oxidoreductase chain 5	3.51E-01	0.646	8.75E-02	1.681
Putative peroxisomal biogenesis factor 19	3.58E-02	0.557	6.47E-02	1.666
CYtochrome P450 family	4.17E-01	0.666	7.45E-02	1.662
V-type proton ATPase 116 kDa subunit a 1	2.47E-02	0.574	6.44E-02	1.656
UPF0642 protein YBL028C	3.62E-01	0.635	3.16E-02	1.649
Protein-tyrosine sulfotransferase A	3.43E-05	0.488	1.01E-04	1.647
Peptidyl-prolyl cis-trans isomerase 10	8.89E-04	0.261	2.14E-01	1.647
5-oxoprolinase	1.59E-01	0.603	1.92E-02	1.637
Uncharacterized protein ZK1073.1	9.35E-02	0.580	3.92E-02	1.635
Esterase CM06B1	1.49E-01	0.604	1.48E-01	1.633
Neuronal calcium sensor 2	1.22E-03	0.512	1.39E-02	1.632
DUF148 domain-containing protein	5.14E-01	0.589	7.46E-02	1.627
Vitelline membrane outer layer protein 1	2.39E-01	0.651	4.20E-01	1.619
DDRGK domain-containing protein 1	1.84E-01	0.604	3.53E-01	1.619
Signal peptidase complex subunit 2	6.36E-03	0.493	5.52E-02	1.618
Malate dehydrogenase	1.57E-02	0.667	3.80E-01	1.617
Uncharacterized protein F36G3.2	6.40E-02	0.435	2.76E-01	1.616
2-methoxy-6-polyprenyl-1,4-benzoquinol methylase, mitochondrial	4.40E-02	0.624	1.83E-01	1.612
Acyl-coenzyme A thioesterase 8	4.68E-01	0.652	1.44E-01	1.608
Probable mitochondrial pyruvate carrier 1	4.86E-01	0.664	2.53E-01	1.595
Glycoside hydrolase 35 catalytic domain-containing protein	1.31E-02	0.594	2.24E-01	1.584

Intestinal acid phosphatase	4.97E-03	0.411	1.28E-01	1.582
mRNA-decapping enzyme 1	1.19E-01	0.501	3.17E-01	1.580
Acidic leucine-rich nuclear phosphoprotein 32-related protein 1	1.00E-01	0.665	4.12E-02	1.577
Histidine phosphatase family protein	9.56E-03	0.643	1.40E-01	1.577
Large ribosomal subunit protein bL9m	9.23E-02	0.547	2.04E-01	1.569
Kynureninase	2.82E-02	0.629	7.88E-02	1.564
Probable mitochondrial import inner membrane translocase subunit tim-17B.1	5.77E-01	0.634	4.76E-02	1.559
mRNA transport homolog 4	2.11E-03	0.475	5.51E-02	1.555
Putative 6-phosphogluconolactonase	8.84E-02	0.630	3.67E-03	1.555
Glutathione S-transferase 4	6.40E-02	0.633	7.06E-02	1.551
Cullin-1	1.81E-03	0.425	8.93E-02	1.551
UBX domain-containing protein 4	1.30E-01	0.418	4.41E-01	1.547
CBS domain-containing protein	1.22E-03	0.439	7.06E-02	1.536
RNA polymerase II transcription factor SIII p18 subunit	4.50E-03	0.370	1.85E-01	1.533
Glycosyl hydrolase family 63 C-terminal domain-containing protein	8.71E-03	0.533	6.78E-02	1.528
Putative UDP-glucuronosyltransferase ugt-46	1.01E-01	0.572	1.87E-01	1.528
Reactive oxygen species modulator 1	8.04E-02	0.587	8.11E-02	1.528
Small ribosomal subunit protein mS31	2.71E-02	0.629	1.26E-02	1.520
BPI1 domain-containing protein	7.37E-03	0.534	3.08E-02	1.511
AB hydrolase-1 domain-containing protein	3.46E-01	0.604	5.02E-02	1.507
Ribulose-phosphate 3-epimerase	1.14E-01	0.649	1.37E-01	1.500
Fibronectin type-III domain-containing protein	8.42E-03	2.861	2.87E-01	0.668
Probable small nuclear ribonucleoprotein Sm D2	2.97E-01	1.691	4.20E-01	0.667
non-specific serine/threonine protein kinase	2.55E-02	1.717	8.42E-02	0.663
Receptor-type guanylate cyclase gcy-23	2.33E-02	1.918	1.35E-01	0.658
HIG1 domain-containing protein	1.06E-01	1.542	1.17E-01	0.657
Cuticle collagen 39	4.59E-02	1.637	9.08E-02	0.643
Ribosomal RNA small subunit methyltransferase nep-1	2.79E-02	1.544	2.51E-02	0.642
Peptidyl-prolyl cis-trans isomerase 4	3.73E-02	1.635	4.66E-02	0.640
Ammonium transporter	1.24E-01	2.297	2.32E-01	0.635
Nuclear pore complex protein npp-16	1.87E-02	3.410	3.17E-01	0.635
RNA-binding S4 domain-containing protein	7.43E-02	1.645	6.41E-02	0.621

NADH dehydrogenase [ubiquinone] 1 alpha subcomplex subunit 1	9.25E-07	2.802	7.80E-03	0.615
Probable dynactin subunit 2	5.56E-02	2.133	2.09E-01	0.614
LIM and SH3 domain protein F42H10.3	7.36E-02	1.728	1.04E-01	0.610
Clathrin light chain	1.77E-04	2.586	3.35E-02	0.610
Protein vem-1	1.05E-02	1.595	7.00E-03	0.609
Protein CASC3	3.22E-01	1.981	3.34E-01	0.608
Histidine-rich glycoprotein-like	3.90E-01	1.652	3.31E-01	0.595
CaLponIn-liKe proteins	8.41E-02	2.397	2.97E-01	0.595
Heat shock protein Hsp-12.2	3.45E-03	2.537	7.18E-02	0.579
G-patch domain-containing protein	4.74E-01	1.763	3.80E-01	0.572
Extracellular superoxide dismutase [Cu-Zn]	5.55E-01	1.557	4.24E-01	0.572
Plasma membrane proteolipid 3	1.85E-01	1.623	1.14E-01	0.559
Transport and Golgi organization protein 1 homolog	3.68E-01	1.590	2.55E-01	0.555
Protein jagunal homolog	2.40E-03	5.416	2.55E-01	0.554
RRM domain-containing protein	1.53E-01	1.725	1.07E-01	0.539
NADH-ubiquinone oxidoreductase chain 4	2.87E-01	1.578	1.44E-01	0.533
DAZ protein 1	1.89E-01	2.254	2.73E-01	0.509
PI31_Prot_N domain-containing protein	1.62E-02	5.933	2.25E-01	0.498
ABC transporter domain-containing protein	2.56E-01	1.618	8.73E-02	0.496
J domain-containing protein	1.88E-01	1.687	8.02E-02	0.495
DUF3456 domain-containing protein	3.96E-03	1.695	3.51E-04	0.495
Endoplasmic reticulum lectin 1	7.78E-05	3.321	3.27E-02	0.484
Proton-coupled zinc antiporter SLC30A5	5.44E-03	3.217	6.68E-02	0.473
V-type proton ATPase subunit e	3.80E-02	2.612	6.67E-02	0.464
Ig-like domain-containing protein	1.67E-01	1.546	1.67E-02	0.463
Serpentine Receptor, class T	9.20E-02	1.774	8.55E-03	0.444
Secreted protein	4.44E-01	1.673	2.27E-01	0.443
Alpha-tubulin N-acetyltransferase 1	1.15E-01	1.765	7.87E-03	0.438
Aspartate dehydrogenase domain-containing protein	5.96E-02	2.348	6.20E-02	0.430
Uterine Lumin Expressed/localized	1.90E-01	1.936	6.04E-02	0.425
ER membrane protein complex subunit 4	2.44E-01	2.400	1.52E-01	0.400
GTP-binding protein	7.07E-02	2.588	6.58E-02	0.379
Fcf2 pre-rRNA processing C-terminal domain-containing protein	3.07E-02	4.312	1.12E-01	0.379
CMP/dCMP-type deaminase domain-containing protein	1.34E-01	2.312	5.10E-02	0.364

Membrane insertase YidC/Oxa/ALB C-terminal domain-containing protein	1.36E-02	2.360	3.73E-03	0.360
Flavin-containing monooxygenase	8.63E-02	2.260	3.90E-02	0.352
39S ribosomal protein L55, mitochondrial	1.37E-03	6.711	3.49E-02	0.315
Protein kinase domain-containing protein		4.287		0.255
Sm domain-containing protein	3.38E-02	7.028	9.86E-02	0.193
Fanconi anemia group I protein	4.83E-01	1.698	2.44E-02	0.184
Cytochrome P450	4.13E-02	5.808	3.42E-02	0.159
JNK-interacting protein	3.34E-02	7.594	8.33E-03	0.132
Fibulin-1	7.44E-03	23.546	3.90E-02	0.112
Nematode cuticle collagen N-terminal domain-containing protein	3.21E-01	2.610	1.89E-03	0.071

Supplemental Table C15 **Rescued proteins (based on fold change) identified by SWATH-MS that are either over- or under-represented in the *Ce*CHIP rescue strain processed by lysis with SDS-based lysis buffer.** Each protein listed below met the fold change cutoff criteria of either ≤ 0.67 or ≥ 1.5 compared to *chn-1(tm2692) C. elegans chn-1* mutants in the *Ce*CHIP rescue strain. Initially, a reference list was created comparing N2 wild-type worms and *chn-1* mutants. Proteins differentially expressed in opposite directions from wild-type to knock-out animals and knock-out to rescue strains were defined as “rescued”. Associated genes for each protein are listed in Supplemental Table C21.

	***chn-1(tm2692)* vs. N2**		***Ce*CHIP rescue 2 vs. *chn-1(tm2692)***	
Protein	***p*-Value**	**Fold Change**	***p*-Value**	**Fold Change**
Nematode cuticle collagen N-terminal domain-containing protein	6.03E-05	0.087	3.11E-01	1.873
PHAF1 protein T01G9.2	1.09E-03	0.127	2.64E-03	6.012
Thioredoxin-like protein	4.98E-04	0.128	5.42E-02	2.715
ATP synthase subunit C lysine N-methyltransferase	1.11E-03	0.145	4.78E-03	4.602
G domain-containing protein	4.77E-04	0.259	2.68E-04	4.367
Peptidyl-prolyl cis-trans isomerase 10	8.89E-04	0.261	4.22E-03	3.578
Prion-like-(Q/N-rich)-domain-bearing protein	4.20E-03	0.263	9.21E-02	1.831
DNA-directed RNA polymerase subunit beta	1.65E-02	0.266	2.42E-01	1.881
ERCC4 domain-containing protein	4.74E-03	0.279	8.32E-03	3.024
Mitochondrial import receptor subunit TOM7 homolog	3.96E-02	0.287	2.23E-02	4.082
Histone H2A	3.27E-02	0.302	9.12E-02	2.544
Glucuronosyltransferase	2.34E-03	0.305	3.27E-02	2.256

SAM domain-containing protein	1.26E-02	0.309	7.79E-02	1.944
Aminopeptidase P N-terminal domain-containing protein	1.93E-02	0.321	2.09E-01	1.800
Peroxidasin homolog pxn-2	5.22E-04	0.323	6.55E-05	3.933
Epoxide hydrolase	1.36E-02	0.326	2.39E-02	2.769
Golgi-specific brefeldin A-resistance guanine nucleotide exchange factor 1 homolog	2.10E-05	0.339	1.47E-04	2.575
Nucleolar protein 9	1.14E-02	0.344	6.26E-02	3.019
Lipase_GDSL domain-containing protein	3.23E-02	0.346	1.62E-01	2.101
RNA uridylyltransferase	1.40E-01	0.347	1.48E-01	2.820
AP-2 complex subunit alpha	5.49E-05	0.356	5.39E-07	3.849
RING-type E3 ubiquitin transferase	1.46E-02	0.361	6.16E-02	2.207
Probable DNA polymerase delta small subunit	6.78E-02	0.361	8.07E-02	2.255
Putative cystathionine gamma-lyase 2	2.00E-03	0.362	4.25E-03	2.529
Molting protein mlt-10	2.76E-02	0.367	1.73E-03	4.398
Tudor domain-containing protein	2.48E-02	0.368	2.13E-02	2.800
Putative glucosylceramidase 1	2.33E-02	0.368	1.66E-02	3.022
C-type lectin domain-containing protein	5.25E-02	0.368	1.62E-01	2.730
Peroxisomal biogenesis factor 3	5.37E-03	0.370	1.20E-02	2.414
RNA polymerase II transcription factor SIII p18 subunit	4.50E-03	0.370	1.71E-03	2.875
DOMON domain-containing protein	7.31E-03	0.373	1.29E-02	2.483
Large ribosomal subunit protein bL17m	1.68E-03	0.375	1.86E-02	2.030
MATH domain-containing protein	4.59E-02	0.379	3.24E-01	1.644
RING-type domain-containing protein	2.11E-01	0.383	6.26E-02	4.336
SURF1-like protein	5.21E-02	0.383	6.87E-02	2.633
Gut esterase 1	1.99E-02	0.385	1.09E-02	2.865
Lipid scramblase CLPTM1L	1.87E-01	0.389	1.74E-02	5.741
Saposin B-type domain-containing protein	1.42E-02	0.389	1.45E-03	3.567
Vesicle-trafficking protein SEC22b	1.00E-02	0.389	1.87E-02	2.347
hydroxyacylglutathione hydrolase	1.16E-02	0.392	1.20E-02	3.008
Probable selenide, water dikinase	6.14E-03	0.394	7.06E-02	1.881
Carboxypeptidase E	3.54E-02	0.395	1.50E-05	10.088
LNS2/PITP domain-containing protein	4.55E-04	0.400	3.03E-03	2.759
Protein-tyrosine-phosphatase	1.56E-02	0.402	2.57E-03	3.511
Intestinal acid phosphatase	4.97E-03	0.411	7.24E-02	1.726
SUI1 domain-containing protein	5.96E-04	0.416	1.19E-03	2.266
UBX domain-containing protein 4	1.30E-01	0.418	8.23E-02	2.741
ubiquitinyl hydrolase 1	6.35E-02	0.422	9.68E-02	2.297
Cullin-1	1.81E-03	0.425	8.54E-02	1.560

KRR1 small subunit processome component	1.68E-01	0.429	3.06E-01	1.552
Uncharacterized protein C29G2.6	1.82E-02	0.433	6.39E-02	1.952
MMS19 nucleotide excision repair protein	3.40E-02	0.435	1.51E-02	2.632
SAM50-like protein gop-3	1.68E-04	0.435	4.40E-03	1.840
Protein LTV1 homolog	1.72E-01	0.439	8.28E-03	5.634
C-type lectin domain-containing protein	5.43E-02	0.441	3.01E-01	1.536
E3 ubiquitin-protein ligase hecd-1	3.29E-03	0.443	2.82E-02	1.814
Dihydropyrimidinase 2	7.73E-03	0.444	2.48E-02	1.959
Extracellular protein	2.82E-01	0.447	6.08E-02	3.586
GTP-binding protein drn-1	2.73E-01	0.452	4.13E-01	2.284
Fatty acyl-CoA reductase	9.97E-03	0.454	5.79E-02	1.761
Ig-like domain-containing protein	3.20E-02	0.458	1.39E-01	1.695
polyribonucleotide nucleotidyltransferase	9.44E-02	0.461	7.20E-03	3.915
DNA-directed RNA polymerase II subunit RPB1	1.18E-02	0.464	1.48E-03	2.725
Dynein heavy chain, cytoplasmic	6.38E-03	0.465	1.04E-01	1.548
mRNA export factor rae-1	1.50E-01	0.467	1.54E-01	2.129
Exosome complex component RRP45	1.86E-01	0.467	1.85E-01	2.146
Innexin-5	1.11E-02	0.472	5.21E-02	1.753
mRNA transport homolog 4	2.11E-03	0.475	4.13E-03	1.988
Vacuolar protein sorting-associated protein 28 homolog	6.62E-02	0.476	3.34E-02	2.291
Putative cuticle collagen 80	4.71E-03	0.476	5.37E-02	2.293
Arf-GAP with ANK repeat and PH domain-containing protein cnt-1	1.69E-01	0.476	1.91E-01	2.239
Splicing factor 3B subunit 1 domain-containing protein	2.72E-02	0.476	9.05E-02	1.748
Dynactin subunit 4	1.19E-01	0.482	7.14E-02	2.344
Proliferating cell nuclear antigen	1.16E-02	0.483	5.73E-03	2.238
sn-1-specific diacylglycerol lipase ABHD11	3.22E-01	0.488	1.38E-01	2.868
tRNA adenine 58-N1-methyltransferase non-catalytic subunit TRM6	9.38E-02	0.488	2.02E-01	1.796
Protein Scribble homolog let-413	1.83E-01	0.490	3.08E-02	3.387
5'-3' exoribonuclease 2 homolog	2.36E-05	0.490	6.24E-05	1.951
Intrinsically Disordered Protein, class C	4.06E-01	0.490	9.50E-04	22.859
Probable 5-formyltetrahydrofolate cyclo-ligase	4.72E-02	0.491	4.09E-02	2.148
Signal peptidase complex subunit 2	6.36E-03	0.493	1.30E-02	1.891
Nudix hydrolase domain-containing protein	2.70E-03	0.495	3.29E-03	1.988
Pre-mRNA-splicing factor ATP-dependent RNA helicase ddx-15	2.72E-02	0.495	1.66E-01	1.536
Ribosomal RNA-processing protein 8	3.85E-02	0.496	1.21E-02	2.477

Spiroplasma plectrovirus-related protein	4.24E-02	0.497	3.50E-02	2.676
Phosphotransferase	4.63E-03	0.497	1.38E-03	2.235
Pinin/SDK/MemA protein domain-containing protein	3.23E-03	0.499	8.33E-05	2.652
Uncharacterized protein B0361.3	1.01E-01	0.499	1.67E-01	1.951
Cysteine protease atg-4.1	7.79E-02	0.500	2.49E-02	2.528
mRNA-decapping enzyme 1	1.19E-01	0.501	1.95E-01	1.505
Tensin homolog	3.54E-01	0.501	2.32E-02	1.750
Glutathione S-transferase	6.11E-04	0.501	3.55E-01	1.816
protein-disulfide reductase	4.21E-02	0.505	4.88E-02	2.501
26S rRNA	1.09E-02	0.507	1.68E-01	1.560
Thioredoxin domain-containing protein 9	7.45E-03	0.510	1.88E-02	1.850
Neuronal calcium sensor 2	1.22E-03	0.512	6.43E-03	1.854
Chromatin target of PRMT1 protein C-terminal domain-containing protein	1.17E-01	0.513	6.14E-04	2.293
ADP-ribosylation factor 6	7.88E-02	0.513	1.17E-01	6.351
Uncharacterized protein T19C3.2	1.64E-02	0.516	5.15E-02	1.588
Tyrosine aminotransferase	8.76E-02	0.516	2.26E-01	1.675
Uncharacterized protein	2.90E-02	0.516	9.13E-02	1.877
Transthyretin-like family protein	2.75E-03	0.517	1.79E-02	1.729
NEDD8-conjugating enzyme ubc-12	3.14E-02	0.517	5.43E-02	2.758
3'-5' exonuclease domain-containing protein	9.24E-03	0.518	1.51E-01	1.974
Not3 domain-containing protein	4.08E-02	0.520	2.55E-02	2.097
Ubiquitin carboxyl-terminal hydrolase	8.07E-02	0.521	2.14E-01	1.725
U5 small nuclear ribonucleoprotein 200 kDa helicase	2.23E-02	0.522	1.17E-01	1.818
Serine/threonine-protein phosphatase 2A activator	1.49E-03	0.524	2.17E-01	1.889
VWFA domain-containing protein	3.42E-01	0.527	9.22E-02	1.509
Cytoplasmic tRNA 2-thiolation protein 1	2.16E-01	0.528	1.51E-02	1.622
Alpha N-terminal protein methyltransferase 1	7.14E-03	0.531	1.37E-02	1.523
Glycosyl hydrolase family 63 C-terminal domain-containing protein	8.71E-03	0.533	4.41E-01	1.686
Protein kinase C-like 2	1.08E-02	0.533	2.77E-02	1.712
Skp1-related protein	2.00E-02	0.534	2.00E-01	1.524
BPI1 domain-containing protein	7.37E-03	0.534	2.26E-02	2.294
NADPH:adrenodoxin oxidoreductase, mitochondrial	4.10E-02	0.537	4.24E-03	1.841
Prolyl Carboxy Peptidase like	8.01E-02	0.538	2.70E-02	1.651
Exportin-2	4.56E-02	0.539	1.07E-02	1.609
Nucleolar complex protein 2 homolog	1.08E-02	0.541	3.59E-03	2.277

Saposin B-type domain-containing protein	3.32E-02	0.541	6.06E-03	1.913
Multifunctional procollagen lysine hydroxylase and glycosyltransferase	7.75E-02	0.542	7.43E-02	2.002
DNA damage-binding protein 1	8.52E-02	0.544	1.87E-01	1.530
Putative thiosulfate sulfurtransferase mpst-1	7.38E-03	0.546	3.21E-01	2.189
Saposin B-type domain-containing protein	1.48E-01	0.546	1.77E-02	2.249
Importin subunit alpha-3	7.07E-02	0.546	2.15E-01	1.907
Large ribosomal subunit protein bL9m	9.23E-02	0.547	5.59E-02	1.947
Integrin-linked protein kinase homolog pat-4	3.43E-02	0.547	2.46E-02	1.837
Protein mac-1	1.08E-01	0.548	1.64E-01	1.517
E3 ubiquitin-protein ligase hrd-1	6.19E-02	0.548	1.02E-01	1.706
Vacuolar H ATPase	3.67E-02	0.550	4.62E-03	5.207
Neuropeptide-Like Protein		0.551	2.02E-02	1.667
60S ribosomal protein L23	2.49E-01	0.554	2.48E-01	1.621
Probable glutathione S-transferase gst-36	2.05E-03	0.554	1.84E-02	2.016
Probable 26S proteasome complex subunit dss-1	4.08E-02	0.555	8.29E-02	1.554
C-type lectin domain-containing protein	7.50E-03	0.557	3.53E-02	1.682
Tetratricopeptide repeat-containing protein trd-1	9.00E-04	0.559	6.31E-04	4.922
EF-hand domain-containing protein	1.38E-02	0.560	3.81E-02	2.028
High mobility group protein hmg-12	6.84E-02	0.560	1.09E-01	2.108
Nuclear hormone receptor family member nhr-49	1.39E-01	0.562	1.53E-02	1.656
CRAL-TRIO domain-containing protein	2.03E-02	0.564	1.38E-02	2.054
Ubiquitin carboxyl-terminal hydrolase	3.56E-01	0.564	4.60E-02	1.581
Protein ctg-1	1.30E-02	0.564	9.36E-02	2.108
Carboxylic ester hydrolase	1.83E-01	0.564	7.71E-02	1.550
DNA topoisomerase 2 top-2	2.70E-02	0.565	9.13E-02	2.011
Nose resistant to fluoxetine protein 5	2.20E-01	0.568	1.19E-01	1.843
Thioredoxin reductase-like selenoprotein T homolog selt-1.1	5.15E-03	0.568	9.50E-04	2.507
MICOS complex subunit MIC60-2	2.35E-01	0.569	3.82E-02	2.190
Proteasome subunit alpha type-7	7.50E-03	0.570	1.18E-02	2.074
Putative ATP synthase subunit epsilon, mitochondrial	2.01E-01	0.570	5.03E-02	1.734
SAP domain-containing protein	2.44E-01	0.571	1.30E-03	1.934
Glutathione S-transferase	3.03E-02	0.572	2.41E-02	2.845
Uncharacterized protein ZK1073.1	9.35E-02	0.580	1.27E-01	1.626
Small ribosomal subunit protein mS26	8.65E-02	0.581	1.72E-01	1.919

MTTase N-terminal domain-containing protein	2.98E-01	0.581		3.945
SUI1 domain-containing protein	1.53E-01	0.583	2.67E-02	2.244
Facilitated glucose transporter protein 1	2.49E-02	0.584	8.38E-02	1.552
Large ribosomal subunit protein uL10m	6.01E-02	0.584	5.18E-03	1.525
KH domain-containing protein akap-1	1.90E-02	0.586	1.17E-02	1.986
Trimeric intracellular cation channel type 1B.1	1.72E-01	0.586	5.89E-02	1.546
Reactive oxygen species modulator 1	8.04E-02	0.587	5.23E-03	2.684
UBX domain-containing protein 3	2.45E-01	0.589	1.96E-04	7.598
Probable Golgi transport protein 1	3.17E-01	0.595	5.12E-02	2.031
Peptidase M16 N-terminal domain-containing protein	1.87E-02	0.597	5.13E-03	1.769
Ig-like domain-containing protein	4.51E-01	0.597	2.98E-02	3.272
Zwei Ig domain protein zig-1	2.93E-02	0.599	9.86E-03	1.756
Glutathione S-transferase	1.01E-01	0.599	1.39E-01	1.680
Ribonucleoside-diphosphate reductase large subunit	1.23E-01	0.601	1.34E-02	2.269
BIG2 domain-containing protein	2.97E-02	0.603	2.39E-02	1.703
Uncharacterized oxidoreductase F53C11.3	1.32E-01	0.604	3.67E-03	1.698
DDRGK domain-containing protein 1	1.84E-01	0.604	1.62E-01	1.900
Phosphatidate cytidylyltransferase, mitochondrial	1.64E-01	0.605	9.02E-02	1.695
Peptidase A1 domain-containing protein	2.24E-01	0.606	5.30E-02	1.563
Metaxin-1 homolog	2.39E-01	0.606	3.09E-03	2.467
Stomatin-1	4.67E-01	0.620	5.44E-03	1.699
Prolyl carboxy peptidase like protein 5	3.25E-01	0.621	2.38E-01	1.585
ER membrane protein complex subunit 1	1.85E-01	0.623	3.53E-01	1.751
Pyridine nucleotide-disulfide oxidoreductase domain-containing protein 2	1.76E-01	0.623	1.34E-01	2.829
alpha-1,2-Mannosidase	7.42E-02	0.624	3.80E-02	1.814
Coatomer subunit epsilon	4.02E-02	0.626	1.49E-02	1.825
DeHydrogenases, Short chain	1.43E-01	0.626	5.03E-02	2.200
Small ribosomal subunit protein mS31	2.71E-02	0.629	1.85E-02	1.567
HEAT repeat-containing protein 1 homolog	2.71E-01	0.631	1.61E-02	1.817
Protein kinase domain-containing protein	1.38E-01	0.633	1.36E-02	2.199
Glutathione S-transferase 4	6.40E-02	0.633	3.66E-02	1.556
Probable mitochondrial import inner membrane translocase subunit tim-17B.1	5.77E-01	0.634	5.65E-02	1.792
UPF0642 protein YBL028C	3.62E-01	0.635	1.22E-03	3.182
F-actin-capping protein subunit alpha	6.41E-02	0.635	5.07E-02	2.276

Protein dif-1	6.36E-02	0.635	2.66E-03	6.086
Methyltransferase domain-containing protein	1.68E-02	0.639	1.18E-01	1.639
Nucleoside-diphosphatase uda-1	3.08E-01	0.640	3.19E-02	2.186
Histidine phosphatase family protein	9.56E-03	0.643	4.00E-01	1.587
Uncharacterized protein C18H9.6	1.95E-01	0.644	3.71E-01	1.548
Probable ubiquitin-conjugating enzyme E2 7	1.73E-01	0.644	9.74E-02	1.660
ER membrane protein complex subunit 2	1.41E-02	0.645	1.71E-01	1.657
NADH-ubiquinone oxidoreductase chain 5	3.51E-01	0.646	6.87E-02	2.654
Probable geranylgeranyl transferase type-2 subunit beta	5.21E-01	0.648	5.39E-08	3.060
HEAT repeat protein	1.98E-01	0.648	2.11E-03	3.922
Acyl-coenzyme A thioesterase 8	4.68E-01	0.652	9.16E-03	2.570
SURF6 homolog gldi-11	1.46E-01	0.655	1.03E-03	1.785
WD_REPEATS_REGION domain-containing protein	6.92E-02	0.656	2.75E-02	2.396
Mitochondrial import inner membrane translocase subunit TIM50	5.34E-02	0.658	8.72E-02	1.517
SUMO-activating enzyme subunit aos-1	2.73E-01	0.658	1.74E-01	1.562
Polypeptide N-acetylgalactosaminyltransferase 5	6.72E-02	0.658	3.35E-02	1.588
D-2-hydroxyglutarate dehydrogenase, mitochondrial	6.32E-03	0.663	2.19E-02	2.499
Esterase C25G4.2	2.03E-01	0.664	2.66E-02	2.330
Probable mitochondrial pyruvate carrier 1	4.86E-01	0.664	1.47E-01	2.980
CYtochrome P450 family	4.17E-01	0.666	1.38E-02	2.045
Sulfhydryl oxidase	2.07E-01	0.667	3.35E-01	1.789
5'-nucleotidase	4.06E-01	0.667	4.03E-03	2.732
Fibulin-1	7.44E-03	23.546	1.32E-02	0.100
JNK-interacting protein	3.34E-02	7.594	1.08E-02	0.160
Sm domain-containing protein	3.38E-02	7.028	7.98E-02	0.213
39S ribosomal protein L55, mitochondrial	1.37E-03	6.711	6.59E-02	0.356
PI31_Prot_N domain-containing protein	1.62E-02	5.933	2.81E-01	0.539
Cytochrome P450	4.13E-02	5.808	6.03E-02	0.202
Fcf2 pre-rRNA processing C-terminal domain-containing protein	3.07E-02	4.312	3.94E-01	0.598
Protein kinase domain-containing protein		4.287		0.416
Endoplasmic reticulum lectin 1	7.78E-05	3.321	8.03E-02	0.556
Proton-coupled zinc antiporter SLC30A5	5.44E-03	3.217	8.57E-02	0.497
Nematode cuticle collagen N-terminal domain-containing protein	1.18E-01	2.942	1.63E-01	0.444
V-type proton ATPase subunit e	3.80E-02	2.612	1.96E-01	0.579

Nematode cuticle collagen N-terminal domain-containing protein	3.21E-01	2.610	4.39E-02	0.191
GTP-binding protein	7.07E-02	2.588	1.99E-02	0.287
CaLponIn-liKe proteins	8.41E-02	2.397	1.93E-01	0.521
Small ribosomal subunit protein uS14m	1.84E-01	2.394	2.55E-01	0.545
Membrane insertase YidC/Oxa/ALB C-terminal domain-containing protein	1.36E-02	2.360	7.03E-04	0.297
Aspartate dehydrogenase domain-containing protein	5.96E-02	2.348	1.44E-01	0.520
Putative UDP-glucuronosyltransferase ugt-47	1.22E-01	2.324	2.78E-02	0.297
CMP/dCMP-type deaminase domain-containing protein	1.34E-01	2.312	1.17E-01	0.467
Ammonium transporter	1.24E-01	2.297	1.21E-01	0.504
Flavin-containing monooxygenase	8.63E-02	2.260	1.20E-02	0.295
DAZ protein 1	1.89E-01	2.254	4.85E-01	0.651
DUF3707 domain-containing protein	8.32E-02	2.162	1.27E-01	0.588
Probable dynactin subunit 2	5.56E-02	2.133	8.52E-02	0.508
EOG090X04TT	1.97E-01	2.026	1.74E-01	0.475
Cytochrome c oxidase copper chaperone	1.09E-01	1.955	2.20E-01	0.601
START domain-containing protein	6.55E-02	1.950	1.32E-02	0.398
Peptidase S28	1.76E-01	1.937	3.34E-01	0.564
Uterine Lumin Expressed/localized	1.90E-01	1.936	2.09E-01	0.531
Large ribosomal subunit protein eL30	5.42E-01	1.862	2.68E-01	0.361
Putative dihydrofolate reductase	9.19E-02	1.859	1.47E-01	0.604
Serpentine Receptor, class T	9.20E-02	1.774	1.90E-01	0.667
G-patch domain-containing protein	4.74E-01	1.763	1.40E-01	0.371
Putative cuticle collagen 91	1.19E-01	1.740	2.65E-01	0.654
RRM domain-containing protein	1.53E-01	1.725	1.07E-02	0.363
Fanconi anemia group I protein	4.83E-01	1.698	6.28E-02	0.265
DUF3456 domain-containing protein	3.96E-03	1.695	1.21E-03	0.549
E3 ubiquitin-protein ligase listerin	2.98E-01	1.692	5.02E-02	0.217
Large ribosomal subunit protein uL14	6.39E-02	1.690	1.18E-02	0.481
J domain-containing protein	1.88E-01	1.687	7.59E-02	0.490
Secreted protein	4.44E-01	1.673	1.99E-01	0.403
Histidine-rich glycoprotein-like	3.90E-01	1.652	1.98E-01	0.501
Probable maleylacetoacetate isomerase	1.21E-01	1.606	7.19E-02	0.575
Transport and Golgi organization protein 1 homolog	3.68E-01	1.590	5.39E-02	0.361
NADH-ubiquinone oxidoreductase chain 4	2.87E-01	1.578	2.62E-01	0.618
Ras-related protein rab-6.2	2.33E-03	1.557	8.52E-09	0.368
Extracellular superoxide dismutase [Cu-Zn]	5.55E-01	1.557	1.10E-01	0.337

Cytochrome c oxidase subunit 1	3.91E-01	1.550	5.42E-01	0.613
UPF0376 protein F10G2.1	1.96E-01	1.522	1.22E-01	0.603
Nucleolar protein 6	3.36E-01	1.512	1.64E-01	0.548
Small ribosomal subunit protein mS23	1.12E-01	1.509	2.12E-02	0.499

Supplemental Table C16 **Genes corresponding to rescued proteins (based on fold change) identified by SWATH-MS that are either over- or under-represented in *h*CHIP rescue strain 1 processed by lysis with CHAPS/urea-based lysis buffer.** Each protein listed below met the fold change cutoff criteria of either ≤ 0.67 or ≥ 1.5 compared to *chn-1(tm2692) C. elegans chn-1* mutants in *h*CHIP rescue strain 1. Initially, a reference list was created comparing N2 wild-type worms and *chn-1* mutants. Proteins differentially expressed in opposite directions from wild-type to knock-out animals and knock-out to rescue strains were defined as "rescued". Associated *p*-values and fold changes for each protein are listed in Supplemental Table C10.

Protein	Gene
Uncharacterized protein D2096.6	*D2096.6*
NADH-ubiquinone oxidoreductase chain 5	*nduo-5*
Nematode cuticle collagen N-terminal domain-containing protein	*dpy-8*
NADH-ubiquinone oxidoreductase chain 3	*nduo-3*
RRM domain-containing protein	*rbm-28*
Nematode cuticle collagen N-terminal domain-containing protein	*col-149*
Vacuolar protein-sorting-associated protein 25	*vps-25*
Proton-coupled zinc antiporter SLC30A5	*slc-30a5*
EOG090X04TT	*cox-15*
Epoxide hydrolase	*W01A11.1*
Iron-sulfur clusters transporter ABCB7, mitochondrial	*abtm-1*
Cytochrome c oxidase subunit 2	*ctc-2*
Tubulin beta chain	*ben-1*
Ragulator complex protein LAMTOR2 homolog	*lmtr-2*
ER membrane protein complex subunit 3	*emc-3*
Long chain fatty acid elongase 6	*elo-6*
Warthog protein 1	*wrt-1*
Putative metallophosphoesterase F40B5.2	*F40B5.2*
mRNA stability protein	*ensa-1*
Ubiquitin-conjugating enzyme E2 1	*ubc-1*
NADH-ubiquinone oxidoreductase chain 1	*nduo-1*
ATP synthase subunit a	*atp-6*
Bestrophin homolog 14	*best-14*
DUF19 domain-containing protein	*nspg-6*
Large ribosomal subunit protein uL10m	*mrpl-10*

Large ribosomal subunit protein mL52	*Y95D11A.1*
Charged multivesicular body protein 1b	*did-2*
Metaxin-1 homolog	*mtx-1*
Surfeit locus protein 4 homolog	*sft-4*
LITAF domain-containing protein	*Y87G2A.19*
carnitine O-palmitoyltransferase	*cpt-1*
Putative 1-acyl-sn-glycerol-3-phosphate acyltransferase acl-1	*acl-1*
Heat shock 70 kDa protein 13	*stc-1*
CRAL-TRIO domain-containing protein	*F20G2.3*
G-patch domain-containing protein	*T23G7.3*
Putative aquaporin-10	*aqp-10*
CRAL-TRIO domain-containing protein	*C11H1.9*
Histone H4	*his-1*
Large ribosomal subunit protein uL5A	*rpl-11.1*
CaDmium Responsive	*cdr-4*
Large ribosomal subunit protein uL5B	*rpl-11.2*
Putative endoplasmic reticulum metallopeptidase 1-A	*B0495.7*
Rab8	*rab-8*
Cytochrome b	*ctb-1*
Histidine-rich glycoprotein-like	*Y39B6A.1*
Casein kinase I gamma	*csnk-1*
Uncharacterized protein	*K03B8.6*
Endoplasmic reticulum lectin 1	*Y105E8A.2*
V-type proton ATPase 21 kDa proteolipid subunit c"	*vha-4*
Probable glycerol-3-phosphate acyltransferase, mitochondrial	*acl-6*
Kunitz/Bovine pancreatic trypsin inhibitor domain protein	*R12A1.3*
Pyr_redox_2 domain-containing protein	*wah-1*
BTB domain-containing protein	*B0496.1*
Translocon-associated protein subunit gamma	*trap-3*
Delta	*fat-2*
Huntington interacting protein related 1	*hipr-1*
BPTI/Kunitz inhibitor domain-containing protein	*C34F6.1*
Retinol dehydrogenase 13	*dhs-24*
Uncharacterized protein	*tag-281*
Acyltransferase 3 domain-containing protein	*ZK899.2*
DeHydrogenases, Short chain	*dhs-14*
Fatty acid-binding protein homolog 4	*lbp-4*
Fungal lipase-like domain-containing protein	*Y54G2A.45*
Long chain fatty acid elongase 2	*elo-2*
Probable manganese-transporting ATPase catp-8	*catp-8*

Excitatory amino acid transporter	*glt-1*
Ectopic P granules protein 3	*epg-3*
ABC transmembrane type-1 domain-containing protein	*haf-3*
Sidoreflexin	*sfxn-1.5*
Probable mitochondrial pyruvate carrier 1	*mpc-1*
J domain-containing protein	*dnj-29*
Long chain fatty acid elongase 5	*elo-5*
CaDmium Responsive	*cdr-6*
Uncharacterized protein C29G2.6	*C29G2.6*
UDP-N-acetylglucosamine/UDP-N-acetylgalactosamine transporter nstp-4	*nstp-4*
DeHydrogenases, Short chain	*F32A5.8*
Odorant response abnormal protein 4	*odr-4*
glucuronosyltransferase	*ugt-1*
EGF-like domain-containing protein	*kola-5*
SOSS complex subunit A homolog	*ints-3*
Glycoside hydrolase 35 catalytic domain-containing protein	*bgal-2*
DnaJ homolog dnj-2	*dnj-2*
Putative UDP-glucuronosyltransferase ugt-46	*ugt-46*
Trimeric intracellular cation channel type 1B.1	*tric-1B.1*
cystathionine gamma-lyase	*cth-1*
NAD-capped RNA hydrolase ndx-9	*ndx-9*
Probable RNA methyltransferase Y17G7B.18	*Y17G7B.18*
Nicalin	*nra-2*
Acyl-coenzyme A diphosphatase FITM2	*fitm-2*
Rab5-interacting protein	*F44E7.9*
Dolichyl-diphosphooligosaccharide--protein glycosyltransferase subunit 2	*ostd-1*
Nucleoside-diphosphatase uda-1	*uda-1*
glucuronosyltransferase	*ugt-29*
TOG domain-containing protein	*F54A3.2*
Putative zinc finger matrin-type protein snu-23	*snu-23*
Dual specificity mitogen-activated protein kinase kinase sek-1	*sek-1*
C2 domain-containing protein	*esyt-2*
START domain-containing protein 10	*T28D6.7*
Prolyl carboxy peptidase like protein 5	*pcp-5*
Putative cuticle collagen 80	*col-80*
Multifunctional methyltransferase subunit TRM112-like protein	*C04H5.1*
Uncharacterized protein C56G2.3	*C56G2.3*
Small RNA 2'-O-methyltransferase	*henn-1*
PUM-HD domain-containing protein	*puf-9*
Nucleolar protein 9	*ZK792.5*

Glutathione peroxidase 3	*gpx-3*
RNA helicase	*eif-4a3*
Helicase SKI2W	*skih-2*
3'-5' exonuclease domain-containing protein	*Y57A10A.13*
DNA-directed RNA polymerase subunit beta	*rpc-2*
Phosphatidate cytidylyltransferase, mitochondrial	*Y71F9B.2*
aralkylamine N-acetyltransferase	*M7.8*
DUF7087 domain-containing protein	*F17E9.5*
UBX domain-containing protein 6	*ubxn-6*
Cysteine protease atg-4.1	*atg-4.1*
Serine racemase	*serr-1*
39S ribosomal protein L55, mitochondrial	*mrpl-55*
GRounDhog	*grd-13*
N-alpha-acetyltransferase 20	*natb-1*
Domain of unknown function DX domain-containing protein	*T10E9.4*
Putative pyridoxal kinase	*pdxk-1*
m7GpppX diphosphatase	*dcs-1*
Anaphase-promoting complex subunit 4-like WD40 domain-containing protein	*aipl-1*
Probable urocanate hydratase	*Y51H4A.7*
Myosin IA	*hum-5*
DeHydrogenases, Short chain	*D1054.8*
Apple domain-containing protein	*T21B6.3*
COP9 signalosome complex subunit 2	*csn-2*
Large ribosomal subunit protein bL17m	*mrpl-17*
Probable glutamine synthetase	*gln-2*
Sjogren's syndrome/scleroderma autoantigen 1	*Y39A1A.3*
Saposin B-type domain-containing protein	*spp-17*
DNA replication licensing factor MCM7	*mcm-7*
Aldehyde dehydrogenase domain-containing protein	*alh-1*
Peptidase S28	*pcp-2*
Tudor domain-containing protein	*ekl-1*
High mobility group protein hmg-12	*hmg-12*
Protein male abnormal 7	*mab-7*
Ribosomal protein S6 kinase beta	*rsks-1*
Glycolipid transfer protein domain-containing protein	*Y82E9BR.14*
Dymeclin	*C47D12.2*
Uncharacterized Golgi apparatus membrane protein-like protein C34D4.4	*C34D4.4*
Cytochrome c oxidase assembly protein COX20, mitochondrial	*C26B2.7*
CMP/dCMP-type deaminase domain-containing protein	*Y48A6B.7*

EB domain-containing protein	*F56B3.2*
C-type lectin domain-containing protein	*clec-51*
Nematode cuticle collagen N-terminal domain-containing protein	*col-124*
Putative choline-phosphate cytidylyltransferase	*pcyt-1*
Nucleotidyl transferase domain-containing protein	*Y47D9A.1*
Retinoid-inducible serine carboxypeptidase	*Y32F6A.5*
JmjC domain-containing protein	*C27F2.9*
DUF3945 domain-containing protein	*Y38E10A.17*
Intestinal acid PHOsphatase	*pho-13*
Probable 26S proteasome non-ATPase regulatory subunit 9	*psmd-9*
Large ribosomal subunit protein mL51	*mrpl-51*
Tubby protein homolog 1	*tub-1*
Ubiquinone biosynthesis monooxygenase COQ6, mitochondrial	*coq-6*
Probable [pyruvate dehydrogenase	*pdhk-2*
Glycoside hydrolase family 1 protein	*klo-1*
Patched-related protein 18	*ptr-18*
PUA domain-containing protein	*C11D2.7*
Probable peptidyl-tRNA hydrolase 2	*C24G6.8*
Small-subunit processome Utp12 domain-containing protein	*T10B5.3*
DUF148 domain-containing protein	*K02F3.9*
Sperm-specific class P protein 34	*ssp-34*
Splicing factor U2AF 35 kDa subunit	*uaf-2*
Elongin-C	*elc-1*
Serine/threonine-protein phosphatase 4 catalytic subunit 1	*pph-4.1*
Acireductone dioxygenase	*F42F12.4*

Supplemental Table C17 **Genes corresponding to rescued proteins (based on fold change) identified by SWATH-MS that are either over- or under-represented in *h*CHIP rescue strain 2 processed by lysis with CHAPS/urea-based lysis buffer.** Each protein listed below met the fold change cutoff criteria of either ≤ 0.67 or ≥ 1.5 compared to *chn-1(tm2692) C. elegans chn-1* mutants in *h*CHIP rescue strain 2. Initially, a reference list was created comparing N2 wild-type worms and *chn-1* mutants. Proteins differentially expressed in opposite directions from wild-type to knock-out animals and knock-out to rescue strains were defined as "rescued". Associated *p*-values and fold changes for each protein are listed in Supplemental Table C11.

Protein	Gene
Dehydrogenase/reductase SDR family member 4	*dhrs-4*
Aralkylamine N-acetyltransferase	*M7.8*
RNA helicase	*eif-4a3*
Tubby protein homolog 1	*tub-1*
DNA-directed RNA polymerase subunit beta	*rpc-2*
PUM-HD domain-containing protein	*puf-9*
Saposin B-type domain-containing protein	*spp-17*
3'-5' exonuclease domain-containing protein	*Y57A10A.13*
Prolyl carboxy peptidase like protein 5	*pcp-5*
Aldehyde dehydrogenase domain-containing protein	*alh-1*
Probable glutamine synthetase	*gln-2*
Serine/threonine-protein phosphatase PP1-gamma	*gsp-3*
Uncharacterized Golgi apparatus membrane protein-like protein C34D4.4	*C34D4.4*
Glycoside hydrolase family 1 protein	*klo-1*
DUF7087 domain-containing protein	*F17E9.5*
Serine/threonine-protein phosphatase 4 catalytic subunit 1	*pph-4.1*
Sjogren's syndrome/scleroderma autoantigen 1	*Y39A1A.3*
Cysteine protease atg-4.1	*atg-4.1*
Intestinal acid PHOsphatase	*pho-13*
Protein male abnormal 7	*mab-7*
Cytochrome c oxidase assembly protein COX20, mitochondrial	*C26B2.7*
Putative choline-phosphate cytidylyltransferase	*pcyt-1*
EB domain-containing protein	*M03F4.6*
Serine racemase	*serr-1*
Myosin IA	*hum-5*
Small RNA 2'-O-methyltransferase	*henn-1*
Putative pyrroline-5-carboxylate reductase 4	*pycr-4*
Ubiquitin fusion degradation protein 1 homolog	*ufd-1*
Probable peptidyl-tRNA hydrolase 2	*C24G6.8*
Methyltransferase BUD23	*C27F2.4*

39S ribosomal protein L55, mitochondrial	*mrpl-55*
Probable urocanate hydratase	*Y51H4A.7*
Nucleolar protein 9	*ZK792.5*
Glyceraldehyde-3-phosphate dehydrogenase 1	*gpd-1*
Putative zinc finger matrin-type protein snu-23	*snu-23*
Putative cuticle collagen 80	*col-80*
Serum response factor-binding protein 1	*F18C12.3*
Probable [pyruvate dehydrogenase acetyl-transferring)] kinase, mitochondrial	*pdhk-2*
COP9 signalosome complex subunit 2	*csn-2*
Protein transport protein sec-16A.1	*sec-16A.1*
Phosphoinositide phospholipase C	*plc-4*
VWFA domain-containing protein	*vwa-8*
DUF3945 domain-containing protein	*Y38E10A.17*
Ribosomal protein S6 kinase beta	*rsks-1*
C-type lectin domain-containing protein	*clec-1*
Corrinoid adenosyltransferase MMAB	*mmab-1*
Putative pyridoxal kinase	*pdxk-1*
Putative thiosulfate sulfurtransferase mpst-4	*mpst-4*
Ubiquinone biosynthesis monooxygenase COQ6, mitochondrial	*coq-6*
m7GpppX diphosphatase	*dcs-1*
C-factor	*dhs-31*
Dymeclin	*C47D12.2*
VWFA domain-containing protein	*C24B9.3*
RING-type E3 ubiquitin transferase	*nhl-2*
U5 small nuclear ribonucleoprotein 40 kDa protein	*snrp-40.1*
Periplasmic protein	*E04F6.9*
Glutathione peroxidase 1	*gpx-1*
Glutathione peroxidase 3	*gpx-3*
CaLponIn-liKe proteins	*clik-3*
DeHydrogenases, Short chain	*D1054.8*
SUPpressor	*sup-36*
Small ribosomal subunit protein mS31	*mrps-31*
Patched-related protein 18	*ptr-18*
Peptidase S28	*pcp-2*
Phosphatidate cytidylyltransferase, mitochondrial	*Y71F9B.2*
Suppressor of forked domain-containing protein	*suf-1*
Uncharacterized protein C56G2.3	*C56G2.3*
MO25-like protein 2	*mop-25.2*
Uridine and thymidine phosphorylase	*upp-1*
COP9 signalosome complex subunit 1	*csn-1*

Domain of unknown function DX domain-containing protein	*T10E9.4*
UBX domain-containing protein 6	*ubxn-6*
Large ribosomal subunit protein bL9m	*mrpl-9*
GRounDhog	*grd-13*
Elongator complex protein 4	*elpc-4*
Arginine kinase	*F32B5.1*
Secretory carrier-associated membrane protein	*scm-1*
High mobility group protein hmg-12	*hmg-12*
Serine protease inhibitor swm-1	*swm-1*
CMP/dCMP-type deaminase domain-containing protein	*Y48A6B.7*
Nose resistant to fluoxetine protein 5	*nrf-5*
Uncharacterized protein D2096.6	*D2096.6*
ADP-ribosylation factor GTPase-activating protein 1	*K02B12.7*
Proton-coupled zinc antiporter SLC30A5	*slc-30a5*
RRM domain-containing protein	*grld-1*
TOG domain-containing protein	*F54A3.2*
Putative aquaporin-10	*aqp-10*
Multidrug resistance protein mrp-7	*mrp-7*
Large ribosomal subunit protein uL5A	*rpl-11.1*
EGF-like domain-containing protein	*kola-5*
Probable mitochondrial pyruvate carrier 1	*mpc-1*
EOG090X04TT	*cox-15*
Putative 1-acyl-sn-glycerol-3-phosphate acyltransferase acl-1	*acl-1*
Long chain fatty acid elongase 6	*elo-6*
Hydroxyacylglutathione hydrolase	*Y17G7B.3*
Putative metallophosphoesterase F40B5.2	*F40B5.2*
Large ribosomal subunit protein uL5B	*rpl-11.2*
NADH-ubiquinone oxidoreductase chain 5	*nduo-5*
Fatty acid-binding protein homolog 4	*lbp-4*
Excitatory amino acid transporter	*glt-1*
DUF3598 domain-containing protein	*C05D2.8*
Probable rho GDP-dissociation inhibitor	*rhi-1*
ATP synthase subunit a	*atp-6*
Uncharacterized protein	*K03B8.6*
Nematode cuticle collagen N-terminal domain-containing protein	*dpy-8*
Acyltransferase 3 domain-containing protein	*ZK899.2*
C3H1-type domain-containing protein	*Y53G8AR.9*
Nematode cuticle collagen N-terminal domain-containing protein	*col-149*
Dynactin subunit 5	*dnc-5*
Protein KRI1 homolog	*F54C9.9*

Kunitz/Bovine pancreatic trypsin inhibitor domain protein	*R12A1.3*
Iron-sulfur clusters transporter ABCB7, mitochondrial	*abtm-1*
Long chain fatty acid elongase 5	*elo-5*
BPTI/Kunitz inhibitor domain-containing protein	*C34F6.1*
NADH-ubiquinone oxidoreductase chain 4	*nduo-4*
NAD-capped RNA hydrolase ndx-9	*ndx-9*
Delta (12) fatty acid desaturase fat-2	*fat-2*
Bestrophin homolog 14	*best-14*
Rab5-interacting protein	*F44E7.9*
NADH-ubiquinone oxidoreductase chain 3	*nduo-3*
Carnitine O-palmitoyltransferase	*cpt-1*
Heat shock 70 kDa protein 13	*stc-1*
Tetratricopeptide repeat protein 38	*Y54G11A.7*
Endoplasmic reticulum lectin 1	*Y105E8A.2*
CHCH domain-containing protein	*T20D3.14*
Lipid scramblase CLPTM1L	*T13H5.8*
Splicing factor 3B subunit 6-like protein	*sftb-6*
CRAL-TRIO domain-containing protein	*F20G2.3*
U3 small nucleolar ribonucleoprotein protein MPP10	*Y75B8A.7*
Retinol dehydrogenase 13	*dhs-24*
ER membrane protein complex subunit 7 homolog	*C35D10.1*
DnaJ homolog dnj-2	*dnj-2*
LEM protein 2	*lem-2*
Probable manganese-transporting ATPase catp-8	*catp-8*
Charged multivesicular body protein 1b	*did-2*
DeHydrogenases, Short chain	*F32A5.8*
SOSS complex subunit A homolog	*ints-3*
Fungal lipase-like domain-containing protein	*Y54G2A.45*
Delta (24)-sterol reductase homolog dhcr-24	*dhcr-24*
Surfeit locus protein 4 homolog	*sft-4*
Abnormal cell migration protein 18-like fibronectin type I domain-containing protein	*T10G3.3*
DNA replication licensing factor mcm-6	*mcm-6*
Glycoside hydrolase 35 catalytic domain-containing protein	*bgal-2*
Diacylglycerol cholinephosphotransferase	*cept-1*
DUF155 domain-containing protein	*ZK1010.2*
Histone H4	*his-1*
DeHydrogenases, Short chain	*dhs-14*
Uncharacterized protein	*tag-281*
Putative endoplasmic reticulum metallopeptidase 1-A	*B0495.7*

Exosome complex component RRP45	*exos-9*
Nicalin	*nra-2*
Ectopic P granules protein 3	*epg-3*
Metaxin-1 homolog	*mtx-1*
J domain-containing protein	*dnj-29*
Mannosyl-oligosaccharide 1,2-alpha-mannosidase mans-2	*mans-2*
tRNA (guanine (26)-N (2))-dimethyltransferase	*trm-1*
Mitochondrial glutamate carrier 1	*slc-25a18.1*
NADH-ubiquinone oxidoreductase chain 1	*nduo-1*
Putative UDP-glucuronosyltransferase ugt-46	*ugt-46*
UDP-glucuronosyltransferase	*ugt-16*
Membrane magnesium transporter	*emc-5*
Endoplasmic reticulum-Golgi intermediate compartment protein 3	*ergi-3*
CaDmium Responsive	*cdr-4*
LITAF domain-containing protein	*Y87G2A.19*
Long chain fatty acid elongase 2	*elo-2*
Ribosome production factor 2 homolog	*Y54E10A.10*
Cleft lip and palate transmembrane protein 1 homolog	*R166.2*
Cytochrome b	*ctb-1*
Sidoreflexin	*sfxn-1.5*
DUF19 domain-containing protein	*nspg-6*
Dolichyl-diphosphooligosaccharide--protein glycosyltransferase subunit 2	*ostd-1*
Translocon-associated protein subunit gamma	*trap-3*
Epoxide hydrolase	*W01A11.1*
Nematode cuticle collagen N-terminal domain-containing protein	*col-174*
Odorant response abnormal protein 4	*odr-4*
Fatty acid amide hydrolase 1	*faah-1*
Nucleolar protein 6	*nol-6*
V-type proton ATPase 21 kDa proteolipid subunit c"	*vha-4*
DOMON domain-containing protein	*Y57G11A.4*
Glucuronosyltransferase	*ugt-29*
Brix domain-containing protein ZK795.3	*ZK795.3*
UDP-N-acetylglucosamine/UDP-N-acetylgalactosamine transporter nstp-4	*nstp-4*
Acyl-coenzyme A diphosphatase FITM2	*fitm-2*
Strictosidine synthase conserved region domain-containing protein	*F57C2.5*
Cytochrome c oxidase subunit 2	*ctc-2*
RRM domain-containing protein	*rbm-28*
ER membrane protein complex subunit 3	*emc-3*
Uridine diphosphate glucose pyrophosphatase NUDT14	*C50F4.16*

Supplemental Table C18 **Genes corresponding to rescued proteins (based on fold change) identified by SWATH-MS that are either over- or under-represented in the *Ce*CHIP rescue strain processed by lysis with CHAPS/urea-based lysis buffer.** Each protein listed below met the fold change cutoff criteria of either ≤ 0.67 or ≥ 1.5 compared to *chn-1(tm2692) C. elegans chn-1* mutants in the *Ce*CHIP rescue strain. Initially, a reference list was created comparing N2 wild-type worms and *chn-1* mutants. Proteins differentially expressed in opposite directions from wild-type to knock-out animals and knock-out to rescue strains were defined as "rescued". Associated *p*-values and fold changes for each protein are listed in Supplemental Table C12.

Protein	Gene
PUM-HD domain-containing protein	*puf-9*
Aldehyde dehydrogenase domain-containing protein	*alh-1*
Probable glutamine synthetase	*gln-2*
Serine/threonine-protein phosphatase PP1-gamma	*gsp-3*
C-type lectin domain-containing protein	*clec-1*
Small RNA 2'-O-methyltransferase	*henn-1*
RNA helicase	*eif-4a3*
RING-type E3 ubiquitin transferase	*nhl-2*
Protein BCCIP homolog	*ZK1127.4*
Uncharacterized Golgi apparatus membrane protein-like protein C34D4.4	*C34D4.4*
Myosin IA	*hum-5*
DNA-directed RNA polymerase subunit beta	*rpc-2*
DUF7087 domain-containing protein	*F17E9.5*
Putative choline-phosphate cytidylyltransferase	*pcyt-1*
Uncharacterized protein C56G2.3	*C56G2.3*
3'-5' exonuclease domain-containing protein	*Y57A10A.13*
Tubby protein homolog 1	*tub-1*
Probable urocanate hydratase	*Y51H4A.7*
Serum response factor-binding protein 1	*F18C12.3*
Gamma-soluble NSF attachment protein	*Y59A8B.8*
FeS cluster biogenesis domain-containing protein	*Y54G11A.9*
CaLponIn-liKe proteins	*clik-3*
Small subunit of serine palmitoyltransferase	*F13H10.8*
GRounDhog	*grd-13*
Dymeclin	*C47D12.2*
Nucleolar protein 9	*ZK792.5*
m7GpppX diphosphatase	*dcs-1*
FACT complex subunit ssrp1-B	*hmg-3*
Serine protease inhibitor swm-1	*swm-1*
Probable peptidyl-tRNA hydrolase 2	*C24G6.8*

Ubiquinone biosynthesis monooxygenase COQ6, mitochondrial	*coq-6*
Patched-related protein 18	*ptr-18*
DUF148 domain-containing protein	*K02F3.9*
Corrinoid adenosyltransferase MMAB	*mmab-1*
High mobility group protein hmg-12	*hmg-12*
COP9 signalosome complex subunit 2	*csn-2*
Calcium-transporting ATPase	*mca-3*
Small ribosomal subunit protein mS31	*mrps-31*
Anaphase-promoting complex subunit 4-like WD40 domain-containing protein	*aipl-1*
Glycoside hydrolase family 1 protein	*klo-1*
Elongin-C	*elc-1*
FErroChelatase-Like	*fecl-1*
Serine racemase	*serr-1*
Glycolipid transfer protein domain-containing protein	*Y82E9BR.14*
mRNA-decapping enzyme 1	*dcap-1*
Probable ubiquitin-conjugating enzyme E2 7	*ubc-7*
C-factor	*dhs-31*
Glutathione peroxidase 1	*gpx-1*
Peptidase S28	*pcp-2*
Seryl-tRNA synthetase	*K03B4.1*
Suppressor of forked domain-containing protein	*suf-1*
Complex 1 LYR protein domain-containing protein	*F53G2.12*
Prolyl carboxy peptidase like protein 5	*pcp-5*
Large ribosomal subunit protein bL17m	*mrpl-17*
Ribosomal protein S6 kinase beta	*rsks-1*
N-alpha-acetyltransferase 20	*natb-1*
COP9 signalosome complex subunit 1	*csn-1*
Serine/threonine-protein phosphatase 4 catalytic subunit 1	*pph-4.1*
Small ribosomal subunit protein uS10 domain-containing protein	*mrpl-48*
NADP-dependent oxidoreductase domain-containing protein	*K07C5.2*
mRNA stability protein	*ensa-1*
C3H1-type domain-containing protein	*Y53G8AR.9*
Uncharacterized protein D2096.6	*D2096.6*
Protein CASC3	*casc-3*
TOG domain-containing protein	*F54A3.2*
ADP-ribosylation factor GTPase-activating protein 1	*K02B12.7*
E3 ubiquitin-protein ligase UBR5	*ubr-5*
EGF-like domain-containing protein	*kola-5*
Uncharacterized protein	*tag-281*

Uncharacterized protein	*K03B8.6*
Large ribosomal subunit protein mL52	*Y95D11A.1*
Large ribosomal subunit protein uL5A	*rpl-11.1*
Cystathionine gamma-lyase	*cth-1*
DeHydrogenases, Short chain	*dhs-14*
Nematode cuticle collagen N-terminal domain-containing protein	*col-149*
Fungal lipase-like domain-containing protein	*Y54G2A.45*
DUF3598 domain-containing protein	*C05D2.8*
BPTI/Kunitz inhibitor domain-containing protein	*C34F6.1*
DOMON domain-containing protein	*Y57G11A.4*
Vacuolar protein-sorting-associated protein 25	*vps-25*
Proton-coupled zinc antiporter SLC30A5	*slc-30a5*
Lipid scramblase CLPTM1L	*T13H5.8*
Rab8	*rab-8*
Bestrophin homolog 14	*best-14*
RRM domain-containing protein	*rbm-28*
Uncharacterized protein C29G2.6	*C29G2.6*
Glycoside hydrolase 35 catalytic domain-containing protein	*bgal-2*
Strictosidine synthase conserved region domain-containing protein	*F57C2.5*
Long chain fatty acid elongase 6	*elo-6*
CaDmium Responsive	*cdr-4*
Nematode cuticle collagen N-terminal domain-containing protein	*dpy-8*
Mitochondrial glutamate carrier 1	*slc-25a18.1*
Carnitine O-palmitoyltransferase	*cpt-1*
ER membrane protein complex subunit 7 homolog	*C35D10.1*
Probable glycerol-3-phosphate acyltransferase, mitochondrial	*acl-6*
Nucleoside-diphosphatase uda-1	*uda-1*
Protein KRI1 homolog	*F54C9.9*
Transthyretin-like family protein	*ttr-35*
DUF19 domain-containing protein	*nspg-6*
Long chain fatty acid elongase 5	*elo-5*
CHCH domain-containing protein	*T20D3.14*
Medium-chain acyl-CoA dehydrogenase	*acdh-8*
Cleft lip and palate transmembrane protein 1 homolog	*R166.2*
Probable DNA-directed RNA polymerases I, II, and III subunit RPABC2	*rpb-6*
CRAL-TRIO domain-containing protein	*C11H1.9*
DNA replication licensing factor mcm-6	*mcm-6*
Protein LTV1 homolog	*T23D8.3*
Uridine diphosphate glucose pyrophosphatase NUDT14	*C50F4.16*
Alpha-mannosidase	*aman-2*

SOSS complex subunit A homolog	*ints-3*
DUF155 domain-containing protein	*ZK1010.2*
Exosome complex component RRP45	*exos-9*
Putative aquaporin-10	*aqp-10*
CRAL-TRIO domain-containing protein	*F20G2.3*
Epoxide hydrolase	*W01A11.1*
DeHydrogenases, Short chain	*F32A5.8*
Heat shock 70 kDa protein 13	*stc-1*
Cytochrome b (Complex III subunit 3)	*ctb-1*
Probable rho GDP-dissociation inhibitor	*rhi-1*
Tetratricopeptide repeat protein 38	*Y54G11A.7*
tRNA (guanine (26)-N (2))-dimethyltransferase	*trm-1*
Ribosome production factor 2 homolog	*Y54E10A.10*
Fatty acid-binding protein homolog 4	*lbp-4*
Retinol dehydrogenase 13	*dhs-24*
Putative 1-acyl-sn-glycerol-3-phosphate acyltransferase acl-1	*acl-1*
Probable manganese-transporting ATPase catp-8	*catp-8*
Putative metallophosphoesterase F40B5.2	*F40B5.2*

Supplemental Table C19 **Genes corresponding to rescued proteins (based on fold change) identified by SWATH-MS that are either over- or under-represented in *h*CHIP rescue strain 1 processed by lysis with SDS-based lysis buffer.** Each protein listed below met the fold change cutoff criteria of either ≤ 0.67 or ≥ 1.5 compared to *chn-1(tm2692) C. elegans chn-1* mutants in *h*CHIP rescue strain 1. Initially, a reference list was created comparing N2 wild-type worms and *chn-1* mutants. Proteins differentially expressed in opposite directions from wild-type to knock-out animals and knock-out to rescue strains were defined as "rescued". Associated *p*-values and fold changes for each protein are listed in Supplemental Table C13.

Protein	Gene
Nematode cuticle collagen N-terminal domain-containing protein	*col-124*
PHAF1 protein T01G9.2	*T01G9.2*
ATP synthase subunit C lysine N-methyltransferase	*Y39A1A.21*
Vitellogenin-1	*vit-1*
Uterine Lumin Expressed/locailized	*ule-3*
Peptidyl-prolyl cis-trans isomerase 10	*cyn-10*
Prion-like-(Q/N-rich)-domain-bearing protein	*C55C3.3*
DNA repair endonuclease XPF	*xpf-1*
Mitochondrial import receptor subunit TOM7 homolog	*tomm-7*
Fungal lipase-like domain-containing protein	*T10B5.7*
Histone H2A	*his-3*
Glucuronosyltransferase	*ugt-13*
DB domain-containing protein	*F55H12.4*
Vitellogenin-5	*vit-5*
Peroxidasin homolog pxn-2	*pxn-2*
Abnormal cell migration protein 18-like fibronectin type I domain-containing protein	*F25E2.2*
Domain of unknown function DX domain-containing protein	*T10E9.4*
Golgi-specific brefeldin A-resistance guanine nucleotide exchange factor 1 homolog	*gbf-1*
TransThyretin-Related family domain	*F17E9.4*
AP-2 complex subunit alpha	*apa-2*
RING-type E3 ubiquitin transferase	*rnf-126*
Putative cystathionine gamma-lyase 2	*cth-2*
Molting protein mlt-10	*mlt-10*
GM2 Activator Protein family member	*gmap-3*
RNA polymerase II transcription factor SIII p18 subunit	*elb-1*
Riboflavin kinase	*rfk-1*
MATH domain-containing protein	*ZC204.12*
SURF1-like protein	*sft-1*
Gut esterase 1	*ges-1*

Saposin B-type domain-containing protein	*spp-17*
Vesicle-trafficking protein SEC22b	*sec-22*
Hydroxyacylglutathione hydrolase	*Y17G7B.3*
Carboxypeptidase E	*egl-21*
Protein-tyrosine-phosphatase	*ptpn-22*
Intestinal acid phosphatase	*pho-1*
SUI1 domain-containing protein	*eif-1*
UBX domain-containing protein 4	*ubxn-4*
Nucleoside hydrolase	*Y43F8C.13*
SAM50-like protein gop-3	*gop-3*
Cystatin domain-containing protein	*C39B5.5*
Protein LTV1 homolog	*T23D8.3*
Vitellogenin-2	*vit-2*
E3 ubiquitin-protein ligase hecd-1	*hecd-1*
Dihydropyrimidinase 2	*dhp-2*
Extracellular protein	*Y54G2A.76*
GTP-binding protein drn-1	*drn-1*
Fatty acyl-CoA reductase	*fard-1*
Polyribonucleotide nucleotidyltransferase	*pnpt-1*
DNA-directed RNA polymerase II subunit RPB1	*ama-1*
Uncharacterized protein byn-1	*byn-1*
Peptidase M14 carboxypeptidase A domain-containing protein	*F02D8.4*
mRNA export factor rae-1	*rae-1*
Nematode cuticle collagen N-terminal domain-containing protein	*col-119*
Innexin-5	*inx-5*
Vacuolar protein sorting-associated protein 28 homolog	*vps-28*
Putative cuticle collagen 80	*col-80*
Splicing factor 3B subunit 1 domain-containing protein	*sftb-1*
Proliferating cell nuclear antigen	*pcn-1*
Vitellogenin-3	*vit-3*
sn-1-specific diacylglycerol lipase ABHD11	*abhd-11.2*
5'-3' exoribonuclease 2 homolog	*xrn-2*
Intrinsically Disordered Protein, class C	*idpc-3*
Signal peptidase complex subunit 2	*spcs-2*
Pre-mRNA-splicing factor ATP-dependent RNA helicase ddx-15	*ddx-15*
Pinin/SDK/MemA protein domain-containing protein	*pnn-1*
Cysteine protease atg-4.1	*atg-4.1*
26S rRNA (cytosine-C (5))-methyltransferase nsun-5	*nsun-5*
Neuronal calcium sensor 2	*ncs-2*

Chromatin target of PRMT1 protein C-terminal domain-containing protein	*Y92H12BR.2*
Tyrosine aminotransferase	*tatn-1*
Transthyretin-like family protein	*ttr-48*
NEDD8-conjugating enzyme ubc-12	*ubc-12*
Putative transcription elongation factor S-II	*T24H10.1*
Not3 domain-containing protein	*ntl-3*
RIIa domain-containing protein	*F39H12.3*
U5 small nuclear ribonucleoprotein 200 kDa helicase	*snrp-200*
Serine/threonine-protein phosphatase 2A activator	*Y71H2AM.20*
VWFA domain-containing protein	*vwa-8*
Cytoplasmic tRNA 2-thiolation protein 1	*tut-1*
Skp1-related protein	*skr-3*
BPI1 domain-containing protein	*F10D11.6*
Prolyl Carboxy Peptidase like	*pcp-4*
Exportin-2	*xpo-2*
Nucleolar complex protein 2 homolog	*pro-2*
Saposin B-type domain-containing protein	*Y66H1A.5*
Multifunctional procollagen lysine hydroxylase and glycosyltransferase	*let-268*
Ribosomal Protein, Small subunit	*rps-15a*
Large ribosomal subunit protein bL9m	*mrpl-9*
Integrin-linked protein kinase homolog pat-4	*pat-4*
C6 domain-containing protein	*Y47G6A.33*
Protein mac-1	*mac-1*
DUF19 domain-containing protein	*T13F3.6*
Uncharacterized protein ZK1320.3	*ZK1320.3*
Probable glutathione S-transferase gst-36	*gst-36*
Probable 26S proteasome complex subunit dss-1	*dss-1*
Proline dehydrogenase 1, mitochondrial	*prdh-1*
Nuclear hormone receptor family member nhr-49	*nhr-49*
CRAL-TRIO domain-containing protein	*cgr-1*
MICOS complex subunit MIC60-2	*immt-2*
Proteasome subunit alpha type-7	*pas-4*
V-type proton ATPase 116 kDa subunit a 1	*unc-32*
Uncharacterized protein C05D11.1	*C05D11.1*
Splicing factor 3B subunit 6-like protein	*sftb-6*
Large ribosomal subunit protein uL10m	*mrpl-10*
Tubulin--tyrosine ligase-like protein 12	*ttll-12*
KH domain-containing protein akap-1	*akap-1*
UBX domain-containing protein 3	*ubxn-3*

Secreted protein	*R105.1*
Glycoside hydrolase 35 catalytic domain-containing protein	*bgal-2*
Probable Golgi transport protein 1	*eas-1*
Major sperm protein	*R10E9.2*
Peptidase M16 N-terminal domain-containing protein	*ucr-2.3*
Ig-like domain-containing protein	*F21C10.7*
Zwei Ig domain protein zig-1	*zig-1*
Ribonucleoside-diphosphate reductase large subunit	*rnr-1*
HECT domain-containing protein	*herc-1*
AB hydrolase-1 domain-containing protein	*K01A2.5*
Uncharacterized oxidoreductase F53C11.3	*decr-1.1*
DDRGK domain-containing protein 1	*ufbp-1*
Phosphatidate cytidylyltransferase, mitochondrial	*Y71F9B.2*
Host cell factor homolog hcf-1	*hcf-1*
Major facilitator superfamily	*C46C2.2*
Ran GTPase-activating protein 2	*ran-2*
Probable 26S proteasome regulatory subunit 6B	*rpt-3*
Probable UDP-N-acetylglucosamine pyrophosphorylase	*C36A4.4*
Glutamine synthetase	*gln-1*
Stomatin-1	*sto-1*
ER membrane protein complex subunit 1	*emc-1*
alpha-1,2-Mannosidase	*ZC506.1*
Dynamin	*dyn-1*
Coatomer subunit epsilon	*cope-1*
DeHydrogenases, Short chain	*R119.3*
PH domain-containing protein	*F42C5.9*
Small ribosomal subunit protein mS31	*mrps-31*
Glutathione S-transferase 4	*gst-4*
Probable mitochondrial import inner membrane translocase subunit tim-17B.1	*timm-17B.1*
F-actin-capping protein subunit alpha	*cap-1*
Large ribosomal subunit protein P2	*rplp-2.2*
Uncharacterized protein C18H9.6	*C18H9.6*
Actin	*arp-1*
Proteasome subunit beta type-1	*pbs-6*
Maestro heat-like repeat-containing protein family member 1 homolog	*hpo-27*
Ribulose-phosphate 3-epimerase	*F08F8.7*
2-hydroxyacyl-CoA lyase 2	*T26C12.1*
Uncharacterized protein R05D3.9	*R05D3.9/R05D3.10*
Nematode Specific Peptide family	*nsph-3.1*

Vitelline membrane outer layer protein 1	*Y57G11A.2*
Acyl-coenzyme A thioesterase 8	*C37H5.13*
Argonaute protein wago-4	*wago-4*
SURF6 homolog gldi-11	*gldi-11*
Ig-like domain-containing protein	*zig-12*
Mitochondrial import inner membrane translocase subunit TIM50	*scpl-4*
SUMO-activating enzyme subunit aos-1	*aos-1*
LIM domain-containing protein unc-95	*unc-95*
Probable mitochondrial pyruvate carrier 1	*mpc-1*
Acidic leucine-rich nuclear phosphoprotein 32-related protein 1	*F33H2.3*
CYtochrome P450 family	*cyp-37a1*
Ubiquinone biosynthesis O-methyltransferase, mitochondrial	*coq-3*
Malate dehydrogenase	*VF13D12L.3*
BTB domain-containing protein	*ivns-1*
Fibulin-1	*fbl-1*
Protein kinase domain-containing protein	*F52B5.2*
Sm domain-containing protein	*atx-2*
JNK-interacting protein	*unc-16*
E3 ubiquitin-protein ligase listerin	*Y54E10A.11*
39S ribosomal protein L55, mitochondrial	*mrpl-55*
PI31_Prot_N domain-containing protein	*F09E5.7*
Cytochrome P450	*cyp-25a2*
Flavin-containing monooxygenase	*fmo-4*
Nematode cuticle collagen N-terminal domain-containing protein	*col-174*
Putative UDP-glucuronosyltransferase ugt-47	*ugt-47*
Fanconi anemia group I protein	*D2030.3*
GTP-binding protein	*raga-1*
V-type proton ATPase subunit e	*vha-17*
Activated in Blocked Unfolded protein response	*abu-13*
Membrane insertase YidC/Oxa/ALB C-terminal domain-containing protein	*oxa-1*
G-patch domain-containing protein	*T23G7.3*
Cytochrome c oxidase subunit 1	*ctc-1*
EOG090X04TT	*cox-15*
Endoplasmic reticulum lectin 1	*Y105E8A.2*
C6 domain-containing protein	*C14A4.9*
Transport and Golgi organization protein 1 homolog	*T22C1.6*
Fcf2 pre-rRNA processing C-terminal domain-containing protein	*Y49F6B.2*
Extracellular superoxide dismutase [Cu-Zn]	*sod-4*
Probable inactive acireductone dioxygenase 1	*T01D1.4*

Metal transporter cnnm-1	*cnnm-1*
Abnormal cell migration protein 18-like fibronectin type I domain-containing protein	*T10G3.3*
Small ribosomal subunit protein uS14m	*mrps-14*
Protein CASC3	*casc-3*
Proton-coupled zinc antiporter SLC30A5	*slc-30a5*
Mannose-6-phosphate isomerase	*C05C8.7*
Serpentine Receptor, class T	*F57G9.3*
BPTI/Kunitz inhibitor domain-containing protein	*F30H5.3*
Cuticle collagen 38	*col-38*
Cuticle collagen 14	*col-14*
Domain of unknown function DB domain-containing protein	*Y65B4BM.3*
NADAR domain-containing protein	*sna-3*
Nematode cuticle collagen N-terminal domain-containing protein	*col-109*
Probable maleylacetoacetate isomerase	*gst-42*
CMP/dCMP-type deaminase domain-containing protein	*Y48A6B.7*
Beta/gamma crystallin 'Greek key' domain-containing protein	*F15B9.8*
Rhodanese domain-containing protein	*dhs-30*
Transthyretin-like family protein	*ttr-31*
Nematode cuticle collagen N-terminal domain-containing protein	*ram-2*
Probable 2,4-dienoyl-CoA reductase 3 [(3E)-enoyl-CoA-producing]	*decr-1.3*
Putative cuticle collagen 145	*col-145*
Nematode cuticle collagen N-terminal domain-containing protein	*dpy-4*
Putative dihydrofolate reductase	*dhfr-1*
Aspartate dehydrogenase domain-containing protein	*F17C8.9*
Nematode cuticle collagen N-terminal domain-containing protein	*col-97*
NADH-ubiquinone oxidoreductase chain 4	*nduo-4*
Large ribosomal subunit protein uL3m	*mrps-18C*
Onchocerca Related Antigen family	*ora-1*
Neprilysin-1	*nep-1*
Warthog protein 4	*wrt-4*
Cuticle collagen 10	*col-10*
Soluble NSF attachment protein 29	*snap-29*
WaRThog	*wrt-10*
Mitochondrial Ribosomal Protein, Large	*mrpl-39*
YKT6 homolog	*ykt-6*
EF-hand domain-containing protein	*H10E21.4*
Putative cuticle collagen 91	*col-91*
Peptidyl-prolyl cis-trans isomerase 4	*cyn-4*
Ribonucleoside-diphosphate reductase small chain	*rnr-2*

Small ribosomal subunit protein mS23	*mrps-23*
Cuticle collagen 1	*sqt-3*
Alpha-tubulin N-acetyltransferase 1	*mec-17*
Histidine-rich glycoprotein-like	*Y39B6A.1*
Uterine Lumin Expressed/localized	*ule-2*
LITAF domain-containing protein	*Y87G2A.19*
ALG-1 INteracting protein	*ain-1*
Heat shock protein Hsp-12.2	*hsp-12.2*
Nematode cuticle collagen N-terminal domain-containing protein	*bli-6*
Nematode cuticle collagen N-terminal domain-containing protein	*rol-1*
Nuclear pore complex protein npp-16	*npp-16*
Uncharacterized protein D2096.6	*D2096.6*
Nuclear pore complex protein 14	*npp-14*
LIM and SH3 domain protein F42H10.3	*F42H10.3*
START domain-containing protein	*C29F5.1*
Probable dynactin subunit 2	*dnc-2*
Protein kinase domain-containing protein	*hpo-34*
Protein jagunal homolog	*K05C4.2*
Glyceraldehyde-3-phosphate dehydrogenase 3	*gpd-3*

Supplemental Table C20 **Genes corresponding to rescued proteins (based on fold change) identified by SWATH-MS that are either over- or under-represented in *h*CHIP rescue strain 2 processed by lysis with SDS-based lysis buffer.** Each protein listed below met the fold change cutoff criteria of either ≤ 0.67 or ≥ 1.5 compared to *chn-1(tm2692) C. elegans chn-1* mutants in *h*CHIP rescue strain 2. Initially, a reference list was created comparing N2 wild-type worms and *chn-1* mutants. Proteins differentially expressed in opposite directions from wild-type to knock-out animals and knock-out to rescue strains were defined as "rescued". Associated *p*-values and fold changes for each protein are listed in Supplemental Table C14.

Protein	Gene
PHAF1 protein T01G9.2	*T01G9.2*
Thioredoxin-like protein	*dib-1*
ATP synthase subunit C lysine N-methyltransferase	*Y39A1A.21*
Transmembrane protein 256 homolog	*Y106G6H.8*
G domain-containing protein	*noa-1*
Peptidyl-prolyl cis-trans isomerase 10	*cyn-10*
Ribosomal RNA-processing protein 7 homolog	*ZC434.4*
DNA repair endonuclease XPF	*xpf-1*
Mitochondrial import receptor subunit TOM7 homolog	*tomm-7*
Fungal lipase-like domain-containing protein	*T10B5.7*
Histone H2A	*his-3*
Glucuronosyltransferase	*ugt-13*
Peroxidasin homolog pxn-2	*pxn-2*
Epoxide hydrolase	*W01A11.1*
Domain of unknown function DX domain-containing protein	*T10E9.4*
Golgi-specific brefeldin A-resistance guanine nucleotide exchange factor 1 homolog	*gbf-1*
AP-2 complex subunit alpha	*apa-2*
Myb-binding protein 1A-like protein	*R02F2.7*
ANK_REP_REGION domain-containing protein	*mtpn-1*
Putative cystathionine gamma-lyase 2	*cth-2*
RNA polymerase II transcription factor SIII p18 subunit	*elb-1*
DOMON domain-containing protein	*Y57G11A.4*
RING-type domain-containing protein	*T20F5.6*
SURF1-like protein	*sft-1*
Gut esterase 1	*ges-1*
Lipid scramblase CLPTM1L	*T13H5.8*
Saposin B-type domain-containing protein	*spp-17*
RRM domain-containing protein	*cpf-2*
Carboxypeptidase E	*egl-21*

Putative metallophosphoesterase F40B5.2	*F40B5.2*
Intestinal acid phosphatase	*pho-1*
SUI1 domain-containing protein	*eif-1*
UBX domain-containing protein 4	*ubxn-4*
Cullin-1	*cul-1*
Uncharacterized protein C29G2.6	*C29G2.6*
Uncharacterized protein F36G3.2	*F36G3.2*
CBS domain-containing protein	*aakg-2*
E3 ubiquitin-protein ligase hecd-1	*hecd-1*
Dihydropyrimidinase 2	*dhp-2*
Extracellular protein	*Y54G2A.76*
Fatty acyl-CoA reductase	*fard-1*
Leucine carboxyl methyltransferase 1	*lcmt-1*
Uncharacterized protein byn-1	*byn-1*
Dynein heavy chain, cytoplasmic	*dhc-1*
Exosome complex component RRP45	*exos-9*
Innexin-5	*inx-5*
mRNA transport homolog 4	*mtr-4*
Dynactin subunit 4	*dnc-4*
Proliferating cell nuclear antigen	*pcn-1*
sn-1-specific diacylglycerol lipase ABHD11	*abhd-11.2*
Protein-tyrosine sulfotransferase A	*tpst-1*
Protein Scribble homolog let-413	*let-413*
5'-3' exoribonuclease 2 homolog	*xrn-2*
Intrinsically Disordered Protein, class C	*idpc-3*
Signal peptidase complex subunit 2	*spcs-2*
Uridine diphosphate glucose pyrophosphatase NUDT14	*C50F4.16*
Pinin/SDK/MemA protein domain-containing protein	*pnn-1*
Cysteine protease atg-4.1	*atg-4.1*
mRNA-decapping enzyme 1	*dcap-1*
Neuronal calcium sensor 2	*ncs-2*
Chromatin target of PRMT1 protein C-terminal domain-containing protein	*Y92H12BR.2*
ADP-ribosylation factor 6	*arf-6*
Uncharacterized protein T19C3.2	*T19C3.2*
Not3 domain-containing protein	*ntl-3*
RIIa domain-containing protein	*F39H12.3*
U5 small nuclear ribonucleoprotein 200 kDa helicase	*snrp-200*
Cytoplasmic tRNA 2-thiolation protein 1	*tut-1*
Probable phosphoribosylformylglycinamidine synthase	*pfas-1*
Glycosyl hydrolase family 63 C-terminal domain-containing protein	*R03E9.2*

Skp1-related protein	*skr-3*
BPI1 domain-containing protein	*F10D11.6*
Prolyl Carboxy Peptidase like	*pcp-4*
Multifunctional procollagen lysine hydroxylase and glycosyltransferase	*let-268*
Large ribosomal subunit protein bL9m	*mrpl-9*
Integrin-linked protein kinase homolog pat-4	*pat-4*
Protein mac-1	*mac-1*
Uncharacterized protein ZK1320.3	*ZK1320.3*
Neuropeptide-Like Protein	*F38B2.6*
60S ribosomal protein L23	*F45E12.5*
Probable glutathione S-transferase gst-36	*gst-36*
Probable 26S proteasome complex subunit dss-1	*dss-1*
Putative peroxisomal biogenesis factor 19	*prx-19*
Sensitive to high expression protein 9, mitochondrial	*C01H6.8*
Nuclear hormone receptor family member nhr-49	*nhr-49*
Ubiquitin carboxyl-terminal hydrolase	*ubh-1*
Protein ctg-1	*ctg-1*
DNA topoisomerase 2 top-2	*top-2*
MICOS complex subunit MIC60-2	*immt-2*
Proteasome subunit alpha type-7	*pas-4*
SAP domain-containing protein	*acin-1*
glutathione transferase	*gst-20*
Putative UDP-glucuronosyltransferase ugt-46	*ugt-46*
V-type proton ATPase 116 kDa subunit a 1	*unc-32*
Splicing factor 3B subunit 6-like protein	*sftb-6*
Uncharacterized protein ZK1073.1	*ZK1073.1*
MTTase N-terminal domain-containing protein	*Y92H12BL.4*
Facilitated glucose transporter protein 1	*fgt-1*
KH domain-containing protein akap-1	*akap-1*
Reactive oxygen species modulator 1	*romo-1*
UBX domain-containing protein 3	*ubxn-3*
DUF148 domain-containing protein	*F40E10.5*
Glycoside hydrolase 35 catalytic domain-containing protein	*bgal-2*
Probable Golgi transport protein 1	*eas-1*
Ribonucleoside-diphosphate reductase large subunit	*rnr-1*
Geranylgeranyl transferase type-2 subunit alpha	*M57.2*
BIG2 domain-containing protein	*npp-12*
5-oxoprolinase	*Y38F2AR.12*
HECT domain-containing protein	*herc-1*
Esterase cest-33	*cest-33*

AB hydrolase-1 domain-containing protein	*K01A2.5*
Uncharacterized oxidoreductase F53C11.3	*decr-1.1*
DDRGK domain-containing protein 1	*ufbp-1*
Major facilitator superfamily	*C46C2.2*
Ran GTPase-activating protein 2	*ran-2*
Stomatin-1	*sto-1*
alpha-1,2-Mannosidase	*ZC506.1*
2-methoxy-6-polyprenyl-1,4-benzoquinol methylase, mitochondrial	*coq-5*
Coatomer subunit epsilon	*cope-1*
Kynureninase	*kynu-1*
Small ribosomal subunit protein mS31	*mrps-31*
Putative 6-phosphogluconolactonase	*Y57G11C.3*
Protein kinase domain-containing protein	*scyl-1*
Glutathione S-transferase 4	*gst-4*
Probable mitochondrial import inner membrane translocase subunit tim-17B.1	*timm-17B.1*
UPF0642 protein YBL028C	*C49H3.3*
Histidine phosphatase family protein	*acp-6*
Uncharacterized protein C18H9.6	*C18H9.6*
Actin	*arp-1*
Proteasome subunit beta type-1	*pbs-6*
NADH-ubiquinone oxidoreductase chain 5	*nduo-5*
Maestro heat-like repeat-containing protein family member 1 homolog	*hpo-27*
Ribulose-phosphate 3-epimerase	*F08F8.7*
Vitelline membrane outer layer protein 1	*Y57G11A.2*
Acyl-coenzyme A thioesterase 8	*C37H5.13*
D-2-hydroxyglutarate dehydrogenase, mitochondrial	*dhgd-1*
Probable mitochondrial pyruvate carrier 1	*mpc-1*
Acidic leucine-rich nuclear phosphoprotein 32-related protein 1	*F33H2.3*
CYtochrome P450 family	*cyp-37a1*
Ubiquinone biosynthesis O-methyltransferase, mitochondrial	*coq-3*
Malate dehydrogenase	*VF13D12L.3*
Nematode cuticle collagen N-terminal domain-containing protein	*col-174*
Fibulin-1	*fbl-1*
JNK-interacting protein	*unc-16*
Cytochrome P450	*cyp-25a2*
Fanconi anemia group I protein	*D2030.3*
Sm domain-containing protein	*atx-2*
Protein kinase domain-containing protein	*F52B5.2*
39S ribosomal protein L55, mitochondrial	*mrpl-55*

Flavin-containing monooxygenase	*fmo-4*
Membrane insertase YidC/Oxa/ALB C-terminal domain-containing protein	*oxa-1*
CMP/dCMP-type deaminase domain-containing protein	*Y48A6B.7*
Fcf2 pre-rRNA processing C-terminal domain-containing protein	*Y49F6B.2*
GTP-binding protein	*raga-1*
ER membrane protein complex subunit 4	*perm-3*
Uterine Lumin Expressed/locailized	*ule-2*
Aspartate dehydrogenase domain-containing protein	*F17C8.9*
Alpha-tubulin N-acetyltransferase 1	*mec-17*
Secreted protein	*Y37D8A.19*
Serpentine Receptor, class T	*F57G9.3*
Ig-like domain-containing protein	*zig-9*
V-type proton ATPase subunit e	*vha-17*
Proton-coupled zinc antiporter SLC30A5	*slc-30a5*
Endoplasmic reticulum lectin 1	*Y105E8A.2*
DUF3456 domain-containing protein	*F01F1.15*
J domain-containing protein	*dnj-7*
ABC transporter domain-containing protein	*pmp-4*
PI31_Prot_N domain-containing protein	*F09E5.7*
DAZ protein 1	*daz-1*
NADH-ubiquinone oxidoreductase chain 4	*nduo-4*
RRM domain-containing protein	*rbm-3.1*
Protein jagunal homolog	*K05C4.2*
Transport and Golgi organization protein 1 homolog	*T22C1.6*
Plasma membrane proteolipid 3	*T23B3.2*
Extracellular superoxide dismutase [Cu-Zn]	*sod-4*
G-patch domain-containing protein	*T23G7.3*
Heat shock protein Hsp-12.2	*hsp-12.2*
CaLponIn-liKe proteins	*clik-3*
Histidine-rich glycoprotein-like	*Y39B6A.1*
Protein CASC3	*casc-3*
Protein vem-1	*vem-1*
Clathrin light chain	*clic-1*
LIM and SH3 domain protein F42H10.3	*F42H10.3*
Probable dynactin subunit 2	*dnc-2*
NADH dehydrogenase [ubiquinone] 1 alpha subcomplex subunit 1	*ndua-1*
RNA-binding S4 domain-containing protein	*C47B2.9*
Nuclear pore complex protein npp-16	*npp-16*
Ammonium transporter	*amt-4*
Peptidyl-prolyl cis-trans isomerase 4	*cyn-4*

Ribosomal RNA small subunit methyltransferase nep-1	*emg-1*
Cuticle collagen 39	*col-39*
HIG1 domain-containing protein	*T20D3.6*
Receptor-type guanylate cyclase gcy-23	*gcy-23*
Non-specific serine/threonine protein kinase	*ttbk-8.2*
Probable small nuclear ribonucleoprotein Sm D2	*snr-4*
Fibronectin type-III domain-containing protein	*let-805*

Supplemental Table C21 **Genes corresponding to rescued proteins (based on fold change) identified by SWATH-MS that are either over- or under-represented in the *Ce*CHIP rescue strain processed by lysis with SDS-based lysis buffer.** Each protein listed below met the fold change cutoff criteria of either ≤ 0.67 or ≥ 1.5 compared to *chn-1(tm2692) C. elegans chn-1* mutants in the *Ce*CHIP rescue strain. Initially, a reference list was created comparing N2 wild-type worms and *chn-1* mutants. Proteins differentially expressed in opposite directions from wild-type to knock-out animals and knock-out to rescue strains were defined as "rescued". Associated *p*-values and fold changes for each protein are listed in Supplemental Table C15.

Protein	**Gene**
Nematode cuticle collagen N-terminal domain-containing protein	*col-124*
PHAF1 protein T01G9.2	*T01G9.2*
Thioredoxin-like protein	*dib-1*
ATP synthase subunit C lysine N-methyltransferase	*Y39A1A.21*
G domain-containing protein	*noa-1*
Peptidyl-prolyl cis-trans isomerase 10	*cyn-10*
Prion-like-(Q/N-rich)-domain-bearing protein	*C55C3.3*
DNA-directed RNA polymerase subunit beta	*rpc-2*
DNA repair endonuclease XPF	*xpf-1*
Mitochondrial import receptor subunit TOM7 homolog	*tomm-7*
Histone H2A	*his-3*
Glucuronosyltransferase	*ugt-13*
SAM domain-containing protein	*F53F8.5*
Aminopeptidase P N-terminal domain-containing protein	*icpp-55*
Peroxidasin homolog pxn-2	*pxn-2*
Epoxide hydrolase	*W01A11.1*
Golgi-specific brefeldin A-resistance guanine nucleotide exchange factor 1 homolog	*gbf-1*
Nucleolar protein 9	*ZK792.5*
Lipase_GDSL domain-containing protein	*W02B12.1*
4Fe-4S ferredoxin-type domain-containing protein	*cid-1*
AP-2 complex subunit alpha	*apa-2*
RING-type E3 ubiquitin transferase	*rnf-126*

Probable DNA polymerase delta small subunit	*F12F6.7*
Putative cystathionine gamma-lyase 2	*cth-2*
Molting protein mlt-10	*mlt-10*
Tudor domain-containing protein	*ekl-1*
Putative glucosylceramidase 1	*gba-1*
C-type lectin domain-containing protein	*clec-51*
Peroxisomal biogenesis factor 3	*prx-3*
RNA polymerase II transcription factor SIII p18 subunit	*elb-1*
DOMON domain-containing protein	*Y57G11A.4*
Large ribosomal subunit protein bL17m	*mrpl-17*
MATH domain-containing protein	*ZC204.12*
RING-type domain-containing protein	*T20F5.6*
SURF1-like protein	*sft-1*
Gut esterase 1	*ges-1*
Lipid scramblase CLPTM1L	*T13H5.8*
Saposin B-type domain-containing protein	*spp-17*
Vesicle-trafficking protein SEC22b	*sec-22*
Hydroxyacylglutathione hydrolase	*Y17G7B.3*
Probable selenide, water dikinase	*seld-1*
Carboxypeptidase E	*egl-21*
LNS2/PITP domain-containing protein	*lpin-1*
Protein-tyrosine-phosphatase	*ptpn-22*
Intestinal acid phosphatase	*pho-1*
SUI1 domain-containing protein	*eif-1*
UBX domain-containing protein 4	*ubxn-4*
Ubiquitin carboxyl-terminal hydrolase 39	*usp-39*
Cullin-1	*cul-1*
KRR1 small subunit processome component	*krr-1*
Uncharacterized protein C29G2.6	*C29G2.6*
MMS19 nucleotide excision repair protein	*mms-19*
SAM50-like protein gop-3	*gop-3*
Protein LTV1 homolog	*T23D8.3*
C-type lectin domain-containing protein	*clec-65*
E3 ubiquitin-protein ligase hecd-1	*hecd-1*
Dihydropyrimidinase 2	*dhp-2*
Extracellular protein	*Y54G2A.76*
GTP-binding protein drn-1	*drn-1*
Fatty acyl-CoA reductase	*fard-1*
Ig-like domain-containing protein	*mrps-27*
Polyribonucleotide nucleotidyltransferase	*pnpt-1*

DNA-directed RNA polymerase II subunit RPB1	*ama-1*
Dynein heavy chain, cytoplasmic	*dhc-1*
mRNA export factor rae-1	*rae-1*
Exosome complex component RRP45	*exos-9*
Innexin-5	*inx-5*
mRNA transport homolog 4	*mtr-4*
Vacuolar protein sorting-associated protein 28 homolog	*vps-28*
Putative cuticle collagen 80	*col-80*
Arf-GAP with ANK repeat and PH domain-containing protein cnt-1	*cnt-1*
Splicing factor 3B subunit 1 domain-containing protein	*sftb-1*
Dynactin subunit 4	*dnc-4*
Proliferating cell nuclear antigen	*pcn-1*
sn-1-specific diacylglycerol lipase ABHD11	*abhd-11.2*
tRNA (adenine(58)-N (1))-methyltransferase non-catalytic subunit TRM6	*trmt-6*
Protein Scribble homolog let-413	*let-413*
5'-3' exoribonuclease 2 homolog	*xrn-2*
Intrinsically Disordered Protein, class C	*idpc-3*
Probable 5-formyltetrahydrofolate cyclo-ligase	*Y106G6E.4*
Signal peptidase complex subunit 2	*spcs-2*
Uridine diphosphate glucose pyrophosphatase NUDT14	*C50F4.16*
Pre-mRNA-splicing factor ATP-dependent RNA helicase ddx-15	*ddx-15*
Ribosomal RNA-processing protein 8	*rrp-8*
Spiroplasma plectrovirus-related protein	*C29E4.17*
Phosphotransferase	*hxk-3*
Pinin/SDK/MemA protein domain-containing protein	*pnn-1*
Uncharacterized protein B0361.3	*B0361.3*
Cysteine protease atg-4.1	*atg-4.1*
mRNA-decapping enzyme 1	*dcap-1*
Tensin homolog	*tns-1*
Glutathione transferase	*gst-13*
Protein-disulfide reductase	*C30H6.8*
26S rRNA (cytosine-C(5))-methyltransferase nsun-5	*nsun-5*
Thioredoxin domain-containing protein 9	*txdc-9*
Neuronal calcium sensor 2	*ncs-2*
Chromatin target of PRMT1 protein C-terminal domain-containing protein	*Y92H12BR.2*
ADP-ribosylation factor 6	*arf-6*
Uncharacterized protein T19C3.2	*T19C3.2*
Tyrosine aminotransferase	*tatn-1*
Uncharacterized protein	*K10G6.9*
Transthyretin-like family protein	*ttr-48*

NEDD8-conjugating enzyme ubc-12	*ubc-12*
3'-5' exonuclease domain-containing protein	*Y57A10A.13*
Not3 domain-containing protein	*ntl-3*
Ubiquitin carboxyl-terminal hydrolase	*ubh-3*
U5 small nuclear ribonucleoprotein 200 kDa helicase	*snrp-200*
Serine/threonine-protein phosphatase 2A activator	*Y71H2AM.20*
VWFA domain-containing protein	*vwa-8*
Cytoplasmic tRNA 2-thiolation protein 1	*tut-1*
Alpha N-terminal protein methyltransferase 1	*homt-1*
Glycosyl hydrolase family 63 C-terminal domain-containing protein	*R03E9.2*
Protein kinase C-like 2	*pkc-2*
Skp1-related protein	*skr-3*
BPI1 domain-containing protein	*F10D11.6*
NADPH:adrenodoxin oxidoreductase, mitochondrial	*Y62E10A.6*
Prolyl Carboxy Peptidase like	*pcp-4*
Exportin-2	*xpo-2*
Nucleolar complex protein 2 homolog	*pro-2*
Saposin B-type domain-containing protein	*Y66H1A.5*
Multifunctional procollagen lysine hydroxylase and glycosyltransferase	*let-268*
DNA damage-binding protein 1	*ddb-1*
Putative thiosulfate sulfurtransferase mpst-1	*mpst-1*
Saposin B-type domain-containing protein	*spp-1*
Importin subunit alpha-3	*ima-3*
Large ribosomal subunit protein bL9m	*mrpl-9*
Integrin-linked protein kinase homolog pat-4	*pat-4*
Protein mac-1	*mac-1*
E3 ubiquitin-protein ligase hrd-1	*sel-11*
Vacuolar H ATPase	*vha-20*
Neuropeptide-Like Protein	*F38B2.6*
60S ribosomal protein L23	*F45E12.5*
Probable glutathione S-transferase gst-36	*gst-36*
Probable 26S proteasome complex subunit dss-1	*dss-1*
C-type lectin domain-containing protein	*clec-150*
Tetratricopeptide repeat-containing protein trd-1	*trd-1*
EF-hand domain-containing protein	*pat-10*
High mobility group protein hmg-12	*hmg-12*
Nuclear hormone receptor family member nhr-49	*nhr-49*
CRAL-TRIO domain-containing protein	*cgr-1*
Ubiquitin carboxyl-terminal hydrolase	*ubh-1*
Protein ctg-1	*ctg-1*

Carboxylic ester hydrolase	*cest-32*
DNA topoisomerase 2 top-2	*top-2*
Nose resistant to fluoxetine protein 5	*nrf-5*
Thioredoxin reductase-like selenoprotein T homolog selt-1.1	*selt-1.1*
MICOS complex subunit MIC60-2	*immt-2*
Proteasome subunit alpha type-7	*pas-4*
Putative ATP synthase subunit epsilon, mitochondrial	*R05D3.6;*
SAP domain-containing protein	*acin-1*
Glutathione transferase	*gst-20*
Uncharacterized protein ZK1073.1	*ZK1073.1*
Small ribosomal subunit protein mS26	*mrps-26*
MTTase N-terminal domain-containing protein	*Y92H12BL.4*
SUI1 domain-containing protein	*eif-2d*
Facilitated glucose transporter protein 1	*fgt-1*
Large ribosomal subunit protein uL10m	*mrpl-10*
KH domain-containing protein akap-1	*akap-1*
Trimeric intracellular cation channel type 1B.1	*tric-1B.1*
Reactive oxygen species modulator 1	*romo-1*
UBX domain-containing protein 3	*ubxn-3*
Probable Golgi transport protein 1	*eas-1*
Peptidase M16 N-terminal domain-containing protein	*ucr-2.3*
Ig-like domain-containing protein	*F21C10.7*
Zwei Ig domain protein zig-1	*zig-1*
Glutathione transferase	*gst-24*
Ribonucleoside-diphosphate reductase large subunit	*rnr-1*
BIG2 domain-containing protein	*npp-12*
Uncharacterized oxidoreductase F53C11.3	*decr-1.1*
DDRGK domain-containing protein 1	*ufbp-1*
Phosphatidate cytidylyltransferase, mitochondrial	*Y71F9B.2*
Peptidase A1 domain-containing protein	*asp-14*
Metaxin-1 homolog	*mtx-1*
Stomatin-1	*sto-1*
Prolyl carboxy peptidase like protein 5	*pcp-5*
ER membrane protein complex subunit 1	*emc-1*
Pyridine nucleotide-disulfide oxidoreductase domain-containing protein 2	*F37C4.6*
alpha-1,2-Mannosidase	*ZC506.1*
Coatomer subunit epsilon	*cope-1*
DeHydrogenases, Short chain	*R119.3*
Small ribosomal subunit protein mS31	*mrps-31*
HEAT repeat-containing protein 1 homolog	*toe-1*

Protein kinase domain-containing protein	*scyl-1*
Glutathione S-transferase 4	*gst-4*
Probable mitochondrial import inner membrane translocase subunit tim-17B.1	*timm-17B.1*
UPF0642 protein YBL028C	*C49H3.3*
F-actin-capping protein subunit alpha	*cap-1*
Protein dif-1	*dif-1*
Methyltransferase domain-containing protein	*metl-13*
Nucleoside-diphosphatase uda-1	*uda-1*
Histidine phosphatase family protein	*acp-6*
Uncharacterized protein C18H9.6	*C18H9.6*
Probable ubiquitin-conjugating enzyme E2 7	*ubc-7*
ER membrane protein complex subunit 2	*emc-2*
NADH-ubiquinone oxidoreductase chain 5	*nduo-5*
Probable geranylgeranyl transferase type-2 subunit beta	*ggtb-1*
Maestro heat-like repeat-containing protein family member 1 homolog	*hpo-27*
Acyl-coenzyme A thioesterase 8	*C37H5.13*
SURF6 homolog gldi-11	*gldi-11*
WD_REPEATS_REGION domain-containing protein	*Y45F10D.7*
Mitochondrial import inner membrane translocase subunit TIM50	*scpl-4*
SUMO-activating enzyme subunit aos-1	*aos-1*
Polypeptide N-acetylgalactosaminyltransferase 5	*gly-5*
D-2-hydroxyglutarate dehydrogenase, mitochondrial	*dhgd-1*
Esterase C25G4.2	*C25G4.2*
Probable mitochondrial pyruvate carrier 1	*mpc-1*
CYtochrome P450 family	*cyp-37a1*
Sulfhydryl oxidase	*T10H10.2*
5'-nucleotidase	*Y10G11A.1*
Fibulin-1	*fbl-1*
JNK-interacting protein	*unc-16*
Sm domain-containing protein	*atx-2*
39S ribosomal protein L55, mitochondrial	*mrpl-55*
PI31_Prot_N domain-containing protein	*F09E5.7*
Cytochrome P450	*cyp-25a2*
Fcf2 pre-rRNA processing C-terminal domain-containing protein	*Y49F6B.2*
Protein kinase domain-containing protein	*F52B5.2*
Endoplasmic reticulum lectin 1	*Y105E8A.2*
Proton-coupled zinc antiporter SLC30A5	*slc-30a5*
Nematode cuticle collagen N-terminal domain-containing protein	*col-120*
V-type proton ATPase subunit e	*vha-17*

Nematode cuticle collagen N-terminal domain-containing protein	*col-174*
GTP-binding protein	*raga-1*
CaLponIn-liKe proteins	*clik-3*
Small ribosomal subunit protein uS14m	*mrps-14*
Membrane insertase YidC/Oxa/ALB C-terminal domain-containing protein	*oxa-1*
Aspartate dehydrogenase domain-containing protein	*F17C8.9*
Putative UDP-glucuronosyltransferase ugt-47	*ugt-47*
CMP/dCMP-type deaminase domain-containing protein	*Y48A6B.7*
Ammonium transporter	*amt-4*
Flavin-containing monooxygenase	*fmo-4*
DAZ protein 1	*daz-1*
DUF3707 domain-containing protein	*F33E2.6*
Probable dynactin subunit 2	*dnc-2*
EOG090X04TT	*cox-15*
Cytochrome c oxidase copper chaperone	*cox-17*
START domain-containing protein	*C29F5.1*
Peptidase S28	*pcp-2*
Uterine Lumin Expressed/locailized	*ule-2*
Large ribosomal subunit protein eL30	*rpl-30*
Putative dihydrofolate reductase	*dhfr-1*
Serpentine Receptor, class T	*F57G9.3*
G-patch domain-containing protein	*T23G7.3*
Putative cuticle collagen 91	*col-91*
RRM domain-containing protein	*rbm-3.1*
Fanconi anemia group I protein	*D2030.3*
DUF3456 domain-containing protein	*F01F1.15*
E3 ubiquitin-protein ligase listerin	*Y54E10A.11*
Large ribosomal subunit protein uL14	*rpl-23*
J domain-containing protein	*dnj-7*
Secreted protein	*Y37D8A.19*
Histidine-rich glycoprotein-like	*Y39B6A.1*
Probable maleylacetoacetate isomerase	*gst-42*
Transport and Golgi organization protein 1 homolog	*T22C1.6*
NADH-ubiquinone oxidoreductase chain 4	*nduo-4*
Ras-related protein rab-6.2	*rab-6.2*
Extracellular superoxide dismutase [Cu-Zn]	*sod-4*
Cytochrome c oxidase subunit 1	*ctc-1*
UPF0376 protein F10G2.1	*F10G2.1*
Nucleolar protein 6	*nol-6*
Small ribosomal subunit protein mS23	*mrps-23*

Bibliography

1 McDonough, H., Patterson, C. J. C. s. & chaperones. CHIP: a link between the chaperone and proteasome systems. **8**, 303 (2003).

2 De Los Rios, P., Ben-Zvi, A., Slutsky, O., Azem, A. & Goloubinoff, P. J. P. o. t. N. A. o. S. Hsp70 chaperones accelerate protein translocation and the unfolding of stable protein aggregates by entropic pulling. **103**, 6166-6171 (2006).

3 Pratt, W. B., Toft, D. O. J. E. b. & medicine. Regulation of signaling protein function and trafficking by the hsp90/hsp70-based chaperone machinery. **228**, 111-133 (2003).

4 Narayan, V., Pion, E., Landré, V., Müller, P. & Ball, K. L. J. J. o. B. C. Docking-dependent ubiquitination of the interferon regulatory factor-1 tumor suppressor protein by the ubiquitin ligase CHIP. **286**, 607-619 (2011).

5 Apriamashvili, G. *et al.* Ubiquitin ligase STUB1 destabilizes IFNγ-receptor complex to suppress tumor IFNγ signaling. **13**, 1923 (2022).

6 Lenhart, K. C. *et al.* Loss of CHIP Expression Perturbs Glucose Homeostasis and Leads to Type II Diabetes Through Defects in Microtubule Polymerization and Glucose Transporter Localization. **30**, 307.307-307.307 (2016).

7 Tawo, R. *et al.* The ubiquitin ligase CHIP integrates proteostasis and aging by regulation of insulin receptor turnover. **169**, 470-482. e413 (2017).

8 Dias, C. *et al.* CHIP-dependent regulation of the actin cytoskeleton is linked to neuronal cell membrane integrity. **24** (2021).

9 Min, J.-N. *et al.* CHIP deficiency decreases longevity, with accelerated aging phenotypes accompanied by altered protein quality control. **28**, 4018-4025 (2008).

10 Chen, D.-H. *et al.* Heterozygous STUB1 missense variants cause ataxia, cognitive decline, and STUB1 mislocalization. **6**, e397 (2020).

11 Hayer, S. N. *et al.* STUB1/CHIP mutations cause Gordon Holmes syndrome as part of a widespread multisystemic neurodegeneration: evidence from four novel mutations. **12**, 1-8 (2017).

12 Lu, E. *et al.* Stub1 ameliorates ER stress-induced neural cell apoptosis and promotes locomotor recovery through restoring autophagy flux after spinal cord injury. **368**, 114495 (2023).

13 Lizama, B. N. *Novel Functions of C-terminus of HSC70-Interacting Protein (CHIP) in Mitophagy and Neuroprotection*, (2018).

14 Chen, B.-H., Chang, Y.-J., Lin, S. & Yang, W. Y. J. N. C. Hsc70/Stub1 promotes the removal of individual oxidatively stressed peroxisomes. **11**, 5267 (2020).

15 Gazulla, J., Izquierdo-Alvarez, S., Sierra-Martínez, E., Marta-Moreno, M. E. & Alvarez, S. J. N. S. Inaugural cognitive decline, late disease onset and novel STUB1 variants in SCAR16. **39**, 2231-2233 (2018).

16 Roux, T. *et al.* Clinical, neuropathological, and genetic characterization of STUB1 variants in cerebellar ataxias: a frequent cause of predominant cognitive impairment. **22**, 1851-1862 (2020).

17 Gwaza, G. P., MacBain, M. M., PlÃ¼ddemann, A. A. & Heneghan, C. J. G. J. o. H. S. The Primary Health Care Approach: Rhetoric or Policy?-A Review of National Health Policies in 8 Countries in Southern Africa. **15**, 1-15 (2023).

18 Koga, H., Kaushik, S. & Cuervo, A. M. J. A. r. r. Protein homeostasis and aging: The importance of exquisite quality control. **10**, 205-215 (2011).
19 Nyström, T. & Liu, B. J. F. y. r. Protein quality control in time and space–links to cellular aging. **14**, 40-48 (2014).
20 Organization, W. H. Ageing. (2020).
21 López-Otín, C., Blasco, M. A., Partridge, L., Serrano, M. & Kroemer, G. J. C. The hallmarks of aging. **153**, 1194-1217 (2013).
22 Aunan, J., Watson, M., Hagland, H. & Søreide, K. J. J. o. B. S. Molecular and biological hallmarks of ageing. **103**, e29-e46 (2016).
23 Friedberg, E. C. J. N. DNA damage and repair. **421**, 436-440 (2003).
24 Moskalev, A. A. *et al.* The role of DNA damage and repair in aging through the prism of Koch-like criteria. **12**, 661-684 (2013).
25 Kryston, T. B., Georgiev, A. B., Pissis, P., Georgakilas, A. G. J. M. R. F. & Mutagenesis, M. M. o. Role of oxidative stress and DNA damage in human carcinogenesis. **711**, 193-201 (2011).
26 Blackburn, E. H., Greider, C. W. & Szostak, J. W. J. N. m. Telomeres and telomerase: the path from maize, Tetrahymena and yeast to human cancer and aging. **12**, 1133-1138 (2006).
27 O'sullivan, R. J. & Karlseder, J. J. N. r. M. c. b. Telomeres: protecting chromosomes against genome instability. **11**, 171-181 (2010).
28 Levy, M. Z., Allsopp, R. C., Futcher, A. B., Greider, C. W. & Harley, C. B. J. J. o. m. b. Telomere end-replication problem and cell aging. **225**, 951-960 (1992).
29 Hayflick, L. & Moorhead, P. S. J. E. c. r. The serial cultivation of human diploid cell strains. **25**, 585-621 (1961).
30 Hahn, W. C. *et al.* Creation of human tumour cells with defined genetic elements. **400**, 464-468 (1999).
31 Kim, N. W. *et al.* Specific association of human telomerase activity with immortal cells and cancer. **266**, 2011-2015 (1994).
32 Allsopp, R. C. *et al.* Telomere shortening is associated with cell division in vitro and in vivo. **220**, 194-200 (1995).
33 Veith, S. & Mangerich, A. J. A. r. r. RecQ helicases and PARP1 team up in maintaining genome integrity. **23**, 12-28 (2015).
34 De Lange, T. J. G. & development. Shelterin: the protein complex that shapes and safeguards human telomeres. **19**, 2100-2110 (2005).
35 Palm, W. & de Lange, T. J. A. r. o. g. How shelterin protects mammalian telomeres. **42**, 301-334 (2008).
36 Fumagalli, M. *et al.* Telomeric DNA damage is irreparable and causes persistent DNA-damage-response activation. **14**, 355-365 (2012).
37 Hewitt, G. *et al.* Telomeres are favoured targets of a persistent DNA damage response in ageing and stress-induced senescence. **3**, 708 (2012).
38 Hagland, H. R., Berg, M., Jolma, I. W., Carlsen, A. & Søreide, K. J. D. s. Molecular pathways and cellular metabolism in colorectal cancer. **30**, 12-25 (2013).
39 Marioni, R. E. *et al.* DNA methylation age of blood predicts all-cause mortality in later life. **16**, 1-12 (2015).

40 Zane, L., Sharma, V. & Misteli, T. J. T. i. c. b. Common features of chromatin in aging and cancer: cause or coincidence? **24**, 686-694 (2014).
41 Issa, J.-P. J. T. J. o. c. i. Aging and epigenetic drift: a vicious cycle. **124**, 24-29 (2014).
42 Marttila, S. *et al.* Ageing-associated changes in the human DNA methylome: genomic locations and effects on gene expression. **16**, 1-17 (2015).
43 Bocklandt, S. *et al.* Epigenetic predictor of age. **6**, e14821 (2011).
44 Hannum, G. *et al.* Genome-wide methylation profiles reveal quantitative views of human aging rates. **49**, 359-367 (2013).
45 Koch, C. M. & Wagner, W. J. A. Epigenetic-aging-signature to determine age in different tissues. **3**, 1018 (2011).
46 Wilkinson, G. S. *et al.* DNA methylation predicts age and provides insight into exceptional longevity of bats. **12**, 1615 (2021).
47 Majchrzak-Celińska, A., Warych, A. & Szoszkiewicz, M. J. G. Novel approaches to epigenetic therapies: from drug combinations to epigenetic editing. **12**, 208 (2021).
48 Horvath, S. *et al.* Obesity accelerates epigenetic aging of human liver. **111**, 15538-15543 (2014).
49 Sawan, C. & Herceg, Z. J. A. i. g. Histone modifications and cancer. **70**, 57-85 (2010).
50 Das, C. & Tyler, J. K. J. B. e. B. A.-G. R. M. Histone exchange and histone modifications during transcription and aging. **1819**, 332-342 (2012).
51 Bartel, D. P. J. c. MicroRNAs: genomics, biogenesis, mechanism, and function. **116**, 281-297 (2004).
52 Lu, J. & Clark, A. G. J. G. r. Impact of microRNA regulation on variation in human gene expression. **22**, 1243-1254 (2012).
53 Bonifacio, L. N. & Jarstfer, M. B. J. P. o. MiRNA profile associated with replicative senescence, extended cell culture, and ectopic telomerase expression in human foreskin fibroblasts. **5**, e12519 (2010).
54 Barzilai, N., Huffman, D. M., Muzumdar, R. H. & Bartke, A. J. D. The critical role of metabolic pathways in aging. **61**, 1315-1322 (2012).
55 Kenyon, C. J. J. N. The genetics of ageing. **464**, 504-512 (2010).
56 Murray, C. J. *et al.* Global, regional, and national disability-adjusted life years (DALYs) for 306 diseases and injuries and healthy life expectancy (HALE) for 188 countries, 1990–2013: quantifying the epidemiological transition. **386**, 2145-2191 (2015).
57 Eisenstein, M. J. N. Molecular biology: Remove, reuse, recycle. **514**, S2-S4 (2014).
58 Brehme, M. *et al.* A chaperome subnetwork safeguards proteostasis in aging and neurodegenerative disease. **9**, 1135-1150 (2014).
59 Ferreiro, D. U., Komives, E. A. & Wolynes, P. G. J. C. o. i. s. b. Frustration, function and folding. **48**, 68-73 (2018).
60 Ferreiro, D. U., Komives, E. A. & Wolynes, P. G. J. Q. r. o. b. Frustration in biomolecules. **47**, 285-363 (2014).
61 Jenik, M. *et al.* Protein frustratometer: a tool to localize energetic frustration in protein molecules. **40**, W348-W351 (2012).

62 Jha, S. K. & Udgaonkar, J. B. J. C. S. Free energy barriers in protein folding and unfolding reactions. 457-475 (2010).
63 Hipp, M. S., Kasturi, P. & Hartl, F. U. J. N. r. M. c. b. The proteostasis network and its decline in ageing. **20**, 421-435 (2019).
64 Hartl, F. U., Bracher, A. & Hayer-Hartl, M. J. N. Molecular chaperones in protein folding and proteostasis. **475**, 324-332 (2011).
65 Sandri, M., Robbins, J. J. J. o. m. & cardiology, c. Proteotoxicity: an underappreciated pathology in cardiac disease. **71**, 3-10 (2014).
66 Lodish, H. *et al.* in *Molecular Cell Biology. 4th edition* (WH Freeman, 2000).
67 Chen, Q. *et al.* Intrasarcoplasmic amyloidosis impairs proteolytic function of proteasomes in cardiomyocytes by compromising substrate uptake. **97**, 1018-1026 (2005).
68 Liu, J. *et al.* Impairment of the ubiquitin-proteasome system in desminopathy mouse hearts. **20**, 362-364 (2006).
69 Liu, J., Tang, M., Mestril, R., Wang, X. J. J. o. m. & cardiology, c. Aberrant protein aggregation is essential for a mutant desmin to impair the proteolytic function of the ubiquitin–proteasome system in cardiomyocytes. **40**, 451-454 (2006).
70 Pattison, J. S. *et al.* Cardiomyocyte expression of a polyglutamine preamyloid oligomer causes heart failure. **117**, 2743-2751 (2008).
71 Su, H., Li, F., Ranek, M. J., Wei, N. & Wang, X. J. C. COP9 signalosome regulates autophagosome maturation. **124**, 2117-2128 (2011).
72 Su, H. *et al.* Perturbation of cullin deneddylation via conditional Csn8 ablation impairs the ubiquitin–proteasome system and causes cardiomyocyte necrosis and dilated cardiomyopathy in mice. **108**, 40-50 (2011).
73 Su, H. *et al.* The COP9 signalosome is required for autophagy, proteasome-mediated proteolysis, and cardiomyocyte survival in adult mice. **6**, 1049-1057 (2013).
74 Thibaudeau, T. A., Anderson, R. T. & Smith, D. M. J. N. c. A common mechanism of proteasome impairment by neurodegenerative disease-associated oligomers. **9**, 1097 (2018).
75 Wang, X. & Wang, H. J. T. i. m. m. Priming the proteasome to protect against proteotoxicity. **26**, 639-648 (2020).
76 Clark, A. R., Lubsen, N. H., Slingsby, C. J. T. i. j. o. b. & biology, c. sHSP in the eye lens: crystallin mutations, cataract and proteostasis. **44**, 1687-1697 (2012).
77 Labbadia, J. & Morimoto, R. I. J. A. r. o. b. The biology of proteostasis in aging and disease. **84**, 435-464 (2015).
78 Sőti, C. & Csermely, P. J. B. Molecular chaperones and the aging process. **1**, 225-233 (2000).
79 Huang, J. *et al.* DAMPs, ageing, and cancer: The 'DAMP Hypothesis'. **24**, 3-16 (2015).
80 Feder, M. E. & Hofmann, G. E. J. A. r. o. p. Heat-shock proteins, molecular chaperones, and the stress response: evolutionary and ecological physiology. **61**, 243-282 (1999).
81 Åkerfelt, M., Morimoto, R. I. & Sistonen, L. J. N. r. M. c. b. Heat shock factors: integrators of cell stress, development and lifespan. **11**, 545-555 (2010).

82 Westerheide, S. D., Anckar, J., Stevens Jr, S. M., Sistonen, L. & Morimoto, R. I. J. S. Stress-inducible regulation of heat shock factor 1 by the deacetylase SIRT1. **323**, 1063-1066 (2009).
83 McConnell, K. W. *et al.* The role of heat shock protein 70 in mediating age-dependent mortality in sepsis. **186**, 3718-3725 (2011).
84 Qu, B. *et al.* The detection and role of heat shock protein 70 in various nondisease conditions and disease conditions: a literature review. **20**, 885-892 (2015).
85 Chondrogianni, N. *et al.* Proteasome activation delays aging in vitro and in vivo. **71**, 303-320 (2014).
86 Chondrogianni, N., Petropoulos, I., Franceschi, C., Friguet, B. & Gonos, E. S. J. E. g. Fibroblast cultures from healthy centenarians have an active proteasome. **35**, 721-728 (2000).
87 Glick, D., Barth, S. & Macleod, K. F. J. T. J. o. p. Autophagy: cellular and molecular mechanisms. **221**, 3-12 (2010).
88 Madeo, F., Zimmermann, A., Maiuri, M. C. & Kroemer, G. J. T. J. o. c. i. Essential role for autophagy in life span extension. **125**, 85-93 (2015).
89 Morselli, E. *et al.* Caloric restriction and resveratrol promote longevity through the Sirtuin-1-dependent induction of autophagy. **1**, e10-e10 (2010).
90 Rubinsztein, D. C., Mariño, G. & Kroemer, G. J. C. Autophagy and aging. **146**, 682-695 (2011).
91 Vidal, R. L., Matus, S., Bargsted, L. & Hetz, C. J. T. i. p. s. Targeting autophagy in neurodegenerative diseases. **35**, 583-591 (2014).
92 Eisenberg, T. *et al.* Induction of autophagy by spermidine promotes longevity. **11**, 1305-1314 (2009).
93 Harrison, D. E. *et al.* Rapamycin fed late in life extends lifespan in genetically heterogeneous mice. **460**, 392-395 (2009).
94 Neff, F. *et al.* Rapamycin extends murine lifespan but has limited effects on aging. **123**, 3272-3291 (2013).
95 Wilkinson, J. E. *et al.* Rapamycin slows aging in mice. **11**, 675-682 (2012).
96 Baur, J. A. *et al.* Resveratrol improves health and survival of mice on a high-calorie diet. **444**, 337-342 (2006).
97 Lane, R. K., Hilsabeck, T. & Rea, S. L. J. B. e. B. A.-B. The role of mitochondrial dysfunction in age-related diseases. **1847**, 1387-1400 (2015).
98 Qin, Z. *et al.* Potentially functional polymorphisms in ATG10 are associated with risk of breast cancer in a Chinese population. **527**, 491-495 (2013).
99 Nicoli, E.-R. *et al.* Determination of autophagy gene ATG16L1 polymorphism in human colorectal cancer. **55**, 57-62 (2014).
100 Tan, C.-C. *et al.* Autophagy in aging and neurodegenerative diseases: implications for pathogenesis and therapy. **35**, 941-957 (2014).
101 Chen, K., Yang, Y.-H., Jiang, S.-D., Jiang, L.-S. J. H. & biology, c. Decreased activity of osteocyte autophagy with aging may contribute to the bone loss in senile population. **142**, 285-295 (2014).
102 Caramés, B., Olmer, M., Kiosses, W. B., Lotz, M. K. J. A. & rheumatology. The relationship of autophagy defects to cartilage damage during joint aging in a mouse model. **67**, 1568-1576 (2015).

103 Riera, C. E. & Dillin, A. J. N. c. b. Tipping the metabolic scales towards increased longevity in mammals. **17**, 196-203 (2015).
104 Barzilai, N., Ferrucci, L. J. J. o. G. S. A. B. S. & Sciences, M. Insulin resistance and aging: a cause or a protective response? **67**, 1329-1331 (2012).
105 Pesce, V. *et al.* Age-related mitochondrial genotypic and phenotypic alterations in human skeletal muscle. **30**, 1223-1233 (2001).
106 Fontana, L., Partridge, L. & Longo, V. D. J. s. Extending healthy life span—from yeast to humans. **328**, 321-326 (2010).
107 Biglou, S. G., Bendena, W. G. & Chin-Sang, I. J. P. An overview of the insulin signaling pathway in model organisms Drosophila melanogaster and Caenorhabditis elegans. **145**, 170640 (2021).
108 Samuels, Y., Waldman, T. J. P.-k. i. H. & 2, D. V. Oncogenic mutations of PIK3CA in human cancers. 21-41 (2011).
109 Anton, S. & Leeuwenburgh, C. J. E. g. Vol. 48 1003-1005 (Elsevier, 2013).
110 Cypser, J. R., Kitzenberg, D. & Park, S.-K. J. E. g. Dietary restriction in C. elegans: recent advances. **48**, 1014-1017 (2013).
111 Lam, Y. Y., Peterson, C. M. & Ravussin, E. J. E. g. Resveratrol vs. calorie restriction: data from rodents to humans. **48**, 1018-1024 (2013).
112 Lee, C. & Longo, V. J. O. Fasting vs dietary restriction in cellular protection and cancer treatment: from model organisms to patients. **30**, 3305-3316 (2011).
113 Zhang, Z. *et al.* The update on transcriptional regulation of autophagy in normal and pathologic cells: A novel therapeutic target. **74**, 17-29 (2015).
114 Wu, W. *The cross-regulation of autophagy and necroptosis*, Dissertation, Düsseldorf, Heinrich-Heine-Universität, 2019, (2019).
115 Kroemer, G., Mariño, G. & Levine, B. J. M. c. Autophagy and the integrated stress response. **40**, 280-293 (2010).
116 Pellegrino, M. W., Nargund, A. M. & Haynes, C. M. J. B. e. B. A.-M. C. R. Signaling the mitochondrial unfolded protein response. **1833**, 410-416 (2013).
117 Haynes, C. M., Fiorese, C. J. & Lin, Y.-F. J. T. i. c. b. Evaluating and responding to mitochondrial dysfunction: the mitochondrial unfolded-protein response and beyond. **23**, 311-318 (2013).
118 Speakman, J. R. *et al.* Uncoupled and surviving: individual mice with high metabolism have greater mitochondrial uncoupling and live longer. **3**, 87-95 (2004).
119 Galgani, J. E., Moro, C., Ravussin, E. J. A. j. o. p.-e. & metabolism. Metabolic flexibility and insulin resistance. (2008).
120 Bitto, A. *et al.* Transient rapamycin treatment can increase lifespan and healthspan in middle-aged mice. **5**, e16351 (2016).
121 Mannick, J. B. *et al.* mTOR inhibition improves immune function in the elderly. **6**, 268ra179-268ra179 (2014).
122 Ross, C. *et al.* Metabolic consequences of long-term rapamycin exposure on common marmoset monkeys (Callithrix jacchus). **7**, 964 (2015).
123 Xue, Q.-L. *et al.* Rapamycin increases grip strength and attenuates age-related decline in maximal running distance in old low capacity runner rats. **8**, 769 (2016).

124 Pantuck, A. J. *et al.* Prognostic relevance of the mTOR pathway in renal cell carcinoma: implications for molecular patient selection for targeted therapy. **109**, 2257-2267 (2007).
125 Kim, J., Kundu, M., Viollet, B. & Guan, K.-L. J. N. c. b. AMPK and mTOR regulate autophagy through direct phosphorylation of Ulk1. **13**, 132-141 (2011).
126 Laplante, M. & Sabatini, D. M. J. C. b. An emerging role of mTOR in lipid biosynthesis. **19**, R1046-R1052 (2009).
127 Peterson, T. R. *et al.* mTOR complex 1 regulates lipin 1 localization to control the SREBP pathway. **146**, 408-420 (2011).
128 Antikainen, H., Driscoll, M., Haspel, G. & Dobrowolski, R. J. A. c. TOR-mediated regulation of metabolism in aging. **16**, 1219-1233 (2017).
129 Fingar, D. C. & Blenis, J. J. O. Target of rapamycin (TOR): an integrator of nutrient and growth factor signals and coordinator of cell growth and cell cycle progression. **23**, 3151-3171 (2004).
130 Dobashi, Y. *et al.* Mammalian target of rapamycin: a central node of complex signaling cascades. **4**, 476 (2011).
131 Guertin, D. A. & Sabatini, D. M. J. T. i. m. m. An expanding role for mTOR in cancer. **11**, 353-361 (2005).
132 Pópulo, H., Lopes, J. M. & Soares, P. J. I. j. o. m. s. The mTOR signalling pathway in human cancer. **13**, 1886-1918 (2012).
133 Kazyken, D. *et al.* AMPK directly activates mTORC2 to promote cell survival during acute energetic stress. **12**, eaav3249 (2019).
134 Shaw, R. J. J. A. p. LKB1 and AMP-activated protein kinase control of mTOR signalling and growth. **196**, 65-80 (2009).
135 Moral-Sanz, J. *et al.* The LKB1–AMPK-α1 signaling pathway triggers hypoxic pulmonary vasoconstriction downstream of mitochondria. **11**, eaau0296 (2018).
136 Hall, J. A., Dominy, J. E., Lee, Y. & Puigserver, P. J. T. J. o. c. i. The sirtuin family's role in aging and age-associated pathologies. **123**, 973-979 (2013).
137 Michan, S. J. F. B. Calorie restriction and NAD+/sirtuin counteract the hallmarks of aging. **19**, 1300-1319 (2014).
138 Brunet, A. *et al.* Stress-dependent regulation of FOXO transcription factors by the SIRT1 deacetylase. **303**, 2011-2015 (2004).
139 Harman, D. J. B. Origin and evolution of the free radical theory of aging: a brief personal history, 1954–2009. **10**, 773-781 (2009).
140 Esparza-Moltó, P. B., Nuevo-Tapioles, C., Cuezva, J. M. J. C. & Sciences, M. L. Regulation of the H+-ATP synthase by IF1: a role in mitohormesis. **74**, 2151-2166 (2017).
141 Yun, J. & Finkel, T. J. C. m. Mitohormesis. **19**, 757-766 (2014).
142 Hekimi, S., Lapointe, J. & Wen, Y. J. T. i. c. b. Taking a "good" look at free radicals in the aging process. **21**, 569-576 (2011).
143 Caldeira da Silva, C. C., Cerqueira, F. M., Barbosa, L. F., Medeiros, M. H. & Kowaltowski, A. J. J. A. c. Mild mitochondrial uncoupling in mice affects energy metabolism, redox balance and longevity. **7**, 552-560 (2008).
144 Durieux, J., Wolff, S. & Dillin, A. J. C. The cell-non-autonomous nature of electron transport chain-mediated longevity. **144**, 79-91 (2011).

145 Onken, B. & Driscoll, M. J. P. o. Metformin induces a dietary restriction–like state and the oxidative stress response to extend C. elegans healthspan via AMPK, LKB1, and SKN-1. **5**, e8758 (2010).
146 Rose, G., Crocco, P., De Rango, F., Montesanto, A. & Passarino, G. J. P. o. Further support to the uncoupling-to-survive theory: the genetic variation of human UCP genes is associated with longevity. **6**, e29650 (2011).
147 Rodgers, J. T. *et al.* Nutrient control of glucose homeostasis through a complex of PGC-1α and SIRT1. **434**, 113-118 (2005).
148 Munkácsy, E. & Rea, S. L. J. E. g. The paradox of mitochondrial dysfunction and extended longevity. **56**, 221-233 (2014).
149 Cid-Castro, C., Hernández-Espinosa, D. R., Morán, J. J. C. & Neurobiology, M. ROS as regulators of mitochondrial dynamics in neurons. **38**, 995-1007 (2018).
150 Nakada, K., Sato, A., Hayashi, J.-I. J. T. i. j. o. b. & biology, c. Mitochondrial functional complementation in mitochondrial DNA-based diseases. **41**, 1907-1913 (2009).
151 Rea, S. L., Ventura, N. & Johnson, T. E. J. P. b. Relationship between mitochondrial electron transport chain dysfunction, development, and life extension in Caenorhabditis elegans. **5**, e259 (2007).
152 Lauritzen, K. H. *et al.* Impaired dynamics and function of mitochondria caused by mtDNA toxicity leads to heart failure. **309**, H434-H449 (2015).
153 van Gisbergen, M. W. *et al.* How do changes in the mtDNA and mitochondrial dysfunction influence cancer and cancer therapy? Challenges, opportunities and models. **764**, 16-30 (2015).
154 Collado, M., Blasco, M. A. & Serrano, M. J. C. Cellular senescence in cancer and aging. **130**, 223-233 (2007).
155 Dimri, G. P. J. C. c. What has senescence got to do with cancer? **7**, 505-512 (2005).
156 Sikora, E., Bielak-Zmijewska, A. & Mosieniak, G. J. C. v. p. Cellular senescence in ageing, age-related disease and longevity. **12**, 698-706 (2014).
157 Tian, X.-L., Li, Y. J. J. o. G. & Genomics. Endothelial cell senescence and age-related vascular diseases. **41**, 485-495 (2014).
158 Van Deursen, J. M. J. N. The role of senescent cells in ageing. **509**, 439-446 (2014).
159 Jeck, W. R., Siebold, A. P. & Sharpless, N. E. J. A. c. a meta-analysis of GWAS and age-associated diseases. **11**, 727-731 (2012).
160 Boquoi, A. *et al.* Reversible cell cycle inhibition and premature aging features imposed by conditional expression of p16Ink4a. **14**, 139-147 (2015).
161 Krishnamurthy, J. *et al.* Ink4a/Arf expression is a biomarker of aging. **114**, 1299-1307 (2004).
162 Ressler, S. *et al.* p16INK4A is a robust in vivo biomarker of cellular aging in human skin. **5**, 379-389 (2006).
163 Waaijer, M. E. *et al.* P16INK4a positive cells in human skin are indicative of local elastic fiber morphology, facial wrinkling, and perceived age. **71**, 1022-1028 (2016).
164 Baker, D. J. *et al.* Clearance of p16Ink4a-positive senescent cells delays ageing-associated disorders. **479**, 232-236 (2011).

165 Angello, J. C., Pendergrass, W. R., Norwood, T. H. & Prothero, J. J. J. o. c. p. Cell enlargement: one possible mechanism underlying cellular senescence. **140**, 288-294 (1989).
166 Campisi, J. J. A. r. o. p. Aging, cellular senescence, and cancer. **75**, 685-705 (2013).
167 Collado, M. *et al.* Senescence in premalignant tumours. **436**, 642-642 (2005).
168 Dimri, G. P. *et al.* A biomarker that identifies senescent human cells in culture and in aging skin in vivo. **92**, 9363-9367 (1995).
169 Kuilman, T., Michaloglou, C., Mooi, W. J., Peeper, D. S. J. G. & development. The essence of senescence. **24**, 2463-2479 (2010).
170 Narita, M. *et al.* Rb-mediated heterochromatin formation and silencing of E2F target genes during cellular senescence. **113**, 703-716 (2003).
171 Newgard, C. B. & Sharpless, N. E. J. T. J. o. c. i. Coming of age: molecular drivers of aging and therapeutic opportunities. **123**, 946-950 (2013).
172 Tchkonia, T., Zhu, Y., Van Deursen, J., Campisi, J. & Kirkland, J. L. J. T. J. o. c. i. Cellular senescence and the senescent secretory phenotype: therapeutic opportunities. **123**, 966-972 (2013).
173 Hoenicke, L. & Zender, L. J. C. Immune surveillance of senescent cells—biological significance in cancer-and non-cancer pathologies. **33**, 1123-1126 (2012).
174 Kang, T.-W. *et al.* Senescence surveillance of pre-malignant hepatocytes limits liver cancer development. **479**, 547-551 (2011).
175 Sagiv, A. & Krizhanovsky, V. J. B. Immunosurveillance of senescent cells: the bright side of the senescence program. **14**, 617-628 (2013).
176 Pera, A. *et al.* Immunosenescence: implications for response to infection and vaccination in older people. **82**, 50-55 (2015).
177 Coppé, J.-P., Desprez, P.-Y., Krtolica, A. & Campisi, J. J. A. r. o. p. m. o. d. The senescence-associated secretory phenotype: the dark side of tumor suppression. **5**, 99-118 (2010).
178 Wang, B., Kohli, J. & Demaria, M. J. T. i. c. Senescent cells in cancer therapy: friends or foes? **6**, 838-857 (2020).
179 Burton, D. G., Krizhanovsky, V. J. C. & Sciences, M. L. Physiological and pathological consequences of cellular senescence. **71**, 4373-4386 (2014).
180 Rera, M. *et al.* Modulation of longevity and tissue homeostasis by the Drosophila PGC-1 homolog. **14**, 623-634 (2011).
181 Molofsky, A. V. *et al.* Increasing p16 INK4a expression decreases forebrain progenitors and neurogenesis during ageing. **443**, 448-452 (2006).
182 vel Szic, K. S., Declerck, K., Vidaković, M. & Vanden Berghe, W. J. C. e. From inflammaging to healthy aging by dietary lifestyle choices: is epigenetics the key to personalized nutrition? **7**, 1-18 (2015).
183 Sergio, G. J. I. R. Exploring the complex relations between inflammation and aging (inflamm-aging): anti-inflamm-aging remodelling of inflamm-aging, from robustness to frailty. **57**, 558-563 (2008).
184 Kumari, M. J. P. I. M. D. i. N. D. A Comprehensive Review of the Ubiquitin-Proteasome System in Synapse Remodeling and Neurodegenerative Diseases. 297-327 (2025).

185 Schlesinger, D. H., Goldstein, G. & Niall, H. D. J. B. Complete amino acid sequence of ubiquitin, an adenylate cyclase stimulating polypeptide probably universal in living cells. **14**, 2214-2218 (1975).
186 Jenson, J., Goldstein, G. & Breslow, E. J. B. e. B. A.-P. S. Physical-chemical properties of ubiquitin. **624**, 378-385 (1980).
187 Lenkinski, R. E., Chen, D. M., Glickson, J. D. & Goldstein, G. J. B. e. B. A.-P. S. Nuclear magnetic resonance studies of the denaturation of ubiquitin. **494**, 126-130 (1977).
188 Schlesinger, D. H. & Goldstein, G. J. N. Molecular conservation of 74 amino acid sequence of ubiquitin between cattle and man. **255**, 423-424 (1975).
189 Hershko, A., Ciechanover, A. & Varshavsky, A. J. N. m. The ubiquitin system. **6**, 1073-1081 (2000).
190 Magnani, M., Crinelli, R., Bianchi, M. & Antonelli, A. J. C. d. t. The ubiquitin-dependent proteolytic system and other potential targets for the modulation of nuclear factor-kB (NF-kB). **1**, 387-399 (2000).
191 Ding, Q. & Shen, H. J. N. The role of ubiquitin-proteasome pathway in synaptic plasticity and memory. **148**, 515-529 (2007).
192 Thrower, J. S., Hoffman, L., Rechsteiner, M. & Pickart, C. M. J. T. E. j. Recognition of the polyubiquitin proteolytic signal. (2000).
193 Koegl, M. *et al.* A novel ubiquitination factor, E4, is involved in multiubiquitin chain assembly. **96**, 635-644 (1999).
194 Stewart, M. D., Ritterhoff, T., Klevit, R. E. & Brzovic, P. S. J. C. r. E2 enzymes: more than just middle men. **26**, 423-440 (2016).
195 Schneider, S. M., Lee, B. H. & Nicola, A. V. J. C. M. Viral entry and the ubiquitin-proteasome system. **23**, e13276 (2021).
196 Celen, A. B. & Sahin, U. J. T. F. j. Sumoylation on its 25th anniversary: mechanisms, pathology, and emerging concepts. **287**, 3110-3140 (2020).
197 Swatek, K. N. & Komander, D. J. C. r. Ubiquitin modifications. **26**, 399-422 (2016).
198 Geoffroy, M.-C. & Hay, R. T. J. N. r. M. c. b. An additional role for SUMO in ubiquitin-mediated proteolysis. **10**, 564-568 (2009).
199 Tatham, M. H. *et al.* RNF4 is a poly-SUMO-specific E3 ubiquitin ligase required for arsenic-induced PML degradation. **10**, 538-546 (2008).
200 Yang, Z. & Klionsky, D. J. J. N. c. b. Eaten alive: a history of macroautophagy. **12**, 814-822 (2010).
201 Boya, P., Reggiori, F. & Codogno, P. J. N. c. b. Emerging regulation and functions of autophagy. **15**, 713-720 (2013).
202 Stolz, A., Ernst, A. & Dikic, I. J. N. c. b. Cargo recognition and trafficking in selective autophagy. **16**, 495-501 (2014).
203 Kerr, J. S. *et al.* Mitophagy and Alzheimer's disease: cellular and molecular mechanisms. **40**, 151-166 (2017).
204 Ntsapi, C. *et al.* New insights into autophagy dysfunction related to amyloid beta toxicity and neuropathology in Alzheimer's disease. **336**, 321-361 (2018).
205 Shang, L. & Wang, X. J. A. AMPK and mTOR coordinate the regulation of Ulk1 and mammalian autophagy initiation. **7**, 924-926 (2011).

206 Hosokawa, N. *et al.* Nutrient-dependent mTORC1 association with the ULK1–Atg13–FIP200 complex required for autophagy. **20**, 1981-1991 (2009).
207 Jung, C. H. *et al.* ULK-Atg13-FIP200 complexes mediate mTOR signaling to the autophagy machinery. **20**, 1992-2003 (2009).
208 Egan, D., Kim, J., Shaw, R. J. & Guan, K.-L. J. A. The autophagy initiating kinase ULK1 is regulated via opposing phosphorylation by AMPK and mTOR. **7**, 643-644 (2011).
209 Dooley, H. C. *et al.* WIPI2 links LC3 conjugation with PI3P, autophagosome formation, and pathogen clearance by recruiting Atg12–5-16L1. **55**, 238-252 (2014).
210 Itakura, E., Kishi, C., Inoue, K. & Mizushima, N. J. M. b. o. t. c. Beclin 1 forms two distinct phosphatidylinositol 3-kinase complexes with mammalian Atg14 and UVRAG. **19**, 5360-5372 (2008).
211 Puri, C., Renna, M., Bento, C. F., Moreau, K. & Rubinsztein, D. C. J. A. ATG16L1 meets ATG9 in recycling endosomes: additional roles for the plasma membrane and endocytosis in autophagosome biogenesis. **10**, 182-184 (2014).
212 Ravikumar, B., Moreau, K., Jahreiss, L., Puri, C. & Rubinsztein, D. C. J. N. c. b. Plasma membrane contributes to the formation of pre-autophagosomal structures. **12**, 747-757 (2010).
213 Mizushima, N., Yoshimori, T., Ohsumi, Y. J. T. i. j. o. b. & biology, c. Role of the Apg12 conjugation system in mammalian autophagy. **35**, 553-561 (2003).
214 Tanida, I., Ueno, T., Kominami, E. J. T. i. j. o. b. & biology, c. LC3 conjugation system in mammalian autophagy. **36**, 2503-2518 (2004).
215 Nixon, R. A. J. N. m. The role of autophagy in neurodegenerative disease. **19**, 983-997 (2013).
216 Nixon, R. A. *et al.* Extensive involvement of autophagy in Alzheimer disease: an immuno-electron microscopy study. **64**, 113-122 (2005).
217 Li, Q., Liu, Y., Sun, M. J. C. & neurobiology, m. Autophagy and Alzheimer's disease. **37**, 377-388 (2017).
218 Dai, Q. *et al.* CHIP activates HSF1 and confers protection against apoptosis and cellular stress. (2003).
219 Lizama, B. N. *et al.* Neuronal preconditioning requires the mitophagic activity of C-terminus of HSC70-interacting protein. **38**, 6825-6840 (2018).
220 McLaughlin, B. *et al.* Haploinsufficiency of the E3 ubiquitin ligase C-terminus of heat shock cognate 70 interacting protein (CHIP) produces specific behavioral impairments. **7**, e36340 (2012).
221 Al-Ramahi, I. *et al.* CHIP protects from the neurotoxicity of expanded and wild-type ataxin-1 and promotes their ubiquitination and degradation. **281**, 26714-26724 (2006).
222 Ko, H. S. *et al.* CHIP regulates leucine-rich repeat kinase-2 ubiquitination, degradation, and toxicity. **106**, 2897-2902 (2009).
223 Petrucelli, L. *et al.* CHIP and Hsp70 regulate tau ubiquitination, degradation and aggregation. **13**, 703-714 (2004).
224 Qian, S.-B., McDonough, H., Boellmann, F., Cyr, D. M. & Patterson, C. J. N. CHIP-mediated stress recovery by sequential ubiquitination of substrates and Hsp70. **440**, 551-555 (2006).

225 KL, B., Ning, J., Nita, E. & Dias, C. J. s. The Functions of CHIP in Age Related Disease. **11**, 12 (2016).
226 Balaji, V., Pokrzywa, W. & Hoppe, T. J. B. Ubiquitylation pathways in insulin signaling and organismal homeostasis. **40**, 1700223 (2018).
227 Landré, V., Pion, E., Narayan, V., Xirodimas, D. P. & Ball, K. L. J. B. J. DNA-binding regulates site-specific ubiquitination of IRF-1. **449**, 707-717 (2013).
228 McLaughlin, B. *et al.* Haploinsufficiency of the E3 ubiquitin ligase C-terminus of heat shock cognate 70 interacting protein (CHIP) produces specific behavioral impairments. **7** (2012).
229 Dai, Q. *et al.* CHIP activates HSF1 and confers protection against apoptosis and cellular stress. **22**, 5446-5458 (2003).
230 Tetzlaff, J. E. *et al.* CHIP targets toxic α-synuclein oligomers for degradation. **283**, 17962-17968 (2008).
231 Kumar, P., Pradhan, K., Karunya, R., Ambasta, R. K. & Querfurth, H. W. J. J. o. n. Cross-functional E3 ligases Parkin and C-terminus Hsp70-interacting protein in neurodegenerative disorders. **120**, 350-370 (2012).
232 LaVoie, M. J., Cortese, G. P., Ostaszewski, B. L. & Schlossmacher, M. G. J. J. o. n. The effects of oxidative stress on parkin and other E3 ligases. **103**, 2354-2368 (2007).
233 Landré, V. *et al.* Regulation of transcriptional activators by DNA-binding domain ubiquitination. **24**, 903-916 (2017).
234 Genis, D. *et al.* Heterozygous STUB1 mutation causes familial ataxia with cognitive affective syndrome (SCA48). **91**, e1988-e1998 (2018).
235 Ronnebaum, S. M., Patterson, C. & Schisler, J. C. J. H. G. V. Emerging evidence of coding mutations in the ubiquitin–proteasome system associated with cerebellar ataxias. **1**, 1-7 (2014).
236 Ballinger, C. A. *et al.* Identification of CHIP, a novel tetratricopeptide repeat-containing protein that interacts with heat shock proteins and negatively regulates chaperone functions. **19**, 4535-4545 (1999).
237 Aravind, L. & Koonin, E. V. J. C. B. The U box is a modified RING finger—a common domain in ubiquitination. **10**, R132-R134 (2000).
238 Dou, H. *et al.* BIRC7–E2 ubiquitin conjugate structure reveals the mechanism of ubiquitin transfer by a RING dimer. **19**, 876-883 (2012).
239 Plechanovová, A., Jaffray, E. G., Tatham, M. H., Naismith, J. H. & Hay, R. T. J. N. Structure of a RING E3 ligase and ubiquitin-loaded E2 primed for catalysis. **489**, 115-120 (2012).
240 Zhang, M. *et al.* Chaperoned ubiquitylation—crystal structures of the CHIP U box E3 ubiquitin ligase and a CHIP-Ubc13-Uev1a complex. **20**, 525-538 (2005).
241 Murata, S., Minami, Y., Minami, M., Chiba, T. & Tanaka, K. J. E. r. CHIP is a chaperone-dependent E3 ligase that ubiquitylates unfolded protein. (2001).
242 Nielsen, M. L. *et al.* Iodoacetamide-induced artifact mimics ubiquitination in mass spectrometry. **5**, 459-460 (2008).
243 Joshi, V. *et al.* A decade of boon or burden: what has the CHIP ever done for cellular protein quality control mechanism implicated in neurodegeneration and aging? **9**, 93 (2016).

244 Wang, G. *et al.* K63-linked ubiquitination in kinase activation and cancer. **2**, 5 (2012).
245 Wu, X. & Karin, M. J. I. r. Emerging roles of Lys63-linked polyubiquitylation in immune responses. **266**, 161-174 (2015).
246 Xu, Z. *et al.* Structure and interactions of the helical and U-box domains of CHIP, the C terminus of HSP70 interacting protein. **45**, 4749-4759 (2006).
247 Xu, Z. *et al.* Interactions between the quality control ubiquitin ligase CHIP and ubiquitin conjugating enzymes. **8**, 1-13 (2008).
248 Andrade, M. A., Perez-Iratxeta, C. & Ponting, C. P. J. J. o. s. b. Protein repeats: structures, functions, and evolution. **134**, 117-131 (2001).
249 Blatch, G. L. & Lässle, M. J. B. The tetratricopeptide repeat: a structural motif mediating protein-protein interactions. **21**, 932-939 (1999).
250 Zeytuni, N. & Zarivach, R. J. S. Structural and functional discussion of the tetra-trico-peptide repeat, a protein interaction module. **20**, 397-405 (2012).
251 Connell, P. *et al.* The co-chaperone CHIP regulates protein triage decisions mediated by heat-shock proteins. **3**, 93-96 (2001).
252 Zhang, H. *et al.* A bipartite interaction between Hsp70 and CHIP regulates ubiquitination of chaperoned client proteins. **23**, 472-482 (2015).
253 Nikolay, R. *et al.* Dimerization of the human E3 ligase CHIP via a coiled-coil domain is essential for its activity. **279**, 2673-2678 (2004).
254 Graf, C., Stankiewicz, M., Nikolay, R. & Mayer, M. P. J. B. Insights into the conformational dynamics of the E3 ubiquitin ligase CHIP in complex with chaperones and E2 enzymes. **49**, 2121-2129 (2010).
255 Narayan, V. *et al.* Protein–protein interactions modulate the docking-dependent E3-ubiquitin ligase activity of Carboxy-terminus of Hsc70-interacting protein (CHIP). **14**, 2973-2987 (2015).
256 Ball, K., Ning, J., Nita, E., Dias, C. J. J. E. & Science, P. The functions of CHIP in age related disease. **1** (2016).
257 Kashyap, V. *et al.* Regulation of stem cell pluripotency and differentiation involves a mutual regulatory circuit of the NANOG, OCT4, and SOX2 pluripotency transcription factors with polycomb repressive complexes and stem cell microRNAs. **18**, 1093-1108 (2009).
258 Levine, B. & Klionsky, D. J. J. D. c. Development by self-digestion: molecular mechanisms and biological functions of autophagy. **6**, 463-477 (2004).
259 Sha, Y., Rao, L., Settembre, C., Ballabio, A. & Eissa, N. T. J. T. E. j. STUB 1 regulates TFEB-induced autophagy–lysosome pathway. **36**, 2544-2552 (2017).
260 Rao, L., Sha, Y., Eissa, N. T. J. M. & oncology, c. The E3 ubiquitin ligase STUB1 regulates autophagy and mitochondrial biogenesis by modulating TFEB activity. **4**, e1372867 (2017).
261 Guo, D. *et al.* Regulation of autophagic flux by CHIP. **31**, 469-479 (2015).
262 Mak, T. W., Hauck, L., Grothe, D. & Billia, F. J. P. o. t. N. A. o. S. p53 regulates the cardiac transcriptome. **114**, 2331-2336 (2017).
263 Naito, A. T. *et al.* Promotion of CHIP-mediated p53 degradation protects the heart from ischemic injury. **106**, 1692-1702 (2010).
264 Vaughan, C. A. *et al.* The oncogenicity of tumor-derived mutant p53 is enhanced by the recruitment of PLK3. **12**, 704 (2021).

265 Li, D. *et al.* Functional inactivation of endogenous MDM2 and CHIP by HSP90 causes aberrant stabilization of mutant p53 in human cancer cells. **9**, 577-588 (2011).
266 Ullah, K. *et al.* The E3 ubiquitin ligase STUB1 attenuates cell senescence by promoting the ubiquitination and degradation of the core circadian regulator BMAL1. **295**, 4696-4708 (2020).
267 Zhu, X. *et al.* Ubiquitination of inositol-requiring enzyme 1 (IRE1) by the E3 ligase CHIP mediates the IRE1/TRAF2/JNK pathway. **289**, 30567-30577 (2014).
268 Palubinsky, A. M. *et al.* CHIP is an essential determinant of neuronal mitochondrial stress signaling. **23**, 535-549 (2015).
269 Shi, Y. *et al.* Identification of CHIP as a novel causative gene for autosomal recessive cerebellar ataxia. **8**, e81884 (2013).
270 Shi, C.-H. *et al.* Ataxia and hypogonadism caused by the loss of ubiquitin ligase activity of the U box protein CHIP. **23**, 1013-1024 (2014).
271 Lizama, B. N., Palubinsky, A. M. & McLaughlin, B. J. N. i. Alterations in the E3 ligases Parkin and CHIP result in unique metabolic signaling defects and mitochondrial quality control issues. **117**, 139-155 (2018).
272 Dai, Q. *et al.* CHIP activates HSF1 and confers protection against apoptosis and cellular stress. **22**, 5446-5458 (2003).
273 Yoo, L. & Chung, K. C. J. J. o. B. C. The ubiquitin E3 ligase CHIP promotes proteasomal degradation of the serine/threonine protein kinase PINK1 during staurosporine-induced cell death. **293**, 1286-1297 (2018).
274 Schisler, J. C., Patterson, C. & Willis, M. S. J. A. j. o. c. p. Skeletal Muscle Mitochondrial Alterations in Carboxyl Terminus of HSC70 Interacting Protein (CHIP)−/− Mice. **6**, 28 (2016).
275 Zilocchi, M. *et al.* Exploring the impact of PARK2 mutations on the total and mitochondrial proteome of human skin fibroblasts. **8**, 423 (2020).
276 Li, J. *et al.* PINK1-parkin-mediated neuronal mitophagy deficiency in prion disease. **13**, 162 (2022).
277 Earnshaw, R. *et al.* Disease-associated mutations in C-terminus of HSP70 interacting protein (CHIP) impair its ability to negatively regulate mitophagy. **200**, 106625 (2024).
278 McDonough, H. *et al.* Stress-dependent Daxx-CHIP Interaction Suppresses the p53 Apoptotic Program*♦. **284**, 20649-20659 (2009).
279 Hwang, J. R., Zhang, C., Patterson, C. J. C. s. & chaperones. C-terminus of heat shock protein 70–interacting protein facilitates degradation of apoptosis signal-regulating kinase 1 and inhibits apoptosis signal-regulating kinase 1–dependent apoptosis. **10**, 147 (2005).
280 Jiang, J., Cyr, D., Babbitt, R. W., Sessa, W. C. & Patterson, C. J. J. o. b. c. Chaperone-dependent regulation of endothelial nitric-oxide synthase intracellular trafficking by the co-chaperone/ubiquitin ligase CHIP. **278**, 49332-49341 (2003).
281 Förstermann, U. & Sessa, W. C. J. E. h. j. Nitric oxide synthases: regulation and function. **33**, 829-837 (2012).
282 Dutta, S. & Sengupta, P. J. L. s. Men and mice: relating their ages. **152**, 244-248 (2016).

283 Metz, G. A. & Whishaw, I. Q. J. J. o. n. m. Cortical and subcortical lesions impair skilled walking in the ladder rung walking test: a new task to evaluate fore-and hindlimb stepping, placing, and co-ordination. **115**, 169-179 (2002).
284 Shiotsuki, H. *et al.* A rotarod test for evaluation of motor skill learning. **189**, 180-185 (2010).
285 Yankelevitch-Yahav, R., Franko, M., Huly, A. & Doron, R. J. J. o. v. e. J. The forced swim test as a model of depressive-like behavior. 52587 (2015).
286 Pitrez, P. R. *et al.* Cellular reprogramming as a tool to model human aging in a dish. **15**, 1816 (2024).
287 Park, S. *et al.* Microphysiological systems for human aging research. **23**, e14070 (2024).
288 Chaffey, N. (Oxford University Press, 2003).
289 Sengupta, P. & Samuel, A. D. J. C. o. i. n. Caenorhabditis elegans: a model system for systems neuroscience. **19**, 637-643 (2009).
290 Currey, H. N. & Liachko, N. F. J. J. o. V. E. Evaluation of motor impairment in C. elegans models of amyotrophic lateral sclerosis. e62699 (2021).
291 Koopman, M. *et al.* Assessing motor-related phenotypes of Caenorhabditis elegans with the wide field-of-view nematode tracking platform. **15**, 2071-2106 (2020).
292 Nawa, M. & Matsuoka, M. J. B.-p. The method of the body bending assay using Caenorhabditis elegans. **2**, e253-e253 (2012).
293 Walker, A. C., Bhargava, R., Brust, A. S., Owji, A. A. & Czyż, D. M. J. B.-p. Time-off-pick assay to measure Caenorhabditis elegans motility. **12**, e4436-e4436 (2022).
294 Chen, H.-Y. *et al.* Clinical and functional characterization of a novel STUB1 frameshift mutation in autosomal dominant spinocerebellar ataxia type 48 (SCA48). **28**, 65 (2021).
295 Alberti, S. *et al.* Ubiquitylation of BAG-1 suggests a novel regulatory mechanism during the sorting of chaperone substrates to the proteasome. **277**, 45920-45927 (2002).
296 Ronnebaum, S. M., Wu, Y., McDonough, H., Patterson, C. J. M. & biology, c. The ubiquitin ligase CHIP prevents SirT6 degradation through noncanonical ubiquitination. **33**, 4461-4472 (2013).
297 Salomoni, P. & Khelifi, A. F. J. T. i. c. b. Daxx: death or survival protein? **16**, 97-104 (2006).
298 McDonough, H. *et al.* Stress-dependent Daxx-CHIP interaction suppresses the p53 apoptotic program. **284**, 20649-20659 (2009).
299 Harman, D. J. P. o. t. N. A. o. S. The aging process. **78**, 7124-7128 (1981).
300 Lehman, N. L. J. A. n. The ubiquitin proteasome system in neuropathology. **118**, 329-347 (2009).
301 Proctor, C. J., Tsirigotis, M. & Gray, D. A. J. B. s. b. An in silico model of the ubiquitin-proteasome system that incorporates normal homeostasis and age-related decline. **1**, 1-18 (2007).
302 VanPelt, J., Page, R. C. J. B. e. B. A.-P. & Proteomics. Unraveling the CHIP: Hsp70 complex as an information processor for protein quality control. **1865**, 133-141 (2017).

303 Paul, I. & Ghosh, M. K. J. B. r. i. The E3 ligase CHIP: insights into its structure and regulation. **2014**, 918183 (2014).
304 Banerjee, P., Joo, J., Buse, J. T., Dawson, G. J. C. & lipids, p. o. Differential solubilization of lipids along with membrane proteins by different classes of detergents. **77**, 65-78 (1995).
305 Theillet, F.-X. *et al.* Physicochemical properties of cells and their effects on intrinsically disordered proteins (IDPs). **114**, 6661-6714 (2014).
306 Zheng, N., Tsai, H. N., Zhang, X., Shedden, K. & Rosania, G. R. J. M. p. The subcellular distribution of small molecules: a meta-analysis. **8**, 1611-1618 (2011).
307 Rampado, R. *et al.* Optimization of a detergent-based protocol for membrane proteins purification from mammalian cells. **219**, 114926 (2022).
308 Das, A., Bysack, A., Raghuraman, H. J. B. & Communications, B. R. Effectiveness of dual-detergent strategy using Triton X-100 in membrane protein purification. **578**, 122-128 (2021).
309 Schröder, L., Senkler, J. & Braun, H. P. J. D. m. i. d. t. Special features of cellular respiration in viscum album. pp 3-pp13 (2020).
310 Smith, S. M. J. P. c. m. & protocols. Strategies for the purification of membrane proteins. 485-496 (2011).
311 Tanca, A., Biosa, G., Pagnozzi, D., Addis, M. F. & Uzzau, S. J. P. Comparison of detergent-based sample preparation workflows for LTQ-O rbitrap analysis of the E scherichia coli proteome. **13**, 2597-2607 (2013).
312 Sagu, S. T., Huschek, G., Homann, T. & Rawel, H. M. J. M. Effect of sample preparation on the detection and quantification of selected nuts allergenic proteins by LC-MS/MS. **26**, 4698 (2021).
313 Vantaggiato, L. *et al.* Protein Extraction Methods Suitable for Muscle Tissue Proteomic Analysis. **12**, 27 (2024).
314 Cruz de Carvalho, R. *et al.* Ecotoxicological effects of the anionic surfactant Sodium Dodecyl Sulfate (SDS) in two marine primary producers: Phaeodactylum tricornutum and ulva lactuca. **10**, 780 (2022).
315 Furmanczyk, E. M. *et al.* Isolation and characterization of Pseudomonas spp. strains that efficiently decompose sodium dodecyl sulfate. **8**, 1872 (2017).
316 Lee, J. Y., Selfridge, K. M., Kohn, E. M., Vaden, T. D. & Caputo, G. A. J. B. Effects of ionic liquid alkyl chain length on denaturation of myoglobin by anionic, cationic, and zwitterionic detergents. **9**, 264 (2019).
317 Tulumello, D. V. & Deber, C. M. J. B. SDS micelles as a membrane-mimetic environment for transmembrane segments. **48**, 12096-12103 (2009).
318 Jeong, W., Kim, M. K. & Kang, H.-W. J. J. o. t. e. Effect of detergent type on the performance of liver decellularized extracellular matrix-based bio-inks. **12**, 2041731421997091 (2021).
319 Kragh-Hansen, U., le Maire, M. & Møller, J. V. J. B. j. The mechanism of detergent solubilization of liposomes and protein-containing membranes. **75**, 2932-2946 (1998).
320 Terrie, L. *et al.* Decellularized tissue exhibits large differences of extracellular matrix properties dependent on decellularization method: novel insights from a standardized characterization on skeletal muscle. **16**, 025033 (2024).

321 Kachuk, C. & Doucette, A. A. J. J. o. p. The benefits (and misfortunes) of SDS in top-down proteomics. **175**, 75-86 (2018).
322 HaileMariam, M. *et al.* S-Trap, an ultrafast sample-preparation approach for shotgun proteomics. **17**, 2917-2924 (2018).
323 Botelho, D. *et al.* Top-down and bottom-up proteomics of SDS-containing solutions following mass-based separation. **9**, 2863-2870 (2010).
324 Unterlander, N. & Doucette, A. A. J. P. Membrane-Based SDS Depletion Ahead of Peptide and Protein Analysis by Mass Spectrometry. **18**, 1700025 (2018).
325 Ngwai, Y. B., Adachi, Y., Ogawa, Y., Ibrahim, K. J. J. o. M., Immunology & Infection. Comparison of immunoblot analysis of emergent multidrug-resistant Salmonella typhimurium definitive phage type 104 with a non-multidrug-resistant definitive phage type 104 strain. **39**, 189-194 (2006).
326 Glatter, T., Ahrné, E. & Schmidt, A. J. J. o. p. r. Comparison of different sample preparation protocols reveals lysis buffer-specific extraction biases in gram-negative bacteria and human cells. **14**, 4472-4485 (2015).
327 Kaleja, P., Emmert, H., Gerstel, U., Weidinger, S. & Tholey, A. J. J. o. p. Evaluation and improvement of protein extraction methods for analysis of skin proteome by noninvasive tape stripping. **217**, 103678 (2020).
328 León, I. R., Schwämmle, V., Jensen, O. N., Sprenger, R. R. J. M. & Proteomics, C. Quantitative assessment of in-solution digestion efficiency identifies optimal protocols for unbiased protein analysis. **12**, 2992-3005 (2013).
329 Steinbach, M. K., Leipert, J., Blurton, C., Leippe, M. & Tholey, A. J. J. o. P. R. Digital microfluidics supported microproteomics for quantitative proteome analysis of single Caenorhabditis elegans nematodes. **21**, 1986-1996 (2022).
330 Zhang, X. J. P. Detergents: Friends not foes for high-performance membrane proteomics toward precision medicine. **17**, 1600209 (2017).
331 Kumar, Y., Yadav, R. & Bhatia, A. J. F. V. Vol. 15 779-782 (Taylor & Francis, 2020).
332 Hjelmeland, L. M., Nebert, D. W. & Chrambach, A. J. A. B. Electrofocusing of integral membrane proteins in mixtures of zwitterionic and nonionic detergents. **95**, 201-208 (1979).
333 Bancells, L., Balsa, D., Gómez, N. & Unzeta, M. J. B. p. Effects of nondenaturating zwitterionic detergent chaps, 3-[(3-cholamido propyl) dimethyl ammonio]-1-propanesulfonate, on rat liver mitochondrial and microsomal monoamine oxidase. **36**, 2539-2546 (1987).
334 Herrera, F. E., Garay, A. S. & Rodrigues, D. E. J. T. J. o. P. C. B. Structural properties of CHAPS micelles, studied by molecular dynamics simulations. **118**, 3912-3921 (2014).
335 Zhang, L. *et al.* Characterization of the aggregated pattern of CHAPS using solvent paramagnetic relaxation enhancements. **555**, 332-338 (2018).
336 Masuda, T., Ito, S. & Ohtsuki, S. J. D. D. T. T. Advances in sample preparation for membrane proteome quantification. **39**, 23-29 (2021).
337 Lau, B. Y. C. & Othman, A. J. P. O. Evaluation of sodium deoxycholate as solubilization buffer for oil palm proteomics analysis. **14**, e0221052 (2019).
338 Broecker, J. & Keller, S. J. L. Impact of urea on detergent micelle properties. **29**, 8502-8510 (2013).

339 Midura, R. J. & Yanagishita, M. J. A. b. Chaotropic solvents increase the critical micellar concentrations of detergents. **228**, 318-322 (1995).
340 Baumeister, R. & Ge, L. J. T. i. b. The worm in us–Caenorhabditis elegans as a model of human disease. **20**, 147-148 (2002).
341 Consortium*, T. C. e. S. Genome Sequence of the Nematode C. elegans: A Platform for Investigating Biology. **282**, 2012-2018, doi:doi:10.1126/science.282.5396.2012 (1998).
342 Conradt, B., MJGBSKOKD, A. C. & Colon-Ramos, D. J. D. C. The power of C. elegans: A tribute to Sydney Brenner. **49**, 496-498 (2019).
343 Corsi, A. K., Wightman, B. & Chalfie, M. J. G. A transparent window into biology: a primer on Caenorhabditis elegans. **200**, 387-407 (2015).
344 Demirci, N., Ustunsoy, R. & Dinc, B. J. P. M. J. Caenorhabditis Elegans in Neuroscience Research. **3**, 101-107 (2021).
345 Gershon, H., Gershon, D. J. M. o. a. & development. Caenorhabditis elegans—a paradigm for aging research: advantages and limitations. **123**, 261-274 (2002).
346 Huang, D. W., Sherman, B. T. & Lempicki, R. A. J. N. p. Systematic and integrative analysis of large gene lists using DAVID bioinformatics resources. **4**, 44-57 (2009).
347 Wisniewski, J. R., Zougman, A., Nagaraj, N. & Mann, M. J. N. m. Universal sample preparation method for proteome analysis. **6**, 359 (2009).
348 Keller, A., Nesvizhskii, A. I., Kolker, E. & Aebersold, R. J. A. c. Empirical statistical model to estimate the accuracy of peptide identifications made by MS/MS and database search. **74**, 5383-5392 (2002).
349 Shteynberg, D. *et al.* iProphet: multi-level integrative analysis of shotgun proteomic data improves peptide and protein identification rates and error estimates. **10** (2011).
350 Deutsch, E. W. *et al.* A guided tour of the Trans-Proteomic Pipeline. **10**, 1150-1159 (2010).
351 Sherman, B. T. *et al.* DAVID: a web server for functional enrichment analysis and functional annotation of gene lists (2021 update). **50**, W216-W221 (2022).
352 Churchward, M. A., Butt, R. H., Lang, J. C., Hsu, K. K. & Coorssen, J. R. J. P. S. Enhanced detergent extraction for analysis of membrane proteomes by two-dimensional gel electrophoresis. **3**, 1-11 (2005).
353 Rodi, P. M., Gianello, M. B., Corregido, M. & Gennaro, A. M. J. B. e. B. A.-B. Comparative study of the interaction of CHAPS and Triton X-100 with the erythrocyte membrane. **1838**, 859-866 (2014).
354 Shen, C.-H. *Diagnostic molecular biology*. (Academic Press, 2019).
355 Nguyen, T. N. *et al.* Comparative Sample Preparation Methods for a Label-Free Proteomic Analysis. **13**, 184-188 (2022).
356 Tanford, C. *The hydrophobic effect: formation of micelles and biological membranes 2d ed*. (J. Wiley., 1980).
357 Wei, J. *et al.* Global proteome discovery using an online three-dimensional LC−MS/MS. **4**, 801-808 (2005).
358 Zhang, N. *et al.* Comparison of SDS-and methanol-assisted protein solubilization and digestion methods for Escherichia coli membrane proteome analysis by 2-D LC-MS/MS. **7**, 484-493 (2007).

359 Wiśniewski, J. R., Zougman, A., Nagaraj, N. & Mann, M. J. N. m. Universal sample preparation method for proteome analysis. **6**, 359-362 (2009).
360 Zhang, N. & Li, L. J. R. C. i. M. S. Effects of common surfactants on protein digestion and matrix-assisted laser desorption/ionization mass spectrometric analysis of the digested peptides using two-layer sample preparation. **18**, 889-896 (2004).
361 Bereman, M. S., Egertson, J. D. & MacCoss, M. J. J. P. Comparison between procedures using SDS for shotgun proteomic analyses of complex samples. **11**, 2931-2935 (2011).
362 Erde, J., Loo, R. R. O. & Loo, J. A. J. J. o. p. r. Enhanced FASP (eFASP) to increase proteome coverage and sample recovery for quantitative proteomic experiments. **13**, 1885-1895 (2014).
363 Jones, M. J. C. S. R. Surfactant interactions with biomembranes and proteins. **21**, 127-136 (1992).
364 Kushnirov, V. V. J. Y. Rapid and reliable protein extraction from yeast. **16**, 857-860 (2000).
365 Speers, A. E. & Wu, C. C. J. C. r. Proteomics of integral membrane proteins theory and application. **107**, 3687-3714 (2007).
366 Trinh, T. H., Kim, J., Lee, C.-H., Ryou, C. J. B. & communications, b. r. Non-ionic detergents Nonidet P-40 and Triton X-100 increase enzymatic activity of plasmin. **512**, 314-318 (2019).
367 Steinbach, M. *Development of miniaturized bioanalytical methods for the qualitative and quantitative analysis of proteins and proteomes by means of digital microfluidics and nanoLC-MS*, (2024).
368 Arakawa, T., Niikura, T., Kita, Y. & Akuta, T. J. C. I. i. M. B. Sodium Dodecyl Sulfate Analogs as a Potential Molecular Biology Reagent. **46** (2024).
369 Asanuma, M., Fukuzawa, S., Matsuda, T. & Hirota, H. J. R. C. i. M. S. A. I. J. D. t. t. R. D. o. U. t. t. M. R. i. M. S. The effect of sodium dodecyl sulfate and anion-exchange silica gel on matrix-assisted laser desorption/ionization mass spectrometric analysis of proteins. **23**, 1647-1653 (2009).
370 Breaux, G. A., Green-Church, K. B., France, A. & Limbach, P. A. J. A. c. Surfactant-aided, matrix-assisted laser desorption/ionization mass spectrometry of hydrophobic and hydrophilic peptides. **72**, 1169-1174 (2000).
371 Fox, J., Stevens Jr, S., Taylor Jr, C. & Poulsen, L. J. A. B. SDS removal from protein by polystyrene beads. **87**, 253-256 (1978).
372 Henderson, L., Oroszlan, S. & Konigsberg, W. J. A. b. A micromethod for complete removal of dodecyl sulfate from proteins by ion-pair extraction. **93**, 153-157 (1979).
373 Van Pijkeren, A. *et al.* Proteome Coverage after Simultaneous Proteo-Metabolome Liquid–Liquid Extraction. **22**, 951-966 (2023).
374 Kim, J.-H. *et al.* C-terminus of HSC70-interacting protein (CHIP) inhibits adipocyte differentiation via ubiquitin-and proteasome-mediated degradation of PPARγ. **7**, 40023 (2017).
375 Lukashchuk, N., Vousden, K. H. J. M. & biology, c. Ubiquitination and degradation of mutant p53. (2007).

376 Quintana-Gallardo, L. *et al.* The cochaperone CHIP marks Hsp70-and Hsp90-bound substrates for degradation through a very flexible mechanism. **9**, 5102 (2019).
377 Wu, H. H. *et al.* Hsp70 acts as a fine-switch that controls E3 ligase CHIP-mediated TAp63 and ΔNp63 ubiquitination and degradation. **49**, 2740-2758 (2021).
378 Chen, J. *et al.* Drosophila CHIP protects against mitochondrial dysfunction by acting downstream of Pink1 in parallel with Parkin. **31**, 5234-5245 (2017).
379 Hahn, K. R., Kwon, H. J., Yoon, Y. S., Kim, D. W. & Hwang, I. K. J. S. R. CHIP ameliorates neuronal damage in H2O2-induced oxidative stress in HT22 cells and gerbil ischemia. **12**, 20659 (2022).
380 Lee, J. *et al.* CHIP has a protective role against oxidative stress-induced cell death through specific regulation of endonuclease G. **4**, e666-e666 (2013).
381 El Khouri, E., Le Pavec, G., Toledano, M. B. & Delaunay-Moisan, A. J. J. o. B. C. RNF185 is a novel E3 ligase of endoplasmic reticulum-associated degradation (ERAD) that targets cystic fibrosis transmembrane conductance regulator (CFTR). **288**, 31177-31191 (2013).
382 Pabarcus, M. K. *et al.* CYP3A4 ubiquitination by gp78 (the tumor autocrine motility factor receptor, AMFR) and CHIP E3 ligases. **483**, 66-74 (2009).
383 Meacham, G. C., Patterson, C., Zhang, W., Younger, J. M. & Cyr, D. M. J. N. c. b. The Hsc70 co-chaperone CHIP targets immature CFTR for proteasomal degradation. **3**, 100-105 (2001).
384 Cook, C. *et al.* Loss of HDAC6, a novel CHIP substrate, alleviates abnormal tau accumulation. **21**, 2936-2945 (2012).
385 Mylvaganam, S., Earnshaw, R., Heymann, G., Kalia, S. K. & Kalia, L. V. J. C. N. C-terminus of Hsp70 interacting protein (CHIP) and neurodegeneration: lessons from the bench and bedside. **19**, 1038-1068 (2021).
386 Al Shweiki, M. R. *et al.* Assessment of label-free quantification in discovery proteomics and impact of technological factors and natural variability of protein abundance. **16**, 1410-1424 (2017).
387 Bai, M. *et al.* LFQ-based peptide and protein intensity differential expression analysis. **22**, 2114-2123 (2023).
388 Li, Q. J. I. j. o. p. Assigning Significance in Label-Free Quantitative Proteomics to Include Single-Peptide-Hit Proteins with Low Replicates. **2010**, 731582 (2010).
389 O'Connell, J. D., Paulo, J. A., O'Brien, J. J. & Gygi, S. P. J. J. o. p. r. Proteome-wide evaluation of two common protein quantification methods. **17**, 1934-1942 (2018).
390 Qin, X., Liu, M., Yang, D. & Zhang, X. J. T. J. o. P. C. B. Concentration-dependent aggregation of CHAPS investigated by NMR spectroscopy. **114**, 3863-3868 (2010).
391 Michaux, C., Pomroy, N. C. & Privé, G. G. J. J. o. m. b. Refolding SDS-denatured proteins by the addition of amphipathic cosolvents. **375**, 1477-1488 (2008).
392 Yamaguchi, H. & Miyazaki, M. J. B. Refolding techniques for recovering biologically active recombinant proteins from inclusion bodies. **4**, 235-251 (2014).

393 Han, S. K. *et al.* OASIS 2: online application for survival analysis 2 with features for the analysis of maximal lifespan and healthspan in aging research. **7**, 56147 (2016).
394 Salemi, M. *et al.* Examples of inverse comorbidity between cancer and neurodegenerative diseases: a possible role for noncoding RNA. **11**, 1930 (2022).
395 Zhao, Y. *et al.* Changes to social feeding behaviors are not sufficient for fitness gains of the Caenorhabditis elegans N2 reference strain. **7**, e38675 (2018).
396 Chen, J. *et al.* A demographic analysis of the fitness cost of extended longevity in Caenorhabditis elegans. **62**, 126-135 (2007).
397 Geens, E. *et al.* Yolk-deprived Caenorhabditis elegans secure brood size at the expense of competitive fitness. **6** (2023).
398 Shabtai, R., Tzur, Y. B. J. F. i. C. & Biology, D. Male-specific roles of lincRNA in C. elegans fertility. **11**, 1115605 (2023).
399 Stobierska, J. & Fernandez, A. G. J. m. B. Low-fecundity dhc-1; mel-28 C. elegans mutants do not have gonad mitosis defects. **2025**, 10.17912/micropub. biology. 001445 (2025).
400 Sutphin, G. L. *et al.* Caenorhabditis elegans orthologs of human genes differentially expressed with age are enriched for determinants of longevity. **16**, 672-682 (2017).
401 Uno, M., Nishida, E. J. n. A. & Disease, M. o. Lifespan-regulating genes in C. elegans. **2**, 1-8 (2016).
402 Dickey, C. A., Patterson, C., Dickson, D. & Petrucelli, L. J. T. i. m. m. Brain CHIP: removing the culprits in neurodegenerative disease. **13**, 32-38 (2007).
403 Ming, R. *et al.* Heat Stress and SCA48 Mutations Reveal the Metamorphic Structure and Function of the Ubiquitin Ligase CHIP.
404 Seo, J., Han, S. Y., Seong, D., Han, H.-J. & Song, J. J. A. o. p. r. Multifaceted C-terminus of HSP70-interacting protein regulates tumorigenesis via protein quality control. **42**, 63-75 (2019).
405 Akutsu, M., Dikic, I. & Bremm, A. J. J. o. c. s. Ubiquitin chain diversity at a glance. **129**, 875-880 (2016).
406 Clague, M. J. & Urbé, S. J. C. Ubiquitin: same molecule, different degradation pathways. **143**, 682-685 (2010).
407 Li, W., Ye, Y. J. C. & Sciences, M. L. Polyubiquitin chains: functions, structures, and mechanisms. **65**, 2397-2406 (2008).
408 Meyer, H.-J. & Rape, M. J. C. Enhanced protein degradation by branched ubiquitin chains. **157**, 910-921 (2014).
409 Mirzaei, H. *et al.* Characterizing the connectivity of poly-ubiquitin chains by selected reaction monitoring mass spectrometry. **6**, 2004-2014 (2010).
410 Xu, P. *et al.* Quantitative proteomics reveals the function of unconventional ubiquitin chains in proteasomal degradation. **137**, 133-145 (2009).
411 Page, R. C., Pruneda, J. N., Amick, J., Klevit, R. E. & Misra, S. J. B. Structural insights into the conformation and oligomerization of E2~ ubiquitin conjugates. **51**, 4175-4187 (2012).
412 Wang, S. *et al.* STUB1 is essential for T-cell activation by ubiquitinating CARMA 1. **43**, 1034-1041 (2013).

413 Dianov, G., Meisenberg, C. & Parsons, J. J. B. Regulation of DNA repair by ubiquitylation. **76**, 69-79 (2011).
414 Gonfloni, S. J. C. c. Vol. 9 217-218 (Taylor & Francis, 2010).
415 Wang, X. *et al.* A positive role for c-Abl in Atm and Atr activation in DNA damage response. **18**, 5-15 (2011).
416 HMA Ramaekers, C. & G Wouters, B. J. C. m. m. Regulatory functions of ubiquitin in diverse DNA damage responses. **11**, 152-169 (2011).
417 Woodruff, T. K. J. N. m. Preserving fertility during cancer treatment. **15**, 1124-1125 (2009).
418 Geisler, S. *et al.* PINK1/Parkin-mediated mitophagy is dependent on VDAC1 and p62/SQSTM1. **12**, 119-131 (2010).
419 van der Laan, L., Ten Voorde, N., Mannens, M. M. & Henneman, P. J. F. i. M. N. Molecular signatures in Mendelian neurodevelopment: a focus on ubiquitination driven DNA methylation aberrations. **17**, 1446686 (2024).
420 Kim, J. *et al.* RAD6-Mediated transcription-coupled H2B ubiquitylation directly stimulates H3K4 methylation in human cells. **137**, 459-471 (2009).
421 Hottinger, A. F. *et al.* (American Society of Clinical Oncology, 2016).
422 Josling, G. A., Selvarajah, S. A., Petter, M. & Duffy, M. F. J. G. The role of bromodomain proteins in regulating gene expression. **3**, 320-343 (2012).
423 Bourgeois, G., Létoquart, J., Van Tran, N. & Graille, M. J. B. Trm112, a protein activator of methyltransferases modifying actors of the eukaryotic translational apparatus. **7**, 7 (2017).
424 Lacoux, C. *et al.* The catalytic activity of the translation termination factor methyltransferase Mtq2-Trm112 complex is required for large ribosomal subunit biogenesis. **48**, 12310-12325 (2020).
425 Das, P. & Golde, T. J. T. J. o. c. i. Dysfunction of TGF-β signaling in Alzheimer's disease. **116**, 2855-2857 (2006).
426 Flanders, K. C., Ren, R. F. & Lippa, C. F. J. P. i. n. Transforming growth factor-βs in neurodegenerative disease. **54**, 71-85 (1998).
427 Tesseur, I. *et al.* Deficiency in neuronal TGF-β signaling promotes neurodegeneration and Alzheimer's pathology. **116**, 3060-3069 (2006).
428 Haque, R. & Nazir, A. J. M. n. SMAD transcription factor, sma-9, attunes TGF-β signaling cascade towards modulating amyloid beta aggregation and associated outcome in transgenic C. elegans. **53**, 109-119 (2016).
429 Wyss-Coray, T. *et al.* TGF-β1 promotes microglial amyloid-β clearance and reduces plaque burden in transgenic mice. **7**, 612-618 (2001).
430 Harris-White, M. E. *et al.* Effects of transforming growth factor-β (isoforms 1–3) on amyloid-β deposition, inflammation, and cell targeting in organotypic hippocampal slice cultures. **18**, 10366-10374 (1998).
431 Mathews, E. A., Mullen, G. P., Hodgkin, J., Duerr, J. S. & Rand, J. B. J. G. Genetic interactions between UNC-17/VAChT and a novel transmembrane protein in Caenorhabditis elegans. **192**, 1315-1325 (2012).
432 Iqbal, K., Flory, M. & Soininen, H. J. J. o. A. s. D. Clinical symptoms and symptom signatures of Alzheimer's disease subgroups. **37**, 475-481 (2013).
433 Traissard, N. *et al.* Combined damage to entorhinal cortex and cholinergic basal forebrain neurons, two early neurodegenerative features accompanying

Alzheimer's disease: effects on locomotor activity and memory functions in rats. **32**, 851-871 (2007).
434 Soond, S. M. & Chantry, A. J. B. How ubiquitination regulates the TGF-β signalling pathway: New insights and new players: New isoforms of ubiquitin-activating enzymes in the E1-E3 families join the game. **33**, 749-758 (2011).
435 Xin, H. *et al.* CHIP controls the sensitivity of transforming growth factor-β signaling by modulating the basal level of Smad3 through ubiquitin-mediated degradation. **280**, 20842-20850 (2005).
436 Shang, Y. *et al.* Hsp70 and Hsp90 oppositely regulate TGF-β signaling through CHIP/Stub1. **446**, 387-392 (2014).
437 Mozdy, A., McCaffery, J. & Shaw, J. J. T. J. o. c. b. Dnm1p GTPase-mediated mitochondrial fission is a multi-step process requiring the novel integral membrane component Fis1p. **151**, 367-380 (2000).
438 Cheng, Z. J. B. J. FoxO transcription factors in mitochondrial homeostasis. **479**, 525-536 (2022).
439 Gao, Z. *et al.* Mitochondrial dynamics controls anti-tumour innate immunity by regulating CHIP-IRF1 axis stability. **8**, 1805 (2017).
440 Liu, B., Han, Y. & Qian, S.-B. J. M. c. Cotranslational response to proteotoxic stress by elongation pausing of ribosomes. **49**, 453-463 (2013).
441 White, J. *et al.* Rab6 coordinates a novel Golgi to ER retrograde transport pathway in live cells. **147**, 743-760 (1999).
442 Matsumura, Y., Sakai, J. & Skach, W. R. J. J. o. B. C. Endoplasmic reticulum protein quality control is determined by cooperative interactions between Hsp/c70 protein and the CHIP E3 ligase. **288**, 31069-31079 (2013).
443 Smith, R. D. *et al.* The COG complex, Rab6 and COPI define a novel Golgi retrograde trafficking pathway that is exploited by SubAB toxin. **10**, 1502-1517 (2009).
444 Kudlyk, T., Willett, R., Pokrovskaya, I. D. & Lupashin, V. J. T. COG6 interacts with a subset of the Golgi SNAREs and is important for the Golgi complex integrity. **14**, 194-204 (2013).
445 Wang, X., Huang, T., Bu, G. & Xu, H. J. M. n. Dysregulation of protein trafficking in neurodegeneration. **9**, 1-9 (2014).
446 Sagona, A. P., Nezis, I. P. & Stenmark, H. J. B. r. i. Association of CHMP4B and autophagy with micronuclei: implications for cataract formation. **2014**, 974393 (2014).
447 Usami, Y. *et al.* Regulation of CHMP4/ESCRT-III function in human immunodeficiency virus type 1 budding by CC2D1A. **86**, 3746-3756 (2012).
448 Hou, J. *et al.* Integrated multi-omics analyses identify anti-viral host factors and pathways controlling SARS-CoV-2 infection. **15**, 109 (2024).
449 Mardi, N. *et al.* Exosomal transmission of viruses, a two-edged biological sword. **21**, 19 (2023).
450 Zhang, Y. *et al.* β-Coronaviruses exploit ESCRT for virion assembly and egress. **16**, e00979-00925 (2025).
451 Diamant, G., Bahat, A. & Dikstein, R. J. N. c. The elongation factor Spt5 facilitates transcription initiation for rapid induction of inflammatory-response genes. **7**, 11547 (2016).

452 Krasnopolsky, S., Novikov, A., Kuzmina, A. & Taube, R. J. B. e. B. A.-G. R. M. CRISPRi-mediated depletion of Spt4 and Spt5 reveals a role for DSIF in the control of HIV latency. **1864**, 194656 (2021).
453 Kuś, K. *et al.* DSIF factor Spt5 coordinates transcription, maturation and exoribonucleolysis of RNA polymerase II transcripts. **16**, 10 (2025).
454 Toth, Z. *et al.* Negative elongation factor-mediated suppression of RNA polymerase II elongation of Kaposi's sarcoma-associated herpesvirus lytic gene expression. **86**, 9696-9707 (2012).
455 Zhao, Z., Tang, K.-W., Muylaert, I., Samuelsson, T. & Elias, P. J. J. o. B. C. CDK9 and SPT5 proteins are specifically required for expression of herpes simplex virus 1 replication-dependent late genes. **292**, 15489-15500 (2017).
456 Norris, A., McManus, C. T., Wang, S., Ying, R. & Grant, B. D. J. P. g. Mutagenesis and structural modeling implicate RME-8 IWN domains as conformational control points. **18**, e1010296 (2022).
457 Norris, A. *et al.* SNX-1 and RME-8 oppose the assembly of HGRS-1/ESCRT-0 degradative microdomains on endosomes. **114**, E307-E316 (2017).
458 Ardley, H. C. & Robinson, P. A. J. E. i. b. E3 ubiquitin ligases. **41**, 15-30 (2005).
459 Jana, N. R. J. N. i. Protein homeostasis and aging: role of ubiquitin protein ligases. **60**, 443-447 (2012).
460 McClellan, A. J. & Frydman, J. J. N. c. b. Molecular chaperones and the art of recognizing a lost cause. **3**, E51-E53 (2001).
461 Li, Q. *et al.* Daxx cooperates with the Axin/HIPK2/p53 complex to induce cell death. **67**, 66-74 (2007).
462 Massaous, J. & Hata, A. J. T. i. c. b. TGF-β signalling through the Smad pathway. **7**, 187-192 (1997).
463 Perlman, R., Schiemann, W. P., Brooks, M. W., Lodish, H. F. & Weinberg, R. A. J. N. c. b. TGF-β-induced apoptosis is mediated by the adapter protein Daxx that facilitates JNK activation. **3**, 708-714 (2001).
464 Cao, Z. *et al.* CHIP: A new modulator of human malignant disorders. **7**, 29864 (2016).
465 Jeong, J. H., An, J. Y., Kwon, Y. T., Li, L. Y. & Lee, Y. J. J. J. o. c. b. Quercetin-induced ubiquitination and down-regulation of Her-2/neu. **105**, 585-595 (2008).
466 Xu, W. *et al.* Chaperone-dependent E3 ubiquitin ligase CHIP mediates a degradative pathway for c-ErbB2/Neu. **99**, 12847-12852 (2002).
467 Wei, C. *et al.* Tripartite motif-containing protein 6 facilitates growth and migration of breast cancer through degradation of STUB1. **65**, 3214 (2021).
468 Kang, S.-A., Cho, H.-S., Yoon, J. B., Chung, I. K. & Lee, S.-T. J. B. J. Hsp90 rescues PTK6 from proteasomal degradation in breast cancer cells. **447**, 313-320 (2012).
469 Fontaine, S. N. *et al.* The active Hsc70/tau complex can be exploited to enhance tau turnover without damaging microtubule dynamics. **24**, 3971-3981 (2015).
470 Arndt, V. *et al.* Chaperone-assisted selective autophagy is essential for muscle maintenance. **20**, 143-148 (2010).
471 Urushitani, M. *et al.* CHIP promotes proteasomal degradation of familial ALS-linked mutant SOD1 by ubiquitinating Hsp/Hsc70. **90**, 231-244 (2004).

472 Dimant, H. *et al.* Direct visualization of CHIP-mediated degradation of alpha-synuclein in vivo: implications for PD therapeutics. **9**, e92098 (2014).
473 Kalia, L. V. *et al.* Ubiquitinylation of α-synuclein by carboxyl terminus Hsp70-interacting protein (CHIP) is regulated by Bcl-2-associated athanogene 5 (BAG5). **6**, e14695 (2011).
474 Shin, Y., Klucken, J., Patterson, C., Hyman, B. T. & McLean, P. J. J. J. o. B. C. The co-chaperone carboxyl terminus of Hsp70-interacting protein (CHIP) mediates α-synuclein degradation decisions between proteasomal and lysosomal pathways. **280**, 23727-23734 (2005).
475 Miller, V. M. *et al.* CHIP suppresses polyglutamine aggregation and toxicity in vitro and in vivo. **25**, 9152-9161 (2005).
476 Zhao, T., Hong, Y., Yin, P., Li, S. & Li, X.-J. J. P. o. t. N. A. o. S. Differential HspBP1 expression accounts for the greater vulnerability of neurons than astrocytes to misfolded proteins. **114**, E7803-E7811 (2017).
477 Singh, A. K. & Pati, U. J. A. C. CHIP stabilizes amyloid precursor protein via proteasomal degradation and p53-mediated trans-repression of β-secretase. **14**, 595-604 (2015).
478 Luan, H. *et al.* CHIP/STUB1 ubiquitin ligase functions as a negative regulator of ErbB2 by promoting its early post-biosynthesis degradation. **13**, 3936 (2021).
479 Koga, D., Ushiki, T. J. A. o. h. & cytology. Three-dimensional ultrastructure of the Golgi apparatus in different cells: high-resolution scanning electron microscopy of osmium-macerated tissues. **69**, 357-374 (2006).
480 Rambourg, A. J. E. J. C. B. Three-dimensional electron microscopy: structure of the Golgi apparatus. **51**, 189-200 (1990).
481 Jarvela, T. & Linstedt, A. D. J. M. b. o. t. c. Isoform-specific tethering links the Golgi ribbon to maintain compartmentalization. **25**, 133-144 (2014).
482 Guo, Y. & Linstedt, A. D. J. T. J. o. c. b. COPII–Golgi protein interactions regulate COPII coat assembly and Golgi size. **174**, 53-63 (2006).
483 Xu, D., Joglekar, A. P., Williams, A. L. & Hay, J. C. J. J. o. B. C. Subunit structure of a mammalian ER/Golgi SNARE complex. **275**, 39631-39639 (2000).
484 Thayanidhi, N. *et al.* α-Synuclein delays endoplasmic reticulum (ER)-to-Golgi transport in mammalian cells by antagonizing ER/Golgi SNAREs. **21**, 1850-1863 (2010).
485 Nichols, W. C. *et al.* Mutations in the ER–Golgi intermediate compartment protein ERGIC-53 cause combined deficiency of coagulation factors V and VIII. **93**, 61-70 (1998).
486 Appenzeller-Herzog, C. & Hauri, H.-P. J. J. o. c. s. The ER-Golgi intermediate compartment (ERGIC): in search of its identity and function. **119**, 2173-2183 (2006).
487 Liu, L., Zhang, M. & Ge, L. J. A. Protein translocation into the ERGIC: an upstream event of secretory autophagy. **16**, 1358-1360 (2020).
488 Tie, H. C., Chen, B., Sun, X., Cheng, L. & Lu, L. J. J. Quantitative localization of a Golgi protein by imaging its center of fluorescence mass. e55996 (2017).
489 Glick, B. S., Nakano, A. J. A. R. o. C. & Developmental. Membrane traffic within the Golgi apparatus. **25**, 113-132 (2009).
490 Suda, Y. & Nakano, A. J. T. The Yeast G olgi Apparatus. **13**, 505-510 (2012).

491 Brandizzi, F. & Barlowe, C. J. N. r. M. c. b. Organization of the ER–Golgi interface for membrane traffic control. **14**, 382-392 (2013).
492 Lowe, M. J. C. o. i. c. b. Structural organization of the Golgi apparatus. **23**, 85-93 (2011).
493 Rohn, W. M., Rouillé, Y., Waguri, S. & Hoflack, B. J. J. o. c. s. Bi-directional trafficking between the trans-Golgi network and the endosomal/lysosomal system. **113**, 2093-2101 (2000).
494 Viotti, C. J. U. p. s. m. & protocols. ER to Golgi-dependent protein secretion: the conventional pathway. 3-29 (2016).
495 Cancino, J., Jung, J. E., Luini, A. J. H. & biology, c. Regulation of Golgi signaling and trafficking by the KDEL receptor. **140**, 395-405 (2013).
496 Goldfischer, S. J. J. o. H. & Cytochemistry. The internal reticular apparatus of Camillo Golgi: a complex, heterogeneous organelle, enriched in acid, neutral, and alkaline phosphatases, and involved in glycosylation, secretion, membrane flow, lysosome formation, and intracellular digestion. **30**, 717-733 (1982).
497 Kulkarni-Gosavi, P., Makhoul, C. & Gleeson, P. A. J. F. l. Form and function of the Golgi apparatus: scaffolds, cytoskeleton and signalling. **593**, 2289-2305 (2019).
498 Deng, S., Liu, J., Wu, X., Lu, W. J. F. i. C. & Biology, D. Golgi apparatus: a potential therapeutic target for autophagy-associated neurological diseases. **8**, 564975 (2020).
499 Shen, J., Chen, X., Hendershot, L. & Prywes, R. J. D. c. ER stress regulation of ATF6 localization by dissociation of BiP/GRP78 binding and unmasking of Golgi localization signals. **3**, 99-111 (2002).
500 Ding, W. *et al.* Endoplasmic reticulum and cis-Golgi localization of human T-lymphotropic virus type 1 p12I: association with calreticulin and calnexin. **75**, 7672-7682 (2001).
501 Nishikawa, S., Hirata, A. & Nakano, A. J. M. b. o. t. c. Inhibition of endoplasmic reticulum (ER)-to-Golgi transport induces relocalization of binding protein (BiP) within the ER to form the BiP bodies. **5**, 1129-1143 (1994).
502 Popoff, V., Adolf, F., Brügger, B. & Wieland, F. J. C. S. H. p. i. b. COPI budding within the Golgi stack. **3**, a005231 (2011).
503 Rabouille, C. & Klumperman, J. J. N. r. M. c. b. The maturing role of COPI vesicles in intra-Golgi transport. **6**, 812-817 (2005).
504 Szul, T. & Sztul, E. J. P. COPII and COPI traffic at the ER-Golgi interface. **26**, 348-364 (2011).
505 Cottam, N. P. & Ungar, D. J. P. Retrograde vesicle transport in the Golgi. **249**, 943-955 (2012).
506 Willett, R., Ungar, D., Lupashin, V. J. H. & biology, c. The Golgi puppet master: COG complex at center stage of membrane trafficking interactions. **140**, 271-283 (2013).
507 Smith, R. D. & Lupashin, V. V. J. C. r. Role of the conserved oligomeric Golgi (COG) complex in protein glycosylation. **343**, 2024-2031 (2008).
508 Foulquier, F. *et al.* Conserved oligomeric Golgi complex subunit 1 deficiency reveals a previously uncharacterized congenital disorder of glycosylation type II. **103**, 3764-3769 (2006).

509 Graves, T. K., Patel, S., Dannies, P. S. & Hinkle, P. M. J. J. o. C. S. Misfolded growth hormone causes fragmentation of the Golgi apparatus and disrupts endoplasmic reticulum-to-Golgi traffic. **114**, 3685-3694 (2001).
510 Tang, F.-L. *et al.* VPS35 in dopamine neurons is required for endosome-to-Golgi retrieval of Lamp2a, a receptor of chaperone-mediated autophagy that is critical for α-synuclein degradation and prevention of pathogenesis of Parkinson's disease. **35**, 10613-10628 (2015).
511 Alvarez, C., Garcia-Mata, R., Hauri, H.-P. & Sztul, E. J. J. o. B. C. The p115-interactive proteins GM130 and giantin participate in endoplasmic reticulum-Golgi traffic. **276**, 2693-2700 (2001).
512 Mancini, M. *et al.* Caspase-2 is localized at the Golgi complex and cleaves golgin-160 during apoptosis. **149**, 603-612 (2000).
513 Miyata, S., Mizuno, T., Koyama, Y., Katayama, T. & Tohyama, M. J. P. O. The endoplasmic reticulum-resident chaperone heat shock protein 47 protects the Golgi apparatus from the effects of O-glycosylation inhibition. **8**, e69732 (2013).
514 Mohan, A. G. *et al.* The Golgi Apparatus: A Voyage through Time, Structure, Function and Implication in Neurodegenerative Disorders. **12**, 1972 (2023).
515 Kim, W. K. *et al.* Golgi Stress Response: New Insights into the Pathogenesis and Therapeutic Targets of Human Diseases. **46**, 191 (2023).
516 Reiling, J. H. *et al.* A CREB3–ARF4 signalling pathway mediates the response to Golgi stress and susceptibility to pathogens. **15**, 1473-1485 (2013).
517 Taniguchi, M. *et al.* TFE3 is a bHLH-ZIP-type transcription factor that regulates the mammalian Golgi stress response. **40**, 13-30 (2015).
518 Taniguchi, M., Yoshida, H. J. C. s. & function. TFE3, HSP47, and CREB3 pathways of the mammalian Golgi stress response. **42**, 27-36 (2017).
519 Machamer, C. E. J. F. i. n. The Golgi complex in stress and death. **9**, 421 (2015).
520 Ciurea, A. V. *et al.* Unraveling Molecular and Genetic Insights into Neurodegenerative Diseases: Advances in Understanding Alzheimer's, Parkinson's, ALS, and Huntington's Disease. (2023).
521 Ferrer, I., Costa, F., Veciana, J. G. J. N. & neurobiology, a. Creutzfeldt-Jacob disease: a Golgi study. **7**, 237-242 (1981).
522 Gonatas, N. K., Stieber, A. & Gonatas, J. O. J. J. o. t. n. s. Fragmentation of the Golgi apparatus in neurodegenerative diseases and cell death. **246**, 21-30 (2006).
523 Simon, D. K., Tanner, C. M. & Brundin, P. J. C. i. g. m. Parkinson disease epidemiology, pathology, genetics, and pathophysiology. **36**, 1-12 (2020).
524 Shah, K. & Rossie, S. J. M. n. Tale of the Good and the Bad Cdk5: Remodeling of the Actin Cytoskeleton in the Brain. **55**, 3426-3438 (2018).
525 Joshi, G., Chi, Y., Huang, Z. & Wang, Y. J. P. o. t. N. A. o. S. Aβ-induced Golgi fragmentation in Alzheimer's disease enhances Aβ production. **111**, E1230-E1239 (2014).
526 Beilina, A. *et al.* The Parkinson's disease protein LRRK2 interacts with the GARP complex to promote retrograde transport to the trans-Golgi network. **31** (2020).
527 Liazoghli, D., Perreault, S., Micheva, K. D., Desjardins, M. & Leclerc, N. J. T. A. j. o. p. Fragmentation of the Golgi apparatus induced by the overexpression of wild-type and mutant human tau forms in neurons. **166**, 1499-1514 (2005).

528 Nguyen, A. P. T. & Moore, D. J. J. L.-R. R. K. Understanding the GTPase activity of LRRK2: Regulation, function, and neurotoxicity. 71-88 (2017).
529 Pérez-Carrión, M. D., Posadas, I., Solera, J. & Ceña, V. J. I. J. o. M. S. LRRK2 and Proteostasis in Parkinson's Disease. **23**, 6808 (2022).
530 Simpson, C. *et al.* Prevalence of ten LRRK2 variants in Parkinson's disease: A comprehensive review. **98**, 103-113 (2022).
531 Waschbüsch, D., Purlyte, E. & Khan, A. R. J. B. J. Dual arginine recognition of LRRK2 phosphorylated Rab GTPases. **120**, 1846-1855 (2021).
532 Xu, L., Nagai, Y., Kajihara, Y., Ito, G. & Tomita, T. J. B. The regulation of rab gtpases by phosphorylation. **11**, 1340 (2021).
533 Zhang, L. *et al.* Spatial proteomics of vesicular trafficking: coupling mass spectrometry and imaging approaches in membrane biology. **21**, 250-269 (2023).
534 Kong, I. C., Ko, K.-S. & Koh, D.-C. J. I. J. o. M. S. Evaluation of the effects of particle sizes of silver nanoparticles on various biological systems. **21**, 8465 (2020).
535 Kuwahara, T. & Iwatsubo, T. J. F. i. n. The emerging functions of LRRK2 and Rab GTPases in the endolysosomal system. **14**, 227 (2020).
536 Shahnawaz, M. *et al.* Discriminating α-synuclein strains in Parkinson's disease and multiple system atrophy. **578**, 273-277 (2020).
537 Mandemakers, W., Morais, V. A. & De Strooper, B. J. J. o. c. s. A cell biological perspective on mitochondrial dysfunction in Parkinson disease and other neurodegenerative diseases. **120**, 1707-1716 (2007).
538 Berg, D., Holzmann, C. & Riess, O. J. N. R. N. 14-3-3 proteins in the nervous system. **4**, 752-762 (2003).
539 Chen, H.-K. *et al.* Interaction of Akt-phosphorylated ataxin-1 with 14-3-3 mediates neurodegeneration in spinocerebellar ataxia type 1. **113**, 457-468 (2003).
540 Tong, Y. *et al.* Loss of leucine-rich repeat kinase 2 causes age-dependent bi-phasic alterations of the autophagy pathway. **7**, 1-16 (2012).
541 Tong, Y. *et al.* Loss of leucine-rich repeat kinase 2 causes impairment of protein degradation pathways, accumulation of α-synuclein, and apoptotic cell death in aged mice. **107**, 9879-9884 (2010).
542 Herzig, M. C. *et al.* LRRK2 protein levels are determined by kinase function and are crucial for kidney and lung homeostasis in mice. **20**, 4209-4223 (2011).
543 Hinkle, K. M. *et al.* LRRK2 knockout mice have an intact dopaminergic system but display alterations in exploratory and motor co-ordination behaviors. **7**, 1-17 (2012).
544 Waschbüsch, D. *et al.* LRRK2 transport is regulated by its novel interacting partner Rab32. **9**, e111632 (2014).
545 Waschbüsch, D. *et al.* Rab32 interacts with SNX6 and affects retromer-dependent Golgi trafficking. **14**, e0208889 (2019).
546 Storrie, B. *et al.* Electron T omography R eveals R ab6 I s E ssential to the T rafficking of trans-G olgi C lathrin and COPI-C oated V esicles and the M aintenance of G olgi C isternal N umber. **13**, 727-744 (2012).
547 Martinez, O. *et al.* GTP-bound forms of rab6 induce the redistribution of Golgi proteins into the endoplasmic reticulum. **94**, 1828-1833 (1997).

548 Liu, S., Storrie, B. J. l. r. o. c. & biology, m. How Rab proteins determine Golgi structure. **315**, 1-22 (2015).
549 Grigoriev, I. *et al.* Rab6 regulates transport and targeting of exocytotic carriers. **13**, 305-314 (2007).
550 Lee, P. L., Ohlson, M. B. & Pfeffer, S. R. J. E. Rab6 regulation of the kinesin family KIF1C motor domain contributes to Golgi tethering. **4** (2015).
551 Goud, B., Zahraoui, A., Tavitian, A. & Saraste, J. J. N. Small GTP-binding protein associated with Golgi cisternae. **345**, 553-556 (1990).
552 Liu, S., Storrie, B. J. C. & sciences, m. l. Are Rab proteins the link between Golgi organization and membrane trafficking? **69**, 4093-4106 (2012).
553 Sun, Y. *et al.* Rab6 regulates both ZW10/RINT-1–and conserved oligomeric Golgi complex-dependent Golgi trafficking and homeostasis. **18**, 4129-4142 (2007).
554 Martinez, O. *et al.* The small GTP-binding protein rab6 functions in intra-Golgi transport. **127**, 1575-1588 (1994).
555 Girod, A. *et al.* Evidence for a COP-I-independent transport route from the Golgi complex to the endoplasmic reticulum. **1**, 423-430 (1999).
556 Kano, F. *et al.* Yip1A regulates the COPI-independent retrograde transport from the Golgi complex to the ER. **122**, 2218-2227 (2009).
557 Lopes, J. E. *et al.* Analysis of FOXP3 reveals multiple domains required for its function as a transcriptional repressor. **177**, 3133-3142 (2006).
558 Nita, E. Role of CHIP in the proteome in a neuronal cell model. (2016).
559 Yang, J.-S. *et al.* OASIS: online application for the survival analysis of lifespan assays performed in aging research. **6**, e23525 (2011).
560 Hoch, E. *et al.* Histidine pairing at the metal transport site of mammalian ZnT transporters controls Zn2+ over Cd2+ selectivity. **109**, 7202-7207 (2012).
561 Kambe, T. *et al.* Cloning and characterization of a novel mammalian zinc transporter, zinc transporter 5, abundantly expressed in pancreatic β cells. **277**, 19049-19055 (2002).
562 Ohana, E. *et al.* Identification of the Zn2+ binding site and mode of operation of a mammalian Zn2+ transporter. **284**, 17677-17686 (2009).
563 Suzuki, T. *et al.* Two different zinc transport complexes of cation diffusion facilitator proteins localized in the secretory pathway operate to activate alkaline phosphatases in vertebrate cells. **280**, 30956-30962 (2005).
564 Suzuki, T. *et al.* Zinc transporters, ZnT5 and ZnT7, are required for the activation of alkaline phosphatases, zinc-requiring enzymes that are glycosylphosphatidylinositol-anchored to the cytoplasmic membrane. **280**, 637-643 (2005).
565 Mourelatos, Z., Gonatas, N. K., Stieber, A., Gurney, M. E. & Dal Canto, M. C. J. P. o. t. N. A. o. S. The Golgi apparatus of spinal cord motor neurons in transgenic mice expressing mutant Cu, Zn superoxide dismutase becomes fragmented in early, preclinical stages of the disease. **93**, 5472-5477 (1996).
566 Joshi, G., Bekier, M. E. & Wang, Y. J. F. i. n. Golgi fragmentation in Alzheimer's disease. **9**, 340 (2015).
567 Rendón, W. O. *et al.* Golgi fragmentation is Rab and SNARE dependent in cellular models of Parkinson’s disease. **139**, 671-684 (2013).

568 Strehlow, A. N., Li, J. Z. & Myers, R. M. J. H. m. g. Wild-type huntingtin participates in protein trafficking between the Golgi and the extracellular space. **16**, 391-409 (2007).
569 Sakurai, A. *et al.* Fragmentation of the Golgi apparatus of the ballooned neurons in patients with corticobasal degeneration and Creutzfeldt-Jakob disease. **100**, 270-274 (2000).
570 Sakurai, A. *et al.* Pathology of the inferior olivary nucleus in patients with multiple system atrophy. **103**, 550-554 (2002).
571 Pottorf, T., Mann, A., Fross, S., Mansel, C. & Vohra, B. P. J. N. I. Nicotinamide Mononucleotide Adenylyltransferase 2 maintains neuronal structural integrity through the maintenance of golgi structure. **121**, 86-97 (2018).
572 van Dis, V. *et al.* Golgi fragmentation precedes neuromuscular denervation and is associated with endosome abnormalities in SOD1-ALS mouse motor neurons. **2**, 1-15 (2014).
573 Joshi, G. & Wang, Y. J. B. Golgi defects enhance APP amyloidogenic processing in Alzheimer's disease. **37**, 240-247 (2015).
574 Covarrubias-Pinto, A. *et al.* Impaired intracellular trafficking of sodium-dependent vitamin C transporter 2 contributes to the redox imbalance in Huntington's disease. **99**, 223-235 (2021).
575 Liu, J. *et al.* The role of the Golgi apparatus in disease. **47**, 38 (2021).
576 Kim, W. K. *et al.* Golgi stress response: new insights into the pathogenesis and therapeutic targets of human diseases. **46**, 191-199 (2023).
577 Barr, F. A. J. C. b. A novel Rab6-interacting domain defines a family of Golgi-targeted coiled-coil proteins. **9**, 381-384 (1999).
578 Barr, F. A. & Short, B. J. C. o. i. c. b. Golgins in the structure and dynamics of the Golgi apparatus. **15**, 405-413 (2003).
579 Fukuda, M., Kanno, E., Ishibashi, K., Itoh, T. J. M. & Proteomics, C. Large scale screening for novel rab effectors reveals unexpected broad Rab binding specificity. **7**, 1031-1042 (2008).
580 Gosavi, N., Lee, H.-J., Lee, J. S., Patel, S. & Lee, S.-J. J. J. o. B. C. Golgi fragmentation occurs in the cells with prefibrillar α-synuclein aggregates and precedes the formation of fibrillar inclusion. **277**, 48984-48992 (2002).
581 Lashuel, H. A. & Hirling, H. J. A. c. b. Rescuing defective vesicular trafficking protects against α-synuclein toxicity in cellular and animal models of Parkinson's disease. **1**, 420-424 (2006).
582 Kim, H. G., Ro, M. H., Hwang, S. H. & Lee, M. J. J. o. C. P. Transformed cells maintain survival by downregulating autophagy at a high cell confluency. **238**, 2468-2480 (2023).
583 Lallemand, D. *et al.* Stress-activated protein kinases are negatively regulated by cell density. (1998).
584 Bahar, R. *et al.* Increased cell-to-cell variation in gene expression in ageing mouse heart. **441**, 1011-1014 (2006).
585 Rai, T. S. *et al.* HIRA orchestrates a dynamic chromatin landscape in senescence and is required for suppression of neoplasia. **28**, 2712-2725 (2014).

586 Coppé, J.-P. *et al.* Senescence-associated secretory phenotypes reveal cell-nonautonomous functions of oncogenic RAS and the p53 tumor suppressor. **6**, e301 (2008).
587 Adams, P. D. J. M. c. Healing and hurting: molecular mechanisms, functions, and pathologies of cellular senescence. **36**, 2-14 (2009).
588 Sisoula, C., Trachana, V., Patterson, C., Gonos, E. S. J. F. R. B. & Medicine. CHIP-dependent p53 regulation occurs specifically during cellular senescence. **50**, 157-165 (2011).
589 Sisoula, C., Gonos, E. S. J. M. o. a. & development. CHIP E3 ligase regulates mammalian senescence by modulating the levels of oxidized proteins. **132**, 269-272 (2011).
590 Grillari, J., Grillari-Voglauer, R., Jansen-Dürr, P. J. P. M. & Aging, H. i. Post-translational modification of cellular proteins by ubiquitin and ubiquitin-like molecules: role in cellular senescence and aging. 172-196 (2010).
591 Ivanschitz, L., De Thé, H. & Le Bras, M. J. F. i. o. PML, SUMOylation, and senescence. **3**, 171 (2013).
592 Vaziri, H. & Benchimol, S. J. O. Alternative pathways for the extension of cellular life span: inactivation of p53/pRb and expression of telomerase. **18**, 7676-7680 (1999).
593 Sen, P., Shah, P. P., Nativio, R. & Berger, S. L. J. C. Epigenetic mechanisms of longevity and aging. **166**, 822-839 (2016).
594 Jang, K. W. *et al.* The C-terminus of Hsp70-interacting protein promotes Met receptor degradation. **6**, 679-687 (2011).
595 Sattler, M. & Salgia, R. J. C. R. M. The expanding role of the receptor tyrosine kinase MET as a therapeutic target in non-small cell lung cancer. **6** (2025).
596 Organ, S. L. & Tsao, M.-S. J. T. a. i. m. o. An overview of the c-MET signaling pathway. **3**, S7-S19 (2011).
597 Brand, M. D. J. E. g. Uncoupling to survive? The role of mitochondrial inefficiency in ageing. **35**, 811-820 (2000).
598 Cottrell, D. A., Turnbull, D. M. J. C. O. i. C. N. & Care, M. Mitochondria and ageing. **3**, 473-478 (2000).
599 Frenzei, H., Feimann, J. J. M. o. a. & development. Age-dependent structural changes in the myocardium of rats. A quantitative light-and electron-microscopic study on the right and left chamber wall. **27**, 29-41 (1984).
600 Liu, Y., Fiskum, G. & Schubert, D. J. J. o. n. Generation of reactive oxygen species by the mitochondrial electron transport chain. **80**, 780-787 (2002).
601 Navarro, A. *et al.* Behavioral dysfunction, brain oxidative stress, and impaired mitochondrial electron transfer in aging mice. **282**, R985-R992 (2002).
602 Trifunovic, A. *et al.* Somatic mtDNA mutations cause aging phenotypes without affecting reactive oxygen species production. **102**, 17993-17998 (2005).
603 Trifunovic, A. *et al.* Premature ageing in mice expressing defective mitochondrial DNA polymerase. **429**, 417-423 (2004).
604 Trounce, I., Byrne, E. & Marzuki, S. J. T. L. Decline in skeletal muscle mitochondrial respiratory chain function: possible factor in ageing. **333**, 637-639 (1989).

605 Yen, T.-C. *et al.* Liver mitochondrial respiratory functions decline with age. **165**, 994-1003 (1989).
606 De Felice, F. G. & Ferreira, S. T. J. D. Inflammation, defective insulin signaling, and mitochondrial dysfunction as common molecular denominators connecting type 2 diabetes to Alzheimer disease. **63**, 2262-2272 (2014).
607 Van Voorhies, W. A. & Ward, S. J. P. o. t. N. A. o. S. Genetic and environmental conditions that increase longevity in Caenorhabditis elegans decrease metabolic rate. **96**, 11399-11403 (1999).
608 Van Voorhies, W. A., Khazaeli, A. A. & Curtsinger, J. W. J. J. o. a. p. Selected contribution: long-lived Drosophila melanogaster lines exhibit normal metabolic rates. **95**, 2605-2613 (2003).
609 Bluher, M., Kahn, B. B. & Kahn, C. R. J. S. Extended longevity in mice lacking the insulin receptor in adipose tissue. **299**, 572-574 (2003).
610 Katic, M. *et al.* Mitochondrial gene expression and increased oxidative metabolism: role in increased lifespan of fat-specific insulin receptor knock-out mice. **6**, 827-839 (2007).
611 Hakimi, P. *et al.* Overexpression of the Cytosolic Form of Phosphoenolpyruvate Carboxykinase (GTP) in Skeletal Muscle Repatterns Energy Metabolism in the Mouse*♦. **282**, 32844-32855 (2007).
612 Puche, J. E. *et al.* Low doses of insulin-like growth factor-I induce mitochondrial protection in aging rats. **149**, 2620-2627 (2008).
613 Hahn, A. *et al.* Misregulation of mitochondrial 6mA promotes the propagation of mutant mtDNA and causes aging in C. elegans. **36**, 2528-2541. e2511 (2024).
614 Leboutet, R. *et al.* LGG-1/GABARAP lipidation is not required for autophagy and development in Caenorhabditis elegans. **12**, e85748 (2023).
615 Chen, H. & Chan, D. C. J. H. m. g. Emerging functions of mammalian mitochondrial fusion and fission. **14**, R283-R289 (2005).
616 Chan, D. C. J. C. Mitochondria: dynamic organelles in disease, aging, and development. **125**, 1241-1252 (2006).
617 Liesa, M., Palacín, M. & Zorzano, A. J. P. r. Mitochondrial dynamics in mammalian health and disease. **89**, 799-845 (2009).
618 Cho, D.-H. *et al.* S-nitrosylation of Drp1 mediates β-amyloid-related mitochondrial fission and neuronal injury. **324**, 102-105 (2009).
619 Van Laar, V. S. & Berman, S. B. J. E. n. Mitochondrial dynamics in Parkinson's disease. **218**, 247-256 (2009).
620 Wang, X. *et al.* Impaired balance of mitochondrial fission and fusion in Alzheimer's disease. **29**, 9090-9103 (2009).
621 Park, Y.-Y. *et al.* Loss of MARCH5 mitochondrial E3 ubiquitin ligase induces cellular senescence through dynamin-related protein 1 and mitofusin 1. **123**, 619-626 (2010).
622 Ong, S.-B. *et al.* Inhibiting mitochondrial fission protects the heart against ischemia/reperfusion injury. **121**, 2012-2022 (2010).
623 Romanello, V. *et al.* Mitochondrial fission and remodelling contributes to muscle atrophy. **29**, 1774-1785 (2010).
624 Cohen, E. *et al.* Temporal requirements of insulin/IGF-1 signaling for proteotoxicity protection. **9**, 126-134 (2010).

625 Hesp, K., Smant, G. & Kammenga, J. E. J. E. g. Caenorhabditis elegans DAF-16/FOXO transcription factor and its mammalian homologs associate with age-related disease. **72**, 1-7 (2015).
626 Kevei, É., Hoppe, T. J. N. s. & biology, m. Ubiquitin sets the timer: impacts on aging and longevity. **21**, 290-292 (2014).